frontiers | Research Topics

Quality control for efficacy and safety of herbal medicinal products, volume II

Edited by
Jian-bo Yang, Zhichao Xu, Wing Lam, Yong Li and Wei Cai

Published in
Frontiers in Pharmacology



FRONTIERS EBOOK COPYRIGHT STATEMENT

The copyright in the text of individual articles in this ebook is the property of their respective authors or their respective institutions or funders. The copyright in graphics and images within each article may be subject to copyright of other parties. In both cases this is subject to a license granted to Frontiers.

The compilation of articles constituting this ebook is the property of Frontiers.

Each article within this ebook, and the ebook itself, are published under the most recent version of the Creative Commons CC-BY licence. The version current at the date of publication of this ebook is CC-BY 4.0. If the CC-BY licence is updated, the licence granted by Frontiers is automatically updated to the new version.

When exercising any right under the CC-BY licence, Frontiers must be attributed as the original publisher of the article or ebook, as applicable.

Authors have the responsibility of ensuring that any graphics or other materials which are the property of others may be included in the CC-BY licence, but this should be checked before relying on the CC-BY licence to reproduce those materials. Any copyright notices relating to those materials must be complied with.

Copyright and source acknowledgement notices may not be removed and must be displayed in any copy, derivative work or partial copy which includes the elements in question.

All copyright, and all rights therein, are protected by national and international copyright laws. The above represents a summary only. For further information please read Frontiers' Conditions for Website Use and Copyright Statement, and the applicable CC-BY licence.

ISSN 1664-8714
ISBN 978-2-8325-6893-4
DOI 10.3389/978-2-8325-6893-4

Generative AI statement
Any alternative text (Alt text) provided alongside figures in the articles in this ebook has been generated by Frontiers with the support of artificial intelligence and reasonable efforts have been made to ensure accuracy, including review by the authors wherever possible. If you identify any issues, please contact us.

About Frontiers

Frontiers is more than just an open access publisher of scholarly articles: it is a pioneering approach to the world of academia, radically improving the way scholarly research is managed. The grand vision of Frontiers is a world where all people have an equal opportunity to seek, share and generate knowledge. Frontiers provides immediate and permanent online open access to all its publications, but this alone is not enough to realize our grand goals.

Frontiers journal series

The Frontiers journal series is a multi-tier and interdisciplinary set of open-access, online journals, promising a paradigm shift from the current review, selection and dissemination processes in academic publishing. All Frontiers journals are driven by researchers for researchers; therefore, they constitute a service to the scholarly community. At the same time, the *Frontiers journal series* operates on a revolutionary invention, the tiered publishing system, initially addressing specific communities of scholars, and gradually climbing up to broader public understanding, thus serving the interests of the lay society, too.

Dedication to quality

Each Frontiers article is a landmark of the highest quality, thanks to genuinely collaborative interactions between authors and review editors, who include some of the world's best academicians. Research must be certified by peers before entering a stream of knowledge that may eventually reach the public - and shape society; therefore, Frontiers only applies the most rigorous and unbiased reviews. Frontiers revolutionizes research publishing by freely delivering the most outstanding research, evaluated with no bias from both the academic and social point of view. By applying the most advanced information technologies, Frontiers is catapulting scholarly publishing into a new generation.

What are Frontiers Research Topics?

Frontiers Research Topics are very popular trademarks of the *Frontiers journals series*: they are collections of at least ten articles, all centered on a particular subject. With their unique mix of varied contributions from Original Research to Review Articles, Frontiers Research Topics unify the most influential researchers, the latest key findings and historical advances in a hot research area.

Find out more on how to host your own Frontiers Research Topic or contribute to one as an author by contacting the Frontiers editorial office: frontiersin.org/about/contact

Quality control for efficacy and safety of herbal medicinal products, volume II

Topic editors

Jian-bo Yang — National Institutes for Food and Drug Control, China
Zhichao Xu — Northeast Forestry University, China
Wing Lam — Yale University, United States
Yong Li — Institute of Materia Medica, Chinese Academy of Medical Sciences and Peking Union Medical College, China
Wei Cai — Hunan University of Medicine, China

Citation

Yang, J.-b., Xu, Z., Lam, W., Li, Y., Cai, W., eds. (2025). *Quality control for efficacy and safety of herbal medicinal products, volume II*. Lausanne: Frontiers Media SA. doi: 10.3389/978-2-8325-6893-4

Table of contents

05 Pre-clinical toxicity assessment of *Artemisia absinthium* extract-loaded polymeric nanoparticles associated with their oral administration
Sana Kauser, Mohd Mughees, Sanskriti Swami and Saima Wajid

22 The pharmacological effects and safety of the raw and prepared folium of *Epimedium brevicornu* Maxim. on improving kidney-yang deficiency syndrome and sexual dysfunction
Kai Wang, Juntao Li, Xinyu Zheng, Jian Xu, Zhe Wang, Senjie Li, Qiang Yang, Yue Wu, Dong-Hua Yang, Shen Yao and Xiangwei Zheng

35 Therapeutic role of Wuda granule in gastrointestinal motility disorder through promoting gastrointestinal motility and decreasing inflammatory level
Zhi Jiang, Qiuping Zou, Qicheng Chen, Junhong Zhang, Hailin Tang, Jingbao Chen, You Qin, Liming Yang, Zhiqiang Chen and Lixing Cao

50 Advancing herbal medicine: enhancing product quality and safety through robust quality control practices
Hongting Wang, Ying Chen, Lei Wang, Qinghui Liu, Siyu Yang and Cunqin Wang

66 Anti-platelet aggregation activities of different grades of *Angelica sinensis* and their therapeutic mechanisms in rats with blood deficiency: insights from metabolomics and lipidomics analyses
Xue Shen, Yangyang Wu, Ping Chen, Yuwei Bai, Yanan Liu, Yihan Jiang, Yawen Zhang and Zhigang Yang

87 Characterization of active peptides derived from three leeches and comparison of their anti-thrombotic mechanisms using the tail vein thrombosis model in mice and metabonomics
Weichao Dong, Huajian Li, Yanan Li, Yuqing Wang, Long Dai and Shaoping Wang

101 Feasibility study on the introduction of Micro-CT technology for the identification of *Radix Bupleuri* and its adulterants
Kehong Chen, Gong Chen, Zhelong Zhuang, Shouhua Luo, Jiaming Liu and Guorong Liu

110 Pharmacokinetics, safety, and efficacy of Fuqi Guben Gao in the treatment of kidney-yang deficiency syndrome: a randomized, double-blind phase I trial
Wei-Yi Cao, Jun-Yu Liu, Min Sun, Jing-Kun Wang, Fang Lu, Qiao-Ning Yang, Wan-Tong Zhang, Ming-Jie Zi, Bai-E Zhang, Hong-Bin Liu, Shu-Ge Wang, Yi Wu, Rong-Zu Wu, Wen-Di Wu, Rui Li, Zhao-Yun Zhu and Rui Gao

125 Barleriside A, an aryl hydrocarbon receptor antagonist, ameliorates podocyte injury through inhibiting oxidative stress and inflammation
Xiao-Jun Li, Yan-Ni Wang, Wen-Feng Wang, Xiaoli Nie, Hua Miao and Ying-Yong Zhao

137 Comparison of the difference in the anti-inflammatory activity of two different color types of Farfarae Flos based on *in vitro*, *in vivo* experiments and untargeted metabolomics
Kexin Zhou, Liang Peng, Yiyao Jing, Yao Luo, Yonggang Yan, Gang Zhang, Qi Guo and Bingyue Yang

151 A review on ethnobotany, phytochemistry, and pharmacology of the genus *Duhaldea* DC
Liangyin Shu, Kailin Li, Suyu Yang, Mengdie Hu, Xinrong Ming, Bingyuan Yan, Liangjun Guan and Shunli Xiao

169 The spectrum-efficacy correlation of Kai-Xin-San for cognition of $A\beta_{42}$ transgenic *Drosophila* and verification of its active ingredients
Jinfu Wu, Hang Sun, Yiyang Zhao, Lian Lian, Hongsheng Bian, Yong Guo, Dan Li and Lili Huang

182 The efficacy and safety of Chinese herbal medicine Shugan Sanjie decoction in the treatment of uterine fibroids: a systematic review and meta-analysis
Yang Zhang, Junfan Wei, Chanchan Gao, Shenyang Feng, Haiying Wang, Junjie Chai, Yini Zhu, Yuan Yuan and Lirong Ren

frontiers | Frontiers in Pharmacology

TYPE Original Research
PUBLISHED 10 July 2023
DOI 10.3389/fphar.2023.1196842

Check for updates

OPEN ACCESS

EDITED BY
Jian-Bo Yang,
National Institutes for Food and Drug Control, China

REVIEWED BY
Laiba Arshad,
Forman Christian College, Pakistan
Muhammad Dawood Shah,
University Malaysia Sabah, Malaysia

*CORRESPONDENCE
Saima Wajid,
swajid@jamiahamdard.ac.in,
wajid.saima@gmail.com

†PRESENT ADDRESS
Mohd Mughees, Department of Breast Medical Oncology, University of Texas MD Anderson Cancer Center, Houston, TX, United States

†These authors have contributed equally to this work and share first authorship

RECEIVED 31 March 2023
ACCEPTED 26 June 2023
PUBLISHED 10 July 2023

CITATION
Kauser S, Mughees M, Swami S and Wajid S (2023), Pre-clinical toxicity assessment of *Artemisia absinthium* extract-loaded polymeric nanoparticles associated with their oral administration. *Front. Pharmacol.* 14:1196842. doi: 10.3389/fphar.2023.1196842

COPYRIGHT
© 2023 Kauser, Mughees, Swami and Wajid. This is an open-access article distributed under the terms of the Creative Commons Attribution License (CC BY). The use, distribution or reproduction in other forums is permitted, provided the original author(s) and the copyright owner(s) are credited and that the original publication in this journal is cited, in accordance with accepted academic practice. No use, distribution or reproduction is permitted which does not comply with these terms.

Pre-clinical toxicity assessment of *Artemisia absinthium* extract-loaded polymeric nanoparticles associated with their oral administration

Sana Kauser†‡, Mohd Mughees†‡, Sanskriti Swami and Saima Wajid *

Department of Biotechnology, School of Chemical and Life Sciences, Jamia Hamdard, New Delhi, India

Background: This study was designed to quantify the composition of the ethanolic extract of *Artemisia absinthium* through gas chromatography–mass spectrometry analysis and ensure *in vivo* safety of *A. absinthium* extract-loaded polymeric nanoparticles (ANPs) before considering their application as a drug carrier via the oral route.

Methods: We synthesized N-isopropylacrylamide, N-vinyl pyrrolidone, and acrylic acid crosslinked polymeric NPs by free-radical polymerization reaction and characterized them by Fourier-transform infrared spectroscopy, transmission electron microscopy, and dynamic light scattering spectroscopy. Different concentrations of extract (50 mg/kg, 300 mg/kg, and 2,000 mg/kg body weight) were encapsulated into the hydrophobic core of polymeric micelles for the assessment of acute oral toxicity and their LD50 cut-off value as per the test procedure of OECD guideline 423. Orally administered female Wistar rats were observed for general appearance, behavioral changes, and mortality for the first 30 min, 4 h, 24 h, and then, daily once for 14 days.

Result: ANPs at the dose of 300 mg/kg body weight were used as an initial dose, and rats showed few short-lived signs of toxicity, with few histological alterations in the kidney and intestine. Based on these observations, the next set of rats were treated at a lower dose of 50 mg/kg and a higher dose of 2,000 mg/kg ANPs. Rats administered with 50 mg/kg ANPs remained normal throughout the study with insignificant histological disintegration; however, rats treated at 2,000 mg/kg ANPs showed some signs of toxicity followed by mortality among all three rats within 24–36 h, affecting the intestine, liver, and kidney. There were no significant differences in hematological and biochemical parameters among rats treated at 50 mg/kg and 300 mg/kg ANPs.

Conclusion: We conclude that the LD50 cut-off value of these ANPs will be 500 mg/kg extract loaded in polymeric NPs.

Abbreviations: GC–MS, gas chromatography–mass spectrometry; NIPAAM, N-isopropyl acrylamide; LCST, lower critical solution temperature; VP, N-vinyl pyrrolidone; AA, acrylic acid; ANPs, *Artemisia absinthium* whole extract-loaded (NIPAAM–VP–AA) polymeric nanoparticles; TEM, transmission electron microscopy; DLS, dynamic light scattering; FT-IR, Fourier-transform infrared spectrophotometry; PDI, polydispersity index; OECD, Organization for Economic Co-operation and Development; and GHS, Globally Harmonized System.

KEYWORDS

Artemisia absinthium, N-isopropyl acrylamide, N-vinyl pyrrolidone, acrylic acid, polymeric nanoparticles, LD50, acute oral toxicity, OECD guidelines 423

1 Introduction

Artemisia absinthium L. (Wormwood), a member of the family Asteraceae, is a perennial herb that is found mainly in the regions of Eurasia, North and South America, and Northern Africa (Bora and Sharma, 2010). This plant is known for its prominent ethnopharmacological significance and is used as a remedy in many diseases due to its antibacterial, antihelminthic, antifungal, antiparasitic, antiseptic, anti-inflammatory, and anticancer activities (Bhat et al., 2018; Mughees et al., 2019). All these activities are ascribed to the presence of different flavonoids, phenolics, and tannins whose type varies with varying geographical origin. The chief components of *A. absinthium* essential oil are β-thujone, β-pinene, (Z)-epoxyocimene, borneol, chrysanthenyl acetate, isobornyl acetate, and methyl hinokiate (Riahi et al., 2015). Oleic and linoleic saturated acids (palmitic and stearic), as well as epoxy oleic acid (oxirane), constitute the fatty acid portion of the essential oil. Phenolic compounds of the plant include p-hydroxyphenylacetic, protocatechuic, fisetin, isorhamnetin, and kaempferol, while phenolic acids include syringic, gallic, p-coumaric, vanillic, caffeic, ferulic, and chlorogenic acids, which are accountable for the antioxidant and free-radical scavenging potential of the plant (Craciunescu et al., 2012; Goud et al., 2015). Flavonoids include artemitin, quercetin, luteolin, apigenin, rutin, myricetin, spinacetin, and glycosides of quercetin, e.g., quercitin 3-glucoside, quercitin 3-rhamnoglucoside, spinacetin 3-glucoside, and spinacetin 3-rhamnoglucoside. Lignans (derived from phenylalanine) are polyphenolic compounds that include diayangambin and epiyangambin (Bora and Sharma, 2010). Volatile oils majorly contain sabinene, myrcene, linalool, and trans-sabinyl acetate. Monoterpene hydrocarbons are the principal component present in the plant with fewer oxygenated monoterpenes, sesquiterpene hydrocarbons, and oxygenated sesquiterpenes. Sesquiterpenes including α-bisabolol, β-curcumene, matricin, and spathulenol are mainly responsible for the antibacterial and antiparasitic activities of the plant (Goud et al., 2015).

Nanotechnology in the field of pharmaceuticals has been implemented to assist site-specific drug delivery by utilizing nanoparticles as a drug carrier which ensures efficient solubility, absorption, and bioavailability of several drugs. Different types of nanoparticles (NPs) are synthesized that vary in their morphology, size, and physical and chemical characteristics, e.g., lipid-based, metallic, ceramic, semiconductor, and polymeric nanoparticles. Among these, polymeric NPs are often preferred over other NPs as they possess good retention time, simple preparation, and less toxicity. Drug-loaded polymeric NPs can pass through the physiological barriers and further stimuli-triggered release of the desired concentration of drug into the intracellular compartment of the target site, thus making it ideal for the drug delivery system (Sur et al., 2019). Self-assembled, double-triggered thermoresponsive, and pH-sensitive crosslinked copolymeric micelles, made of N-isopropyl acrylamide (NIPAAM), N-vinyl pyrrolidone (VP), and acrylic acid (AA), are non-toxic and biocompatible and have been used previously with several drugs (e.g., ketorolac and riluzole) to ensure site-specific delivery of the formulation (Gupta et al., 2000; Verma et al., 2016). Copolymerization of the acrylic acid provides a carboxylic group, which makes it pH-sensitive and responsive when the pH is changed at the particular cell or tissue in the body. Similarly, NIPAAM, being a thermoresponsive polymer, has been known to have lower critical solution temperature (LCST) (32°C) near physiological temperature, and its copolymerization increases its LCST above which its polymeric form collapsed. The anticancer therapeutic potential of *A. absinthium* ethanolic extract-loaded NIPAAM–VP–AA NPs against breast cancer cell lines (MCF-7 and MDA MB-231) was previously evaluated by our research team (Mughees et al., 2020). The tumor microenvironment (leaky vasculature with irregular epithelial cells, elevated temperature around cancerous cells due to inflammation, and low physiological pH due to an acidic environment) was utilized for the targeted drug delivery system employing pH and thermoresponsive polymeric nanoparticles for *in vitro* breast cancer treatment.

The *A. absinthium* extract in conjugation with NIPAAM–VP–AA NPs would aid the establishment of potential drug with enhanced bioavailability, retention time, and efficacy of the extract due to site-specific drug delivery. The *in vivo* behavior of these NPs and their capability to cross certain biological barriers after oral administration have not been scrutinized previously. The oral utilization of nanoformulations with a larger surface-area-to-volume ratio provides greater surface area for mucosal interaction and adherence, protecting entrapped therapeutic agents from extreme pH conditions and enzymatic degradation and facilitating sustained release and enhanced systemic absorption of drugs or intact NPs in the gastrointestinal (GI) tract. However, the fate of NPs in the GI tract and further distribution throughout the body depends on their size, shape, composition, surface charge, conformation, and concentration (Peppas and Kavimandan, 2006; Hua, 2020). As inadequate information is available in the scientific literature about *in vivo* oral administration of the *A. absinthium* ethanolic extract and NIPAAM–VP–AA polymeric NPs, thus, the investigation of the *in vivo* safety of *A. absinthium* ethanolic extract-loaded NIPAAM–VP–AA NPs (ANPs) is a prerequisite before considering their clinical implication as a drug carrier via the oral route.

The main objectives of the present study were to identify the composition of the ethanolic extract of *A. absinthium* grown in the Indian subcontinent and the evaluation of the acute oral toxicity of these *A. absinthium* extract-loaded polymeric nanoparticles in rats as per the OECD guidelines for the Testing of Chemicals (423), Acute Oral Toxicity—Acute Toxic Class Method. This guideline will also allow the determination of the LD50 cut-off value of these ANPs and their further ranking for classification purposes and hazard assessment.

2 Materials and methods

2.1 Reagents

N-isopropyl acrylamide (NIPAAM) was procured from Sigma-Aldrich (United States) and recrystallized with N-hexane before use. N-vinyl pyrrolidone (VP) was purchased from Acros Organics,

which was freshly distilled before use. Acrylic acid (AA) and N, N′-methylenebisacrylamide (MBA) were procured from Sigma-Aldrich (United States). Ferrous ammonium sulfate (FAS) and ammonium persulfate (APS) were purchased from SRL Pvt. Ltd. and Hi-media. Absolute ethanol was purchased from Merck (Germany).

2.2 Plant material and preparation of the ethanolic extract

Plant *A. absinthium* (vegetative stage) was obtained during mid-summer from Jamia Hamdard Herbal Garden. It was thoroughly washed to remove dust or dirt, and its different parts (root, leaf, and aerial portion) were shade-dried. Whole plant extract synthesis was carried out through maceration of 5 gm dried powdered sample mixed with 20 mL ethanol (1:5 = drug:solvent ratio) at 28°C ± 2°C for 24 h in an incubator shaker. This procedure was repeated three times consecutively, and the final collected solvent was filtered through Whatman filter paper no. 45. A rotary evaporator was used to concentrate the filtrate under vacuum pressure at 40°C until 5 mL solvent was left (with extraction yield = 3.06%), which was further filtered through a 0.22 μm Millipore syringe filter and stored at 4°C for further use.

2.3 Gas chromatography–mass spectrometry analysis

The types of active compounds present in the whole plant ethanolic extract of *A. absinthium* grown in the Indian subcontinent have not been reported previously. Therefore, it needs to be addressed before their therapeutic application. Thus, the separation and identification of compounds in the *A. absinthium* ethanolic extract were performed using a GC/MS QP 2010 (Shimadzu) equipped with an auto-injector (AOC-20i + s) mass selective detector having an ion source temperature of 220°C, interface temperature of 270°C, solvent cut time of 3.50 min, threshold of 1,000 eV, and mass range of 40–650 m/z. Compounds were separated using an Rxi-5 Sil MS capillary column (Restek Company, Bellefonte, United States) having dimensions 30 m × 0.25 mm × 0.25 μm (film thickness). The split injection mode was used at a split ratio of 10:1 having an injection temperature of 260°C. 1.0 μL of ethanolic extract was fixed as the injected volume. Oven temperature program started from 80°C (3 min) and further increased to 300°C at a rate of 10°C/min (16 min hold). Helium was used as the carrier gas at a linear flow velocity of 40.5 cm/s with a total and column flow fixed at 16.3 and 1.21 mL/min, respectively. Compounds were identified by the comparison of their relative retention time and mass spectra with those in the NIST libraries and literature data.

2.4 Synthesis and characterization of polymeric nanoparticles

Polymeric nanoparticles were synthesized as described previously (Mughees et al., 2020). Monomeric NIPAAM, VP, and AA were used in the molar ratio of 90:10:5. This protocol is based on the free-radical mechanism where MBA was used for crosslinking the monomers, FAS was used as an activator, and APS as an initiator in the polymerization reaction. Then, 180 mg NIPAAM, 20 μL VP, and 10 μL AA were dissolved in 20 mL double distilled water with vigorous vortexing. For crosslinking the monomers, 100 μL MBA (0.049 g/mL) was added and nitrogen gas was passed for 1 h to remove dissolved oxygen from the reaction. Then, 60 μL FAS (5 mg/mL) and 100 μL APS (saturated) were added in the reaction to trigger polymerization that lasted for 24 h at 32°C under nitrogen atmosphere. After completion, the final solution was dialyzed through a cellulose dialyzing membrane (cut-off 12 kDa) and lyophilized for further use.

Synthesized NPs were characterized for their average size distribution and polydispersity index (PDI) by Zetasizer Nano ZS Ver. 7.13, (Malvern Instruments Ltd., Worcestershire, United Kingdom) through dynamic scattering light (DLS) spectroscopy. 2 mL aqueous solution was used for measurement employing a laser beam (wavelength of 633 nm) passing through the solution at 25°C with a detection angle of 90°.

Transmission electron microscopy (TEM) was performed on Tecnai G20 HR-TEM (Thermo Scientific) operated at a voltage of 200 kV to analyze the size and morphology of synthesized NPs. A drop of NPs was placed on a carbon-coated copper grid, and 2% uranyl acetate was added. The grid was air-dried, and TEM images were obtained through a high-resolution digital CCD camera with image processing software (Olympus Soft Imaging System, Germany).

Fourier-transform infrared (FTIR) spectra of NIPAAM, VP, and AA and synthesized NPs were recorded through a Varian 7000 FTIR Spectrometer with a Varian 600 UMA Microscope using the KBr pellet method. Each monomer and NPs were scanned at wavenumbers in the range of 4,000 cm^{-1} to 400 cm^{-1} with a resolution of 2 cm^{-1} and 16 scans per sample.

2.5 Animals

Twenty-one 8–12-week-old (100–150 gm) healthy female Wistar rats were procured from the Central Animal House Facility (CAHF), Jamia Hamdard, New Delhi, and randomly housed in a group of three per cage under standard conditions (20 ± 2°C; 50 ± 10% relative humidity; and 12 h of light/dark cycles) for acclimatization to ideal laboratory conditions 7 days before the start of the experiment. The rats were provided free access to food and water *ad libitum*. All the experiments were approved and performed in compliance with the Institutional Animal Ethics Committee (IAEC) constituted through the Committee for the Purpose of Control and Supervision of Experiments on Animals (173/GO/Re/S/2000/CPCSEA) under the Ministry of Animal Welfare Division, Government of India, New Delhi.

2.6 Acute oral toxicity study

The toxicological assessment was conducted according to the procedures of the Organization for Economic Co-operation and

Development (OECD) guideline for the Testing of Chemicals (423), Acute Oral Toxicity—Acute Toxic Class Method, which is a (single dose) 14-day acute oral study using three female Wistar rats per step. The range of acute toxicity of the test substance depends on the mortality incidence of the animals which assists in finding the toxicity category of the tested drug defined by fixed LD50 cut-off values. For animal welfare reasons, the OECD guideline 423 recommends using 300 mg/kg body weight as a starting dose, when sufficient information is not available about the substance to be tested. Lyophilized NPs were dissolved in distilled water, and the extract was added slowly with continuous vortexing and mild sonication to facilitate its physical entrapment inside the hydrophobic core of NPs. Different concentrations of *A. absinthium* ethanolic extract were loaded into NPs as per the body weight of each rat, and food but not water was withheld overnight before dosing. Group CN (n = 6) served as the control that received distilled water via oral gavage, while group ANP_{300} (n = 6) received *A. absinthium* ethanolic extract-loaded NPs at an initial dose of 300 mg/kg body weight. The rats were critically observed for general appearance, behavioral changes, and mortality rate for the first 30 min, 4 h, 24 h, and then, daily once for 14 days. The body weight of each rat was monitored and recorded periodically throughout the study.

Based on the absence or presence of mortality, group ANP_{2000} (n = 3) received the next higher dose of 2,000 mg/kg body weight ANPs. With a minor modification to the OECD guideline 423 due to the presence of few toxic signs among ANP_{300}-treated animals, another group ANP_{50} (n = 6) received the next lower dose of 50 mg/kg body weight ANPs. On the 15th day, blood was drawn from the tail vein in EDTA-coated sterilized vials and anticoagulant free vials for whole blood and serum collection, respectively. The rats were euthanized by CO_2 inhalation for procuring all the vital organs (stomach, intestine liver, kidney, spleen, heart, and brain) for necropsy, macroscopic examination, and histopathological analysis.

2.7 Hematological and biochemical parameters

Whole blood was processed immediately to examine hematological parameters using an automatic hematological analyzer (Sysmex XP 100, Transasia, India). The hematological parameters measured were hemoglobin (Hb), total leucocyte count (TLC), neutrophil, lymphocyte, eosinophil, monocyte, basophil, and red blood cell count (RBC), hematocrit (PCV/HCT), mean corpuscular volume (MCV), mean corpuscular Hb (MCH), mean corpuscular Hb concentration (MCHC), and platelet count. Anticoagulant-free vials were left undisturbed for 30 min to coagulate and then centrifuged for 15 min at 4,500 rpm for serum separation. Serum was used to investigate biochemical parameters using an automatic chemistry analyzer (ERBACHEM 7X, Transasia, India) comprising total bilirubin, direct bilirubin, indirect bilirubin, serum glutamic-oxaloacetic transaminase (SGOT), serum glutamic pyruvic transaminase (SGPT), alkaline phosphatase, total protein, albumin, globulin, urea, creatinine, uric acid, serum calcium, sodium, potassium, and chloride.

2.8 Histopathology

Various vital organs (stomach, intestine liver, kidney, spleen, heart, and brain) were fixed in a 10% buffered formalin solution before embedding in paraffin wax. From these blocks, 3–4 μm sections were made and stained with hematoxylin and eosin (H&E). Histopathology was carried out to identify any morphological and degenerative changes in different organs due to ANP administration.

2.9 Statistical analysis

The data obtained from all the groups were statistically analyzed by GraphPad Prism Version 7 and expressed as the mean ± standard deviation. Differences in hematology and biochemistry data were analyzed using one-way ANOVA followed by Dunnett's multiple comparison tests. However, body weight results were analyzed using two-way ANOVA followed by Dunnett's multiple comparison tests, and p-value < 0.05 was considered statistically significant.

3 Results

3.1 Gas chromatography–mass spectrometry analysis

Forty-five compounds were identified in the *A. absinthium* ethanolic extract through gas chromatography–mass spectrometry (GC–MS) analysis as shown in Figure 1 (chromatogram). The list of the active compounds, their retention time, molecular formula, and area % are shown in Table 1. All the detected compounds belong to diverse classes of phytochemicals with ethnomedical benefits, namely, polysaccharides, terpenoids, flavonoids, phytosterols, lignans, and fatty acid esters. Out of the forty-five compounds, some biologically important and prevalent compounds include mome inositol (11.83%), tetracontane (2.26%), stigmasta-5,22-dien-3-ol (3.34%), gamma-sitosterol (9.55%), cycloartenol (1.07%), yangambin (34.44%), 24-methylenecycloartanol (1.08%), and sesartemin (5.28%), while compounds like neophytadiene (0.25%), 6,10,14-trimethyl-2-pentadecanone (0.16%), hexadecanoic acid, ethyl ester (0.23%), alpha-curcumene (0.24%), reynosin (0.54%), phytol (0.48%), 9,12-octadecadienoic acid (Z,Z)-, methyl ester (0.25%), isogeraniol (0.47%), 1-docosanol (0.48%), 2-methyloctacosane (0.23%), squalene (0.67%), ergost-5-en-3-ol, (3Beta,24R) (0.87%), and artemetin (0.61%) were present in trace amount as shown in Table 2. Phytosterols, including gamma-sitosterol (Sundarraj et al., 2012), campesterol, and stigmasta-5,22-dien-3-ol (Shahzad et al., 2017; Vezza et al., 2020), have the potential to trigger the production of anti-inflammatory cytokine, hepatoprotective, hypercholesterolemic, antidiabetic, and anticancer activities. The two most dominant lignans, namely, yangambin (Monte et al., 2007; Bala et al., 2015) and sesartemin (Dixit and Reddy, 2017; Ickovski et al., 2020), tend to exhibit analgesic, antianaphylactic, antiallergic, antileishmanial, anti-PAF, and anticancer activities and can act as an inhibitor of cytochrome P450-linked oxygenase. Polysaccharide-like mome inositol has been reported with antiallopathic, anticirrhotic, antineuropathic,

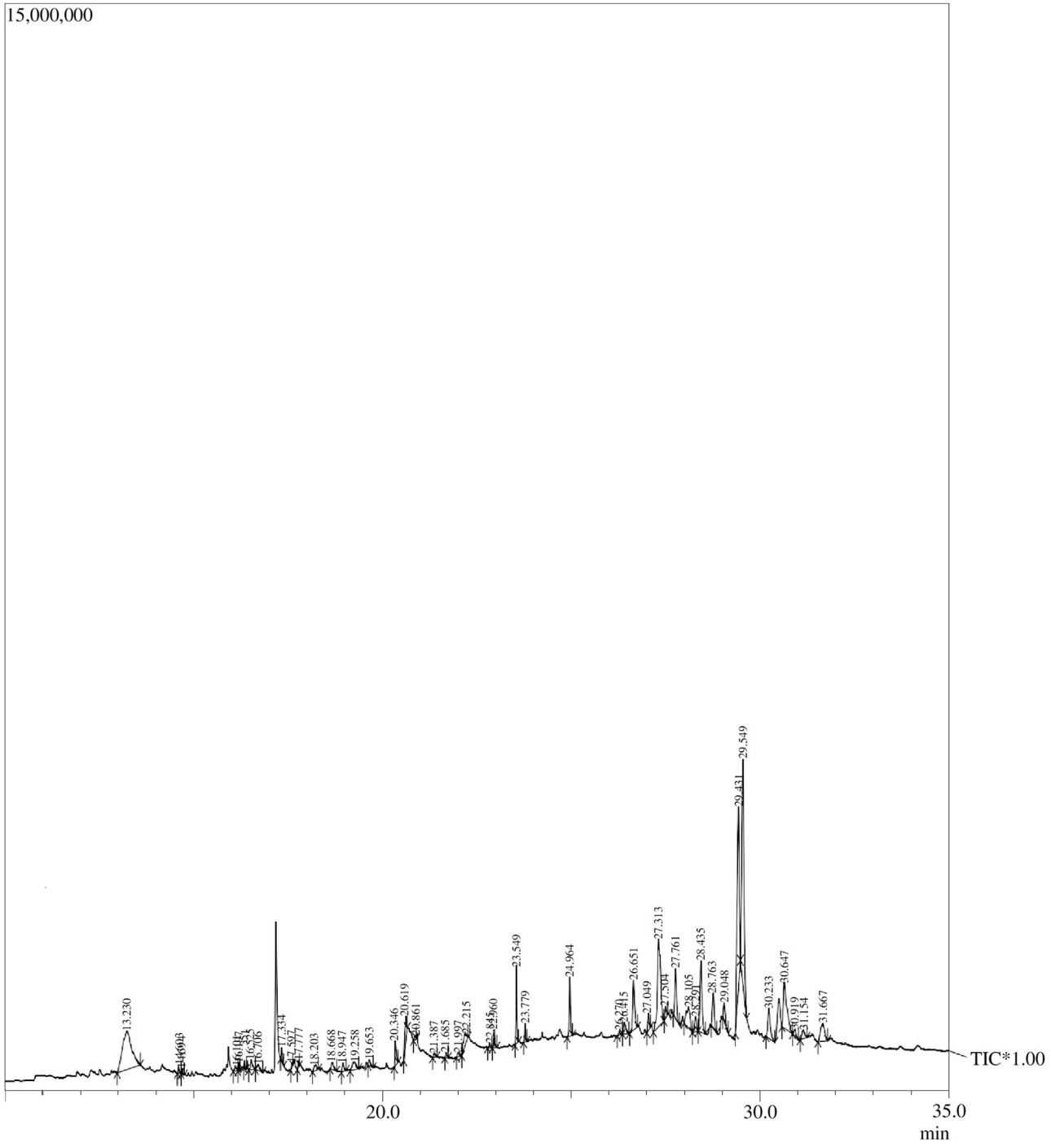


FIGURE 1
GC–MS chromatogram: Peaks of the *Artemisia absinthium* ethanolic extract obtained through GC–MS analysis.

cholesterolytic, and lipotropic activities (Das et al., 2014). Flavonoids like artemetin possess antioxidant, hepatoprotective, and antiedematogenic activities (Bayeux et al., 2002). Palmitic and linoleic acid esters, namely, hexadecanoic acid, ethyl ester, and 9,12-octadecadienoic acid (Z, Z)-, methyl ester, also have antioxidant, anti-inflammatory, hypocholesterolemic, cancer preventive, insectifuge, antiarthritic, hepatoprotective, antiandrogenic, nematicide, and antihistaminic properties (Krishnamoorthy and Subramaniam, 2014). Compounds belonging to different classes of terpenes, such as neophytadiene (Bhardwaj et al., 2020), 6,10,14-trimethyl-2-pentadecanone (Chen et al., 2022), alpha-curcumene (Obrenovich et al., 2010), reynosin (Lim et al., 2013), phytol (Krishnamoorthy and Subramaniam, 2014), isogeraniol (Lei et al., 2019), squalene, cycloartenol, and 24-methylenecycloartenol (Wu et al., 2022), have been found to encompass antioxidant, anti-inflammatory, antimicrobial, antiproliferative, immunostimulant, chemopreventive,

TABLE 1 Compounds identified in *Artemisia absinthium* whole plant ethanolic extract through GC–MS analysis.

Peak	R.Time	Area	Name	Formula	Area %
1	13.230	8,993,640	Mome inositol	$C_7H_{14}O_6$	11.83
2	14.603	190,918	Neophytadiene	$C_{20}H_{38}$	0.25
3	14.694	119,615	6,10,14-Trimethyl-2-pentadecanone	$C_{18}H_{36}O$	0.16
4	16.101	205,452	4-tert-Butyl-2,6-diisopropylphenol	$C_{16}H_{26}O$	0.27
5	16.197	178,382	Hexadecanoic acid, ethyl ester	$C_{18}H_{36}O_2$	0.23
6	16.351	179,208	alpha-Curcumene	$C_{15}H_{22}$	0.24
7	16.525	488,604	Cyclohexanemethanol, 4-ethenyl-alpha.,.Alpha.,4-Trimethyl-3-(1-methylethenyl)-, [1R (1.Alpha.,3.Alpha.,4.Beta.)]	$C_{15}H_{26}O$	0.64
8	16.706	408,294	Reynosin	$C_{15}H_{20}O_3$	0.54
9	17.334	363,358	Phytol	$C_{20}H_{40}O$	0.48
10	17.597	121,731	3,5-Dimethylcyclohex-1-ene-4-carboxaldehyde	$C_9H_{14}O$	0.16
11	17.777	189,641	9,12-Octadecadienoic acid (Z,Z)-, methyl ester	$C_{19}H_{34}O_2$	0.25
12	18.203	368,050	11-Heneicosanone	$C_{21}H_{42}O$	0.48
13	18.668	359,300	Isogeraniol	$C_{10}H_{18}O$	0.47
14	18.947	362,183	1-Docosanol	$C_{22}H_{46}O$	0.48
15	19.258	718,469	13,21-Cyclo-18-norpregnan-20-ol, 20-methyl-, (5.alpha.,20S	$C_{21}H_{34}O$	0.95
16	19.653	294,295	p-Undecyloxybenzoic acid	$C_{18}H_{28}O3$	0.39
17	20.346	934,622	Silane, dimethyl(3-ethylphenoxy)heptyloxy-	$C_{17}H_{30}O_2Si$	1.23
18	20.619	1,168,896	1-Heneicosanol	$C_{21}H_{44}O$	1.54
19	20.861	129,421	Palmitic acid, TMS derivative	$C_{19}H_{40}O_2Si$	0.17
20	21.387	174,184	2-Methyloctacosane	$C_{29}H_{60}$	0.23
21	21.685	168,280	(E)-3,7-dimethylocta-2,6-dien-1-yl stearate	$C_{28}H_{52}O_2$	0.22
22	21.997	202,569	1H-indole-3-acetic acid	$C_{10}H_9NO_2$	0.27
23	22.215	982,203	Hexanoic acid, heptadecyl ester	$C_{23}H_{46}O_2$	1.29
24	22.845	172,657	Pentacontanoic acid, ethyl ester	$C_{52}H_{104}O_2$	0.23
25	22.960	507,808	Squalene	$C_{30}H_{50}$	0.67
26	23.549	1,766,666	Pentacosane	$C_{25}H_{52}$	2.32
27	23.779	445,163	2,2-Dimethyl-3-(3,7,16,20-tetramethyl-heneicosa-3,7,11,15, 19-pentaenyl)-oxirane	$C_{29}H_{48}O$	0.59
28	24.964	1,715,947	Tetracontane	$C_{40}H_{82}$	2.26
29	26.270	177,153	2,4-Diamino-5-[3,4,5-trimethoxybenzoxy]pyrimidine	$C_{14}H_{16}N_4O_5$	0.23
30	26.415	664,124	Ergost-5-en-3-ol, (3Beta,24R)-	$C_{28}H_{48}O$	0.87
31	26.651	2,537,184	Stigmasta-5,22-dien-3-ol	$C_{29}H_{48}O$	3.34
32	27.049	643,954	Ergosta-8,24(28)-dien-3-Ol, 4,14-dimethyl-, (3.Beta.,4.Alpha.,5.Alpha.)	$C_{30}H_{50}O$	0.85
33	27.313	7,256,424	gamma-Sitosterol	$C_{29}H_{50}O$	9.55
34	27.504	459,989	4H-1-benzopyran-4-one, 2-(3,4-dimethoxyphenyl)-5-hydroxy-3,6,7-trimethoxy; artemetin	$C_{20}H_{20}O_8$	0.61
35	27.761	2,265,533	3-Debenzoyl-tetrahydrocarpesterol	$C_{30}H_{54}O_3$	2.98
36	28.105	2,022,248	5-Chloro-3-(4-methoxyphenyl)-1-methylpyrazole-4-carboxaldehyde	$C_{12}H_{11}ClN_2O_2$	2.66
37	28.291	812,278	9,19-Cyclolanost-24-en-3-ol, (3.beta.)-; cycloartenol	$C_{30}H_{50}O$	1.07

(Continued on following page)

TABLE 1 (*Continued*) Compounds identified in *Artemisia absinthium* whole plant ethanolic extract through GC–MS analysis.

Peak	R.Time	Area	Name	Formula	Area %
38	87.415	26,175,102	Yangambin	$C_{24}H_{30}O_8$	34.44
39	28.763	1,641,286	Cholesterol epoxide	$C_{27}H_{46}O_2$	2.16
40	29.048	822,805	24-Methylenecycloartenol	$C_{31}H_{52}O$	1.08
41	30.233	1,870,633	1-Meyhyl-2,4,6-triphenyl-1-[2-phenyl-(E)-ethenyl]-.Lambda(5).-Phosphinine	$C_{32}H_{27}P$	2.46
42	30.647	4,011,010	Sesartemin	$C_{23}H_{26}O_8$	5.28
43	30.919	349,032	3-(1,5-Dimethyl-hexyl)-3a,10,10,12b-tetramethyl-1,2,3,3a,4,6,8,9,10,10a,11,12,12a,12b-tetradecahydro-benzo[4,5]cyclohepta[1,2-E]inde ne	$C_{30}H_{50}$	0.46
44	31.154	551,541	Dimethyl 2-[(1′,4′-dimethoxy-9′,10′-dioxo-9′,10′dihydroanthracen-2′-Yl)Methylene]Butanedioate	$C_{23}H_{22}O_8$	0.73
45	31.667	1,831,203	4.alpha.,14-dimethyl-5.alpha.-ergosta-8,24(28)-dien-3.beta-ol	$C_{30}H_{50}O$	2.41

lipoxygenase-inhibitor, pesticide, and diuretic activities. Polycosanols including 1-docosanol and tetracontane (Vergara et al., 2015) have anti-inflammatory, antiproliferative, analgesic, and antiviral activities, while isononacosane-like 2-methyloctacosane has an antimicrobial activity (Barretto and Vootla, 2018).

3.2 Synthesis and characterization of the synthesized polymeric nanoparticles

The free-radical polymerization process was exploited for the copolymerization of NIPAAM, VP, and AA monomers resulting in the formation of amphiphilic micelles with an external hydrophilic shell and an inner hydrophobic core. This hydrophobic core of the micelles was utilized as the carrier of the plant extract. The average particle size of NPs was found to be 131 nm with PDI 0.2 at 25°C as determined by DLS, indicating monodispersity in solution [Figure 2I]. TEM analysis revealed prominent spherical-shaped morphology of NPs with an average size of 117 nm ± 4.04 nm as shown in Figure 2II. FTIR spectra of monomeric NIPAAM, VP, AA, and synthesized polymeric NPs are shown in Figure 2III. FTIR spectra of NIPAAM [Figure 2IIIa] show characteristic absorption peaks at 3,297 cm^{-1} corresponding to N–H stretching vibrations of the secondary amide group. Absorption peaks in the range of 2,970–2,875 cm^{-1} correspond to C–H bond stretching vibrations of methyl and isopropyl groups in NIPAAM. The absorption peak at 1,659 cm^{-1} and 1,548 cm^{-1} occurred due to amide I-associated C=O stretching vibrations and amide II-associated N–H bending with C–N stretching vibrations, respectively. A medium-intensity absorption peak at 1,620 cm^{-1} originated from the stretching vibrations of the C=C bond, while peaks in the range of 963–809 cm^{-1} appeared due to the out-of-plane bending vibrations of = C–H bond in the vinyl group of NIPAAM. Other less-intense peaks in the range of 1,369–1,307 cm^{-1} correspond to vibrations from the isopropyl group of NIPAAM. FTIR spectra of VP [Figure 2IIIb] had characteristic absorption peaks at 3,484 cm^{-1} and 1,711 cm^{-1} occurring due to O–H and amide C=O stretching vibrations, respectively. Absorption peaks in the range 2,985–2,885 cm^{-1} and 1,634 cm^{-1} correspond to C–H and C=C stretching vibrations, respectively. Peaks at 1,420 cm^{-1} and 1,460 cm^{-1} occurred due to = C–H and aromatic ring stretching vibrations. FTIR spectra of AA [Figure 2IIIc] represent characteristic absorption peaks at 3,074 cm^{-1} and 1,704 cm^{-1} due to carbonyl O–H bond and C=O bond stretching vibrations, respectively. Additionally, absorption peaks at 1,636 cm^{-1} and 985 cm^{-1} are designated to C=C and = C–H stretching vibrations, respectively. However, FTIR spectra of synthesized polymeric NPs [Figure 2IIId] depict changes in the peaks corresponding to specific functional groups in monomers indicating the formation of new interactions. There were no peaks in the range of 800–1,000 cm^{-1} corresponding to stretching vibrations of vinyl double bond indicating that polymerization has occurred among monomers via breaking of the C=C bond (Larrañaga et al., 2011; Verma et al., 2016). Absorption peaks at 1,639 cm^{-1} and 1,720 cm^{-1} correspond to C=O stretching vibrations from all three monomeric units in the polymer. Another broad and intense peak at 3,445 cm^{-1} represents O–H stretching vibration due to attached water of hydration with the polymer (Gupta et al., 2000; Mughees et al., 2020). In comparison with the monomer, declination in the absorption peaks in the range of 1,369–1,307 cm^{-1} corresponding to vibrations from the isopropyl group implies their involvement as the crosslinking points.

3.3 Acute oral toxicity study

All rats were observed individually for several clinical signs of toxicity including loss of appetite, skin and fur change, sitting at the corner, mortality, convulsion, drowsiness, salivation, respiratory depression/irregular respiratory pattern, lacrimation, abnormal sleeping pattern, tremors, diarrhea, aggressiveness, and piloerection and recorded as shown in Table 3. Group ANP_{300} treated at an initial dose of 300 mg/kg appeared less active and drowsy, sat at the corners of the cage with loss of appetite for the first 30 min of the oral administration compared to control, and then, appeared normal afterward. The presence of these few clinical signs but no mortality in animals treated at 300 mg/kg led us to proceed to the next higher dose of 2,000 mg/kg and the next lower dose of 50 mg/kg. Group ANP_{2000} showed few signs of toxicity in the first 30 min which included loss of appetite, sitting at the corner, and drowsiness.

TABLE 2 Activity of some important bioactive compounds found in *Artemisia absinthium* whole plant ethanolic extract.

Peak	Name	Compound nature	Activity
1.	Mome inositol	Polysaccharide	Anticirrhotic, antineuropathic, antioxidant, cholesterolytic, and lipotropic; Das et al. (2014)
2.	Neophytadiene	Diterpene	Anti-inflammatory and antimicrobial; Bhardwaj et al. (2020)
3.	6,10,14-Trimethyl-2-pentadecanone	Sesquiterpene	Anti-inflammatory and antibacterial; Chen et al. (2022)
4.	Hexadecanoic acid, ethyl ester	Palmitic acid	Antioxidant and anti-inflammatory; Krishnamoorthy and Subramaniam, (2014)
5.	alpha-Curcumene	Sesquiterpene	Antioxidant, anti-inflammatory, antimicrobial, cytotoxic, and antiviral; Obrenovich et al. (2010)
6.	Reynosin	Sesquiterpene	Hepatoprotective, anti-inflammatory, and antimicrobial; Lim et al. (2013)
7.	Phytol	Diterpene	Antimicrobial, anti-inflammatory anticancer, diuretic, antitumor, chemopreventive, and antimicrobial; Krishnamoorthy and Subramaniam, (2014)
8.	9,12-Octadecadienoic acid (Z, Z)-, methyl ester	Linoleic acid ester	Anti-inflammatory, hypocholesterolemic, cancer preventive, insectifuge, antiarthritic, hepatoprotective, antiandrogenic, nematicide, and antihistaminic; Krishnamoorthy and Subramaniam, (2014)
9.	Isogeraniol	Terpene	Flavoring agent and antifungal; Lei et al. (2019)
10.	1-Docosanol	Polycosanols	Antiproliferative and antiviral; Vergara et al. (2015)
11.	2-Methyloctacosane	Hydrocarbon	Antimicrobial; Barretto and Vootla, (2018)
12.	Squalene	Triterpene	Antibacterial, antioxidant, antitumor, cancer preventive, immunostimulant, chemopreventive, lipoxygenase-inhibitor, and pesticide; Wu et al. (2022)
13.	Tetracontane	Polycosanols	Anti-inflammatory and analgesic; Vergara et al. (2015)
14.	Ergost-5-en-3-ol, (3Beta,24R)-; campesterol	Phytosterol	Protection against liver diseases (e.g., jaundice), atherosclerosis, and anticancer; Shahzad et al. (2017); Vezza et al. (2020)
15.	Stigmasta-5,22-dien-3-ol	Phytosterol	Anti-inflammatory, antihypercholestrolemic, antitumor antioxidant, antiarthritic antiasthma, diuretic, antibacterial, and antiviral; Shahzad et al. (2017); Vezza et al. (2020)
16.	gamma-Sitosterol	Phytosterols	Antimicrobial, antidiabetic, and anticancer; Sundarraj et al. (2012)
17.	4H-1-benzopyran-4-one, 2-(3,4-dimethoxyphenyl)-5-hydroxy-3,6,7-trimethoxy; artemetin	Flavonoids	Antioxidant, hepatoprotective, and antiedematogenic; Bayeux et al. (2002)
18.	9,19-Cyclolanost-24-en-3-ol, (3.beta.)-; cycloartenol	Triterpenoid	Antioxidant and antimicrobial; Wu et al. (2022)
19.	Yangambin	Lignan	Analgesic, antianaphylactic, antiallergic, antileishmanial, anti-PAF, and anticancer; Monte et al. (2007); Bala et al. (2015)
20.	24-Methylenecycloartenol	Triterpenoid	Antiproliferative, arousal-effect, and anti-inflammatory; Wu et al. (2022)
21.	Sesartemin	Lignin	Inhibitor of cytochrome P450-linked oxygenase and cytotoxic; Dixit and Reddy, (2017); Ickovski et al. (2020)

Group ANP_{2000} animals were excluded as major toxicity signs appeared after 4 h of dosing that included lacrimation, diarrhea, aggressiveness, respiratory depression, and abnormal sleeping pattern, and all three animals died within 24–36 h. Macroscopic examination of organs dissected from dead animals did not reveal any necrosis, hemorrhage, or changes in size, shape, and color. Group ANP_{50} remains active and normal without showing any adverse signs of toxicity. As per the principle of the OECD guideline 423 shown in "Annexure 2c," for all three animals dying at 2,000 mg/kg dose within 24–48 h, while all the animals surviving at 300 mg/kg dose during the study, the LD50 cut-off value of ANPs will be 500 mg/kg body weight extract loaded in polymeric NPs.

A statistically significant increase in the mean value of body weight gain was observed in the control ($p < 0.01$), as well as group ANP_{50} treated at 50 mg/kg ($p < 0.05$) up to the 14th day as shown in Figure 3. However, the mean body weight of animals treated at 300 mg/kg ANPs remained quite stagnant, and no statistical change occurred till the seventh day, although weight gain resumed after 7 days and significantly increased till the 14th day ($p < 0.001$).

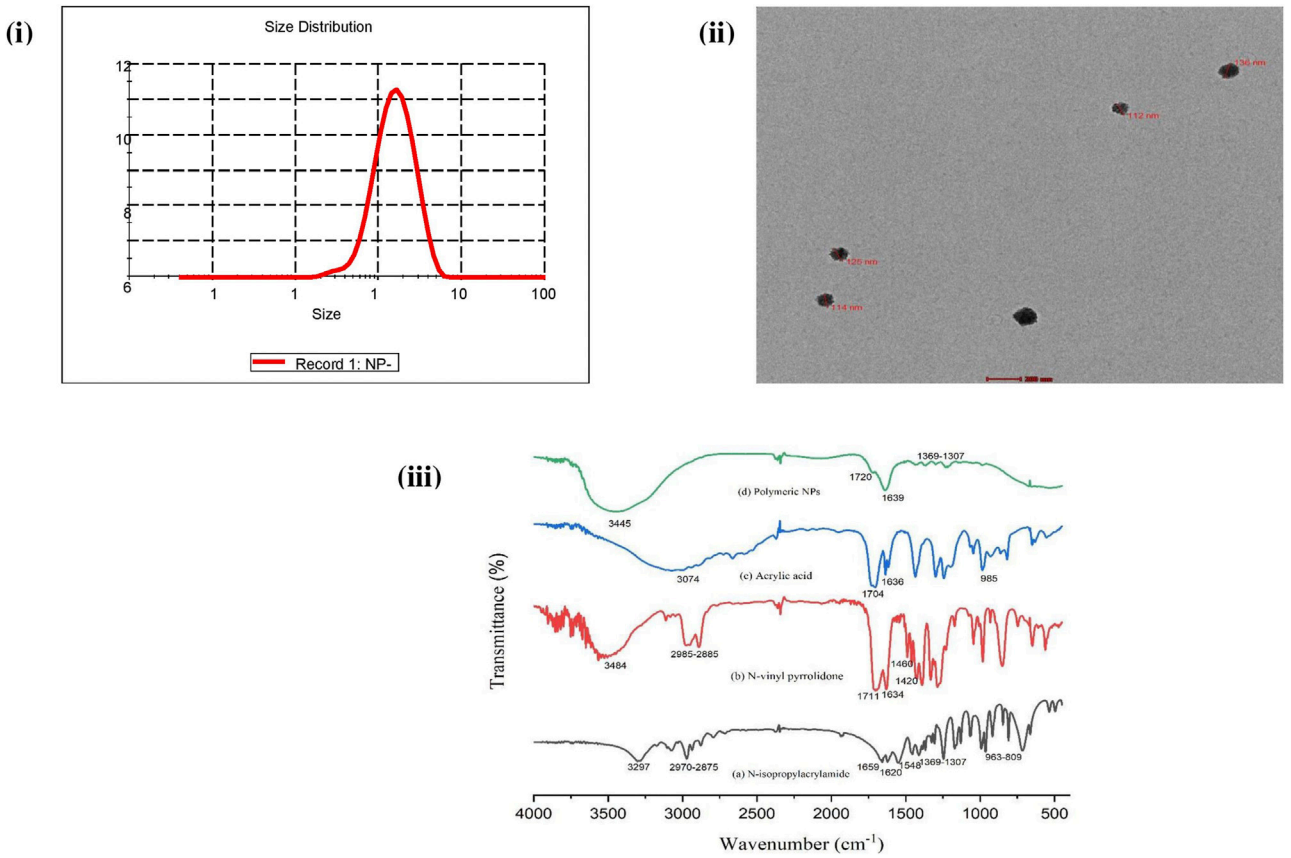


FIGURE 2
Characterization of synthesized NIPAAM–VP–AA polymeric nanoparticles: **(i)** DLS analysis showing the average size and PDI. **(ii)** TEM analysis showing the shape and size (scale bar = 0.2 μm). **(iii)** FT-IR spectroscopy analysis showing the IR spectra of (a) NIPAAM, (b) N-vinyl pyrrolidone (VP), (c) acrylic acid (AA), and (d) synthesized polymeric nanoparticles. Data are presented as the mean ± SD.

3.4 Histopathology

Microscopic histopathological observations of the intestine, liver, and kidney of all the groups are shown in Figure 4. Figure 4A shows a normal intestinal architecture of group CN, and Figure 4B shows the normal intestinal architecture of group ANP_{50} with insignificant inflammatory cell infiltrate. Figure 4C shows minor ulceration and inflammatory cell infiltrate in the lamina propria, and Figure 4D shows ulceration of intestinal mucosa with dense mixed inflammatory infiltrates in the lamina propria of group ANP_{300} and ANP $_{2000}$, respectively. Necropsy analysis of animals treated at 2,000 mg/kg ANPs reveals that a small amount of ANPs was deposited in the lumen of the intestine. These degenerative and corrosive effects of ANPs at intestinal pH can be attributed to the fact that ANPs were able to pass through the intestinal epithelium and reached the lamina propria. Representative photomicrographs of the liver [Figures 4E–G] from groups CN, ANP_{50}, and ANP_{300} represent the preserved hepatic lobular architecture, normal cell plate thickness, and polarity of hepatic parenchyma without necrosis, biliary cell damage, or inflammatory infiltrate. However, dilatation of sinusoids and a few central veins with interspersed congested blood vessels without necrosis or inflammatory infiltrate were seen in all the groups which could be due to the impaired venous drainage at the time of death. Figures 4I–L belong to sections from the kidney comprising of the cortex and medulla of groups CN, ANP_{50}, ANP_{300}, and ANP_{2000} showing normal histological features of renal tubules and glomeruli with no evidence of ischemia or necrosis. However, Figure 4J of ANP_{50} shows focal areas of the cortex with inflammatory infiltrates. Figures 4K, L shows focal areas of hemorrhage in the renal cortex without any other architectural distortion in animals treated at 300 mg/kg and 2,000 mg/kg, respectively. After entering systemic circulation, the kidney could be the major site of action for these ANPs where they would have accumulated causing renal toxicity.

Histological changes were not observed in the stomach, heart, brain, and spleen of treated groups as compared to the control. The stomach and heart sections from groups CN, ANP_{50}, ANP_{300}, and ANP_{2000} showed the normally arranged gastric architecture and maintained polarity of myocytes arranged in muscle bundles [Figures 5A–H]. The brain from groups CN, ANP_{50}, ANP_{300}, and ANP_{2000} did not suffer any alteration and had normally arranged astrocytes, oligodendrocytes, axons, and interspersed capillaries in a fibrillary background [Figures 5I–L]. The spleen of groups CN, ANP_{50}, ANP_{300}, and ANP_{2000} showed white and red pulp with variable lymphoid population and no significant changes [Figures 5M–P].

TABLE 3 Clinical signs of toxicity in Group CN (control), ANP_{50} (50 mg/kg), ANP_{300} (300 mg/kg), and ANP_{2000} (2,000 mg/kg) during the acute oral toxicity study of *Artemisia absinthium* whole extract-loaded nanoparticles using the OECD guideline 423.

	30 minutes				4 hours				24 hours				7 days				14 days			
Signs	CN	ANP_{50}	ANP_{300}	ANP_{2000}	CN	ANP_{50}	ANP_{300}	ANP_{2000}	CN	ANP_{50}	ANP_{300}	ANP_{2000}	CN	ANP_{50}	ANP_{300}	ANP_{2000}	CN	ANP_{50}	ANP_{300}	ANP_{2000}
Loss of appetite	-	-	+	+	-	-	-	+	-	-	-	+	-	-	-	N.A.	-	-	-	N.A.
Skin and fur change	-	-	-	-	-	-	-	-	-	-	-	-	-	-	-	N.A.	-	-	-	N.A.
Sitting at the corner	-	-	+	+	-	-	-	+	-	-	-	+	-	-	-	N.A.	-	-	-	N.A.
Mortality	-	-	-	-	-	-	-	-	-	-	-	3/3	-	-	-	N.A.	-	-	-	N.A.
Convulsion	-	-	-	-	-	-	-	-	-	-	-	-	-	-	-	N.A.	-	-	-	N.A.
Drowsiness	-	-	+	+	-	-	-	+	-	-	-	+	-	-	-	N.A.	-	-	-	N.A.
Salivation	-	-	-	-	-	-	-	-	-	-	-	-	-	-	-	N.A.	-	-	-	N.A.
Respiratory depression	-	-	-	-	-	-	-	+	-	-	-	+	-	-	-	N.A.	-	-	-	N.A.
Lacrimation	-	-	-	-	-	-	-	+	-	-	-	+	-	-	-	N.A.	-	-	-	N.A.
Abnormal sleeping pattern	-	-	-	-	-	-	-	+	-	-	-	+	-	-	-	N.A.	-	-	-	N.A.
Tremors	-	-	-	-	-	-	-	-	-	-	-	-	-	-	-	N.A.	-	-	-	N.A.
Diarrhea	-	-	-	-	-	-	-	+	-	-	-	+	-	-	-	N.A.	-	-	-	N.A.
Aggressiveness	-	-	-	-	-	-	-	+	-	-	-	+	-	-	-	N.A.	-	-	-	N.A.
Piloerection	-	-	-	-	-	-	-	-	-	-	-	-	-	-	-	N.A.	-	-	-	N.A.

(–): absence of sign, (+): presence of sign, (3/3): three out of three rats died within 24 h, (N.A.): not applicable as rats died.

10.3389/fphar.2023.1196842

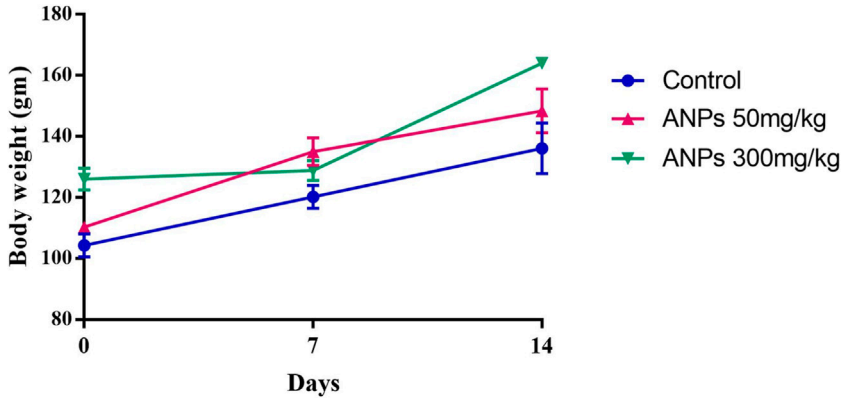


FIGURE 3
Increase in the mean value of body weight among control and treated groups. Significant increase in body weight was noted in control and groups treated at 50 mg/kg throughout 14 days. No significant growth was noticed in animals treated at 300 mg/kg till the 7th day, although weight gain resumed and continued till the 14th day. Values are expressed as the mean ± SD (N = 3); *$p < 0.05$ compared to the control.

3.5 Hematological and biochemical parameters

All the hematological and biochemical parameters for Group CN, ANP_{50}, and ANP_{300} were under normal physiological range and did not show any significant differences compared with the control group as shown in Table 4. As all the parameters were normal, no metabolic perturbations caused by these prolonged circulating ANPs were perceived in the study. Analysis of hematological and biochemical parameters for group ANP_{2000} could not be carried out as all animals succumbed to the highest dose.

4 Discussion

The GC–MS analysis of the *A. absinthium* ethanolic extract revealed forty-five well-known terpenoids (alpha-curcumene, reynosin, phytol, isogeraniol, squalene, cycloartenol, and 24-methylenecycloartenol), phytosterols (campesterol, stigmasta-5,22-dien-3-ol, and gamma-sitosterol), flavonoids (Artemetin), and lignan (yangambin and sesartemin) that have promising antioxidant, anti-inflammatory, antimicrobial, anticancer, and antiviral properties, attributing to the medicinal potency of the plant (Gonzalez-Burgos and Gómez-Serranillos, 2012). There is no previously available information about the toxicity assessment of a single oral dose of *A. absinthium* extract-loaded NIPAAM–VP–AA polymeric NPs that can cause severe complications in rodents. In this study, we first synthesized NIPAAM–VP–AA polymeric NPs by the free-radical polymerization reaction which was further confirmed by TEM, DLS, and FTIR spectroscopy. Different concentrations of the ethanolic extract of *A. absinthium* were encapsulated into the hydrophobic core of polymeric micelles for their acute toxicological assessment as per the OECD guideline 423.

NIPAAM–VP–AA NPs loaded with a variety of therapeutic compounds (e.g., ketorolac, riluzole, and curcumene) were administered via different routes, namely, ocular, intraperitoneal, and intranasal (Gupta et al., 2000; Bisht et al., 2010; Ahmad et al., 2013; Verma et al., 2016). This is the first study, in our knowledge, that was engaged in the evaluation of the LD50 cut-off value and exposure range of these polymeric ANPs for oral administration. Different studies have reported varying LD50 values of the *A. absinthium* alcoholic extract, i.e., 2,499 mg/kg, 3,700 mg/kg, and more than 5,000 mg/kg b.wt. (Parra et al., 2001; Mahmoudi et al., 2009; Daradka et al., 2014). As per our observations and the test procedure of the OECD guideline 423, ANPs exhibit dose-dependent toxicity as all three animals died at the highest dose of 2,000 mg/kg, and their LD50 cut-off value will be 500 mg/kg body weight. According to the Globally Harmonized System, the substance having LD50 > 300–2,000 belongs to "category 4." Thus, the evaluation of obtained data enabled us to conclude that *A. absinthium* extract-loaded NIPAAM–VP–AA polymeric NPs lie under Globally Harmonized System (GHS) "category 4," i.e., moderately toxic. A subacute toxicity study demonstrated that orally administered poly (N-isopropyl acrylamide) copolymerized with acrylic acid (PNIPAAm-co-AAc) did not cause any toxicity in mice up to 2,000 mg/kg (Malonne et al., 2005). Therefore, we anticipated the involvement of the *A. absinthium* ethanolic extract to be responsible for the toxicity caused by ANPs at 2,000 mg/kg.

Modifications that occurred in the animal body weight during toxicity studies are reliable predictors of metabolic unfavorable effects of the test substance under investigation (da Silva Oliveira et al., 2016). There was a gradual weight gain in control as well as in animals treated at 50 mg/kg throughout the study. However, the body weight of animals treated at 300 mg/kg ANPs remained quite stagnant for up to 1 week, which significantly increased during the next week. Moreover, mild intestinal inflammation was also found in these animals, which corroborates our result, indicating that 300 mg/kg ANPs could compromise nutrient absorption and subsequent weight gain (da Silva Oliveira et al., 2018). However, this pathological and metabolic perturbation was short-lived and reversible. Similarly, behavioral symptoms of toxicity including drowsiness and loss of appetite, which were observed among these animals, also persisted for a short period. Meanwhile, there were no adverse clinical signs observed in animals treated at 50 mg/kg ANPs.

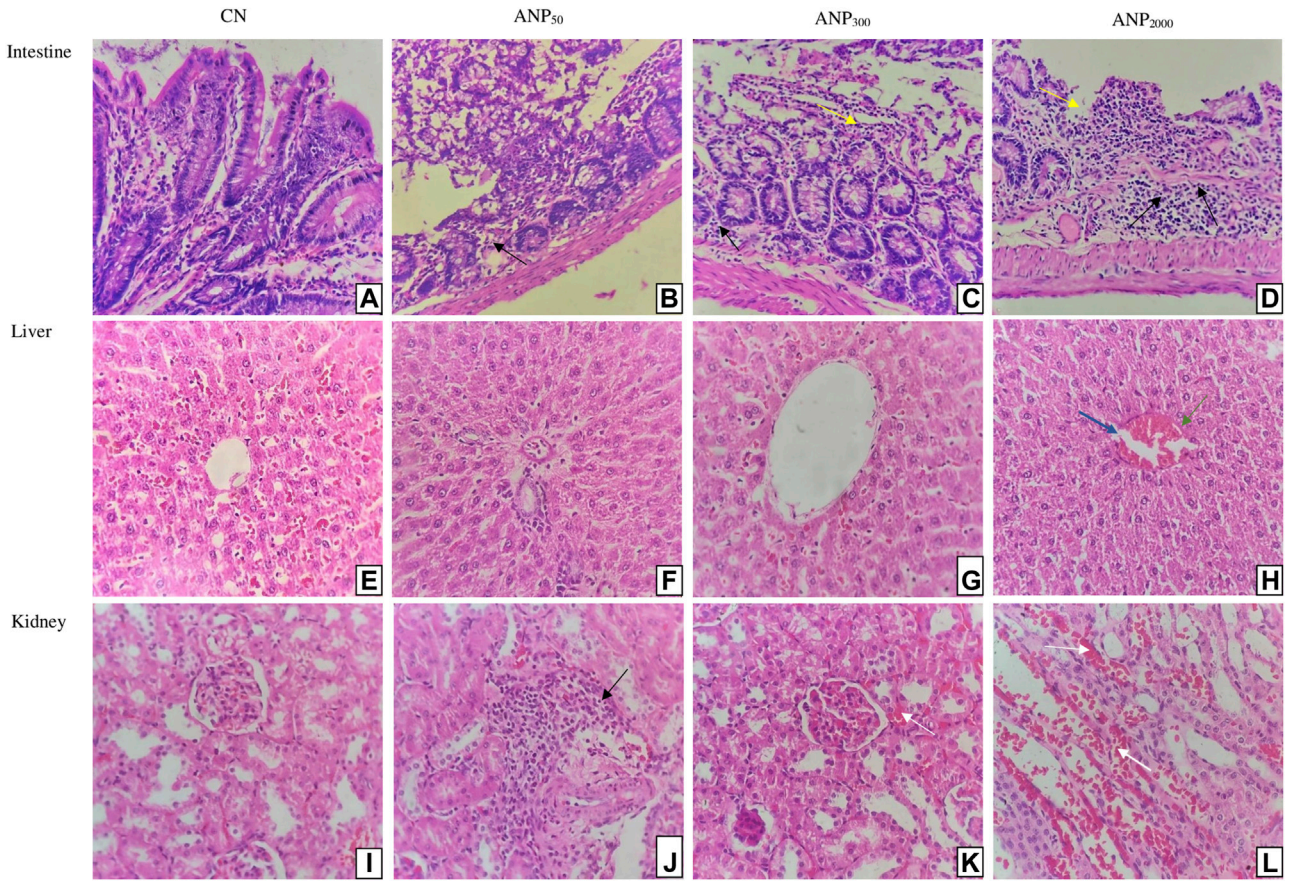


FIGURE 4
Histological sections of the intestine, liver, and kidney of rats (Hematoxylin and eosin stain, magnification 400×): Sections of Group **(A)** CN (control) and **(B)** ANP_{50} treated at 50 mg/kg show normal intestinal mucosa, submucosa, and muscularis propria; although ANP_{50} had insignificant inflammatory cell infiltrate; **(C)** ANP_{300} treated at 300 mg/kg show mild ulceration (Yellow arrow) with inflammatory infiltrates (Black arrows) in lamina propria; **(D)** ANP_{2000} treated at 2,000 mg/kg had ulceration (Yellow arrow) of intestinal mucosa with dense mixed inflammatory infiltrates (Black arrows) comprising of plasma cells, lymphocytes, and eosinophils in lamina propria (Yellow arrow depict ulceration of intestine and black arrows depict inflammatory infiltrates). Sections of Group **(E)** CN (control), **(F)** ANP_{50} treated at 50 mg/kg, **(G)** ANP_{300} treated at 300 mg/kg, and **(H)** ANP_{2000} treated at 2,000 mg/kg represents maintained lobular architecture, normal cell plate thickness, and polarity of hepatic parenchyma without necrosis, biliary cell damage or inflammatory infiltrate; although dilatation of sinusoids (Blue arrow) and few central veins with interspersed congested blood vessels (Green arrow) were also seen in all the groups (Blue arrow indicate dilated sinusoids and green arrow indicate congested central veins). Sections of Group **(I)** CN (control), **(J)** ANP_{50} treated at 50 mg/kg, **(K)** ANP_{300} treated at 300 mg/kg, and **(L)** ANP_{2000} treated at 2,000 mg/kg represent the kidney comprising of cortex and medulla where cortex shows numerous normal glomeruli having normal capillary loops and normal mesangial matrix deposition, normal proximal convoluted tubules, distal convoluted tubules, the loop of Henle and interstitium without any area of ischemia or necrosis; although **(J)** had focal areas of renal cortex with mild inflammatory infiltrate (Black arrow); **(K)** and **(L)** had focal areas of hemorrhage in the cortex (White arrow) (White arrow depict haemorrhage and black arrow depict inflammatory infiltrates).

Analysis of the *in vivo* hemocompatibility of ANPs and their interaction with the cellular components of blood, namely, erythrocytes, platelets, and leukocytes, is a prerequisite to ensure its safety for effective translation to clinical implication. Assessment of hematological and biochemical parameters is crucial to monitor the toxicity profile of different chemicals which was carried out in our study to evaluate the effect of these prolonged circulating ANPs on the hematopoietic system. The hematopoietic system is extremely sensitive to toxic compounds and serves as an indicator of the physiological and pathological status of animals in toxicological studies (da Silva Oliveira et al., 2016). Once entering system circulation, polymeric micelles of amphiphilic nature with the hydrophilic outer shell (>200 nm) possess prolonged circulating time and biocompatibility by evading reticuloendothelial systems (RESs) (Liu et al., 2005; Ashraf et al., 2018). Previously, 400 nm-sized NIPAAM–VP–AA NPs showed high cytotoxicity and apoptosis in the murine macrophage cell line J774 compared to 100 nm-sized NPs, confirming macrophage activation and recruitment of the inflammatory cascade (Ashraf et al., 2018). In our study, there were no significant differences in hematological parameters among animals treated at the dose of 50 mg/kg and 300 mg/kg ANPs as compared to control after 14 days. However, there was an apparent treatment-related insignificant increase in the total leukocyte count (TLC) and platelet count in animals treated at the dose of 50 mg/kg and 300 mg/kg after 14 days of dosing. Increment in TLC indicates the activation of the immune system of animals either due to stimulated or disturbed lymphopoiesis (Çetin et al., 2010; Otuechere et al., 2014). The finding of our study with minor increment in TLC and platelet count suggests immunomodulatory and wound healing properties of *A. absinthium*

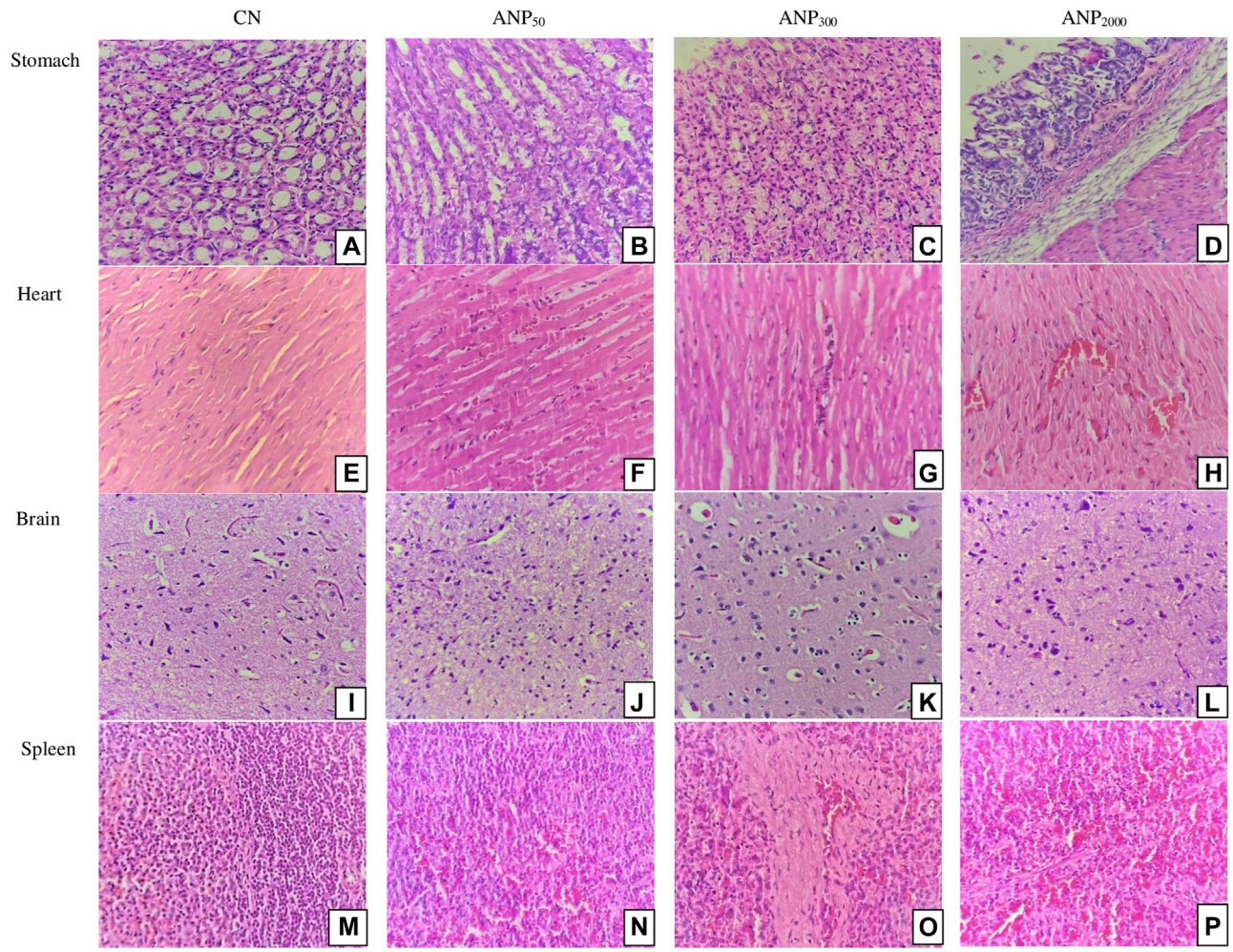


FIGURE 5
Histological sections of the stomach, heart, brain, and spleen of rats (hematoxylin and eosin stain, magnification ×400). Sections of group **(A)** CN (control), **(B)** ANP_{50} treated at 50 mg/kg, **(C)** ANP_{300} treated at 300 mg/kg, and **(D)** ANP_{2000} treated at 2,000 mg/kg show normal gastric mucosa comprising foveolar epithelium without any inflammation or necrosis. Micrographs of group **(E)** CN (control), **(F)** ANP_{50} treated at 50 mg/kg, **(G)** ANP_{300} treated at 300 mg/kg, and **(H)** ANP_{2000} treated at 2,000 mg/kg display normally arranged and maintained polarity of myocytes arranged in muscle bundles. Sections of group **(I)** CN (control), **(J)** ANP_{50} treated at 50 mg/kg **(K)** ANP_{300} treated at 300 mg/kg, and **(L)** ANP_{2000} treated at 2,000 mg/kg show normally arranged astrocytes, oligodendrocytes, axons, and interspersed capillaries in a fibrillary background. Micrographs of group **(M)** CN (control), **(N)** ANP_{50} treated at 50 mg/kg, **(O)** ANP_{300} treated at 300 mg/kg, and **(P)** ANP_{2000} treated at 2,000 mg/kg show normal white and red pulp of the spleen with a profused lymphoid population.

extract-loaded NPs at lower doses (Yamthe et al., 2012), which is in agreement with the previous study of Amat et al. that demonstrated immunomodulatory effects of *A. absinthium* extracts in mice indicating toward its antiradical and antioxidant activity (Amat et al., 2010). Therefore, we suggest that ANPs with 100–200 nm hydrodynamic size are hemocompatible and do not cause lethal alterations in hematological parameters at a single low dose. Liver- and kidney-related biochemical enzymes are reliable indicators of possible toxicity caused by exposure to different drugs (Farag et al., 2006). All the liver- and kidney-related enzymes, as well as electrolyte levels, were normal in animals treated at the dose of 50 mg/kg and 300 mg/kg ANPs. Therefore, we suggest that neither metabolic disturbance nor renal dysfunction was caused by ANPs at low doses in the rats. However, the impact of 2,000 mg/kg ANPs on hematological and biochemical parameters could not be inferred as all the animals died during the experiment.

In our study, histological evidence reveals the toxic potential of ANPs mainly in the intestine and kidney. Orally administered small NPs (50–100 nm) can move through the intestinal epithelium to lamina propria of the GI tract via a transcellular pathway comprising enterocytes to finally enter the systemic circulation, while large NPs (>100 nm) are taken up by M cells (Pridgen et al., 2015; Reinholz et al., 2018). It is also reported that NPs may experience direct and indirect movement in systemic circulation through the intestinal lymphatic system and hepatic portal system, respectively (Hua, 2020). We observed that a single oral dose of ANPs at 300 mg/kg caused mild intestinal inflammation, while 2,000 mg/kg caused ulceration of intestinal mucosa and inflammatory response in the

TABLE 4 Effect of single oral administration of different doses of *Artemisia absinthium* extract-loaded NPs on the hematological parameters, liver profile, kidney profile, and body weight of female Wistar rats after 14 days of acute oral toxicity study.

Parameters	Group CN	Group ANP_{50}	Group ANP_{300}
Hematological test			
Hemoglobin (Hb) (gm/dL)	14.03 ± 0.15	13.67 ± 0.25	14 ± 0.26
TLC (/cumm)	11,400 ± 818.5	13,066 ± 4,821.13	16,933.33 ± 5,839.8
Neutrophil (%)	4.17 ± 0.97	9.16 ± 2.31	7.68 ± 4.72
Lymphocyte (%)	93.23 ± 1.2	88.16 ± 3.17	88.47 ± 6.17
Eosinophil (%)	0.79 ± 0.02	1.08 ± 0.15	1.23 ± 0.55
Monocyte (%)	1.56 ± 0.21	1.86 ± 0.34	2.24 ± 1.3
Basophil (%)	0.37 ± 0.05	0.32 ± 0.19	0.39 ± 0.18
RBC (red blood cell count) (millions/cmm)	6.7 ± 0.40	6.55 ± 0.62	7.18 ± 0.70
PCV/HCT (hematocrit) (%)	47.03 ± 0.35	45.87 ± 1.2	46.3 ± 2.45
MCV (mean corpuscular volume) (fL)	68.2 ± 0.62	68.27 ± 6.67	68.57 ± 5.24
MCH (mean corpuscular Hb) (pg)	20.7 ± 0.75	20.67 ± 1.61	20.7 ± 0.79
MCHC (mean corpuscular Hb concentration) (gm/dL)	30.93 ± 0.50	30.27 ± 1.02	30.33 ± 2.1
Platelet count (lacs/cmm)	6.04 ± 0.34	8.19 ± 1.57	8.89 ± 1.29
Liver function test			
Total bilirubin (mg/dL)	0.38 ± 0.06	0.45 ± 0.20	0.45 ± 0.19
Direct bilirubin (mg/dL)	0.123 ± 0.03	0.18 ± 0.09	0.18 ± 0.1
Indirect bilirubin (mg/dL)	0.25 ± 0.04	0.26 ± 0.10	0.26 ± 0.09
SGOT (U/L)	139.37 ± 46	140.6 ± 35.69	148 ± 86.33
SGPT (U/L)	46.27 ± 9.7	45.5 ± 6.73	40.57 ± 7.81
Alkaline phosphatase (U/L)	272.17 ± 60.7	312.6 ± 125.38	194.4 ± 45.78
Total protein (gm/dL)	6.75 ± 0.10	7.09 ± 0.29	7.22 ± 0.74
Albumin (gm/dL)	3.13 ± 0.27	3.75 ± 0.29	4.03 ± 0.76
Globulin (gm/dL)	3.51 ± 0.18	3.35 ± 0.30	3.19 ± 0.51
Kidney function test			
Urea (mg/dL)	36.3 ± 6.45	33.63 ± 2.5	42.03 ± 3.02
Serum creatinine (mg/dL)	0.61 ± 0.06	0.72 ± 0.13	0.63 ± 0.07
Uric acid (mg/dL)	1.59 ± 0.31	1.98 ± 0.88	2.31 ± 1.22
Serum calcium (mg/dL)	8.64 ± 3.34	10.04 ± 2.15	9.99 ± 2.19
Sodium (mmol/L)	148.67 ± 2.30	139.33 ± 0.58	146.33 ± 9.29
Potassium (mmol/L)	4.98 ± 0.23	6.35 ± 0.30	6.47 ± 0.53
Chloride (mmol/L)	104 ± 0.58	103.67 ± 0.58	107.33 ± 2.30
Body weight (gm)			
0th day	104.33 ± 3.78	110.33 ± 1.52	126 ± 3.6
7th day	120.17 ± 3.81**	135 ± 4.58****	128.83 ± 3.25
14th day	136.17 ± 8.25**	148.33 ± 7.23*	164 ± 1.32****

Values are expressed as the mean ± SD. *$p < 0.05$, **$p < 0.01$, and ***$p < 0.001$ compared to the normal control group. TLC, total leucocyte count; RBC, red blood cell count; PCV/HCT, hematocrit; MCV, mean corpuscular volume; MCH, mean corpuscular hb; MCHC, mean corpuscular hb concentration; SGOT, serum glutamic-oxaloacetic transaminase; SGPT, serum glutamic pyruvic transaminase.

lamina propria which, in turn, indicates that ANPs increased gut permeability in rats. Additionally, adverse clinical signs, including diarrhea and loss of appetite, were seen in group ANP $_{2000}$, which was consistent with our finding of intestinal ulceration and inflammation, indicating disturbed intestinal function accompanied by diarrhea at a high dose of ANPs (Wang et al., 2019). Necropsy analysis of animals treated at 2,000 mg/kg also revealed the deposition of a small amount of ANPs in the lumen of the intestine. These findings can be correlated with an *in vitro* release study that reported a remarkable increment in LCST of the pH- and temperature-responsive, insulin-loaded NIPAAM and AA derivative-based hydrogels under the condition of neutral artificial intestinal fluid (pH 6.8), resulting in hydrogel swelling and fast release of insulin (Gao et al., 2013). Thus, we can anticipate that ANPs would also have experienced an increase in LCST (>37°C) at intestinal pH, eventually collapsing and releasing its content. However, our study cannot infer the amount of ANPs collapsing at intestinal pH and the amount of ANPs entering the systemic circulation and eventually getting eliminated from the body.

Several studies suggested that NPs entering systemic circulation are further distributed to different organs triggering further pathological changes (Chen et al., 2006). In this study, the liver of rats from all the groups showed dilatation of sinusoids and few central veins with interspersed congested blood vessels as a functional consequence of impaired blood flow. The kidney is the blood-filtering organ that receives a major portion of the systemic circulation; thus, direct exposure and accumulation of NPs can be responsible for renal tissue rupture or hemorrhage. In this study, the kidneys of animals treated at 300 mg/kg and 2,000 mg/kg showed focal areas of hemorrhage in the renal cortex without traces of ischemia, necrosis, or any other structural disintegration. The kidneys of animals treated at 50 mg/kg were also histopathologically normal with focal areas of inflammatory infiltrates in the cortex. Thus, we can postulate that these morphological and structural changes were associated with the fact that ANPs were able to pass through the intestinal epithelium and reached the lamina propria through which they are phagocytosed and transported to the kidney causing acute renal injury. These pathological changes due to a single oral dose persisted among animals treated at 50 mg/kg and 300 mg/kg ANPs even after 14 days of acute exposure advocate toward their capacity to cause moderate-to-mild renal toxicity. However, no pathological damage or toxicity of these ANPs was found in the stomach, heart, brain, or spleen. Therefore, the *in vivo* behavior, role of hydrodynamic size, nature of interaction with the intestinal tract, and fate in the GI tract require further investigation.

5 Conclusion

The findings of our study demonstrate that *A. absinthium* extract-loaded NIPAAM–VP–AA polymeric NPs (ANPs) have LD50 cut-off value equal to 500 mg/kg body weight and belong to 'category 4' of the GHS, with moderately toxic nature as high dose caused intestinal and renal injury in rats. Our preliminary study exhibits limitations being only concerned with the assessment of the LD50 cut-off value of ANPs, although providing a new insight into the understanding of immunostimulation by ANPs and emphasizing the need of investigating the hemocompatibility and chronic toxicity of ANPs for clinical application. However, an appropriate dose of these NPs presents a promising site-specific drug delivery system that could be employed against different medical disorders.

Data availability statement

The original contributions presented in the study are included in the article/Supplementary Material. Further inquiries can be directed to the corresponding author.

Ethics statement

The animal study was reviewed and approved by the Institutional Animal Ethics Committee (IAEC) constituted through the Committee for the Purpose of Control and Supervision of Experiments on Animals (173/GO/Re/S/2000/CPCSEA) under the Ministry of Animal Welfare Division, Government of India, New Delhi.

Author contributions

SK was involved in data curation, formal analysis, investigation, methodology, validation, visualization, funding acquisition, writing—original draft, and writing—review and editing. MM was involved in methodology, project administration, and writing—review and editing. SS helped in investigation, methodology, and writing—review and editing. SW was involved in conceptualization, formal analysis, funding acquisition, investigation, methodology, project administration, resources, supervision, validation, visualization, and writing—review and editing. All authors contributed to the article and approved the submitted version.

Funding

The authors acknowledge the financial assistance by the Council of Scientific and Industrial Research (CSIR), India, by providing fellowship to SK and SS with award letter no. 09/591(0158)/2018-EMR-I and 09/591(0159)/2018-EMR-I, respectively.

Acknowledgments

The authors would like to thank Jamia Hamdard for it's immense support and for providing necessary research facilities for conducting the experiments.

Conflict of interest

The authors declare that the research was conducted in the absence of any commercial or financial relationships that could be construed as a potential conflict of interest.

Publisher's note

All claims expressed in this article are solely those of the authors and do not necessarily represent those of their affiliated organizations, or those of the publisher, the editors, and the reviewers. Any product that may be evaluated in this article, or claim that may be made by its manufacturer, is not guaranteed or endorsed by the publisher.

References

Ahmad, N., Umar, S., Ashafaq, M., Akhtar, M., Iqbal, Z., Samim, M., et al. (2013). A comparative study of PNIPAM nanoparticles of curcumin, demethoxycurcumin, and bisdemethoxycurcumin and their effects on oxidative stress markers in experimental stroke. *Protoplasma* 250 (6), 1327–1338. doi:10.1007/s00709-013-0516-9

Amat, N., Upur, H., and Blažeković, B. (2010). *In vivo* hepatoprotective activity of the aqueous extract of Artemisia absinthium L. against chemically and immunologically induced liver injuries in mice. *J. Ethnopharmacol.* 131 (2), 478–484. doi:10.1016/j.jep.2010.07.023

Ashraf, M. D., Farooqi, J. A., and Javed, K. (2018). Evaluation of macrophage injury and activation by amphotericin B-loaded polymeric nanoparticles. *Int. J. Polym. Mater. Polym. Biomaterials* 67 (5), 297–306. doi:10.1080/00914037.2017.1323216

Bala, M., Pratap, K., Verma, P. K., Singh, B., and Padwad, Y. (2015). Validation of ethnomedicinal potential of Tinospora cordifolia for anticancer and immunomodulatory activities and quantification of bioactive molecules by HPTLC. *J. Ethnopharmacol.* 175, 131–137. doi:10.1016/j.jep.2015.08.001

Barretto, D. A., and Vootla, S. K. (2018). Gc-Ms Analysis of bioactive compounds and antimicrobial activity of Cryptococcus rajasthanensis Ky627764 isolated from *Bombyx mori* gut microflora. *Int. J. Adv. Res.* 6 (3), 525–538. doi:10.21474/ijar01/6700

Bayeux, M. C., Fernandes, A. T., Foglio, M. A., and Carvalho, J. E. (2002). Evaluation of the antiedematogenic activity of artemetin isolated from Cordia curassavica DC. *Braz. J. Med. Biol. Res.* 35, 1229–1232. doi:10.1590/s0100-879x2002001000017

Bhardwaj, M., Sali, V. K., Mani, S., and Vasanthi, H. R. (2020). Neophytadiene from Turbinaria ornata suppresses LPS-induced inflammatory response in RAW 264.7 macrophages and Sprague Dawley rats. *Inflammation* 43, 937–950. doi:10.1007/s10753-020-01179-z

Bhat, M. Y., Gul, M. Z., Lohamror, L. R., Qureshi, I. A., and Ghazi, I. A. (2018). An *in vitro* study of the antioxidant and antiproliferative properties of Artemisia absinthium-A potent medicinal plant. *Free Radicals Antioxidants* 8 (1), 18–25. doi:10.5530/fra.2018.1.4

Bisht, S., Mizuma, M., Feldmann, G., Ottenhof, N. A., Hong, S. M., Pramanik, D., et al. (2010). Systemic administration of polymeric nanoparticle-encapsulated curcumin (NanoCurc) blocks tumor growth and metastases in preclinical models of pancreatic cancer. *Mol. cancer Ther.* 9 (8), 2255–2264. doi:10.1158/1535-7163.MCT-10-0172

Bora, K. S., and Sharma, A. (2010). Phytochemical and pharmacological potential of Artemisia absinthium linn. And Artemisia asiatica nakai: A review. *J. Pharm. Res.* 3 (2), 325–328. doi:10.1016/j.jep.2010.04.030

Çetin, E., Kanbur, M., Silici, S., and Eraslan, G. (2010). Propetamphos-induced changes in haematological and biochemical parameters of female rats: Protective role of propolis. *Food Chem. Toxicol.* 48 (7), 1806–1810. doi:10.1016/j.fct.2010.04.010

Chen, G., Li, X., Minghui, J., Masood, T., Safir, W., Khan, M. A., et al. (2022). Comparison of phytochemical constituents and pharmacological activities of various solvent extracts obtained from Millettia speciosa stem powder. *BioMed Res. Int.* 2022, 2486979. doi:10.1155/2022/2486979

Chen, Z., Meng, H., Xing, G., Chen, C., Zhao, Y., Jia, G., et al. (2006). Acute toxicological effects of copper nanoparticles *in vivo*. *Toxicol. Lett.* 163 (2), 109–120. doi:10.1016/j.toxlet.2005.10.003

Craciunescu, O., Constantin, D., Gaspar, A., Toma, L., Utoiu, E., and Moldovan, L. (2012). Evaluation of antioxidant and cytoprotective activities of Arnica Montana L. and Artemisia absinthiumL. ethanolic extracts. *Chem. Central J.* 6 (1), 97–101. doi:10.1186/1752-153X-6-97

da Silva Oliveira, G. L., Machado, K. C., Machado, K. C., Feitosa, C. M., and de Castro Almeida, F. R. (2018). Non-clinical toxicity of β-caryophyllene, a dietary cannabinoid: Absence of adverse effects in female Swiss mice. *Regul. Toxicol. Pharmacol.* 92, 338–346. doi:10.1016/j.yrtph.2017.12.013

da Silva Oliveira, G. L., Medeiros, S. C., Sousa, A. M., da Silva Lopes, L., David, J. M., da Costa Junior, J. S., et al. (2016). Pre-clinical toxicology of garcinielliptone FC, a tautomeric pair of polyprenylated benzophenone, isolated from Platonia insignis Mart seeds. *Phytomedicine* 23 (5), 477–482. doi:10.1016/j.phymed.2016.02.013

Daradka, H. M., Abas, M. M., Mohammad, M. A., and Jaffar, M. M. (2014). Antidiabetic effect of Artemisia absinthium extracts on alloxan-induced diabetic rats. *Comp. Clin. Pathol.* 23 (6), 1733–1742. doi:10.1007/s00580-014-1963-1

Das, S., Vasudeva, N., and Sharma, S. (2014). Chemical composition of ethanol extract of Macrotyloma uniflorum (Lam) Verdc. using GC-MS spectroscopy. *Org. Med. Chem. Lett.* 4 (1), 13–14. doi:10.1186/s13588-014-0013-y

Dixit, D., and Reddy, C. R. (2017). Non-targeted secondary metabolite profile study for deciphering the cosmeceutical potential of red marine macro alga jania rubens—an LCMS-based approach. *Cosmetics* 4 (4), 45. doi:10.3390/cosmetics4040045

Farag, R. S., Mahmoud, E. A., Basuny, A. M., and Ali, R. F. (2006). Influence of crude olive leaf juice on rat liver and kidney functions. *Int. J. food Sci. Technol.* 41 (7), 790–798. doi:10.1111/j.1365-2621.2006.01093.x

Gao, X., Cao, Y., Song, X., Zhang, Z., Xiao, C., He, C., et al. (2013). pH-and thermo-responsive poly (N-isopropylacrylamide-co-acrylic acid derivative) copolymers and hydrogels with LCST dependent on pH and alkyl side groups. *J. Mater. Chem. B* 1 (41), 5578–5587. doi:10.1039/c3tb20901f

Gonzalez-Burgos, E., and Gómez-Serranillos, M. P. (2012). Terpene compounds in nature: A review of their potential antioxidant activity. *Curr. Med. Chem.* 19 (31), 5319–5341. doi:10.2174/092986712803833335

Goud, B. J., Dwarakanath, V., and Swamy, B. K. (2015). A review on history, controversy, traditional use, ethnobotany, phytochemistry and pharmacology of Artemisia absinthium Linn. *Int. J. Adv. Res. Eng. Appl. Sci.* 4 (5), 77–107.

Gupta, A. K., Madan, S., Majumdar, D. K., and Maitra, A. (2000). Ketorolac entrapped in polymeric micelles: Preparation, characterisation and ocular anti-inflammatory studies. *Int. J. Pharm.* 209 (1-2), 1–14. doi:10.1016/s0378-5173(00)00508-1

Hua, S. (2020). Advances in oral drug delivery for regional targeting in the gastrointestinal tract-influence of physiological, pathophysiological and pharmaceutical factors. *Front. Pharmacol.* 11, 524. doi:10.3389/fphar.2020.00524

Ickovski, J. D., Pavlović, J. L., Mitić, M. N., Palić, I. R., Kostić, D. A., Petrović, G. M., et al. (2020). Furofuran lignans of Artemisia genus: Isolation, biosynthesis and biological activity. *J. Serbian Chem. Soc.* 85 (5), 575–600. doi:10.2298/jsc191210009i

Krishnamoorthy, K., and Subramaniam, P. (2014). Phytochemical profiling of leaf, stem, and tuber parts of Solena amplexicaulis (Lam) Gandhi using GC-MS. *Int. Sch. Res. notices* 2014, 567409. doi:10.1155/2014/567409

Larrañaga, A., Petisco, S., Villanueva, R., Iturri, J. J., Moya, S., Meaurio, E., et al. (2011). "Physicochemical properties of plasma polymerized acrylic acid, ε-caprolactone and lactic acid films," in Proceedings of the European Technical Conference-Society of Plastic Engineers, Boston, Massachusetts, May 1-5, 2011.

Lei, Y., Fu, P., Jun, X., and Cheng, P. (2019). Pharmacological properties of geraniol–a review. *Planta medica.* 85 (1), 48–55. doi:10.1055/a-0750-6907

Lim, S., Lee, S. J., Nam, K. W., Kim, K. H., and Mar, W. (2013). Hepatoprotective effects of reynosin against thioacetamide-induced apoptosis in primary hepatocytes and mouse liver. *Archives pharmacal Res.* 36, 485–494. doi:10.1007/s12272-013-0039-0

Liu, S. Q., Tong, Y. W., and Yang, Y. Y. (2005). Incorporation and *in vitro* release of doxorubicin in thermally sensitive micelles made from poly (N-isopropylacrylamide-co-N, N-dimethylacrylamide)-b-poly (D, L-lactide-co-glycolide) with varying compositions. *Biomaterials* 26 (24), 5064–5074. doi:10.1016/j.biomaterials.2005.01.030

Mahmoudi, M., Ebrahimzadeh, M. A., Ansaroudi, F., Nabavi, S. F., and Nabavi, S. M. (2009). Antidepressant and antioxidant activities of Artemisia absinthium L. at flowering stage. *Afr. J. Biotechnol.* 8 (24).

Malonne, H., Eeckman, F., Fontaine, D., Otto, A., De Vos, L., Moës, A., et al. (2005). Preparation of poly (N-isopropylacrylamide) copolymers and preliminary assessment of their acute and subacute toxicity in mice. *Eur. J. Pharm. Biopharm.* 61 (3), 188–194. doi:10.1016/j.ejpb.2005.05.007

Monte, R. L., Barbosa, J. M., Sousa, L. M., Athayde, P. F., Dias, C. S., and Oliveira, M. R. (2007). Crude ethanolic extract, lignoid fraction and yangambin from Ocotea duckei (Lauraceae) show antileishmanial activity. *Zeitschrift fur Naturforschung. C, J. Biosci.* 62 (5-6), 348–352. doi:10.1515/znc-2007-5-605

Mughees, M., Samim, M., Ahmad, S., and Wajid, S. (2019). Comparative analysis of the cytotoxic activity of extracts from different parts of A. absinthium L. on breast cancer cell lines and correlation with active compounds concentration. *Plant Biosystems-An Int. J. Deal. all Aspects Plant Biol.* 153 (4), 569–579. doi:10.1080/11263504.2018.1527792

Mughees, M., Wajid, S., and Samim, M. (2020). Cytotoxic potential of Artemisia absinthium extract loaded polymeric nanoparticles against breast cancer cells: Insight into the protein targets. *Int. J. Pharm.* 586, 119583. doi:10.1016/j.ijpharm.2020.119583

Obrenovich, M. E., Nair, N. G., Beyaz, A., Aliev, G., and Reddy, V. P. (2010). The role of polyphenolic antioxidants in health, disease, and aging. *Rejuvenation Res.* 13 (6), 631–643. doi:10.1089/rej.2010.1043

Otuechere, C. A., Abarikwu, S. O., Olateju, V. I., Animashaun, A. L., and Kale, O. E. (2014). Protective effect of curcumin against the liver toxicity caused by propanil in rats. *Int. Sch. Res. notices* 2014, 853697. doi:10.1155/2014/853697

Parra, A. L., Yhebra, R. S., Sardiñas, I. G., and Buela, L. I. (2001). Comparative study of the assay of and the estimate of the medium lethal dose (LD50 value) in mice, to determine oral acute toxicity of plant extracts. *Phytomedicine* 8 (5), 395–400. doi:10.1078/0944-7113-00044

Peppas, N. A., and Kavimandan, N. J. (2006). Nanoscale analysis of protein and peptide absorption: Insulin absorption using complexation and pH-sensitive hydrogels as delivery vehicles. *Eur. J. Pharm. Sci.* 29 (3-4), 183–197. doi:10.1016/j.ejps.2006.04.014

Pridgen, E. M., Alexis, F., and Farokhzad, O. C. (2015). Polymeric nanoparticle drug delivery technologies for oral delivery applications. *Expert Opin. drug Deliv.* 12 (9), 1459–1473. doi:10.1517/17425247.2015.1018175

Reinholz, J., Landfester, K., and Mailänder, V. (2018). The challenges of oral drug delivery via nanocarriers. *Drug Deliv.* 25 (1), 1694–1705. doi:10.1080/10717544.2018.1501119

Riahi, L., Ghazghazi, H., Ayari, B., Aouadhi, C., Klay, I., Chograni, H., et al. (2015). Effect of environmental conditions on chemical polymorphism and biological activities among Artemisia absinthium L. essential oil provenances grown in Tunisia. *Industrial Crops Prod.* 66, 96–102. doi:10.1016/j.indcrop.2014.12.036

Shahzad, N., Khan, W., Shadab, M. D., Ali, A., Saluja, S. S., Sharma, S., et al. (2017). Phytosterols as a natural anticancer agent: Current status and future perspective. *Biomed. Pharmacother.* 88, 786–794. doi:10.1016/j.biopha.2017.01.068

Sundarraj, S., Thangam, R., Sreevani, V., Kaveri, K., Gunasekaran, P., Achiraman, S., et al. (2012). γ-Sitosterol from Acacia nilotica L. induces G2/M cell cycle arrest and apoptosis through c-Myc suppression in MCF-7 and A549 cells. *J. Ethnopharmacol.* 141 (3), 803–809. doi:10.1016/j.jep.2012.03.014

Sur, S., Rathore, A., Dave, V., Reddy, K. R., Chouhan, R. S., and Sadhu, V. (2019). Recent developments in functionalized polymer nanoparticles for efficient drug delivery system. *Nano-Structures Nano-Objects* 20, 100397. doi:10.1016/j.nanoso.2019.100397

Vergara, M., Olivares, A., and Altamirano, C. (2015). Antiproliferative evaluation of tall-oil docosanol and tetracosanol over CHO-K1 and human melanoma cells. *Electron. J. Biotechnol.* 18 (4), 291–294. doi:10.1016/j.ejbt.2015.05.004

Verma, S. K., Arora, I., Javed, K., Akhtar, M., and Samim, M. (2016). Enhancement in the neuroprotective power of riluzole against cerebral ischemia using a brain targeted drug delivery vehicle. *ACS Appl. Mater. Interfaces* 8 (30), 19716–19723. doi:10.1021/acsami.6b01776

Vezza, T., Canet, F., de Marañón, A. M., Bañuls, C., Rocha, M., and Víctor, V. M. (2020). Phytosterols: Nutritional health players in the management of obesity and its related disorders. *Antioxidants* 9 (12), 1266. doi:10.3390/antiox9121266

Wang, W., Dong, Z., Zhang, J., Zhou, X., Wei, X., Cheng, F., et al. (2019). Acute and subacute toxicity assessment of oxyclozanide in Wistar rats. *Front. Veterinary Sci.* 6, 294. doi:10.3389/fvets.2019.00294

Wu, L., Zhao, J., Wu, L., Zhang, Y., and Li, J. (2022). Simultaneous determination of squalene, tocopherols and phytosterols in edible vegetable oil by SPE combined with saponification and GC-MS. *LWT* 169, 114026. doi:10.1016/j.lwt.2022.114026

Yamthe, L. R., David, K., and Ngadena, Y. M. (2012). Acute and chronic toxicity studies of the aqueous and ethanol leaf extracts of Carica papaya Linn in Wistar rats. *J. Nat. Prod. Plant Resour.* 2, 617–627.

frontiers | Frontiers in Pharmacology

TYPE Original Research
PUBLISHED 14 July 2023
DOI 10.3389/fphar.2023.1233468

Check for updates

OPEN ACCESS

EDITED BY
Wei Cai,
Hunan University of Medicine, China

REVIEWED BY
Olha Mykhailenko,
University College London,
United Kingdom
Hailin Tang,
Sun Yat-sen University Cancer Center (SYSUCC), China
Yan Zhang,
Shanghai Jiao Tong University, China

*CORRESPONDENCE
Dong-Hua Yang,
dong-hua.yang@nyctcm.edu
Shen Yao,
13916260830@163.com
Xiangwei Zheng,
zhengxwsh@hotmail.com

†These authors have contributed equally to this work and share first authorship

RECEIVED 02 June 2023
ACCEPTED 06 July 2023
PUBLISHED 14 July 2023

CITATION
Wang K, Li J, Zheng X, Xu J, Wang Z, Li S, Yang Q, Wu Y, Yang D-H, Yao S and Zheng X (2023), The pharmacological effects and safety of the raw and prepared folium of *Epimedium brevicornu* Maxim. on improving kidney-yang deficiency syndrome and sexual dysfunction. *Front. Pharmacol.* 14:1233468. doi: 10.3389/fphar.2023.1233468

COPYRIGHT
© 2023 Wang, Li, Zheng, Xu, Wang, Li, Yang, Wu, Yang, Yao and Zheng. This is an open-access article distributed under the terms of the Creative Commons Attribution License (CC BY). The use, distribution or reproduction in other forums is permitted, provided the original author(s) and the copyright owner(s) are credited and that the original publication in this journal is cited, in accordance with accepted academic practice. No use, distribution or reproduction is permitted which does not comply with these terms.

The pharmacological effects and safety of the raw and prepared folium of *Epimedium brevicornu* Maxim. on improving kidney-yang deficiency syndrome and sexual dysfunction

Kai Wang[1†], Juntao Li[2†], Xinyu Zheng[2†], Jian Xu[3†], Zhe Wang[3], Senjie Li[2], Qiang Yang[3], Yue Wu[3], Dong-Hua Yang[4*], Shen Yao[5*] and Xiangwei Zheng[2*]

[1]Science and Technology Experiment Center, Shanghai University of Traditional Chinese Medicine, Shanghai, China, [2]Engineering Research Center of Modern Preparation Technology of Traditional Chinese Medicine, Ministry of Education, Innovation Research Institute of Traditional Chinese Medicine, Shanghai University of Traditional Chinese Medicine, Shanghai, China, [3]Hubei Provincial Key Laboratory of Quality and Safety of Traditional Chinese Medicine Health Food, Jing Brand Research Institute, Jing Brand Co., Ltd., Daye, Hubei, China, [4]New York College of Traditional Chinese Medicine, Mineola, NY, United States, [5]Sanlin Community Health Service Center of Shanghai Pudong New District, Shanghai, China

Background: Kidney-Yang deficiency syndrome (KDS) is a group of diseases related to hypothalamic-pituitary-adrenal (HPA) axis and sexual dysfunction. The folium of *Epimedium brevicornu* Maxim. (FEB) includes raw and prepared slices, named RFEB and PFEB, respectively. PFEB is traditionally believed to be good for tonifying kidney-Yang and improving sexual dysfunction. However, there are few studies comparing the pharmacological effects of RFEB and PFEB, and their underlying mechanisms. In this study, we aimed to compare the effects and safety of RFEB and PFEB on the HPA axis and sexual function. Additionally, the mechanisms of their roles in relation to the neuroendocrine-immune (NEI) network in the KDS model mice were explored.

Methods: Male adult C57BL/6 mice were treated with corticosterone to establish a KDS mouse model, and RFEB and PFEB were administered intragastrically. Corticotropin releasing hormone (CRH), adrenocorticotropic hormone (ACTH), cyclic adenosine monophosphate (cAMP), cyclic guanosine monophosphate (cGMP), testosterone levels and oxidative damage indexes were measured. The mRNA and protein levels of *CRH* and *ACTH* in hypothalamus and pituitary, endothelial nitric oxide synthase (eNOS) and phosphodiesterase 5 (PDE5) in corpus cavernosum were examined. TNFα, IL-6, NF-κB, eNOS and PDE5 were investigated in mouse corpus cavernosum.

Results: Our results showed that PFEB was more effective than RFEB in increasing corticosterone-suppressed *ACTH* levels, enhancing *CRH* levels and cAMP/cGMP ratio, and reducing oxidative damage. *In vivo*, PFEB significantly increased eNOS and inhibited PDE5 expression in corpus cavernosum. PFEB showed stronger protective effect on normal spleen lymphocytes from apoptosis both *in vitro* and *in vivo*. Additionally, it noticeably inhibited the levels of inflammatory cytokines in corpus cavernosum. Both RFEB and PFEB were safe and did not cause any clinical

signs of toxicity in mice at the dosage of 20 times dosages of that in the Chinese Pharmacopeia.

Conclusion: We demonstrated that PFEB was better than RFEB at tonifying the kidney-Yang by comparing their effects on improving the NEI network, which includes the HPA axis, immune system and corpus cavernosum. This study revealed that PFEB could significantly improve the sexual function of KDS mice by regulating the HPA axis and activating the immune system through the NEI network.

KEYWORDS

processed folium of *Epimedium brevicornu* Maxim, raw folium of *Epimedium brevicornu* Maxim, hypothalamus-pituitary-adrenal axis, sexual dysfunction, neuroendocrine-immune network

1 Introduction

In Traditional Chinese medicine (TCM), the "kidney-Yang" governs growth, development, and aging of human body. Clinical symptoms of kidney-Yang deficiency commonly include sexual dysfunction, waist and knees soreness, tinnitus and deafness, tooth loss, and others. Modern medical research shows that patients with kidney-Yang deficiency syndrome (KDS) are frequently accompanied with different diseases related to dysfunction of hypothalamic-pituitary-adrenal (HPA) axis and sexual organs (Shen, 2012). Previous pathological and pharmacological studies have demonstrated that KDS is closely associated with the HPA axis and the regulating center located in hypothalamus could be the target organ of kidney-Yang tonifying (Shen, 2012). It was also found that herbs tonifying the kidney-Yang are involved in neuroendocrine-immune (NEI) network and could activate immune system, and promote secretion of sex hormone and growth hormone (Shen, 2005; Shen, 2012; Huang et al., 2013b). Therefore, KDS animal model can be established by intake a large-dose of glucocorticoids (GCs) to induce HPA axis disorders (Shen, 2012; Dai et al., 2017).

Epimedii Folium (EF), known as Yinyanghuo in Chinese, has been commonly used as a TCM over the last two thousand of years for the treatment of various diseases. The *Epimedium genus* includes at least 68 species that exist as herbs, present in land around the Mediterranean and east Asia, and there are approximately 58 species in China (Xu et al., 2020). Various medicinal materials and preparations of Yinyanghuo as Chinese medicine and dietary supplements are traded to Japan, South Korea, Europe and America from China.

The folium of *Epimedium brevicornu* Maxim. (FEB) from a variety of Yinyanghuo, was recorded in the 2020 edition of Chinese Pharmacopoeia. And it is increasingly valued by pharmacognosticians because of its abundant wild resources and relatively stable quality of medicinal components (Xu et al., 2008). By TCM theory, the prepared slice of FEB (PFEB) is beneficial in reinforcing the kidney-Yang whereas the raw products (RFEB) have the advantage of strengthening tendons and bones. Thus, the PFEB is commonly used to treat sexual dysfunction, and RFES is used for treatment of osteoporosis. However, there are few studies comparing their effect on HPA axis and the sexual function of KDS animal model. Moreover, it is not clear how the FEB regulation of HPA axis links to the restoration of sexual function in the entire NEI network.

There were only two experimental studies reported the protective effects of FEB on HPA axis in KDS rat model (Huang et al., 2013a; An et al., 2015): The extract of FEB is beneficial in treating hydrocortisone-induced-KDS rats through improving HPA axis and endocrine system, which involved in releasing corticotropin releasing hormone from hypothalamus, producing serum adrenocorticotropic hormone in anterior pituitary, and secreting corticosteroids from adrenal cortex. FEB flavonoids affect GCs-induced-HPA axis-suppression by upregulation of *ACTH* and insulin-like growth factor II. Additionally, there are a few literature reports on how Yinyanghuo improves sexual function in the experimental animals: It was found that PFEB significantly promoted the growth and endocrine function of the testicular tissues in normal rat (Niu, 1989). The water and alcohol extracts of both RFEB and PFEB could significantly inhibit the atrophy of accessory organs of castrated mice (Wang et al., 2005). Preliminary clinical trials had shown that FEB granules could effectively improve the sperm number and motility in male infertility patients with abnormal semen (Gu et al., 2018). Chiu et al. (2006) revealed that the mechanism on FEB treatment on Erectile Dysfunction (ED) is involved in relaxing the corpus cavernosum smooth muscle through activation of NO/cGMP/PDE5 signaling pathway.

At present, there was no systematic study on the mechanism of prepared slices of EF on regulating HPA axis and immune system in the NEI network in KDS animal model. As part of the series of research on the mechanism of action of the processed products of Yinyanghuo, this study aimed to compare the difference of RFEB and PFEB in the effects and safety involving HPA axis, immune system and sexual function in KDS mice. Additionally, the internal connection of these systems will be discuss. This study will provide rationale for the application of Yinyanghuo.

2 Materials and methods

2.1. Plant sources

The folium of *E. brevicorn*. was purchased and identified by Dr. *Jian Xu* in Jing Brand Co., Ltd., Hubei Province, China, in May 2019. The specimen vouchers (20190502) had been stored in the Hubei Provincial Key Laboratory for Quality and Safety of Traditional Chinese Medicine.

2.2 Preparation of the RFEB and PFEB extract

According to Chinese Pharmacopoeia, processing procedures of the folium of *E. brevicorn* include eliminating foreign matter, pick the

leaves, spray with water, soften slightly, cut into slivers and dried. Stir-bake the slivers of FEB with refined suet by gentle heating until an evenlustre is produced, then remove and cool the slivers. Using 20 kg of refined suet per 100 kg of FEB, the PFEB (5 kg) were extracted with 50% EtOH (the solvent multiples were 8 times and 7 times in turn, 1.5 h, each time) at 83°C and with 95% EtOH at 78°C. RFEB were extracted by the same method without suet. Then RFEB and PFEB were concentrated in the rotary evaporator, eventually dried into powder in the vacuum drying box, and their extraction rate was 7.5%.

2.3 Dectection of the total flavonoid content in RFEB and PFEB

According to the detection method for the total flavonoid content of Yinyanghuo in the 2020 edition of the Chinese Pharmacopoeia, The detection steps were as follows:

Preparation of reference solution: Icariin, accurately weighed, added with methanol to produce 0.1 mg per 1 mL. The solution is used as the mother liquor for backup.

Preparation of sample solution: Accurately weigh 0.2 g of RFEB and PFEB dry extract powder and place them in a 50 mL volumetric flask. Add an appropriate amount of methanol to completely dissolve and replenish it to the mark. Shake well and serve as the test solution.

2.4 Animal grouping and sample collection

Forty eight-week-old C57BL/6 mice were acquired from Charles River (Beijing, China) and kept in cages with room temperature of 22°C–25°C and 70% humidity. Animal welfare and experimental procedures were followed in accordance with the institutional guidelines for the care and use of laboratory animals and related ethical regulations of Shanghai University of Traditional Chinese Medicine (2022011). The mice were divided into the control group, KDS group, RFEB group, and PFEB group, 10 mice in each group. The control group was subcutaneously injected with 0.2 mL of normal saline (NS) each day, while the other three groups were subcutaneously injected with 20 mg/kg of corticosterone in 1% dimethyl sulfoxide (DMSO) each day. Based on the pharmaceutical results achieved in the preliminary experiment, as well as the human clinical dosage of 9 g of the folium of *E. brevicorn* per 70 kg body weight (China Pharmacopoeia Committee, 2015), mice in RFEB group and PFEB group were correspondingly gavaged with a dosage of 2.25 g extract of RFEB and PFEB per kg body weight daily, equating 2 times of the human clinical dosage, for consecutive 21 days. (The two kinds of extract are about 1.486 g crude drug per milliliter). The control group and KDS group were given distilled water of the same volume.

On 8:00 a.m. of the 22nd day, the mice were weighed and anesthetized. Blood samples were collected from the fundus venous plexus, and blood serum was isolated. The cavernous body was removed and divided into two even parts. One-half was fixed with 4% paraformaldehyde solution, while the other half was frozen with liquid nitrogen. The thymus gland and the spleen were weighed and calculated for organ coefficient.

TABLE 1 List of primer sequences.

Name	Primer sequence
CRH-F1	ACCTTCTGCGGGAAGTCTTG
CRH-R1	TTTTGGCCAAGCGCAACATT
ACTH-R1	CGTACTTCCGGGGGTTTTCA
ACTH-F1	GGCTTGCAAACTCGACCTCT
eNOS-F	GCACATTTGGCAATGGGGAT
eNOS-R	CGGGCCTGACATTTCCATGA
PDE5A1-F	CAACTCCGTGCGGTCG
PDE5A1-R	TCTCTGAAAACCATGCGTTGA
GAPDH-F1	GAGTCAACGGATTTGGTCGT
GAPDH-R1	TTGATTTTGGAGGGATCTCG

Organ Coefficient (mg/g) = Organ Weight (mg)/Body Weight (g)

2.5 Serum hormonal indicators

By ELISA, the serum samples were tested for *ACTH* (Cusabio Technology, Wuhan, China) and testosterone (Elabscience, Wuhan, China) levels, according to the procedures given in the manufacturer's manuals. The serum samples were tested for cAMP and cGMP levels using the cAMP GsHiRange kit and the cGMP HTRF kit (PerkinElmer, United States), and then the cAMP/cGMP ratios were calculated. Following blood biochemistry analysis, the serum samples were tested for superoxide dismutase (SOD) and MDA levels (Jiancheng, Nanjing, China.)

2.6 qRT-PCR

The hypothalamus, pituitary, and cavernous body tissues were individually ground in liquid nitrogen and lysed with cell lysis buffer. The total RNA was extracted using Trizol and tested for purity, and then reverse transcribed into cDNA using Super RT cDNA Synthesis Kit (Cwbio, Beijing, China). The cDNA was then amplified using the Ultra SYBR One Step RT-qPCR Kit (Cwbio). See Table 1 for the primer sequences. The amplification conditions were 95°C for 2 min, 38 cycles of 95°C for 30 s and 60°C for 30 s and finally 74°C for 30 s. The mRNA levels of eNOS, PDE5A1, *ACTH*, and *CRH* were calculated using the $2^{-\triangle\triangle Ct}$ method.

2.7 Western blot

The hypothalamus, pituitary, and cavernous body tissues were individually ground, homogenized using RIPA lysis buffer. The homogenates were rested on ice for 30 min, and immediately subjected to centrifugation with 12,000 × g in 4°C for 15 min, then the supernatant was collected. The total protein concentration in supernatant was determined according to the BCA Protein Assay Kit (Cwbio). 50 μg of total protein was separated using SDS-PAGE.

The electrophoresis peptides were transferred to the PVDF membranes. The PVDF membranes were then blocked for 2 h using 5% nonfat dried milk and probed with antibodies at 4°C. After washing 3 times using TBST, the PVDF membranes were incubated for 2 h using horseradish peroxidase-conjugated secondary antibodies, and then ECL (a chemiluminescence agent) was used to develop the protein bands. The signal intensity was analyzed using Gel-Pro Analyzer 4.0 software (Media Cybernetics, Silver spring, MD, United States). The GAPDH was used as an internal control to assess the protein loading equivalence. The eNOS antibodies (1:500,ab300071), PDE5A1 antibodies (1:500, ab259945), *ACTH* antibodies (1:500, ab32893), *CRH* antibodies (1:500, ab184238), and GAPDH antibodies were purchased from Abcam.

2.8 PDE5A1 inhibition assays

This test adopted the method we have published previously (Li et al., 2022). Briefly, all samples were diluted in assay buffer which contained 100 mM $MgCl_2$ and 50 mM Tris-HCl (pH 8.0). 30μL PDE5A1 solution (0.0625 μg/mL, ab56614 Abcam) and 30 uL extraction solution were mixed at room temperature and incubated for 5 min, followed by addition of 30 μL cGMP solution (7.5 μg/mL, G6129, Sigma), and the reaction was carried out at 35°C for 90 min. The PDE5A1 inhibitors were diluted to 7 concentration series with a; 2-fold gradient. After the reaction, each vial was incubated in 100°C boiling water for 5 min to inactivate PDE5A1 activity, and then cooled to be tested with HPLC. Percentage inhibition was calculated using the peak area of HPLC. Two individual operations were performed on different dates as the repetition.

The half maximal inhibitory concentration (IC50) of each extraction solution towards PDE5A1 was evaluated.

2.9 Isolation of splenic lymphocytes and apoptosis analysis

The mouse spleen was isolated aseptically, and minced into small pieces and filtered through 100-um nylon mesh to acquire the cell suspension. Splenic lymphocytes were isolated after centrifugation at 250 *g* for 10 min and cell fractionation on lymphocyte separation medium (density = 1.081). After the white blood cell layer was collected and washed, the cells were cultured in RPMI-1640 medium containing 10% Fetal bovine serum (FBS) for 2 h, then the non-adherent cells (splenic lymphocytes) were harvested and adjusted to 1 × 106 cells/mL in the culture medium.

Splenic lymphocytes were labeled with Annexin V and Propridium Iodide (PI), and left to react at room temperature for 30 min in the dark. The apoptosis rate was detected by fluorescence-activated cell sorting (FACS) analysis.

2.10 CCK-8 assay on splenic lymphocytes proliferation

The splenic lymphocytes were adjusted to a concentration of 2 × 10^6/mL, and 100 μL was added to each well in a 96-well culture plate. Concanavalin A (Con A) of 3 μg/mL and the extract of different concentrations were added. The lymphocytes were cultured for 72 h in 5% CO_2 at 37°C. The cell viability was measured using Cell Counting Kit-8 (CCK-8) method.

2.11 Immunohistochemistry analysis

The paraformaldehyde-fixed cavernous body was dehydrated, embedded in paraffin, and cut into 5-um thick sections. The sections were deparaffinized, hydrated, incubated for 10 min in 3% H_2O_2 at room temperature to stop endogenous peroxidase activity. The sections were blocked for 30 min in 10% goat blood serum, and then incubated in a specific primary antibody solution overnight at 4°C. Next, the sections were incubated in a biotinylated secondary antibody solution at room temperature for 30 min, then incubated in a streptavidin-horseradish peroxidase complex diluted by 1:200 at room temperature for 30 min. Finally, using DAB solution (3,3′-diaminobenzidine tetrahydrochloride solution), the sections were observed under microscope for color development. Finally, the sections were counterstained with hematoxylin, dehydrated, and mounted with resin. The eNOS antibody (ab300071), PDE5A1 antibody (ab259945), TNF-α antibody (ab1793), IL-6 antibody (ab290735), and NF-κB antibody (ab32536) were purchased from Abcam.

2.12 Toxicity evaluation

Mice (five mice per group) were orally administered with the FEB extract at 22.5 g/kg BW every day for 2 weeks. The mice in control group were given distilled water. Mortality, and body weight were monitored. The major organs, such as heart, liver, stomach, and kidneys were collected for evaluations after 14 days. Blood samples were subjected to centrifugation (10 min at 1,400 g) for serum separation. Biochemical assay was used to assess alanine aminotransferase (ALT), aspartate aminotransferase (AST) and lactate dehydrogenase (LDH) activity determination, and urea and creatinine concentration, by clinical analyzer (HITACHI 7180, Japan).

2.13 Statistical processing

Statistical software SPSS 17.0 was used for analysis, and the data were expressed as mean ± standard deviation (x ± sd). One-way ANOVA and LSD-t test were used for comparison between multiple groups, with a significant difference defined at $p < 0.05$.

3 Results

3.1 Flavonoid content in RFEB and PFEB

Take the mother liquor under "*2.3*" and place it in a 10 mL volumetric flask. Add methanol to prepare solutions with concentrations of 0.0055, 0.0073, 0.011, 0.0165, and 0.022 mg/mL, respectively. With methanol as the blank, refer to Ultraviolet–visible spectroscopy (Appendix VA in the

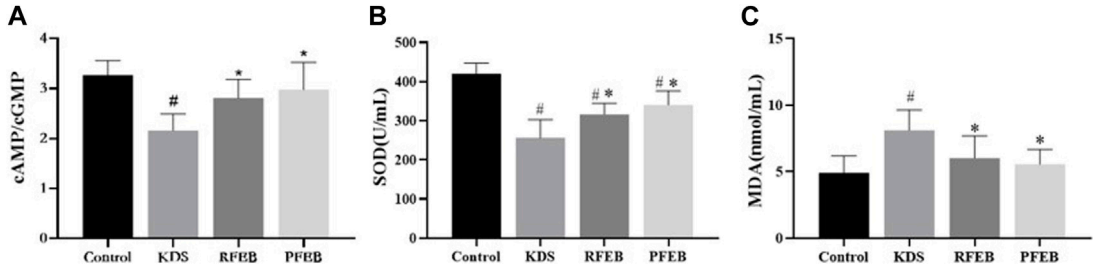


FIGURE 1
Effects of RFEB and PFEB on the changes in the second messengers and oxidative stress molecules in KDS mice. **(A)** Serum cAMP/cGMP Tatio. **(B)** Serum S0D-activity. **(C)** Serum MDA content. Mean ± SD (n = 10/group), #p < 0.05 vs. control; *p < 0.05 vs. KDS, ANOVA, LSD-t-test.

2020 edition of the Chinese Pharmacopoeia), measure the absorbance at the wavelength of 270 nm, take the concentration of the reference solution as the abscissa, and the absorbance value as the ordinate, to obtain the linear regression equation: y = 52.425x -0.0649 (r = 0.9997, linear range 0.0052 ~ 0.026 mg/mL). Based on this, the total flavonoid contents of RFEB and PFEB were measured as follows: 4.98, 5.40 (%) (n = 3).

3.2 The effect of FEB extracts on KDS treatment

After treatment with RFEB or PFEB, some changes were observed in the KDS mice. Figure 1 showed the changes in the biochemical indices in rat serum. Cyclin AMP is the second messenger with the strongest effect among those induced by *ACTH* in the HPA axis, which affects downstream signaling pathways. Cyclin GMP is another second messenger in the HPA axis. Since cAMP and cGMP have been shown to link to the Yin-Yang theory and the suppression of cAMP/cGMP ratio was shown to be a manifestation of Yang deficiency, we evaluated the ratio of cAMP/cGMP in serum (Goldberg et al., 1975; Brian et al., 1990; Jin et al., 2020). SOD and MDA are indicators reflecting oxidative stress levels. Corticosterone caused cAMP/cGMP ratio (Figure 1A) and SOD level (Figure 1B) to decrease, and MDA level to increase (Figure 1C); while RFEB and PFEB both raised cAMP/cGMP ratio and SOD level, and decreased MDA level. Both cAMP/cGMP ratio and MDA levels returned to normal range after treatment.

3.3 The comparative effect of RFEB and PFEB on hormone secretion in the HPA axis of KDS mice

As Figure 2 showed, KDS mice showed a decrease in both *CRH* levels in the hypothalamus, as well as *ACTH* levels in the pituitary and serum, compared to control mice (p < 0.05). After RFEB and PFEB treatment, both mRNA and protein levels of *CRH* and *ACTH* markedly increased, and the treatment with PFEB increased *CRH* and *ACTH* mRNA by PFEB to the similar level of control group. Compared to the RFEB treatment group, the *ACTH* mRNA and protein levels in the pituitary of PFEB treatment group increased with a statistically significant difference (p < 0.05).

3.4 The comparative effect of RFEB and PFEB on the corpus cavernosum of KDS mice

Testosterone, eNOS and PDE5 are important indicators reflecting ED symptom. As shown in Figure 3A, the serum testosterone level in KDS mice was significantly lower than that of control mice (p < 0.05), whereas mice treated with PFEB had testosterone level significantly higher than KDS mice (p < 0.05). Compared to control group, the mRNA and protein levels of eNOS and PDE5A1 of corpus cavernosum increased in KDS mice. (p < 0.05). As shown in Figures 3B–E, with the RFEB and PFEB treatment, the expression of eNOS in corpus cavernosum showed progressive increase, with PFEB group having higher levels than RFEB group (p < 0.05). Figures 3D, E showed that RFEB and PFEB treatment markedly decrease PDE5A expression which was raised by corticosterone, and PDE5A returned to normal range by PFEB treatment. Figure 3F showed the eNOS and PDE5A expression in corpus cavernosum by immunohistochemistry, which showed similar change.

3.5 Comparisons of the inhibitory potency of FEB extracts on PDE5A1 in vitro

Figure 4 showed the 50% inhibitive concentration (IC50) of different types of FEB extracts on PDE5A1 activity. Both the RFEB and the PFEB extract, using 50% and 95% ethanol, inhibited PDE5A1 activity. The four types of extracts have IC50s between 0.13 mg/mL - 0.28 mg/mL, and there was no significant difference in their inhibiting potency on PDE5A1 *in vitro*.

3.6 The comparative effect of FEB extracts on KDS mouse immune cell response *in vivo* and *in vitro*

As shown in Figures 5A, B, the spleen index and thymus index of KDS mice were noticeably lower than those of control mice

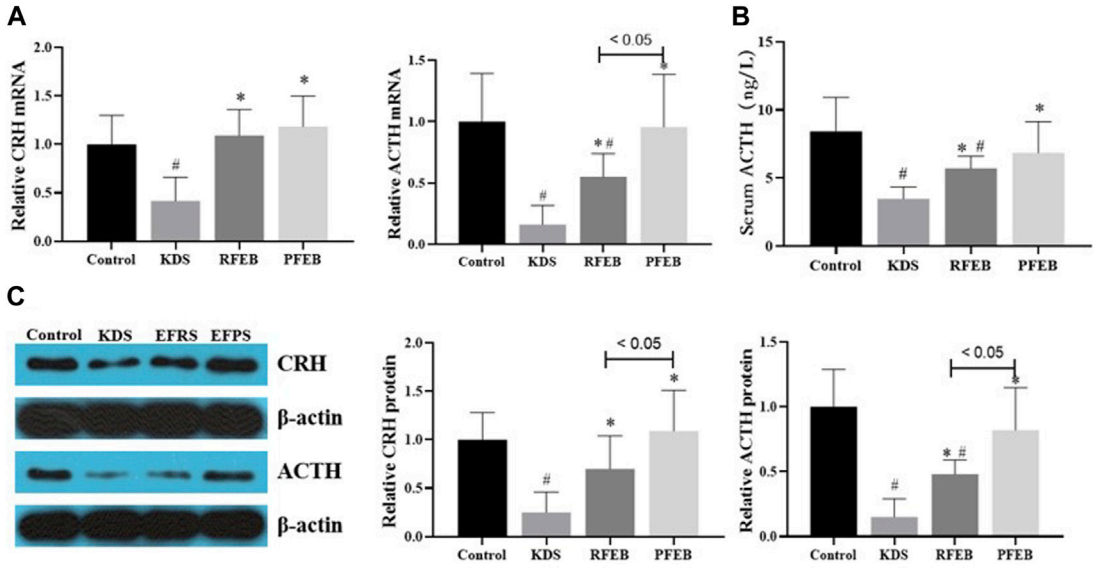


FIGURE 2
Effect of RFEB and FEB on hormone secretion inthe HPA axis of KDS mice. **(A)** CRH mRNA.levels in the hypothalamus and ACTH RNA in thepituitary. **(B)** Serum ACTH content. **(C)** CRH protein levels in the hypothalamus and ACTH protein levels in the pituitary. Mean ± SD (n = 10/group), #p < 0.05 vs. control; *p < 0.05 vs. KDS, ANOVA, LSD-t test.

(p < 0.05). RFEB and PFEB significantly attenuated spleen and thymus atrophy induced by corticosterone, indicated by the increases of spleen index and thymus index (p < 0.05). Concanavalin A (Con A) acts as a mitogen, stimulating the receptors on the lymphocyte membrane and inducing lymphocyte proliferation and immune response. The level of lymphocyte proliferation can reflect the strength of the body's immune response; therefore, in the present study this indicator was used to examine the effect of RFEB and PFEB on immune regulation. Figures 5C, D showed the proliferation and apoptosis of spleen lymphocytes *in vitro*. Compared to the lymphocytes of control mice, the *in vitro* lymphocyte proliferation of KDS mice was markedly low, while apoptosis was more significant. RFEB and PFEB increased lymphocyte proliferation and decreased apoptosis to different degrees, and PFEB showed better performance than RFEB. The effect of RFEB and PFEB on normal lymphocyte proliferation *in vitro* was compared and shown in Figure 5E, after 48 h of cell culture, compared to the lymphocytes of control mice, Con A noticeably increased cell proliferation (p < 0.05). When RFEB concentration was below 5 ug/mL, or when PFEB concentration was below 10 ug/mL, as concentration increases, OD value gradually increased. When dosage was higher than 2.5 μg/mL, PFEB showed better performance in stimulating lymphocyte proliferation compared to RFEB with the same concentration (p < 0.05). When concentration of RFEB was higher than 5 ug/mL, or when PFEB was higher than 10 ug/mL, OD value decreased as concentration increased. Microscopic observation showed no significant change in morphology. There was no sign of cytoplastic shrinkage or other kinds of cytotoxicity. Therefore, the decrease in lymphocyte proliferation should not be attributed to cytotoxicity.

3.7 The comparative effect of RFEB and PFEB on inflammatory cytokines in corpus cavernosum of KDS mice

As Figure 6 showed, the inflammation in corpus cavernosum were observed. Both RFEB and PFEB inhibited the up-regulated inflammatory cytokines (TNFα, IL-6 and NF-κB) in corpus cavernosum of KDS mice (p < 0.05), and the down-regulated level of PFEB treatment was more obvious than that of RFEB (p <0.05).

3.8 Toxicity evaluation

All the mice remained normal under FEB treatment at the dosage of 20 times the human clinical dosage, with no any adverse behavioral changes. Animals treated with PFEB or RFEB showed weight gain equivalent to control mice. No changes in organ coefficient, morphology, or color were observed during analysis of the heart, liver, stomach, and kidneys (data not shown). Except for AST, all serum parameters (ALT, urea, creatinine, LDH) were in normal range and there was no difference between the groups. AST treated with RFEB (185.0 ± 12.4 U/L) were higher than control (150.5 ± 18.3U/L) and PFEB (160.1 ± 26.4U/L) group (Figure 7).

4 Discussion

4.1 FEB improve KDS via NEI network

After almost half of a century's research, Zi-yin Shen suggested that the pathogenesis of KDS in TCM was associated with HPA axis,

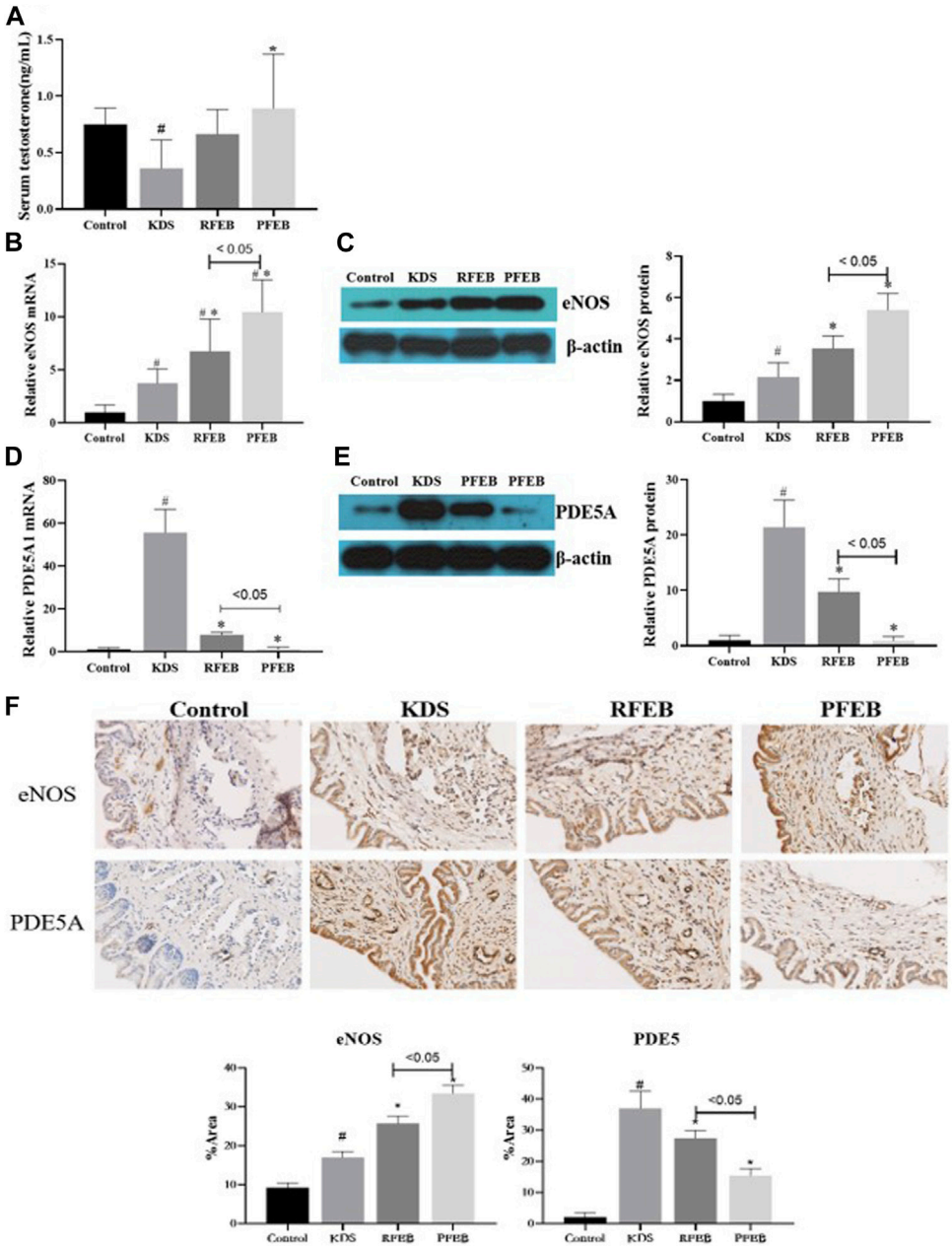


FIGURE 3
Effect of RFEB and PFEB affect the expression of sex hormones, eNOS and PDE5A in the KDS mice. **(A)** Serum testosterone content. eNOS mRNA **(B)** and protein levels **(C)** incorpus cavernosum. PDE5A mRNA **(D)** and protein levels **(E)**. **(F)** incorpus cavernosum. eNOS and PDE5A expression incorpus cavernosum by immunohistochemistry. Mean ± SD (n = 10/group), #p < 0.05 vs. control; *p < 0.05 vs. KDS, ANOVA, LSD-t test.

and the organs involved in the adrenal gland, gonads, and thyroidgland (Shen, 2005). The *ACTH*, cortisol (CORT) and cAMP level in Yang deficiency subjects declined significantly in comparison to healthy ones (Wang et al., 2008; Hu et al., 2018). Through the systematical analysis of the relationship between kidney-Yang deficiency and TCM clinical symptoms and related genes, it is found that the gene *CRH* is closely related to KDS. TCM clinical studies have confirmed that *Epimedium* flavonoids can reconstruct the balance of NEI network by increasing serum *ACTH* levels (Zha, 1982), recovering gonadal function and serum cortisol (Hua et al., 2003; Thomas et al., 2008; Xiong et al., 2009), as well as regulating cell apoptosis and proliferation in KDS patients (Xiao et al., 2000; Lin et al., 2002; Jin et al., 2010; Shen, 2012; Gong et al., 2015; Tan et al., 2017).

The Kidney-tonifying treatment based on the theory of the "HPA axis" has explained its underlying mechanism in treating kidney-Yang deficiency diseases and obtained clinical effectiveness, and KDS may have the potential relationship with ED (Gong et al., 2015). However, no study has reported the systemic organ changes and mechanism of TCM in tonifying

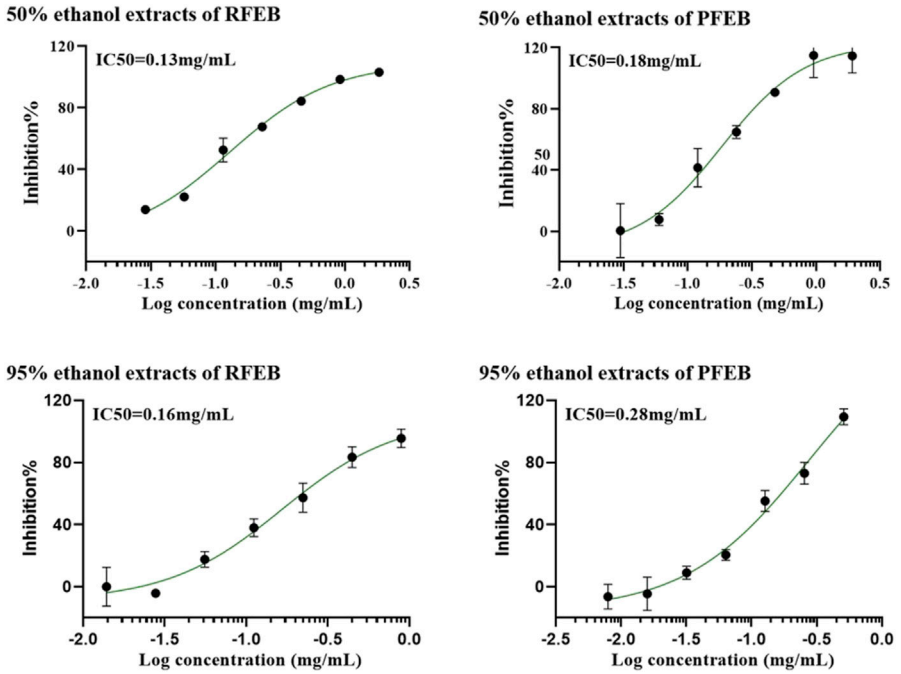


FIGURE 4
In vitro IC_{50} curve of various EF extract of PDE5A1.

kidney-Yang and the treatment of ED, which makes this research of important value for healthcare guidance and clinical application.

4.1.1 Deregulation of endocrine and immune function, and sexual dysfunction co-exist in KDS

In this study, subcutaneous injection of corticosterone was used to disrupt HPA axis in KDS mice. The apparent decrease of serum cAMP/cGMP ratio and increase of oxidative stress markers confirmed the presence of KDS. Decreased levels of *CRH* in the hypothalamus and *ACTH* in the pituitary and serum indicated damage to the HPA axis. Decreased spleen index and thymus index indicated that kidney-Yang deficiency and HPA damage caused the atrophy of immune organs. In addition, the increased expression levels of eNOS and PDE5 in the corpus cavernosum and the decreased serum testosterone indicated that they also caused dysfunction of sexual organs. These data suggested that the KDS mouse model was successfully established, and their endocrine secretion, immune and sexual functions were impaired.

4.1.2 FEB improves the neuroendocrine system of HPA axis and KDS index

Clinical studies have found that *Epimedium* extract increases *ACTH* and corticosterone levels in the plasma of patients who took prednisone (Cai et al., 1998). This present study found that FEB could not only increase corticosterone-suppressed *ACTH* levels *in vivo*, but also enhance *CRH* levels and cAMP/cGMP ratio, and reduce oxidative damage. This study was the first to compare the effects of RFEB and PFEB on the improvement of HPA endocrine secretion and KDS. PFEB showed a stronger effect than RFEB on the improvement of *CRH* levels, cAMP/cGMP ratio and oxidative damage at the indicated doses. PFEB was more effective than RFEB in improving *ACTH* levels.

4.1.3 FEB reduces eNOS uncoupling and inhibit PDE5

In the concept of TCM, patients with HPA axis disorders have ED symptoms (Citron et al., 1996; Salvio et al., 2021). Moreover, in TCM clinical practice, sexual dysfunction is one of the typical symptoms of kidney-Yang deficiency. This study confirmed that FEB increased the level of eNOS induced by HPA axis disorders, and the effect of PFEB was significantly better than that of RFEB. It has been reported that eNOS coupling means normal electron transfer and function, while uncoupled eNOS under pathological conditions results in a decrease in NO, an increase in superoxide anion (O^{2-}), and aggravation of oxidative stress, resulting in endothelial dysfunction (Scmidt and Alp, 2007; Perlins et al., 2012). For example, interleukin-1β (IL-1β) stimulus and noise exposure cause the uncoupling and dysregulation of eNOS by over-activating the HPA axis, which in turn leads to increased ROS and vascular dysfunction (Gadek-Michalska et al., 2012; Daiberab et al., 2020). In this study, the HPA axis disorders increased the eNOS level and serum oxidative stress biomarkers in the corpus cavernosum, however, FEB treatment reduced ROS and further increased eNOS expression. eNOS uncoupling might explain the relationship between the two changes. It was speculated that as FEB treatment increased eNOS expression and simultaneously reduced eNOS uncoupling, then to enhance NO, and therefore reduced oxidative stress. Further experiments are required to confirm this speculation. The result confirmed that the HPA axis disorders in

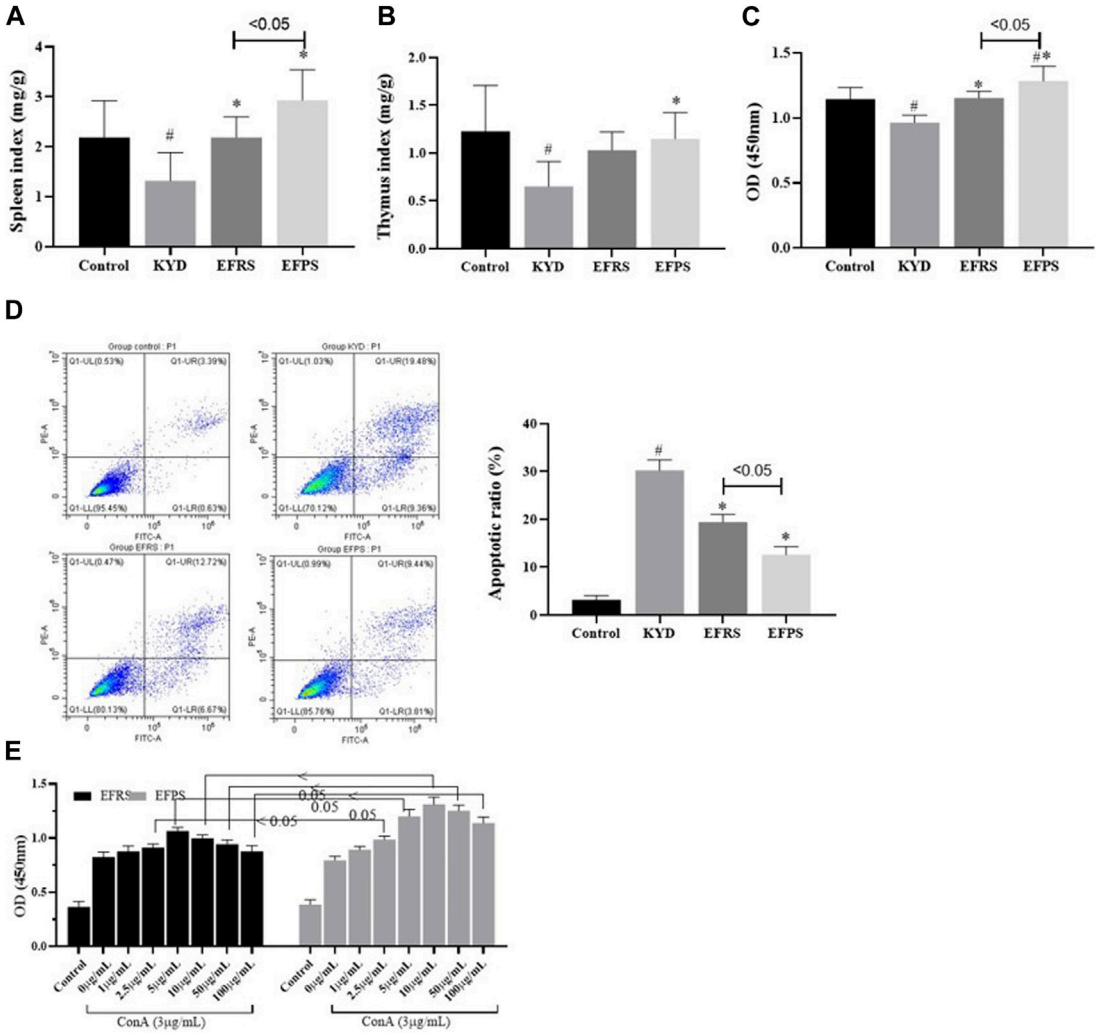


FIGURE 5
Effect of RFEB and PFEB on KDS mouse immune response. Spleen index **(A)** and thymus index **(B)** (n = 0/group). The proliferation **(C)** and apoptosis **(D)** of spleen lymphocytes of various groups *in vitro*. (n = 5/group). **(E)** The proliferation of normal lymphocytes (n = 5/group). Mean ± SD# $p < 0.05$ vs. control; $p < 0.05$ vs. KDS, ANOVA, LSD-t test.

KDS caused ED-like changes in the first messenger of the corpus cavernosum, and FEB had a protective effect against ED.

In addition, FEB reduced the level of PDE5 *in vivo*. PDE5 is highly expressed in the corpus cavernosum and has become a noteworthy target for drug screening in ED. Sildenafil (Viagra) is a representative drug for the treatment of ED. In this study, the *in vitro* inhibitive activities against PDE5 were similar to that using RFEB and PFEB usage, and interestingly, the *in vivo* inhibition on PDE5 expression by PFEB was better than that by RFEB. This *in vivo* pharmacological effect results are similar to the clinicalefficacy of PFEB in treating ED. It indicates that the different anti-ED effect between RFEB and PFEB was determined not by their enzyme inhibitory activity but by other mechanisms.

4.1.4 FEB improve the immune system of KDS mice

The neuroendocrine system and the immune system are essential components that regulate the physiological activities of mammals, and they play important roles in the regulation of metabolism and fighting against infection and disease. There are dynamic and interactive transfer of signaling molecules between the two systems, which coordinate their activities. It is well known that glucocorticoids can inhibit the immune response of the body. If the HPA axis is severely dysfunctional, endocrine homeostasis and glucocorticoids released from the adrenal cortex will be disturbed, which in turn affects the immune system of the body and increases disease susceptibility of target organs.

In this study, it was found that FEB effectively increased the thymus index and spleen index of KDS mice and reduced the ratio of apoptotic lymphocytes in the spleen, and the protective effect of PFEB was stronger than that of RFEB. The results of the *in vitro* and *in vivo* experiments were consistent. Compared with RFEB, PFEB had a stronger effect on protecting immune organs and cells. In addition, the levels of inflammation-related cytokines TNFα, IL-6, and NF-κB in the corpus cavernosum were inhibited by FEB, especially PFEB. Similar results have been

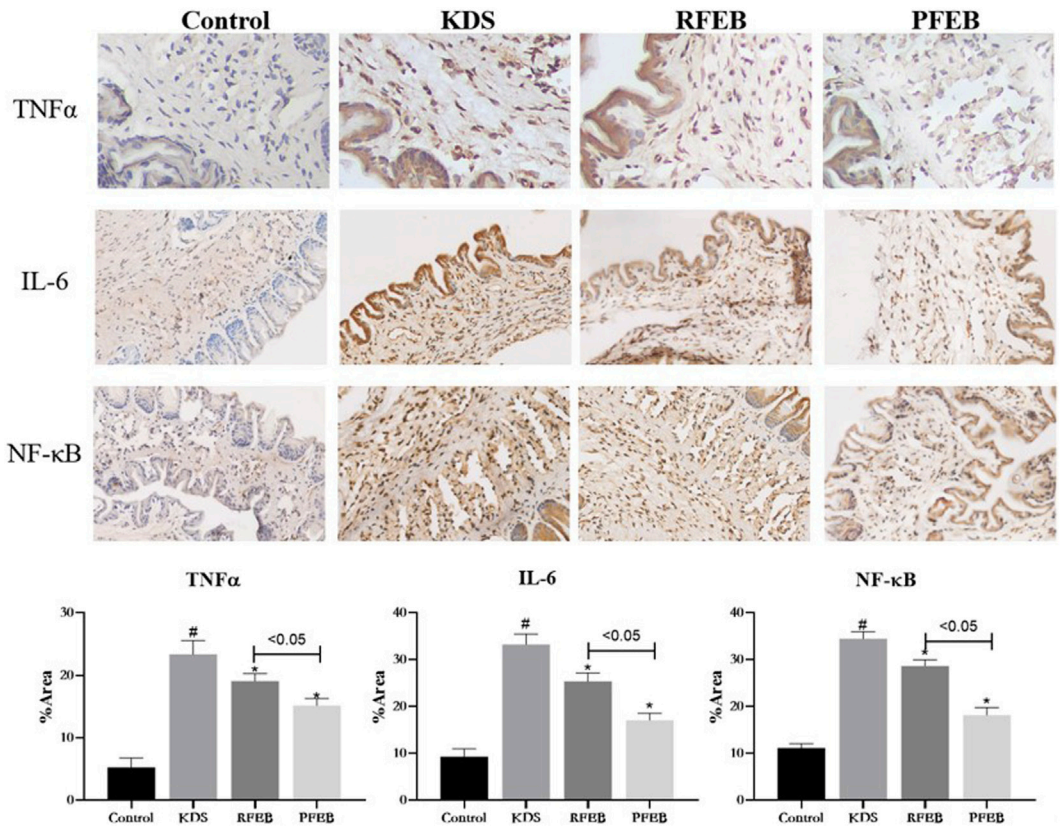


FIGURE 6
Effect of RFEB and IFEB on TNFα IL-6 and NF-κB expression in-corpus cavernosum of mice. Mean ± SD < (*n* = 10 group), #*p* < 0.05 control; vs. KDS, ANOVA, LSD-t test.

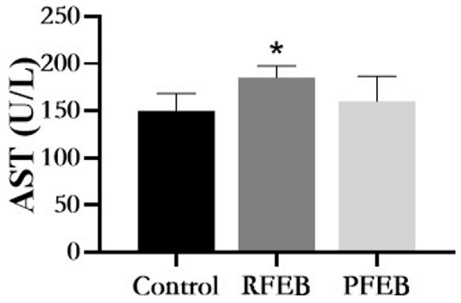


FIGURE 7
Effect of RFEB and PFEB on serum AST of mice. Mean ± SD (*n* = 5/group), **p* < 0.05 vs., control, ANSOVA, LSD t-test.

reported that *Epimedium* flavonoids significantly upregulate levels of FSH, sex hormones and lymphocytes amount in aged rats by secretion of GnRH, which is a powerful information transmission factor in NEI network (Huang et al., 2013a; An et al., 2015). Thus, in this study, it was speculated that FEB could act on the corpus cavernosum by regulating the HPA axis of the KDS animal model and activating the immune system through the signaling pathway of NEI network (Shen et al., 2004). The strong protective effect of PFEB on the NEI network might be the underlying mechanism that it was more efficient than RFEB in the treatment of kidney-Yang deficiency.

4.2 The composition changes of PFEB and RFEB, and the future prospects

The characteristic chemical components of *Epimedium* are 8-isopentenyl flavonoids in that icariin shows its protective effects on hydrocortisone-induced-KDS mice by regulating the HPA axis and endocrine system. Icariin also exhibit an IC_{50} value of 5.9 μM against PDE5A1 *in vitro* (Mario et al., 2008). It was worth noting that there were a few reports on the qualitative and quantitative analysis for the composition changes in the prepared slices of Yinyanghuo compared to raw products. The content of aglycones and secondary glycosides of flavonoids in Yinyanghuo increased due to the desugarization reactions in frying (Jing et al., 2009), and it was confirmed by some studies that the content of epimedin A, B and C decreased, while icariin increased when the herb was processed (Xie et al., 2011; Chen and Luo, 2013; Zhang et al., 2018; XU et al., 2021). And the increased icariin was proved to be a hydrolysis product of 3′′′-carbonyl-2′′-β-L-quinovosyl icariin instead of epimedin A, B and C (Sun et al., 2018). In addition, two (Sun et al., 2014), (Li et al., 2014) literature reported the compound formation mechanism in the processing of Yinyanghuo: During the processing, the increase of secondary glycosides and the formation of self-assembled micelles could be

attributed to the absorption of isopentenyl flavonoid glycosides, which leads to the enhancement of warming kidney-Yang. The literature generally confirmed that the raw and processed Yinyanghuo showed the difference of substance components, which is the reason for the difference in their action effects and pharmacological mechanisms. However, a great deal of composition analysis should be researched and enriched for FEB, especially for PFEB. In addition, for the exploration of pharmacological mechanism, further efforts should be paid on signaling pathways and the connecting molecules among the neuroendocrine system, immune system, and target organs. These studies are necessary to reveal the mechanism of their different pharmacological effects. The current research could not fully explain the pharmacological effect and mechanism of FEB against KDS. Therefore, further study on its complex pharmacological effects, especially after processing, is warranted.

5 Conclusion

By comparing the pharmacological effects and mechanism of RFEB and PFEB on kidney-Yang deficiency mice, this study found that PFEB was more effective than RFEB in improving the HPA axis function, reducing symptoms of kidney-Yang deficiency, enhancing functions of gonadal and corpus cavernosum, and maintaining balance of immune system. Moreover, no toxicity was observed, suggesting the safety of RFEB and PFEB for clinical use.

Data availability statement

The original contributions presented in the study are included in the article/Supplementary Materials, further inquiries can be directed to the corresponding authors.

Ethics statement

The animal study was reviewed and approved by The Shanghai University of Traditional Chinese Medicine (2022011).

Author contributions

The study was designed by XGZ, SY, and D-HY. KW, JL, XYZ, SL, and KW analyzed the data and wrote the first draft of the manuscript. D-HY, SY, and XGZ guided and supervised the experiments, and revised the manuscript. All data were generated in-house, and no paper mill was used. All authors agree to be accountable for all aspects of the work and ensure its integrity and accuracy. All authors contributed to the article and approved the submitted version.

Funding

This study received funding from the Natural Science Foundation of Hubei Province [grant number 2019CFB829].

Conflict of interest

Authors JX, ZW, QY, and YW were employed by Jing Brand Research Institute. The authors declare that this study received funding from Jing Brand Research Institute, Jing Brand Co., Ltd. The funder had the following involvement with the study: Establishment of animal model.

The remaining authors declare that the research was conducted in the absence of any commercial or financial relationships that could be construed as a potential conflict of interest.

Publisher's note

All claims expressed in this article are solely those of the authors and do not necessarily represent those of their affiliated organizations, or those of the publisher, the editors and the reviewers. Any product that may be evaluated in this article, or claim that may be made by its manufacturer, is not guaranteed or endorsed by the publisher.

References

An, R., Li, B., You, L. S., and Wang, X. H. (2015). Improvement of kidney yang syndrome by icariin through regulating hypothalamus-pituitary-adrenal Axis. *Chin. J. Integr. Med.* 21, 765–771. doi:10.1007/s11655-015-2063-z

Brian, H., Machteld, C., and Joshua, T. (1990). Lithium modulation of cortical cyclic nucleotides: Evidence for the yin-yang hypothesis. *Eur. J. Pharmacol.* 175, 129–136. doi:10.1016/0014-2999(90)90223-s

Cai, D. F., Shen, S. M., Chen, X. H., Shen, Z. Y., Zhang, L. J., and Liu, Y. F. (1998). Clinical and experimental research of Epimedium brevicornum in relieving neuroendocrino-immunological effect inhibited by exogenous glucocorticoid. *Zhongguo Zhong Xi Yi Jie He Za Zhi* 18, 4–7.

China Pharmacopoeia Committee (2015). Epimedium. Available at: https://db.ouryao.com/yd2015/view.php?id=520.

Chen, N., Luo, L. C., Kim, C. H., Noh, M., and Lee, A. Y. (2013). Glucosamine induces activated T cell apoptosis through reduced T cell receptor. *Tillage Cultiv.* 78, 17–27. doi:10.1111/sji.12056

Chiu, J. H., Chen, K. K., Chien, T. M., Chiou, W. F., Chen, C. C., Wang, J. Y., et al. (2006). *Epimedium brevicornum* Maxim extract relaxes rabbit corpus cavernosum through multitargets on nitric oxide/cyclic guanosine monophosphate signaling pathway. *Int. J. Impot. Res.* 18, 335–342. doi:10.1038/sj.ijir.3901437

Citron, J. T. E., Rubinoff, B., Ettinger, H., Minkoff, V. M., Hom, J., Kan, F., et al. (1996). Prevalence of hypothalamic-pituitary imaging abnormalities in impotent men with secondary hypogonadism. *J. Urology* 529, 529–533. doi:10.1097/00005392-199602000-00033

Dai, B., Zhang, J. N., Yang, M. L., Li, Y. X., Xiao, Z. Z., Yang, L., et al. (2017). Establishment of a mouse model of kidney deficiency induced by oral administration of hydrocortisone and evaluation of related factors. *Acta lab. anim. Sci. sin.* 2017, 70–73.

Daiberab, A., Kröller-Schöna, S., Oelzea, M., Hahadab, O., Lic, H., Schulzd, R., et al. (2020). Oxidative stress and inflammation contribute to traffic noise-induced vascular and cerebral dysfunction via uncoupling of nitric oxide synthases. *Redox Biol.* 34, 101506. doi:10.1016/j.redox.2020.101506

Gadek-Michalska, A., Tadeusz, J., Rachwalska, P., Spyrka, J., and Bugajski, J. (2012). Brain nitric oxide synthases in the interleukin-1β-induced activation of hypothalamic-pituitary-adrenal axis. *Pharmacol. Rep.* 64, 1455–1465. doi:10.1016/s1734-1140(12)70943-x

Goldberg, N. D., Haddox, M. K., Nicol, S. E., Glass, D. B., Sanford, C. H., Kuehl, F. A., Jr, et al. (1975). Biologic regulation through opposing influences of cyclic GMP and cyclic AMP: The yin yang hypothesis. *Adv. Cycl. nucleotide Res.* 5, 307–330.

Gong, Y., Liu, L. X., He, X. J., Zhao, H. Y., Yang, J., Li, L., et al. (2015). The th17/treg immune balance in ulcerative colitis patients with two different Chinese syndromes: Dampness-heat in large intestine and spleen and kidney yang deficiency syndrome. *Evidence-based complementary Altern. Med.* 2015, 264317. doi:10.1155/2015/264317

Gu, S., Zhou, R., and Wang, X. Y. (2018). Comparison of enhanced male mice sexual function among three medicinal materials. *Andrologia* 50, e13087. doi:10.1111/and.13087

Hu, X. W., Deng, C. Y., Tang, L. M., Qiu, F. F., Huang, P., Geng, L. L., et al. (2018). Ginger-separated snake moxibustion improves Yang deficiency constitution by up-regulating serum adrenocorticotropic hormone and cortisol levels in Yang deficiency constitution volunteers. *Zhen Ci Yan Jiu* 43, 773–776. doi:10.13702/j.1000-0607.180513

Hua, L., Wu, Y. N., and Zhang, J. M. (2003). Clinical study of yishen jianpi yangxue tongli therapy in treating polycystic ovary syndrome. *Chin. J. Of Integr. Traditional And West. Med.* 23, 819–822.

Huang, J. H., Li, J. J., Zheng, S., Wu, J. Z., Zhang, W., Sun, T., et al. (2013a). Epimedium flavonoids counteract the side effects of glucocorticoids on hypothalamic-pituitary-adrenal axis. *Evid. Based Complement. Altern. Med.* 2013, 938425. doi:10.1155/2013/938425

Huang, J. H., Shen, Z. Y., Cai, W. J., and Zhou, W. J. (2013b). Hypothalamic-pituitary-adrenal axis programming and its application in research of 'ZHENG' of traditional Chinese medicine. *China J. Traditional Chin. Med. Pharm.* 28, 3620–3623.

Jin, F. Q., Qin, H., Liu, H., and Wang, Z. L. (2020). Influence of acupuncture combined with rehabilitation therapy on limb motor function and serum c AMP and cGMP in patients with hemiplegia of cerebral ischemic stroke. *Chin. Acupunct. Moxibustion* 40, 581–585. doi:10.13703/j.0255-2930.20190613-k0001

Jin, R., Lin, Q., Liu, S. M., Zhao, Q., Zhang, Q., and Zhang, B. (2010). Mathematical analysis of the relationship between yang deficiency syndrome in traditional Chinese medicine and its objective indicators in clinical literature. *J. Chin. Integr. Med.* 8, 678–683. doi:10.3736/jcim20100712

Jing, X. Y., Jia, X. B., Sun, E., Wang, J. J., Chen, Y., and Cai, B. C. (2009). Research on variation regularity of five main flavonoids contents in *Epimedium* and processed *Epimedium*. *China J. Chin. Mater Med.* 34, 2738–2742.

Li, J., Sun, E., Zhang, Z. H., Jiang, J., Xu, F. J., and Jia, X. B. (2014). Effect of suet oil on formation of self-assembled micelles of flavonoids in *Epimedium*. *Zhongguo Zhong Yao Za Zhi* 39, 3278–3282.

Li, J. T., Wu, Y., Yu, X. X., Zheng, X. Y., Xian, J. C., Li, S. J., et al. (2022). Isolation, bioassay and 3D-QSAR analysis of 8-isopentenyl flavonoids from Epimedium sagittatum maxim. as PDE5A inhibitors. *Chin. Med.* 17, 147. doi:10.1186/s13020-022-00705-5

Lin, B. H., Fang, S. Q., and Ye, Y. (2002). Exploration on essence of spleen-kidney deficiency in middle-aged patients. *Chin. J. Of Integr. Traditional And West. Med.* 22, 33–36.

Mario, D. A., V, G. G., Esther, D. C., Federica, B., Riccardo, M., Elisa, Z., et al. (2008). Potent inhibition of human phosphodiesterase-5 by icariin derivatives. *J. Nat. Prod.* 71, 1513–1517. doi:10.1021/np800049y

Niu, R. (1989). Action of the drug herba *Epimedii* on testosterone of the mouse plasma and its accessory sexual organ before and after processing. *China J. Chin. materia medica* 20, 18–20+62.

Perlins, A. A. A., Sailesh, P., Qian, C., Sloane, M., S, A. J., Christopher, Z., et al. (2012). The effects of modulating eNOS activity and coupling in ischemia/reperfusion (I/R). *Schmiedeb. Arch. Pharmacol.* 385, 27–38. doi:10.1007/s00210-011-0693-z

Salvio, G., Martino, M., Giancola, G., Arnaldi, G., and Balercia, G. (2021). Hypothalamic-pituitary diseases and erectile dysfunction. *J. Clin. Med.* 10, 2551. doi:10.3390/jcm10122551

Scmidt, S. T., and Alp, J. N. (2007). Mechanisms for the role of tetrahydrobiopterin in endothelial function and vascular disease. *Clin. Sci.* 113, 47–63. doi:10.1042/CS20070108

Shen, Z. Y. (2012). A review of studies on kidney essence of integrated traditional Chinese and Western medicine. *Chin. J. Integr. Med.* 32, 304–306.

Shen, Z. Y., Chen, Y., Huang, J. H., and Hu, Z. W. (2004). The gene expression profile in hypothalamus-pituitaty-adrenal-thymus(HPAT) axis from EF-treated old rats. *Zhongguo Mianyixue Zazhi* 24, 59–62.

Shen, Z. Y. (2005). Studies of gene networks and singal transduction of kidney deficiency syndrome by syndrome differentiation through drug effects. *Chin. J. Integr. Tradit. West Med. Chin. Ed.* 25, 1125–1128.

Sun, E., Wei, Y. J., Zhang, Z. H., Cui, L., Xu, F. J., and Jia, X. B. (2014). Processing mechanism of Epimedium fried with suet oil based on absorption and metabolism of flavonoids. *Chin. J. Traditional Chin. Med.* 39, 383–390.

Sun, X. G., Li, Q., Zhang, J., Zheng, W., Ding, Q. Z., Yang, J., et al. (2018). The reason leading to the increase of icariin in Herba Epimedii by heating process. *J. Pharm. Biomed. Anal.* 149, 525–531. doi:10.1016/j.jpba.2017.11.050

Tan, C. E., Huang, X. Y., and Wang, M. X. (2017). Serum proteomic analysis and construction of protein-protein interaction networks about ejaculation praecox with shen-yang deficiency. *Zhongguo Zhong Xi Yi Jie He Za Zhi* 37, 438–442.

Thomas, R., Petra, K., Frauke, M., Jürgen, D. G., Klose, P., Musial, F., et al. (2008). Menopause in German and Chinese women—an analysis of Symptoms,TCM-diagnosis and hormone status. *Chin. J. Integr. Med.* 14, 194–196. doi:10.1007/s11655-008-0194-1

Wang, Q., Yao, S. L., Dong, J., Wu, H. D., Wu, C. Y., Xia, Z. Y., et al. (2008). Changes of endocrine and immune function in subjects of yang deficiency constitution. *Zhong Xi Yi Jie He Xue Bao* 6, 1226–1232. doi:10.3736/jcim20081204

Wang, S. Y., Qing, M. Z., Li, F., Gao, Y. K., and Ma, X. J. (2005). Effects of the crude and processed *Epimedium Sagittatum* Maxim on castrated mice. *Chin. Tradit. Pat. Med.* 2005, 59–60.

Xiao, X. C., Zhu, X. F., Ni, J. H., and Luo, X. X. (2000). Effect of intravascular laser irradiation of blood and traditional Chinese medical therapy on immune function in senile cerebral infarction patients of kidney deficiency type. *Zhongguo Zhong Xi Yi Jie He Za Zhi* 2000, 264–266.

Xie, J. P., Xiang, J. M., and Wang, H. D. (2011). Effects of different processed products on the main ingredient of *Epimedin* C and icariin of *Epimedium wushanense*. *Chin. J. Pharm. Anal.* 31, 674–677.

Xiong, G. B., Yao, W. L., and Wu, F. H. (2009). Shenfu Qiangjing decoction improves non-inflammatory and non-liquefied semen in kidney-yang deficiency men. *Zhonghua Nan Ke Xue* 1138.

Xu, J. Y., Yuan, H. C., Wang, C. P., Zhang, Y. H., Feng, Z. L., and Chen, W. (2021). Study on the changes of flavonoids content in *Epimedium Wushanensis* during processing. *Mod. Chem. Res.* 2021, 24–26.

Xu, Y. Q., Jiang, Y., Huang, H., Li, R. Q., Li, F. Q., Liu, Y., et al. (2020). Taxonomic study of Epimedium L.: Status, issues and prospect. *Guihaia* 40, 601–617.

Xu, Y. Q., Li, Z. Z., Zhang, X. J., Chen, J. J., Zhou, J. F., and Wang, Y. (2008). Geographic distribution and resource status of three important medicinal *Epimedium* species. *Plant Sci. J.* 2008, 91–98.

Zha, L. L. (1982). The application of plasma ACTH radioimmunoassay in patients with Shen Yang Xu. *Zhonghua Nei Ke Za Zhi* 21, 202–205.

Zhang, Q., Ouyang, L. Q., Yang, L., and Hu, W. H. (2018). Effects of different processing methods on chemical constituents and product quality of *Epimedum*. *J. Hubei Univ. Chin. Med.* 20, 52–56.

Glossary

ACTH	adrenocorticotropic hormone
CAMP	cyclic adenosine monophosphate
CCK-8	cell Counting Kit-8
CGMP	cyclic guanosine monophosphate
ConA	concanavalin A
CRH	corticotropin-releasing hormone
DMSO	dimethyl sulfoxide
EF	epimedii Folium
eNOS	endothelin nictric oxide synthase
FACS	fluorescence-activated cell sorting
FEB	the folium of Epimedium brevicornu Maxim.
FSB	fetal bovine serum
GADPH	glyceraldehyde-3-phosphate dehydrogenase
GCs	glucocorticoids
HPA	hypothalamic-pituitary-adrenal
HPLC	high performance liquid chromatography
IC50	half maximal inhibitory concentration
IL-6	interleukin-6
KDS	kidney-Yang deficiency syndrome
MDA	malondialdehyde
NEI	neuroendocrine-immune
NF-κB	nuclear factor kappa-B
NO	nitric oxide
NS	normal saline
PDE 5	phosphodiesterase type-5
PFEB	prepared slice of the folium of Epimedium brevicornu Maxim.
PI	propridium Iodide
RFEB	raw slices of the folium of Epimedium brevicornu Maxim.
SOD	superoxide dismutase
TCM	traditional Chinese medicine
TNF-α	tumor necrosis factor-α

frontiers | Frontiers in Pharmacology

TYPE Original Research
PUBLISHED 21 August 2023
DOI 10.3389/fphar.2023.1237686

Check for updates

OPEN ACCESS

EDITED BY
Wing Lam,
Yale University, United States

REVIEWED BY
Xiaofang Guo,
University of South Florida, United States
Baoguo Sun,
The First Affiliated Hospital of Sun Yat-sen University, China

*CORRESPONDENCE
Zhiqiang Chen,
zhi57@163.com
Lixing Cao,
wssq@gzucm.edu.cn

†These authors have contributed equally to this work

RECEIVED 09 June 2023
ACCEPTED 18 July 2023
PUBLISHED 21 August 2023

CITATION
Jiang Z, Zou Q, Chen Q, Zhang J, Tang H, Chen J, Qin Y, Yang L, Chen Z and Cao L (2023), Therapeutic role of Wuda granule in gastrointestinal motility disorder through promoting gastrointestinal motility and decreasing inflammatory level.
Front. Pharmacol. 14:1237686.
doi: 10.3389/fphar.2023.1237686

COPYRIGHT
© 2023 Jiang, Zou, Chen, Zhang, Tang, Chen, Qin, Yang, Chen and Cao. This is an open-access article distributed under the terms of the Creative Commons Attribution License (CC BY). The use, distribution or reproduction in other forums is permitted, provided the original author(s) and the copyright owner(s) are credited and that the original publication in this journal is cited, in accordance with accepted academic practice. No use, distribution or reproduction is permitted which does not comply with these terms.

Therapeutic role of Wuda granule in gastrointestinal motility disorder through promoting gastrointestinal motility and decreasing inflammatory level

Zhi Jiang[1†], Qiuping Zou[1,2†], Qicheng Chen[1], Junhong Zhang[3], Hailin Tang[4], Jingbao Chen[1], You Qin[5], Liming Yang[5], Zhiqiang Chen[1*] and Lixing Cao[1*]

[1]Department of Perioperative Research Centre of Chinese Medicine, The Second Affiliated Hospital of Guangzhou University of Chinese Medicine, Guangzhou, China, [2]Emergency Department, Dongguan People's Hospital, Dongguan, China, [3]Department of Research Public Service Center, The Second Affiliated Hospital of Guangzhou University of Chinese Medicine, Guangzhou, China, [4]State Key Laboratory of Oncology in South China, Sun Yat-Sen University Cancer Center, Guangzhou, China, [5]Department of Minimally Invasive Surgery, The Second Affiliated Hospital of Guangzhou University of Chinese Medicine, Guangzhou, China

Introduction: Previous studies indicated that Wuda Granule (WDG) has been applied in the treatment of gastrointestinal motility disorder (GMD), but the effect and underlying mechanisms is yet to be elucidated. This study aimed to explore the mechanism and pharmacological effect of WDG for GMD via network analysis, verification of animal experiments and clinical experiments.

Methods: The chemical components of WDG were identified from the Traditional Chinese Medicine Systems Pharmacology Database (TCMSP, http://lsp.nwu.edu.cn/index.php), and the Encyclopedia of Traditional Chinese Medicine (ETCM, http://www.tcmip.cn/ETCM/index.php/Home/Index/) according to oral bioavailability (OB) ≥ 20% and drug-likeness (DL) ≥ 0.10. The targets of WDG compounds were retrieved from the Swiss Target Prediction database (http://www.swisstargetprediction.ch/) and targets related to GMD were retrieved from GeneCards database (https://www.genecards.org/). Network analysis were performed to screen the key active compounds of WDG and its hub targets. Then the pharmacological effect of WDG were verified via vivo experiments in rats and clinical experiments.

Results: The results showed that 117 effective active compounds of WDG were screened and 494 targets of WDG compounds targeting GMD were selected. These targets were involved in the biological process of inflammatory regulation and the regulation of gastrointestinal motility. The mechanism was mainly involved in the regulation of PI3K-Akt signaling pathway and Rap1 signaling pathway. In addition, molecular docking analysis suggested that eight key active compounds of WDG may be mainly responsible for the effect of WDG on GMD by targeting HARS, AKT, and PIK3CA, respectively. Animal experiments

Abbreviations: DL, Drug-likeness; GMD, Gastrointestinal motility disorders; GO, Gene ontology; HCT, Herbal-compounds-targets; KEGG, Kyoto Encyclopedia of Gene and Genome; MI, Motor index; MMC, Migrating motor complex; OB, Oral bioavailability; POI, Postoperative ileus; PPI, Protein-protein interaction; TCM, Traditional Chinese medicine; WDG, Wuda granule.

and clinical trials both suggested that WDG could exert therapeutical effect on GMD via inhibiting inflammation and promoting gastrointestinal motility, it could also improve digestive function of patients with laparoscopic colorectal cancer after surgery.

Conclusion: This study was the first to demonstrate that WDG improved GMD mainly via inhibiting inflammatory level and promoting gastrointestinal motility, providing new insights for the understanding of WDG for GMD, inspiration for future research and reference for clinical strategy in terms of the treatment of GMD.

KEYWORDS

gastrointestinal motility disorders, network analysis, Wuda granule, molecule docking, Chinese herb medicine

1 Introduction

Gastrointestinal motility disorder (GMD), affecting millions of patients worldwide (Madl and Madl, 2018), is an important mechanism of functional gastrointestinal diseases and mainly presents as debilitating symptoms, delayed gastric emptying, and unexpected severe gastric symptoms (Suresh et al., 2021). Especially for the majority of patients undergoing gastrointestinal surgery, GMD may directly lead to bowel failure (Foong et al., 2020). The incidence of GMD is increasing with aging society (Singh et al., 2022), and is associated with the functional degradation or loss of neurons in the enteric nervous system as well as the intrinsic innervation of the bowel, which is a major contributing factor to gastrointestinal motility. In addition, GMD can be secondary to other neurological, autoimmune, or metabolic diseases, paraneoplastic syndromes, endocrine disorders, and infectious diseases. However, there is a lack of approved and efficacious drugs for GMD (Docsa et al., 2022), which highlights the need for the development and deployment of new or alternative drugs with potential effectiveness.

Traditional Chinese medicine (TCM), with thousands of years of practice and experience, is a major source of new drugs. It is mainly comprised of natural products, and has been used in the prevention and treatment of human diseases (Yang et al., 2013). Wuda granule (WDG), a traditional Chinese patent medicine, is consists of the following five herbal medicines: *Arecae Semen* [Arecaceae; Areca catechu L.], *Panax ginseng* [Araliaceae; Ginseng Radix et Rhizoma], *Lindera aggregata* (Sims) *Kosterm* [Lauraceae; Linderae Radix], *Persicae Semen* [Rosaceae; Prunus persica (L.) Batsch] and *Fructus amomi* [Zingiberaceae; Amomum villosum Lour.] (Jiang et al., 2020). The major components of WDG are ginsenoside Rc, ginsenoside Rd, ginsenoside Rg1, quercetin, quercitrin, isoquercitrin, laetrile, norisoboldine, linderane, and *arecoline*, etc. (Wang et al., 2020). Additionally, it mainly comprises four alkaloids, including arecoline, norisoboldine, and boldine (Wang et al., 2020). It has been proved that WDG treatment for GMD can improve gastrointestinal function in practice (Jiang et al., 2017; Zeng et al., 2022), but the underlying mechanism still lacks further verification and remains to be elucidated.

Network analysis is an effective method for comprehensively analyzing complex networks using high-throughput analyses and computerized calculations (Wang et al., 2021). The holistic philosophy of TCM is consistent with the key ideas of emerging network analysis and the requirements for treating complex diseases (Li and Zhang, 2013). This approach can be used to explore interactions between various compounds, diseases, genes, and proteins (Lai et al., 2020). Recently, an increasing number of studies have used network analysis to reveal the mechanisms and effects of TCM in the treatment of diseases. The aim of this study was to explore the possible biological function of WDG and its mechanism of action in GMD via the network analysis and virtual molecular docking analyses, the findings of which were further verified via *in vivo* experiments and clinical trials.

2 Materials and methods

2.1 Network analysis

2.1.1 Identification of WDG compounds and their targets

The chemical components of WDG were identified from the Traditional Chinese Medicine Systems Pharmacology Database (TCMSP, http://lsp.nwu.edu.cn/index.php), and the Encyclopedia of Traditional Chinese Medicine (ETCM, http://www.tcmip.cn/ETCM/index.php/Home/Index/). Candidate compounds with oral bioavailability (OB) ≥ 20% and drug-likeness (DL) ≥ 0.10 of WDG were screened. The chemical structure formulae of the screened compounds was obtained from the PubChem database, and the targets of WDG compounds were retrieved from the Swiss Target Prediction database (http://www.swisstargetprediction.ch/).

2.1.2 Identification of targets related to GMD and screening by venn analysis

The therapeutic targets of GMD were retrieved from GeneCards database (https://www. genecards. org/), which is a comprehensive multifunctional database containing the therapeutic targets of all known human diseases. The query keywords used were “gastrointestinal mobility disorder”, “gastrointestinal motility, or “gastrointestinal peristalsis”. To exclude the interference of targets with low correlation with GMD, only targets with a relevance score greater than or equal to the median value of all the targets were included. Intersection targets between GMD proteins and WDG targets were screened by Venn analysis, and were considered as targets of WDG compounds with potential pharmacological therapeutic effects on GMD.

2.1.3 Analysis of protein-protein interaction network

The protein-protein interaction (PPI) of intersection targets was retrieved from the STRING database (https://string-db.org/), which was used to search and predict protein-protein interactions, and identify core regulatory genes in the PPI network. Core targets with functional interactions were screened according to the degree value in the network after network topology analysis.

2.1.4 Construction of networks

The herbal-compounds-targets (HCT) and PPI networks were constructed, visualized, and analyzed using the open-source Cytoscape software (Version 3.7.1). Network topology analysis was conducted to determine important compounds and core targets of WDG in the HCT and PPI networks, respectively, which calculated the value of the degree between the nodes, thereby suggesting the interaction strength between the compounds, targets, or herbs.

2.1.5 Gene ontology enrichment and kyoto encyclopedia of gene and genome pathway enrichment

To elucidate the potential mechanisms of action of WDG in the treatment of GMD, targets with twice more than the median value of degree in the PPI network were selected for gene ontology (GO) enrichment and Kyoto Encyclopedia of Gene and Genome (KEGG) pathway enrichment analyses using the DAVID database (DAVID 6.8, https://david.ncifcrf.gov/). An adjusted p value less than 0.05 indicated that the GO terms and the pathway were significantly associated with WDG. Finally, the results of GO and KEGG enrichment were visualized via the bubble plot using the "ggplot2" package of R software 4.2.0.

2.1.6 Verification of the key active compounds and key targets of WDG by molecular docking

In order to determine whether the screened active compounds of WDG could bind to the core target, thus providing evidence for our predicted results on the active compounds of WDG and their potential therapeutical targets, we conducted molecular docking analysis to verify the results. The structures of the core targets were obtained from the PDB database (https://www.rcsb.org/) and * SDF format files of the screened active WDG compounds were downloaded from the PubChem database (https://pubchem.ncbi.nlm.nih.gov/). The bioactive compounds of WDG (ligands) were examined for their putative antibacterial activities against key targets to determine efflux protein-ligand interactions through molecular docking analysis using the Schrodinger software suite.

2.2 Verification by *in vivo* experiments

Recent studies have demonstrated a link between the immune inflammatory response and the occurrence and development of gastrointestinal dysfunction. Our network analysis also indicated that WDG might exert a therapeutic effect on GMD through its anti-inflammatory effects. Rat models were chosen to validate the anti-inflammatory effect of WDG on GMD because the immune system is activated in GMD rat models and large number of inflammatory factors are increasingly released during the stress response (Patil et al., 2019; Accarie and Vanuytsel, 2020).

2.2.1 Animals

Forty specific pathogen free grade SD rats (weighing 150–200 g each) were purchased from the Guangdong Medical Laboratory Animal Center (animal quality certificate: 44007200051802). Ethics approval for the study protocol was obtained from the Institutional Animal Care and Ethics Committee of Guangdong Provincial Hospital of Chinese Medicine (certificate number: 2017041).

2.2.2 Experimental design

Forty rats were randomly divided into four groups: control group (normal rat + 0.9% NaCl), Postoperative ileus (POI) group (POI rat + 0.9% NaCl), WDG group (POI rat + Wuda granule 500 mg/kg), and prucalopride group (POI rat + prucalopride 2 mg/kg). Rats in the control and POI groups were administered 100 μ L of 0.9% NaCl solution, whereas those in the WDG and prucalopride groups were administered the same volume of 500 mg/kg WDG and 2 mg/kg prucalopride, respectively, at 6, 12, 18, and 24 h after the surgery.

2.2.3 Surgical procedures

Before POI induction, the rats were denied food for 12 h and kept water-free for 6 h. After anesthesia, the rats were placed in the supine position and immobilized using tape following which their hair was shaved, the abdomen was sterilized with iodine solution, and the abdominal cavity was opened with surgical scissors. Thereafter, the small intestine to the cecum region was placed on sterilized gauze, and the entire small intestine was massaged three times using a sterile cotton swab (Kalff et al., 1998). Finally, the abdomen was sutured, and the duration of the entire operation did not exceed 10 min. Rats were gavaged with the corresponding drugs at the same time points (6, 12, 18, or 24 h) postoperatively. Specimens were collected 24 h after surgery, including the mesenteric tissue and blood from the abdominal aorta.

2.2.4 Detection of serum VIP and cytokines

Blood collected from each group was placed in a centrifuge tube which was incubated at 4°C for 3 h and then centrifuged at 3000 rpm for 15 min. The upper serum was collected and used for Enzyme Linked Immunosorbent Assay (ELISA) of VIP and IL-10 according to the manufacturer's instructions. Optical density was measured at 450 nm using a SpectraMax M5 autoreader.

2.2.5 Preparation of gastrointestinal smooth muscle specimen

Half an hour before the preparation of the rat gastrointestinal smooth muscle specimen, cold water was added to the external circulation bath of the HV-4 isothermal tissue-organ perfusion system to maintain the temperature at 37°C. Thereafter, 10 mL of Krebs solution was injected into the bath, and a mixture of 95% O_2 and 5% CO_2 was continuously injected into the bath via the gas supply device. After 4 h of reperfusion, the rats were anesthetized by an intraperitoneal injection of 7% chloral hydrate. The abdomen was opened and the gastric antrum, duodenum, and jejunum were rinsed with Krebs solution at room temperature. Thereafter, the tissues were fixed to the bottom of a glass dish using a silicone plate, and the chassis was filled with Krebs solution. Finally, the mucosal layer was removed using tweezers. Based on the direction of the longitudinal muscle fiber, 8 mm × 2 mm longitudinal smooth muscle strips were cut using a blade following which each longitudinal muscle strip was suspended in the

tissue chamber. One end of the strip was fixed to a hook at the bottom of the chamber and the other was connected to an external isometric force transducer. The strips were subjected to an initial tension of 1 g and were balanced for 60 min. The Krebs solution was replaced every 15 min during the balancing process, and the spontaneous contraction frequency and area under the curve were calculated. After the muscle strips contracted smoothly, 100 μL of acetylcholine (5–10 mol/L) was added to the muscle groove. The amplitude index, contraction tension, and contraction frequency of the muscle strips before and after the administration were recorded by Protowin.

2.3 Clinical experiment

Gastrointestinal motility disorder (GMD) is a common gastrointestinal disease that severely affects the patient's life and physical wellbeing (Raubinger et al., 2022). It is the main complication or symptom of irritable bowel syndrome and other functional gastrointestinal disorders, particularly in patients undergoing gastrointestinal surgery (Wang et al., 2019). Thus in order to validate the effect of WDG and understand its potential mechanism, we recruited patients with colon or rectal cancer who had undergone colorectal cancer surgery. According to the results of the network analysis, WDG may exert a therapeutic effect on GMD via its anti-inflammatory effects and by promoting gastrointestinal motility. In practice, GMD is a common complication among patients with colon or rectal cancer who have undergone colorectal cancer surgery.

2.3.1 Ethical statement

Informed consent was obtained from all the participants, and the study protocol was approved by the Ethics Committee of Guangdong Provincial Hospital of Chinese Medicine (approval number: B2016-046-01). This study was registered with the Chinese Clinical Trial Registry (registration number: ChiCTR-IPR-16008599). All participants were informed about the trial content and signed an informed consent form before the trial.

2.3.2 Participants in the experiment

Patients were recruited according to the following criteria:1) diagnosed with distinct histopathological evidence of colon or rectal cancer; 2) underwent colorectal cancer surgery at the Guangdong Provincial Hospital of TCM (The Second Affiliated Hospital of Guangzhou University of TCM); 3) the duration of the surgical procedure was within 2–4 h; 4) the duration under anesthesia was within 2.5–4.5 h; 5) did not experience serious complications, infections, adverse events, or secondary surgery during treatment; and 6) levels of serum albumin >27 g/L and prealbumin > 0.14 g/L.

Forty patients with who had undergone laparoscopic colorectal cancer surgery were included in this study. Of these, 26 patients (14 of the WDG and 12 of the placebo group) completed the entire experiment, while 14 dropped out. Of the 14 who dropped out, eight patients were of the placebo group and six were of the WDG group. Of the eight patients of the placebo group who dropped out, three patients withdrew because the duration of surgery exceeded the time stipulated in the inclusion criteria, three patients withdrew because they could not tolerate the piezometric tube after the surgery, and two patients accidentally pulled out the piezometric tube due to pain and irritation at the port of surgery. Of the six patients of the WDG group who dropped out, three patients withdrew because the duration of surgery for these exceeded the time stipulated in the inclusion criteria, and three patients were unwilling to continue participating in the trial after surgery and voluntarily withdrew. All 26 patients who completed the entire experiment received the same fundamental treatment. The WDG treatment group received fundamental treatment plus WDG, whereas the placebo group received fundamental treatment only.

2.3.3 Gastrointestinal pressure measurement

Gastrointestinal pressure was measured using a gastrointestinal motility instrument (MMS, Netherlands) comprising a 24-channel high-resolution pressure measurement system. A gastrointestinal piezometer tube was sterilized and placed in the abdomen of the patient a day before surgery. Briefly, after topical anesthesia was administered to the nasal cavity, the tube was slowly inserted from one side of the nasal cavity. After successful placement, the tube was fixed. Monitoring of the gastrointestinal motility of the patient was initiated 2–3 h before the surgery. After surgery, gastrointestinal motility was monitored for 2–3 h on an empty stomach for 1–3 days. To measure gastrointestinal pressure, the patient was intubated, and the tube was located at the proximal end of the jejunum using radiography. According to the characteristics of the contraction wave, the pressure wave of the gastric antrum was wide with a high amplitude and that of the duodenum was narrow and sharp. The frequency of sinus contractions was approximately 3 contractions/min, and that of the duodenum and jejunum was 8–12 times/min.

2.3.4 Measurement of postoperative related indicators

Migrating motor complex (MMC) parameters of the gastric antrum, duodenum, and jejunum, including the duration of phases I and II, the contraction amplitude and frequency of phase III, were mainly determined using the measurements of high-resolution gastrointestinal pressure. The MMC parameters were also related to the motor index (MI) of the jejunum, duration, MMCII phase amplitude, and MI. Clinical evaluation indicators of postoperative gastrointestinal motility recovery included the first postoperative gas level, duration of defecation, duration of postoperative liquid and semi-liquid diet recovery, duration of hospitalization, and hospitalization expenses.

2.3.5 Determination of cytokine level and endotoxin in serum and colon tissue

Blood samples were collected from the patients at 8:00 a.m. on the first, second, third, and seventh postoperative days. Each sample was centrifuged at 3000 rpm for 10 min at 4°C, following which 1.5 mL of the supernatant was transferred to a fresh centrifuge tube and stored at −80°C. Levels of IL-4, IL-6, TNF-α and endotoxin in serum and colon tissue were measured by ELISA kits according to the manufacturer's instructions.

2.4 Statistical analyses

All experimental data was presented as the mean ± standard deviation and was analyzed by one-way ANOVA test followed by Bonferroni test for multiple comparisons using GraphPad Prism software. Student's t-tests and Mann–Whitney U tests was used to

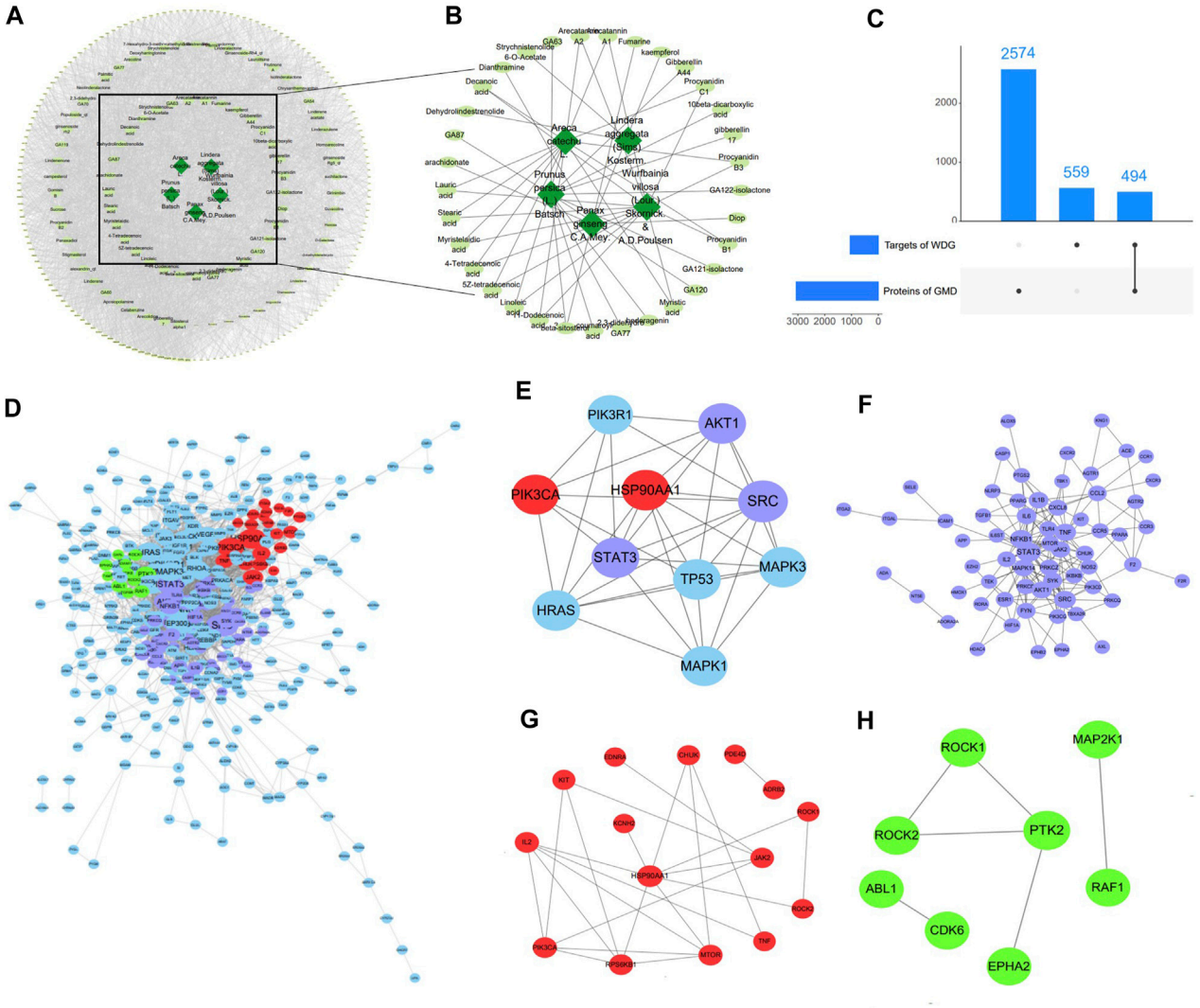


FIGURE 1
WDG may exert therapeutical effect on GMD via multi-compounds and multi-targets. ((**A**) Herbs-Compounds-Targets network of WDG; **(B)** Screened active compounds of WDG; **(C)** Intersection targets between proteins of GMD and targets of WDG compounds; **(D)** PPI networks of intersection targets; Green: targets related to gastrointestinal motility; Red: targets related to regulation of gastrointestinal smooth muscle contraction; Purple: targets related to regulation of inflammation; **(E)** 10 hub targets with node degrees 5.64 fold greater than the average node degree; **(F)** Network of targets related to regulation of inflammation; **(G)** Network of targets related to regulation of gastrointestinal smooth muscle contraction; **(H)** Network of targets related to regulation of gastrointestinal motility).

assess statistical significance between two groups (version 8.0, GraphPad Software Inc., United States). Two-factor ANOVA was used to compare different time points. A value of $p < 0.05$ was considered statistically significant.

3 Results

3.1 WDG may exert therapeutical effect on GMD via multi-compounds

After removing duplication, 117 compounds of WDG were obtained according to OB ≥ 20% and DL ≥ 0.10. A total of 1053 predicted targets of the 117 WDG compounds were then identified. As shown in Figure 1A, the Herbs-Compounds-Targets network consisted of 255 nodes and 4043 edges, the average degree node of the common compounds was 48.23, and eight hub compounds, whose node degrees were 2.11fold greater than the average degree in this network, were identified. The respective nodes for these were 107 for beta-sitosterol (PubChem CID: 222284), 102 for 5Z-tetradecenoic acid (PubChem CID: 5312400), 102 for 4-tetradecenoic acid (PubChem CID: 5282739), 102 for myristelaidic acid (PubChem CID:5312402), 102 for stearic acid (PubChem CID:5281), 102 for 11-dodecenoic acid (PubChem CID:125207), 102 for lauric acid (PubChem CID: 3893), and 102 for linoleic acid (PubChem CID:5280450)), suggesting that these eight hub compounds might represent the main active compounds of WDG, and further suggesting that

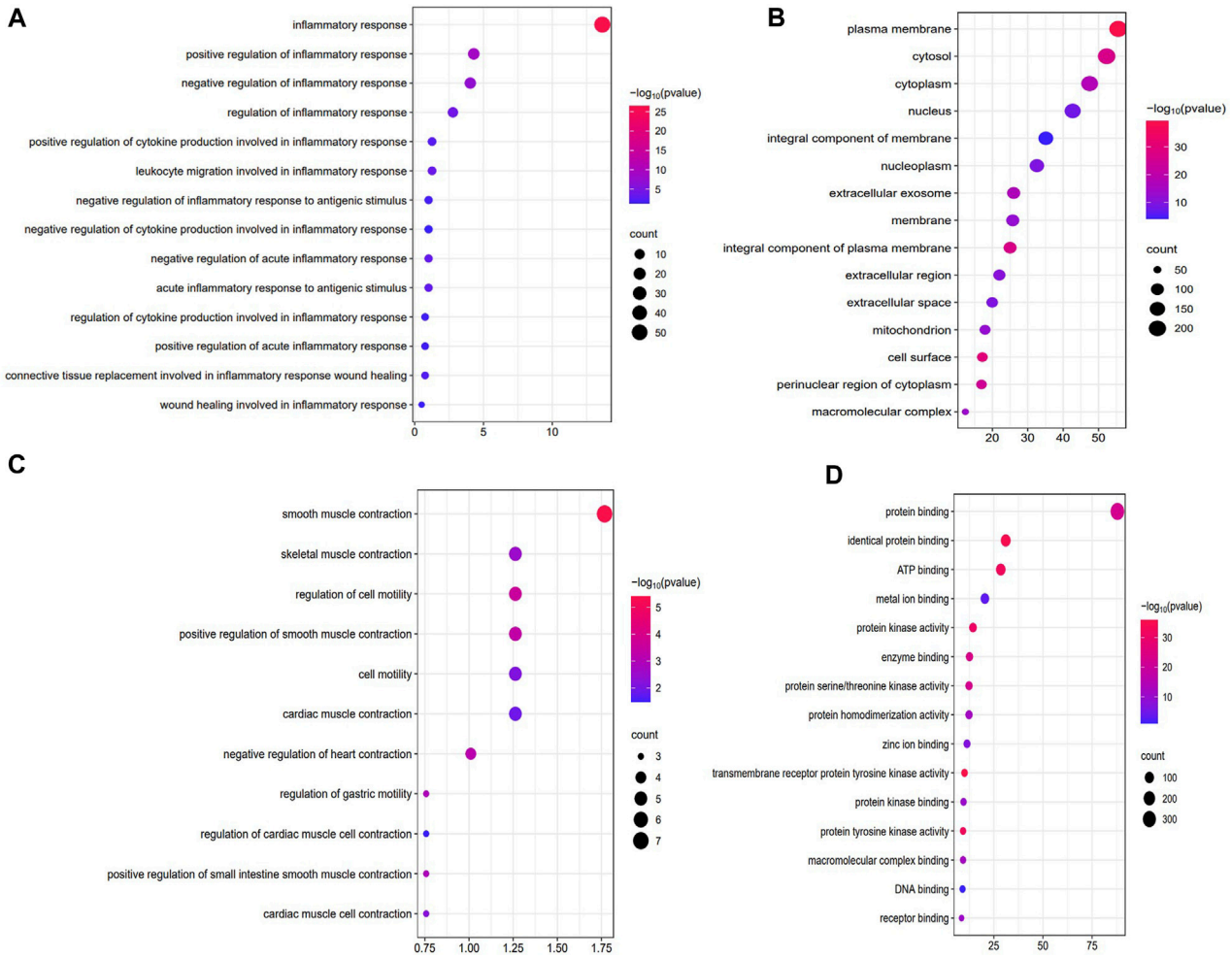


FIGURE 2
WDG may exert therapeutic effect on GMD via the regulation of inflammation and gastrointestinal motility in the GO enrichment of Biological processes (BP), Cellular component (CC), Molecular function (MF). (**(A)** Regulation of inflammation of biological processes (BP); **(B)** Regulation of inflammation of biological processes (BP); **(C)** Results of cellular component (CC); **(D)** Results of molecular function (MF)).

WDG may exert a therapeutic effect on GMD via multi-compounds (Figure 1B).

3.2 WDG may exert therapeutical effect on GMD via multi-targets

A total of 3073 GMD targets were screened in the GeneCards database after removing duplication. Subsequently, 494 intersection targets were selected via Venn analysis between the targets of the WDG compounds and GMD targets (Figure 1C). The intersection targets were regarded as targets of the WDG compounds targeting GMD. The PPI network of intersection targets was retrieved with a minimum required interaction score > 0.9, as shown in Figure 1D, which contained 396 nodes and 2038 edges with an average degree of 10.29. A total of 10 hub targets were identified (Figure 1D) with degrees greater than 58 and 5.64fold greater than the average node degree in this network (82 for SRC, 67 for PIK3R1, 67 for TP53, 66 for HSP90AA1, 64 for STAT3, 61 for PIK3CA, 60 for MAPK1, 60 for MAPK3, 59 for HRAS, and 58 for AKT1) (Figure 1E). Multi-targets related to the regulation of inflammation, gastrointestinal smooth muscle contraction, and gastrointestinal motility were clustered in the PPI network (Figures 1F–H). These results indicated that WDG may serve as an agent with multi-compounds and exerts therapeutic effects on GMD via multi-targets.

3.3 WDG may exert therapeutic effect on GMD via the regulation of inflammation and gastrointestinal motility

Figure 2 showed the results of the GO enrichment analysis of targets in the PPI network. Among the biological processes, the intersection targets were mainly enriched in the inflammatory process, including inflammatory response, regulation of inflammatory response, leukocyte migration involved in

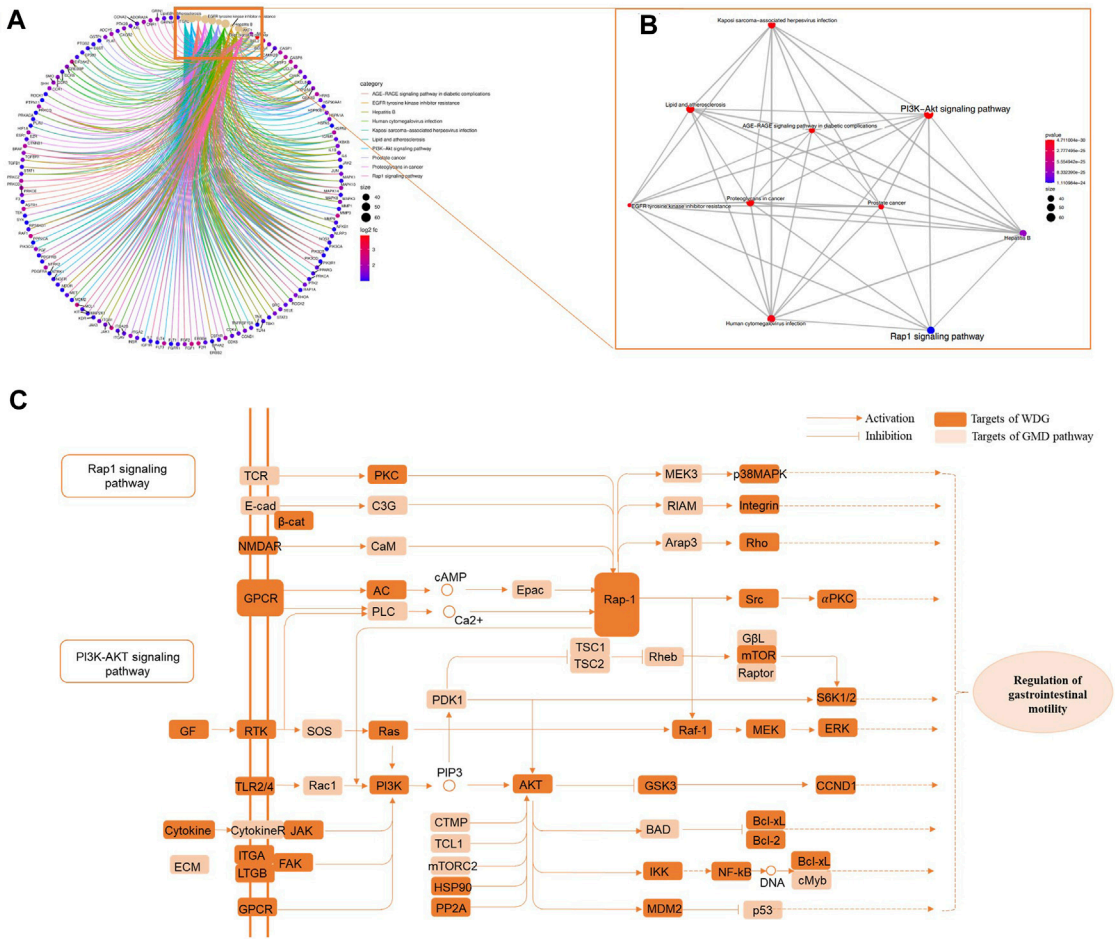


FIGURE 3
WDG may exert potential therapeutical effect on GMD via regulating multi-pathways. ((**A**) Results of KEGG pathway enrichment; (**B**) gene-concept network analysis on KEGG enrichment; and (**C**) "GMD-pathway" network of pathway crosstalk between PI3K-Akt signaling pathway and Rap1 signaling pathway).

inflammatory response, regulation of acute inflammatory response, acute inflammatory response to antigenic stimulus, regulation of cytokine production involved in inflammatory response, regulation of inflammatory response to antigenic stimulus, and regulation of cytokine production involved in inflammatory response (Figure 2A). The targets were also enriched in the regulation of gastrointestinal motility, including smooth muscle contraction, positive regulation of smooth muscle contraction, positive regulation of small intestine smooth muscle contraction, skeletal muscle contraction, regulation of cell motility, and regulation of gastric motility (Figure 2B). In addition, targets enriched in molecular function mainly included protein binding, ATP binding, protein kinase activity, enzyme binding, DNA binding, and receptor binding (Figure 2C). Further, targets enriched in cellular component, mainly included the plasma membrane, cytosol, nucleus, extracellular region, and mitochondria (Figure 2C). These results suggested that WDG may regulate the inflammation process and gastrointestinal motility via protein binding, ATP binding, and protein kinase activity in the plasma membrane, cytosol, nucleus, extracellular region, and mitochondria, etc.

3.4 WDG may exert therapeutic effect on GMD via the regulation of multi-pathways

The results of KEGG pathway enrichment showed that WDG was mainly involved in the regulation of the PI3K-Akt and Rap1 signaling pathways (Figures 3A, B), after excluding specific pathways related to specific diseases, such as lipid and atherosclerosis, the AGE-RAGE signaling pathway in diabetic complications, prostate cancer, and Hepatitis B. Figure 3C showed that intersection of pathway crosstalk between PI3K-Akt signaling pathway and Rap1 signaling pathway were integrated into an "GMD-pathway" network, which indicated that WDG may exert therapeutic effect on GMD via the regulation of multi-pathways.

3.5 WDG decreased inflammation in POI rats

To verify the results of the network analysis, the regulation of inflammation and gastrointestinal motility by WDG was verified *in vivo*. The results showed that compared with the control group, the

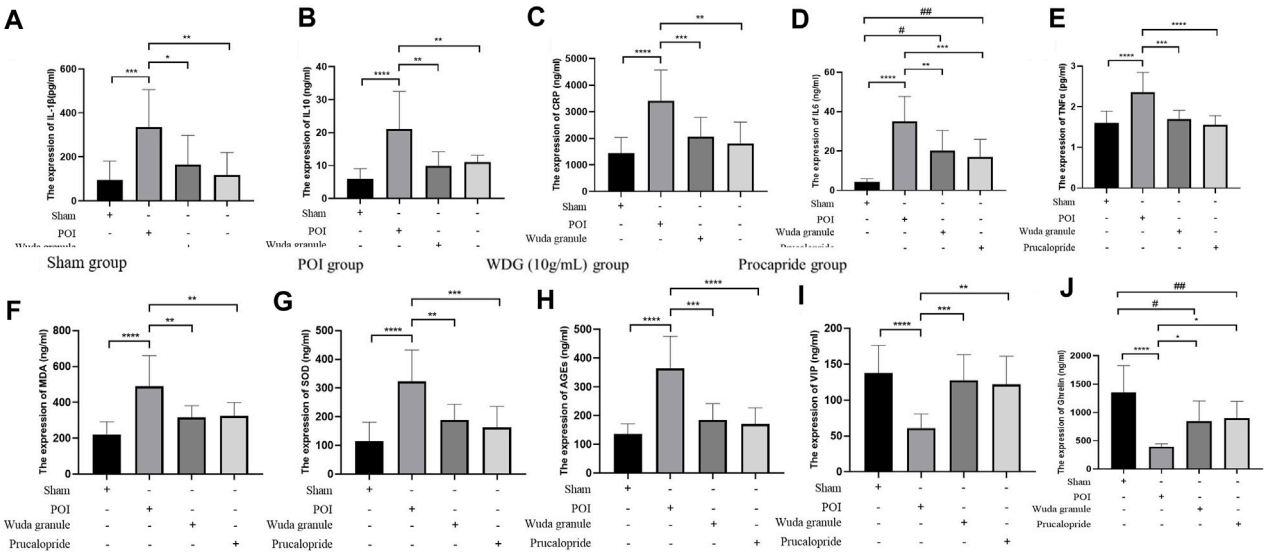


FIGURE 4
WDG decreased inflammation expression and improved gastrointestinal motility in Rats. ((**A**) The expression level of IL-1β; **(B)** The expression level of IL-10; **(C)** The expression level of CRP; **(D)** The expression level of IL-6; **(E)** The expression level of TNF *α*; **(F)** The expression level of MDA; **(G)**: The expression level of SOD; **(H)** The expression level of AGEs; **(I)** The expression level of VIP; **(J)** The expression level of Ghrelin; ***: $p < 0.001$, **: $p < 0.01$, *: $p < 0.05$).

levels of TNF *α* (Figure 4E), IL-1β (Figure 4A), CRP (Figure 4C), IL-6 (Figure 4D), IL-10 (Figure 4B), MDA (Figure 4F), and SOD (Figure 4G) were significantly higher in the POI group, but there were lower in the WDG and Procapride groups, which showed that WDG decreased inflammation in POI rats, and oxidative stress level.

3.6 WDG improved gastrointestinal motility in POI rats

Compared to that in the sham group, the expression of AGEs, VIP and ghrelin was lower in the POI group, but higher in the WDG and the Procapride groups (Figures 4H–J), indicating that symptoms of GMD could be alleviated by WDG, similar to the effect of Procapride, a drug proven for improving gastrointestinal motility in the clinic. These results were further verified by observing the contraction parameters of the gastric antrum, duodenum, and jejunum in the POI rat model. The results showed that the amplitude, tension, and frequency of contraction were reduced in the POI group after intervention, whereas in the WDG and Procapride groups, these were improved (Figures 5A–I), indicating that GMD could be successfully induced in the POI rats, and that WDG improved gastrointestinal motility.

3.7 Clinical characteristics of patients who had undergone laparoscopic colorectal cancer surgery

Among the 26 patients who had undergone laparoscopic colorectal cancer surgery, no significant difference in clinical characteristics was observed between the 12 patients of the placebo group and 14 of the WDG group ($p > 0.05$; Table 1). During the digestive process, MMC was the main form of gastrointestinal motility, it also had no significant difference between the two groups before treatment ($p > 0.05$; Table 1).

3.8 WDG improved gastrointestinal motility in patients

The duration of the MMC phase I was significantly increased; further, 1 day after surgery, the duration of MMC phase II, the number of MMC, and the contractive amplitude and motility of the gastric antrum, duodenum, and jejunum, were decreased compared to the levels before surgery ($p < 0.05$; Figures 6A–I). However, compared with the placebo group, the above results were reversed with a time-dependent tendency for the WDG group, and on the third day after surgery, the gastrointestinal motility was significantly restored ($p < 0.05$), which indicated that WDG exerted a pharmacological effect on GMD by improving gastrointestinal motility.

3.9 WDG improved digestive function and reduced inflammation in patients

The levels of IL4, IL6, and TNFα (Figures 7G–1) was significantly higher after surgery in patients, but were lower in the WDG group, especially on the third and seventh days after surgery. In addition, the levels of ghrelin and motilin were lower in the WDG group 1 day after surgery, which was further lowered with an increasing number of days (Figures 7E–F). Compared to the

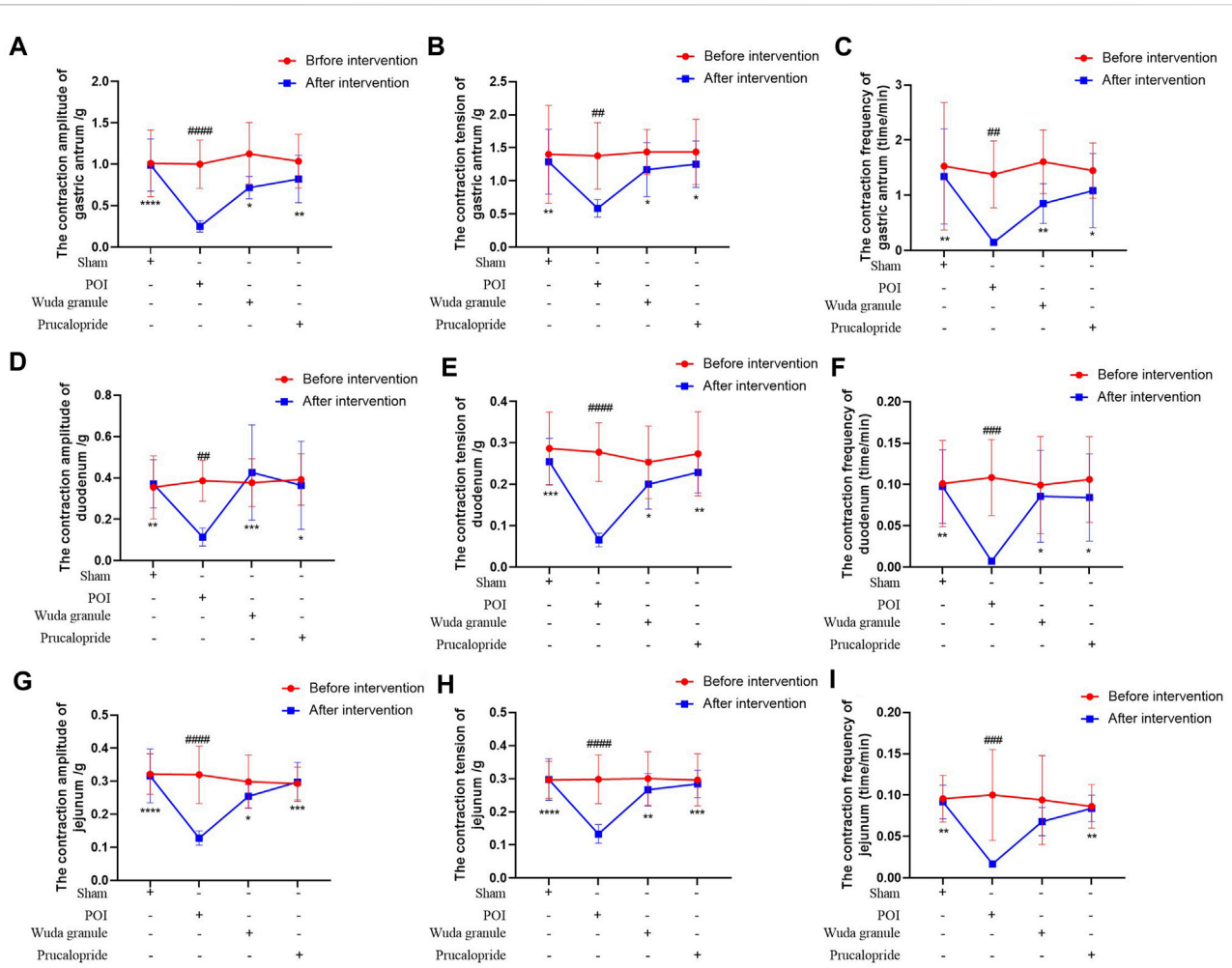


FIGURE 5
WDG improved the contraction amplitude, tension and frequency of gastric antrum, duodenum and jejunum in POI rats. ((**A**) The contraction amplitude of gastric antrum; **(B)** The contraction tension of gastric antrum; **(C)** The contraction frequency of gastric antrum; **(D)** The contraction amplitude of duodenum; **(E)** The contraction tension of duodenum; **(F)** The contraction frequency of duodenum; **(G)** The contraction amplitude of jejunum; **(H)** The contraction tension of jejunum; **(I)** The contraction frequency of jejunum; ***: Compared with 1 day after surgery; ###: Compared with before surgery; ΔΔΔ: Comparison between WDG group and placebo group).

placebo administration, WDG treatment decreased the duration of postoperative intestinal exhaust and defecation, as well as the duration of postoperative liquid and semi-liquid diet recovery (Figures 7A–D). These results suggested that WDG exerts therapeutic effects on GMD by improving digestive function and reducing inflammation.

3.10 Screened key compounds of WDG could target core hub-targets of GMD

The prerequisite for efficacy of a drug is its ability to bind with specific proteins or receptors. Therefore, we verified whether the screened key compounds of WDG could bind with the hub targets of GMD. Network analysis identified beta-sitosterol, linoleic acid, 4-tetradecenoic acid, 5Z-tetradecenoic acid, myristelaidic acid, stearic acid, lauric acid and 11-dodecenoic acid as the key active components of WDG. Further, HSP90AA1, AKT, HRAS, MAPK1, MAPK3, PIK3CA, PIK3R1, SRC, STAT3, and TP53 were screened as the key targets. The results of molecular docking showed that linoleic acid, 4-tetradecenoic acid, 5Z-tetradecenoic acid, myristelaidic acid, lauric acid, and 11-dodecenoic acid had higher docking scores with HRAS; further, stearic acid and beta-sitosterol could dock with AKT and PIK3CAwith high docking scores respectively, indicating that these eight compounds of WDG may exert anti-GMD effects by targeting HRAS, AKT, and PIK3CA (Figures 8A–R). These results provided new insights for further research to explore the pharmacological compounds of WDG.

4 Discussion

Gastrointestinal motility disorder (GMD) is a common gastrointestinal disease that severely affects the patient's life and physical wellbeing (Raubinger et al., 2022). It can cause incoordination of the gastrointestinal delay, delay gastric emptying, affect enteral feed intolerance, and even functionally obstruct the small or large intestines. GMD is a common public health issue worldwide

TABLE 1 The characteristics of included patients before intervention (n/%, M/P_{25}-P_{75} or $\bar{x}\pm$ s).

Indicators	Placebo group (n = 12)	WDG group (n = 14)	X^2/t/Z	*p*
Sex (male)	7/58.3%	5/35.7%	1.330	0.249
Age(y)	61.4 ± 8.1	56.9 ± 7.3	−1.501	0.146
Total flow time (d)	1(0.5–1.5)	1 (1–2)	0.930	0.352
Fasting time (h)	12 (12–12)	12 (12–24)	1.280	0.201
Anesthesia time (h)	4 (3.5–4)	4 (3–4)	−0.728	0.467
Operation time (h)	3.00 ± 0.74	2.79 ± 0.80	−0.704	0.488
Intraoperative flushing volume (mL)	1650 (1000–2100)	2000 (1600–2000)	1.196	0.232
Indwelling drainage tube time (d)	6 (5.5–7)	5.5(4–7)	−1.370	0.171
Indwelling catheter time (d)	3.17 ± 1.70	2.71 ± 1.38	−0.749	0.461
Number of MMC (per 2h)	1.33 ± 0.65	1.07 ± 0.62	−1.053	0.303
Time of phase I (min)	36.00 ± 46.01	23.71 ± 40.67	−0.723	0.477
Time of phase II (min)	46.83 ± 9.90	51.86 ± 11.51	1.182	0.249
Amplitude of phase II (mmHg)				
Antrum gastricum	45.98 ± 12.86	51.05 ± 11.87	1.044	0.307
Duodenum	25.58 ± 5.44	26.90 ± 5.76	0.596	0.557
Jejunum	24.31 ± 5.92	24.62 ± 4.39	0.155	0.878
Motility index of phase II (mmHg/min)				
Antrum gastricum	4828.92 ± 1286.39	3960.21 ± 1173.82	1.800	0.084
Duodenum	7204.67 ± 2721.35	7116.40 ± 2052.87	0.094	0.926
Jejunum	7411(6165.5–8902)	6177.5 (5644–7693)	−0.874	0.382

Note: Continuous variable data with normal distribution was presented as the mean ± standard deviation and was analyzed by Student's t-tests, Continuous variable data with non-normal distribution was presented as M/P_{25}-P_{75} and was analyzed by Mann–Whitney U tests. Categorical variable was presented as frequency/percentage (n/%) and was analyzed by Chi-squared test or fisher exact test. A value of $p < 0.05$ was considered statistically significant.

and is the main complication or symptom of irritable bowel syndrome and other functional gastrointestinal disorders, particularly in patients undergoing gastrointestinal surgery (Wang et al., 2019). Presently, Western medical treatment cannot effectively target the pathogenesis of the disease because of its limited effect (Zhang and Bai, 2022). In this study, we aimed to explore the pharmacological mechanism of WDG in GMD via network analysis and experimental validation.

4.1 WDG alleviated GMD via an anti-inflammatory effect

Gastrointestinal symptoms, are significant non-motor symptoms of GMD, and are represented by inflammation (Zou et al., 2022), which is considered as an aggravating factor and manifestation of GMD (Villanacci et al., 2008). Gastrointestinal disorders promote inflammatory cell infiltration of the mucosa and/or myenteric plexus (Bassotti et al., 2009), which leads to abnormalities in the enteric nervous system, and alterations in normal motor function and visceral reflexes of the gut (Bassotti et al., 2014). Inflammation and GMD have been proposed as factors confounding with each other (Peuhkuri et al., 2010). Various studies have shown that the release of inflammatory cytokines accelerates the development of gastrointestinal disorders (Docsa et al., 2022), which can activate resident macrophages and T helper cells and recruit neutrophils into the smooth muscle to propagate the spread of motility dysfunction along the gastrointestinal tract (Wehner et al., 2007). Thus, specific or combined inflammatory mediators such as C-X-C motif chemokine ligand 1 (also known as GroA and upregulated in developed ileus), are believed to be viable biomarkers for the early detection of gastrointestinal disorders (Docsa et al., 2020). In this study, we predicted that inflammation may be the main biological process in GMD that is targeted by WDG. Experiments using the POI rat model showed that WDG did decrease the expression of inflammatory markers IL-10, IL-6, IL-1β, CRP, and TNF-α. Further, the clinical experiment revealed that treatment with WDG could also decrease the levels of IL-6, IL4, and TNF-α. These results proved that WDG exerts an anti-inflammatory effect in GMD, thus elucidating one of the mechanisms for the pharmacological effect of WDG on GMD.

4.2 WDG alleviated GMD by improving gastrointestinal motility

Gastrointestinal motility disorder is considered an idiopathic symptom of other diseases and is characterized by abnormal gastrointestinal contractions, dysphagia, gastroesophageal reflux

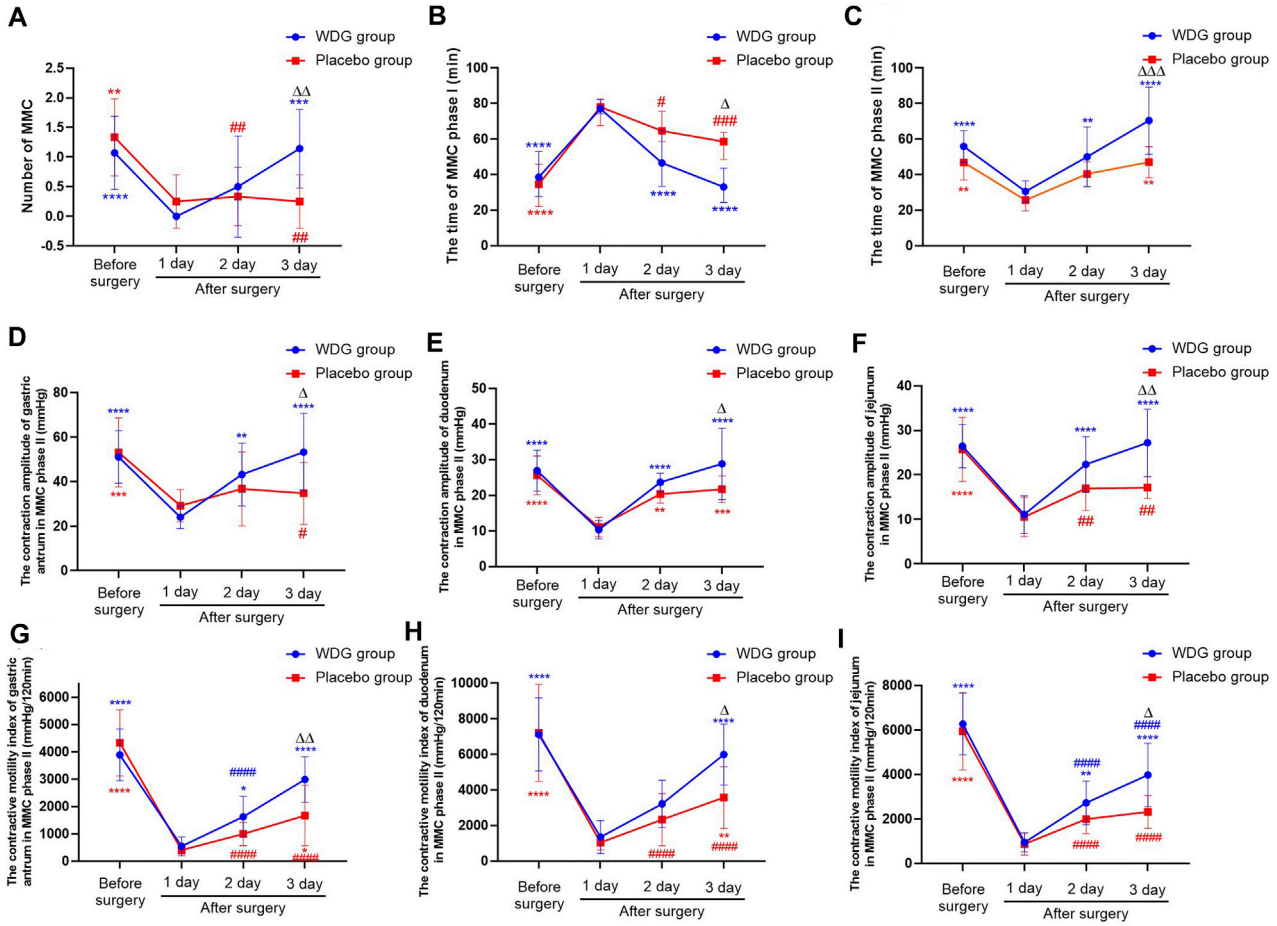


FIGURE 6
WDG improved gastrointestinal motility in patients. ((**A**) The numbers of MMC in the two groups; **(B)** The time of MMC phase I; **(C)** The time of MMC phase II; **(D)** The contraction amplitude of gastric antrum in MMC phase II (mmHg); **(E)** The contraction amplitude of duodenum in MMC phase II (mmHg); **(F)** The contraction amplitude of jejunum in MMC phase II (mmHg); **(G)** The contractive motility index of gastric antrum in MMC phase II (mmHg/120min); **(H)** The contractive motility index of duodenum in MMC phase II (mmHg/120min); **(I)** The contractive motility index of jejunum in MMC phase II (mmHg/120min); ***: Compared with 1 day after surgery; ###: Compared with before surgery; ΔΔΔ: Comparison between WDG group and placebo group).

disease, flatulence, severe constipation, vomiting, and abdominal distension (Fukuda et al., 2022). In GMD, gastrointestinal motility is impaired mainly because of problems within the muscles that control peristalsis or with the nerves or hormones that govern muscle contractions. It has been reported that prokinetic motility drugs can alleviate the symptoms of patients with GMD by promoting gastric emptying and accommodation rates (Shrestha et al., 2021). Commonly, gastrointestinal motility drugs have certain curative effects; however, all of these cause different degrees of side effects and do not effectively reduce the recurrence rate following drug withdrawal (Wang et al., 2022). Traditional Chinese medicines are believed to play an important role in regulating gastrointestinal motility and alleviating GMD symptoms (Zhang et al., 2022). These medicines can increase the function of muscles, nerves, and hormones by regulating excitatory neurotransmission (Chen et al., 2022), gut microbiota (Yang et al., 2022), intestinal glial cell apoptosis (Wang et al., 2022), and nitrergic neurons (Li et al., 2022). Thus, these medicines can potentially improve GMD by enhancing the motility of muscle contraction. In this study, treatment with WDG increased the levels of motilin, AGEs, VIP, and ghrelin, which are the indicators for the assessment of gastrointestinal motility. In addition, WDG treatment improved the contraction of the gastric antrum, duodenum, and jejunum in the POI rat model, decreased the duration of the MMCI phase, and increased the duration of MMC phase II, the number of MMC, and the contractive amplitude and motility index of the gastric antrum, duodenum, and jejunum. Interestingly, WDG treatment also reduced the duration of postoperative intestinal exhaust and defecation, as well as the duration of postoperative liquid and semi-liquid diet recovery.

4.3 WDG alleviates GMD via multi-compounds, multi-targets, and multi-pathways

Chinese herbal medicines, which consist of natural medicinal herbs, possess various complex chemical compositions owing to

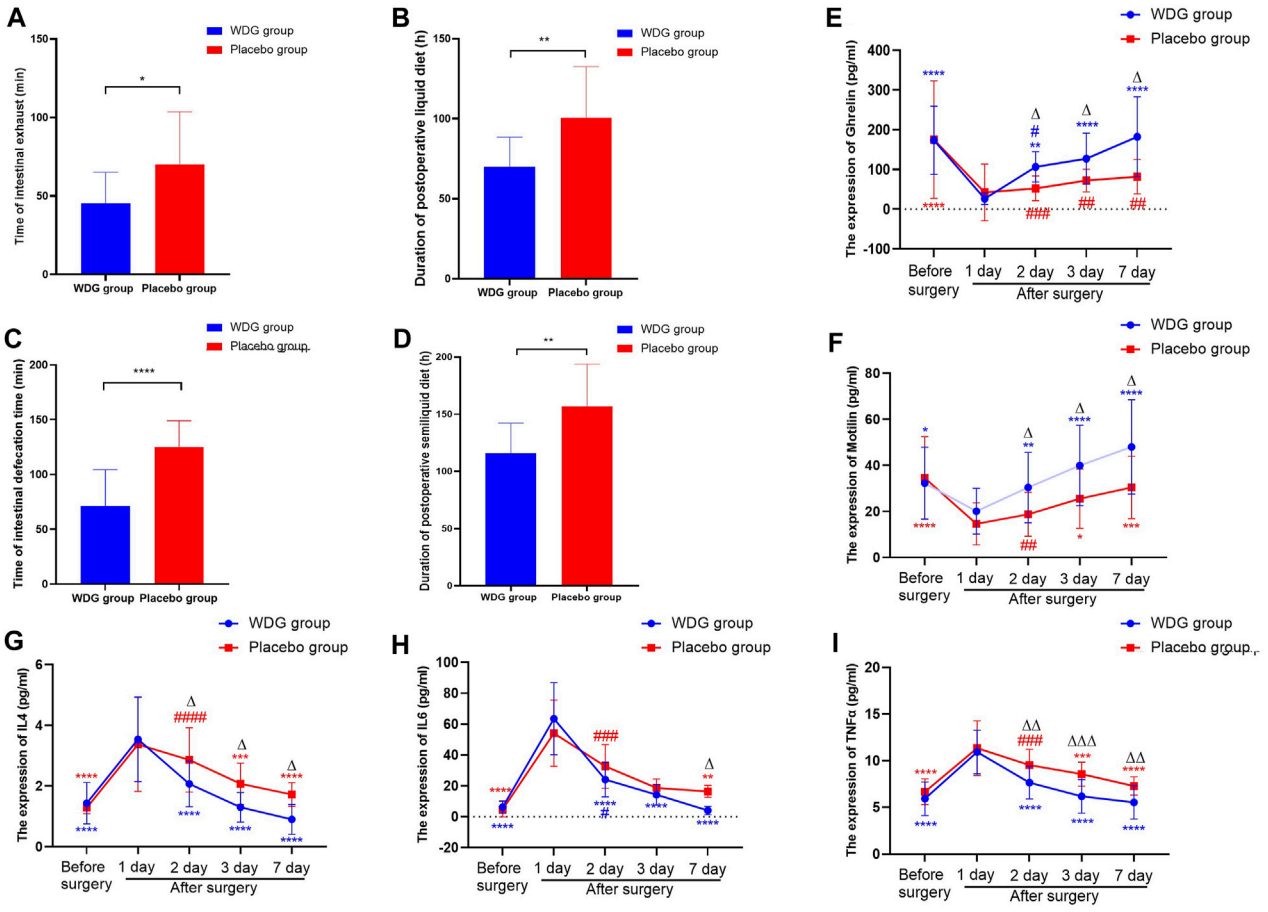


FIGURE 7
WDG improved gastrointestinal function and reduced inflammation in patients. **(A)** The time of intestinal exhaust (min) in the two groups; **(B)** The time of intestinal defecation time (min) in the two groups; **(C)** The duration of postoperative liquid diet (h) after surgery in the two groups; **(D)** The duration of postoperative semiliquid diet (h) after surgery in the two groups; **(E)** The expression level of Ghrelin (pg/mL); **(F)** The expression level of Motilin (pg/mL); **(G)** The expression level of IL4 (pg/mL); **(H)** The expression of IL-6 (pg/mL); **(I)** The expression level of TNF-α (pg/mL); ***: Compared with 1 day after surgery; ###: Compared with before surgery; ΔΔΔ: Comparison between WDG group and placebo group).

the herbal combinations, making it difficult to elucidate the mechanism of their therapeutic effects. A single herb or Chinese medicinal formula contains many phytochemical compounds, including alkaloids, terpenoids, and flavonoids. These medicines achieve the desired pharmacological effects mainly through a combination of various compounds. Many effective drugs in the clinic have been derived from Chinese herbal medicines, such as artemisinin (named qinghaosu in China, derived from Artemisia annua L. [Asteraceae]), which not only increase the pharmacological effect, but also reduce the cost for patients and make the pharmacokinetics clearer. Thus, identifying the main chemical constituents responsible for the therapeutic function of Chinese herbal medicine is vital. In this study, we predicted eight key active compounds in WDG that may be responsible for its therapeutic effects. Previous studies have reported that beta-sitosterol (Kasirzadeh et al., 2021), stearic acid (Sobocinska et al., 2022), linoleic acid (Zhang et al., 2021), and lauric acid (Li et al., 2022) exert pharmacological effects on the regulation of intestinal inflammation and the intestinal gut function, both of which are consistent with the mechanism of GMD. However, there remains a lack of reports on the effect of 4-tetradecenoic acid, 5Z-tetradecenoic acid, myristelaidic acid, and 11-dodecenoic acid on gastrointestinal disorders, prompting us to focus on these drugs with potential functions in GMD in future studies. In addition, results of the molecular docking analysis suggested that these eight key compounds target different proteins, thus suggesting that these compounds may be responsible for the therapeutic effects of WDG on GMD mainly by targeting multitargets.

4.4 Implications on prospective research and limitations of present study

This study aimed to explore the potential pharmacological effects of WDG on GMD, and their underlying mechanisms, providing insight for the research on the mechanism of WDG on GMD. It firstly explored the mechanism of action of WDG in treating postoperative GMD through network analysis, animal experiments, and small sample clinical controlled studies. The

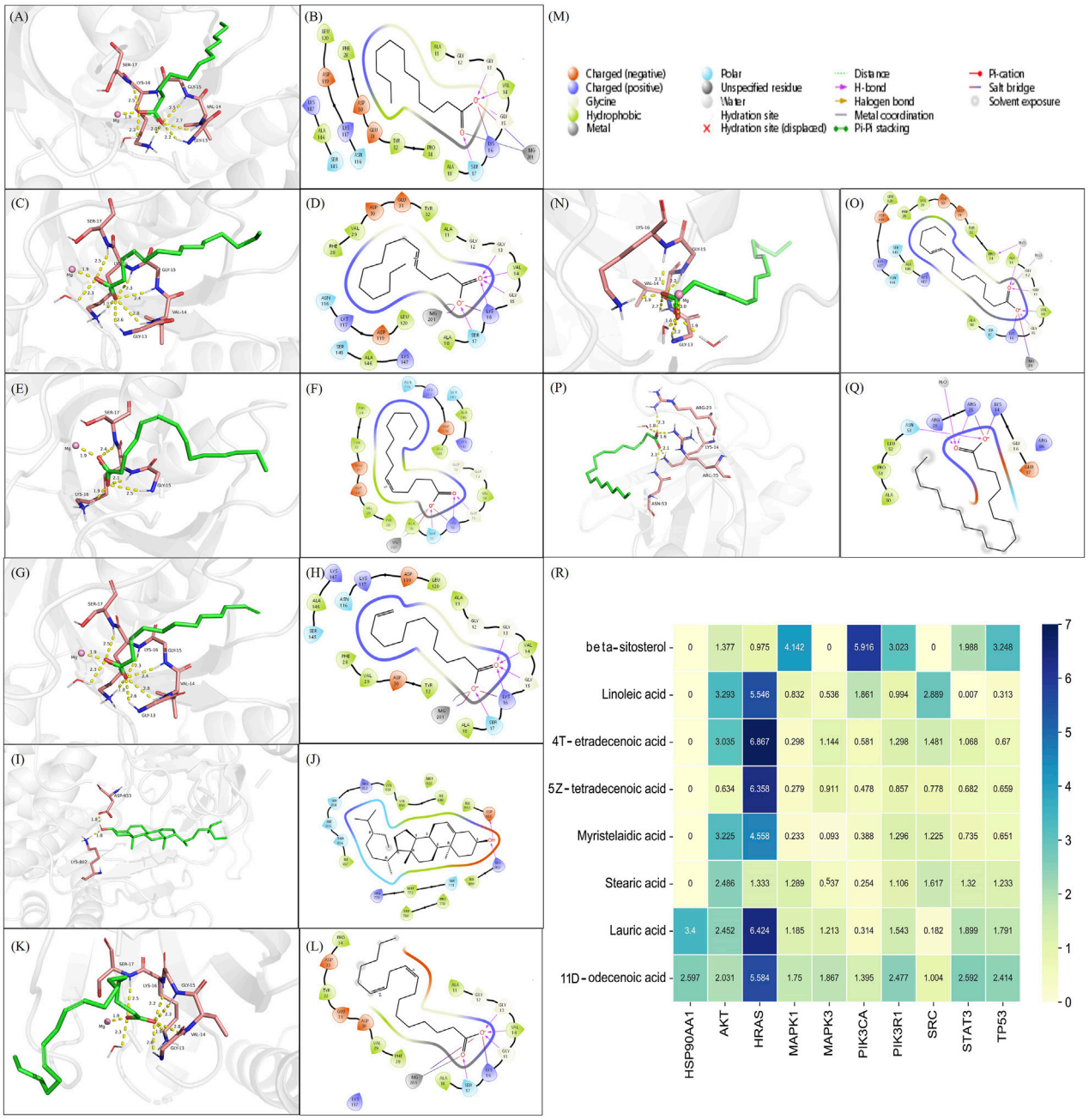


FIGURE 8
The active compounds of WDG had preferable docking ability with Hub-Target of GMD. **(A)** 3D docking structure of Lauric acid docked with HRAS; **(B)** 2D docking structure of Lauric acid docked with HRAS; **(C)** 3D docking structure of 4-Tetradecenoic acid docked with HRAS; **(D)** 2D docking structure of 4-Tetradecenoic acid docked with HRAS; **(E)** 3D docking structure of 5Z-tetradecenoic acid docked with HRAS; **(F)** 2D docking structure of 5Z-tetradecenoic acid docked with HRAS; **(G)** 3D docking structure of 11-Dodecenoic acid docked with HRAS; **(H)** 2D docking structure of 11-Dodecenoic acid docked with HRAS; **(I)** 3D docking structure of beta-sitosterol docked with PIK3CA; **(J)** 2D docking structure of beta-sitosterol docked with PIK3CA; **(K)** 3D docking structure of Linoleic acid docked with HRAS; **(L)** 2D docking structure of Linoleic acid docked with HRAS; **(M)** Type of interaction between identified compounds and their docking targets; **(N)** 3D docking structure of Myristelaidic acid docked with HRAS; **(O)** 2D docking structure of Myristelaidic acid docked with HRAS; **(P)** 3D docking structure of Stearic acid docked with AKT; **(Q)** 2D docking structure of Stearic acid docked with AKT; **(R)** Heat map of docking score of key WDG components docked with Hub-Target of GMD).

results showed that WDG could promote the recovery of postoperative gastrointestinal motility via inhibiting the inflammatory process and promoting postoperative gastrointestinal motility recovery, providing the biochemical basis of WDG's clinical efficacy. Although the results were encouraging, there still exist some limitations in this study. As a preliminary exploration, the relationship and crosstalk between the inflammatory mechanism of Wuda granules and the promoting gastrointestinal motility effect still lack further verification, which should be verified in the future research. Network analysis was

mainly depended on compute calculation, it may lead to a very speculative hypothesis, which may result in false positives, further verification on the compounds of herbs should be conducted to confirm the results. Thus, in future, the research should be designed according to the following directions: 1) the pathway involving in inhibiting inflammation and promoting gastrointestinal motility by WDG should be designed to further verify the potential pathway of WDG based on the results of network analysis. 2) In clinic, high-quality RCT with large sample and multiple center should be designed to assess the anti-inflammation effect and effect of promoting gastrointestinal motility based on the small sample results of this study. 3) with multitopic analysis and sequencing techniques, the mechanism involving in the therapeutical effect of WDG should be confirmed with human sample. 4) as various effective compounds has been derived from Chinese herds medicine in recent years, the eight key compounds screened in this study should be further explored for their role in the alleviation of GMD with the purpose of developing plant-derived compounds that may have better therapeutic effects.

5 Conclusion

This study firstly demonstrated that treatment with WDG alleviates GMD mainly by reducing inflammation and promoting gastrointestinal motility, multi-compounds and multi-targets are involved in this process, providing new insights to understand the effect of WDG treatment on GMD, which can inspire future research, and serve as a reference to devise clinical strategies in the treatment of GMD.

Data availability statement

The datasets presented in this study can be found in online repositories. The names of the repository/repositories and accession number(s) can be found in the article/Supplementary Material.

Ethics statement

The studies involving human participants were reviewed and approved by the Ethics Committee of Guangdong Provincial Hospital of Chinese Medicine (approval number: B2016-046-01).The patients/participants provided their written informed consent to participate in this study. The animal study was reviewed and approved by Ethics approval for the study protocol was obtained from the Institutional Animal Care and Ethics Committee of Guangdong Provincial Hospital of Chinese Medicine (certificate number: 2017041).

Author contributions

ZJ designed and performed the experiments, analysed the data, QZ and JZ prepared the figures and revised the manuscript; LC, HT, and QC analysed the data, JC, YQ, and LY prepare and revised the figures and revised the manuscript; ZC and LC revised the figures and manuscript; ZJ revised the figures and data analysis, designed the experiments and wrote the manuscript. All authors contributed to the article and approved the submitted version.

Funding

This work was financially supported by the National Natural Science Foundation of China (No.82204716), Department of Science and Technology of Guangdong Province (No. 2021A1515110773, 2022A1515220198), Guangzhou Basic and Applied Basic Research Foundation (No. 2023A03J0759) and Guangzhou Municipal Science and Technology Bureau (No.202201011785), and the Traditional Chinese Medicine Bureau of Guangdong Province (No.20225012, 20231363), and also the Special Project for Clinical Research of Guangdong Provincial Hospital of Chinese Medicine (YN10101902), the Guangdong Administration for Market Regulation (Guangdong Intellectual Property Administration) [No. (2022)158].

Conflict of interest

The reviewer BS declared a shared parent affiliation with the author HT to the handling editor at the time of review.

The authors declare that the research was conducted in the absence of any commercial or financial relationships that could be construed as a potential conflict of interest.

Publisher's note

All claims expressed in this article are solely those of the authors and do not necessarily represent those of their affiliated organizations, or those of the publisher, the editors and the reviewers. Any product that may be evaluated in this article, or claim that may be made by its manufacturer, is not guaranteed or endorsed by the publisher.

Supplementary material

The Supplementary Material for this article can be found online at: https://www.frontiersin.org/articles/10.3389/fphar.2023.1237686/full#supplementary-material

References

Accarie, A., and Vanuytsel, T. (2020). Animal models for functional gastrointestinal disorders. *Front. PSYCHIATRY* 11, 509681. doi:10.3389/fpsyt.2020.509681

Bassotti, G., Antonelli, E., Villanacci, V., Salemme, M., Coppola, M., and Annese, V. (2014). Gastrointestinal motility disorders in inflammatory bowel diseases. *World J. Gastroenterol.* 20, 37–44. doi:10.3748/wjg.v20.i1.37

Bassotti, G., Villanacci, V., Nascimbeni, R., Cadei, M., Fisogni, S., Antonelli, E., et al. (2009). Enteric neuroglial apoptosis in inflammatory bowel diseases. *J. CROHNS COLITIS* 3, 264–270. doi:10.1016/j.crohns.2009.06.004

Chen, W., Liao, L., Huang, Z., Lu, Y., Lin, Y., Pei, Y., et al. (2022). Patchouli alcohol improved diarrhea-predominant irritable bowel syndrome by regulating excitatory

neurotransmission in the myenteric plexus of rats. *Front. Pharmacol.* 13, 943119. doi:10.3389/fphar.2022.943119

Docsa, T., Bhattarai, D., Sipos, A., Wade, C. E., Cox, C. J., and Uray, K. (2020). CXCL1 is upregulated during the development of ileus resulting in decreased intestinal contractile activity. *Neurogastroenterol. Motil.* 32, e13757. doi:10.1111/nmo.13757

Docsa, T., Sipos, A., Cox, C. S., and Uray, K. (2022). The role of inflammatory mediators in the development of gastrointestinal motility disorders. *Int. J. Mol. Sci.* 23, 6917. doi:10.3390/ijms23136917

Foong, D., Zhou, J., Zarrouk, A., Ho, V., and O'Connor, M. D. (2020). Understanding the biology of human interstitial cells of cajal in gastrointestinal motility. *Int. J. Mol. Sci.* 21, 4540. doi:10.3390/ijms21124540

Fukuda, H., Sato, H., Fujiyoshi, Y., Abe, H., Okada, H., Shiota, J., et al. (2022). Risks of refractory chest pain after peroral endoscopic myotomy in achalasia-related esophageal motility disorders: Short-term results from a multicenter study in Japan. *Gastrointest. Endosc.* 96, 620–629.e4. doi:10.1016/j.gie.2022.04.1347

Jiang, Z., Cao, L. X., Liu, B., Chen, Q. C., Shang, W. F., Zhou, L., et al. (2017). Effects of Chinese herbal medicine Xiangbin prescription on gastrointestinal motility. *World J. Gastroenterol.* 23, 2987–2994. doi:10.3748/wjg.v23.i16.2987

Jiang, Z., Chen, Q., Zhang, J., Cao, L., and Chen, Z. (2020). Wuda granule, a traditional Chinese herbal medicine, ameliorates postoperative ileus by anti-inflammatory action. *Pathol. Res. Pract.* 216, 152605. doi:10.1016/j.prp.2019.152605

Kalff, J. C., Schraut, W. H., Simmons, R. L., and Bauer, A. J. (1998). Surgical manipulation of the gut elicits an intestinal muscularis inflammatory response resulting in postsurgical ileus. *Ann. Surg.* 228, 652–663. doi:10.1097/00000658-199811000-00004

Kasirzadeh, S., Ghahremani, M. H., Setayesh, N., Jeivad, F., Shadboorestan, A., Taheri, A., et al. (2021). *β*-Sitosterol alters the inflammatory response in CLP rat model of sepsis by modulation of NFκB signaling. *Biomed. Res. Int.* 2021, 5535562. doi:10.1155/2021/5535562

Lai, X., Wang, X., Hu, Y., Su, S., Li, W., and Li, S. (2020). Editorial: Network pharmacology and traditional medicine. *Front. Pharmacol.* 11, 1194. doi:10.3389/fphar.2020.01194

Li, S., and Zhang, B. (2013). Traditional Chinese medicine network pharmacology: Theory, methodology and application. *Chin. J. Nat. Med.* 11, 110–120. doi:10.1016/S1875-5364(13)60037-0

Li, X., Yi, Y., Wu, J., Yang, Q., Tan, B., Chi, S., et al. (2022a). Identification of a chromosome 1 substitution line B6-Chr1BLD as a novel hyperlipidemia model *via* phenotyping screening. *Metabolites* 12, 1276. doi:10.3390/metabo12121276

Li, Y. R., Li, Y., Jin, Y., Xu, M., Fan, H. W., Zhang, Q., et al. (2022b). Involvement of nitrergic neurons in colonic motility in a rat model of ulcerative colitis. *World J. Gastroenterol.* 28, 3854–3868. doi:10.3748/wjg.v28.i29.3854

Madl, C., and Madl, U. (2018). Gastrointestinal motility in critically ill patients. *Med. Klin. Intensivmed. Notfmed* 113, 433–442. doi:10.1007/s00063-018-0446-6

Patil, K. R., Mahajan, U. B., Unger, B. S., Goyal, S. N., Belemkar, S., Surana, S. J., et al. (2019). Animal models of inflammation for screening of anti-inflammatory drugs: Implications for the discovery and development of phytopharmaceuticals. *Int. J. Mol. Sci.* 20, 4367. doi:10.3390/ijms20184367

Peuhkuri, K., Vapaatalo, H., and Korpela, R. (2010). Even low-grade inflammation impacts on small intestinal function. *World J. Gastroenterol.* 16, 1057–1062. doi:10.3748/wjg.v16.i9.1057

Raubinger, S., Allworth, S., and Carey, S. (2022). When you are living and dying at the same time" - a qualitative exploration of living with gastrointestinal motility disorders. *J. Hum. Nutr. Diet.* 36, 622–631. doi:10.1111/jhn.13114

Shrestha, D. B., Budhathoki, P., Subedi, P., Khadka, M., Karki, P., Sedhai, Y. R., et al. (2021). Acotiamide and functional dyspepsia: A systematic review and meta-analysis. *Cureus* 13, e20532. doi:10.7759/cureus.20532

Singh, R., Zogg, H., Ghoshal, U. C., and Ro, S. (2022). Current treatment options and therapeutic insights for gastrointestinal dysmotility and functional gastrointestinal disorders. *Front. Pharmacol.* 13, 808195. doi:10.3389/fphar.2022.808195

Sobocinska, M., Fichna, J., Gieldon, A., Skowron, P., and Kamysz, E. (2022). N-terminally lipidated sialorphin analogs-synthesis, molecular modeling, *in vitro* effect on enkephalins degradation by NEP and treatment of intestinal inflammation in mice. *Int. J. Mol. Sci.* 23, 14450. doi:10.3390/ijms232214450

Suresh, H., Zhou, J., and Ho, V. (2021). The short-term effects and tolerability of low-viscosity soluble fibre on gastroparesis patients: A pilot clinical intervention study. *NUTRIENTS* 13, 4298. doi:10.3390/nu13124298

Villanacci, V., Bassotti, G., Nascimbeni, R., Antonelli, E., Cadei, M., Fisogni, S., et al. (2008). Enteric nervous system abnormalities in inflammatory bowel diseases. *Neurogastroenterol. Motil.* 20, 1009–1016. doi:10.1111/j.1365-2982.2008.01146.x

Wang, S., Yan, M., Guo, Y., Sun, R., Jin, H., and Gong, Y. (2020a). *In vivo* and *in vitro* effects of Salsola collina on gastrointestinal motility in rats. *Iran. J. BASIC Med. Sci.* 23, 383–389. doi:10.22038/IJBMS.2019.40613.9605

Wang, T., Xu, Y., Chen, Q., Zheng, W., Wang, J., Zeng, H., et al. (2020b). Metabolomics analysis of laparoscopic surgery combined with Wuda granule to promote rapid recovery of patients with colorectal cancer using UPLC/Q-TOF-MS/MS. *Evid. Based Complement. Altern. Med.* 2020, 5068268. doi:10.1155/2020/5068268

Wang, X., Liu, H., Li, W., and Xiao, H. (2022a). Bibliometric analysis of functional dyspepsia research trends over the past 20 years. *Front. Public Health* 10, 1019110. doi:10.3389/fpubh.2022.1019110

Wang, X. M., Lv, L. X., Qin, Y. S., Zhang, Y. Z., Yang, N., Wu, S., et al. (2022b). Ji-Chuan decoction ameliorates slow transit constipation via regulation of intestinal glial cell apoptosis. *World J. Gastroenterol.* 28, 5007–5022. doi:10.3748/wjg.v28.i34.5007

Wang, X., Wang, Z. Y., Zheng, J. H., and Li, S. (2021). TCM network pharmacology: A new trend towards combining computational, experimental and clinical approaches. *Chin. J. Nat. Med.* 19, 1–11. doi:10.1016/S1875-5364(21)60001-8

Wang, X., Zhang, C., Zheng, M., Gao, F., Zhang, J., and Liu, F. (2019). Metabolomics analysis of L-arginine induced gastrointestinal motility disorder in rats using UPLC-MS after magnolol treatment. *Front. Pharmacol.* 10, 183. doi:10.3389/fphar.2019.00183

Wehner, S., Behrendt, F. F., Lyutenski, B. N., Lysson, M., Bauer, A. J., Hirner, A., et al. (2007). Inhibition of macrophage function prevents intestinal inflammation and postoperative ileus in rodents. *GUT* 56, 176–185. doi:10.1136/gut.2005.089615

Yang, L., Wang, Y., Zhang, Y., Li, W., Jiang, S., Qian, D., et al. (2022). Gut microbiota: A new avenue to reveal pathological mechanisms of constipation. *Appl. Microbiol. Biotechnol.* 106, 6899–6913. doi:10.1007/s00253-022-12197-2

Yang, M., Chen, J. L., Xu, L. W., and Ji, G. (2013). Navigating traditional Chinese medicine network pharmacology and computational tools. *Evid. Based Complement. Altern. Med.* 2013, 731969. doi:10.1155/2013/731969

Zeng, H., Wang, W., Cao, L., Wu, Y., Ouyang, W., Diao, D., et al. (2022). Effect of Wuda granule on gastrointestinal function recovery after laparoscopic intestinal resection: A randomized-controlled trial. *Gastroenterol. Rep. (Oxf)* 10, goac004. doi:10.1093/gastro/goac004

Zhang, J., Wang, X., Wang, F., and Tang, X. (2022). Xiangsha Liujunzi Decoction improves gastrointestinal motility in functional dyspepsia with spleen deficiency syndrome by restoring mitochondrial quality control homeostasis. *PHYTOMEDICINE* 105, 154374. doi:10.1016/j.phymed.2022.154374

Zhang, Q., Zhong, D., Ren, Y. Y., Meng, Z. K., Pegg, R. B., and Zhong, G. (2021). Effect of konjac glucomannan on metabolites in the stomach, small intestine and large intestine of constipated mice and prediction of the KEGG pathway. *FOOD Funct.* 12, 3044–3056. doi:10.1039/d0fo02682d

Zhang, X. P., and Bai, X. H. (2022). Analysis on the gastrointestinal motility disorder of gastroesophageal reflux disease and the mechanism of acupuncture-moxibustion from the perspective of autonomic nervous system. *Zhongguo Zhen Jiu* 42, 1299–1303. doi:10.13703/j.0255-2930.20220608-k0007

Zou, Y., Ye, F., Kong, Y., Hu, X., Deng, X., Xie, J., et al. (2022). The single-cell landscape of intratumoral heterogeneity and the immunosuppressive microenvironment in liver and brain metastases of breast cancer. *Adv. Sci. (Weinh)* 10, e2203699. doi:10.1002/advs.202203699

frontiers | Frontiers in Pharmacology

TYPE Review
PUBLISHED 25 September 2023
DOI 10.3389/fphar.2023.1265178

Check for updates

OPEN ACCESS

EDITED BY
Jian-Bo Yang,
National Institutes for Food and Drug Control, China

REVIEWED BY
Martin Fitzgerald,
University of Westminster, United Kingdom
Yongsheng Chen,
Jinan University, China

*CORRESPONDENCE
Hongting Wang,
leonasuper@icloud.com
Cunqin Wang,
wcq5188b@163.com

RECEIVED 22 July 2023
ACCEPTED 15 September 2023
PUBLISHED 25 September 2023

CITATION
Wang H, Chen Y, Wang L, Liu Q, Yang S and Wang C (2023), Advancing herbal medicine: enhancing product quality and safety through robust quality control practices.
Front. Pharmacol. 14:1265178.
doi: 10.3389/fphar.2023.1265178

COPYRIGHT
© 2023 Wang, Chen, Wang, Liu, Yang and Wang. This is an open-access article distributed under the terms of the Creative Commons Attribution License (CC BY). The use, distribution or reproduction in other forums is permitted, provided the original author(s) and the copyright owner(s) are credited and that the original publication in this journal is cited, in accordance with accepted academic practice. No use, distribution or reproduction is permitted which does not comply with these terms.

Advancing herbal medicine: enhancing product quality and safety through robust quality control practices

Hongting Wang*, Ying Chen, Lei Wang, Qinghui Liu, Siyu Yang and Cunqin Wang*

Anhui Provincial Engineering Laboratory for Screening and Re-evaluation of Active Compounds of Herbal Medicines in Southern Anhui, Anhui Provincial Engineering Research Center for Polysaccharide Drugs, Anhui Innovative Center for Drug Basic Research of Metabolic Diseases, School of Pharmacy, Wannan Medical College, Wuhu, China

This manuscript provides an in-depth review of the significance of quality control in herbal medication products, focusing on its role in maintaining efficiency and safety. With a historical foundation in traditional medicine systems, herbal remedies have gained widespread popularity as natural alternatives to conventional treatments. However, the increasing demand for these products necessitates stringent quality control measures to ensure consistency and safety. This comprehensive review explores the importance of quality control methods in monitoring various aspects of herbal product development, manufacturing, and distribution. Emphasizing the need for standardized processes, the manuscript delves into the detection and prevention of contaminants, the authentication of herbal ingredients, and the adherence to regulatory standards. Additionally, it highlights the integration of traditional knowledge and modern scientific approaches in achieving optimal quality control outcomes. By emphasizing the role of quality control in herbal medicine, this manuscript contributes to promoting consumer trust, safeguarding public health, and fostering the responsible use of herbal medication products.

KEYWORDS

herbal medication products, quality control, standardization, quality assurance protocols, quality control methods

Abbreviations: AAS, Atomic absorption spectroscopy; *E. coli*, *Escherichia coli*; FTIR, Fourier transform infrared spectroscopy; GC, Gas chromatography; GC-MS, Gas Chromatography-Mass Spectrometry; GMP, Good manufacturing practices; HEPA, High-efficiency particulate air; HPLC, High-performance liquid chromatography; HPTLC, High-performance thin-layer chromatography; ICP-MS, Inductively coupled plasma-mass spectrometry; IRS, Infrared spectroscopy; IoT, Internet of things; LC, Liquid chromatography; MS, Mass spectrometry; NMR, Nuclear magnetic resonance; NMRS, Nuclear magnetic resonance spectroscopy; TCM, Traditional chinese medicine; TLC, Thin-Layer Chromatography; TCC, Total coliform counts; TOC, Total organic carbon; TVC, Total viable counts; TYMC, Total yeast and mould counts; UVVS, UV-Vis spectroscopy.

1 Introduction

Herbal medication products have been utilized for centuries as a primary form of healthcare in many cultures worldwide (Motti, 2021). Derived from plants and plant-derived materials, these products offer a rich source of bioactive compounds with potential therapeutic benefits (Chrysant and Chrysant, 2017). The use of herbal medicines spans diverse traditional systems, such as traditional Chinese medicine (TCM), ayurveda, and indigenous healing practices (Liu et al., 2012; Kabak and Dobson, 2017). One of the key reasons for the enduring popularity of herbal medication products is their perceived natural origin and historical use. Many societies have a long-established tradition of utilizing herbal remedies to address a wide range of ailments and promote overall wellbeing (Liu et al., 2006; Alipour et al., 2022). This traditional knowledge has been passed down through generations, offering valuable insights into the healing properties of various plant species (Cho and Kim, 2020). Herbal medication products have demonstrated therapeutic potential across various health conditions, including digestive disorders, respiratory ailments, chronic pain, and immune system support (Ernst, 1998; Kaefer and Milner, 2008; Shaikh et al., 2020). Their bioactive constituents, such as alkaloids, flavonoids, terpenes, and polyphenols, can interact with biological systems, offering potential therapeutic benefits (Wu et al., 2005; Wang and Liu, 2014; Brown, 2017). However, the growing demand for herbal medication products also raises concerns about quality control, safety, and efficacy (Osman et al., 2019; Zhou et al., 2019; Tao et al., 2023). Ensuring the consistent quality and standardization of herbal products is crucial to guarantee their safety, efficacy, and reproducibility (Rahath Kubra et al., 2016). Rigorous quality control measures are essential to protect the health and safety of consumers (Deutch et al., 2019). By implementing stringent testing and quality assurance protocols, potential risks such as contamination, adulteration, and the presence of harmful substances can be minimized, ensuring that the herbal medication products are safe for consumption (Giacometti et al., 2018). Insufficient quality control can pose serious safety risks to consumers. Contaminants, adulterants, or incorrect formulations in herbal medication products may lead to adverse reactions, toxicity, or other health complications (Chen et al., 2018; Cai et al., 2019). Inadequate quality control may result in inconsistent levels of active compounds in herbal medication products (Liu et al., 2020). This inconsistency can lead to variable therapeutic effects, making it challenging for healthcare professionals to prescribe and manage patient treatments effectively (Ma et al., 2022). Quality control measures help maintain consistency in the composition and potency of herbal medication products (Yago and Pla, 2020). Through standardized manufacturing processes and testing methods, the levels of active compounds can be monitored and controlled, ensuring that the products deliver the desired therapeutic effects consistently (Parr et al., 2001; Braga et al., 2020). This commitment helps build trust among consumers, healthcare professionals, and regulatory authorities. The purpose of the review is to provide a comprehensive overview of the importance, methods, and considerations involved in ensuring the quality, efficiency, and safety of herbal medication products.

2 Overview of herbal medication products

Herbal medication products, also known as herbal medicines or phytotherapeutic products, refer to medicinal products derived from plants or plant materials (Liu et al., 2013). These products utilize the therapeutic properties of various plant species, including their leaves, flowers, roots, stems, or extracts, to promote health and treat or prevent diseases (Sinha et al., 2015). Herbal medication products often contain a combination of active compounds, such as alkaloids, flavonoids, terpenes, and phenolic compounds, which contribute to their pharmacological effects (Chang, 2000; Ranasinghe et al., 2015). Herbal medication products can be classified based on different criteria. Based on different classification methods, we summarize the classification rules of traditional Chinese herbal medicine (Figure 1). Traditional Chinese medicine (TCM) and Ayurvedic herbal medication products have both holistic system of healthcare and healing that has been practiced for over 2,000 years in China and other parts of East Asia (Balachandran and Govindarajan, 2005; Joshi et al., 2017; Prasad et al., 2021). TCM uses a wide range of medicinal herbs, minerals, and animal products to restore balance and treat various health conditions (Wang et al., 2022). These natural substances have been used for centuries for their therapeutic properties and health benefits (Dina et al., 2022). Herbal formulas are often prescribed based on the individual's unique pattern of disharmony (Zhu et al., 2019). Different herbs have specific chemical compounds that exert various effects on the body. For example, echinacea is used to boost the immune system, ginger for digestive issues, and ginkgo biloba for cognitive function (Karsch-Völk et al., 2014; Sharifi-Rad et al., 2018). Certain minerals and mineral-rich substances are used in traditional medicine for their therapeutic effects. For instance, calcium, magnesium, iron, sulphur, and zinc were supplied for bone health and muscle function, the treatment of anemia and to boost hemoglobin levels, skin conditions like acne and eczema, the immune system, and wound healing (Harper et al., 1987; Song et al., 2021; Xiao et al., 2022). Traditional medicine systems, particularly in

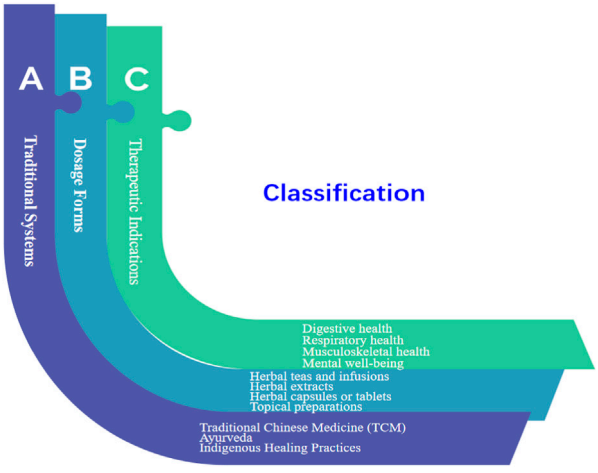


FIGURE1
A classification of herbal medication products.

East Asia, have used animal products for their medicinal properties (Cheng et al., 2022). Some examples include deer antler velvet which is used to strengthen the body, improve energy, and support joint health, and bear bile used in some traditional Chinese remedies, though the use of bear bile is controversial due to animal cruelty concerns (Wu et al., 2013; Yu et al., 2017). Cordyceps is a fungus that parasitizes insects and is used for various health benefits, including respiratory support and energy enhancement (Chen et al., 2017; Lou et al., 2019; Ashraf et al., 2020; Yang et al., 2020). It is essential to note that while traditional medicine systems have been using these substances for generations, the safety and efficacy of medicinal herbs, minerals, and animal products are not always supported by modern scientific evidence (Yuan et al., 2016). Some of these substances may interact with medications or have potential side effects (Saini et al., 2022). Therefore, it is crucial to consult with qualified healthcare professionals, such as herbalists or traditional medicine practitioners, who have knowledge and experience in the safe use of these natural remedies. In modern times, there is an increasing interest in studying traditional medicinal practices and evaluating the therapeutic potential of these natural substances through rigorous scientific research (Schwabl and Vennos, 2015; Jaiswal et al., 2016). It is precisely because of the diversity of Chinese herbal medicines that the quality control of the herbal medicine industry is particularly important for the efficiency and safety of herbal medication products (Kankanamalage et al., 2014). So, integrative medicine approaches seek to combine the best practices from traditional and modern medicine to provide comprehensive and personalized healthcare solutions.

3 Quality control for herbal medication products

Quality control is a systematic approach that involves monitoring and controlling various aspects of herbal product development, manufacturing, and distribution to guarantee consistent product quality (Ding et al., 2008). Quality control measures are essential in any industry or organization as they play a significant role in ensuring that products or services meet the expected standards and specifications (Osman et al., 2019; Chen et al., 2023). Effective quality control measures involve evaluating processes and identifying areas for improvement (Qin et al., 2012; Zhao et al., 2018; Gong et al., 2023). By streamlining operations, eliminating bottlenecks, and addressing inefficiencies, organizations can enhance productivity and achieve higher output levels with fewer resources (Gong et al., 2023).

3.1 Standardization and identification of herbs

The first step is to built standardization and identification of herbs for effective quality control measures. Standardization and identification of herbs involve establishing consistent and reliable levels of active compounds or markers in herbal medication products (Aleksieva and Yordanov, 2018). It aims to minimize batch-to-batch variability and ensure that each product meets predetermined quality standards (Ketai et al., 2000). Identify the key active compounds or markers in the herb that contribute to its therapeutic properties. Some key aspects of them involve active compound identification, quantitative analysis, and reference standards, which can be done through scientific research, traditional knowledge, or existing literature (Zhao et al., 2022). Develop methods to quantitatively measure the levels of active compounds or markers (An et al., 2022). This can involve techniques such as chromatography (HPLC, GC), spectroscopy (UV-Vis, IR), or specific chemical assays (Pan et al., 2018). Establish reference standards or reference materials that represent the desired levels of active compounds or markers (Xiong et al., 2022). These standards act as benchmarks for comparison during quality control testing and help ensure consistency across batches (Jin et al., 2018). Standardization provides a means to monitor and control the quality and efficacy of herbal medication products, enabling healthcare professionals to prescribe treatments with confidence.

Authenticity testing methods are essential in quality control for herbal medication products to ensure the accurate identification and verification of the herbs used to ensure that the correct herb is being used, as different species or plant parts may have varying therapeutic properties and safety profiles (Zhang et al., 2022). Herb identification is the process of accurately identifying the botanical species or plant material used in herbal medication products (Lo and Shaw, 2019). Some commonly employed authenticity testing methods involve macroscopic examination, microscopic examination, thin-layer chromatography, high-performance liquid chromatography, DNA Barcoding, and chemical profiling (Figure 2).

Macroscopic Examination involves visual inspection and examination of the physical characteristics of the herb, including its color, shape, size, texture, and any unique features (K et al., 2021). Macroscopic examination helps in identifying the herb and distinguishing it from other similar-looking plants. Microscopic examination involves the use of a microscope to examine the cellular structures and characteristic features of the herb (Xiong et al., 2019). This method helps in identifying specific plant parts, such as leaves, stems, or roots, and verifying their authenticity. TLC is a technique used to separate and analyze the chemical constituents of a herb. It involves applying a thin layer of the herb extract onto a solid support, which is then developed using a suitable solvent system (Poole, 2003; Cheng et al., 2011). The resulting chromatogram can be compared to reference standards to identify the herb and detect any adulterants or contaminants (Del Bubba et al., 2013). HPLC is a powerful analytical technique that separates and quantifies the chemical compounds in a herb (Sontag et al., 2019). It can be used to determine the presence and concentration of specific marker compounds or active ingredients, ensuring the consistency and quality of herbal medication products (Malherbe et al., 2012). DNA testing, specifically DNA barcoding, is a molecular technique used to authenticate and identify herbal species (Li et al., 2015). It involves sequencing a specific region of the herb's DNA, such as the barcode region, which is unique to each species. By comparing the obtained DNA sequence with a reference database, the herb's genetic identity can be determined, ensuring the use of the correct species and detecting any potential adulteration or substitution (DeSalle et al., 2005; Senapati et al., 2022). DNA testing provides a highly reliable method for herb

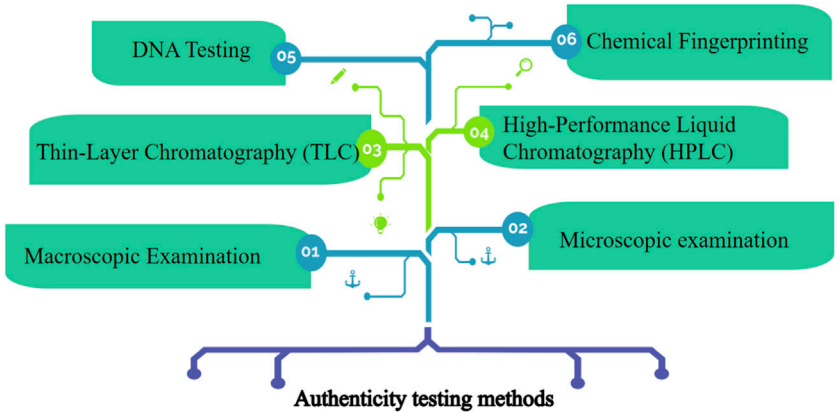


FIGURE2
The quality control methods for the accurate identification and verification of the herbs.

identification and is particularly useful when the herbs are in processed or powdered forms. Next, chemical fingerprinting involves analyzing the chemical constituents of herbs using analytical techniques such as high-performance liquid chromatography (HPLC), gas chromatography-mass spectrometry (GC-MS), or nuclear magnetic resonance (NMR) (Wibowo et al., 2015; Li et al., 2022). By comparing the chemical profiles obtained from a herb sample with established reference profiles, manufacturers can verify the authenticity, consistency, and quality of the herbs. Chemical fingerprinting helps identify specific marker compounds or active ingredients, ensuring the desired potency and therapeutic efficacy of herbal medication products (Gainza et al., 2020). Chemical fingerprinting and DNA testing provide objective and scientific data for quality control in herbal medication products (Yin et al., 2022). By integrating these techniques into quality control processes, manufacturers can establish robust standards, maintain consistency, meet regulatory requirements, verify the authenticity of herbal ingredients, detect any adulterations or contaminants, and ensure the consistency and safety of herbal medication products. It is worth noting that macroscopic and microscopic examination should be complemented with other testing methods, such as Thin-Layer Chromatography (TLC), High-Performance Liquid Chromatography (HPLC), DNA barcoding, or chemical profiling, to provide a comprehensive quality control approach for herbal medication products (Chen et al., 2006; Hu et al., 2021). These authenticity testing methods help ensure the accurate identification and quality control of herbs used in herbal medication products that may compromise the safety and efficacy of the products.

3.2 Processing and manufacturing controls

Extraction methods play a crucial role in obtaining the desired active compounds from herbs during the manufacturing process of herbal medication products (Boutron et al., 2007; Abeillé et al., 2020). Optimizing extraction methods is critical to ensure the efficient extraction of bioactive compounds from herbs, which directly impacts the potency and efficacy of herbal medication products (Zhu et al., 2006). Some key points regarding extraction methods and optimization involve selection of solvent, pre-processing of herbal material, ratio of solvent to herbal material, temperature and time, extraction techniques, multiple extractions, pH adjustment, use of co-solvents or enhancers, quality control, safety considerations, sustainability, validation and reproducibility (Hawthorne et al., 2000; Boateng et al., 2023). The selection of the appropriate extraction technique depends on factors such as the nature of the herb, targeted bioactive compounds, desired product characteristics, and manufacturing scale (Gollahon and Holt, 2000). Each technique has its advantages and limitations, and it is important to choose the most suitable method for efficient extraction (Silva et al., 2022). First of all, the choice of solvent is crucial for successful extraction (Brennan et al., 2009). Different solvents have varying polarities and can selectively extract different compounds (Kalkan et al., 2019). Common solvents used include water, ethanol, methanol, and their mixtures. The solvent selection should consider the solubility of target compounds, potential toxicity, environmental impact, and regulatory requirements (Tasfiyati et al., 2022). It is important to optimize the solvent-to-herb ratio to achieve optimal extraction efficiency. Besides, optimization of extraction parameters such as temperature, time, and pressure is essential to maximize the extraction of bioactive compounds while maintaining their stability and minimizing degradation (Ma et al., 2021). These parameters can vary depending on the herb and its targeted compounds. Factors like temperature and extraction duration should be carefully controlled to prevent the loss of heat-sensitive compounds or the degradation of thermally unstable components (Feldmann and Bondemark, 2006). Apparently, pre-treatment techniques, such as size reduction (grinding, milling), drying, or specific treatments like blanching, can influence the efficiency of extraction (Wibowo et al., 2015; An et al., 2022). These techniques help in breaking down the plant matrix, facilitating the release of bioactive compounds and improving their accessibility to the extraction solvent (Dai et al., 2022). Once the extraction method is established, process validation should be performed to ensure consistent and reproducible

TABLE 1 Extraction methods and optimization factors.

Advanced extractions techniques	Ultrasound-assisted extraction (UAE)	Microwave-assisted extraction (MAE)	Pressurized liquid extraction	Supercritical fluid extraction	References
Sample	√	√	√	-	Wolle and Conklin (2018); Pradhan et al. (2019); Woolman and Liu (2022)
Extraction solvent	√	√	√	-	Rodsamran and Sothornvit (2019); Gil-Díaz et al. (2021)
Pressure	-	-	√	√	Chan and Choo (2013); Ma et al. (2017); Silva et al. (2022)
Extraction temperature	√	√	√	-	Brennan et al. (2009); Elfgen et al. (2020); Gil-Díaz et al. (2021)
Size	-	-	√	-	El Maangar et al. (2020); da Cunha et al. (2021); Ma et al. (2021)
PH	-	-	√	-	Feldmann and Bondemark (2006); Gupta and Sinha (2007); Spineli (2017); Tasfiyati et al. (2022)
Flow rate	-	-	√	-	Du et al. (2009); Backes et al. (2018); da Cunha et al. (2021)
Extraction time	√	√	√	√	Xie and Dreisinger (2009); González et al. (2021); Tsiaka et al. (2023)
Ultrasound power	√	-	-	-	Mulinacci et al. (2011); Boyd et al. (2012); Speltini et al. (2021)
Frequency	√	-	-	-	Hawthorne et al. (2000); Zhu et al. (2006); Silva et al. (2022)
Intensity	√	-	-	-	Backes et al. (2018); Speltini et al. (2021); Yin et al. (2022)
Microwave power	-	√	-	-	Byrd et al. (1991); Gollahon and Holt (2000); Ege and Demirkol (2021)
Plant matrix characteristic	-	√	-	-	Pihlström et al. (2002); El Maangar et al. (2020); González et al. (2021)

extraction results. Process validation involves confirming that the extraction process consistently meets predetermined quality standards, including extraction efficiency, yield, and the presence of desired bioactive compounds (González et al., 2021; Kapadia et al., 2022). Validation parameters may include analytical testing, comparison with reference samples, and statistical analysis (Campuzano and González-Martínez, 2017; Onishi et al., 2018). Various extraction techniques and extraction parameters are listed, including maceration, percolation, reflux, Soxhlet extraction, ultrasound-assisted extraction, and supercritical fluid extraction (Table 1).

3.3 Quality assessment during processing

Quality assessment during processing is a crucial aspect of ensuring the safety, efficacy, and consistency of herbal medication products (Fillingim et al., 2016). It involves monitoring and evaluating various parameters and factors throughout the manufacturing process (Sargeant et al., 2022). Here, some key points regarding quality assessment were summarized during processing (Table 2).

3.3.1 Raw material evaluation

The quality assessment starts with a thorough evaluation of the raw materials, which are the herbs used in the product (Liang et al., 2023). Raw material evaluation methods includes checking the identity, authenticity, purity, and quality of the herbs, which involve a combination of techniques and tests to assess the quality, authenticity, and safety of raw materials used in the production of herbal medication products (Sridharan et al., 2016; Benedetti et al., 2019). First of all, it is an organoleptic evaluation that involves the examination of raw materials using the senses, including sight, smell, taste, and touch (Sridharan et al., 2016). It helps identify any abnormalities or inconsistencies in appearance, odor, and taste. Next, a microscopic examination of plant material can help verify its identity and detect any adulteration or foreign substances (Saletnik et al., 2021; Zhang et al., 2021). High-performance thin-layer chromatography (HPTLC) is used to separate and identify different chemical components in a sample. It is often employed to verify the presence of specific markers or active compounds in herbal raw materials (Vestal, 1984; Hussain et al., 2015; Sontag et al., 2019). Fourier transform infrared spectroscopy (FTIR) is used to identify functional groups in raw materials, helping to assess their chemical composition (Agustika

TABLE 2 Quality management practices.

Quality assessment	Parameters	Methods	References
Raw Material Evaluation	Botanical Identity	Visual inspections Macroscopic examinations Microscopic examinations Chemical analyses	Stringham et al. (2009); Sridharan et al. (2016); Benedetti et al. (2019); Liang et al. (2023)
	Purity and Authenticity		
	Plant Part		
	Geographic Origin		
	Moisture Content		
	Foreign Matter		
	Chemical Composition		
	Microbial Contamination		
	Heavy Metal Content		
	Residual Solvents		
Good Manufacturing Practices (GMP)	Proper documentation Personnel training Hygiene practices Quality control procedures	Facility Design and Maintenance	Velagaleti et al. (2002); Burcham et al. (2018); Crimi et al. (2021); Lai et al. (2022)
		Personnel Training and Qualification	
		Standard Operating Procedures	
		Raw Material Control	
		Equipment Calibration and Maintenance	
		Batch Records and Documentation	
		In-process Quality Control	
		Product Testing and Release	
		Stability Testing	
		Recall Procedures	
		Validation and Qualification	
Process Control	Temperature	Cleaning and Sanitization Environmental Conditions Quality Control Testing Macroscopic examinations Microscopic examinations	Davids and Bagley (2014); Cox et al. (2019); Huaulmé et al. (2020); Kjelkenes et al. (2022)
	Time pH		
	Pressure		
	Solvent-to-Solid Ratio		
	Mixing Intensity		
	Drying Conditions		
	Particle Size		
In-process Testing	Moisture Content	Chemical analysis Microbial testing Dissolution testing Physical measurements	Sridharan et al. (2016); Benedetti et al. (2019); Kjelkenes et al. (2022); Liang et al. (2023)
	Solvent Concentration pH Level		
	Mixing Time		
	Particle Size		
	Homogeneity		
	Pressure		
	Temperature		
	Weight Variation		
	Disintegration Time		
	Uniformity of Dosage Units		
	Residual Solvents		

(Continued on following page)

TABLE 2 (*Continued*) Quality management practices.

Quality assessment	Parameters	Methods	References
Contamination Control	Microbial Contamination	Aseptic techniques	Dworkin et al. (2018); Noh et al. (2018); Ling et al. (2021); Prata et al. (2021); Jenner et al. (2022)
	Heavy Metals	Environmental Monitoring	
	Pesticide Residues	Equipment Cleaning and Sanitization	
	Mycotoxins	Packaging Material Evaluation	
	Solvent Residues	Good Manufacturing Practices	
	Foreign Matter	Quality Control Testing	
	Cross-Contamination		

et al., 2022; Barnes et al., 2023). Atomic absorption spectroscopy (AAS) is employed to detect and quantify the presence of heavy metals in raw materials, ensuring they are within safe limits (Qu et al., 2016; Ortegón et al., 2022). High-performance liquid chromatography is utilized for quantitative analysis of active compounds in herbal materials, ensuring that they meet specified quality standards (Olsson et al., 2014; Xie et al., 2014). And total organic carbon (TOC) analysis is used to determine the total amount of organic carbon present in a sample, which can indicate the presence of contaminants (Shao et al., 2022; Lee et al., 2023). By using a combination of these raw material evaluation methods, manufacturers can ensure the quality, authenticity, and safety of the herbal ingredients used in their products. These evaluations are crucial for maintaining consistent product quality, meeting regulatory standards, and providing consumers with safe and effective herbal medication products.

3.3.2 Good manufacturing practices for herbal products

Good Manufacturing Practices (GMP) guidelines are essential to the herbal industry to maintain product quality and protect consumer health (Lesch et al., 2021). GMP for herbal products is a set of guidelines and principles that ensure the quality, safety, and consistency of herbal medicines, supplements, and other herbal products (Castiglia et al., 2018). It involves raw material sourcing and identification, facility and equipment, standard operating procedures, batch records and documentation, quality control testing, validation and qualification, stability testing, recalls and complaints, regulatory compliance, and continuous improvement (Boyd, 1994; Jacquemart et al., 2016; Cundell et al., 2023). GMP also involve proper documentation, personnel training, hygiene practices, and quality control procedures to ensure consistent quality throughout the manufacturing process (Castiglia et al., 2018). GMP requires the use of high-quality, authentic, and properly identified herbal raw materials. Suppliers should be carefully selected and qualified to ensure the consistency and purity of the ingredients (Lesch et al., 2021). GMP-compliant facilities should be designed, maintained, and operated in a manner that prevents cross-contamination, ensures cleanliness, and provides a controlled environment for manufacturing (Melethil, 2006; Bai et al., 2022). GMP emphasizes the development and implementation of written standard operating procedures for all critical manufacturing processes (Shukla and Gottschalk, 2013). These procedures help ensure consistent and controlled production. Detailed batch records and documentation should be maintained for each product manufactured (Mager et al., 2007). This includes information about raw materials, manufacturing steps, quality control tests, and any deviations or corrective actions taken during production (Deagle et al., 2017; Smith, 2020). GMP requires routine quality control testing of raw materials, in-process samples, and finished products (Morgan et al., 2015). Testing may include the identification of herbal ingredients, quantitative analysis of active compounds, and evaluation of contaminants. Processes, equipment, and analytical methods used in herbal product manufacturing should be validated to demonstrate their effectiveness and accuracy (Williams et al., 2012). Herbal products should undergo stability testing to determine their shelf life and storage conditions (Cundell et al., 2023). This helps ensure that the product retains its quality and potency throughout its designated shelf life. Regular audits, self-inspections, and reviews of manufacturing processes help identify areas for enhancement and ensure ongoing compliance with GMP principles (Deagle et al., 2017). Finally, adhering to good manufacturing practices is essential for the herbal products industry to maintain product quality, safety, and consistency. GMP guidelines promote the use of standardized procedures, robust quality control, and proper documentation to ensure that herbal products meet the required standards and are safe for consumers (Smith, 2020). By following GMP principles, manufacturers can build trust with consumers, healthcare professionals, and regulatory authorities, contributing to the growth and acceptance of herbal products in the healthcare market.

3.3.3 Process control

Monitoring and controlling critical parameters during processing is essential to maintain product quality (Qu et al., 2021). This includes parameters such as temperature, pressure, pH, mixing time, and drying conditions (Morgan et al., 2015). Regular monitoring and documentation of these parameters help identify any deviations from the desired specifications and allow for necessary adjustments or corrective actions to ensure product consistency (Wasalathanthri et al., 2020). Temperature control is

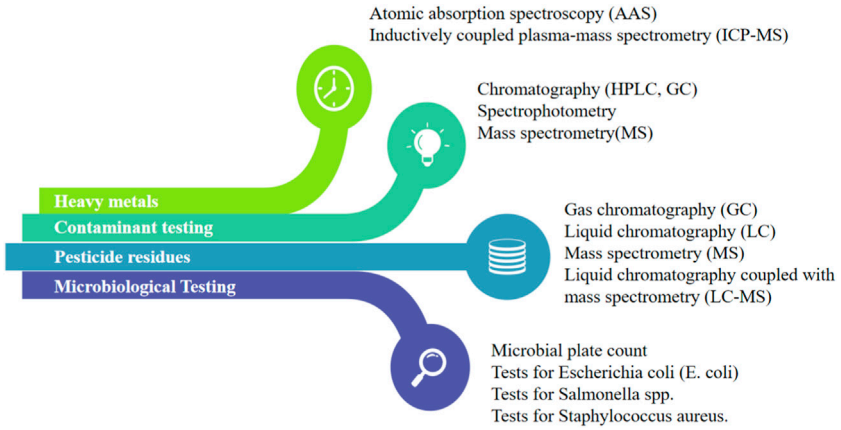


FIGURE 3
The quality control methods for contaminants, heavy metals, pesticide residues, and microbiology.

vital in many processes as it directly impacts chemical reactions, phase changes, and microbial growth (Reischauer et al., 2009). Precise temperature control ensures that reactions proceed as intended, preventing unwanted by-products and ensuring the desired product quality. In pharmaceutical manufacturing, maintaining the correct temperature during drug synthesis helps produce stable and effective medications (Pan et al., 2019). Pressure control is particularly important in processes involving gases or liquids (Seo and Shin, 2022). Too much or too little pressure can affect reaction rates, solubility, and the overall efficiency of the process. In applications like chemical reactions, pressure control helps maintain a safe operating environment and prevents equipment failures (Schmidt et al., 2023). pH is a measure of acidity or alkalinity and significantly influences the stability and functionality of many products (Wright, 2021). In industries like food and beverage production, pharmaceuticals, and cosmetics, maintaining the correct pH level is critical for product preservation, taste, and effectiveness (Wiseman et al., 2022). For instance, certain enzymes are only active within specific pH ranges, making pH control essential during enzyme-based processes (Daniel et al., 2022). In processes involving mixing or blending, the duration and intensity of mixing time directly affect product homogeneity and consistency (Hernandez and Perera, 2022). Controlling the mixing time ensures uniform distribution of ingredients, which is crucial in formulations such as pharmaceutical tablets or food products (Adra et al., 2022). Drying is a common step in herbal medication industries, such as product processing, pharmaceuticals, and chemical manufacturing. Controlling drying conditions can change product defects, increase shelf life, or even keep fresh, which involves temperature, humidity, airflow, moisture content, texture, and stability (da Cunha et al., 2021). Quality testing for herbal medication products involves rigorous analysis to ensure the absence of contaminants, heavy metals, pesticide residues, and microbiological safety evaluation (Figure 3). By controlling critical parameters, manufacturers can achieve consistent product quality across different batches, leading to reliable and predictable outcomes, reducing waste and production time, avoiding product defects and minimizing rejections, and increasing its market value and consumer satisfaction.

3.3.4 In-process testing

In-process testing involves performing quality tests at various stages of the manufacturing process to assess the product's quality and consistency (Silva et al., 2022). These tests may include chemical analysis, microbial testing, dissolution testing, or physical measurements. In-process testing helps identify any variations or issues during processing, allowing for timely corrective actions and ensuring the final product meets the desired quality standards (Chan and Choo, 2013). The presence of contaminants, heavy metals, pesticide residues, and microbiological safety evaluation is a crucial major concern in herbal medication products (Omeje et al., 2021). Therefore, the detection of pollutants, pesticides, microbiological counts, and heavy metals in the environment is key to ensuring the quality of herbal medication products (Varol and Sünbül, 2017). Contaminant testing includes assessing the presence of impurities such as aflatoxins, mycotoxins, residual solvents, and environmental pollutants (Simpson and McKelvie, 2009). Various analytical techniques like chromatography (HPLC, GC), spectrophotometry, and mass spectrometry are employed to detect and quantify these contaminants (Levy et al., 2018). Heavy metals such as lead, mercury, arsenic, and cadmium can pose health risks if present in herbal medication products. Testing methods such as atomic absorption spectroscopy or inductively coupled plasma-mass spectrometry (ICP-MS) are utilized to measure heavy metal content and ensure compliance with permissible limits (Lockwood et al., 2021). Pesticide residues can result from agricultural practices or contamination during cultivation. Analytical techniques like gas chromatography (GC) or liquid chromatography (LC) coupled with mass spectrometry (MS) are employed for pesticide residue analysis, ensuring adherence to regulatory standards (Lockwood et al., 2021). Microbiological testing assesses the presence of harmful microorganisms in herbal medication products (Levy et al., 2018). It includes testing for total microbial counts, specific pathogens, and the absence of certain indicator organisms (Levy et al., 2018). Common methods include microbial plate count, tests for *E. coli* (*Escherichia coli*), *Salmonella* spp., and *Staphylococcus aureus* (York et al., 2000). The microbial evaluation for total coliform counts (TCC), total viable counts (TVC), and total yeast and mold counts (TYMC) was evaluated using the method described in the compendium of methods for microbiological testing of herb medication products

described by Hervert and Alles (2016) with minor modifications. These tests ensure product safety and compliance with microbial limits set by regulatory authorities.

Analytical techniques are employed to determine the presence, identity, and concentration of active constituents in herbal medication products (Seo and Shin, 2022). High-Performance liquid chromatography is widely employed to separate, identify, and quantify individual chemical components, including active compounds, in herbal extracts (Wright, 2021). It provides precise measurements and is useful for standardization and quality control. Gas chromatography-mass spectrometry is used for volatile compounds and essential oils analysis in herbal medication products (Silva et al., 2022). It enables the identification and quantification of specific compounds based on their mass spectra and retention times. Thin-Layer Chromatography is a rapid and cost-effective technique used for qualitative analysis and identification of compounds in herbal medicines (Del Bubba et al., 2013). It involves separating components based on their differential migration on a thin layer of adsorbent material. Spectroscopic Techniques like UV-Vis spectroscopy, infrared (IR) spectroscopy, and nuclear magnetic resonance (NMR) spectroscopy are employed for qualitative and quantitative analysis of herbal constituents. They provide information on chemical structures, functional groups, and concentrations. These quality testing and analytical techniques help ensure the safety, efficacy, and consistency of herbal medication products. By performing these tests, manufacturers can identify potential contaminants, verify active constituent content, and ensure compliance with regulatory requirements, thereby ensuring the quality and safety of the products.

3.3.5 Contamination control

Contamination control is a critical aspect of various herbal medication industries, ensuring safety, product quality, and environmental protection (Raeisossadati et al., 2016). Contamination control methods are techniques and practices employed to prevent, minimize, or eliminate the presence of harmful or unwanted substances in a specific environment, product, or process (Edberg et al., 1989; Simpson and McKelvie, 2009). These methods vary depending on the industry and the nature of the contamination. This includes implementing measures such as cleaning and sanitation, sterilization, disinfection, hand hygiene, cleanroom technology, air filtration, regulatory compliance, and environmental monitoring (Wan et al., 2019). Regular cleaning and sanitation of surfaces, equipment, and facilities are fundamental contamination control methods. Proper cleaning removes dirt, debris, and potential contaminants, reducing the risk of cross-contamination. Sterilization is a critical method used in healthcare settings and the pharmaceutical industry to eliminate all viable microorganisms, including bacteria, viruses, and spores. Techniques like autoclaving, irradiation, and chemical sterilization are commonly used. Disinfection involves the use of chemical agents to reduce the number of microorganisms on surfaces and objects. It is commonly used in healthcare settings and food production to control the spread of pathogens. Clean-rooms are controlled environments designed to minimize airborne particulates and microorganisms (Safra, 2019). They are widely used in industries like semiconductor manufacturing, aerospace, and pharmaceuticals. High-efficiency particulate air (HEPA) filters are used in ventilation systems to remove airborne particles, including microorganisms and other contaminants. In industries like food production and healthcare, pest control measures are essential to prevent contamination from insects and rodents. Many industries have specific regulations and standards related to contamination control (Panteghini et al., 2001). Compliance with these regulations is essential to ensure public safety, product quality, and environmental protection. Regular monitoring of environmental conditions, such as temperature, humidity, and air quality, can help identify potential sources of contamination and ensure appropriate control measures are in place (Omeje et al., 2021). Contamination control methods encompass a range of practices and techniques aimed at preventing or reducing contamination in herbal medication products industries (Levy et al., 2018). These methods are critical to ensure the safety, quality, and efficacy of products, protect public health, and preserve the environment.

4 Discussion

Despite the growing recognition of herbal medicines' therapeutic potential, the field of quality control in this domain faces several critical gaps and challenges that warrant diligent attention. One notable challenge is the significant variability in product composition and quality due to factors such as geographical variations, cultivation methods, and post-harvest processing. This inherent diversity poses a unique hurdle for establishing consistent quality standards across different herbal products. Rapid advancements in analytical technologies, such as mass spectrometry and DNA barcoding, have transformed the landscape of quality control in other industries, yet their integration into herbal medicine quality assessment has been sporadic and inconsistent. We propose the utilization of molecular fingerprinting techniques, such as DNA bar-coding and metabolic, to authenticate herbal ingredients. These approaches offer accurate species identification and enable the detection of adulterants or contaminants. Secondly, we advocate for the incorporation of real-time monitoring and Internet of Things (IoT) devices along the herbal supply chain. This enables continuous data collection on environmental conditions, ensuring the preservation of botanical integrity and product quality. Besides, Data-driven predictive modeling is also necessary for quality control practices in the herbal industry. Introducing data-driven predictive models, including machine learning and artificial intelligence, can forecast the impact of processing variables on herbal product quality. This empowers manufacturers to optimize production processes for consistent outcomes. Finally, the collaboration between regulatory bodies, herbal practitioners, and manufacturers is proposed to establish comprehensive industry standards. These standards would encompass cultivation, harvesting, processing, and quality control, ensuring adherence to best practices. Moreover, the under-utilization of traditional knowledge is a missed opportunity for elevating the quality control process. Traditional healers and local communities possess invaluable insights into the therapeutic properties and usage of herbs. Integrating this wisdom with modern scientific approaches could enrich the quality control paradigm and enhance product efficacy. In response to these challenges, a holistic approach to quality control is needed—one that bridges the gaps between traditional practices and modern innovations, streamlines regulatory oversight, and nurtures collaborative partnerships among stakeholders. To illustrate the interplay of these elements, a diagram of the road map is presented below in Figure 4. By following this roadmap, herbal medicine manufacturers and regulators can strengthen

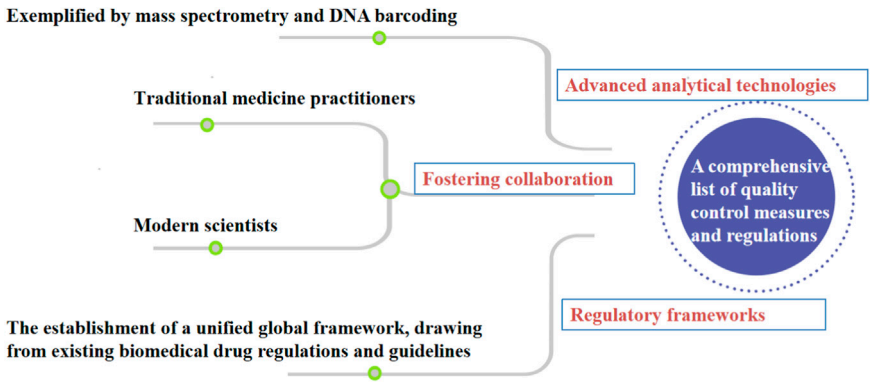


FIGURE 4
A diagram of the road map for the comprehensive list of quality control measures and regulations applied to herbal medicines.

TABLE 3 A potential evolution of quality control measures.

Quality control aspect	Current practices	Biomedical drug products	Herbal medicines	Enhanced approach for herbal medicines
Analytical Testing Methods	Visual inspection, basic impurity tests	High-precision tests, such as HPLC and GC-MS, to identify and quantify active compounds	Traditional visual inspection and basic tests for impurities and contaminants	Adoption of advanced technologies like mass spectrometry and DNA barcoding to authenticate herbal components
Regulatory Framework	Varied regional regulations	Stringent global regulations and guidelines (e.g., FDA, EMA) for drug approval and manufacturing	Varied regulations across regions, with potential gaps in standardization	Establishment of a unified global framework based on international guidelines and good manufacturing practices
Collaboration & Knowledge	Limited collaboration between stakeholders	Collaboration between scientists, researchers, and pharmaceutical companies	Limited integration of traditional knowledge and modern research	Encouragement of multidisciplinary partnerships between traditional practitioners, scientists, and regulators, harnessing both traditional knowledge and modern expertise

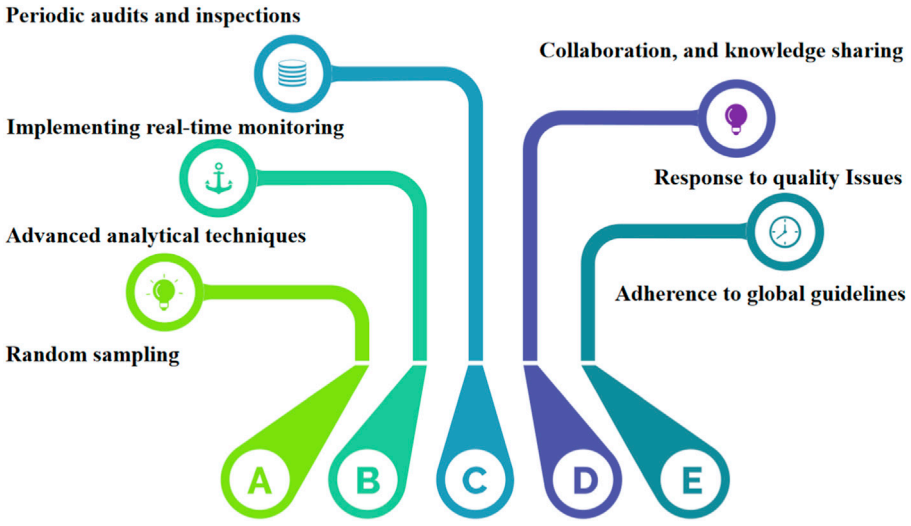


FIGURE 5
A map for the quality of herbal medicine products control of enterprises.

the safety and efficacy of herbal medication products, thereby instilling confidence in consumers and fostering the responsible growth of the herbal medicine industry. The road map also serves as a foundation for continuous research, improvement, and knowledge-sharing, ultimately contributing to the advancement of quality control practices for herbal medicines. medicines.

Herbal medicines often draw from centuries of traditional knowledge, which should be thoughtfully integrated into modern quality control practices. It is worth noting that some of the quality control advances suggested for herbal medicines are already well-established practices in the context of biomedical drug products. Building upon the insights highlighted by previous researchers, strategic integration of cutting-edge analytical techniques, harmonized global standards, and collaborative partnerships emerges as the pathway forward. While some aspects of biomedical drug quality control can serve as a model for herbal medicines, there are specific differences between the two domains. Although adopting certain aspects of biomedical drug quality control can be beneficial for the quality control of herbal medicines, the application of such measures to herbal medicines raises distinct considerations. By juxtaposing the existing practices with the proposed enhancements, we underscore the potential evolution of quality control measures for herbs (Table 3). By embracing these enhancements, we hold the promise of transforming the herbal medicine landscape and instilling newfound confidence in consumers seeking natural remedies.

By synthesizing a comprehensive understanding of the challenges and opportunities within the realm of herbal medicine quality control, we equip enterprises with actionable insights to enhance their practices such as a comprehensive review of quality control measures, identification of gaps and challenges, recommendations for enhancements, integration of modern techniques, regulatory harmonization, collaborative approach, continuous improvement, and innovation (Figure 5). Enterprises learn how to maintain uniformity in active ingredients, dosage forms, and potency and improve the core aspects of GMP, including cleanliness, personnel training, documentation, and equipment maintenance. This knowledge empowers enterprises to conduct rigorous quality assessments before products reach the market. By underscoring the role of quality control in ensuring safety, the text assists enterprises in identifying potential risks associated with herbal medicine production. Enterprises are encouraged to regularly review and update their quality control processes in light of emerging research, technological advancements, and changing consumer preferences. By implementing the insights provided in the text, enterprises can confidently navigate the complexities of herbal medicine production and contribute to the availability of safe and consistent products for consumers.

5 Conclusion

Quality control for the efficiency and safety of herbal medication products is of significant importance to safeguard consumer health, establish reliable treatment options, comply with regulations, and foster the growth of the herbal medicine industry. The efficacy of herbal medications depends on the presence and concentration of active compounds. Quality control processes should focus on establishing standardized procedures for sourcing, processing, and formulating herbal ingredients. Besides, regular monitoring of raw materials and finished products, quantitative analysis of these compounds to guarantee consistent therapeutic effects, rigorous testing for potential contaminants, implementing GMP principles in the production process, and post-market surveillance are often attributed to ensure safety and efficacy. With continuous quality control measures in place, any issues related to product quality or safety can be identified and addressed promptly. Advanced techniques such as DNA barcoding can be employed to verify the authenticity of herbs used in the products. This proactive approach minimizes the risk of widespread product recalls or adverse events.

Ensuring the quality, efficiency, and safety of herbal medication products involves standardization, authentication, contaminant testing, quantification of active compounds, adherence to regulations, stability testing, GMP implementation, validated methods, post-market surveillance, and open collaboration among stakeholders. These key findings and takeaways provide a road map for establishing robust quality control processes for herbal medication products.

In conclusion, this comprehensive review underscores the pivotal role of quality control in herbal medication products, emphasizing its significance in ensuring efficiency and safety. The use of robust quality control methods ensures the authenticity and therapeutic value of herbal remedies, fostering consumer trust and promoting the responsible integration of herbal medicine into modern healthcare practices. Continued research and collaboration between traditional knowledge and modern science will undoubtedly enhance the quality and acceptance of herbal medication products, further benefiting public health and wellbeing.

Author contributions

HW: Data curation, Formal Analysis, Funding acquisition, Software, Validation, Writing–original draft, Writing–review and editing. YC: Data curation and editing. LW: Data curation. QL: Investigation and Software. SY:Data curation, Investigation, Software. CW: Formal Analysis, Writing–review and editing.

Funding

The authors declare financial support was received for the research, authorship, and/or publication of this article. This work was supported by the Nature Science Research Project of Anhui Province fund (2023AH040268, 2023AH040257).

Acknowledgments

The authors would like to acknowledge the contributions of Anhui Provincial Engineering Research Center for Polysaccharide Drugs that aided the efforts of the authors.

Conflict of interest

The authors declare that the research was conducted in the absence of any commercial or financial relationships that could be construed as a potential conflict of interest.

Publisher's note

All claims expressed in this article are solely those of the authors and do not necessarily represent those of their affiliated organizations, or those of the publisher, the editors and the reviewers. Any product that may be evaluated in this article, or claim that may be made by its manufacturer, is not guaranteed or endorsed by the publisher.

References

Abeillé, A., Hemforth, B., Winckel, E., and Gibson, E. (2020). Extraction from subjects: differences in acceptability depend on the discourse function of the construction. *Cognition* 204, 104293. doi:10.1016/j.cognition.2020.104293

Adra, H. J., Zhi, J., Luo, K., and Kim, Y. R. (2022). Facile preparation of highly uniform type 3 resistant starch nanoparticles. *Carbohydr. Polym.* 294, 119842. doi:10.1016/j.carbpol.2022.119842

Agustika, D. K., Mercuriani, I., Purnomo, C. W., Hartono, S., Triyana, K., Iliescu, D. D., et al. (2022). Fourier transform infrared spectrum pre-processing technique selection for detecting PYLCV-infected chilli plants. *Spectrochim. Acta A Mol. Biomol. Spectrosc.* 278, 121339. doi:10.1016/j.saa.2022.121339

Aleksieva, K. I., and Yordanov, N. D. (2018). Various approaches in EPR identification of gamma-irradiated plant foodstuffs: A review. *Food Res. Int. Ott. Ont.)* 105, 1019–1028. doi:10.1016/j.foodres.2017.11.072

Alipour, R., Marzabadi, L. R., Arjmand, B., Ayati, M. H., and Namazi, N. (2022). The effects of medicinal herbs on gut microbiota and metabolic factors in obesity models: A systematic review. *Diabetes Metab. Syndr.* 16, 102586. doi:10.1016/j.dsx.2022.102586

An, Y. L., Wei, W. L., and Guo, D. A. (2022). Application of analytical technologies in the discrimination and authentication of herbs from fritillaria: A review. *Crit. Rev. Anal. Chem.* 1-22, 1–22. doi:10.1080/10408347.2022.2132374

Ashraf, S. A., Elkhalifa, A., Siddiqui, A. J., Patel, M., Awadelkareem, A. M., Snoussi, M., et al. (2020). Cordycepin for health and wellbeing: A potent bioactive metabolite of an entomopathogenic cordyceps medicinal fungus and its nutraceutical and therapeutic potential. *Molecules* 25, 2735. doi:10.3390/molecules25122735

Backes, E., Pereira, C., Barros, L., Prieto, M. A., Genena, A. K., Barreiro, M. F., et al. (2018). Recovery of bioactive anthocyanin pigments from Ficus carica L. peel by heat, microwave, and ultrasound based extraction techniques. *Food Res. Int. Ott. Ont.)* 113, 197–209. doi:10.1016/j.foodres.2018.07.016

Bai, R., Sun, Q., He, Y., Peng, L., Zhang, Y., Zhang, L., et al. (2022). Ceramic toughening strategies for biomedical applications. *Front. Bioeng. Biotechnol.* 10, 840372. doi:10.3389/fbioe.2022.840372

Balachandran, P., and Govindarajan, R. (2005). Cancer-an ayurvedic perspective. *Pharmacol. Res.* 51, 19–30. doi:10.1016/j.phrs.2004.04.010

Barnes, M., Sulé-Suso, J., Millett, J., and Roach, P. (2023). Fourier transform infrared spectroscopy as a non-destructive method for analysing herbarium specimens. *Biol. Lett.* 19, 20220546. doi:10.1098/rsbl.2022.0546

Benedetti, A., Khoo, J., Sharma, S., Facco, P., Barolo, M., and Zomer, S. (2019). Data analytics on raw material properties to accelerate pharmaceutical drug development. *Int. J. Pharm.* 563, 122–134. doi:10.1016/j.ijpharm.2019.04.002

Boateng, I. D., Kuehnel, L., Daubert, C. R., Agliata, J., Zhang, W., Kumar, R., et al. (2023). Updating the status quo on the extraction of bioactive compounds in agro-products using a two-pot multivariate design. A comprehensive review. *Food Funct.* 14, 569–601. doi:10.1039/d2fo02520e

Boutron, I., Guittet, L., Estellat, C., Moher, D., Hróbjartsson, A., and Ravaud, P. (2007). Reporting methods of blinding in randomized trials assessing nonpharmacological treatments. *PLoS Med.* 4, e61. doi:10.1371/journal.pmed.0040061

Boyd, A. R., Champagne, P., McGinn, P. J., MacDougall, K. M., Melanson, J. E., and Jessop, P. G. (2012). Switchable hydrophilicity solvents for lipid extraction from microalgae for biofuel production. *Bioresour. Technol.* 118, 628–632. doi:10.1016/j.biortech.2012.05.084

Boyd, L. H. (1994). Regulation of drugs and chemicals used by the poultry industry. Good manufacturing practices. *Poult. Sci.* 73, 1419–1422. doi:10.3382/ps.0731419

Braga, F., Pasqualetti, S., Aloisio, E., and Panteghini, M. (2020). The internal quality control in the traceability era. *Clin. Chem. Lab. Med.* 59, 291–300. doi:10.1515/cclm-2020-0371

Brennan, A. A., You, J., and Lydy, M. J. (2009). Comparison of cleanup methods for fipronil and its degradation products in sediment extracts. *TALANTA* 78, 1408–1413. doi:10.1016/j.Talanta.2009.02.034

Brown, A. C. (2017). Liver toxicity related to herbs and dietary supplements: Online table of case reports. Part 2 of 5 series. *Food Chem. Toxicol.* 107, 472–501. doi:10.1016/j.fct.2016.07.001

Burcham, C. L., Florence, A. J., and Johnson, M. D. (2018). Continuous manufacturing in pharmaceutical process development and manufacturing. *Annu. Rev. Chem. Biomol. Eng.* 9, 253–281. doi:10.1146/annurev-chembioeng-060817-084355

Byrd, C. L., Schwartz, S. J., Hedin, N., and Beach, M. (1991). Intravascular techniques for extraction of permanent pacemaker leads. *J. Thorac. Cardiovasc. Surg.* 101, 989–997. doi:10.1016/s0022-5223(19)36615-2

Cai, Z., Wang, C., Zou, L., Liu, X., Chen, J., Tan, M., et al. (2019). Comparison of multiple bioactive constituents in the flower and the caulis of *Lonicera japonica* based on UFLC-QTRAP-MS/MS combined with multivariate statistical analysis. *Molecules* 24, 1936. doi:10.3390/molecules24101936

Campuzano, R., and González-Martínez, S. (2017). Influence of process parameters on the extraction of soluble substances from OFMSW and methane production. *Waste Manag. (New York, N.Y.)* 62, 61–68. doi:10.1016/j.wasman.2017.02.015

Castiglia, S., Adamini, A., Rustichelli, D., Castello, L., Mareschi, K., Pinnetta, G., et al. (2018). Cytokines induced killer cells produced in good manufacturing practices conditions: Identification of the most advantageous and safest expansion method in terms of viability, cellular growth and identity. *J. Transl. Med.* 16, 237. doi:10.1186/s12967-018-1613-5

Chan, S. Y., and Choo, W. S. (2013). Effect of extraction conditions on the yield and chemical properties of pectin from cocoa husks. *Food Chem.* 141, 3752–3758. doi:10.1016/j.foodchem.2013.06.097

Chang, J. (2000). Medicinal herbs: Drugs or dietary supplements. *Biochem. Pharmacol.* 59, 211–219. doi:10.1016/s0006-2952(99)00243-9

Chen, C., Liu, Z., Zou, L., Liu, X., Chai, C., Zhao, H., et al. (2018). Quality evaluation of apocyni veneti folium from different habitats and commercial herbs based on simultaneous determination of multiple bioactive constituents combined with multivariate statistical analysis. *Molecules* 23, 573. doi:10.3390/molecules23030573

Chen, J., Wang, F., Lee, F. S., Wang, X., and Xie, M. (2006). Separation and identification of water-soluble salvianolic acids from Salvia miltiorrhiza Bunge by high-speed counter-current chromatography and ESI-MS analysis. *TALANTA* 69, 172–179. doi:10.1016/j.Talanta.2005.09.041

Chen, R., Liu, F., Zhang, C., Wang, W., Yang, R., Zhao, Y., et al. (2023). Trends in digital detection for the quality and safety of herbs using infrared and Raman spectroscopy. *Front. Plant Sci.* 14, 1128300. doi:10.3389/fpls.2023.1128300

Chen, Y. C., Chen, Y. H., Pan, B. S., Chang, M. M., and Huang, B. M. (2017). Functional study of cordyceps sinensis and cordycepin in male reproduction: A review. *J. Food Drug Anal.* 25, 197–205. doi:10.1016/j.jfda.2016.10.020

Cheng, S. C., Huang, M. Z., and Shiea, J. (2011). Thin layer chromatography/mass spectrometry. *J. Chromatogr. A* 1218, 2700–2711. doi:10.1016/j.chroma.2011.01.077

Cheng, W. J., Yang, H. T., Chiang, C. C., Lai, K. H., Chen, Y. L., Shih, H. L., et al. (2022). Deer velvet antler extracts exert anti-inflammatory and anti-arthritic effects on human rheumatoid arthritis fibroblast-like synoviocytes and distinct mouse arthritis. *Am. J. Chin. Med.* 50, 1617–1643. doi:10.1142/S0192415X22500689

Cho, E. C., and Kim, K. (2020). A comprehensive review of biochemical factors in herbs and their constituent compounds in experimental studies on alopecia. *J. Ethnopharmacol.* 258, 112907. doi:10.1016/j.jep.2020.112907

Chrysant, S. G., and Chrysant, G. S. (2017). Herbs used for the treatment of hypertension and their mechanism of action. *Curr. Hypertens. Rep.* 19, 77. doi:10.1007/s11906-017-0775-5

Cox, S., Cleves, A., Clementel, E., Miles, E., Staffurth, J., and Gwynne, S. (2019). Impact of deviations in target volume delineation - time for a new RTQA approach. *Radiother. Oncol.* 137, 1–8. doi:10.1016/j.radonc.2019.04.012

Crimi, C., Impellizzeri, P., Campisi, R., Nolasco, S., Spanevello, A., and Crimi, N. (2021). Practical considerations for spirometry during the COVID-19 outbreak: Literature review and insights. *Pulmonology* 27, 438–447. doi:10.1016/j.pulmoe.2020.07.011

Cundell, T., Atkins, J. W., and Lau, A. F. (2023). Sterility testing for hematopoietic stem cells. *J. Clin. Microbiol.* 61, e0165422. doi:10.1128/jcm.01654-22

da Cunha, R. S., Amorim, K. S., Gercina, A. C., de Oliveira, A., Dos Santos Menezes, L., Groppo, F. C., et al. (2021). Herbal medicines as anxiolytics prior to third molar surgical extraction. A randomized controlled clinical trial. *Clin. Oral Investig.* 25, 1579–1586. doi:10.1007/s00784-020-03468-1

Dai, Y. L., Li, Y., Wang, Q., Niu, F. J., Li, K. W., Wang, Y. Y., et al. (2022). Chamomile: A review of its traditional uses, chemical constituents, pharmacological activities and quality control studies. *Molecules* 28, 133. doi:10.3390/molecules28010133

Daniel, S., Kis, Z., Kontoravdi, C., and Shah, N. (2022). Quality by Design for enabling RNA platform production processes. *Trends Biotechnol.* 40, 1213–1228. doi:10.1016/j.tibtech.2022.03.012

Davids, J. R., and Bagley, A. M. (2014). Identification of common gait disruption patterns in children with cerebral palsy. *J. Am. Acad. Orthop. Surg.* 22, 782–790. doi:10.5435/JAAOS-22-12-782

Deagle, R. C., Wee, T. E., and Brown, C. M. (2017). Reproducibility in light microscopy: Maintenance, standards and SOPs. *Int. J. Biochem. Cell Biol.* 89, 120–124. doi:10.1016/j.biocel.2017.06.008

Del Bubba, M., Checchini, L., and Lepri, L. (2013). Thin-layer chromatography enantioseparations on chiral stationary phases: A review. *Anal. Bioanal. Chem.* 405, 533–554. doi:10.1007/s00216-012-6514-5

DeSalle, R., Egan, M. G., and Siddall, M. (2005). The unholy trinity: Taxonomy, species delimitation and DNA barcoding. *Philos. Trans. R. Soc. Lond., B, Biol. Sci.* 360, 1905–1916. doi:10.1098/rstb.2005.1722

Deutch, M. R., Grimm, D., Wehland, M., Infanger, M., and Krüger, M. (2019). Bioactive candy: Effects of licorice on the cardiovascular system. *Foods* 8, 495. doi:10.3390/foods8100495

Dina, E., Vontzalidou, A., Cheilari, A., Bagatzounis, P., Agapidou, E., Giannenas, I., et al. (2022). Sustainable use of Greek herbs by-products, as an alternative source of biologically active ingredients for innovative products. *Front. Nutr.* 9, 867666. doi:10.3389/fnut.2022.867666

Ding, L., Luo, X. B., Tang, F., Yuan, J. B., Guo, M., and Yao, S. Z. (2008). Quality control of medicinal herbs Fructus gardeniae, Common Andrographis Herb and their preparations for their active constituents by high-performance liquid chromatography-photodiode array detection-electrospray mass spectrometry. *TALANTA* 74, 1344–1349. doi:10.1016/j.Talanta.2007.09.001

Du, F. Y., Xiao, X. H., Luo, X. J., and Li, G. K. (2009). Application of ionic liquids in the microwave-assisted extraction of polyphenolic compounds from medicinal plants. *TALANTA* 78, 1177–1184. doi:10.1016/j.Talanta.2009.01.040

Dworkin, J. P., Adelman, L. A., Ajluni, T., Andronikov, A. V., Aponte, J. C., Bartels, A. E., et al. (2018). OSIRIS-REx contamination control strategy and implementation. *Space Sci. Rev.* 214, 19. [pii]. doi:10.1007/s11214-017-0439-4

Edberg, S. C., Allen, M. J., and Smith, D. B. (1989). National field evaluation of a defined substrate method for the simultaneous detection of total coliforms and *Escherichia coli* from drinking water: Comparison with presence-absence techniques. *Appl. Environ. Microbiol.* 55, 1003–1008. doi:10.1128/aem.55.4.1003-1008.1989

Ege, B., and Demirkol, M. (2021). Is the only buccal infiltration anesthesia enough for extraction of mandibular anterior incisors and premolar teeth? A split-mouth randomized clinical trial. *Clin. Oral Investig.* 25, 3077–3085. doi:10.1007/s00784-020-03628-3

El Maangar, A., Theisen, J., Penisson, C., Zemb, T., and Gabriel, J. P. (2020). A microfluidic study of synergic liquid-liquid extraction of rare earth elements. *Phys. Chem. Chem. Phys.* 22, 5449–5462. doi:10.1039/c9cp06569e

Elfgen, R., Gehrke, S., and Hollóczki, O. (2020). Ionic liquids as extractants for nanoplastics. *ChemSusChem* 13, 5449–5459. doi:10.1002/cssc.202001749

Ernst, E. (1998). Harmless herbs? A review of the recent literature. *Am. J. Med.* 104, 170–178. doi:10.1016/s0002-9343(97)00397-5

Feldmann, I., and Bondemark, L. (2006). Orthodontic anchorage: A systematic review. *Angle Orthod.* 76, 493–501. doi:10.1043/0003-3219(2006)076[0493:OA]2.0.CO;2

Fillingim, R. B., Loeser, J. D., Baron, R., and Edwards, R. R. (2016). Assessment of chronic pain: Domains, methods, and mechanisms. *J. Pain* 17, T10–T20. doi:10.1016/j.jpain.2015.08.010

Gainza, P., Sverrisson, F., Monti, F., Rodolà, E., Boscaini, D., Bronstein, M. M., et al. (2020). Deciphering interaction fingerprints from protein molecular surfaces using geometric deep learning. *Nat. Methods* 17, 184–192. doi:10.1038/s41592-019-0666-6

Giacometti, J., Bursać Kovačević, D., Putnik, P., Gabrić, D., Bilušić, T., Krešić, G., et al. (2018). Extraction of bioactive compounds and essential oils from mediterranean herbs by conventional and green innovative techniques: A review. *Food Res. Int. Ott. Ont.)* 113, 245–262. doi:10.1016/j.foodres.2018.06.036

Gil-Díaz, M., Luchsinger-Heitmann, A., García-Gonzalo, P., Alonso, J., and Lobo, M. C. (2021). Selecting efficient methodologies for estimation of as and Hg availability in a brownfield. *Environ. Pollut. (Barking, Essex 1987)* 270, 116290. doi:10.1016/j.envpol.2020.116290

Gollahon, L. S., and Holt, S. E. (2000). Alternative methods of extracting telomerase activity from human tumor samples. *Cancer Lett.* 159, 141–149. doi:10.1016/s0304-3835(00)00544-9

Gong, L., Xie, J. B., Luo, Y., Qiu, Z. D., Liu, J. R., Mei, N. J., et al. (2023). Research progress of quality control for the seed of Ziziphus jujuba var. spinosa (Bunge) Hu ex H.F. Chow (Suan-Zao-Ren) and its proprietary Chinese medicines. *J. Ethnopharmacol.* 307, 116204. doi:10.1016/j.jep.2023.116204

González, F., Quintero, J., Del Río, R., and Mahn, A. (2021). Optimization of an extraction process to obtain a food-grade sulforaphane-rich extract from broccoli (*Brassica oleracea* var. italica). *Molecules* 26, 4042. doi:10.3390/molecules26134042

Gupta, A. K., and Sinha, S. (2007). Assessment of single extraction methods for the prediction of bioavailability of metals to Brassica juncea L. Czern. (var. Vaibhav) grown on tannery waste contaminated soil. *J. Hazard. Mat.* 149, 144–150. doi:10.1016/j.jhazmat.2007.03.062

Harper, D. S., Osborn, J. C., Clayton, R., and Hefferren, J. J. (1987). Modification of food cariogenicity in rats by mineral-rich concentrates from milk. *J. Dent. Res.* 66, 42–45. doi:10.1177/00220345870660010901

Hawthorne, S. B., Grabanski, C. B., Martin, E., and Miller, D. J. (2000). Comparisons of soxhlet extraction, pressurized liquid extraction, supercritical fluid extraction and subcritical water extraction for environmental solids: Recovery, selectivity and effects on sample matrix. *J. Chromatogr. A* 892, 421–433. doi:10.1016/s0021-9673(00)00091-1

Hernandez, G. A., and Perera, R. M. (2022). Autophagy in cancer cell remodeling and quality control. *Mol. Cell* 82, 1514–1527. doi:10.1016/j.molcel.2022.03.023

Hervert, C. J., Alles, A. S., Martin, N. H., Boor, K. J., and Wiedmann, M. (2016). Evaluation of different methods to detect microbial hygiene indicators relevant in the dairy industry. *J. Dairy Sci.* 99, 7033–7042. doi:10.3168/jds.2016-11074

Hu, G., Li, X., Zhang, J., Zhang, L., Qi, J., and Yu, B. (2021). An integrated strategy for the identification and screening of anti-allergy components from natural products based on calcium fluctuations and cell extraction coupled with HPLC-Q-TOF-MS. *Anal. Bioanal. Chem.* 413, 6253–6266. doi:10.1007/s00216-021-03580-5

Huaulmé, A., Jannin, P., Reche, F., Faucheron, J. L., Moreau-Gaudry, A., and Voros, S. (2020). Offline identification of surgical deviations in laparoscopic rectopexy. *Artif. Intell. Med. Conf. Artif. Intell. Med.* 104, 101837. doi:10.1016/j.artmed.2020.101837

Hussain, S. A., Panjagari, N. R., Singh, R. R., and Patil, G. R. (2015). Potential herbs and herbal nutraceuticals: Food applications and their interactions with food components. *Crit. Rev. Food Sci. Nutr.* 55, 94–122. doi:10.1080/10408398.2011.649148

Jacquemart, R., Vandersluis, M., Zhao, M., Sukhija, K., Sidhu, N., and Stout, J. (2016). A single-use strategy to enable manufacturing of affordable biologics. *Comput. Struct. Biotechnol. J.* 14, 309–318. doi:10.1016/j.csbj.2016.06.007

Jaiswal, Y., Liang, Z., and Zhao, Z. (2016). Botanical drugs in ayurveda and traditional Chinese medicine. *J. Ethnopharmacol.* 194, 245–259. doi:10.1016/j.jep.2016.06.052

Jenner, L. C., Rotchell, J. M., Bennett, R. T., Cowen, M., Tentzeris, V., and Sadofsky, L. R. (2022). Detection of microplastics in human lung tissue using μFTIR spectroscopy. *Sci. Total Environ.* 831, 154907. doi:10.1016/j.scitotenv.2022.154907

Jin, Y., Ma, Y., Xie, W., Hou, L., Xu, H., Zhang, K., et al. (2018). UHPLC-Q-TOF-MS/MS-oriented characteristic components dataset and multivariate statistical techniques for the holistic quality control of Usnea. *RSC Adv.* 8, 15487–15500. doi:10.1039/c8ra00081f

Joshi, V. K., Joshi, A., and Dhiman, K. S. (2017). The Ayurvedic Pharmacopoeia of India, development and perspectives. *J. Ethnopharmacol.* 197, 32–38. doi:10.1016/j.jep.2016.07.030

Kabak, B., and Dobson, A. D. (2017). Mycotoxins in spices and herbs-An update. *Crit. Rev. Food Sci. Nutr.* 57, 18–34. doi:10.1080/10408398.2013.772891

Kaefer, C. M., and Milner, J. A. (2008). The role of herbs and spices in cancer prevention. *J. Nutr. Biochem.* 19, 347–361. doi:10.1016/j.jnutbio.2007.11.003

Kalkan, E., Maness, N. O., and Chrz, D. R. (2019). Partial propane extraction of aromatic compounds from dehydrated basils (Ocimum Lamiaceae). *J. Sci. Food Agric.* 99, 3776–3784. doi:10.1002/jsfa.9592

Kankanamalage, T. N., Dharmadasa, R. M., Abeysinghe, D. C., and Wijesekara, R. G. (2014). A survey on medicinal materials used in traditional systems of medicine in Sri Lanka. *J. Ethnopharmacol.* 155, 679–691. doi:10.1016/j.jep.2014.06.016

Kapadia, P., Newell, A. S., Cunningham, J., Roberts, M. R., and Hardy, J. G. (2022). Extraction of high-value chemicals from plants for technical and medical applications. *Int. J. Mol. Sci.* 23, 10334. doi:10.3390/ijms231810334

Karsch-Völk, M., Barrett, B., Kiefer, D., Bauer, R., Ardjomand-Woelkart, K., and Linde, K. (2014). Echinacea for preventing and treating the common cold. *Cochrane database Syst. Rev.* 2014, CD000530. doi:10.1002/14651858.CD000530.pub3

Ketai, W., Huitao, L., Yunkun, Z., Xingguo, C., Zhide, H., Yucheng, S., et al. (2000). Separation and determination of alantolactone and isoalantolactone in traditional Chinese herbs by capillary electrophoresis. *Talanta* 52, 1001–1005. doi:10.1016/s0039-9140(00)00467-7

Kjelkenes, R., Wolfers, T., Alnæs, D., Norbom, L. B., Voldsbekk, I., Holm, M., et al. (2022). Deviations from normative brain white and gray matter structure are associated with psychopathology in youth. *Dev. Cogn. Neurosci.* 58, 101173. doi:10.1016/j.dcn.2022.101173

Lai, J. J., Chau, Z. L., Chen, S. Y., Hill, J. J., Korpany, K. V., Liang, N. W., et al. (2022). Exosome processing and characterization approaches for research and technology development. *Adv. Sci. (Weinheim, Baden-Wurttemberg, Ger.* 9, e2103222. doi:10.1002/advs.202103222

Lee, E. J., Lee, S. C., Lee, K., Cha, J. Y., Han, Y. N., Kim, S. G., et al. (2023). Properties of river organic carbon affected by wastewater treatment plants. *Sci. Total Environ.* 858, 159761. doi:10.1016/j.scitotenv.2022.159761

Lesch, H. P., Valonen, P., and Karhinen, M. (2021). Evaluation of the single-use fixed-bed bioreactors in scalable virus production. *Biotechnol. J.* 16, e2000020. doi:10.1002/biot.202000020

Levy, J. H., Neal, M. D., and Herman, J. H. (2018). Bacterial contamination of platelets for transfusion: Strategies for prevention. *Crit. care (London, Engl.* 22, 271. doi:10.1186/s13054-018-2212-9

Li, M., Xu, J., Zheng, Q., Guo, C., and Chen, Y. (2022). Chemical-based surface plasmon resonance imaging of fingerprints. *Anal. Chem.* 94, 7238–7245. doi:10.1021/acs.analchem.2c00389

Li, X., Yang, Y., Henry, R. J., Rossetto, M., Wang, Y., and Chen, S. (2015). Plant DNA barcoding: From gene to genome. *Biol. Rev. Camb Philos. Soc.* 90, 157–166. doi:10.1111/brv.12104

Liang, X., Dang, W., Yang, G., and Zhang, Y. (2023). Environmental feasibility evaluation of cement co-production using classified domestic waste as alternative raw material and fuel: A life cycle perspective. *J. Environ. Manag.* 326, 116726. doi:10.1016/j.jenvman.2022.116726

Ling, J., Xu, Y., Lu, C., Hou, W., Liu, Q., Wang, F., et al. (2021). Microbial contamination control mechanism in lipid production using distillery wastewater and oleaginous yeast - antimicrobial compounds in wastewater as a double-edged sword. *J. Environ. Manag.* 291, 112672. doi:10.1016/j.jenvman.2021.112672

Liu, H., Lu, X., Hu, Y., and Fan, X. (2020). Chemical constituents of Panax ginseng and Panax notoginseng explain why they differ in therapeutic efficacy. *Pharmacol. Res.* 161, 105263. doi:10.1016/j.phrs.2020.105263

Liu, X., Zhang, M., He, L., and Li, Y. (2012). Chinese herbs combined with Western medicine for severe acute respiratory syndrome (SARS). *Cochrane database Syst. Rev.* 10, CD004882. doi:10.1002/14651858.CD004882.pub3

Liu, X., Zhang, M., He, L., Li, Y. P., and Kang, Y. K. (2006). Chinese herbs combined with Western medicine for severe acute respiratory syndrome (SARS). *Cochrane database Syst. Rev.* 2006, CD004882. doi:10.1002/14651858.CD004882.pub2

Liu, Y., Yin, H., and Chen, K. (2013). Platelet proteomics and its advanced application for research of blood stasis syndrome and activated blood circulation herbs of Chinese medicine. *Sci. China Life Sci.* 56, 1000–1006. doi:10.1007/s11427-013-4551-8

Lo, Y. T., and Shaw, P. C. (2019). Application of next-generation sequencing for the identification of herbal products. *Biotechnol. Adv.* 37, 107450. doi:10.1016/j.biotechadv.2019.107450

Lockwood, T. E., Westerhausen, M. T., and Doble, P. A. (2021). Pew(2): Open-Source imaging software for laser ablation-inductively coupled plasma-mass spectrometry. *Anal. Chem.* 93, 10418–10423. doi:10.1021/acs.analchem.1c02138

Lou, H., Lin, J., Guo, L., Wang, X., Tian, S., Liu, C., et al. (2019). Advances in research on Cordyceps militaris degeneration. *Appl. Microbiol. Biotechnol.* 103, 7835–7841. doi:10.1007/s00253-019-10074-z

Ma, K., Wu, Z. Z., Wang, G. L., and Yang, X. P. (2021). Separation and purification of pyrroloquinoline quinone from Gluconobacter oxydans fermentation broth using supramolecular solvent complex extraction. *Food Chem.* 361, 130067. doi:10.1016/j.foodchem.2021.130067

Ma, L., Yang, Z., Kong, Q., and Wang, L. (2017). Extraction and determination of arsenic species in leafy vegetables: Method development and application. *Food Chem.* 217, 524–530. doi:10.1016/j.foodchem.2016.09.015

Ma, P. Y., Li, X. Y., Wang, Y. L., Lang, D. Q., Liu, L., Yi, Y. K., et al. (2022). Natural bioactive constituents from herbs and nutraceuticals promote browning of white adipose tissue. *Pharmacol. Res.* 178, 106175. doi:10.1016/j.phrs.2022.106175

Mager, S. R., Oomen, M. H., Morente, M. M., Ratcliffe, C., Knox, K., Kerr, D. J., et al. (2007). Standard operating procedure for the collection of fresh frozen tissue samples. *Eur. J. cancer* 43, 828–834. doi:10.1016/j.ejca.2007.01.002

Malherbe, C. J., De Beer, D., and Joubert, E. (2012). Development of on-line high performance liquid chromatography (HPLC)-biochemical detection methods as tools in the identification of bioactives. *Int. J. Mol. Sci.* 13, 3101–3133. doi:10.3390/ijms13033101

Melethil, S. (2006). Proposed rule: Current good manufacturing practice in manufacturing, packing, or holding dietary ingredients and dietary supplements. *LIFE Sci.* 78, 2049–2053. doi:10.1016/j.lfs.2005.12.020

Morgan, L., New, S., Robertson, E., Collins, G., Rivero-Arias, O., Catchpole, K., et al. (2015). Effectiveness of facilitated introduction of a standard operating procedure into routine processes in the operating theatre: A controlled interrupted time series. *BMJ Qual. Saf.* 24, 120–127. doi:10.1136/bmjqs-2014-003158

Motti, R. (2021). Wild plants used as herbs and spices in Italy: An ethnobotanical review. *Plants (Basel, Switz.* 10, 563. doi:10.3390/plants10030563

Mulinacci, N., Innocenti, M., Bellumori, M., Giaccherini, C., Martini, V., and Michelozzi, M. (2011). Storage method, drying processes and extraction procedures strongly affect the phenolic fraction of rosemary leaves: An HPLC/DAD/MS study. *TALANTA* 85, 167–176. doi:10.1016/j.Talanta.2011.03.050

Noh, W., Kim, J., Lee, S. J., Ryu, B. G., and Kang, C. M. (2018). Harvesting and contamination control of microalgae Chlorella ellipsoidea using the bio-polymeric flocculant α-poly-l-lysine. *Bioresour. Technol.* 249, 206–211. doi:10.1016/j.biortech.2017.09.157

Olsson, P., Holmbäck, J., and Herslöf, B. (2014). A single step reversed-phase high performance liquid chromatography separation of polar and non-polar lipids. *J. Chromatogr. A* 1369, 105–115. doi:10.1016/j.chroma.2014.10.010

Omeje, K. O., Ezema, B. O., Okonkwo, F., Onyishi, N. C., Ozioko, J., Rasaq, W. A., et al. (2021). Quantification of heavy metals and pesticide residues in widely consumed Nigerian food crops using atomic absorption spectroscopy (AAS) and gas chromatography (GC). *Toxins (Basel)* 13, 870. doi:10.3390/toxins13120870

Onishi, T., Kadohira, T., and Watanabe, I. (2018). Relation extraction with weakly supervised learning based on process-structure-property-performance reciprocity. *Sci. Technol. Adv. Mater* 19, 649–659. doi:10.1080/14686996.2018.1500852

Ortegón, S., Peñaranda, P. A., Rodríguez, C. F., Noguera, M. J., Florez, S. L., Cruz, J. C., et al. (2022). Magnetic torus microreactor as a novel device for sample treatment via solid-phase microextraction coupled to graphite furnace atomic absorption spectroscopy: A route for arsenic pre-concentration. *Molecules* 27, 6198. doi:10.3390/molecules27196198

Osman, A. G., Haider, S., Chittiboyina, A. G., and Khan, I. A. (2019). Utility of alkaloids as chemical and biomarkers for quality, efficacy, and safety assessment of botanical ingredients. *Phytomedicine* 54, 347–356. doi:10.1016/j.phymed.2018.03.064

Pan, C., Chen, S., Hao, S., and Yang, X. (2019). Effect of low-temperature preservation on quality changes in pacific white shrimp, Litopenaeus vannamei: A review. *J. Sci. Food Agric.* 99, 6121–6128. doi:10.1002/jsfa.9905

Pan, M., Pei, W., Yao, Y., Dong, L., and Chen, J. (2018). Rapid and integrated quality assessment of organic-inorganic composite herbs by FTIR spectroscopy-global chemical fingerprints identification and multiple marker components quantification of indigo naturalis (qing dai). *Molecules* 23, 2743. doi:10.3390/molecules23112743

Panteghini, M., Ceriotti, F., Schumann, G., and Siekmann, L. (2001). Establishing a reference system in clinical enzymology. *Clin. Chem. Lab. Med.* 39, 795–800. doi:10.1515/CCLM.2001.131

Parr, L. F., Anderson, A. L., Glennon, B. K., and Fetherston, P. (2001). Quality-control issues on high-resolution diagnostic monitors. *J. Digit. Imaging* 14, 22–26. doi:10.1007/BF03190289

Pihlström, T., Isaac, G., Waldebäck, M., Osterdahl, B. G., and Markides, K. E. (2002). Pressurised fluid extraction (PFE) as an alternative general method for the determination of pesticide residues in rape seed. *Analyst* 127, 554–559. doi:10.1039/b110814j

Poole, C. F. (2003). Thin-layer chromatography: Challenges and opportunities. *J. Chromatogr. A* 1000, 963–984. doi:10.1016/s0021-9673(03)00435-7

Pradhan, R., Hoaglin, D. C., Cornell, M., Liu, W., Wang, V., and Yu, H. (2019). Automatic extraction of quantitative data from ClinicalTrials.gov to conduct meta-analyses. *J. Clin. Epidemiol.* 105, 92–100. doi:10.1016/j.jclinepi.2018.08.023

Prasad, S., Kulshreshtha, A., Lall, R., and Gupta, S. C. (2021). Inflammation and ROS in arthritis: management by ayurvedic medicinal plants. *Food Funct.* 12, 8227–8247. doi:10.1039/d1fo01078f

Prata, J. C., Reis, V., da Costa, J. P., Mouneyrac, C., Duarte, A. C., and Rocha-Santos, T. (2021). Contamination issues as a challenge in quality control and quality assurance in microplastics analytics. *J. Hazard. Mat.* 403, 123660. doi:10.1016/j.jhazmat.2020.123660

Qin, Y., Wang, J. B., Zhao, Y. L., Shan, L. M., Li, B. C., Fang, F., et al. (2012). Establishment of a bioassay for the toxicity evaluation and quality control of Aconitum herbs. *J. Hazard. Mat.* 199-200, 350–357. doi:10.1016/j.jhazmat.2011.11.029

Qu, C. C., Sun, X. Y., Sun, W. X., Cao, L. X., Wang, X. Q., and He, Z. Z. (2021). Flexible wearables for plants. *Small* 17, e2104482. doi:10.1002/smll.202104482

Qu, Z., Steinvall, E., Ghorbani, R., and Schmidt, F. M. (2016). Tunable diode laser atomic absorption spectroscopy for detection of potassium under optically thick conditions. *Anal. Chem.* 88, 3754–3760. doi:10.1021/acs.analchem.5b04610

Raeisossadati, M. J., Danesh, N. M., Borna, F., Gholamzad, M., Ramezani, M., Abnous, K., et al. (2016). Lateral flow based immunobiosensors for detection of food contaminants. *Biosens. Bioelectron.* 86, 235–246. doi:10.1016/j.bios.2016.06.061

Rahath Kubra, I., Kumar, D., and Jagan Mohan Rao, L. (2016). Emerging trends in microwave processing of spices and herbs. *Crit. Rev. Food Sci. Nutr.* 56, 2160–2173. doi:10.1080/10408398.2013.818933

Ranasinghe, S., Ansumana, R., Lamin, J. M., Bockarie, A. S., Bangura, U., Buanie, J. A., et al. (2015). Herbs and herbal combinations used to treat suspected malaria in Bo, Sierra Leone. *J. Ethnopharmacol.* 166, 200–204. doi:10.1016/j.jep.2015.03.028

Reischauer, C., Staempfli, P., Jaermann, T., and Boesiger, P. (2009). Construction of a temperature-controlled diffusion phantom for quality control of diffusion measurements. *J. Magn. Reson Imaging* 29, 692–698. doi:10.1002/jmri.21665

Rodsamran, P., and Sothornvit, R. (2019). Microwave heating extraction of pectin from lime peel: Characterization and properties compared with the conventional heating method. *Food Chem.* 278, 364–372. doi:10.1016/j.foodchem.2018.11.067

Safra, P. (2019). Importance of photographic standardization. *Am. J. Orthod. Dentofac. Orthop.* 155, 756–757. doi:10.1016/j.ajodo.2019.03.014

Saini, R., Sharma, N., Oladeji, O. S., Sourirajan, A., Dev, K., Zengin, G., et al. (2022). Traditional uses, bioactive composition, pharmacology, and toxicology of Phyllanthus emblica fruits: A comprehensive review. *J. Ethnopharmacol.* 282, 114570. doi:10.1016/j.jep.2021.114570

Saletnik, A., Saletnik, B., and Puchalski, C. (2021). Overview of popular techniques of Raman spectroscopy and their potential in the study of plant tissues. *Molecules* 26, 1537. doi:10.3390/molecules26061537

Sargeant, J. M., Brennan, M. L., and O'Connor, A. M. (2022). Levels of evidence, quality assessment, and risk of bias: Evaluating the internal validity of primary research. *Front. Vet. Sci.* 9, 960957. doi:10.3389/fvets.2022.960957

Schmidt, R. L., Moore, R. A., Walker, B. S., and Rudolf, J. W. (2023). Precision quality control: A dynamic model for risk-based analysis of analytical quality. *Clin. Chem. Lab. Med.* 61, 679–687. doi:10.1515/cclm-2022-1094

Schwabl, H., and Vennos, C. (2015). From medical tradition to traditional medicine: A Tibetan formula in the European framework. *J. Ethnopharmacol.* 167, 108–114. doi:10.1016/j.jep.2014.10.033

Senapati, A., Basak, S., and Rangan, L. (2022). A review on application of DNA barcoding technology for rapid molecular diagnostics of adulterants in herbal medicine. *Drug Saf.* 45, 193–213. doi:10.1007/s40264-021-01133-4

Seo, C. S., and Shin, H. K. (2022). Simultaneous analysis of 19 marker components for quality control of oncheong-eum using HPLC-DAD. *Molecules* 27, 2992. doi:10.3390/molecules27092992

Shaikh, A. S., Thomas, A. B., and Chitlange, S. S. (2020). Herb-drug interaction studies of herbs used in treatment of cardiovascular disorders-A narrative review of preclinical and clinical studies. *Phytother. Res.* 34, 1008–1026. doi:10.1002/ptr.6585

Shao, H., Dong, H., Liu, Y., Zhou, G., and Guan, X. (2022). Chemiluminescence quenching capacity as a surrogate for total organic carbon in wastewater. *J. Hazard. Mat.* 440, 129765. doi:10.1016/j.jhazmat.2022.129765

Sharifi-Rad, M., Mnayer, D., Morais-Braga, M., Carneiro, J., Bezerra, C. F., Coutinho, H., et al. (2018). Echinacea plants as antioxidant and antibacterial agents: From traditional medicine to biotechnological applications. *Phytother. Res.* 32, 1653–1663. doi:10.1002/ptr.6101

Shukla, A. A., and Gottschalk, U. (2013). Single-use disposable technologies for biopharmaceutical manufacturing. *Trends Biotechnol.* 31, 147–154. doi:10.1016/j.tibtech.2012.10.004

Silva, D., Silva, M. S., Coelho, T., Dantas, C., Lopes Júnior, C. A., Caldas, N. M., et al. (2022). Combining high intensity ultrasound and experimental design to improve carotenoid extraction efficiency from Buriti (Mauritia flexuosa). *Ultrason. Sonochem* 88, 106076. doi:10.1016/j.ultsonch.2022.106076

Simpson, M. J., and McKelvie, J. R. (2009). Environmental metabolomics: new insights into earthworm ecotoxicity and contaminant bioavailability in soil. *Anal. Bioanal. Chem.* 394, 137–149. doi:10.1007/s00216-009-2612-4

Sinha, R., Abnet, C. C., White, O., Knight, R., and Huttenhower, C. (2015). The microbiome quality control project: baseline study design and future directions. *Genome Biol.* 16, 276. doi:10.1186/s13059-015-0841-8

Smith, W. S. (2020). Standardizing brain death globally. *JAMA Neurol.* 77, 1353–1354. doi:10.1001/jamaneurol.2020.1243

Song, P., Zhou, F., Li, F., Han, Z., Wang, L., Xu, J., et al. (2021). Superfine pulverisation pretreatment to enhance crystallinity of cellulose from Lycium barbarum L. leaves. *Carbohydr. Polym.* 253, 117207. doi:10.1016/j.carbpol.2020.117207

Sontag, G., Pinto, M. I., Noronha, J. P., and Burrows, H. D. (2019). Analysis of food by high performance liquid chromatography coupled with coulometric detection and related techniques: A review. *J. Agric. Food Chem.* 67, 4113–4144. doi:10.1021/acs.jafc.9b00003

Speltini, A., Merlo, F., Maraschi, F., Villani, L., and Profumo, A. (2021). HA-C@silica sorbent for simultaneous extraction and clean-up of steroids in human plasma followed by HPLC-MS/MS multiclass determination. *TALANTA* 221, 121496. doi:10.1016/j.Talanta.2020.121496

Spineli, L. M. (2017). Missing binary data extraction challenges from Cochrane reviews in mental health and Campbell reviews with implications for empirical research. *Res. Synth. Methods* 8, 514–525. doi:10.1002/jrsm.1268

Sridharan, B., Mohan, N., Berkland, C. J., and Detamore, M. S. (2016). Material characterization of microsphere-based scaffolds with encapsulated raw materials. *Mater Sci. Eng. C Mater Biol. Appl.* 63, 422–428. doi:10.1016/j.msec.2016.02.038

Stringham, R. W., Lynam, K. G., Mrozinski, P., Kilby, G., Pelczer, I., and Kraml, C. (2009). High performance liquid chromatographic evaluation of artemisinin, raw material in the synthesis of artesunate and artemether. *J. Chromatogr. A* 1216, 8918–8925. doi:10.1016/j.chroma.2009.10.056

Tao, Y., Bao, J., Zhu, F., Pan, M., Liu, Q., and Wang, P. (2023). Ethnopharmacology of rubus idaeus linnaeus: A critical review on ethnobotany, processing methods, phytochemicals, pharmacology and quality control. *J. Ethnopharmacol.* 302, 115870. doi:10.1016/j.jep.2022.115870

Tasfiyati, A. N., Antika, L. D., Dewi, R. T., Septama, A. W., Sabarudin, A., and Ernawati, T. (2022). An experimental design approach for the optimization of scopoletin extraction from *Morinda citrifolia* L. using accelerated solvent extraction. *TALANTA* 238, 123010. doi:10.1016/j.Talanta.2021.123010

Tsiaka, T., Lantzouraki, D. Z., Polychronaki, G., Sotiroudis, G., Kritsi, E., Sinanoglou, V. J., et al. (2023). Optimization of ultrasound- and microwave-assisted extraction for the determination of phenolic compounds in peach byproducts using experimental design and liquid chromatography-tandem mass spectrometry. *Molecules* 28, 518. doi:10.3390/molecules28020518

Varol, M., and Sünbül, M. R. (2017). Organochlorine pesticide, antibiotic and heavy metal residues in mussel, crayfish and fish species from a reservoir on the Euphrates River, Turkey. *Environ. Pollut. (Barking, Essex 1987)* 230, 311–319. doi:10.1016/j.envpol.2017.06.066

Velagaleti, R., Burns, P. K., Gill, M., and Prothro, J. (2002). Impact of current good manufacturing practices and emission regulations and guidances on the discharge of pharmaceutical chemicals into the environment from manufacturing, use, and disposal. *Environ. Health Perspect.* 110, 213–220. doi:10.1289/ehp.02110213

Vestal, M. L. (1984). High-performance liquid chromatography-mass spectrometry. *Science* 226, 275–281. doi:10.1126/science.6385251

Wan, Q., Yiner-Lee Leemaqz, S., Pederson, S. M., McCullough, D., McAninch, D. C., Jankovic-Karasoulos, T., et al. (2019). Quality control measures for placental sample purity in DNA methylation array analyses. *Placenta* 88, 8–11. doi:10.1016/j.placenta.2019.09.006

Wang, X., and Liu, Z. (2014). Prevention and treatment of viral respiratory infections by traditional Chinese herbs. *Chin. Med. J.* 127, 1344–1350. doi:10.3760/cma.j.issn.0366-6999.20132029

Wang, Y. Y., Sun, Y. P., Yang, B. Y., Wang, Q. H., and Kuang, H. X. (2022). Application of metabolomics and network analysis to reveal the ameliorating effect of four typical "hot" property herbs on hypothyroidism rats. *Front. Pharmacol.* 13, 955905. doi:10.3389/fphar.2022.955905

Wasalathanthri, D. P., Rehmann, M. S., Song, Y., Gu, Y., Mi, L., Shao, C., et al. (2020). Technology outlook for real-time quality attribute and process parameter monitoring in biopharmaceutical development-A review. *Biotechnol. Bioeng.* 117, 3182–3198. doi:10.1002/bit.27461

Wibowo, S., Grauwet, T., Kebede, B. T., Hendrickx, M., and Van Loey, A. (2015). Study of chemical changes in pasteurised orange juice during shelf-life: A fingerprinting-kinetics evaluation of the volatile fraction. *Food Res. Int. Ott. Ont.)* 75, 295–304. doi:10.1016/j.foodres.2015.06.020

Williams, D. J., Thomas, R. J., Hourd, P. C., Chandra, A., Ratcliffe, E., Liu, Y., et al. (2012). Precision manufacturing for clinical-quality regenerative medicines. *Philos. Trans. A Math. Phys. Eng. Sci.* 370, 3924–3949. doi:10.1098/rsta.2011.0049

Wiseman, R. L., Mesgarzadeh, J. S., and Hendershot, L. M. (2022). Reshaping endoplasmic reticulum quality control through the unfolded protein response. *Mol. Cell* 82, 1477–1491. doi:10.1016/j.molcel.2022.03.025

Wolle, M. M., and Conklin, S. D. (2018). Speciation analysis of arsenic in seafood and seaweed: Part I-evaluation and optimization of methods. *Anal. Bioanal. Chem.* 410, 5675–5687. doi:10.1007/s00216-018-0906-0

Woolman, M., and Liu, K. (2022). Simplified analysis and expanded profiles of avenanthramides in oat grains. *Foods* 11, 560. doi:10.3390/foods11040560

Wright, J. F. (2021). Quality control testing, characterization and critical quality attributes of adeno-associated virus vectors used for human gene therapy. *Biotechnol. J.* 16, e2000022. doi:10.1002/biot.202000022

Wu, F., Li, H., Jin, L., Li, X., Ma, Y., You, J., et al. (2013). Deer antler base as a traditional Chinese medicine: A review of its traditional uses, chemistry and pharmacology. *J. Ethnopharmacol.* 145, 403–415. doi:10.1016/j.jep.2012.12.008

Wu, T., Chen, X., Duan, X., Juan, N., Liu, G., Qiao, J., et al. (2005). Chinese medicinal herbs for acute bronchitis. *Cochrane database Syst. Rev.* 2005, CD004560. doi:10.1002/14651858.CD004560.pub2

Xiao, Z., Yang, L., Chen, C., Chen, D., and Zhou, X. (2022). Redox reaction between solid-phase humins and Fe(III) compounds: Toward a further understanding of the redox properties of humin and its possible environmental effects. *J. Environ. Manag.* 310, 114793. doi:10.1016/j.jenvman.2022.114793

Xie, F., and Dreisinger, D. (2009). Studies on solvent extraction of copper and cyanide from waste cyanide solution. *J. Hazard. Mat.* 169, 333–338. doi:10.1016/j.jhazmat.2009.03.102

Xie, Y. Y., Xiao, X., Luo, J. M., Fu, C., Wang, Q. W., Wang, Y. M., et al. (2014). Integrating qualitative and quantitative characterization of traditional Chinese medicine injection by high-performance liquid chromatography with diode array detection and tandem mass spectrometry. *J. Sep. Sci.* 37, 1438–1447. doi:10.1002/jssc.201400129

Xiong, C., Huang, C. H., Wu, L., Xu, R., Xue, J. P., Liu, Z. G., et al. (2022). Identification of Andrographis Herba and its common products using mini-barcode. *Chin. J. Nat. Med.* 20, 393–400. doi:10.1016/S1875-5364(22)60157-2

Xiong, R., Li, Y., Zheng, K., Zhang, T., Gao, M., Li, Y., et al. (2019). Er Shen Wan extract alleviates polyuria and regulates AQP 2 and AVPR 2 in a rat model of spleen-kidney Yang deficiency-induced diarrhea. *Biomed. Pharmacother.* 110, 302–311. doi:10.1016/j.biopha.2018.11.147

Yago, M., and Pla, C. (2020). Reference-mean-centered statistical quality control. *Clin. Chem. Lab. Med.* 58, 1517–1523. doi:10.1515/cclm-2019-1034

Yang, S., Yang, X., and Zhang, H. (2020). Extracellular polysaccharide biosynthesis in Cordyceps. *Crit. Rev. Microbiol.* 46, 359–380. doi:10.1080/1040841X.2020.1794788

Yin, F., Song, Z., He, Z., Qin, B., John, G. F., Zhang, L., et al. (2022). Chemical fingerprinting and characterization of spilled oils and burnt soot particles - a case study on the Sanchi oil tanker collision in the East China Sea. *Sci. Total Environ.* 824, 153896. doi:10.1016/j.scitotenv.2022.153896

York, M. K., Baron, E. J., Clarridge, J. E., Thomson, R. B., and Weinstein, M. P. (2000). Multilaboratory validation of rapid spot tests for identification of *Escherichia coli*. *J. Clin. Microbiol.* 38, 3394–3398. doi:10.1128/JCM.38.9.3394-3398.2000

Yu, Y., Jin, Y., Wang, F., Yan, J., Qi, Y., and Ye, M. (2017). Protein digestomic analysis reveals the bioactivity of deer antler velvet in simulated gastrointestinal digestion. *Food Res. Int. Ott. Ont.)* 96, 182–190. doi:10.1016/j.foodres.2017.04.002

Yuan, H., Ma, Q., Ye, L., and Piao, G. (2016). The traditional medicine and modern medicine from natural products. *Molecules* 21, 559. doi:10.3390/molecules21050559

Zhang, B., Gao, Y., Zhang, L., and Zhou, Y. (2021). The plant cell wall: Biosynthesis, construction, and functions. *J. Integr. Plant Biol.* 63, 251–272. doi:10.1111/jipb.13055

Zhang, D. Y., Peng, R. Q., Wang, X., Zuo, H. L., Lyu, L. Y., Yang, F. Q., et al. (2022). A network pharmacology-based study on the quality control markers of antithrombotic herbs: Using Salvia miltiorrhiza - ligusticum chuanxiong as an example. *J. Ethnopharmacol.* 292, 115197. doi:10.1016/j.jep.2022.115197

Zhao, M., Dai, Y., Li, Q., Li, P., Qin, X. M., and Chen, S. (2018). A practical quality control method for saponins without UV absorption by UPLC-QDA. *Front. Pharmacol.* 9, 1377. doi:10.3389/fphar.2018.01377

Zhao, N., Liu, D., Wang, Y., Zhang, X., and Zhang, L. (2022). Screening and identification of anti-acetylcholinesterase ingredients from Tianzhi granule based on ultrafiltration combined with ultra-performance liquid chromatography-mass spectrometry and *in silico* analysis. *J. Ethnopharmacol.* 298, 115641. doi:10.1016/j.jep.2022.115641

Zhou, S. S., Hu, J. W., Kong, M., Xu, J. D., Shen, H., Chen, H. B., et al. (2019). Less SO(2) residue may not indicate higher quality, better efficacy and weaker toxicity of sulfur-fumigated herbs: Ginseng, a pilot study. *J. Hazard. Mat.* 364, 376–387. doi:10.1016/j.jhazmat.2018.10.038

Zhu, X. R., Wang, H., Sun, J., Yang, B., Duan, X. W., and Jiang, Y. M. (2019). Pericarp and seed of litchi and longan fruits: Constituent, extraction, bioactive activity, and potential utilization. *J. Zhejiang Univ. Sci. B* 20, 503–512. doi:10.1631/jzus.B1900161

Zhu, X., Su, Q., Cai, J., and Yang, J. (2006). Optimization of microwave-assisted solvent extraction for volatile organic acids in tobacco and its comparison with conventional extraction methods. *Anal. Chim. Acta* 579, 88–94. doi:10.1016/j.aca.2006.07.005

frontiers | Frontiers in Pharmacology

TYPE Original Research
PUBLISHED 03 January 2024
DOI 10.3389/fphar.2023.1230861

Check for updates

OPEN ACCESS

EDITED BY
Jian-Bo Yang,
National Institutes for Food and Drug Control, China

REVIEWED BY
Huaben Bo,
Guangdong Pharmaceutical University, China
Yue Liu,
Beijing University of Chinese Medicine, China

*CORRESPONDENCE
Zhigang Yang,
yangzg@lzu.edu.cn

RECEIVED 29 May 2023
ACCEPTED 30 November 2023
PUBLISHED 03 January 2024

CITATION
Shen X, Wu Y, Chen P, Bai Y, Liu Y, Jiang Y, Zhang Y and Yang Z (2024), Anti-platelet aggregation activities of different grades of *Angelica sinensis* and their therapeutic mechanisms in rats with blood deficiency: insights from metabolomics and lipidomics analyses.
Front. Pharmacol. 14:1230861.
doi: 10.3389/fphar.2023.1230861

COPYRIGHT
© 2024 Shen, Wu, Chen, Bai, Liu, Jiang, Zhang and Yang. This is an open-access article distributed under the terms of the Creative Commons Attribution License (CC BY). The use, distribution or reproduction in other forums is permitted, provided the original author(s) and the copyright owner(s) are credited and that the original publication in this journal is cited, in accordance with accepted academic practice. No use, distribution or reproduction is permitted which does not comply with these terms.

Anti-platelet aggregation activities of different grades of *Angelica sinensis* and their therapeutic mechanisms in rats with blood deficiency: insights from metabolomics and lipidomics analyses

Xue Shen[1], Yangyang Wu[1], Ping Chen[1], Yuwei Bai[1], Yanan Liu[1], Yihan Jiang[1], Yawen Zhang[1,2] and Zhigang Yang[1,2,3]*

[1]School of Pharmacy, Lanzhou University, Lanzhou, China, [2]Collaborative Innovation Center for Northwestern Chinese Medicine, Lanzhou University, Lanzhou, China, [3]State Key Laboratory of Applied Organic Chemistry, Lanzhou University, Lanzhou, China

In traditional Chinese medicine, the radix of *Angelica sinensis* (Oliv.) Diels (RAS) is mainly used to replenish and invigorate the blood circulation. This study investigated anti-platelet aggregation activities were used by New Zealand rabbits, and high-performance liquid chromatography data were obtained to determine the spectrum–effect relationship for different commercial grades of RAS. Plasma and urine metabolites were examined using ultra-performance liquid chromatography coupled with quadrupole time-of-flight tandem mass spectrometry-based metabolomics to elucidate the mechanisms underlying the role of these metabolites in a rat model of blood deficiency (BD). Plasma and spleen metabolites were additionally examined using ultra-performance liquid chromatography plus Q-Exactive tandem mass spectrometry-based lipidomics to clarify the mechanisms of RAS in treating BD. The third grade of RAS exhibited the best activity in replenishing and invigorating blood *in vitro* and *in vivo*. Ferulic acid, ligustilide, senkyunolide I, uridine, and guanine are quality markers of anti-platelet aggregation activity. Based on the metabolomics results, 19 potential biomarkers were screened in plasma, and 12 potential metabolites were detected in urine. In lipidomics analyses, 73 potential biomarkers were screened in plasma, and 112 potential biomarkers were screened in the spleen. RAS may restore lipid metabolism by regulating disorders of glycerophospholipid and sphingolipid metabolism, the tricarboxylic acid cycle, amino acid metabolism (thereby improving energy metabolism), and arachidonic acid metabolism (thereby promoting blood circulation). These results provide a deeper understanding of the effects of different grades of RAS and a scientific reference for the establishment of grading standards and for the clinical use of RAS.

KEYWORDS

***Angelica sinensis*, different commodity grades, anti-platelet aggregation activity, blood deficiency rat, Metabolomics, lipidomics, Q-marker**

1 Introduction

The raw materials employed in traditional Chinese medicine (TCM) exhibit a dual nature, serving as medicinal components and commercial commodities. The commercial-grade specification of TCM components plays a vital role in determining a product's medicinal value within the market (Wei et al., 2022). To ensure the quality and premium pricing of TCM materials, it has become imperative to enhance the criteria and standards for these commodities (Qian et al., 2019). The critical commodity classification method, referred to as "distinguishing appearance and quality," assesses various attributes such as shape, size, color, surface characteristics, texture, section features, and scent to gauge quality (He et al., 2022). However, it is often the case that there is no clear scientific correlation between commodity grade specifications and the bioactivities of TCM raw materials. For instance, low-grade *Panax notoginseng* exhibits superior hemostatic activity compared to its high-grade counterpart (Liu et al., 2016). Consequently, the accurate utilization of high-quality Chinese herbal medicines presents a significant challenge that must be addressed to ensure optimal clinical efficacy.

The radix of *Angelica sinensis* (Oliv.) Diels (RAS) replenishes and invigorates blood circulation, regulates menstruation, relieves pain, and moistens the intestines, as claimed by the Pharmacopoeia of the People's Republic of China in 2020. RAS is categorized into different grades based on weight, as specified by T/CACM in 2018. RAS of the first to fourth grades was used in this study. It has been discovered that there is a positive correlation between blood tonic activity and RAS weight, a negative correlation between polysaccharide and RAS weight, and no association between ligustilide and RAS weight (Yang, 2017).

The clinical signs of hemolytic anemia in TCM include pale skin, a white tongue, palpitations, dizziness, and frequent bleeding (Hwang et al., 2022). A combination of acetylphenylhydrazine (APH) and cyclophosphamide (CTX) has been used to develop models of blood deficiency (BD) (Song et al., 2014). Previous studies have demonstrated that RAS can enhance peripheral blood indices in rat models of BD (Hua et al., 2017). RAS extracts have also been found to significantly inhibit platelet aggregation (Chen et al., 2019). However, there is no evidence for variance in effectiveness or differences in the therapeutic mechanisms among the different grades of RAS in replenishing and invigorating blood circulation.

Metabolomics examines the variations in small-molecule metabolites produced under various intervention conditions in order to detect the differences among creatures' metabolisms after treating with TCM (Cui et al., 2022). Herbs are multifaceted components with diverse targeting properties. Research has demonstrated the principles underlying TCM treatments using metabolomics in numerous studies (Chang et al., 2016). Additionally, lipidomics plays a crucial role in identifying key lipid biomarkers in metabolic regulation and in elucidating the roles of lipids in various physiological processes (Yang and Han, 2016).

In this study, we investigated the effects of various grades of RAS in terms of replenishing and invigorating blood circulation, both *in vitro* and *in vivo*. We employed untargeted metabolomics and lipidomic profiling of plasma, urine, and spleen samples to unveil potential therapeutic mechanisms.

2 Material and methods

2.1 Reagents and materials

RAS was collected from Min Country of Gansu Province, China, in November 2020. All of the plant materials were authenticated as *A. sinensis* (Oliv.) Diels by Professor Zhigang Yang. Polymerase chain reaction (PCR) tests were performed to identify the RAS (Liu et al., 2018). The PCR results are shown in Supplementary Figure S1. Voucher specimens (No. DG202009001) were stored at the School of Pharmacy, Lanzhou University. The weights per RAS for specimens falling into the first to fourth grades were more than 60.0 g, 25.0–60.0 g, 15.0–25.0 g, and 10.0–15.0 g, respectively.

Ferulic acid, ligustilide, senkyunolide I, chlorogenic acid, levistolide A, uridine, adenosine, guanine, and *L*-tryptophan were purchased from Chengdu Pufeide Biotech Co., Ltd. (Chengdu, China) as reference compounds. Acetonitrile and Methanol were purchased from CNW Technologies GmbH. Formic acid was purchased from Merck (Darmstadt, Germany). Double-distilled water (ddH_2O) was obtained using a laboratory water purifier. APH, CTX, and ATPase were purchased from Beijing Solarbio Science and Technology Co., Ltd. (Beijing, China). Adenosine diphosphate (ADP) and arachidonic acid (AA) were purchased from Shandong Tailixin Medical Technology Co., Ltd. (Shandong, China). Finally, aspirin was provided by the CSPC Pharmaceutical Group Co., Ltd.

2.2 Metabolite extraction from RAS and drug administration

RAS powders (100.0 g) of different grades were weighed and extracted with 1,000 mL of deionized water by refluxing in a hot water bath for 1 h. Subsequently, the sediment was filtered and soaked for 1 h in an 8-fold deionized water for the second extraction. The obtained filtrates were mixed and concentrated. The concentration of the water extracts of RAS used in BD model rats was 7.5 mg/mL (7.5 mg of RAS per milliliter of deionized water). Reference compounds were weighed and dissolved in ddH_2O to a final concentration of 5 mg/mL for high-performance liquid chromatography (HPLC).

2.3 Animals and preparation of the BD model

Healthy New Zealand rabbits (20 weeks, 2.5–3.0 kg) and male Wistar rats (8 weeks, 180 ± 20 g) were obtained from the Animal Center of Lanzhou University. All animal procedures were performed in accordance with the Guidelines for the Care and Use of Laboratory Animals of Lanzhou University and were approved by the Animal Ethics Committee of Lanzhou University: SCXK (gan) 2018–0002.

The healthy male Wistar rats were initially allowed to freely consume water and food under constant temperature (24°C ± 2°C), humidity (70% relative humidity), and light–dark cycles (12 h light/dark) in the Specific Pathogen Free Laboratory. The rats were fed standard commercial chow and purified water was available *ad libitum*. After 1 week of acclimation, 81 Wistar rats were randomly

divided into nine groups with nine rats in each: 1) a control group (C); 2) the model group (M); 3) the aspirin group (P, positive control drug, 7.5 mg/mL); 4) the first-grade RAS group (F, 7.5 mg/mL); 5) the second-grade RAS group (S, 7.5 mg/mL); (6) the third-grade RAS group (T, 7.5 mg/mL); 7) the fourth-grade RAS group (Fo, 7.5 mg/mL); 8) the high-dose third-grade RAS group (H, 15 mg/mL); and 9) the low-dose third-grade RAS group (L, 3.5 mg/mL). As the clinical dosage of RAS is 6–12 g per day (Committee, 2020), the clinically equivalent dose was calculated according to the animal experimental dose. The animal drug dose calculated based on the body mass of the RAS decoction was 0.01 mL/g, and oral gavage was administered once daily continuously for 7 days from day 1. The rats in the control and model groups were administered an equal volume of normal saline. The M, P, F, S, T, and Fo groups were hypodermically injected with 4 mg/mL APH saline solution on days 1–3 at a dose of 20 mg/kg. After a 2 h hypodermic injection on day 3, the rats were intraperitoneally injected with 4 mg/mL CTX saline solution on days 3–6 at 20 mg/kg. All the rats were allowed free access to feed and water during the experiment, and the entire experiment lasted for 7 days. Their body weight was measured and recorded daily during the experiment.

2.4 High-performance liquid chromatography analysis of water extracts of RAS

All water extracts of RAS were analyzed using an Agilent 1260 HPLC system (Agilent Technologies, Santa Clara, CA, United States). Separation was carried out on an HPLCONE-5C18D column (250 mm × 4.6 mm, 5 μm), which was maintained at 30°C and eluted at a flow rate of 1 mL/min. The mobile phase consisted of water containing 0.1% formic acid (A) and acetonitrile (B) for gradient elution. A linear gradient of 0–5 min, 3%–10% (B); 5–15 min, 15% (B); 15–25 min, 25% (B); 25–35 min, 35% (B); 35–40 min, 70% (B); 40–55 min, 95% (B); 55–60 min, 100% (B) was used. The injection volume and detection wavelength were 10 μL and 280 nm, respectively.

2.5 Anti-platelet aggregation assay

The anti-platelet aggregation assay was carried out according to methods reported in our previous research (Zhang et al., 2022a).

2.6 Peripheral hemogram assay and histopathology analysis

Twelve hours after the last administration, blood was taken from the abdominal aorta, and the plasma was separated into several portions (200 μL each) and stored at −80°C for further analysis. Levels of red blood cells (RBC, 10^{12}/L), white blood cells (WBC, 10^{9}/L), hemoglobin (HGB, g/L), hematocrit (HCT, %), platelets (PLT, 10^{9}/L), lymphocytes (LY, %), monocytes (MO, %) and neutrophils (NE, %) were also examined using an auto-hemocytome with a Hemavet 950FS automatic blood analyzer (Ellis, Beijing, China). After the animals were euthanized, their organs were separated, fixed in formalin, and embedded in paraffin. Samples were cut into thin slices and stained with hematoxylin–eosin (HE). Organ histological changes were observed using a BX53 light microscope (Olympus, Tokyo, Japan). Spleen samples were collected and weighed. Spleen indices were calculated using the organ index formula (organ index (g/g) = organ weight/body weight), and spleen indices were calculated. All organ samples were kept at −80°C until analysis.

2.7 Determination of ATPase content in the erythrocyte membrane

The ATPase content in the rat erythrocyte membranes was measured according to the instructions of the ATPase kit.

2.8 Untargeted metabolomics analysis

For rat plasma samples, approximately 200 μL was mixed with 800 μL of acetonitrile in a 2-mL conical tube. After vigorous vortexing for 2 min and subsequent centrifugation (15 min, 15,000 rpm, 4°C), the supernatant was filtered through a 0.22-μm membrane filter. The filtered liquid was then evaporated using a nitrogen blower. Subsequently, 25 μL of 40% acetonitrile was introduced to redissolve the samples. Following another round of vortexing (2 min) and centrifugation (15 min, 15,000 rpm, 4°C), the supernatant was collected for further analysis.

For urine samples, approximately 1.2 mL was mixed with 3.6 μL of acetonitrile in a 10-mL conical tube. After thorough vortexing for 2 min and subsequent centrifugation (15 min, 15,000 rpm, 4°C), the supernatant was evaporated using a nitrogen blower. Next, 400 μL of acetonitrile (40%) was added to redissolve the samples. After another round of vortexing (2 min) and centrifugation (15 min, 15,000 rpm, 4°C), the supernatant was collected and prepared for filtering and analysis.

To ensure the stability of the analytical methods and instruments, quality control (QC) samples were prepared using 5 μL from each plasma sample. These QC samples were analyzed alongside every set of six samples throughout the entire analysis process.

Sample analysis was carried out using an Agilent 6560 QTOF mass spectrometer (Agilent Technologies, Santa Clara, CA, United States). Chromatographic separation was achieved with an ACQUITY BEH C18 column (2.1 mm × 50 mm, 1.7 μm, Waters, United States) maintained at 40°C. The mobile phase consisted of water containing 0.1% formic acid (A) and acetonitrile containing 0.1% formic acid (B), following gradient elution at a 0.3 mL/min flow rate. A linear gradient sequence was applied as follows: 0–1 min, 5% (B); 1–6 min, 5%–20% (B); 6–9 min, 20%–50% (B); 9–15 min, 50%–95% (B); 15–20 min, 95% (B); 20–23 min, 95%–100% (B); 23–25 min, 100%–5% (B); 25–30 min, 5% (B). The injection volume and detection wavelength were 4 nm and 280 nm, respectively.

The ion-source parameters were optimized and set as follows: capillary voltage, 3,500 V; drying gas temperature, 225°C; drying gas flow rate, 10 L/min; nebulizer pressure, 25 psig; sheath gas temperature, 400°C; sheath gas flow rate, 12 L/min. Data were

acquired at a rate of 1 spectrum/s with a scanning range of 20–1,500 m/*z*.

2.9 Untargeted lipidomic analysis

For plasma samples, approximately 40 μL was mixed with 300 μL of acetonitrile in a 2-mL conical tube and vortex-shaken for 1 min. Subsequently, 1,000 μL of methyl tert-butyl ether (MTBE) was added, and the mixture was shaken for 1 h. A subsequent step involved adding 250 μL of ddH2O and vortex-shaking for 1 min. The sample was then centrifuged (10 min, 12,000 rpm, 4°C), and 400 μL of the supernatant was collected. This liquid was concentrated using a vacuum concentrator until dry. Finally, 100 μL of isopropanol/acetonitrile (1/1) solution was added for sonic reconstitution for 1 min. The reconstituted sample was then filtered through a 0.22-μm membrane filter and prepared for analysis.

For spleen samples, one steel ball and 20 ceramic beads were added to each sample, which was then ground for 1 min. Subsequently, 300 μL of methanol and 1 mL of MTBE were added, and the mixture was shaken for 60 min to ensure thorough mixing. Afterward, the sample was centrifuged (10 min, 12,000 rpm, 4°C), and 300 μL of the supernatant was collected for concentration in a vacuum concentrator. A final step involved adding 100 μL of isopropanol/acetonitrile (1/1) solution for sonic reconstitution for 1 min. The reconstituted sample was filtered through a 0.22-μm membrane filter for analysis.

The samples were tested using the Thermo Scientific U3000 (Agilent Technologies, Santa Clara, CA, United States). Chromatographic separation was performed with an ACQUITY UPLC BEH C8 (2.1 mm × 100 mm, 1.7 μm, Waters, United States) and samples were maintained at 50°C. For the plasma samples, the mobile phase consisted of water/acetonitrile at 6/4, containing 0.1% formic acid and 5 mM ammonium formate (A), and isopropanol/acetonitrile at 1/9, containing 0.1% formic acid and 5 mM ammonium formate (B), in gradient elution at 0.3 mL/min. For ESI^+, a linear gradient of 0–2 min, 0%–30% B; 2–9 min, 30%–70% B; 9–11 min, 70%–95% B; 11–12 min, 95%–100% B was employed. For ESI^-, the linear gradient was 0–3 min, 10%–35% B; 3–6 min, 35%–85% B; 6–8 min, 85%–100% B. The injection volume and flow velocity were 1.0 μL and 0.3 mL/min, respectively.

The ion-source parameters were optimized and set as follows: capillary voltage, ESI^+ 3.7 kV, ESI^- 3.5 kV; drying gas temperature, 320°C; drying gas flow rate, 10 L/min; nebulizer pressure, 30 psig; sheath gas temperature, 300°C; sheath gas flow rate, 12 L/min. Data were acquired at a rate of 1 spectrum/s in the scanning range of 150–1,500 m/*z*.

2.10 Statistical analysis

The chromatograms of 30 samples of water extract of RAS were input into the *Similarity Evaluation System for Chromatographic Fingerprint of TCMs* software package (Chinese Pharmacopoeia Commission, version 2012.130723) to generate the standard fingerprints of RAS of different grades. Chemometric analysis, including multivariate data analysis, was performed using the SIMCA 14.1 software package. One-way analysis of variance, followed by the Student's t-test, was conducted to determine the statistical significance of differences between groups. The threshold for statistical significance was set at $p < 0.05$.

3 Results

3.1 High-performance liquid chromatography fingerprints and the nine main compounds in RAS

The results of this methodological investigation are presented in Supplementary Table S1. All results indicated that the HPLC analysis method was valid and satisfactory. The HPLC profiles of 30 batches of RAS water extract are shown in Figure 1A. Seventeen coexisting peaks were detected in all analyzed samples; these were labeled 1–17 according to the standard fingerprint of RAS of different grades (Figure 1B). Indices of similarity among the samples of different grades were in the range of 0.871–0.997 (Table 1). These high degrees of similarity indicated that the compounds found in different grades of RAS were similar.

Nine reference compounds were quantitatively analyzed: ferulic acid, ligustilide, senkyunolide I, chlorogenic acid, levistolide A, uridine, adenosine, guanine, and *L*-tryptophan. Among the four RAS grades (Table 2), the third group showed the highest average values for ferulic acid, ligustilide, senkyunolide I, levistolide A, uridine, adenosine, and guanine.

3.2 Anti-platelet aggregation activity

The percentage of activities inhibiting platelet aggregation varied with RAS grade. As shown in Figure 2, illustrating the anti-platelet aggregation activity induced by ADP or AA of water extract samples with different grades of RAS *in vitro*, the ordering of different grades of RAS by IC_{50} was as follows: fourth-grade > first-grade > second-grade > third-grade ($p < 0.001$).

3.3 Spectrum–effect analysis

As shown in Table 3, nine main compounds were identified as bioactive compounds with anti-platelet aggregation activity through grey relational analysis. Levistolide A and senkyunolide I exerted the strongest influence on ADP- and AA-induced platelet aggregation activity, respectively. As shown in Figure 3A,C, the segregation produced via 3D principal component analysis (PCA) was between anti-platelet aggregation activity and the content of the different grades of RAS. Senkyunolide I, uridine, guanine, and ligustilide showed the greatest influence on ADP- and AA-induced platelet aggregation based on their variable importance in projection (VIP) scores (Figures 3B,D, respectively).

3.4 Body weight and spleen index

The functions of the spleen include hematogenesis, and the spleen plays a dominant role in blood control in TCM. The effects of BD on the spleen were evaluated by examining the spleen index. As

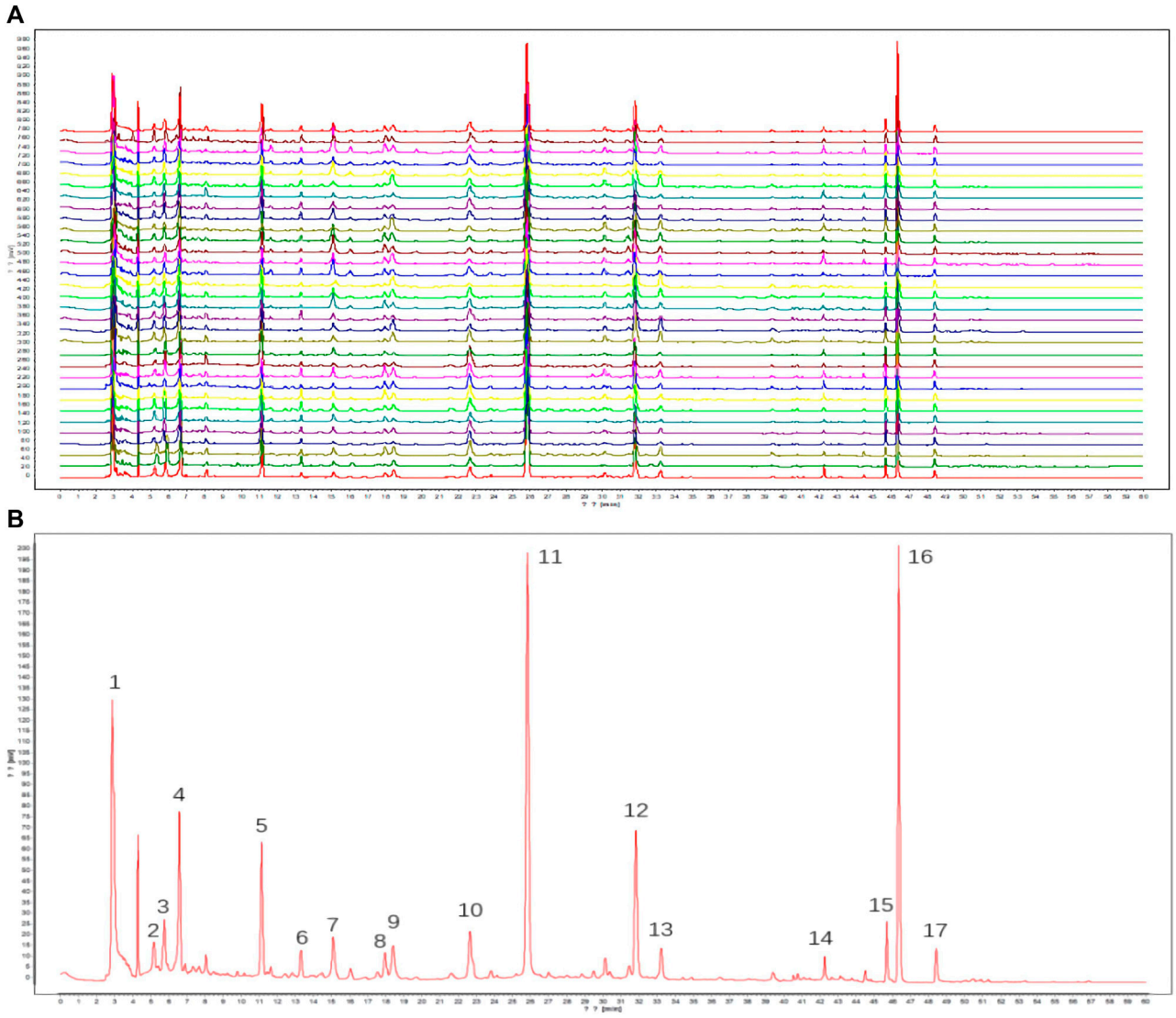


FIGURE 1
HPLC fingerprints of samples. (**(A)** Fingerprints of different grades of RAS; **(B)** Standard fingerprint of different grades of RAS. 1: unknown; 2: uridine; 3: adenosine; 4: guanine; 5: tryptophan; 6: unknown; 7: chlorogenic acid; 8: unknown; 9: unknown; 10: unknown; 11: ferulic acid; 12: senkyunolide I; 13: unknown; 14: unknown; 15: unknown; 16: ligustilide; 17: levistolide A).

shown in Figure 4A, the body weight of the model rats was significantly lower than that of the control rats. The RAS and positive control groups gained more body weight than the model rats. As shown in Figure 4B, the organ index for the spleen was significantly higher among the model group than the control group. The spleen index in the control group was 2.95 ± 0.55, while its value was 5.20 ± 0.32 in the model group. It was clear that the spleen index recovered to the normal level in the third-grade RAS dose group and the high-dose group, whereas it fell between the normal and model levels in the other RAS groups. All RAS groups were significantly different from the model group. It is worth mentioning that the aspirin group exhibited a decreased spleen index but also exhibited significantly decreased body weight, which indicated a lack of curative effect. These results suggest that water extract of RAS, especially third-grade RAS, could improve spleen enlargement in a rat model of BD.

3.5 Peripheral blood cells

WBC, RBC, PLT, LY, MO, NE, HGB, and HCT are important indicators in routine blood examinations that can directly reflect the status of hematopoietic function in the rat model of BD. The results of these analyses are shown in Figures 5A–H. WBC, RBC, PLT, HGB, and HCT levels were significantly lower in the model group than in the control group ($p < 0.0001$), indicating that the BD model was successfully replicated. After treatment with RAS, these levels increased to varying degrees ($p < 0.01$), and the PLT index

TABLE 1 Similarity of different grades of RAS.

Sample	Similarity	Sample	Similarity
1	0.979	16	0.997
2	0.988	17	0.871
3	0.985	18	0.991
4	0.993	19	0.954
5	0.983	20	0.983
6	0.994	21	0.986
7	0.982	22	0.981
8	0.973	23	0.996
9	0.990	24	0.994
10	0.969	25	0.979
11	0.969	26	0.981
12	0.994	27	0.991
13	0.933	28	0.992
14	0.978	29	0.982
15	0.980	30	0.963

recovered to normal levels ($p < 0.01$), which is consistent with anti-platelet aggregation activity *in vitro*. Notably, levels of LY, MO, and NE in the third-grade RAS group were similar to those in the control group, and there were significant differences between the third-grade group and the other RAS groups.

3.6 Pathological morphology of the heart, kidney, and spleen

HE staining results for each group are shown in Figure 6. Differences in pathological morphology slices between the model and control groups were clearly observed for the heart, kidney, and spleen. However, there were no clear abnormalities in the liver slices. The heart endometrium, the myocardium, the epicardial structure, and horizontal stripes of myocardial cells were clearly observed in the control group, and the myocardial fibers were evenly colored. The model group showed significant changes in neutrophilic granulocyte augmentation and interstitial edema. The control group exhibited normal renal morphology without pathological lesions; however, vacuoles and focal segmental sclerosis were observed in the glomeruli of the model group. In the spleen slices, the purplish-red part represents the red pulp; the white pulp, formed by the aggregation of lymphocytes, was dyed blue. The proportion of white pulp was significantly reduced in the model group. There was significant recovery from damage in the other groups, whether they were treated with RAS or with aspirin. Specifically, the effect in rats in the RAS groups, with the exceptions of the fourth-grade and low-dose third-grade groups, was better than that observed in the positive control group. Moreover, the spleen was significantly larger in the model group than in the other groups. After treatment with RAS and aspirin, the spleen decreased in size. The third-grade RAS group exhibited excellent therapeutic effects on lesions of the heart, kidney, and spleen. These findings were similar to the results on anti-platelet aggregation activity *in vitro*.

3.7 Activity of ATPase in plasma

The standard enzyme-linked immunosorbent assay curve is shown in Figure 7A. ATPase content was 3.54 ± 0.17 U/mL for the control group and 1.51 ± 0.22 U/mL for the model group. Relative to the control group, the ATPase content observed in the model group was significantly decreased ($p < 0.01$). In contrast, ATPase content was increased in the RAS and aspirin groups. In particular, ATPase content in the third-grade group increased to the level of the control group, indicating that the third-grade group exhibited a superior effect in terms of the development of ATPase content (Figure 7B).

3.8 Multivariate statistical analysis of metabolomics

Total ion chromatograms (TICs) of plasma and urine from different groups in positive mode are shown in Supplementary Figure S2. Endogenous metabolites in the plasma and urine of the BD model rats were selected using VIP scores. The differential endogenous metabolites of plasma and urine, screened for VIP >1.5 and $p < 0.05$, along with information on their identification, are presented in Tables 4, 5, respectively. The peak area and retention time of ions, determined using Profinder B.08.00, were imported into the SIMCA 14.1 software package. Permutation plots of plasma in positive mode were constructed to verify the reliability of the multidimensional statistical model, and the permutation test showed that the model was not overfitting. All plasma and urine samples were subjected to OPLS-DA based on the differential metabolites identified. A summary of the various chemometric models used in the analysis of the UPLC-QTOF-mass spectra is provided in Supplementary Table S2. As shown in Figures 8A,B, OPLS-DA score plots of plasma and urine in the control, model, aspirin, third-grade RAS, and QC groups in positive mode were clearly separated, indicating that blood deficiency occurred after injection with APH and CTX, and that RAS was able to improve the metabolic disturbance induced by BD. Clear separation between the first-to fourth-grade groups can be observed in Figures 8C,D, showing that different influences on plasma and urine were in effect under each grade of RAS. The constructed model fit the obtained data well, with Q^2Y suggesting that the model could accurately predict new data for plasma and urine according to a permutation test with 200 repetitions, as shown in Figures 8E–H.

Based on their VIP scores, *p*-values, and S-plot results, 19 potential endogenous metabolites (Table 4) in plasma were screened and identified, based on MS/MS fragments, retention behavior, and online databases such as Metlin (http://metlin.scripps.edu/), LIPID MAPS (http://www.lipidmaps.org), and the Human Metabolome Database (HMDB, http://www.hmdb.ca), as

TABLE 2 The content (mg/g) of nine components in different grades of RAS.

Grade	No.	Ferulic acid	Ligustilide	Senkyunolide I	Chlorogenic acid	Levistolide A	Uridine	Adenosine	Guanine	*L*-tryptophan
First grade	1	9.97	27.20	1.85	2.57	12.78	19.00	96.27	54.65	17.24
	2	13.90	18.37	2.48	3.39	11.84	18.38	80.12	53.60	18.02
	3	9.22	20.83	0.88	1.83	12.58	14.13	71.65	38.20	11.88
	4	12.19	24.93	1.81	2.62	13.09	13.12	57.09	34.39	9.42
	5	8.26	15.96	0.95	3.43	12.46	21.14	86.53	51.98	13.38
	6	10.47	23.61	1.38	3.32	13.17	21.83	90.40	57.89	15.97
	7	13.25	21.41	2.94	2.63	12.97	14.94	60.22	42.57	3.98
	8	12.83	21.66	1.74	4.99	12.84	18.58	95.48	53.49	14.01
Second grade	9	17.40	23.57	1.92	3.09	11.04	15.18	62.50	41.40	11.70
	10	11.06	32.84	1.79	2.36	13.72	7.23	60.67	39.21	11.76
	11	14.25	19.59	2.45	4.13	12.43	15.92	82.70	53.08	9.79
	12	16.62	20.36	1.39	1.36	12.68	11.67	71.13	34.90	23.13
	13	6.52	16.98	0.87	3.41	12.97	11.54	67.11	39.48	10.79
	14	8.68	14.93	1.03	2.44	10.78	13.20	50.06	45.97	8.20
	15	12.78	21.04	1.34	3.47	13.48	15.84	85.54	42.70	14.32
	16	14.35	28.88	1.43	2.34	13.92	12.08	76.37	38.05	18.01
Third grade	17	15.50	31.56	3.58	3.71	13.09	20.93	82.93	51.92	18.02
	18	9.44	23.19	4.11	4.43	14.12	21.82	92.86	59.63	12.54
	19	13.36	34.74	1.43	2.91	14.18	20.46	111.55	58.18	14.54
	20	14.57	17.16	2.16	7.88	13.81	19.65	71.87	45.18	9.51
	21	13.85	29.20	2.90	4.71	13.42	19.19	94.86	54.75	13.70
	22	11.62	26.08	3.96	2.93	13.35	24.01	71.22	46.01	10.60
	23	11.05	21.98	4.64	6.79	15.07	13.34	81.86	37.77	12.56
Fourth grade	24	5.48	11.90	1.85	3.92	13.16	22.12	73.00	58.22	17.73
	25	13.74	20.27	1.64	7.03	13.46	13.47	81.79	46.06	12.79
	26	6.94	19.40	2.97	5.02	13.37	11.76	69.16	48.28	7.88
	27	8.98	16.07	2.37	9.01	13.24	11.69	54.19	42.11	10.79
	28	9.80	20.48	2.76	8.20	12.32	21.48	79.59	60.84	14.06
	29	10.80	21.07	1.14	3.47	13.97	14.64	99.98	44.04	12.23
	30	10.70	17.08	2.50	12.27	13.21	15.58	72.25	43.72	14.02

10.3389/fphar.2023.1230861

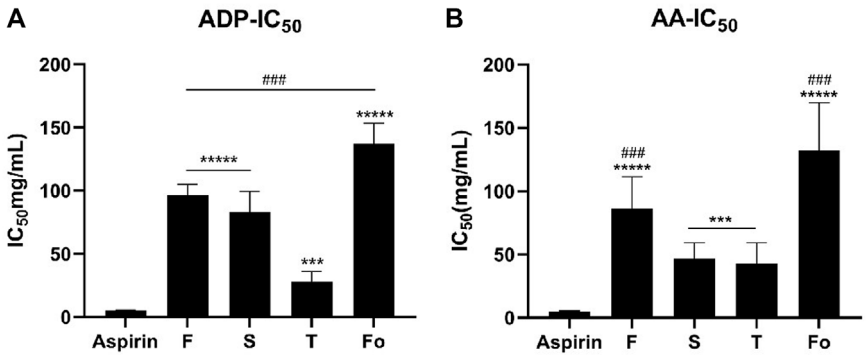


FIGURE 2
The IC50 of platelet aggregation activity induced by ADP or AA of 30 batches of RAS ((**A**) The IC50 of platelet aggregation activity induced by ADP; (**B**) The IC50 of platelet aggregation activity induced by AA). ***$p < 0.001$, *****$p < 0.00001$ vs Aspirin; $^{###}p < 0.001$, $^{#####}p < 0.00001$ vs the third-grade group.

TABLE 3 Grey relational analysis and ranking results of nine bioactive components on ADP- and AA-induced anti-platelet aggregation activity.

Peak no.	Compound	$\gamma_{0,\ i}$	
		ADP	AA
1	Uridine	0.6439	0.7121
2	Adenosine	0.6588	0.7037
3	Guanine	0.6825	0.7079
4	Tryptophan	0.6715	0.6838
5	Chlorogenic acid	0.6452	0.7104
6	Ferulic acid	0.6254	0.7007
7	Senkyunolide I	0.6127	0.7194
8	Ligustilide	0.6334	0.6929
9	Levistolide A	0.6915	0.7069

differential metabolites associated with the rat model of BD. Compared with the control group, 11 metabolites were significantly upregulated ($p < 0.01$) in the model group, including lysophosphatidylcholine LysoPC(17:0), sphingomyelin SM(d20:1/20:4 (5Z,7E,11Z, 14Z)-OH(9)), phosphatidylcholine PC(18:1 (9Z)-O (12,13)/P-16:0), LysoPC(0:0/18:0), arachidonic acid, LysoPA (20:2 (11Z, 14Z)/0:0), phosphatidyl ethanolamine PE (15:0/22:2 (13Z, 16Z)), diisobutyl phthalate, *L*-alanine, and ceramide. In contrast, the levels of eight metabolites were clearly downregulated ($p < 0.01$): these were caffeoylcycloartenol, DG (PGE2/0:0/10:0), chenodeoxycholic acid, *L*-carnitine, citrulline, dihydrothymine, *L*-leucine, and *L*-glutamine. Twelve differential metabolites were detected in urine samples. Four metabolites were upregulated in the model group, including endoperoxide G2, PA (LTE4/*i*-15:0), and PA (*i*-19:0/PGE1); and eight metabolites were downregulated in the model group, including hippuric acid, citric acid, and galabiosylceramide. Figures 9A,B show heatmap images of the differential metabolites in plasma and urine, respectively. After treatment with RAS, the metabolites showed different degrees of increase or decrease in the process of recovery to control levels. The MetaboAnalyst 4.0 (https://www.metaboanalyst.ca/MetaboAnalyst/home.xhtml) system was used to analyze the pathways of plasma and urine metabolites in the rat model of BD. As shown in Figure 9C, the important pathways of plasma metabolites in relation to RAS treatment in the rat model of BD included arachidonic acid metabolism; arginine biosynthesis; alanine, aspartate, and glutamate metabolism; sphingolipid metabolism; and glycerophospholipid metabolism. Four main metabolic pathways were identified in urine: the tricarboxylic acid (TCA) cycle, sphingolipid metabolism, arachidonic acid metabolism, and glyoxylate and dicarboxylate metabolism (Figure 9D).

3.9 Multivariate statistical analysis of lipidomics

TICs in the plasma and spleen are shown in Supplementary Figure S3. All groups of plasma and spleen were re-analyzed via PCA and orthogonal projections to latent structures discriminant analysis (OPLS-DA) using the SIMCA 14.1 software package. A summary of the various chemometric models used in the analysis of the UPLC-Q-exactive-mass spectra is shown in Supplementary Table S3. As shown in Figures 10A,B, PCA score plots for the plasma and spleen in the positive and negative modes showed clear separation in the control, model, aspirin, and third-grade RAS groups. OPLS-DA score plots for the plasma and spleen in positive and negative modes in the control and model groups are shown in Figures 10C,D. The constructed model fit the obtained data well, with Q^2Y suggesting that the model could accurately predict new data based on 200 permutation tests, as shown in Figures 10E,F. Endogenous metabolites in the plasma and spleen of the BD model rats were selected using VIP scores. The differential endogenous metabolites of plasma and spleen, screened for VIP >1.5 and $p < 0.05$, are shown in Supplementary Tables S4, S5, respectively.

Approximately 73 potential biomarkers were screened in plasma. Polyunsaturated fatty acids and glycerophospholipids were the two most clearly evident changes observed in the plasma lipidomics of BD rats. Twenty-eight metabolites were

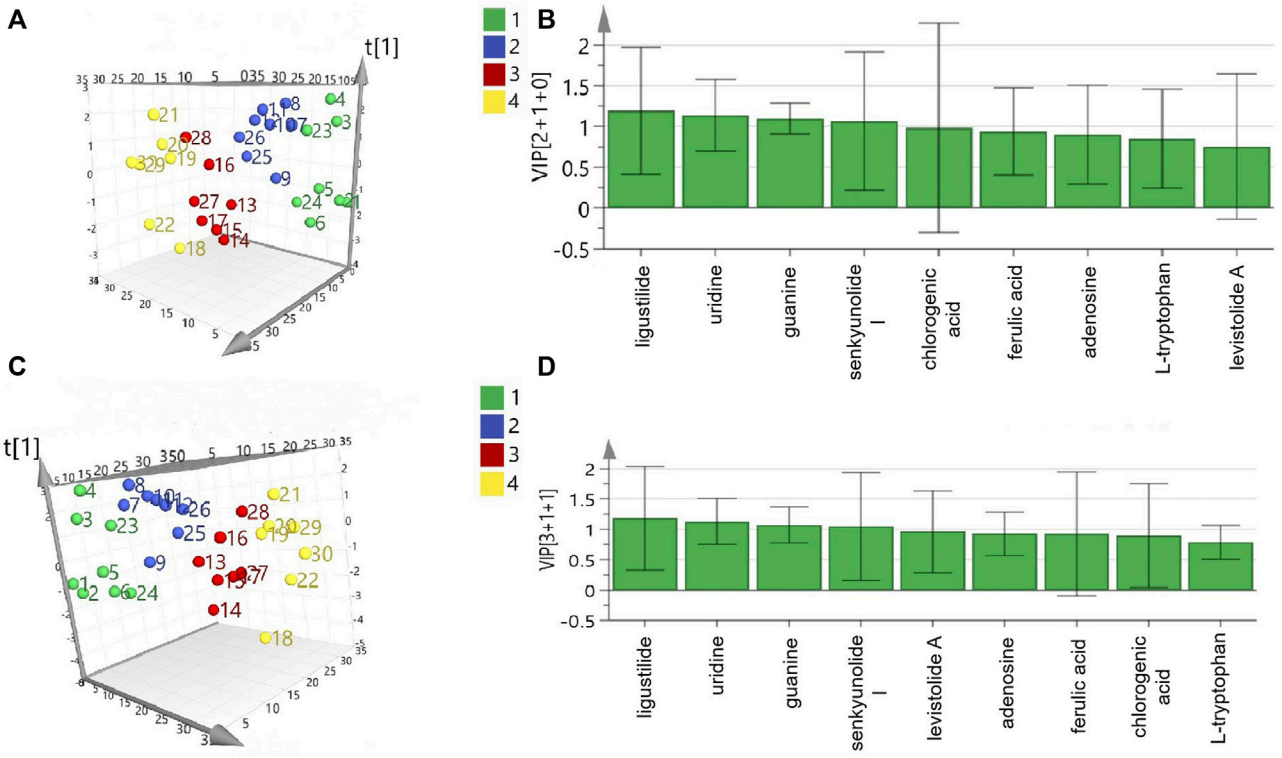


FIGURE 3
Result of PCA analysis of coexisting peaks and antiplatelet aggregation activities of different grades of RAS: adenosine diphosphate, PCA 3D plot **(A)** and VIP **(B)**; arachidonic acid, PCA 3D **(C)** and VIP **(D)**.

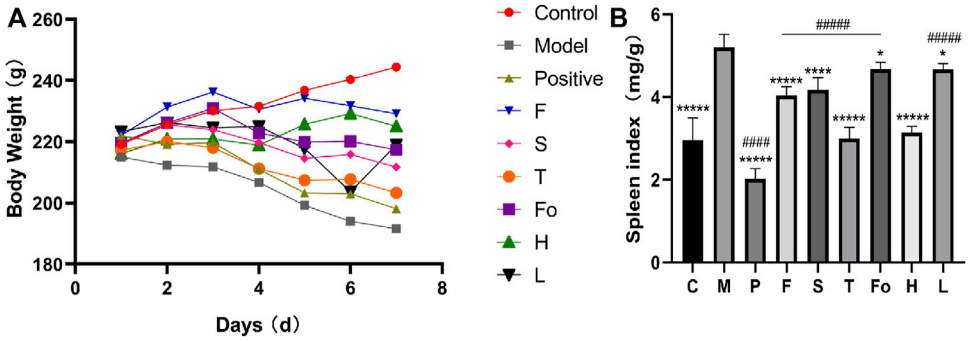


FIGURE 4
The body weight and the effect of RAS on spleen index in BD rats ((**A**) The body weight of rats; **(B)** The effect of RAS on spleen index in rats with blood deficiency. mean ± SD, n = 6) ****$p < 0.0001$, *****$p < 0.00001$ vs model group; ####$p < 0.0001$, #####$p < 0.00001$ vs the third-grade group.

upregulated in plasma in the model group, including PC (P-18:0/18:3), triglyceride TG (16:0/16:0/16:0), and PE (20:5/18:0); and 45 metabolites were downregulated, including PC (22:2/20:5), α-linolenic acid, and linoleic acid. Each RAS group exhibited regulation of 73 potential biomarkers. A total of 112 potential biomarkers were identified in the spleen. The two most prominent substances were TG. Twenty-one metabolites, including PE (20:4/22:2), PC (P-18:0/22:5), and LysoPC (P-18:0/0:0), were upregulated in the spleen in the model group, and 91 metabolites were downregulated, including LysoPC (20:2/0:0), TG (14:0/16:0/20:4), and PE (20:1/0:0). These 112 potential biomarkers were upregulated in each treatment group. Figures 11A,B show heatmap images of the differential metabolites in the plasma and spleen, respectively. As shown in Figure 11C, three main metabolic pathways for plasma were screened for with MetPA: α-linolenic acid metabolism, glycerophospholipid metabolism, and

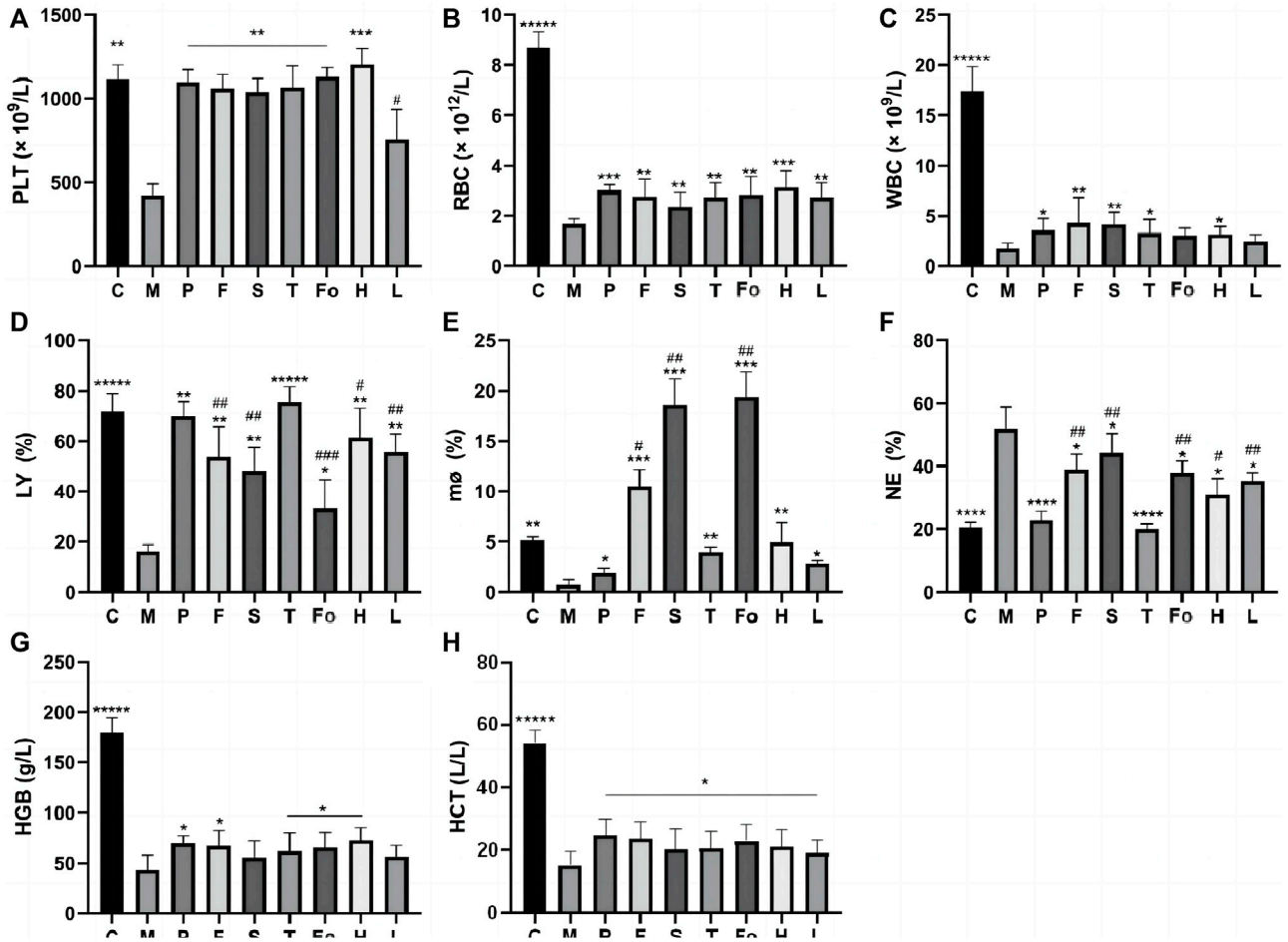


FIGURE 5
Effect of RAS on Peripheral Blood Cells in BD rats (mean ± SD, n = 6) *$p < 0.05$, ** $p < 0.01$, ***$p < 0.001$, *****$p < 0.00001$ vs model group; $^{\#}p < 0.05$, $^{\#\#}p < 0.01$ vs the third-grade group.

linoleic acid metabolism. Five major metabolic pathways in the spleen were identified: glycerophospholipid metabolism, sphingolipid metabolism, glycerolipid metabolism, glycosylphosphatidylinositol-anchor biosynthesis, and ether lipid metabolism (Figure 11D).

4 Discussion

The use of RAS for enhancing blood circulation has a long history in TCM. The commercial grade specification for TCM is crucial in ensuring high-quality and premium price TCM materials. Distinguishing between commodity grades in terms of the differences in quality is essential, as it helps to improve commodity standards.

In the current study, we employed HPLC fingerprints and *in vitro* anti-platelet aggregation assays to identify the active components within different grades of RAS. Grey correlation analysis revealed that nine components exhibited inhibitory effects on ADP-induced and AA-induced platelet aggregation. Notably, there was a consistent correlation between anti-platelet aggregation activity and the content of different grades of RAS. Specifically, third-grade RAS demonstrated the most significant potential for enhancing blood circulation, particularly with regard to ADP- and AA-induced platelet aggregation activity. Conversely, fourth-grade RAS was associated with lower content of these components, mirroring its reduced anti-platelet aggregation activity. First- and second-grade RAS exhibited moderate effects on anti-platelet aggregation activity and fell in the middle range concerning the associated content of the relevant components among the various grades. Senkyunolide I, uridine, guanine, and ligustilide emerged as pivotal components for enhancing blood circulation in ADP- and AA-induced platelet aggregation. This corroborates our earlier findings, which identified senkyunolide I, uridine, guanine, ferulic acid, and adenosine as potential Q-markers for RAS (Zhang et al., 2022b). Additionally, our previous research identified ferulic acid, ligustilide, and senkyunolide I as Q-markers for anti-platelet aggregation and Ca^{2+} antagonistic activities using near-infrared reflectance spectroscopy (Gao et al., 2022). In other studies, ferulic acid, ligustilide, and levistilide A have also been identified as Q-markers for RAS through effective component-bioactivity network analysis (Liu et al., 2021). Furthermore,

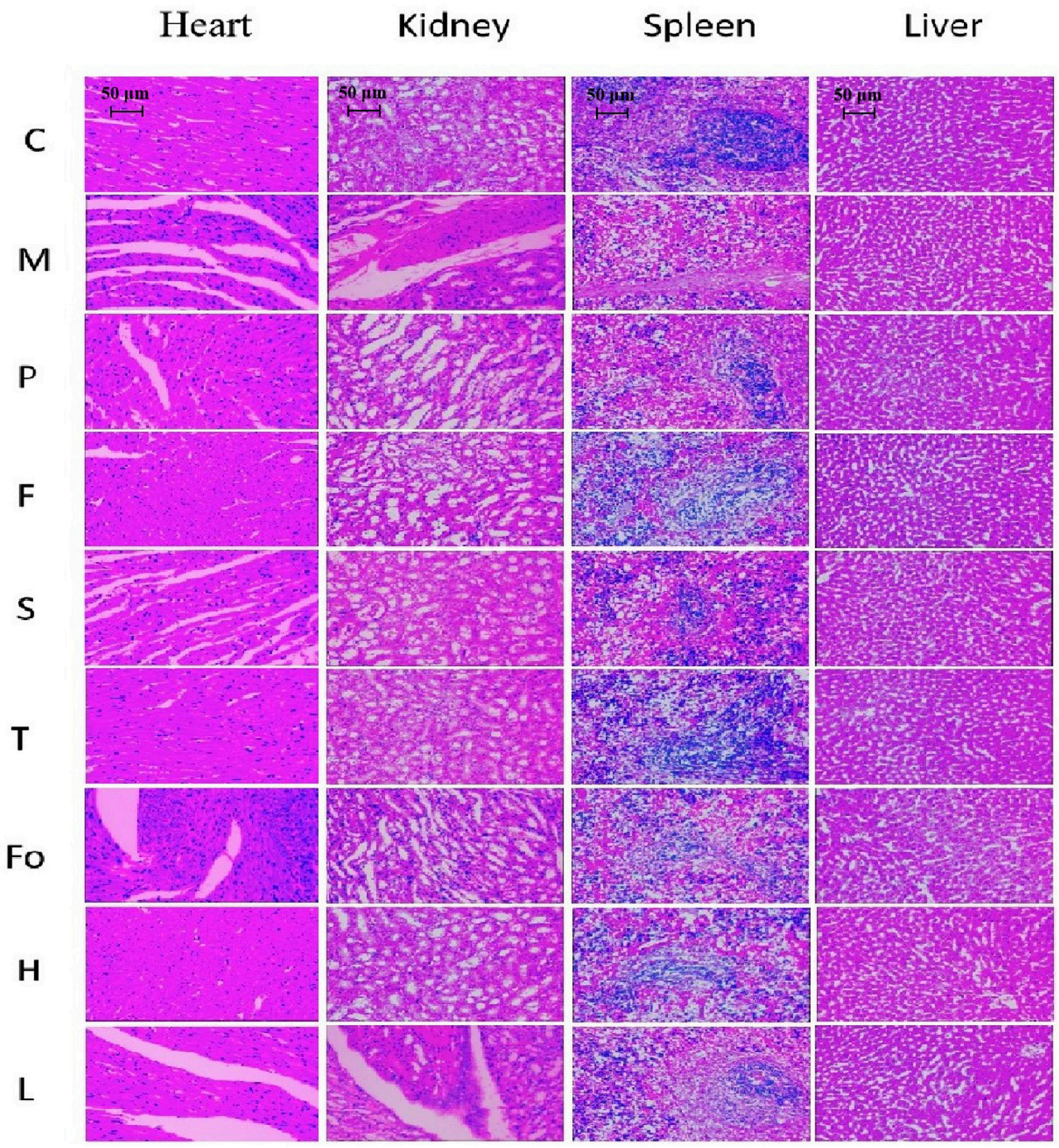


FIGURE 6
Effect of RAS on the heart, kidney, spleen, and liver in BD rats (H & E staining, × 200).

ferulic acid, levistilide I, and levistilide A have been found to alleviate RBC aggregation (Hong et al., 2003). In this study, we selected ferulic acid, ligustilide, senkyunolide I, uridine, and guanine as Q-markers of RAS to assess their impact on blood circulation.

In a rat model of BD, APH and CTX were administered to assess the efficacy of TCM in enhancing blood circulation (Lu, 2015). APH, known for its potent oxidizing properties, inflicts oxidative damage on RBCs, leading to hemolytic anemia within the organism (Roth et al., 1979). Conversely, CTX serves as a cytotoxic agent that targets bone marrow cells. The destruction of these bone marrow cells prompts the spleen (Pi) to assume responsibility for immune hematopoiesis, resulting in enlargement of the spleen (Wang et al., 2009). However, this enlargement of the spleen can lead to hypersplenism and impairment of immune functions. In TCM, the spleen is regarded as crucial in managing blood and enhancing blood circulation. In modern medical science, the spleen is recognized as a

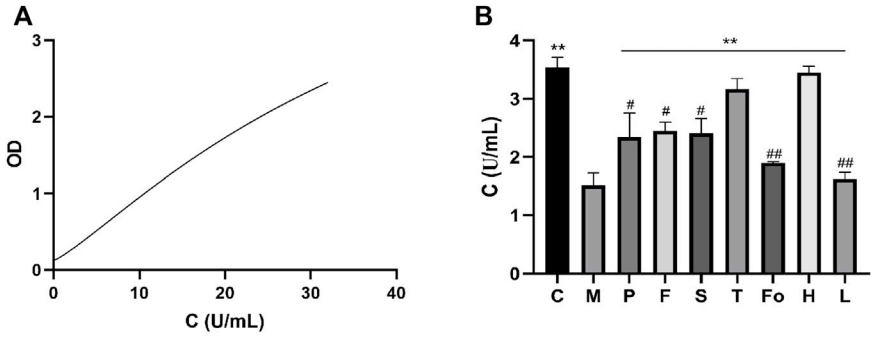


FIGURE 7
Effect of RAS on the content of ATPase activity in BD rats (mean ± SD, n = 3). **$p < 0.01$, vs model group; #$p < 0.05$, ##$p < 0.01$, vs the third-grade group.

TABLE 4 Information on the identification of differential endogenous metabolites in the plasma of rats with blood deficiency (trend: model vs. control group).

No.	T_R (time)	Observed m/z (ESI+)	VIP	Molecular formula	Metabolites	MS/MS fragment ion (m/z)	Trend
1	11.28	560.3367 [M + FA + Li] $^+$	10.66	$C_{25}H_{52}NO_7P$	LysoPC(17:0) (Wang et al., 2022)	86.0963, 104.1069, 184.0732, 500.2446, 524.3130, 542.3235	↑
2	10.82	818.5822 [M + Na]$^+$	6.33	$C_{45}H_{83}N_2O_7P$	SM(d20:1/20:4 (5Z,7E,11Z,14Z)-OH(9))	337.2517, 355.2627, 373.2733, 799.5704	↑
3	20.45	759.5700 [M + H]$^+$	5.41	$C_{42}H_{80}NO_8P$	PC(18:1 (9Z)-O (12,13)/P-16:0)	184.0732	↑
4	15.37	546.3528 [M + Na]$^+$	4.45	$C_{26}H_{54}NO_7P$	LysoPC(0:0/18:0)	86.0946, 91.0535, 184.0655, 238.0989, 261.1334	↑
5	9.54	305.2983 [M + H]$^+$	4.4	$C_{20}H_{32}O_2$	Arachidonic acid (Bian et al., 2023)	44.9971	↑
6	15.48	611.4128 [M + Na]$^+$	4.18	$C_{39}H_{56}O_4$	Caffeoylcycloartenol	89.0608, 207.0626, 269.2481	↓
7	15.31	613.4323 [M + CH_3OH + H]$^+$	3.47	$C_{33}H_{56}O_8$	DG (PGE2/0:0/10:0)	46.0655, 287.2359, 331.2636	↓
8	10.45	464.2823 [M + H]$^+$	3.29	$C_{22}H_{23}O_{11}$	LysoPA (20:2 (11Z,14Z)/0:0)	97.9759,105.0332, 207.0816, 311.1207, 405.2041	↑
9	11.23	393.5709 [M + H]+	3.06	$C_{24}H_{40}O_4$	Chenodeoxycholic acid (Zhan et al., 2012)	82.0012, 128.1031	↓
10	8.98	162.1985 [M + H]$^+$	2.92	$C_7H_{15}NO_3$	*L*-Carnitine (Wu et al., 2016)	74.0486, 89.0711	↓
11	14.78	759.5778 [M + H]$^+$	2.04	$C_{42}H_{80}NO_8P$	PE (15:0/22:2 (13Z,16Z))	86.0964, 184.0730	↑
12	7.16	301.1412 [M + Na]$^+$	1.78	$C_{16}H_{22}O_4$	Diisobutyl phthalate	45.0338, 67.0544, 89.0602	↑
13	1.06	90.0555 [M + H]$^+$	1.73	$C_3H_7NO_2$	*L*-Alanine (Huang et al., 2018)	116.0936	↑
14	11.03	637.5191 [M + H]$^+$	1.73	$C_{41}H_{81}NO_3$	Ceramide (Li et al., 2022)	74.0459, 312.2797, 398.3083	↑
15	6.32	176.0951 [M + H]$^+$	1.66	$C_6H_{13}N_3O_3$	Citrulline (Zhang, 2020)	143.7347, 156.9812	↓
16	8.53	129.0658 [M + H]$^+$	1.65	$C_5H_8N_2O_2$	Dihydrothymine	76.1312	↓
17	1.74	132.1735 [M + H]$^+$	1.64	$C_6H_{13}NO_2$	*L*-Leucine (Zhu et al., 2020)	102.1044	↓
18	3.61	147.0773 [M + H]$^+$	1.63	$C_5H_{10}N_2O_3$	*L*-Glutamine (Yang et al., 2013; Wang et al., 2015)	155.4121	↓
19	15.59	482.2997 [M + H]$^+$	1.52	$C_{28}H_{37}N_2O_5$	Unknown	325.2018, 461.1941	↑

vital central immune organ, housing cytotoxic T lymphocytes and delayed-type hypersensitive T lymphocytes (Yao et al., 2021). RAS has been found to elevate PLT levels, restore spleen indices, alleviate organ damage, and enhance ATPase activity in erythrocyte membranes. In this study, histopathological results revealed an increase in neutrophilic granulocytes and interstitial edema in the

TABLE 5 Information on the identification of differential endogenous metabolites in the urine of rats with blood deficiency (trend: model vs. control group).

No.	T_R (time)	Adduct *m/z* (ESI^+)	VIP	Molecular formula	Metabolites	MS/MS fragment ion (m/z)	Trend
1	13.16	751.5080 $[M + Na]^+$	4.39	$C_{41}H_{76}O_8P$	Cardiolipins (CL)	329.2477, 603.5331, 738.5012	↓
2	0.66	369.4645 $[M + H]^+$	1.91	$C_{20}H_{32}O_6$	Endoperoxide G2	295.1094	↑
3	7.34	315.2060 $[M + H]^+$	1.89	$C_{19}H_{26}N_2O_2$	Unknown	286.1544	↓
4	6.71	289.2260 $[M + Li]^+$	1.79	$C_{19}H_{26}N_2$	Aspidospermidine (Feng, 2019)	41.0386, 255.1809, 267.1809	↓
5	8.32	338.1875 $[M + K]^+$	1.78	$C_{20}H_{29}NO$	Unknown	83.0851	↑
6	8.30	132.1019 $[M + H]^+$	1.72	$C_6H_{13}NO_2$	*L*-lsoleucine	86.0979, 91.0541	↓
7	5.32	180.1727 $[M + H]^+$	1.61	$C_9H_9NO_3$	hippuric acid (Yang, 2019)	91.1137, 119.0007	↓
8	1.21	819.4525 $[M + H]^+$	1.61	$C_{41}H_{72}NO_{11}PS$	PA (LTE4/*i*-15:0)	189.0935, 391.2663	↑
9	1.07	216.1233 $[M + Na + H]^+$	1.59	$C_6H_8O_7$	Citric acid (Huang et al., 2020)	133.0137	↓
10	4.93	863.6179 $[M + H]^+$	1.57	$C_{46}H_{87}NO_{13}$	Galabiosylceramide (Ferraris et al., 2022)	145.0501,163.0598, 708.5770	↓
11	7.19	234.0516 $[M+2Na]^+$	1.54	$C_7H_{12}N_2O_4$	Glycylhydroxyproline	44.9965	↓
12	13.14	795.9741 $[M + Li]^+$	1.52	$C_{42}H_{77}O_{11}P$	PA (*i*-19:0/PGE1)	96.9685	↑

heart, vacuoles and focal segmental sclerosis in the glomerulus, and a significant reduction in the white pulp in the spleen of the model group. Different grades of RAS exhibited varying degrees of efficacy in promoting blood circulation. Notably, third-grade RAS demonstrated the most favorable activity, aligning with the findings of the compound content analyses and *in vivo* and *in vitro* experiments.

Metabolomics and lipidomics analyses were conducted on BD rats, focusing on glycerophospholipids, amino acids, and polyunsaturated fatty acids (PUFAs), among other components, in comparison to the model group. Following treatment with RAS, the levels of metabolites and lipids were restored to normal. Notably, RAS was found to regulate the levels of certain glycerophospholipids in BD rats. Glycerophospholipids, including LysoPCs and PCs, are the most abundant phospholipids in the endoplasmic reticulum. They play crucial roles in cell membrane protein recognition, signal transduction, maintaining the body's energy metabolism, and promoting material transport. LysoPCs, a subset of lysoglycerophospholipids, are particularly abundant in the blood, especially in plasma. When combined with a protein carrier, LysoPC plays a key role in facilitating the transfer of fatty acids for the growth and development of the brain and the body. It also serves as a fundamental component for synthesizing nerve cell membranes (Han et al., 2016). In an extracellular context, elevated concentrations of LysoPC can disrupt cell membrane integrity, leading to membrane rupture and subsequent toxicity (Ma et al., 2019). LysoPC is a significant pharmacodynamic marker associated with RAS efficacy in BD rats. It activates transient receptor potential 6 (TRPC6) channels, which in turn trigger the lipid-cleaving enzyme phospholipase A2 (PLA2) to release AA from cellular membranes, allowing calcium influx (Putta et al., 2021). The activation of the arachidonate lipoxygenase-15/12-hydroxyeicosatetraenoic acid (Alox15/12-HETE) signaling pathway during AA lipoxygenase metabolism serves to protect calcified blood vessels (Han et al., 2021). Furthermore, previous research has demonstrated that RAS obtained from geoherbs exhibits robust calcium-antagonistic activity (Zhang et al., 2019a).

LysoPC is recognized as a critical proinflammatory cytokine in atherosclerosis (AS), impacting endothelium-dependent vasorelaxation and vascular smooth muscle cells, and influencing platelet aggregation and coagulation pathways (Matsumoto et al., 2007). Importantly, LysoPCs possess hypoglycemic and anti-inflammatory properties. PCs and PEs, primarily found in cell membranes and lipoproteins, constitute over 50% of glycerophospholipids. PC, in particular, can inhibit inflammation (Guzzolino et al., 2018), influence macrophage phagocytosis strength, regulate immunity, and impact organelle biosynthesis, secretion, and endocytosis (Sasset et al., 2016). Simultaneously, PC contributes to the removal of peroxides from the plasma, breaks down cholesterol and fatty acids, reduces cholesterol and neutral fat levels in the blood, accelerates the excretion of fat, shortens its retention time, and restores the elasticity of blood vessel walls (Snider et al., 2018). In contrast, the accumulation of SM in whole blood increases viscosity and is considered a risk factor for coronary heart disease (Sasset et al., 2016). The reduction in SM levels indicates that RAS may decrease whole-blood viscosity, potentially preventing cardiovascular disease.

Furthermore, L-glutamine exerts its influence by inhibiting the production of reactive oxygen species, specifically oxygen-free radicals. It accomplishes this by activating the nuclear factor erythroid-2 related factor 2/antioxidant response element (Nrf2/ARE) signaling pathway, which in turn regulates levels of superoxide dismutase and glutathione (Xue et al., 2018). In the present study, L-glutamine and citrulline, both critical for arginine synthesis, were found to be downregulated in the model group. This downregulation results in significant inhibition of mitochondrial biosynthesis and

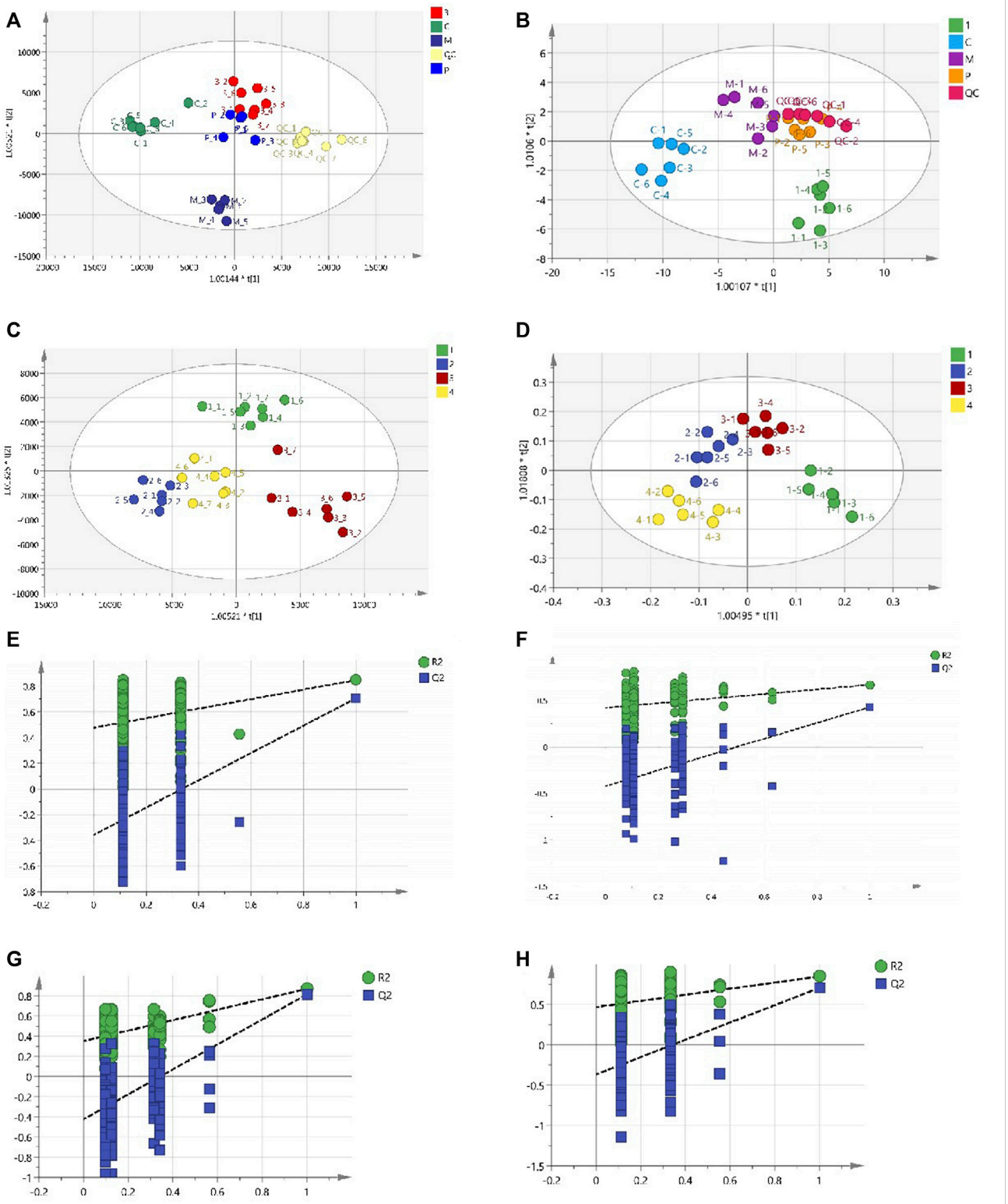


FIGURE 8
OPLS-DA score plot and ermutation test plot of the OPLS-DA models. ((**A**) OPLS-DA score plot of the control group, model group, positive group, the third-grade group of RAS, and QC group in plasma; **(B)** OPLS-DA score plot of the control group, model group, positive group, the first-grade group of RAS, and QC group in urine; **(C)** OPLS-DA score plot of different grade groups of RAS in plasma; **(D)** OPLS-DA score plot of different grade groups of RAS in urine; **(E)** The control group, model group, positive group, the third-grade group of RAS, and QC group samples of 200 permutation times in plasma; **(F)** The different grade samples of 200 permutation times in plasma; **(G)** The control group, model group, positive group, the first-grade group of RAS, and QC group samples of 200 permutation times in urine; **(H)** The different grade samples of 200 permutation times in urine).

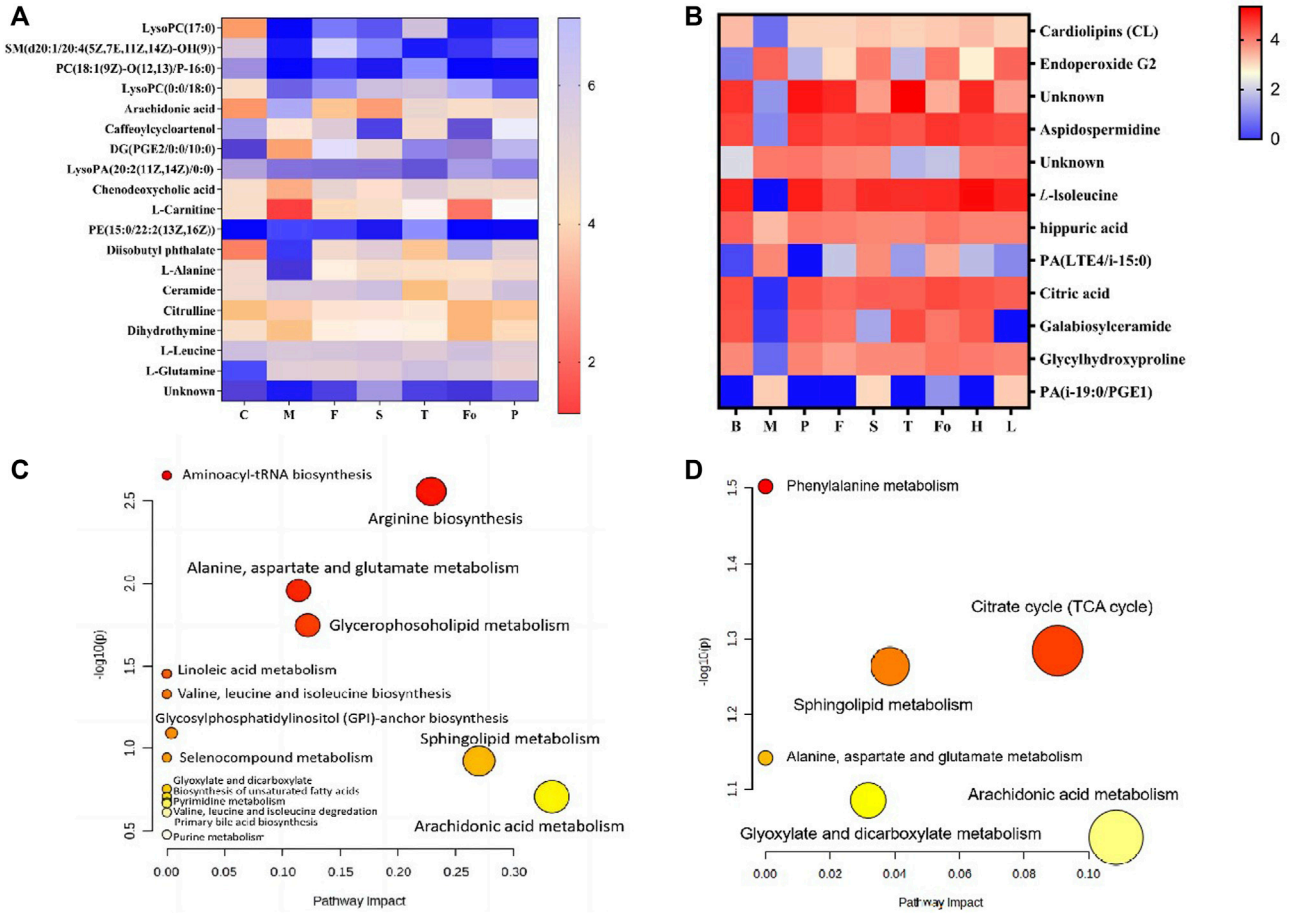


FIGURE 9
The heatmap visualization of the differential metabolites in plasma **(A)** and urine **(B)**, altered metabolomic pathways observed in plasma sample after RAS treatment in plasma **(C)** and urine **(D)**.

ATP production (Hai, 2009). Furthermore, excessive pyruvate and other metabolites, along with disruptions in arginine and proline metabolism, interferes with the TCA cycle (Wang et al., 2013), ultimately reducing hemoglobin production (Hao and Yan, 2015). Additionally, an excess of ceramide accumulation was noted, causing disturbances in sphingolipid metabolism. Sphingolipids are implicated in potential mechanisms underlying cardiovascular disease (Jia et al., 2022). RAS can rectify sphingolipid metabolism by downregulating ceramide from a disordered state to normal levels. The breakdown of lipids into acetyl-CoA also impacts the TCA cycle and ATP production (Hua et al., 2017). Notably, nineteen potential endogenous metabolites primarily participated in five metabolic pathways. RAS has been demonstrated to enhance blood circulation by modulating the metabolism of arachidonic acid; arginine biosynthesis; alanine, aspartate, and glutamate metabolism; sphingolipid metabolism; and glycerophospholipid metabolism. Managing energy metabolism is considered to be a fundamental strategy in preventing hemolysis and treating BD (Zhang et al., 2022a). This approach involves regulating the osmotic pressure of blood cells and bolstering their synthesis. In summary, RAS effectively reduces the accumulation of AA, thereby shortening the period of activity of TRPC6 channels, enhancing calcium antagonistic activity, and participating in five key metabolic pathways.

BD model rats have been reported to exhibit metabolic disturbances in their blood. RAS has been shown to exert regulatory effects on various metabolic pathways, including the ornithine cycle, platelet biochemical pathways, fructose metabolism, lipid metabolism, the folate cycle, and energy metabolism (Hua et al., 2017). Furthermore, Angelica sinensis polysaccharides (ASP) and phthalides have demonstrated significant impact on the BD model. ASP, for instance, inhibits Wnt/β-catenin signaling pathway-mediated premature senescence and oxidative stress in hematopoietic cells, thereby mitigating oxidative damage and regulating perivascular niche function (Niu et al., 2023). Additionally, ASP protects hematopoietic stem/progenitor cells and prevents hematopoietic regression by enhancing the hematopoietic microenvironment (Jing et al., 2023). Ligustilide, a compound with a crucial role in enhancing blood circulation, offers protection against nerve damage caused by ischemic stroke. It accomplishes this by modulating the Drp1-mediated mitochondrial fission pathway by activating AMP-

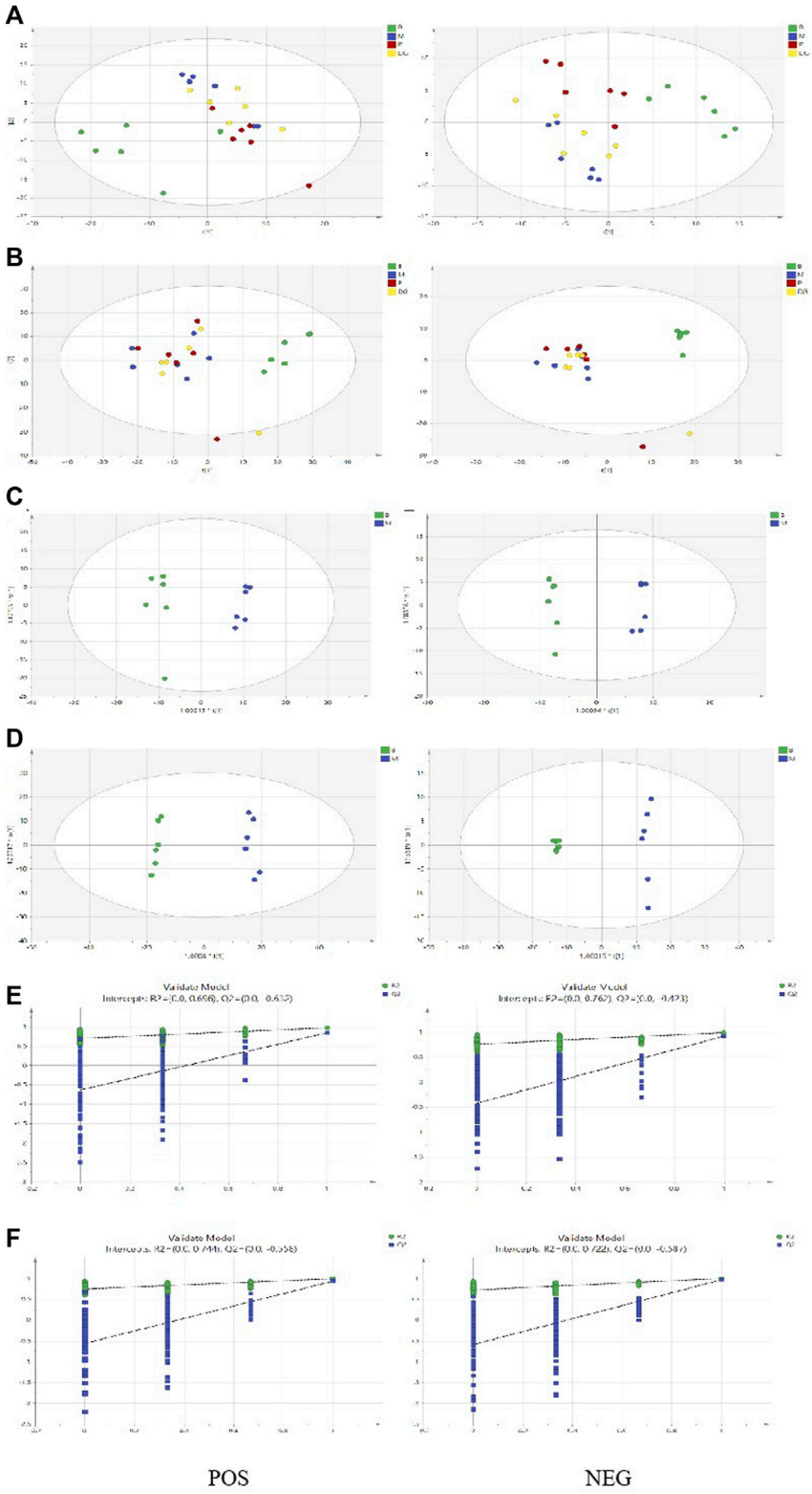


FIGURE 10
PCA score plot, OPLSDA score plot, and ermutation test plot of the OPLS-DA models. ((**A**) PCA score plot of the control group, model group, positive group, and the third-grade group of RAS in plasma via positive and negative model; **(B)** PCA score plot of the control group, model group, positive group, and the third-grade group of RAS in urine via positive and negative model; **(C)** OPLS-DA score plot of the control group and model group in plasma via positive and negative model; **(D)** OPLS-DA score plot of the control group and model group in urine via positive and negative model; **(E)** The control group and model group samples of 200 permutation times in plasma via positive and negative model; **(F)** The control group and model group samples of 200 permutation times in urine via positive and negative model).

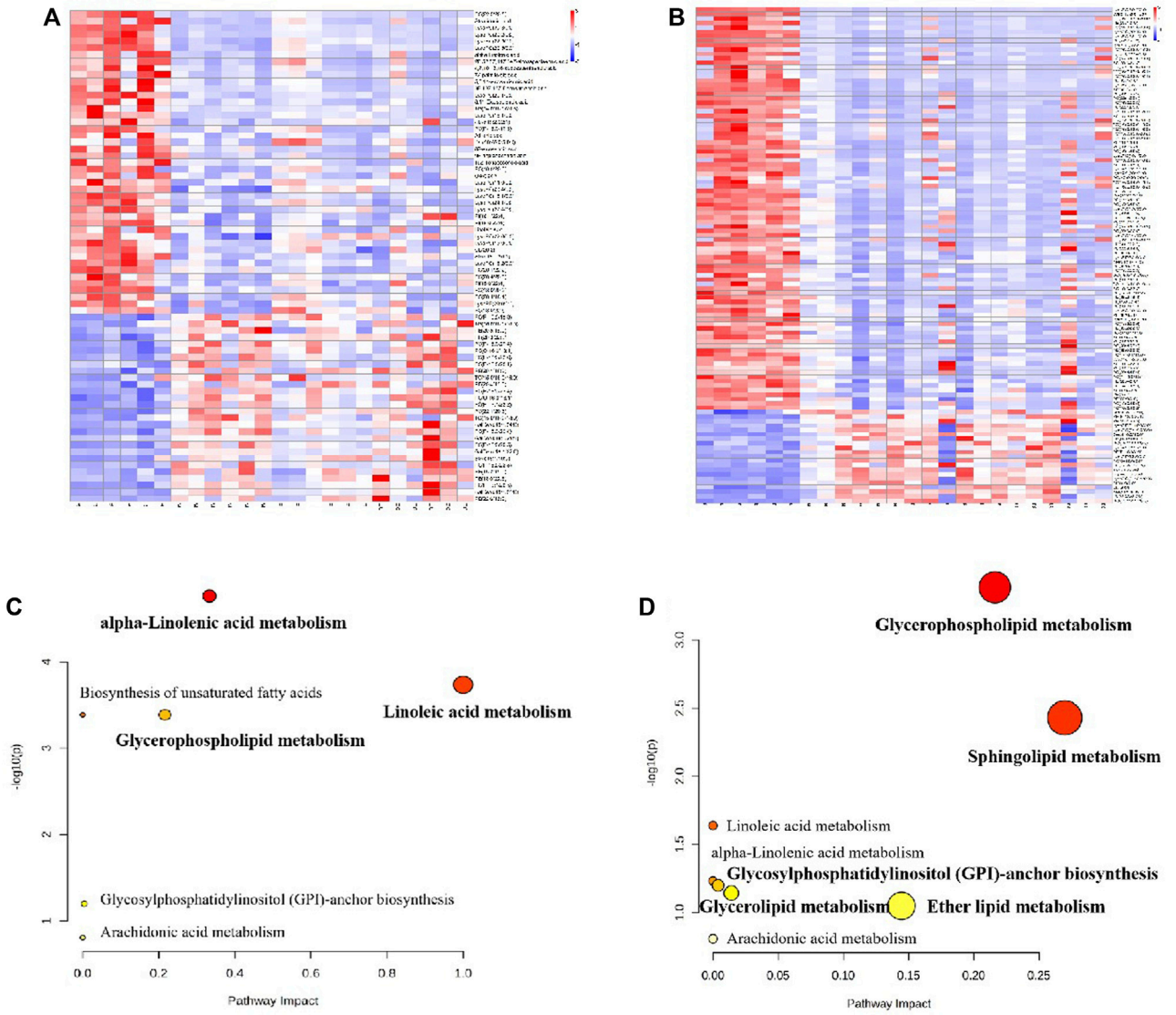


FIGURE 11
The heatmap visualization of the differential lipid metabolites in plasma **(A)** and urine **(B)**, altered lipid metabolomic pathways observed in plasma sample after RAS treatment in plasma **(C)** and urine **(D)**.

activated protein kinase (AMPK) signaling (Wu et al., 2022b). Ligustilide also safeguards vascular endothelial cells from oxidative stress by acting as an effective activator of Nrf2 (Liang et al., 2021). Ferulic acid can alleviate atherosclerotic plaques by inhibiting the proliferation of vascular smooth muscle cells (Wu et al., 2022a). Additionally, ferulic acid can impede the synthesis of triglycerides and cholesterol by upregulating adenosine monophosphate or ATP, which is sensed by AMPK (Gao et al., 2022). Finally, senkyunolide I has been shown to protect the brain from focal cerebral ischemia-reperfusion injury by binding to a promoter known as ARE, leading to the upregulation of several antioxidant and detoxification genes (Hu et al., 2015).

Urine constitutes a significant component in the body's metabolic processes, and investigating differences in metabolites holds profound importance in comprehending the overall integrity of these processes. Citric acid, a vital precursor for the synthesis of essential fatty acids and a source of inflammatory mediators like prostaglandin and nitric oxide (Hu et al., 2015), plays a crucial role in metabolism. Amino acid metabolism is a carbon source for the energy cycle (Hao and Yan, 2015). Glutamine can be enzymatically broken down by glutaminase into glutamic acid and α-ketoglutaric acid, which in turn provide energy for the TCA cycle (Hao and Yan, 2015). The TCA cycle, a convergence point for the catabolism of sugars, fats, and amino acids, draws on intermediates from various biosynthetic pathways (Hua, 2014). Consequently, changes in the TCA cycle may reflect shifts in overall energy metabolism. Observing the citric acid content in the model group in the present study, we noted a decrease followed by an increase after treatment, indicating that RAS has the potential to enhance glycolysis, strengthen the energy cycle, and bolster energy

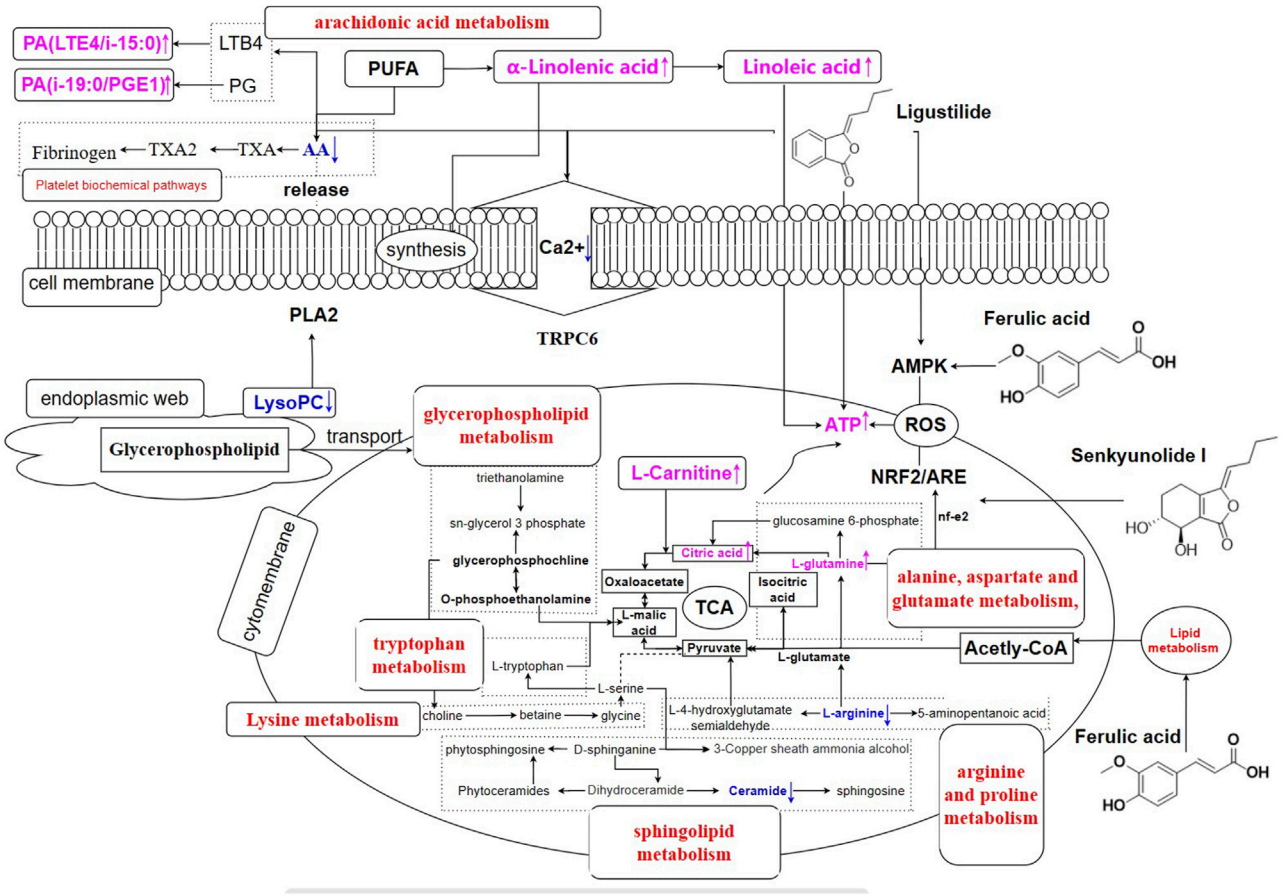


FIGURE 12
Regulation on metabolic network of RAS in BD rats (control vs. model group, the purple towards up-regulating; the blue towards down-regulating).

provision in the body. Galabiosylceramide, a ceramide dihexoside, is derived from sphingosine and is subject to degradation by α-galactosidase A in lysosomes, resulting in X-linked lysosomal storage disorder (Kamzolova et al., 2003). Notably, sphingosine is involved in cancer cell apoptosis via stimulation of phospholipase C-protein kinase C and activation of phospholipase D, serving as a metabolic marker for metabolic and chronic diseases (Dowdy et al., 2020; Akiyama et al., 2021).

The increase in galabiosylceramide content in BD rats post-treatment suggests that RAS may effectively treat metabolic diseases associated with BD syndrome by regulating sphingolipid metabolism. Arachidonic acid metabolism is a core pathway in inflammatory metabolism, exerting a significant influence on immune function (Wang et al., 2020). Under the influence of lipoxygenase, this pathway leads to the production of immunomodulatory factors such as prostaglandin E2 (PGE2) and leukotriene B4 (LTB4). LTB4 finally forms the metabolite LTE4 via leukotriene C4 synthase and protease processing (Li et al., 2014). Prostaglandin E1 (PGE1), in particular, increases the content of cAMP in vascular smooth muscle cells, leading to vasodilation (Löfgren et al., 2020); enhances the deformability of RBC; activates immunoreactive cells (Amberger et al., 2019); and inhibits platelet aggregation activity, thereby avoiding the formation of AS plaques, reducing the incidence of AS, and providing protection from ischemic myocardial cell injury (Gu et al., 1985). The enhancement of arachidonic acid metabolism in BD rats, as indicated by the increase in endoperoxide G2 and PA (LTE4/i-15:0), gives rise to inflammatory reactions. RAS, however, can regulate arachidonic acid metabolism, inhibiting the release of inflammatory factors, regulating the production of immune regulatory factors, and reducing the body's inflammatory response. The elevation of PA (i-19:0/PGE1) suggests an increase in production of PGE1, which effectively inhibits platelet aggregation, enhances erythrocyte deformation ability, and holds promise for the effective treatment of BD syndrome. Furthermore, some researchers have identified a connection between RAS and the regulation of ketone synthesis, degradation, and pyruvate metabolism, findings that align with the results of this study corroborating the blood-enriching mechanisms of RAS.

The downstream metabolites of PUFA in the body include AA, prostaglandins (PG), thromboxane, interleukin leukotrienes (LTs), and various other inflammatory factors (Chemello et al., 2022). Linolenic acid, an essential fatty acid in the body, is a precursor for prostaglandin synthesis (Liu et al., 2023). Under the action of desaturase and elongation enzymes, α-linolenic acid is gradually converted to linolenic acid. Eicosapentaenoic acid (EPA) and docosahexaenoic acid (DHA) can produce a series of specific anti-inflammatory mediators through the catalysis of

cyclooxygenases, lipoxygenases, and cytochrome P450 oxidases, which have significant physiological effects on the body (Li et al., 2006). α-linolenic acid exhibits an inhibitory effect on lipoprotein synthesis in the liver and enhances metabolic rates, contributing to improved resistance to thrombosis. The increase in α-linolenic acid content after treatment indicates that RAS effectively exerts anti-inflammatory effects by influencing linolenic acid metabolism. Moreover, EPA, catalyzed by cyclooxygenases (COX), produces thromboxane A3, which inhibits platelet aggregation and prostacyclin I3, promoting vasodilation, PGE3, and leukotriene LT5, with anti-inflammatory properties (Anand and Kaithwas, 2014). Linoleic acid protects cardiovascular and cerebrovascular processes, cell membrane synthesis, cholesterol synthesis, and metabolism. In its absence, the body experiences cholesterol metabolism disorders, leading to gradual deposition of cholesterol in the vascular walls, ultimately resulting in atherosclerosis (AS). Accumulated PUFA, on the other hand, primarily serves to prevent AS. RAS effectively reduces the accumulation of PUFA and thus prevents AS. By regulating energy metabolism, linoleic acid inhibits fat deposition in mice (Cao et al., 2018). The increase in linoleic acid content post-treatment signifies that RAS can impact energy metabolism by regulating linoleic acid content, addressing BD syndrome.

The spleen is a primary immune organ. RAS can regulate the levels of glycerophospholipids in the spleen, enhance the body's immune system, and effectively fight inflammation. Cyclophosphamide induces immune inhibition through lipid metabolism disorder (Simpson et al., 2021). Lipid metabolism disorders are one of the factors that induce AS. RAS can regulate the increase in TG content that occurs in the spleen of BD rats and regulate lipid metabolism, which returns to normal, indicating that RAS can effectively prevent AS, thus reducing the probability of diseases such as myocardial infarction and stroke. In contrast, when the body is in an ischemic state, the spleen can release a large number of monocytes into the plasma, activate the angiotensin II signaling pathway (Li et al., 2015), induce cell migration to the heart, kidney, and other organs, and maintain the everyday activities of the body (Leuschner et al., 2010). Conversely, several marrow progenitor cells migrate out of the bone marrow and accumulate in the spleen, resulting in extramedullary hematopoietic function. Simultaneously, several red blood cells accumulate in the spleen, aggravating anemia and resulting in a significant increase in the spleen index and splenomegaly (Shen, 2016). As an important source of inflammatory cells, the spleen restores lipid metabolism and enhances immunity. RAS can treat bone marrow perivascular mesenchymal progenitor cell damage and enhance the effects on the blood (Zhang et al., 2019b), restoring splenomegaly. The potential mechanism of action of RAS in the treatment of blood-deficient rats is shown in Figure 12.

5 Conclusion

In this study, we have extensively explored the attributive classification of various grades of RAS through a combination of *in vivo* and *in vitro* assessments. We have also investigated the therapeutic mechanisms underpinning the effectiveness of RAS in replenishing and invigorating blood circulation. To the best of our knowledge, this research marks the first attempt to elucidate the bioactive features associated with different grades of RAS. Our key findings reveal that the third grade of RAS exhibits a significantly superior capacity to replenish and invigorate blood circulation. Furthermore, we have identified ferulic acid, ligustilide, senkyunolide I, uridine, and guanine as valuable Q-markers for assessment and and enhancement of the blood circulation effects of RAS. The metabolic pathways investigated in our study, including glycerophospholipid metabolism, sphingolipid metabolism, arachidonic acid metabolism, the TCA cycle, and amino acid metabolism, form the core avenues through which RAS addresses BD syndrome. This intricate understanding of metabolic interactions and the impact of RAS within these pathways has provided valuable insights into the relevant therapeutic mechanisms. Moreover, our findings suggest that RAS may be crucial in restoring lipid metabolism. It achieves this by effectively regulating glycerophospholipid and sphingolipid metabolic processes, optimizing the TCA cycle and amino acid metabolism, and ultimately enhancing energy metabolism. The regulation of arachidonic acid metabolism further promotes blood circulation, addressing the core issues associated with BD. In summary, this study has substantially contributed to the scientific classification of commercial grades of RAS, which holds significant promise in TCM. As the research field evolves, our findings offer a reasonable methodological reference for the establishment of standardized grading in TCM.

Data availability statement

The original contributions presented in the study are included in the article/Supplementary Material, further inquiries can be directed to the corresponding author.

Ethics statement

The animal study was approved by the Animal Ethics Committee of Lanzhou University. The study was conducted in accordance with the local legislation and institutional requirements.

Author contributions

XS: methodology, investigation, data curation, writing–review and editing, and visualization. YW: methodology and investigation. PC: investigation and writing of the original draft. YB: investigation and writing of the original draft. YL: conceptualization and visualization. YJ: conceptualization and visualization. YZ: visualization, review, and editing. ZY: methodology, conceptualization, resources, supervision, review, and editing. All authors contributed to the article and approved the submitted version.

Funding

This research was supported by the Major International S&T Cooperation Project, Ministry of Science and Technology of the

People's Republic of China (2016YFE0129000), the Key Project of the NMPA Key Laboratory for Quality Control of Traditional Chinese Medicine (2020GSMPA-KL11 and 2022GSMPA0010), Fundamental Research Funds for the Central Universities (lzujbky-2022-sp09), and the Medical Innovation and Development Project of Lanzhou University (lzuyxcx-2022-176).

Conflict of interest

The authors declare that the research was conducted in the absence of any commercial or financial relationships that could be construed as a potential conflict of interest.

Publisher's note

All claims expressed in this article are solely those of the authors and do not necessarily represent those of their affiliated organizations, or those of the publisher, the editors and the reviewers. Any product that may be evaluated in this article, or claim that may be made by its manufacturer, is not guaranteed or endorsed by the publisher.

Supplementary material

The Supplementary Material for this article can be found online at: https://www.frontiersin.org/articles/10.3389/fphar.2023.1230861/full#supplementary-material

References

Akiyama, H., Ide, M., Yamaji, T., Mizutani, Y., Niimi, Y., Mutoh, T., et al. (2021). Corrigendum to "Galabiosylceramide is present in human cerebrospinal fluid. *Biochem. Biophys. Res. Commun.* 543 (5), 96. doi:10.1016/j.bbrc.2021.01.065

Amberger, D. C., Doraneh-Gard, F., Gunsilius, C., Weinmann, M., Möbius, S., Kugler, C., et al. (2019). PGE(1)-containing protocols generate mature (leukemia-derived) dendritic cells directly from leukemic whole blood. *Int. J. Mol. Sci.* 20 (18), 4590. doi:10.3390/ijms20184590

Anand, R., and Kaithwas, G. (2014). Anti-inflammatory potential of alpha-linolenic acid mediated through selective COX inhibition: computational and experimental data. *Inflammation* 37 (34), 1297–1306. doi:10.1007/s10753-014-9857-6

Bian, Z. H., Zhang, W. M., Tang, J. Y., Fei, Q. Q., Hu, M. M., Chen, X. W., et al. (2023). Effective substances and mechanism of Yishen Guluo Mixture in treatment of chronicglomerulonephritis based on metabolomics and serum pharmacochemistry. *China J. Chin. Mat. Med.* 48 (02), 492–506. doi:10.19540/j.cnki.cjcmm.20220905.705

Cao, Y., Wang, W. Q., Chen, C., Qin, Y. T., and Guo, X. M. (2018). Structure and metabolism of w-3 polyunsaturated fatty acid and its relationship withatherosclerosis. *Chin. J. Arterioscler.* 26 (06), 633–643.

Chang, C. W., Chen, Y. M., Hsu, Y. J., Huang, C. C., Wu, Y. T., and Hsu, M. C. (2016). Protective effects of the roots of Angelica sinensis on strenuous exercise-induced sports anemia in rats. *J. Ethnopharmacol.* 193, 169–178. doi:10.1016/j.jep.2016.08.010

Chemello, K., Chan, D. C., Lambert, G., and Watts, G. F. (2022). Recent advances in demystifying the metabolism of lipoprotein(a). *Atherosclerosis* 349, 82–91. doi:10.1016/j.atherosclerosis.2022.04.002

Chen, E. L., Li, X. X., Wu, S. N., Wang, X., Niu, M., Wang, J. B., et al. (2019). Study on quality evaluation of Angelica sinensis based on biological titer of activating blood. *J. Chin. Med. Mat.* 42 (04), 818–821. doi:10.13863/j.issn1001-4454.2019.04.024

Cui, F. Y., Yang, J. Y., Wang, Z. G., Li, X. Y., Chen, P., Yang, H. J., et al. (2022). Application and prospect of metabolomics in traditional Chinese medicine research. *Chin. Tradit. Herb. Drugs* 53 (14), 4512–4526.

Dowdy, T., Zhang, L., Celiku, O., Movva, S., Lita, A., Ruiz-Rodado, V., et al. (2020). Sphingolipid pathway as a source of vulnerability in IDH1^{mut} glioma. *Cancers (Basel)* 12 (10), 2910. doi:10.3390/cancers12102910

Feng, Y. L. (2019). *Effective constituents and mechanism of plantaginis semen against Aryl Hydrocarbon receptor-mediated renal Fibrosis Doctor dissertation*. USA, Northwest University.

Ferraris, Q., Alcazar, A., and Qian, M. C. (2022). Profiling polar lipids in whey protein phospholipid concentrate by LC-HRMS/MS. *Foodchem* 374, 131495. doi:10.1016/j.foodchem.2021.131495

Gao, J., Gu, X., Zhang, M., Zu, X., Shen, F., Hou, X., et al. (2022). Ferulic acid targets ACSL1 to ameliorate lipid metabolic disorders in db/db mice. *J. Funct. Foods* 91, 105009. doi:10.1016/j.jff.2022.105009

Gu, Y. Q., Jiang, M. T., Chen, G. R., Yang, X. h., Chen, D., Fu, F. H., et al. (1985). Prostaglandin E_1 inhibits platelet aggregation and thromboxane biosynthesis. *J. Norman Bethune Univ. Med. Sci.* (01), 9–12+21. doi:10.13481/j.1671-587x.1985.01.004

Guzzolino, E., Chiavacci, E., Ahuja, N., Mariani, L., Evangelista, M., Ippolito, C., et al. (2018). Post-transcriptional modulation of Sphingosine-1-Phosphate Receptor 1 by miR-19a affects cardiovascular development in zebrafish. *Front. Cell. Dev. Biol.* 6, 58. doi:10.3389/fcell.2018.00058

Hai, C. X. (2009). *Aasymmetric dimethylarginine inhibits mitochondrialbiosynthesis in myocardial of type 2 diabetic rats and its mechanism* Master thesis. China, Central South University.

Han, Y. C., Zhang, J. C., Zhang, C. C., and Du, J. (2021). Arachidonic acid Alox15/12-HETE signaling inhibits vascular calcification. *Acta Physiol. Sin.* 73 (04), 571–576. doi:10.13294/j.aps.2021.0051

Han, Y. Z., Jiang, Y., Lin, M., Li, Y., Li, M., and Liu, X. (2016). Determination of glutamine in human plasma by liquid chromatography-tandem massspectrometry. *J. Shenyang Pharm. Univ.* 33 (07), 572–576+580. doi:10.14066/j.cnki.cn21-1349/r.2016.07.011

Hao, J. N., and Yan, B. (2015). Recyclable lanthanide-functionalized MOF hybrids to determine hippuric acid in urine as a biological index of toluene exposure. *Chem. Commun. (Camb)* 51 (77), 14509–14512. doi:10.1039/c5cc05219j

He, P., Li, Z. Y., Liu, Y. T., Wang, Z. C., Du, G. H., and Qin, X. M. (2022). Study on commodity specification and grade standard of multi-effect herbs based onquality markers of Chinese materia medica. *Chin. Tradit. Herb. Drugs* 53 (06), 1868–1874.

Hong, M., Dong, Z. B., and Zhu, Q. (2003). Effects of ferulic acid,senkyunolide H and senkyunolide I on erythrocytes. *Lishizhen Med. Mat. Med. Res.* (12), 738–739.

Hu, Y., Duan, M., Liang, S., Wang, Y., and Feng, Y. (2015). Senkyunolide I protects rat brain against focal cerebral ischemia-reperfusion injury by up-regulating p-Erk1/2, Nrf2/HO-1 and inhibiting caspase 3. *Brain Res.* 1605, 39–48. doi:10.1016/j.brainres.2015.02.015

Hua, Y., Yao, W., Ji, P., and Wei, Y. (2017). Integrated metabonomic-proteomic studies on blood enrichment effects of Angelica sinensis on a blood deficiency mice model. *Pharm. Biol.* 55 (1), 853–863. doi:10.1080/13880209.2017.1281969

Hua, Y. L. (2014). *Study the metabolite and metabolic pathways of inflammation induce by LPS and intervention of Angelica sinensis volatile oil Doctor dissertation*. China, Gansu Agricultural University.

Huang, J. F., Xun, Z. Q., Wang, C. X., Guo, X. D., Xian, Y. P., Lu, Y. J., et al. (2018). Simultaneous determination of Choline, L-Carnitine, Taurine and Inositol in infant formula MilkPowder by HPLC-MS/MS. *J. Instrum. Anal.* 37 (06), 702–707.

Huang, Y. W., Jin, Y. X., Bao, X., Zhang, M. L., Wen, C. C., and Wang, X. Q. (2020). UPLC-MS/MS simultaneous determination of citric acid,succinic acid,fumaric acid,lactic acid,pyruvic acid,malic acid and fructose in rat urine and its application. *Strait Pharm. J.* 32 (04), 33–36.

Hwang, S. R., Saliba, A. N., and Wolanskyj-Spinner, A. P. (2022). Immunotherapy-associated autoimmune hemolytic anemia. *Hematol./Oncol. Clin. North Am.* 36 (2), 365–380. doi:10.1016/j.hoc.2021.11.002

Jia, Z. X., Pan, M. X., Liu, L. R., Zhu, M. X., Fang, C., Yu, Z. Y., et al. (2022). Mechanisms of Suxiao Jiuxin Pills against myocardial ischemia based on metabolomics. *Chin. Tradit. Herb. Drugs.* 53 (15), 4719–4729.

Jing, P., Song, X., Xiong, L., Wang, B., Wang, Y., and Wang, L. (2023). Angelica sinensis polysaccharides prevents hematopoietic regression in D-Galactose-Induced aging model via attenuation of oxidative stress in hematopoietic microenvironment. *Mol. Biol. Rep.* 50 (1), 121–132. doi:10.1007/s11033-022-07898-w

Kamzolova, S. V., Shishkanova, N. V., Morgunov, I. G., and Finogenova, T. V. (2003). Oxygen requirements for growth and citric acid production of Yarrowia lipolytica. *FEMS Yeast Res.* 3 (2), 217–222. doi:10.1016/S1567-1356(02)00188-5

Leuschner, F., Panizzi, P., Chico-Calero, I., Lee, W. W., Ueno, T., Cortez-Retamozo, V., et al. (2010). Angiotensin-converting enzyme inhibition prevents the release of monocytes from their splenic reservoir in mice with myocardial infarction. *Circ. Res.* 107 (11), 1364–1373. doi:10.1161/circresaha.110.227454

Li, C. L., Shang, J. F., Liao, Z. H., Cai, L. R., Yi, B. X., and Ma, X. N. (2022). Determination of L-alanine isopropyl ester in tenofovir alafenamide fumarate by LC-MS method. *Cent. South Pharm.* 20 (10), 2399–2402.

Li, J., Lin, W., Lin, W., Xu, P., Zhang, J., Yang, H., et al. (2015). Metabolic profiling study on potential toxicity and immunotoxicity-biomarker discovery in rats treated with cyclophosphamide using HPLC-ESI-IT-TOF-MS. *Biomed. Chromatogr.* 29 (5), 768–776. doi:10.1002/bmc.3355

Li, J. L., Shi, B. L., Yan, S. M., Jin, L., Xu, Y. Q., Li, T. Y., et al. (2014). Effects of different chitosan concentrations in medium on arachidonic acid metabolism in peripheral blood lymphocytes of weaner piglets. *Chin. J. Anim. Nutr.* 26 (01), 184–189.

Li, J. X., Zhang, C., and Luo, X. L. (2006). Research advances of o-Linolenic acid. *Cereals&Oils* (02), 10–12.

Liang, B., Zhu, Y., and Gu, N. (2021). Z-ligustilide protects vascular endothelial cells from oxidative stress and rescues high fat diet-induced atherosclerosis by activating multiple NRF2 downstream genes. *Atheroscler. Amst. Neth.)* 331, e19. doi:10.1016/j.atherosclerosis.2021.06.060

Liu, D. H., Xu, N., Guo, L. P., Jin, Y., Cui, X. M., Yang, Y., et al. (2016). Qualitative characteristics and classification study on commodity specification and grade standard of Panax notoginseng. *China J. Chin. Mat. Med.* 41 (05), 776–785. doi:10.4268/cjcmm20160504

Liu, Q. L., Yang, L., Liu, S., and Wang, S. (2023). Polyunsaturated fatty acid metabolism and its relationship with atherosclerosis. *Chin. J. Arterioscler.* 1-17.

Liu, X. X., Ou, Q. M., Shi, Y. T., Xin, T. Y., Song, J. Y., Luo, J. J., et al. (2018). Ldentification of Angelica sinensis and its adulterants based on ITS2 sequence. *Zhong Cao Yao* 49 (20), 4877–4883.

Liu, Y. R., Tang, Z. S., Song, Z. X., Liu, F., Duan, J. a., Chen, L., et al. (2021). Q-Marker screening method for Angelicae Sinensis Radix depending on effective components-bioactivity-efficacy network integration analysis. *Chin. Tradit. Herb. Drugs* 52 (09), 2626–2637.

Löfgren, L., Forsberg, G.-B., Davidsson, P., Eketjäll, S., and Whatling, C. (2020). Development of a highly sensitive liquid chromatography–mass spectrometry method to quantify plasma leukotriene E 4 and demonstrate pharmacological suppression of endogenous 5-LO pathway activity in man. *Prostagl. Other Lipid Mediat.* 150, 106463. doi:10.1016/j.prostaglandins.2020.106463

Lu, S. T. (2015). Detection and evaluation of experimental animal models with blood deficiency. *Chin. J. Inf. Tradit. Chin. Med.* 22 (03), 127–131.

Ma, G., Wang, T., Korhonen, P. K., Young, N. D., Nie, S., Ang, C. S., et al. (2019). Dafachronic acid promotes larval development in *Haemonchus contortus* by modulating dauer signalling and lipid metabolism. *PLoS Pathog.* 15 (27), e1007960. doi:10.1371/journal.ppat.1007960

Matsumoto, T., Kobayashi, T., and Kamata, K. (2007). Role of lysophosphatidylcholine (LPC) in atherosclerosis. *Curr. Med. Chem.* 14 (30), 3209–3220. doi:10.2174/092986707782793899

Niu, Y., Xiao, H., Wang, B., Wang, Z., Du, K., Wang, Y., et al. (2023). Angelica sinensis polysaccharides alleviate the oxidative burden on hematopoietic cells by restoring 5-fluorouracil-induced oxidative damage in perivascular mesenchymal progenitor cells. *Pharm. Biol.* 61 (1), 768–778. doi:10.1080/13880209.2023.2207592

Putta, P., Smith, A. H., Chaudhuri, P., Guardia-Wolff, R., Rosenbaum, M. A., and Graham, L. M. (2021). Activation of the cytosolic calcium-independent phospholipase A(2) β isoform contributes to TRPC6 externalization via release of arachidonic acid. *J. Biol. Chem.* 297 (4), 101180. doi:10.1016/j.jbc.2021.101180

Qian, X. Y., Nie, L. X., Dai, Z., and Ma, S. C. (2019). Research progress on evaluation of quality grade of traditional Chinese medicine. *Chin. J. Pharm. Anal.* 39 (10), 1724–1737. doi:10.16155/j.0254-1793.2019.10.01

Roth, E. F., Jr., Grossman, H. A., Tanowitz, H., and Nagel, R. L. (1979). Reticulocytes contain increased amounts of reduced glutathione except when produced by acetylphenylhydrazine. *Biochem. Med.* 21 (3), 333–341. doi:10.1016/0006-2944(79)90087-5

Sasset, L., Zhang, Y., Dunn, T. M., and Di Lorenzo, A. (2016). Sphingolipid *de novo* biosynthesis: a rheostat of cardiovascular homeostasis. *Trends Endocrinol. Metab.* 27 (11), 807–819. doi:10.1016/j.tem.2016.07.005

Shen, Y. (2016). *Spleen ischemia conditioning attenuatesrenal ischemia-reperfusion injury in rats Doctor dissertation*. Wuhan, Wuhan University.

Simpson, F. C., McTiernan, C. D., Islam, M. M., Buznyk, O., Lewis, P. N., Meek, K. M., et al. (2021). Collagen analogs with phosphorylcholine are inflammation-suppressing scaffolds for corneal regeneration from alkali burns in mini-pigs. *Commun. Biol.* ;24(21):608. doi:10.1038/s42003-021-02108-y

Snider, S. A., Margison, K. D., Ghorbani, P., LeBlond, N. D., O'Dwyer, C., Nunes, J. R. C., et al. (2018). Choline transport links macrophage phospholipid metabolism and inflammation. *J. Biol. Chem.* 293 (229), 11600–11611. doi:10.1074/jbc.RA118.003180

Song, C. C., Wang, Z. B., Su, B., Guo, Y. D., Gao, Y., Zuo, Z. P., et al. (2014). Study on commonly used rat model of blood stasis syndrome. *J. Beijing Univ. Tradit. Chin. Med.* 37 (02), 94–98.

Wang, H., Tian, Q., Zhang, J., Liu, H., Zhang, X., Cao, W., et al. (2020). Population-based case-control study revealed metabolomic biomarkers of suboptimal health status in Chinese population-potential utility for innovative approach by predictive, preventive, and personalized medicine. *EPMA J.* 11 (22), 147–160. doi:10.1007/s13167-020-00200-7

Wang, T., Jiang, X. H., and Wang, L. (2015). HPLC-MS/MS method for determination of Glutamine in rat plasma and application to pharmacokinetic study. *Chin. Pharm. J.* 50 (03), 253–257.

Wang, Y., Meng, Q., Qiao, H., Jiang, H., and Sun, X. (2009). Role of the spleen in cyclophosphamide-induced hematosuppression and extramedullary hematopoiesis in mice. *Arch. Med. Res.* 40 (4), 249–255. doi:10.1016/j.arcmed.2009.04.003

Wang, Y., Wang, Y., Li, M., Xu, P., Gu, T., Ma, T., et al. (2013). (1)H NMR-based metabolomics exploring biomarkers in rat cerebrospinal fluid after cerebral ischemia/reperfusion. *Mol. Biosyst.* 9 (3), 431–439. doi:10.1039/c2mb25224d

Wang, Y. Y., Feng, W. S., Wang, Q. H., and Kuang, H. X. (2022). Metabolomic profiling reveals blood-tonifying effect of Rehmanniae Radix Praeparatabased on theory of activating spleen and generating blood. *China J. Chin. Mat. Med.* 47 (13), 3562–3568. doi:10.19540/j.cnki.cjcmm.202220220322.401

Wei, F., Cheng, X. L., Jing, W. G., Chen, J., Yu, K., Zhang, P., et al. (2022). Some concerns about the standard establishment of Chinese medicinal medicines and decoction pieces. *Chin. Pharm. J.* 57 (18), 1493–1503.

Wu, C. X., Miao, M. X., Wang, Y. B., and Guan, L. (2016). Pharmacokinetics of ursodeoxycholic acid and chenodeoxycholic acid in bear gall powder extract by LC-MS in rats. *Cent. South Pharm.* 14 (07), 716–720.

Wu, Q., Liu, J., Mao, Z., Tian, L., Wang, N., Wang, G., et al. (2022a). Ligustilide attenuates ischemic stroke injury by promoting Drp1-mediated mitochondrial fission via activation of AMPK. *Phytomedicine* 95, 153884. doi:10.1016/j.phymed.2021.153884

Wu, X., Hu, Z., Zhou, J., Liu, J., Ren, P., and Huang, X. (2022b). Ferulic acid alleviates atherosclerotic plaques by inhibiting VSMC proliferation through the NO/p21 signaling pathway. *J. Cardiovasc. Transl. Res.* 15 (4), 865–875. doi:10.1007/s12265-021-10196-8

Xue, S., He, W., Zeng, X., Tang, Z., Feng, S., Zhong, Z., et al. (2018). Hypothermic machine perfusion attenuates ischemia/reperfusion injury against rat livers donated after cardiac death by activating the Keap1/Nrf2-ARE signaling pathway. *Mol. Med. Rep.* 18 (1), 815–826. doi:10.3892/mmr.2018.9065

Yang, B. W. (2017). *Study on grades quality and species identification among various Danggui roots* Master thesis. Chengdu, Chengdu University of Traditional Chinese Medicine.

Yang, F., Wang, H. Y., Hu, B., and Jiang, J. (2013). Quantitative determination of leucine concentration and the abundance of ^{13}C-leucine in humanplasma by LC-MS/MS. *Chin. J. Pharm. Anal.* 33 (08), 1322–1325+1330. doi:10.16155/j.0254-1793.2013.08.025

Yang, K., and Han, X. (2016). Lipidomics: techniques, applications, and outcomes related to biomedical sciences. *Trends biochem. Sci.* 41 (11), 954–969. doi:10.1016/j.tibs.2016.08.010

Yang, Z. (2019). Magnetic moleculary imprinted polymer-magnetic solid phase extraction coupled with ultra performance liquid chromatography-tandem mass spectrometry for the determination of hippuic acid and methyhippuric acid in urine samples. *Master Thesis. Univ. South China*.

Yao, J. H., Zhao, M., and Xia, X. J. (2021). Discussion on the spleen and blood. *Clin. J. Chin. Med.* 13 (12), 22–23.

Zhan, T. Y., Shi, L., Zhao, S. J., Zeng, X. H., He, B. X., and Guan, H. (2012). HPLC-MS/MS determination of arachidonic acid in human plasma. *Chin. J. Pharm. Anal.* 32 (03), 388–391+382. doi:10.16155/j.0254-1793.2012.03.029

Zhang, K., Shen, X., Yang, L., Chen, Q., Wang, N., Li, Y., et al. (2022a). Exploring the Q-markers of Angelica sinensis (Oliv.) Diels of anti-platelet aggregation activity based on spectrum-effect relationships. *Biomed. Chromatogr.* 36 (9), e5422. doi:10.1002/bmc.5422

Zhang, K., Yan, M., Han, S., Cong, L., Wang, L., Zhang, L., et al. (2019a). Identification of chemical markers for the discrimination of Radix Angelica sinensis grown in geoherb and non-geoherb regions using UHPLC-QTOF-MS/MS based metabolomics. *Molecules* 24 (19), 3536. doi:10.3390/molecules24193536

Zhang, L., Yu, R., Zong, Z. W., Ye, Z., Zhong, X., Jia, Y. J., et al. (2022b). Preliminary observation on the effects of myocardial energy metabolism-promoted resuscitation strategy on hemorrhagic induced cardiac arrest in rabbits. *J. Army Med. Univ.* 44 (16), 1629–1635. doi:10.16016/j.2097-0927.202201109

Zhang, R. (2020). *Establishmemt of LC-MS/MS based ceramide quantification platform and its application in patients with coronary heart disease*, Master thesis. Beijing, Beijing University of Chemical Technology.

Zhang, Z., Zhang, Y., Gao, M., Cui, X., Yang, Y., van Duijn, B., et al. (2019b). Steamed Panax notoginseng attenuates anemia in mice with blood deficiency syndrome via regulating hematopoietic factors and JAK-STAT pathway. *Front. Pharmacol.* 10, 1578. doi:10.3389/fphar.2019.01578

Zhu, G. H., Pang, W., Cheng, X. F., and Hu, J. N. (2020). Correlation between citrulline concentration and gastrointestinal injury in patients with multiple injuries by HPLC-MS/MS. *Cent. South Pharm.* 18 (08), 1344–1347.

frontiers | Frontiers in Pharmacology

TYPE Original Research
PUBLISHED 25 January 2024
DOI 10.3389/fphar.2023.1324418

Check for updates

OPEN ACCESS

EDITED BY
Wei Cai,
Hunan University of Medicine, China

REVIEWED BY
Xiangui Mei,
Shandong Agricultural University, China
Mallikarjuna Rao Pichika,
International Medical University, Malaysia

*CORRESPONDENCE
Long Dai,
2665275709@qq.com
Shaoping Wang,
wsp.0104@163.com

†These authors have contributed equally to this work

RECEIVED 19 October 2023
ACCEPTED 26 December 2023
PUBLISHED 25 January 2024

CITATION
Dong W, Li H, Li Y, Wang Y, Dai L and Wang S (2024), Characterization of active peptides derived from three leeches and comparison of their anti-thrombotic mechanisms using the tail vein thrombosis model in mice and metabonomics.
Front. Pharmacol. 14:1324418.
doi: 10.3389/fphar.2023.1324418

COPYRIGHT
© 2024 Dong, Li, Li, Wang, Dai and Wang. This is an open-access article distributed under the terms of the Creative Commons Attribution License (CC BY). The use, distribution or reproduction in other forums is permitted, provided the original author(s) and the copyright owner(s) are credited and that the original publication in this journal is cited, in accordance with accepted academic practice. No use, distribution or reproduction is permitted which does not comply with these terms.

Characterization of active peptides derived from three leeches and comparison of their anti-thrombotic mechanisms using the tail vein thrombosis model in mice and metabonomics

Weichao Dong[1,2†], Huajian Li[1,3†], Yanan Li[2†], Yuqing Wang[2], Long Dai[1*] and Shaoping Wang[1*]

[1]School of Pharmacy, Binzhou Medical University, Yantai, China, [2]School of Pharmacy, Shandong University of Traditional Chinese Medicine, Jinan, China, [3]School of Pharmacy, ZheJiang Chinese Medicial University, Hangzhou, China

Background and aims: The increasing incidence of cardiovascular diseases has created an urgent need for safe and effective anti-thrombotic agents. Leech, as a traditional Chinese medicine, has the effect of promoting blood circulation and removing blood stasis, but its real material basis and mechanism of action for the treatment of diseases such as blood stasis and thrombosis have not been reported.

Methods: In this study, *Whitmania Pigra Whitman* (WPW), *Hirudo nipponica Whitman* (HNW) and *Whitmania acranutata Whitman* (WAW) were hydrolyzed by biomimetic enzymatic hydrolysis to obtain the active peptides of WPW (APP), the active peptides of HNW (APH) and the active peptides of WAW (APA), respectively. Then their structures were characterized by sykam amino acid analyzer, fourier transform infrared spectrometer (FT-IR), circular dichroism (CD) spectrometer and LC-MS. Next, the anti-thrombotic activities of APP, APH and APA were determined by carrageenan-induced tail vein thrombosis model in mice, and the anti-thrombotic mechanisms of high-dose APP group (HAPP), high-dose APH group (HAPH) and high-dose APA group (HAPA) were explored based on UHPLC-Q-Exactive Orbitrap mass spectrometry.

Results: The results showed that the amino acid composition of APP, APH and APA was consistent, and the proportion of each amino acid was few different. The results of FT-IR and CD showed that there were no significant differences in the proportion of secondary structures (such as β-sheet and random coil) and infrared absorption peaks between APP, APH and APA. Mass spectrometry data showed that there were 43 common peptides in APP, APH and APA, indicating that the three have common material basis. APP, APH and APA could significantly inhibit platelet aggregation, reduce black-tail length, whole blood viscosity (WBV), plasma viscosity (PV), and Fibrinogen (FIB), and prolong coagulation time, including activated partial thrombin time (APTT), prothrombin time (PT) and thrombin time (TT). In addition, 24 metabolites were identified as potential biomarkers associated with thrombosis development. Among these, 19, 23, and 20 metabolites were significantly normalized after administration of HAPP, HAPH, and HAPA in the mice, respectively. Furthermore, the

intervention mechanism of HAPP, HAPH and HAPA on tail vein thrombosis mainly involved in linoleic acid metabolism, primary bile acid biosynthesis and ether lipid metabolism.

Conclusion: Our findings suggest that APP, APH and APA can exert their anti-blood stasis and anti-thrombotic activities by interfering with disordered metabolic pathways *in vivo*, and there is no significant difference in their efficacies.

KEYWORDS

leech, active peptide, tail vein thrombosis, mechanism, metabonomics, UHPLC-Q-exactive orbitrap mass spectrometer

1 Introduction

In recent years, the incidence rates of cardiovascular and cerebrovascular diseases have increased significantly, especially in the middle-aged and elderly subjects, because of modern living standards and food habits (Zeng et al., 2022). Thrombosis is one of the main causes of cardiovascular and cerebrovascular diseases. It is defined as the partial or complete blocking of the blood vessels by the thrombi or blood clots, which subsequently causes serious and life-threatening complications, including myocardial infarction and stroke (Setiabakti et al., 2023). Thrombosis is classified into arterial thrombosis and venous thrombosis based on the location and mechanism of thrombus formation. Arterial thrombosis is implicated in myocardial infarction and cerebral infarction, whereas venous thrombosis causes deep vein thrombosis and pulmonary embolism (Zhou et al., 2021). Thrombosis is generally caused by cardiovascular endothelial cell injury, abnormal blood flow, and increased blood coagulation (Chen et al., 2023). The incidence rates of venous thrombosis are significantly higher than those of arterial thrombosis in the human population; the venous/arterial thrombosis ratio is reported to be 4:1 (Warkentin, 2018). The commonly used anti-thrombotic drugs, such as warfarin and aspirin, are associated with serious adverse effects (Lee et al., 2023). Therefore, development of new anti-thrombotic drugs without serious adverse effects is a hotspot area in scientific research.

Leeches were first recorded in the Shennong's Herbal Classic, an ancient book of traditional Chinese medicine (TCM) from the Han Dynasty, as treatment for improving blood circulation by removing blood stasis (Tang et al., 2018). Several studies have reported that leeches are associated with anticoagulant, anti-inflammatory, and anti-tumor effects (Han et al., 2020). The Chinese Pharmacopoeia (version 2020) has included 3 leeches, namely, *Whitmania Pigra Whitman* (WPW), *Hirudo nipponica Whitman* (HNW) and *Whitmania acranutata Whitman* (WAW), for use in clinical treatments (Chinese Pharmacopoeia Commission, 2020). Macro-molecular components such as proteins are the main therapeutics in animal-based medicines; however, proteins cannot be directly absorbed into cells because of their high molecular weight and complex structure (You et al., 2023). Therefore, it is necessary to take corresponding methods to improve its bioavailability and efficacy. Previous studies have shown that proteins can be well absorbed by cells after being hydrolyzed into peptides or amino acids by enzymes, thus improving their bioavailability and efficacy (Li et al., 2023; Xu et al., 2023). Several bioactive peptides and proteins have been reported from the in-depth studies on leeches. Ren *et al* identified a 11 amino-acid bioactive peptide (NH_2-His-Asp-Phe-Leu-Asn-Asn-Lys-Leu-Glu-Tyr-Glu-COOH) with high anticoagulant activity from WPW, a leech that is commonly used in TCM (Ren et al., 2016). Huang et al. screened potential bioactive constituents from WPW and HNW and identified a 16 amino-acid peptide sequence (SYELPDGQVITIGNER) with potent anti-thrombin properties (Huang et al., 2020). These data suggested that small molecule peptides may be the main bioactive components of protein-based animal medicines.

Metabonomics refers to a systematic analysis of the dynamic changes in the low molecular weight metabolites at a cellular or organismal level in response to pathophysiological stimuli, genetic perturbations, or environmental factors (Yang et al., 2023). The dynamic changes in the metabolite profile will help identify perturbations at the genomic and protein levels that cause disease and are closely associated with phenotypic changes. Furthermore, comprehensive analyses of metabolite biomarkers, metabolic pathway profiles, and drug-target interactions can be used to elucidate the pathogenetic mechanisms underlying specific human diseases and the mechanism of action of drugs and other treatments (Lang et al., 2023; McMillen et al., 2023). Metabolic profiling has also been used to discover novel biomarkers and assess the holistic effects of many therapeutic components in various TCM preparations.

In the present study, we used a mimetic enzymatic method consisting of pepsin and trypsin to digest WPW, HNW, and WAW and obtain the active peptides of WPW (APP), the active peptides of HNW (APH), and the active peptides of WAW (APA), respectively. Then, we performed structural analyses of APP, APH, and APA using chemical analysis and other methods. Subsequently, we used the carrageenan-induced tail vein thrombosis model in mice to analyze the effects of APP, APH, and APA on the black tail percentage (BTP), hemorheology and four specific blood coagulation parameters. Finally, we performed metabonomics of plasma samples from the control group (Con), model group (Mod), high-dose APP group (HAPP), high-dose APH group (HAPH), and high-dose APA group (HAPA) treated mice to determine the mechanism of tail vein thrombosis and the potential anti-thrombotic mechanisms of HAPP, HAPH, and HAPA. We also screened for potential plasma metabolite biomarkers of thrombosis by analyzing the metabolic pathways.

2 Materials and methods

2.1 Materials and reagents

We purchased 3 types of leeches (WPW, HNW, and WAW) from the Hebei Hongsen Pharmaceutical Co., Ltd (Hebei, China).

Their identities were confirmed by Prof. Long Dai from the Binzhou Medical University. Their specimens were preserved at the Chemical laboratory of the Binzhou Medical University. We purchased kits from the Beijing Zhongchi Weiye Technology Development Co., Ltd. (Beijing, China) to estimate prothrombin time (PT, Lot No. F-3114040), activated partial thrombin time (APTT, Lot No. L-3122030), fibrinogen (FIB, Lot No. F-3142050), and thrombin time (TT, Lot No. F-3134011). Pepsin (2,500 U/mg, Lot#E2128141), trypsin (5,000 U/mg, Lot#I2110298), and epinephrine hydrochloride (EH, Lot#F2110069) were purchased from the Shanghai Aladdin Biochemical Technology Co., Ltd (Shanghai, China). HPLC-grade formic acid and acetonitrile were supplied by Fisher (Waltham, MA, USA). Deionized water was obtained using a Milli-Q system (Merck, USA).

2.2 Isolation and purification of APP, APH, and APA

WPW was crushed and added with 2 times the amount of petroleum ether, and degreased three times by ultrasonic (40°C, 30 min, 50 Hz). After degreasing, the petroleum ether was evaporated. We mixed 500 g of degreased WPW with deionized water (10 times weight/volume). The mixture was boiled for 15 min. Subsequently, the boiled mixture was cooled to 37°C. Then, the pH was adjusted to 1.5 with diluted hydrochloric acid and hydrolyzed with 1% pepsin at 37°C for 1 h. Then the pH of the hydrolysate was adjusted to 8.0 using a solution of NaOH. Subsequently, the mixture was hydrolyzed with 1% trypsin at 37°C for 3 h. The solution was boiled for 15 min to inactivate trypsin. The hydrolysate was neutralized and centrifuged at 4,500 r/min for 10 min. The supernatant was collected and desalted using a 500 Da dialysis bag. APP were then obtained by ultrafiltration using a membrane with a molecular weight cut-off of <3,000 Da at 0.8 MPa. Finally, the filtrate was concentrated and freeze-dried (Jiang et al., 2022).

HNW and WAW were also processed using the same method and their products were named as the APH and APA, respectively.

2.3 Structural characterization of APP, APH, and APA

2.3.1 Amino acid analysis

We mixed freeze-dried powders of APP (0.1240 g) with 5 mL of 6 mol/L hydrochloric acid, and the mixture was solidified under liquid nitrogen and vacuum. Then, the mixture was hydrolyzed in a constant temperature drying oven at 110°C for 24 h. The impurities were removed by filtration. Subsequently, 0.5 mL of the filtrate was vacuum dried, dissolved in 1 mL deionized water, and dried again. This process was repeated twice. Finally, the powder was dissolved in sample buffer, filtered, and analyzed by an automatic amino acid analyzer (Sykam, Germany) using a LCA K06/Na chromatographic column (4.6 mm × 150 mm) with 0.12 N sodium citrate solution (pH 3.45) and 0.2 N sodium citrate solution (pH 10.85) as mobile phases A and B, respectively. Flow rates of the eluting and derivative pumps were 0.45 mL/min and 0.25 mL/min, respectively. The detection wavelengths were 570 nm and 440 nm. The injection volume was 0.05 mL. The gradient temperature control set to 58°C–74°C. The pressure of the column was maintained at 30–40 bar (Liu et al., 2016).

The amino acid analyses of APA (0.1190 g) and APH (0.1520 g) were also processed by the same method.

2.3.2 Circular dichroism (CD) analysis

The freeze-dried powders of APP (10 mg) were dissolved in deionized water to obtain a 0.1 mg/mL solution. The solution was filtered using a 0.45 μm microporous membrane. The secondary microstructure of APP, including α-helix and β-sheet, were analyzed by CD, which was performed at an ambient temperature of 20°C. The thickness of the quartz cell was 0.1 cm. The scanning range was 190–260 nm. The scanning speed was 50 nm/min. The data interval was 0.2 nm. The bandwidth was 2 nm. The sensitivity was 20 mdeg. The response time was 0.5 s. The proportion of secondary structures (α-helix, β-sheet, β-turn and random coil) in APP were analyzed using the CDNN version 2.1 software (Applied Photophysics Ltd., Leatherhead, UK) (Han et al., 2024).

The CD analyses of APA (10 mg) and APH (10 mg) were also processed by the same method.

2.3.3 Fourier transform-infrared (FT-IR) spectroscopy analysis

The freeze-dried powders of APP (5 mg) were mixed with 200 mg of dried KBr. The mixture was pressed into discs at 15.0 MPa for 3 min. Then the mixture was loaded in the sample holder of the 470 FT-IR spectrometer (Nicolet, USA) and the spectra in the range of 4,000 to 400 cm^{-1} were recorded (Fu et al., 2023).

The FT-IR spectroscopy analyses of APA (5 mg) and APH (5 mg) were also processed by the same method.

2.3.4 Peptide spectroscopy analysis

The freeze-dried powders of APP (5 mg) were dissolved in 200 μL of 25 mmol/L ammonium bicarbonate. The extract was centrifuged and the supernatant was harvested. Then, 2 μL of 1 mol/L dithiothreitol (DTT) was added to the supernatant and the solution was incubated in a water bath at 60°C for 40 min. Subsequently, we added 8 μL of freshly prepared 1 mol/L iodoacetamide to the solution, incubated in the dark for 30 min at room temperature, and desalinated. Then the freeze-dried sample was dissolved in 10 μL of loading buffer and analyzed by LC-MS/MS using the Easy nLC1200-QEaxtive plus system (Thermo Scientific, USA) in a Thermo Scientific C18 column (50 mm × 150 mm, 3 μm) with a flow rate of 300 nL/min. The mobile phase was composed of solution A (aqueous solution of 0.1% formic acid) and solution B (0.1% formic acid in 80% acetonitrile). The following gradient elution program was used: 0–3 min, 2%–8% B; 3–42 min, 8%–20% B; 42–48 min, 20%–35% B; 48–49 min, 35%–100% B; 49–60 min, 100% B. The chromatographic peaks were monitored in the ESI^+ mode. The Orbitrap analyser acquired a high-resolution mass spectrum at full scan (m/z 200-1,600) with resolution of 70,000. The product ions were measured at a resolution of 17,500. The capillary temperature was 275°C and the spray voltage was 1,800 V. The maximum filling time for the entire scan and the MS/MS scan was set at 50 ms and 45 ms, respectively. The dynamic exclusion time was set at 30 s. We identified and selected peptide sequences with a false discovery rate (FDR) ≤ 1%.

The peptide spectroscopy analyses of APA (5 mg) and APH (5 mg) were also processed by the same method.

2.4 Animals experiments

2.4.1 Animal model generation and treatments

We purchased 54 male Kunming mice (SPF level, weighing 18–20 g) from the Jinan Pengyue Experimental Animal Breeding Co., Ltd (Shandong, China, SYXK (LU)2019-0003). All the animals were housed under standard animal room conditions (temperature 24°C ± 2°C, humidity 55%–60%, 12/12 h light/dark cycles) with standard food and water *ad libitum*. All the protocols for the animal experiments were performed according to the National Institutes of Health (NIH) guidelines for the care and use of experimental animals and were approved by the Institutional Animal Care and Use Committee, School of Pharmacy, Bin Zhou Medical University (Ethics Approval Number: 2021-087).

After 7 days of adaptive feeding, the animals were randomly divided into the following 9 groups (n = 6 each): Con; Mod; aspirin group (Asp, 40 mg/kg); low-dose APP group (LAPP, 100 mg/kg); HAPP (200 mg/kg); low-dose APH group (LAPH, 100 mg/kg); HAPH (200 mg/kg); low-dose APA group (LAPA, 100 mg/kg); and HAPA (200 mg/kg). The mice were treated via intragastric administration for 10 days and the mice in the Con and Mod were administered the same volumes of normal saline. After 10 days, mice from all the other groups except the Con were intraperitoneally injected with 0.5% carrageenan (type I) solution after the last gavage to establish the thrombus model (Yang et al., 2022). After 48 h of modeling, the mice were anesthetized with 10% chloral hydrate and blood samples were obtained from the abdominal aorta. The whole blood was divided into two parts: (1) half of the whole blood was added into an anticoagulant tube containing heparin; (2) the remaining whole blood was added into an anticoagulant tube containing 3.2% sodium citrate.

2.4.2 Determination of BTP

The total tail lengths (L_1) and the black tail lengths (L_2) were recorded for all the mice in the 9 groups after blood collection. The BTP was estimated with the following formula:

$$BTP\ (\%) = L_2/L_1 \times 100\%$$

2.4.3 Measurement of hemorheological and coagulation indices

We collected 400 μL of whole blood from anticoagulant tubes with heparin sodium. Then, we measured the high, medium and low shear values of the whole blood using a rheometer (XL1000, Zhongchi Weiye Technology Development Co., Ltd, China). The plasma viscosity was also measured. The blood samples in the sodium citrate-containing vacuum tubes were centrifuged at 3,500 r/min for 15 min at 4°C. The supernatant was harvested as a plasma sample to be used. Then, we measured the PT, APTT, TT, and FIB for all the groups using the plasma samples with an automatic coagulation analyzer (MEN-C100A, Shandong Meiyilin Electronic Instrument Co., Ltd, China) and commercial kits according to manufacturers' instructions. These indicators were used to evaluate the anti-coagulant efficacies of APP, APH, and APA.

2.5 Metabonomics analysis of plasma

2.5.1 Sample collection and preparation

We incubated 100 μL of blood plasma from the vacuum tubes with heparin sodium with 300 μL of cold ethanol for 10 min. Then, the extract was centrifuged at 4,000 rpm for 15 min at 4°C. The supernatant was harvested for use. 1 mL of the supernatant was dried by nitrogen blowing at 4°C. Then, it was re-dissolved using 100 μL of 80% methanol, centrifuged at 15,000 rpm for 15 min at 4°C, and the supernatant was stored for further analysis.

2.5.2 Chromatographic conditions

Chromatographic separation was performed on a Dionex Ultimate 3000 UHPLC system equipped with a WPS-3000 TRS autosampler, a TCC-3000RS column oven, and an HPG-3400RS binary pump (Dionex Softron GmbH-Part of Thermo Fisher Scientific, Germany). An ACQUITY UPLC BEH C18 column (150 mm × 2.1 mm, 1.7 μm) was operated at 40°C. The mobile phase was composed of (A) 0.1% FA in water and (Setiabakti et al.) ACN with a flow rate of 0.3 mL/min. The elution parameters were as follows: 0.00–1.00 min, 5% B; 1.00–4.00 min, 5%–30% B; 4.00–10.00 min, 30% B; 10.00–11.00 min, 30%–75% B; 11.00–13.00 min, 75%–90% B; 13.00–15.10 min, 90%–5% B; and 15.10–17.00 min, 5% B.

2.5.3 Mass spectrometry conditions

The LC-MS/MS analysis was performed on a Q-Exactive Focus Orbitrap MS (Thermo Electron, Germany) equipped with a heated electrospray ionization (HESI) source. In a single analytical run, the peaks were monitored in both the positive and negative ion modes. The ion source parameters were as follows: (1) ion spray voltages were set at 3.5 kV in the positive ion mode and 3.0 kV in the negative ion mode; (2) Nitrogen (purity ≥99.99%) was used as the sheath gas and the auxiliary gas at a flow rate of 30 and 10 arbitrary units, respectively; (3) capillary temperature was set at 320°C and vaporizer temperature was set at 400°C. The orbitrap mass analyzer was used to acquire a high-resolution mass spectrum at full scan in a mass range of m/z 70-1,050 at a resolution of 70,000 (Shi et al., 2023).

2.5.4 Multivariate analysis of LC-MS/MS data

The LC-MS/MS data was processed using the Compound Discoverer 3.0 software (Thermo Fisher Scientific, MA, USA) for noise cancellation, baseline correction and normalization so that reliable data was obtained for parameters, including m/z, peak intensity and retention time. At the same time, some data were verified by manual screening in the process of data processing to ensure the accuracy and reliability of the results. Then, principal component analysis (PCA) and orthogonal to partial least squares-discriminate analysis (OPLS-DA) was performed for the processed datasets using the SIMCA-P 14.0 software (Umetrics, Sweden). S-plots were used to screen differential metabolites in the tail vein thrombosis model after treatment with HAPP, HAPH, and HAPA in combination with other judgment methods, such as variable importance in projection (VIP) (generated in the OPLS-DA mode) and *p*-value (formed from relative intensity). Finally, we extracted further information for the differential metabolites, including molecular formulas, molecular weights and codes, using the HMDB dataset (http://www.hmdb.ca/), KEGG dataset (https://www.kegg.jp/), and VMH dataset (http://www.vmh.life).

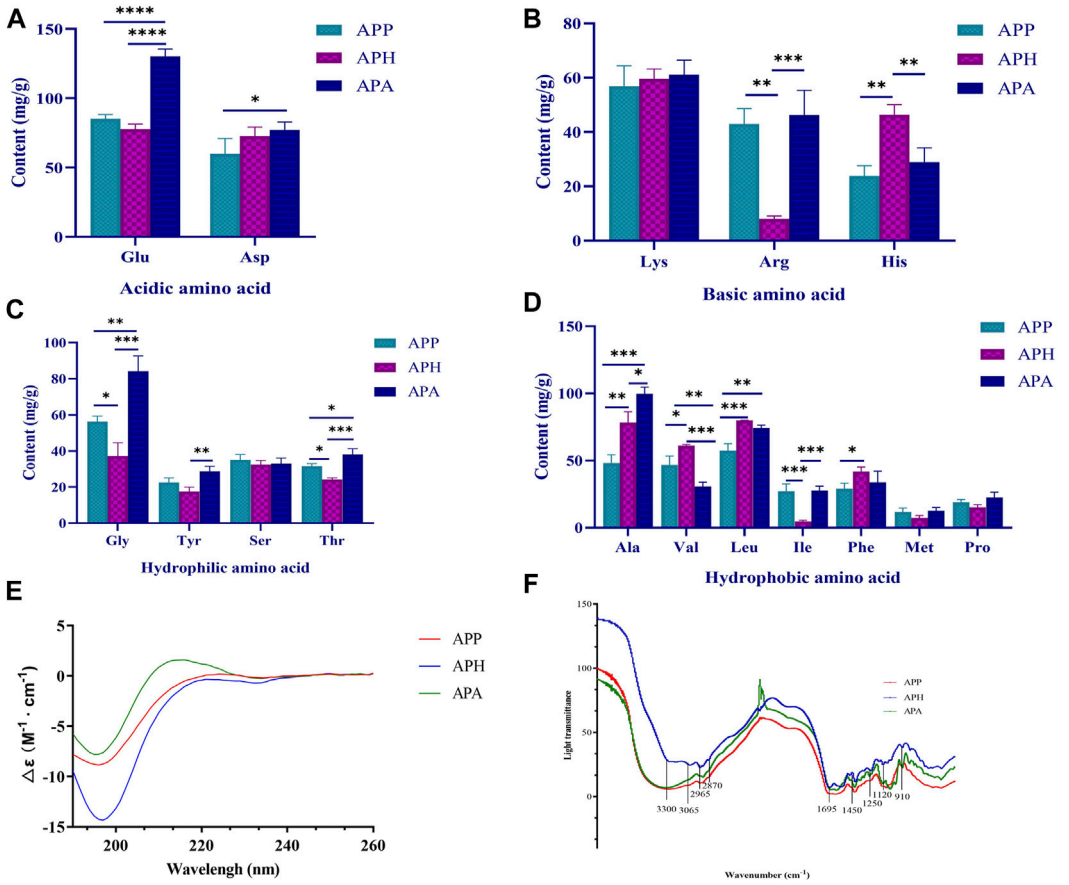


FIGURE 1
Structural characterization of APP, APH and APA. **(A)** Acidic amino acid compositions in APP, APH and APA. **(B)** Basic amino acid compositions in APP, APH and APA. **(C)** Hydrophilic amino acid compositions in APP, APH and APA. **(D)** Hydrophobic amino acid compositions in APP, APH and APA. **(E)** Circular dichrograms of APP, APH and APA. **(F)** Infrared absorption spectra of APP, APH and APA. *$p < 0.05$, **$p < 0.01$, ***$p < 0.001$, ****$p < 0.0001$. The significance level of the test results between different groups were assessed by ANOVA. All data are shown as mean ± SD ($n = 3$).

2.6 Statistical analysis

Statistical analysis was performed using the SPSS 26.0 software (SPSS Inc., Chicago, IL, USA). The data were expressed as mean ± standard deviation (S.D.). The data between two groups was compared using a two-tailed Student's t-test, whereas data between three or more groups was analyzed using the one-way analysis of variance (ANOVA) followed by Dunnett's *post hoc* tests. The differences were considered significant at the following *p*-values: $p < 0.05$, $p < 0.01$, $p < 0.001$ and $p < 0.0001$. GraphPad Prism 8.0.2 software (San Diego, CA, USA) was used to visualize data.

3 Results

3.1 Structures and amino acid compositions of APP, APH, and APA

3.1.1 Amino acid compositions of APP, APH, and APA

The amino acid compositions of APP, APH, and APA are shown in Figures 1A–D. We detected 16 amino acids in APP, APH, and APA, including 2 acidic amino acids (Figure 1A), 3 basic amino acids (Figure 1B), 7 hydrophobic amino acids (Figure 1D) and 4 hydrophilic amino acids (Figure 1C). The total amino acid content of APP was 653.359 mg/g with higher levels of Glu (13.03%), Asp (9.15%), and Leu (8.78%), and lower levels of Pro (2.90%) and Met (1.82%). The total amino acid content of APA was 829.027 mg/g with higher levels of Glu (15.70%), Ala (12.03%), and Gly (10.17%), and lower levels of Pro (2.70%) and Met (1.51%). The total amino acid content of APH was 663.553 mg/g with higher levels of Leu (12.04%), Ala (11.81%), and Glu (11.56%), and lower levels of Met (1.10%) and Ile (0.71%). The structures and functions of the proteins or peptides are determined by the composition and sequence of the amino acids (Perron et al., 2019). Therefore, the comparison of the activity of APP, APH and APA with similar amino acid composition will be further revealed.

3.1.2 CD analysis of APP, APH, and APA

CD is often used to rapidly determine the secondary structure, folding, and binding properties of the macromolecules, including proteins or peptides (Yoo et al., 2023). The CD spectra of most disordered or unfolded proteins show a negative peak in the region of 190–200 nm (Miles et al., 2021). As shown in Figure 1E, the CD

spectrum of APP exhibited a strong negative band at 196 nm and a positive band at 224 nm. The CD spectrum of APH exhibited a strong negative band at 197 nm and a positive band at 250 nm. The CD spectrum of APA exhibited a strong negative band at 195 nm and a positive band at 216 nm. Further analysis using the CDNN software showed that the α-helix, β-sheet, β-turn and random coil of APP accounted for 16.7%, 44.2%, 21.0% and 42.6%, respectively; the α-helix, β-sheet, β-turn and random coil of APA accounted for 16.6%, 44.1%, 20.9% and 43.0%, respectively; and the α-helix, β-sheet, β-turn and random coil of APH accounted for 16.7%, 45.1%, 21.1% and 42.2%, respectively. Therefore, the proportion of the secondary structures in APP, APH and APA did not show significant differences.

3.1.3 FT-IR analysis of APP, APH and APA

FT-IR spectroscopy is a valuable tool for studying the secondary structural composition and changes in the proteins. A peptide generates the following infrared-active amide vibrational modes under normal conditions: amide A (3,300 cm^{-1}), amide B (3,100-3,050 cm^{-1}), amide I (1,700-1,600 cm^{-1}), and amide II (1,570-1,540 cm^{-1}). Amide I band mostly consists of C=O stretching vibrations and C-N groups. Amide II band consists primarily of N-H bending, but also C-N and C-C stretching vibrations (Bicak, 2023). As shown in Figure 1F, the bands around 3,300 cm^{-1} and 3,065 cm^{-1} were generated by Fermi resonances between amide II and N-H stretching vibrations, whereas the strong band at 1,695 cm^{-1} represented the signal of amide I absorption peak. The FT-IR spectra of APP, APH, and APA exhibited absorption peak signals at 2,870 cm^{-1} and 2,965 cm^{-1}, which represented the CH_3 stretching vibrations. They also exhibited a spectral band at 1,405 cm^{-1} for the C-N stretching vibrations. The absorption peaks at 1,250 cm^{-1} and 1,120 cm^{-1} represented the C-O stretching vibrations in the alcohol and carboxylic acid groups, respectively. The presence of broad absorption peaks at 910 cm^{-1} and 1,450 cm^{-1} suggested presence of a benzene ring in APP, APH, and APA. In summary, the infrared absorption spectra were similar for APP, APH and APA.

3.1.4 Peptide spectroscopy analysis of APP, APH and APA

The mass spectra of APP, APH, and APA were analyzed with the PEAKS StudioX software (BSI, Canada). Firstly, peptides with low confidence based on $-10\log p < 20$ and peak area = 0 were removed from the analysis. Subsequently, we identified 1,688 peptides (length: 3–27 amino acids; molecular weight: 300–2,900 Da) in APP, 959 peptides (length: 7–22 amino acids; molecular weight: 600–2,300 Da) in APA, and 313 peptides (length: 7–24 amino acids; molecular weight: 750–2,700 Da) in APH. Furthermore, we identified 171 identical peptides between APP and APA, 78 identical peptides between APP and APH, and 107 identical peptides between APH and APA. The identical polypeptide in APP, APA, and APH are shown in Supplementary Table S1.

3.2 Analysis of the anti-thrombotic effects of APP, APH, and APA using the tail vein thrombosis model in mice

Next, we analyzed the therapeutic efficacies of APP, APH, and APA against tail vein thrombosis in mice. We measured the BTP by dividing the black tail length with the full tail length of each mouse to negate the individual differences between mice. We injected carrageenan to stimulate tail vein thrombosis and BTP was analyzed after 48 h in different groups of mice. As shown in Figures 2A, B, the Mod mice showed an average BTP of 33.42%. However, we observed significant reduction in the BTP of mice belonging to the ASP, LAPP, HAPP, LAPH, HAPH, LAPA, and HAPA ($p < 0.01$) (Figure 2B). Furthermore, we compared BTP in mice treated with high and low doses of APP, APH, and APA. Our data showed that APP, APH, and APA alleviated mice tail vein thrombus in a dose-dependent manner (Figure 2B). Then, we analyzed the whole blood viscosity (WBV) and plasma viscosity (PV) to evaluate the degree of blood stasis and the treatment effects in different groups of mice. As shown in Figures 2C–F, Mod showed significantly higher WBV at the low, medium and high shear rates compared with the Con; moreover, Mod showed significantly higher PV compared with the Con ($p < 0.0001$). WBV was significantly lower in the ASP, HAPP, HAPH, and HAPA compared with the Mod at high, medium, and low shear rates; PV was also significantly lower in the ASP, HAPP, HAPH, and HAPA compared with the Mod ($p < 0.05$; Figures 2C–F). Whole blood of the LAPP, LAPH, and LAPA showed lower PV and WBV at the high, medium and low shear rates compared with the Mod, but the data was not statistically significant. Then, we analyzed the status of blood coagulation by estimating PT, APTT, TT, and FIB using the automatic coagulation analyzer and commercial kit. The coagulation function of Mod mice was abnormal and their plasma showed significantly reduced PT, APTT and TT ($p < 0.01$), and increased levels of FIB ($p < 0.01$) compared with the Con (Figures 2G–J). Compared with the Mod, plasma of the LAPP, HAPP, LAPH, HAPH, LAPA, and HAPA showed higher PT, TT, and APTT, and decreased levels of FIB ($p < 0.05$). Therefore, the therapeutic efficacies of APP, APH, and APA against tail vein thrombosis in mice was comparable and significant.

3.3 Metabonomics of the plasma samples from the mice tail vein thrombosis model with or without treatments with HAPP, HAPH, and HAPA

3.3.1 Plasma metabonomics analysis

Metabonomics was used to investigate the mechanisms underlying the anti-thrombotic effects of HAPP, HAPH and HAPA in the mice tail vein thrombosis model. Plasma samples from the Con, Mod, HAPP, HAPH, and HAPA were analyzed in the ESI^+ and ESI^- modes using the UHPLC-Q-Exactive Orbitrap MS/MS, and their base peak ions (BPI) diagrams of the Con, Mod, HAPP, HAPH and HAPA were depicted in Supplementary Figure S1, which exhibited clear separation of all peaks within a span of 15 min in both ESI^+ and ESI^- modes. Furthermore, the metabolic profiles of various groups showed significant differences. This suggested that the treatments altered the plasma metabolite profiles in each group. The differences in the plasma metabolite profiles of the Con, Mod, HAPP, HAPH, and HAPA were analyzed using the PCA score plots. As shown in Figures 3A, B, the five groups of samples showed a clear separation trend in ESI^+ and ESI^- modes. In the ESI^+ and ESI^- modes, samples from the Con and Mod showed clear separation. Furthermore, samples from the treatment groups

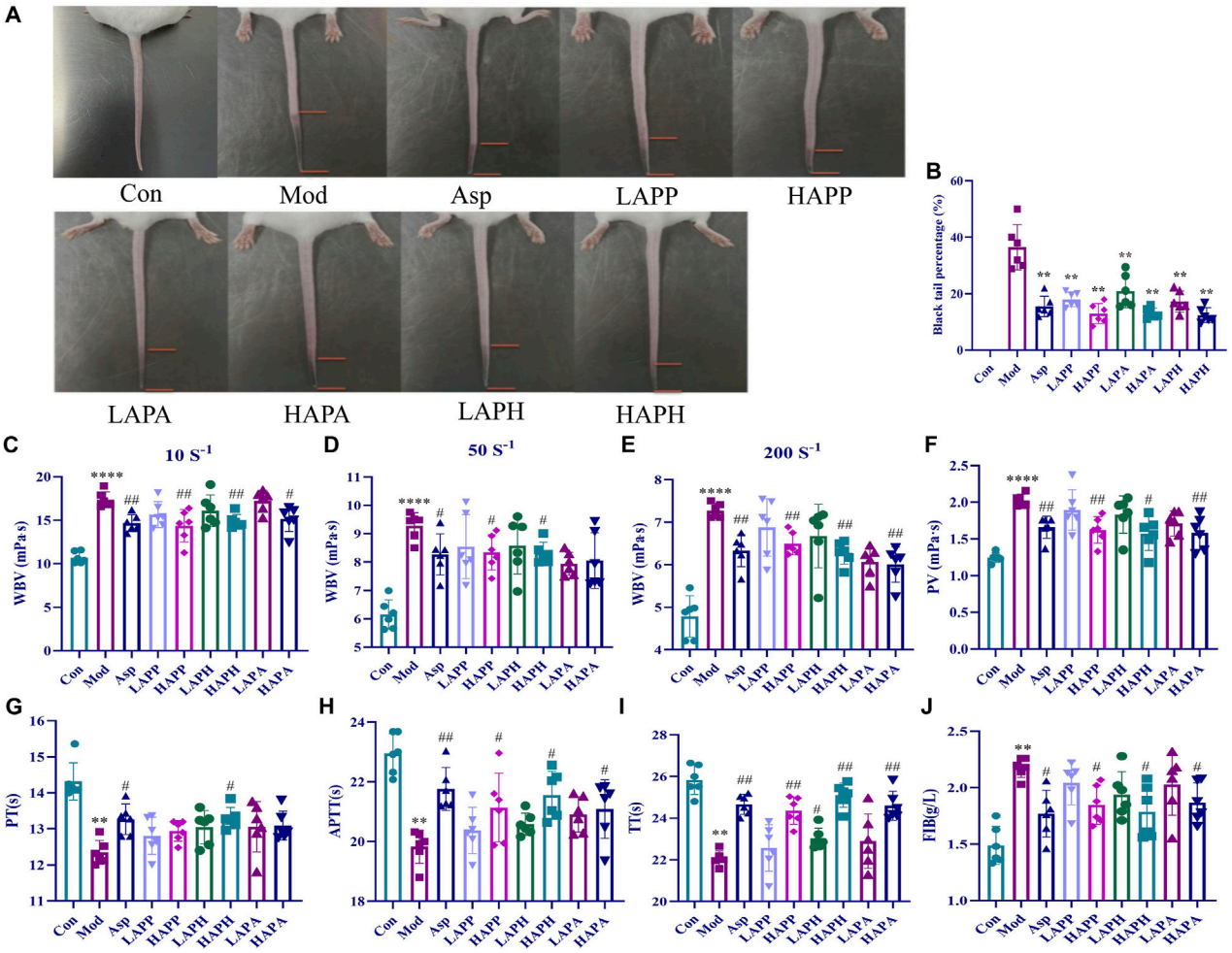


FIGURE 2
Effects of APP, APH and APA on black-tail length, hemorheological indexes and coagulation indexes of mice induced by carrageenan for 48 h. Representative images **(A)** and BTP **(B)** showing the tails of mice in Con, Mod and treatment groups. Effects of APP, APH and APA on WBV at low (10 s^{-1}) shear rate **(C)**, medium (50 s^{-1}) shear rate **(D)** and high (200 s^{-1}) shear rate **(E)**. Effects of APP, APH and APA on PV **(F)**, PT **(G)**, APTT **(H)**, TT **(I)**, FIB **(J)**. ****$p <$ 0.0001: Con *versus* Mod; $^{\#}p < 0.05$, $^{\#\#}p < 0.01$: Mod *versus* treatment groups. The significance level of the test results between different groups were assessed by ANOVA. All data are shown as mean ± SD (n = 6).

were clearly separated from the Mod samples. These results demonstrated significant differences in the endogenous metabolites between the Mod and the Con, HAPP, HAPH, and HAPA.

3.3.2 Identification of potential plasma metabolite biomarkers

The supervised OPLS-DA model was used to identify potential biomarker metabolites between the Con, Mod, HAPP, HAPH, and HAPA. The plasma metabolite profile of the Mod showed significantly differences from the plasma metabolite profiles of the Con, HAPP, HAPH, and HAPA in both ESI^+ and ESI^- modes (Figures 3C–J). The reliability of the OPLS-DA model was assessed using the R^2Y and Q^2 parameters (Supplementary Table S2). In ESI^+ mode, the R^2Y and Q^2 values were 0.981 and 0.852, respectively, while in ESI^- mode, the corresponding values were 0.988 and 0.876. In general, when the values of R^2Y and Q^2 are close to 1, it shows that the model is reliable and stable (Wei et al., 2023). Furthermore, seven-round cross validation and 200 time-permutation testing also showed the robustness of OPLS-DA models (Supplementary Figure S2). The S-plot scores (Supplementary Figure S3) were used to screen and identify the potential metabolic biomarkers in the OPLS-DA model. The differential metabolites between groups were evaluated using VIP >1 and t-test $p < 0.05$ as threshold parameters. The molecular information was then imported into the HMDB database and compared with the relevant values retrieved by HMDB. The theoretical fragments were used to infer the structure and fragment attribution of the compounds and potential biomarkers related to tail vein thrombosis were identified. Based on this comprehensive analysis, we identified 24 compounds with significant differences in their plasma concentrations between the Con and the Mod. These included bile acids, fatty acids, glycerophospholipids, and others (Supplementary Table S3; Figure 4). Among these, 19, 23, and 20 metabolites were significantly normalized after administration of HAPP, HAPH, and HAPA in the mice, respectively. Venn diagram showed that 16 of the 24 metabolites overlapped between

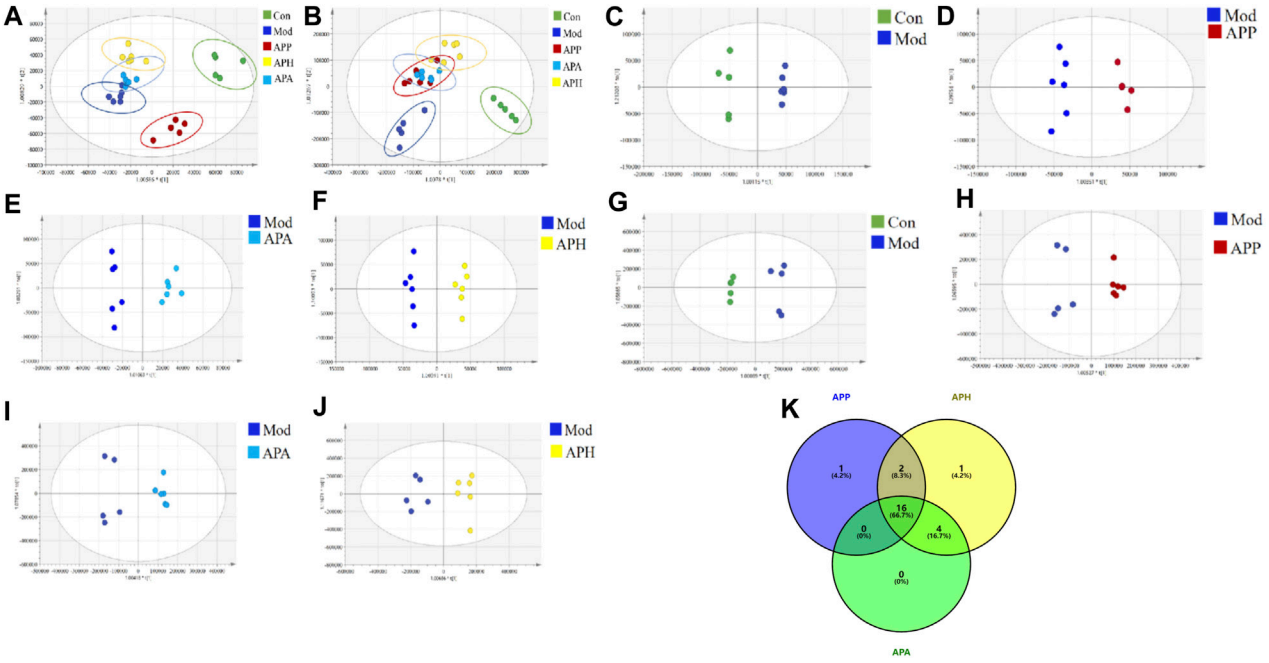


FIGURE 3
PCA and OPLS-DA scores of plasma samples in different groups (n = 6). **(A)** PCA score plot in ESI⁻ mode. **(B)** PCA score plot in ESI⁺ mode. **(C)** OPLS-DA score plots of Con and Mod in ESI⁻ mode. **(D)** OPLS-DA score plots of Mod and APP in ESI⁻ mode. **(E)** OPLS-DA score plots of Mod and APA in ESI⁻ mode. **(F)** OPLS-DA score plots of Mod and APH in ESI⁻ mode. **(G)** OPLS-DA score plots of Con and Mod in ESI⁺ mode. **(H)** OPLS-DA score plots of Mod and APP in ESI⁺ mode. **(I)** OPLS-DA score plots of Mod and APA in ESI⁺ mode. **(J)** OPLS-DA score plots of Mod and APH in ESI⁺ mode. **(K)** The Venn diagram of metabolites in mice with tail vein thrombosis was intervened by APP, APH and APA.

HAPP, HAPH, and HAPA, accounting for 66.7% of the total differential metabolites (Figure 3K). It is suggested that HAPP, HAPH and HAPA might have a common mechanism in the treatment of tail vein thrombosis.

3.3.3 Metabolic pathway analysis of the plasma metabolite biomarkers

We identified significant differences in the plasma levels of 24 metabolites between the Mod and the Con ($p < 0.05$; Figure 4). The Mod showed significantly lower levels of glycochenodeoxycholic acid, cholic acid, chenodeoxycholic acid, LysoPE (0:0/16:0), eicosapentaenoic acid, linoleic acid, 1-oleoyl-2-hydroxy-sn-glycero-3-phosphoethanolamine, deoxycholic acid, 1-hydroxy-2-eicosadienoyl-sn-glycero-3-phosphoethanolamine, and 1-Stearoyl-2-hydroxy-sn-glycero-3-phosphoethanolamine ($p < 0.05$) and significantly higher levels of L-alpha-lysophosphatidylcholine, 1-[(9Z)-hexadecenoyl]-sn-glycero-3-phosphocholine, PC (O-18:1 (9Z)/2:0), 1-homo-gamma-linolenoyl-glycero-3-phosphocholine, palmitoylcarnitine, platelet-activating factor, 1-octadecyl-Sn-glycero-3-phosphocholine, phosphatidylcholine, 1-icosanoyl-sn-glycero-3-phosphocholine, 1-alpha-linolenoyl-2-linoleoyl-phosphatidylcholine, cis-5-tetradecenoylcarnitine, 1-heptadecanoyl-sn-glycero-3-phosphocholine, 1-[(11Z,14Z)]-icosadienoyl-sn-glycero-3-phosphocholine and 1-arachidonoyl-sn-glycero-3-phosphocholine compared with the Con ($p < 0.05$). Subsequently, we imported the information about these metabolites into the MetaboAnalyst 5.0 database (http://www.metaboanalyst.ca/) to predict the thrombus-related metabolic pathways in mice. The 24 metabolites with significant differences between the Mod and Con correlated with linoleic acid metabolism, primary bile acid biosynthesis, ether lipid metabolism, and glycerophospholipid metabolism (Figure 5A).

The differences in the plasma metabolites between the HAPP, HAPH, and HAPA and the Mod were analyzed to determine their potential therapeutic effects and mechanism of action. The results revealed that the intervention of HAPP resulted in the reversal of 19 metabolites among the 24 potential biomarkers listed in Supplementary Table S3, including glycochenodeoxycholic acid, cholic acid, chenodeoxycholic acid, L-alpha-lysophosphatidylcholine, 1-[(9Z)-hexadecenoyl]-sn-glycero-3-phosphocholine, PC(O-18:1 (9Z)/2:0), 1-homo-gamma-linolenoyl-glycero-3-phosphocholine, LysoPE (0:0/16:0), palmitoylcarnitine, platelet-activating factor, 1-Octadecyl-sn-glycero-3-phosphocholine, eicosapentaenoic acid, linoleic acid, phosphatidylcholine, 1-icosanoyl-sn-glycero-3-phosphocholine, 1-alpha-linolenoyl-2-linoleoyl-phosphatidylcholine, 1-Oleoyl-2-hydroxy-sn-glycero-3-phosphoethanolamine, deoxycholic acid, and 1-hydroxy-2-eicosadienoyl-sn-glycero-3-phosphoethanolamine. Likewise, 23 metabolites among the 24 potential biomarkers were significantly reversed after the intervention of HAPH, including glycochenodeoxycholic acid, cholic acid, chenodeoxycholic acid, L-alpha-lysophosphatidylcholine, 1-[(9Z)-hexadecenoyl]-sn-glycero-3-phosphocholine, PC(O-18:1 (9Z)/2:0), 1-homo-gamma-linolenoyl-glycero-3-phosphocholine, LysoPE (0:0/16:0), palmitoylcarnitine, platelet-activating factor, 1-Octadecyl-sn-glycero-3-phosphocholine, eicosapentaenoic acid, linoleic acid, phosphatidylcholine, 1-icosanoyl-sn-glycero-3-phosphocholine, 1-alpha-linolenoyl-2-linoleoyl-phosphatidylcholine, cis-5-Tetradecenoylcarnitine, deoxycholic acid, 1-hydroxy-2-eicosadienoyl-sn-glycero-3-phosphoethanolamine, 1-Stearoyl-2-hydroxy-sn-glycero-3-phosphoethanolamine, 1-

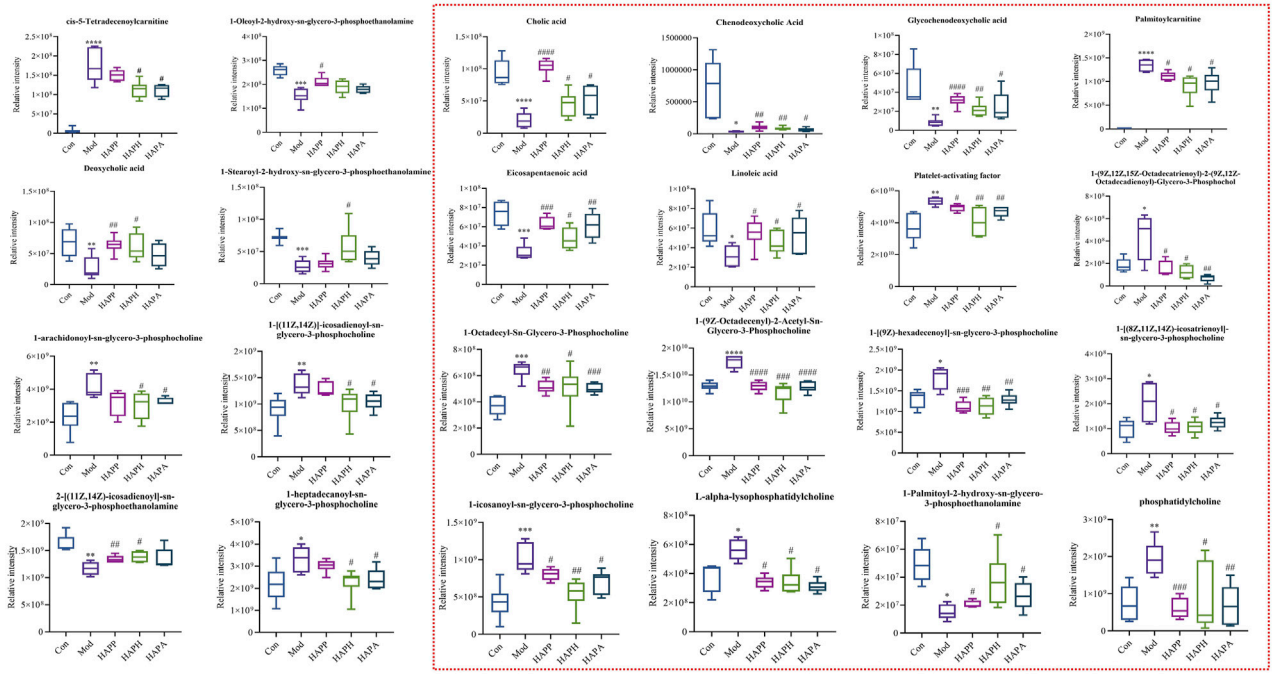


FIGURE 4
Results of 24 differential metabolites among Con, Mod, HAPP, HAPH and HAPA. *$p < 0.05$, **$p < 0.01$, ***$p < 0.001$, ****$p < 0.0001$: Con *versus* Mod; $^{\#}p < 0.05$, $^{\#\#}p < 0.01$, $^{\#\#\#}p < 0.001$, $^{\#\#\#\#}p < 0.0001$: Mod *versus* treatment groups. Inside the red dotted line were the common significant differential metabolites of HAPP, HAPH and HAPA. The significance level of the test results between different groups were assessed by ANOVA. All data are shown as mean ± SD (n = 6).

heptadecanoyl-sn-glycero-3-phosphocholine, 1-[(11Z,14Z)]-icosadienoyl-sn-glycero-3-phosphocholine, and 1-arachidonoyl-sn-glycero-3-phosphocholine. There were 20 metabolites among the 24 differential metabolites are significantly reversed after the intervention of HAPA, including glycochenodeoxycholic acid, cholic acid, chenodeoxycholic acid, L-alpha-lysophosphatidylcholine, 1-[(9Z)-hexadecenoyl]-sn-glycero-3-phosphocholine, PC(O-18:1 (9Z)/2:0), 1-homo-gamma-linolenoyl-glycero-3-phosphocholine, LysoPE (0:0/16:0), palmitoylcarnitine, platelet-activating factor, 1-Octadecyl-sn-glycero-3-phosphocholine, eicosapentaenoic acid, linoleic acid, phosphatidylcholine, 1-icosanoyl-sn-glycero-3-phosphocholine, 1-alpha-linolenoyl-2-linoleoyl-phosphatidylcholine, cis-5-Tetradecenoylcarnitine, 1-heptadecanoyl-sn-glycero-3-phosphocholine, 1-[(11Z,14Z)]-icosadienoyl-sn-glycero-3-phosphocholine, and 1-arachidonoyl-sn-glycero-3-phosphocholine. As shown in Figures 5B–D, HAPP, HAPH and HAPA could reverse the disorder of linoleic acid metabolism, primary bile acid biosynthesis and ether lipid metabolism induced by tail vein thrombosis in mice. The above results suggested significant anti-thrombotic effects of HAPP, HAPH, and HAPA. Furthermore, the anti-thrombotic mechanisms of HAPP, HAPH, and HAPA were similar.

4 Discussion

Leech has been used since ancient times in TCM for removing blood stasis. The basic research has shown that the activity of leeches mainly comes from a variety of natural molecules contained in their saliva, such as enzymes, anticoagulants and anti-inflammatory substances (Tong et al., 2022). In fact, the active substances are mostly exist in the form of macromolecular proteins, while only a few exist in the form of natural peptides in animals. However, macromolecular proteins cannot be directly absorbed *in vivo*, and can only be easily absorbed into the circulatory system with the form of peptides. Several studies have established that the anti-thrombotic effects of leeches are associated with the bioactive polypeptides and proteins. The biological activities of these proteins and polypeptides can vary because of differences in the amino acid composition and molecular weights (Tang et al., 2018; Cheng et al., 2019). In this study, we prepared APP, APH, and APA using bio-mimetic enzymatic hydrolysis. We selected proteins and peptides with specific range of molecular weights using specific molecular weight filtering. Then, the structures of the potential bioactive peptides were characterized by multiple methods. Our data showed that the amino acid compositions of APP, APH and APA were similar and the proportions of different amino acids varied between APP, APH, and APA. The activity of polypeptides is affected by the amino acid content, spatial conformation, molecular weight, and charge distribution. Therefore, we analyzed the secondary structures of APP, APH, and APA by CD. Our data showed that there was no significant difference in the proportion of secondary structures between APP, APH and APA, and that APP, APH and APA are mainly dominated by β-sheet and random coil. The β-sheet fragments penetrate into the platelet aggregation factors and other related proteins, or directly bind to the receptors on the platelet surface, thereby activating or inhibiting platelet function and regulating platelet aggregation or agglutination (David et al., 2023). FT-IR analysis also showed that the infrared absorption peaks and spectra were similar between APP, APH and APA. Our data

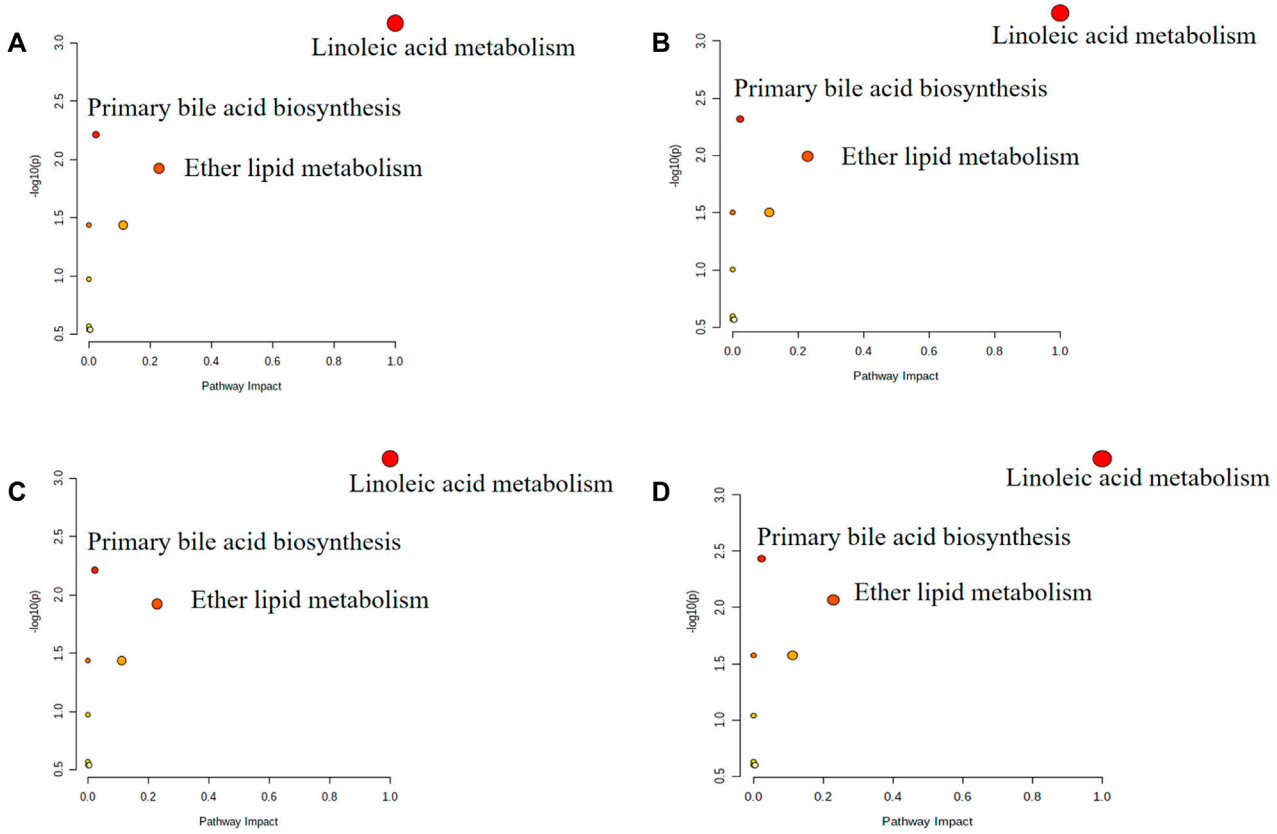


FIGURE 5
Pathway analysis of significantly altered metabolites. **(A)** Metabolic pathway analysis of Con and Mod plasma samples. **(B)** Metabolic pathway analysis of Mod and HAPP plasma samples. **(C)** Metabolic pathway analysis of Mod and HAPA plasma samples. **(D)** Metabolic pathway analysis of Mod and HAPH plasma samples. The color of the circle denotes the *p*-values and size of each circle denotes the pathway impact values.

identified 43 common polypeptides in APP, APH and APA. Most of the amino acid residues at the C-terminus of these peptide sequences were basic amino acids such as arginine and lysine. Several studies have shown that basic amino acids modulate the growth, protein synthesis, energy storage, lymphocyte transformation, and immune function in most animals (Zhang et al., 2013; Chen et al., 2021). Therefore, the rapid absorption and therapeutic effects of APP, APH, and APA may be related to their characteristics, including low molecular weight, abundant amino acids, and basic amino acids at the terminals.

Carrageenan induces diffuse intravascular clotting and thrombus formation in the tail of mice. Therefore, the extent of black tail is an important experimental index to intuitively judge the degree of tail vein thrombosis in mice. In this study, we analyzed the therapeutic effects of APP, APH and APA on the mice tail vein thrombosis using the carrageenan-induced black tail model. Our data showed that APP, APH and APA alleviated thrombosis and decreased the formation of black tail in a dose-dependent manner. The effects of APP, APH and APA were comparable with the effects of ASP, a common anti-thrombotic drug.

Thrombus formation in the arteries or veins blocks the flow of blood and alters the blood rheology. The increased WBV decreases blood flow and may lead to cardiovascular diseases (Hur et al., 2023). APTT is an indicator of the endogenous coagulation pathway activity. PT is an indicator of the extrinsic coagulation pathway activity. TT is a measure of the time for blood clotting and is used to detect the activities of both the intrinsic and extrinsic coagulation pathways. FIB is essential protein for the thrombus formation (Wu et al., 2021; Wang et al., 2022). This study showed that treatments with APP, APH, and APA significantly increased PT, TT, and APTT, and decreased the levels of FIB ($p < 0.05$) as well as WBV and PV ($p < 0.05$). There was no significant difference in hemorheology and coagulation indexes among APP, APH and APA, which was contrary to the results determined in the Chinese Pharmacopoeia (2020 Edition) (Chinese Pharmacopoeia Commission, 2020). The reason was that APP, APH and APA were carried out *in vivo* experiments and reflected the true state of three leeches in the treatment of diseases through *in vivo* metabolism. Our results suggested that the anti-coagulant activities of APP, APH, and APA improved the dysfunctional characteristics of blood caused by tail vein thrombosis. These data provided further information regarding the potential anti-thrombotic mechanisms of APP, APH, and APA in the clinical treatment of thrombosis.

UHPLC-Q-Exactive Orbitrap MS was used to identify the differentially expressed plasma metabolites to determine the potential anti-thrombotic mechanisms of HAPP, HAPH and HAPA. In the Mod, we identified 24 plasma metabolites that were significantly altered compared with the plasma metabolites of the Con. Furthermore, administration of HAPP, HAPH and HAPA normalized the plasma levels of 19, 23, and 20 metabolites, respectively. Pathway analysis demonstrated that linoleic acid metabolism, primary bile acid biosynthesis, and ether lipid metabolism were significantly altered in

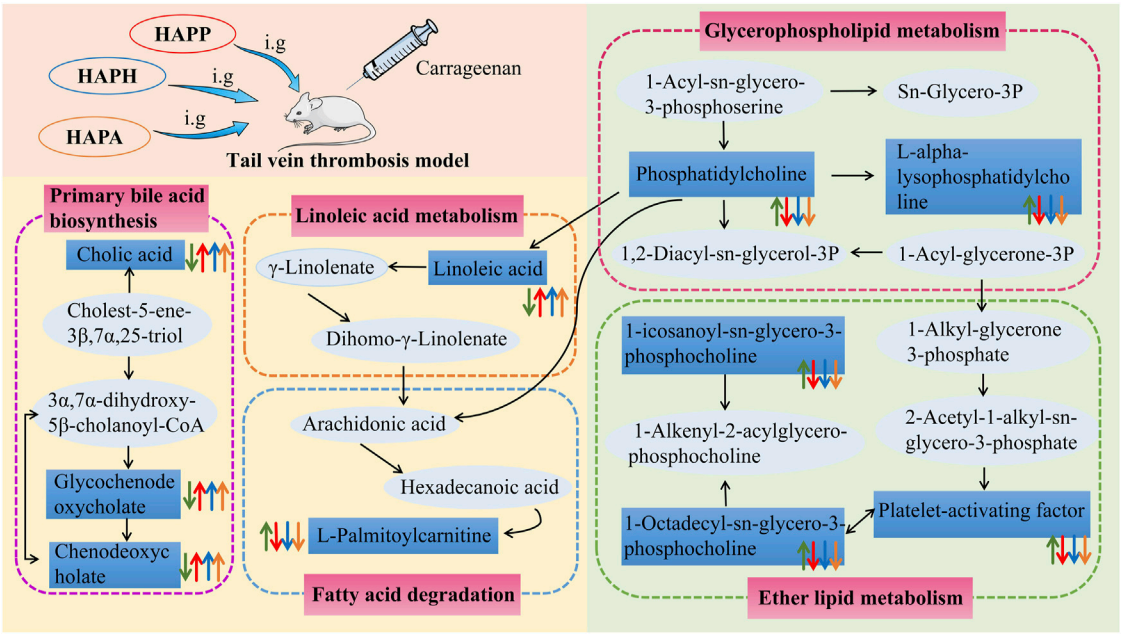


FIGURE 6
The intervention of HAPP, HAPH and HAPA on plasma metabolic pathways in mouse tail vein thrombosis model. The green arrow represents the change trend of metabolites in plasma of mice with tail vein thrombosis. The red arrow represents the change trend of metabolites in plasma after HAPP intervention. The blue arrow represents the change trend of metabolites in plasma after HAPH intervention. The yellow arrow represents the change trend of metabolites in plasma after HAPA intervention. Pink-filled boxes represent related metabolic pathways.

the Mod and were normalized by HAPP, HAPH and HAPA treatments. The changes of plasma metabolites and related pathways after HAPP, HAPH and HAPA intervention were summarized in Figure 6. Ether lipid metabolism plays a very important role in several physiological processes. For example, ether lipids are essential components of the cell membranes, which plays an important role in regulating the structure and function of cell membrane, cell signal transduction, apoptosis and immune response. Ether lipids are also used as energy sources in the human body. Previous studies have shown that ether lipids inhibit agonist-induced platelet aggregation, Rap1-GTP loading, protein kinase C (PKC) activation, and *ex vivo* thrombus growth (Holly et al., 2019; Liao et al., 2021). 3 of the 24 differential metabolites, namely, 1-icosanoyl-sn-glycero-3-phosphocholine, platelet-activating factor, and 1-octadecyl-sn-glycero-3-phosphocholine were related to ether lipid metabolism and were significantly increased in the Mod but normalized in the HAPP, HAPH and HAPA. In general, thrombosis promotes the release and activation of platelet-activating factors, which bind to the receptors on the surface of platelets and alter the platelet membrane phosphatidylinositol metabolism and increase the intracellular Ca^{2+} levels, thereby inducing platelet activation and aggregation (Ding et al., 2023). Two of the ether lipids identified as biomarkers in this study, namely, 1-icosanoyl-sn-glycero-3-phosphocholine and 1-octadecyl-sn-glycero-3-phosphocholine are glycerophosphates. Glycerophospholipids are major and essential components of the cell membranes and include lipid molecules such as phosphatidylcholine, phosphatidylethanolamine, and others (Wu et al., 2023). Previous studies have shown that some phospholipids are associated with thrombosis. For example, exposure of phosphatidylserine, an intracellular phospholipid, to the outer surface of the cell membrane triggers platelet aggregation and coagulation cascades, which promote thrombosis (Atsou et al., 2023). Lyso-phosphatidylcholine downregulates NOS transcript levels and inhibits the transcriptional activity of NF-κB and tissue factor, thereby inducing thrombosis by disrupting the normal functioning of the vascular endothelial cells (Curcic et al., 2017). Therefore, this study showed that thrombus formation may be caused by aberrant alterations in the ether lipid metabolism. However, treatment with APP, APH and APA restored the ether lipid metabolic pathway to normal, thereby alleviating thrombosis.

Linoleic acid is a key fatty acid in the human body and its metabolism mainly occurs in the liver and the muscle tissues. Typically, fatty acids such as linoleic acid are oxidized to provide cellular energy (Burr et al., 2023). Modern pharmacological studies have shown that linoleic acid reduces the levels of cholesterol, triglycerides, low-density lipoproteins, and very low-density lipoproteins in blood (Yang et al., 2023). They also decreased the levels of inflammation-related factors such as IL-1β, TNF-α, and NO, thereby inhibiting thrombosis (Zhang et al., 2023). In this study, linoleic acid levels were reduced in the Mod compared with the Con but were significantly increased ($p < 0.05$) in the HAPP, HAPH, and HAPA compared with the Mod. This suggested that HAPP, HAPH, and HAPA could exert anticoagulant activity by regulating linoleic acid metabolism. Furthermore, cholic acid, glycochenodeoxycholic acid, and chenodeoxycholic acid levels were reduced in the Mod compared with the Con, but these effects were reversed by treatment with HAPP, HAPH, and HAPA. This suggested that tail vein thrombosis was caused by alterations in the primary bile acid biosynthesis, but these effects were restored to normal by treatment with HAPP, HAPH, and HAPA. Previous studies have demonstrated that bile acids are signaling molecules that activate several intracellular signaling pathways. For example, elevated levels of bile acid in the plasma activate the

farnesoid X receptor (FXR) and regulate intrahepatic bile acid biosynthesis and secretion as well as lipid and glucose metabolism (Song et al., 2023). Thrombus formation is initiated in the arterial wall and is involved in the induction of blood stasis. Furthermore, cholesterol and lipid levels show positive correlation with the risk of thrombosis (Shi et al., 2023). Therefore, our data suggested that HAPP, HAPH and HAPA may alleviate tail vein thrombosis by improving primary bile acid biosynthesis.

In summary, our data showed that the structural features of APP, APH, and APA were similar. APP, APH, and APA could significantly alleviated tail vein thrombosis in mice. Metabonomics data showed that HAPP, HAPH and HAPA ameliorated tail vein thrombosis in mice by modulating linoleic acid metabolism, primary bile acid biosynthesis, and ether lipid metabolism. Our data showed similar effects for APP, APH, and APA. This may be caused by the formation of active peptides from macromolecular proteins that are similar to hirudin because of enzymatic hydrolysis. However, we also realized that there were some limitations and shortcomings in our study. In our research, we detected 24 different metabolites in Con and Mod, and 19, 23, and 20 metabolites were significantly normalized after administration of HAPP, HAPH, and HAPA in the mice, respectively. Therefore, we will verify the antithrombotic efficacy of metabolites that have been significantly reversed after HAPP, HAPH and HAPA treatment. In addition, the saliva of leeches contains a variety of toxins and biologically active components, possibly including venom polypeptides. Since the specific composition and activity of venom polypeptides may vary depending on the leech species. Therefore, we will further study the polypeptide components in leech venom and explore its potential pharmacological effects to promote innovation and development in related fields.

5 Conclusion

In this study, we obtained APP, APH, and APA after enzymatic hydrolysis of WPW, HNW, and WAW, respectively. The structural characterization of APP, APH and APA was performed by CD, FT-IR, and other methods. Subsequently, we used an untargeted metabonomics technique based on UHPLC-Q-Exactive Orbitrap MS to explore the mechanisms of HAPP, HAPH, and HAPA in treating tail vein thrombosis in mice. 24 differential metabolites were identified from the plasma samples of the Mod. Among these, 19, 23, and 20 metabolites were significantly normalized after administration of HAPP, HAPH, and HAPA in the mice, respectively, and the pathways are mainly involved in linoleic acid metabolism, primary bile acid biosynthesis, and ether lipid metabolism. These findings elucidate the pharmacodynamic material basis of WPW, HNW and WAW, and also provide a basis for the development of APP, APH and APA in the treatment of thrombosis.

Data availability statement

The original contributions presented in this study are publicly available. The data presented in the study are deposited in the MetaboLights Human Metabolome Database, accession number MTBLS9306. This data can be found here: https://www.ebi.ac.uk/metabolights/MTBLS9306.

Ethics statement

The animal study was approved by the Institutional Animal Care and Use Committee at Bin Zhou Medical University (No. 2021-087). The study was conducted in accordance with the local legislation and institutional requirements.

Author contributions

WD: Data curation, Formal Analysis, Methodology, Visualization, Writing–original draft. HL: Data curation, Methodology, Writing–original draft, Investigation, Project administration. YL: Data curation, Investigation, Methodology, Writing–review and editing. YW: Investigation, Project administration, Writing–review and editing. LD: Conceptualization, Data curation, Funding acquisition, Writing–review and editing. SW: Conceptualization, Data curation, Funding acquisition, Writing–review and editing.

Funding

The author(s) declare financial support was received for the research, authorship, and/or publication of this article. This research was funded by the National Natural Science Foundation of China (NO. 82304815), the Collaborative Innovation Transformation Project for High-Quality Development of Chinese Medicine (CX2H202201), the Special Project of Central Guidance for Local Science and Technology Development (YDZX2021050), Shandong Provincial Natural Science Foundation Youth Project (No. ZR2021QH009) and the Yantai Campus Integration Development Project (NO. 2019XDRHXMPT18).

Conflict of interest

The authors declare that the research was conducted in the absence of any commercial or financial relationships that could be construed as a potential conflict of interest.

Publisher's note

All claims expressed in this article are solely those of the authors and do not necessarily represent those of their affiliated organizations, or those of the publisher, the editors and the reviewers. Any product that may be evaluated in this article, or claim that may be made by its manufacturer, is not guaranteed or endorsed by the publisher.

Supplementary material

The Supplementary Material for this article can be found online at: https://www.frontiersin.org/articles/10.3389/fphar.2023.1324418/full#supplementary-material

References

Atsou, S., Schellenberg, C., Lagrange, J., Lacolley, P., Lenting, P. J., Denis, C. V., et al. (2023). Thrombin generation on vascular cells in the presence of factor VIII and/or emicizumab. *J. Thromb. Haemost.* S1538-7836, 00719–725. doi:10.1016/j.jtha.2023.09.017

Bicak, B. (2023). Structural, spectroscopic, molecular docking, ADME, molecular dynamics studies of Val-Trp dipeptide. *J. Biomol. Struct. Dyn.* 1, 13873–13890. doi:10.1080/07391102.2023.2183041

Burr, S. D., Chen, Y., Hartley, C. P., Zhao, X., and Liu, J. (2023). Replacement of saturated fatty acids with linoleic acid in western diet attenuates atherosclerosis in a mouse model with inducible ablation of hepatic LDL receptor. *Sci. Rep.* 13, 16832. doi:10.1038/s41598-023-44030-9

Chen, J., Yang, Y., Wang, S., and Zhang, K. (2023). Crocin improves lower extremity deep venous thrombosis by regulating the PIM1/FOXO3a axis. *Cell Mol. Biol. (Noisy-le-grand)* 69, 183–188. doi:10.14715/cmb/2023.69.9.28

Chen, K., Yuan, S., Wang, D., Liu, Y., Chen, F., and Qi, D. (2021). Basic amino acid-modified lignin-based biomass adjuvants: synthesis, emulsifying activity, ultraviolet protection, and controlled release of avermectin. *Langmuir* 37, 12179–12187. doi:10.1021/acs.langmuir.1c02113

Cheng, R. M., Tang, X. P., Long, A. L., Mwangi, J., Lai, R., Sun, R. P., et al. (2019). Purification and characterization of a novel anti-coagulant from the leech Hirudinaria manillensis. *Zool. Res.* 40, 205–210. doi:10.24272/j.issn.2095-8137.2019.037

Chinese Pharmacopoeia Commission. (2020). *Pharmacopoeia of the People's Republic of China (Part One)*. China Medical Science Press: Beijing, China. 87.

Curcic, S., Holzer, M., Pasterk, L., Knuplez, E., Eichmann, T. O., Frank, S., et al. (2017). Secretory phospholipase A_2 modified HDL rapidly and potently suppresses platelet activation. *Sci. Rep.* 7, 8030. doi:10.1038/s41598-017-08136-1

David, V., Wermelinger, L. S., Frattani, F. S., Lima, A. G. F., Santos, Y. F. S., Mourão, P. A. S., et al. (2023). rJararacin, a recombinant disintegrin from *Bothrops jararaca* venom: exploring its effects on hemostasis and thrombosis. *Arch. Biochem. Biophys.* 738, 109557. doi:10.1016/j.abb.2023.109557

Ding, Y., Gui, X., Chu, X., Sun, Y., Zhang, S., Tong, H., et al. (2023). MTH1 protects platelet mitochondria from oxidative damage and regulates platelet function and thrombosis. *Nat. Commun.* 14, 4829. doi:10.1038/s41467-023-40600-7

Fu, L., Tan, S., Si, R., Qiang, Y., Wei, H., Huang, B., et al. (2023). Characterization, stability and antioxidant activity of curcumin nanocomplexes with soy protein isolate and pectin. *Curr. Res. Food Sci.* 6, 100530. doi:10.1016/j.crfs.2023.100530

Han, J., Pang, X., Zhang, Y., Peng, Z., Shi, X., and Xing, Y. (2020). Hirudin protects against kidney damage in streptozotocin-induced diabetic nephropathy rats by inhibiting inflammation via P38 MAPK/NF-κB pathway. *Drug Des. Devel Ther.* 14, 3223–3234. doi:10.2147/dddt.S257613

Han, L., Li, J., Jiang, Y., Lu, K., Yang, P., Jiang, L., et al. (2024). Changes in the structure and functional properties of soybean isolate protein: effects of different modification methods. *Food Chem.* 432, 137214. doi:10.1016/j.foodchem.2023.137214

Holly, S. P., Gera, N., Wang, P., Wilson, A., Guan, Z., Lin, L., et al. (2019). Ether lipid metabolism by AADACL1 regulates platelet function and thrombosis. *Blood Adv.* 3, 3818–3828. doi:10.1182/bloodadvances.2018030767

Huang, Q., Gao, Q., Chai, X., Ren, W., Zhang, G., Kong, Y., et al. (2020). A novel thrombin inhibitory peptide discovered from leech using affinity chromatography combined with ultra-high performance liquid chromatography-high resolution mass spectroscopy. *J. Chromatogr. B Anal. Technol. Biomed. Life Sci.* 1151, 122153. doi:10.1016/j.jchromb.2020.122153

Hur, W. S., Kawano, T., Mwiza, J. M. N., Paul, D. S., Lee, R. H., Clark, E. G., et al. (2023). Mice expressing nonpolymerizable fibrinogen have reduced arterial and venous thrombosis with preserved hemostasis. *Blood*, 2023020805. doi:10.1182/blood.2023020805

Jiang, S., Dong, W., Zhang, Z., Xu, J., Li, H., Zhang, J., et al. (2022). A new iron supplement: the chelate of pig skin collagen peptide and Fe^{2+} can treat iron-deficiency anemia by modulating intestinal flora. *Front. Nutr.* 9, 1055725. doi:10.3389/fnut.2022.1055725

Lang, J., Li, L., Quan, Y., Tan, R., Zhao, J., Li, M., et al. (2023). LC-MS-based metabolomics reveals the mechanism of anti-gouty arthritis effect of Wuwei Shexiang pill. *Front. Pharmacol.* 14, 1213602. doi:10.3389/fphar.2023.1213602

Lee, H., Hong, J. H., and Seo, K. D. (2023). Long-term stroke and major bleeding risk in patients with non-valvular atrial fibrillation: a comparative analysis between non-vitamin K antagonist oral anticoagulants and warfarin using a clinical data warehouse. *Front. Neurol.* 14, 1058781. doi:10.3389/fneur.2023.1058781

Li, W., Lv, M., Zhang, T., Zhou, M., Zheng, L., Song, T., et al. (2023). Peptide characterization of bovine myocardium hydrolysates and its ameliorative effects on doxorubicin-induced myocardial injury in H9c2 cells and in mice. *J. Agric. Food Chem.* 71, 14562–14574. doi:10.1021/acs.jafc.3c02339

Liao, L., Zhou, M., Wang, J., Xue, X., Deng, Y., Zhao, X., et al. (2021). Identification of the antithrombotic mechanism of leonurine in adrenalin hydrochloride-induced thrombosis in zebrafish via regulating oxidative stress and coagulation cascade. *Front. Pharmacol.* 12, 742954. doi:10.3389/fphar.2021.742954

Liu, W. H., Chen, Y., Bai, X. W., Yao, H. M., Zhang, X. G., Yan, X. W., et al. (2016). Identification and characterization of a novel neuropeptide (neuropeptide Y-HS) from leech salivary gland of Haemadipsa sylvestris. *Chin. J. Nat. Med.* 14, 677–682. doi:10.1016/s1875-5364(16)30080-2

McMillen, T. S., Leslie, A., Chisholm, K., Penny, S., Gallant, J., Cohen, A., et al. (2023). A large-scale, targeted metabolomics method for the analysis and quantification of metabolites in human plasma via liquid chromatography-mass spectrometry. *Anal. Chim. Acta* 1279, 341791. doi:10.1016/j.aca.2023.341791

Miles, A. J., Janes, R. W., and Wallace, B. A. (2021). Tools and methods for circular dichroism spectroscopy of proteins: a tutorial review. *Chem. Soc. Rev.* 50, 8400–8413. doi:10.1039/d0cs00558d

Perron, U., Kozlov, A. M., Stamatakis, A., Goldman, N., and Moal, I. H. (2019). Modeling structural constraints on protein evolution via side-chain conformational states. *Mol. Biol. Evol.* 36, 2086–2103. doi:10.1093/molbev/msz122

Ren, Y., Yang, Y., Wu, W., Zhang, M., Wu, H., and Li, X. (2016). Identification and characterization of novel anticoagulant peptide with thrombolytic effect and nutrient oligopeptides with high branched chain amino acid from Whitmania pigra protein. *Amino Acids* 48, 2657–2670. doi:10.1007/s00726-016-2299-8

Setiabakti, N. M., Tarlac, V., Larsson, P., and Hamilton, J. R. (2023). PI3KC2α inhibition is antithrombotic in blood from hypercholesterolemic mice. *J. Thromb. Haemost.* S1538-7836, 00732–00738. doi:10.1016/j.jtha.2023.09.030

Shi, C., Mammadova-Bach, E., Li, C., Liu, D., and Anders, H. J. (2023a). Pathophysiology and targeted treatment of cholesterol crystal embolism and the related thrombotic angiopathy. *Faseb J.* 37, e23179. doi:10.1096/fj.202301316R

Shi, Z., Ge, X., Zheng, S., Zeng, P., Su, Z., Li, X., et al. (2023b). Mangiferin reduces uric acid via regulation of amino acid and lipid metabolism. *J. Funct. Foods* 108, 105716. doi:10.1016/j.jff.2023.105716

Song, J., Lu, X., Liu, D., Zhang, Y., Zhai, X., Zhou, L., et al. (2023). Fucogalactan sulfate (FS) from laminaria japonica regulates lipid metabolism in diet-induced humanized dyslipidemia mice via an intestinal FXR-FGF19-CYP7A1/CYP8B1 pathway. *J. Agric. Food Chem.* 71, 14027–14037. doi:10.1021/acs.jafc.3c04683

Tang, X., Chen, M., Duan, Z., Mwangi, J., Li, P., and Lai, R. (2018). Isolation and characterization of poecistasin, an anti-thrombotic antistasin-type serine protease inhibitor from leech poecilobdella manillensis. *Toxins (Basel).* 10, 429. doi:10.3390/toxins10110429

Tong, L., Dai, S. X., Kong, D. J., Yang, P. P., Tong, X., Tong, X. R., et al. (2022). The genome of medicinal leech (Whitmania pigra) and comparative genomic study for exploration of bioactive ingredients. *BMC Genomics* 23, 76. doi:10.1186/s12864-022-08290-5

Wang, H., He, D., Duan, L., Lv, L., Gao, Q., Wang, Y., et al. (2022). *In vivo* anticoagulant and antithrombic activity of depolymerized glycosaminoglycan from apostichopus japonicus and dynamic effect-exposure relationship in rat plasma. *Mar. Drugs* 20, 631. doi:10.3390/md20100631

Warkentin, T. E. (2018). Heparin-induced thrombocytopenia-associated thrombosis: from arterial to venous to venous limb gangrene. *J. Thromb. Haemost.* 16, 2128–2132. doi:10.1111/jth.14264

Wei, S., He, T., Zhao, X., Jing, M., Li, H., Chen, L., et al. (2023). Alterations in the gut microbiota and serum metabolomics of spontaneous cholestasis caused by loss of FXR signal in mice. *Front. Pharmacol.* 14, 1197847. doi:10.3389/fphar.2023.1197847

Wu, S., Liang, C., Xie, X., Huang, H., Fu, J., Wang, C., et al. (2021). Hsp47 inhibitor Col003 attenuates collagen-induced platelet activation and cerebral ischemic-reperfusion injury in rats. *Front. Pharmacol.* 12, 792263. doi:10.3389/fphar.2021.792263

Wu, X. Y., Xie, L. J., He, J. J., Yan, X. X., Zhang, F. F., Xu, Y. Y., et al. (2023). Lipidomics reveals the lipid metabolism disorders in Fructus Psoraleae-induced hepatotoxicity in rats with kidney-yin deficiency syndrome. *J. Chromatogr. B Anal. Technol. Biomed. Life Sci.* 1229, 123898. doi:10.1016/j.jchromb.2023.123898

Xu, Y., Yang, Y., Ma, C. M., Bian, X., Liu, X. F., Wang, Y., et al. (2023). Characterization of the structure, antioxidant activity and hypoglycemic activity of soy (Glycine max L.) protein hydrolysates. *Food Res. Int.* 173, 113473. doi:10.1016/j.foodres.2023.113473

Yang, H. R., Hwang, D. H., Prakash, R. L. M., Kim, J. H., Hong, I. H., Kim, S., et al. (2022). Exploring the fibrin(ogen)olytic, anticoagulant, and antithrombotic activities of natural cysteine protease (ficin) with the κ-carrageenan-induced rat tail thrombosis model. *Nutrients* 14, 3552. doi:10.3390/nu14173552

Yang, N., Zhang, J., Guo, J., Xiang, Q., Huang, Y., Wen, J., et al. (2023a). Revealing the mechanism of Zanthoxylum armatum DC. extract-induced liver injury in mice based on lipidomics. *J. Ethnopharmacol.* 319, 117086. doi:10.1016/j.jep.2023.117086

Yang, Q., Zhao, Y., Li, N., Wu, J. L., Huang, X., Zhang, M., et al. (2023b). Identification of polyunsaturated fatty acids as potential biomarkers of osteoarthritis after sodium hyaluronate and mesenchymal stem cell treatment through metabolomics. *Front. Pharmacol.* 14, 1224239. doi:10.3389/fphar.2023.1224239

Yoo, S., Yeon, J., Kim, E., and Kim, Y. (2023). Important features for protein foldings in two acyl carrier proteins from *Enterococcus faecalis*. *J. Microbiol. Biotechnol.* 34, 1–10. doi:10.4014/jmb.2309.09006

You, H., Li, J., Li, Y., Wang, W., Yu, Z., Liu, J., et al. (2023). Absorption of egg white hydrolysate in the intestine: clathrin-dependent endocytosis as the main transport route. *Food Res. Int.* 173, 113480. doi:10.1016/j.foodres.2023.113480

Zeng, S., Yi, R., Tan, F., Sun, P., Cheng, Q., and Zhao, X. (2022). Lactobacillus plantarum HFY05 attenuates carrageenan-induced thrombosis in mice by regulating NF-κB pathway-associated inflammatory responses. *Front. Nutr.* 9, 813899. doi:10.3389/fnut.2022.813899

Zhang, B., Luo, S., Wu, S., Li, J., He, F., Luo, R., et al. (2023). Anti-inflammatory and anti-osteoclastogenesis activities of different kinds of zanthoxylum bungeanum seed oil *in vitro*. *Chem. Biodivers.* 20, e202201157. doi:10.1002/cbdv.202201157

Zhang, X., Zhao, X., Zhang, Y., Niu, S., Qu, F., Zhang, Y., et al. (2013). N-terminal basic amino acid residues of Beet black scorch virus capsid protein play a critical role in virion assembly and systemic movement. *Virol. J.* 10, 200. doi:10.1186/1743-422x-10-200

Zhou, Y., Tao, W., Shen, F., Du, W., Xu, Z., and Liu, Z. (2021). The emerging role of neutrophil extracellular traps in arterial, venous and cancer-associated thrombosis. *Front. Cardiovasc Med.* 8, 786387. doi:10.3389/fcvm.2021.786387

frontiers | Frontiers in Pharmacology

TYPE Original Research
PUBLISHED 28 February 2024
DOI 10.3389/fphar.2024.1347316

Check for updates

OPEN ACCESS

EDITED BY
Zhichao Xu,
Northeast Forestry University, China

REVIEWED BY
Xun Wang,
China University of Petroleum (East China), China
Yang Xiu,
Changchun University of Chinese Medicine, China

*CORRESPONDENCE
Gong Chen,
cracracra@126.com
Shouhua Luo,
luoshouhua@seu.edu.cn

RECEIVED 30 November 2023
ACCEPTED 12 February 2024
PUBLISHED 28 February 2024

CITATION
Chen K, Chen G, Zhuang Z, Luo S, Liu J and Liu G (2024), Feasibility study on the introduction of Micro-CT technology for the identification of *Radix Bupleuri* and its adulterants. *Front. Pharmacol.* 15:1347316. doi: 10.3389/fphar.2024.1347316

COPYRIGHT
© 2024 Chen, Chen, Zhuang, Luo, Liu and Liu. This is an open-access article distributed under the terms of the Creative Commons Attribution License (CC BY). The use, distribution or reproduction in other forums is permitted, provided the original author(s) and the copyright owner(s) are credited and that the original publication in this journal is cited, in accordance with accepted academic practice. No use, distribution or reproduction is permitted which does not comply with these terms.

Feasibility study on the introduction of Micro-CT technology for the identification of *Radix Bupleuri* and its adulterants

Kehong Chen[1], Gong Chen[1,2]*, Zhelong Zhuang[1], Shouhua Luo[3]*, Jiaming Liu[3] and Guorong Liu[1]

[1]School of Artificial Intelligence and Information Technology, Nanjing University of Chinese Medicine, Nanjing, Jiangsu, China, [2]Affiliated Hospital of Nanjing University of Traditional Chinese Medicine, Nanjing, Jiangsu, China, [3]School of Biological & Medical Engineering, Southeast University, Nanjing, Jiangsu, China

Background: *Radix Bupleuri*, a kind of Chinese herbal medicine with great clinical use, is often confused with its adulterants, and it is difficult to identify it without certain knowledge. The existing identification methods have their own drawbacks, so a new method is needed to realize the identification of *Radix Bupleuri* and its adulterants.

Methods: We used Micro Computed Tomography (Micro-CT) to perform tomography scans on *Radix Bupleuri* and its adulterants, performed data screening and data correction on the obtained DICOM images, and then applied 3D reconstruction, data augmentation, and ResNext deep learning model for the classification study.

Results: The DICOM images after data screening, data correction, and 3D reconstruction can observe the differences in the microstructure of *Radix Bupleuri* and its adulterants, thus enabling effective classification and analysis. Meanwhile, the accuracy of classification using the ResNext model reached 75%.

Conclusion: The results of this study showed that Micro-CT technology is feasible for the authentication of *Radix Bupleuri*. The pre-processed and 3D reconstructed tomographic images clearly show the microstructure and the difference between *Radix Bupleuri* and its adulterants without damaging the internal structure of the samples. This study concludes that Micro-CT technology provides important technical support for the reliable identification of *Radix Bupleuri* and its adulterants, which is expected to play an important role in the quality control and clinical application of herbs.

KEYWORDS

Micro-CT technology, *Radix Bupleuri*, microstructure, identification, 3D reconstruction, data augmentation, ResNeXt

1 Introduction

According to the *Chinese Pharmacopoeia*, *Radix Bupleuri*, also called "Chaihu" in Chinese, is derived from the dried roots of *Bupleurum chinense DC.* and *Bupleurum scorzonerifolium Willd.* (Editorial Committee of Chinese Pharmacopoeia, 2020). According to different characters, it is called "North-chaihu" and "South-chaihu," which has the effect

of evacuating and reducing fever, soothing the liver and relieving depression, and lifting Yang qi. It is often used to treat cold and fever, cold and heat exchange, chest and hypogastric pain, menstrual irregularity, uterine prolapse, and anal prolapse (Yang et al., 2017). In recent years, with a deeper insight into the relevant research, it has been found that *Radix Bupleuri* has anti-inflammatory, antiviral, liver and gallbladder protective effects, prevents and treats cancer, balances different organs and energy in the body, strengthens the digestive tract, improves the function of the liver and circulatory system, and relieves liver tension, among others (Ma et al., 2016). However, the safety and effectiveness of the use of *Radix Bupleuri* are challenging to guarantee for two reasons: first, because the efficacy of *Radix Bupleuri* is significant, some merchants illegally mix the products for some profits, which seriously affects the regular operation of the medicinal material market and dramatically undermines the safety and effectiveness of the use of *Radix Bupleuri*; second, the seeds of *Radix Bupleuri* tend to be mixed with those of its adulterants when planting, and it is difficult to distinguish after growth. *Radix Bupleuri* and its adulterants share a similar morphological appearance, but the chemicals they contain differ considerably, including *Bupleurum longiradiatum Turcz.* with toxic ingredients and *Bupleurum hamiltonii Balak* with almost undetectable saikosaponin contents (Chao et al., 2014). More seriously, *B. longiradiatum Turcz.* has been reported by Heilongjiang Institute for Drug Control for mistakenly confusing commercial *Radix Bupleuri* preparations and causing poisoning incidents (Shen et al., 2024). Therefore, identifying and classifying *Radix Bupleuri* and its adulterants are particularly important in order to prevent similar incidents.

At present, the identification methods for *Radix Bupleuri* and its adulterants include character identification (Editorial Committee of Chinese Pharmacopoeia, 2020), DNA barcode identification (Feng et al., 2015), TLC identification (Yen et al., 1991), HPLC identification (Qian, 2012), and microscopic identification (Miao et al., 2017). Existing identification methods have their advantages and disadvantages: character identification is simple but requires rich knowledge of traditional Chinese medicine identification; DNA barcode identification, thin-layer chromatography identification, HPLC identification, and microscopic identification features high accuracy, but the operation is too complicated. Therefore, it is of great importance to introduce Micro Computed Tomography (Micro-CT) technology as a new method for *Radix Bupleuri* identification.

Micro-CT technology differs from clinical CT technology in that the X-ray emission tube of Micro-CT is a micro-focus X-ray tube, that can realize the imaging of small/micro-volume samples at a resolution level of 1–100 μm. It has a good "microscopic effect," which can be applied to show the nuanced structural differences in small samples. Micro-CT is widely recognized as the preferred method for studying the microstructure, spatial volume, and structural changes of bones. Meanwhile, Micro-CT technology is an advanced, non-destructive 3D imaging technology that has been researched and applied in many fields, such as medicine, geological research, materials, and agriculture (Wong et al., 2010; van Raamsdonk et al., 2019; Feng et al., 2021; Ma et al., 2021; Xie et al., 2021). Different from ordinary clinical CT, it is a technology used for scanning and analyzing images of living small animals, various complex tissues and related soft tissues with a micro-focus X-ray tube. However, Micro-CT technology is rarely used in plants and Chinese medicine (Starosolski et al., 2015; Su and Xiao, 2020). Micro-CT technology can scan *Radix Bupleuri* and its adulterants products, and corresponding DICOM images are obtained and studied. In addition, Micro-CT technology can not only accurately obtain the internal microstructure of traditional Chinese medicine (TCM) decoction pieces but also preserve the integrity of the sample to the greatest extent to facilitate future follow-up studies of the sample (Zhang et al., 2020).

In addition, Micro-CT can be combined with 3D reconstruction technology to obtain clear and precise 3D deconstructed images of the test specimen. The FDK algorithm (Feldkamp-Davis-Kress) used in this study is the most commonly used reconstruction algorithm for CT images. The FDK algorithm, first proposed by Feldkamp, Davis, and Kress in 1984, is an approximate reconstruction algorithm for cone-beam CT circular-trajectory scans, and has been the most practical algorithm for cone-beam circular-trajectory reconstruction to date (Feldkamp et al., 1984). DICOM images after FDK 3D reconstruction are able to generate high-quality 3D reconstructed images, reducing artifacts and image distortions and improving the spatial resolution and geometric accuracy of the images. At the same time, the image after FDK 3D reconstruction can retain multi-layered information about the structure of the dissection, preserving the 2D slice features while permitting the formation of a 3D model to study its 3D structural features if needed.

What's more, ResNext (Residual Next) used in this study is a deep neural network architecture that extends and improves on ResNet (Residual Network) (Xie et al., 2016). The design goal of ResNext is to increase the expressive power of the model while maintaining its simplicity, thus improving the performance in various computer vision tasks. ResNext, we introduce the concept of "cardinality" to the idea of residual learning in ResNet. In ResNext, the branches within each residual block are divided into multiple paths, each with the same convolutional layers but different weight parameters. This structure allows the network to learn features in multiple dimensions, and the complexity of the model can be increased by increasing the number of cardinalities.

Hence, this study aims to provide a new method for the authenticity identification of *Radix Bupleuri* and its adulterants products by analyzing and identifying DICOM images obtained after Micro-CT imaging. The application of Micro-CT technology provides us with a unique perspective that allows us to explore the microstructure of *Radix Bupleuri* and its adulterants in depth, thus discovering small but important differences between them. This method not only improves the quality control of *Radix Bupleuri* herbs, but also is expected to play a key role in the field of Chinese herbal medicine identification to ensure the safety of medication. By combining DICOM image analysis and advanced 3D reconstruction techniques and deep learning techniques, we will be able to achieve reliable classification and identification of *Radix Bupleuri* and its adulterants, providing new tools and perspectives for quality management and monitoring of Chinese herbal medicines. This study is expected to bring innovative advances in quality control and applications in the field of Chinese herbal medicine.

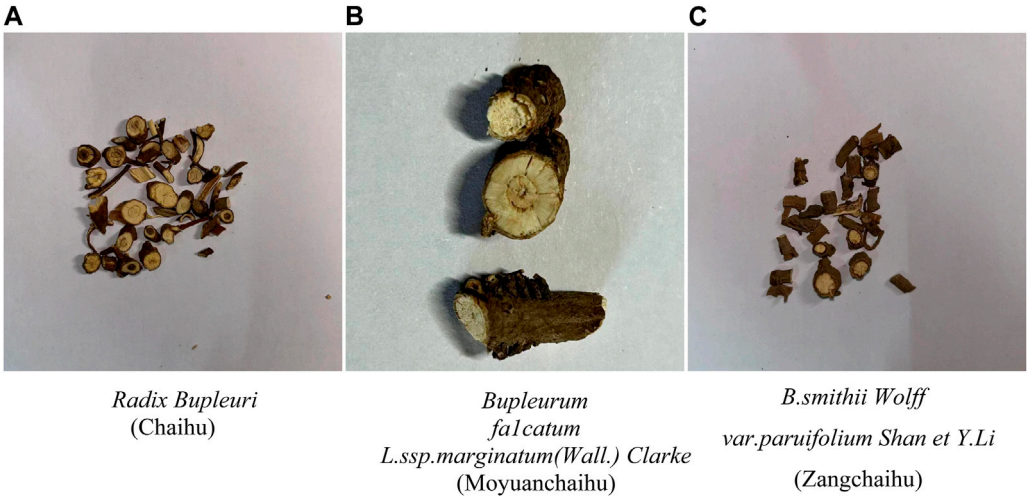


FIGURE 1
Optical photographs of three types of *Radix Bupleuri*. **(A)** *Shows the optical image of Radix Bupleuri* (Chaihu). **(B)** Shows the microstructure of the *Bupleurum fa1catum L. ssp.marginatum(Wall.) Clarke* (Moyuanchaihu). **(C)** Shows the microstructure of *B. smithii Wolff var. paruifolium Shan et Y.Li* (Zangchaihu). From the above images, it can be observed that the three types of *Radix Bupleuri* and its adulterants are more difficult to be classified and identified under normal visual observation, including the cross-section of the external features.

2 Materials and methods

2.1 Experimental materials

This study collected nine samples of *Radix Bupleuri* (Chaihu), *Bupleurum fa1catum L. ssp.marginatum (Wall.) Clarke* (Moyuanchaihu), and *B. smithii Wolff var. paruifolium Shan et Y.Li* (Zangchaihu). Among them, Moyuanchaihu and Zangchaihu have been identified. Jiangsu Provincial Hospital of Traditional Chinese Medicine identified all samples. Optical photographs of three types of *Radix Bupleuri* and its adulterants used in this study are shown in Figure 1.

2.2 Equipment and data collection

The Micro-CT machine used in this study was provided by Southeast University. In addition, the hardware information of the experimental platform used in this study is as follows: 13th Gen Intel(R) Core (TM) i9-13900KF, NVIDIA GeForce RTX 4090 24 GB. The software information of the experimental platform used in this study is as follows: the operating system is Windows 10, the programming language is Python 3.7.12, and the deep learning framework is Pytorch 1.13.1. Among the three types of *Radix Bupleuri* and its adulterants, three samples of each type were randomly taken, totaling nine samples, the bottom end of which was ground flat and placed into Micro-CT for scanning at a scanning set voltage of 45kv, current of 175μA, exposure time of 5s. After scanning and screening, three samples of each type of *Radix Bupleuri*, with 33, 33, and 34 images were selected respectively. A total of 100 images were retained, so there were 300 images for the three types of *Radix Bupleuri*. Those images were exported to DICOM file format, each with a size of approximately 7 M. The DICOM file format is a medical image format that defines the quality and can meet the clinical needs for data exchange, including crucial information such as the original size of the sample, window level, and window width.

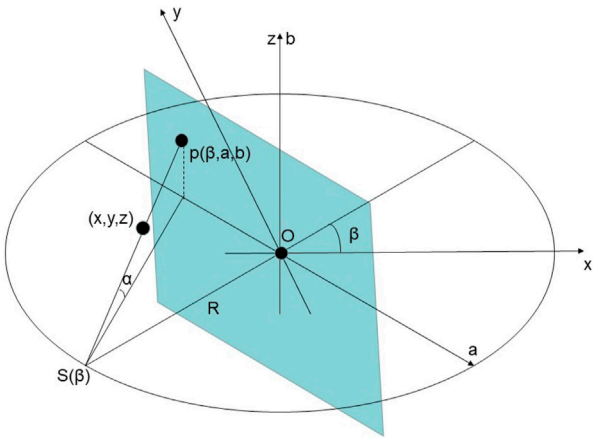


FIGURE 2
The Schematic of A Conventional Cone-beam CT Scan. ***Oxyz*** is the Cartesian coordinate system, and ***S*** is the X-ray source, rotating circularly about the *z*-axis with a rotation radius of R, i.e., the distance from the ray source to the center of the sample. The X-rays and their projections can be determined by $\boldsymbol{p}(\boldsymbol{\beta},\boldsymbol{a},\boldsymbol{b})$, where $\boldsymbol{\beta}$ is an angular parameter.

2.3 Data correction

In the actual Micro-CT scanning process, some defects in the detector itself will have an impact on the scanning results, leading to a particular gap between the ideal situation and pixel response distortion. Therefore, it is necessary to correct the scanned image to

restore the actual image to the maximum extent. In this study, geometric correction and light-field correction were performed for the Micro-CT machine used, and the true scanning image was restored to a large extent (Prell et al., 2009).

2.4 3D reconstruction

Micro-CT combined with 3D reconfiguration technology can obtain clear and precise three-dimensional deconstructed structural images of test samples in medicine, biology, geology, etc. (Su and Xiao, 2020). Figure 2 shows the schematic of a conventional cone-beam CT scan. The FDK algorithm is an FBP (2-D fan-beam filtered-back projection) algorithm of the 3-D extension. According to the conical beam CT geometry shown in Figure 2, it can be rewritten as:

$$f(x,y,z) = \frac{1}{2}\int_0^{2\pi} \frac{R^2}{(R + x\cos\beta + y\sin\beta)^2}\tilde{p}(\beta, a(x,y,\beta), b(x,y,z,\beta))d\beta$$

$$\tilde{p}(\beta,a,b) = \left(\frac{R}{\sqrt{R^2+a^2+b^2}}\cdot p(\beta,a,b)\right)^{*}h(a) \quad (2)$$

$$a(x,y,\beta) = R\frac{-x\sin\beta + y\cos\beta}{R + x\cos\beta + y\sin\beta} \quad (3)$$

$$b(x,y,z,\beta) = \frac{zR}{R + x\cos\beta + y\sin\beta} \quad (4)$$

where h(a) is the ramp-filter. The FDK algorithm is implemented in three main steps: data pre-weighting, row-by-row one-dimensional convolution, and weighted three-dimensional back-projection. The FDK algorithm has been widely used because of its simplicity and ease of implementation and has become the most commonly used algorithm in cone-beam reconstruction.

In this study, the FDK algorithm is implemented using ASTRA Toolbox, an open-source toolkit dedicated to reconstructing and analyzing projection data, which is particularly suitable for imaging applications such as computed tomography (CT) (Flouris et al., 2022). The open-source nature of the ASTRA Toolbox allows users to freely access and modify the source code to meet the specific needs of different application scenarios. In addition, the toolkit features powerful GPU acceleration, which significantly improves the computational speed of the FDK algorithm, making it particularly suitable for applications that deal with large-scale projection data and real-time reconstruction (Palenstijn et al., 2017).

In this study, the Micro-CT detector used has a pixel count of 2048 × 2048 with each pixel size of 13.5 μm. In addition, the distance from the X-ray source to the detector is 45.37 cm. These detailed experimental setups provided an accurate basis for the study, ensuring accurate modelling of the Micro-CT system and reliability of the reconstruction process.

2.5 Data augmentation

In the process of deep learning, the larger the amount of data, the better the generalization ability of the neural network model, as well as the more stable the ability to classify images. Therefore, the enhancement of images can improve the performance of deep learning models and increase the stability of the model to prevent overfitting. The data enhancement methods adopted in this study included image rotation, image masking, and noise addition.

The image rotation used in this study mainly employs random angle rotation by randomly selecting angles in 90°, 180°, and 270° for clockwise rotation. Taking the center point of the image as the origin $O(0,0)$, let the corresponding end of $P(x_0, y_0)$ after selecting the angle θ ($\theta \in \{90°, 180°, 270°\}$) for rotation be $Q(x,y)$. The coordinates obtained after clockwise rotation of $P(x_0, y_0)$ by θ angle are $(x_0\cos(\theta) + y_0\sin(\theta), -x_0\sin(\theta) + y_0\cos(\theta))$ and its matrix expression is shown in Equation (5). The features of its image do not change before and after rotation.

$$\begin{bmatrix} x \\ y \\ 1 \end{bmatrix} = \begin{bmatrix} \cos(\theta) & \sin(\theta) & 0 \\ -\sin(\theta) & \cos(\theta) & 0 \\ 0 & 0 & 1 \end{bmatrix}\begin{bmatrix} x_0 \\ y_0 \\ 1 \end{bmatrix} \quad (5)$$

In addition, this study used random masking for data augmentation. An arbitrary point in the image was taken as the starting point; both the length and width were randomly selected between 10pixel and 100pixel, which were used to form a rectangular region, and the gray value of the image within the rectangular area was set to 0, to achieve occlusion of the image.

The last selected data augmentation method is to add noise to the image; in this study, Gaussian noise was added to the DICOM image. Hussain et al. previously added Gaussian noise for data enhancement, and by using Gaussian noise, Gaussian blurring was applied to the images requiring data enhancement, and the accuracy obtained was also improved compared to the previous one (Hussain et al., 2017). The core idea of Gaussian blurring is to replace each pixel value in an image with a weighted average of the pixel values around it, with the weights determined by a Gaussian function. The Gaussian function is the largest at the center and decreases the further away from the center; therefore, pixels closer to the center are weighted more heavily. The Gaussian function has two main parameters: the standard deviation (σ) and pixel value at the center. The core of performing Gaussian blurring is to create a matrix called a filter based on the Gaussian function, the elements of this matrix are the weights calculated by the Gaussian function, and then the filter is applied to each pixel in the image. The pixel values in and around this centroid are weighted and averaged; in this study, the standard deviation (σ) was set to 1.0.

2.6 ResNext

A significant advantage of ResNext over ResNet is its ability to improve the model performance without significantly increasing model complexity. By expanding the cardinality number, ResNext can balance the depth of the model and width to a certain extent. A comparison between the network structures of ResNext and ResNet is shown in Table 1.

As shown in Table 1, the network structure of ResNet-50 is shown on the left, and that of ResNext-50 ($32 \times 4d$) on the right. The shapes of the residual blocks are in parentheses, the number of stacked blocks is outside the parentheses, and $C = 32$ indicates that the convolution is divided into 32 groups. The Bottleneck structure

TABLE 1 Network structure comparison table.

Stage	Output	ResNet-50	ResNext-50 (32 × 4*d*)
Conv1	112 × 112	7 × 7,64, stride 2	7 × 7,64, stride 2
Conv2	56 × 56	3 × 3 max pool, stride 2	3 × 3 max pool, stride 2
		$\begin{bmatrix} 1\times1, 64 \\ 3\times3, 64 \\ 1\times1, 256 \end{bmatrix}\times3$	$\begin{bmatrix} 1\times1, 128 \\ 3\times3, 128, \ C=32 \\ 1\times1, 256 \end{bmatrix}\times3$
Conv3	28 × 28	$\begin{bmatrix} 1\times1, 128 \\ 3\times3, 128 \\ 1\times1, 512 \end{bmatrix}\times4$	$\begin{bmatrix} 1\times1, 256 \\ 3\times3, 256, \ C=32 \\ 1\times1, 512 \end{bmatrix}\times4$
Conv4	14 × 14	$\begin{bmatrix} 1\times1, 256 \\ 3\times3, 256 \\ 1\times1, 1024 \end{bmatrix}\times6$	$\begin{bmatrix} 1\times1, 512 \\ 3\times3, 512, \ C=32 \\ 1\times1, 1024 \end{bmatrix}\times6$
Conv5	7 × 7	$\begin{bmatrix} 1\times1, 512 \\ 3\times3, 512 \\ 1\times1, 2048 \end{bmatrix}\times3$	$\begin{bmatrix} 1\times1, 1024 \\ 3\times3, 1024, \ C=32 \\ 1\times1, 2048 \end{bmatrix}\times3$
	1 × 1	global average pool 1000-day fc, softmax	global average pool 1000-day fc, softmax

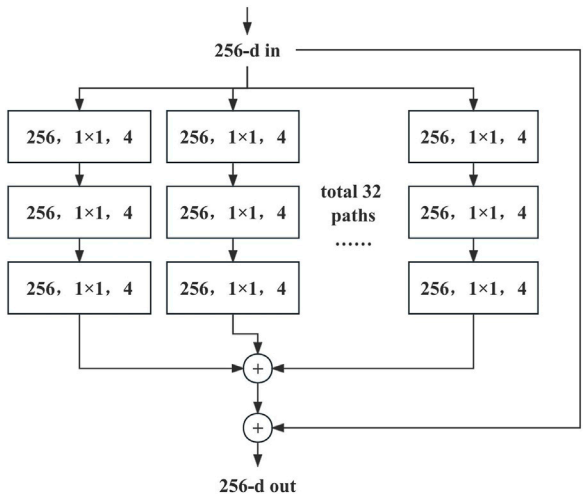


FIGURE 3
A block of ResNext-50 with cardinality = 32, with roughly the same complexity. The figure illustrates a Bottleneck structure in ResNext-50. The initial input has 256 channels, which undergoes dimensionality reduction to 128 channels using a 1 × 1 convolution. Subsequently, the 128 channels are divided into 32 groups, each containing 4 channels. Finally, dimensionality expansion is performed using a 1 × 1 convolution, resulting in the final output.

in ResNext-50 is shown in Figure 3. The Bottleneck module structure enhances the network's expressive power and computational efficiency by introducing 1 × 1 convolutions, 3 × 3 grouped convolutions, and another round of 1 × 1 convolutions in each module. This design allows the network to maintain lower computational complexity while learning complex features, enabling ResNext-50 to perform exceptionally well in handling large-scale image data and complex tasks. In the original study, ResNext was implemented to improve the accuracy of the model with approximately the same amount of computation as ResNet. Therefore, the deep learning model chosen in this study was ResNext50, and each parameter is listed in Table 2.

TABLE 2 Network parameter details.

Parameter	Category/Category/value
Loss Function	Cross-Entropy Loss Function
Optimizer	Stochastic Gradient Descent (SGD)
Activation Function	ReLU
Learning Rate	0.0002
Batch Size	16
epoch	160

In addition, this study used NVIDIA Apex Automatic Mixed Precision (AMP) in the model to improve training efficiency (Micikevicius et al., 2017). AMP allows training and inference to be performed using low-precision floating-point numbers while keeping the model values stable, thus speeding up the training and reducing the memory footprint.

3 Results

3.1 Results of 3D reconstruction

After 3D reconstruction of the image data in the DICOM file format using the FDK algorithm, a relatively clear tomographic image can be obtained, as shown in Figure 4. Figure 4 shows the tomographic structure of *Radix Bupleuri*, and all structures correspond to the microstructure of *Radix Bupleuri* in the *Identification of Traditional Chinese Medicines* (Feng, 2020). The cork layer is located in the outermost layer, which consists of several rows of cells and plays a protective role; the cortex is located inside the cork layer, and there are oil chamber fissures

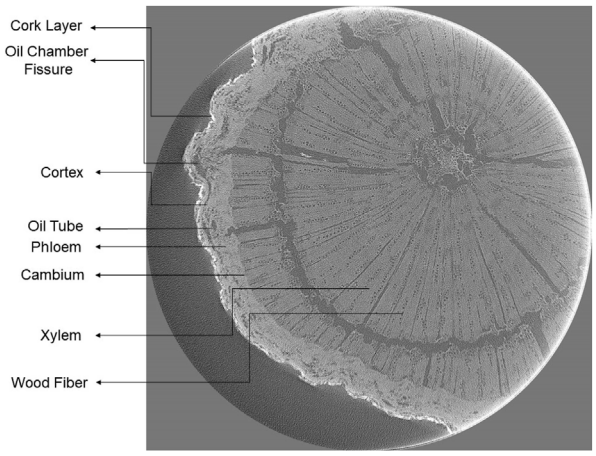


FIGURE 4
Microstructure of *Radix Bupleuri*. The structures in order from the outside to the inside are: cork layer, cortex, phloem, cambium, and xylem. Among these are oil chamber fissures scattered in the cortex, oil tubes scattered in the phloem, and wood fibers in the xylem.

scattered in the cortex of *Radix Bupleuri*, oil tubes are scattered in the phloem, and the sieve tubes are inconspicuous; the cambium shows a ring-like shape, which consists of three to four rows of parenchyma cells; the ducts of the xylem are sparse and dispersed, and the bundles of wood fibers are arranged in intermittent rings, with radial fissures as xylem rays.

According to the microscopic identification method recorded in *Identification of Traditional Chinese Medicines*, the most apparent difference between North-chaihu and South-chaihu is the number and arrangement of wood fibers in the xylem. The xylem conduits of North-chaihu are sparse and scattered, the wood fiber bundles are arranged in intermittent rings in the middle of the xylem, and the fibers mostly show a polygonal shape. In contrast, the wood fibers in the xylem of South-chaihu are fewer and scattered, and most of them are distributed in the outer part of the xylem.

Extending this finding to *Radix Bupleuri* and its adulterants, a significant difference was observed between the wood fibers in the microstructure of *Radix Bupleuri* and its adulterants, as shown in Figure 5. Figure 5A shows the cross-section of the tomography of *Radix Bupleuri*, and it can be clearly seen that the wood fibers in the xylem are arranged in an interrupted ring, which is consistent with the microstructural characteristics of North-chaihu in the book. Figure 5B shows the cross-section of *Bupleurum fa1catum L. ssp.marginatum (Wall.) Clarke* (Moyuanchaihu), whose wood fibers are distributed in a manner that is quite different from that of *Radix Bupleuri*. The wood fibers of Moyuanchaihu have a certain degree of aggregation. The aggregation points are mainly distributed near the formation layer, and the wood fibers in the middle of the xylem are relatively aggregated. Figure 5C shows the cross-section of *B. smithii W. var. paruifolium Shan et Y.Li* (Zangchaihu). Compared with the above two wood fiber distribution patterns, there is a noticeable difference: the wood fibers of Zangchaihu are irregularly arranged in the middle of the xylem, which is more similar to that of the wood fiber of *Radix Bupleuri*, but is more disordered; the most significant difference from the previous two distribution patterns is that the wood fibers of Zangchaihu are mostly aggregated in the middle part of Zangchaihu, which forms a medullary-like part. Based on the above distribution, it can be put into ResNext for training, which can achieve the classification of *Radix Bupleuri* and its adulterants.

3.2 Results of the classification

In this study, 1200 DICOM images of 1,024 pixel×1,024 pixel were obtained by data enhancement of the 3D reconstructed

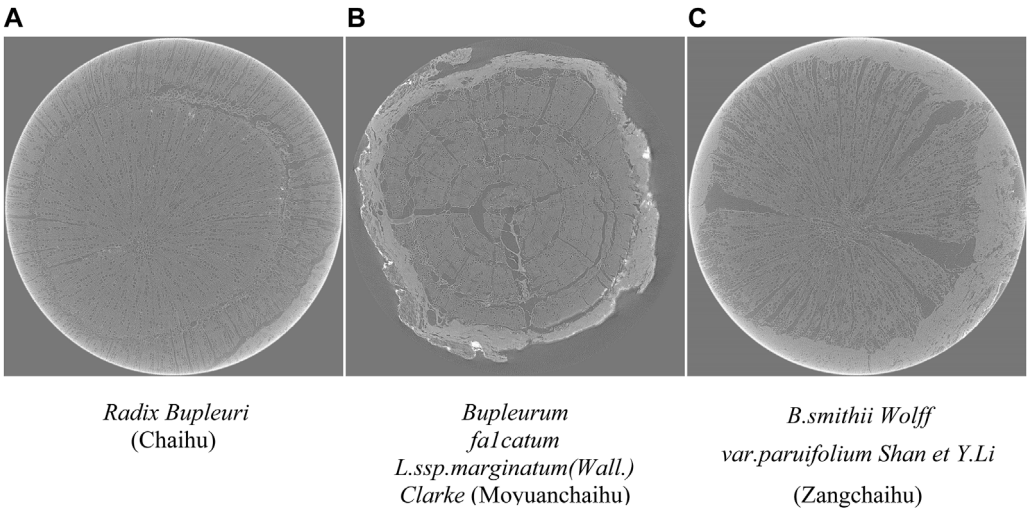


FIGURE 5
Cross-section of *Radix Bupleuri* and Its Adulterants. The images shown above are all from a single sample and can correspond one-to-one with the optical image in Figure 1. **(A)** shows the microstructure of *Radix Bupleuri* (Chaihu), which is characterized by the interrupted ring-like structure of wood fiber bundles in the xylem. **(B)** shows the microstructure of the *Bupleurum fa1catum L. ssp.marginatum(Wall.) Clarke* (Moyuanchaihu), which is characterized by the aggregation of wood fibers near the formation layer. **(C)** shows the microstructure of *B. smithii Wolff var. paruifolium Shan et Y.Li* (Zangchaihu), characterized by the aggregation of wood fibers in the middle of xylem.

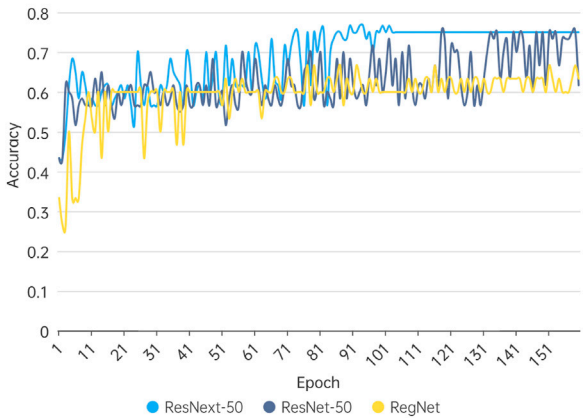


FIGURE 6
The Iterative Process of Validation Accuracy of Each Model. The horizontal coordinate is the number of epochs and the vertical coordinate is the accuracy. As the number of epochs increases, the accuracy rate increases and stabilizes.

DICOM images, of which, 300 images were original images and 900 images were obtained by data enhancement of original images. The training and testing sets were randomly assigned in the ratio of 8:2, i.e., the number of images in the training set was 960, and that of images in the testing set was 240. All the DICOM images were trained and tested using ResNext50, and, a classification accuracy of 75% was obtained. In this study, ResNet-50 and RegNet models were also used to train and validate the same images and compare the results with ResNext-50 model training. The iterative process of validation accuracy of each model is shown in Figure 6.

As shown in Figure 6, the accuracy rate gradually increased with the increase of training epochs. The ResNext-50 model achieves 75% accuracy rate after 70 epochs, stabilizing at this level after 100 epochs. In contrast, ResNet-50, although also capable of reaching 75% accuracy, requires 120 epochs to do so and demonstrates less stability compared to ResNext-50. However, the RegNet network model, which is a classification model with strong generalization ability, does not exhibit satisfactory training results in this study. The validation accuracy increases with the number of epochs and reaches 67% around the 150th epoch.

4 Discussion

In this study, data acquisition of *Radix Bupleuri* and its adulterants was carried out by Micro-CT technology, followed by data correction, FDK 3D reconstruction, data augmentation, and finally put into the ResNext50 model for training and testing, which ultimately yielded an accuracy of 75%, and this result can help the doctors to some extent to carry out the research on the identification of *Radix Bupleuri*. In this study, Micro-CT technology was introduced for the identification of *Radix Bupleuri* and its adulterants, which, to a certain extent, made up for the regret that Micro-CT technology was seldom applied in research related to plants and traditional Chinese medicines, and also confirmed the feasibility of using Micro-CT technology in the field of plants and traditional Chinese medicines. After data correction and FDK 3D reconstruction, the DICOM image was clear and obvious so that its microstructures could be distinguished more obviously, and its microscopic features; could be obtained more accurately to identify its authenticity.

Micro-CT has several advantages over electron microscopy: Micro-CT technology does not require slicing of the sample; tomography does not destroy the internal structure of the sample, which allows for the repeated use of the sample and other future studies on the same sample; the sample can be reconstructed in three dimensions if required; Micro-CT technology can be applied to live animals and plants without affecting their growth; Micro-CT can be applied to live animals and plants without affecting their growth; and because the scanning environment of Micro-CT is closed and dark, it can avoid the influence of the surrounding environment on the scanning results.

The significance of this study is to provide a new method for the identification of *Radix Bupleuri* and its adulterants, and the identification and classification of *Radix Bupleuri* and its adulterants were realized based on microscopic features using the ResNext50 model. In general, the images scanned by the Micro-CT technology showed the following microscopic features: the wood fibers in the xylem of *Radix Bupleuri* were arranged in interrupted rings, the wood fibers of Zangchaihu were clustered in the middle, and the wood fibers of Moyuanchaihu were clustered around the forming layer. The results of this study provide a new method for the identification and characterization of *Radix Bupleuri* and even traditional Chinese medicine.

The future work of this study is divided into two main parts. The first part is to use other different deep learning models and optimize these deep learning models to improve the accuracy of model classification. The second part is to scan and classify other kinds of Chinese medicine tablets and their mixed forgeries, and ultimately to realize the ability to classify and identify all Chinese medicine tablets.

5 Conclusion

This study highlights the significant potential of Micro-CT technology as a crucial tool in the authentication of Traditional Chinese Medicine (TCM), with a specific focus on *Radix Bupleuri*. The introduction of Micro-CT technology represents a groundbreaking step in providing doctors with an innovative and supplementary diagnostic method for determining the authenticity of medicinal herbs. The capability of Micro-CT to visualize the internal structure of samples offers a unique advantage in discerning microscopic features that aid in the accurate identification of *Radix Bupleuri* and its adulterants.

Moreover, the study recognizes the promising avenue of incorporating deep learning techniques into the analysis of data obtained through Micro-CT scans. Deep learning, with its remarkable achievements in image analysis, is identified as a key direction for future research. The application of deep learning in addressing the authentication challenges of traditional Chinese medicine is anticipated to enhance the precision and efficiency of

identification processes. Through the training of neural network models, the potential for automated authentication of TCM is envisioned, providing robust support for the sustainable development of the traditional Chinese medicine industry.

Taken together, the application of Micro-CT technology brings new perspectives and tools for authentication of TCM, whereas the combination of deep learning and other technologies will further enhance the accuracy and efficiency of TCM authentication. This developmental trend is of great significance for the quality control of Chinese medicines. Through more accurate identification methods, the circulation of counterfeit and substandard Chinese medicines can be prevented, and the safety and effectiveness of public medication can be guaranteed. The application of Micro-CT technology also injects new impetus for the sustainable development of the TCM industry. By upgrading the technical level of TCM identification, the TCM industry will become more competitive and provide strong support for the inheritance and innovative development of TCM.

Data availability statement

The datasets presented in this study can be found in online repositories. The names of the repository/repositories and accession number(s) can be found here: https://figshare.com/articles/dataset/_/25239973.

Author contributions

KC: Data curation, Project administration, Validation, Writing–original draft, Writing–review and editing. GC: Conceptualization, Funding acquisition, Methodology, Supervision, Writing–review and editing. ZZ: Data curation, Supervision, Validation, Writing–review and editing. SL: Conceptualization, Methodology, Supervision, Writing–review and editing. JL: Data curation, Project administration, Supervision, Writing–review and editing. GL: Data curation, Supervision, Validation, Writing–review and editing.

Funding

The author(s) declare financial support was received for the research, authorship, and/or publication of this article. This study was supported by the National Natural Science Funds of China (51832001), and the National Natural Science Funds of China (61871126). The funders have no role in the research design, data collection, analysis, or decision to publish or prepare manuscripts.

Acknowledgments

This is a short text to acknowledge the contributions of specific colleagues, institutions, or agencies that aided the efforts of the authors.

Conflict of interest

The authors declare that the research was conducted in the absence of any commercial or financial relationships that could be construed as a potential conflict of interest.

Publisher's note

All claims expressed in this article are solely those of the authors and do not necessarily represent those of their affiliated organizations, or those of the publisher, the editors and the reviewers. Any product that may be evaluated in this article, or claim that may be made by its manufacturer, is not guaranteed or endorsed by the publisher.

References

Chao, Z., Zeng, W., Liao, J., Liu, L., Liang, Z., and Li, X. (2014). DNA barcoding Chinese medicinal Bupleurum. *Phytomedicine* 21 (13), 1767–1773. Epub 20141015. doi:10.1016/j.phymed.2014.09.001

Editorial Committee of Chinese Pharmacopoeia (2020). *Chinese Pharmacopoeia*. Beijing: Medical Science and Technology Press.

Feldkamp, L. A., Davis, L. C., and Kress, J. W. (1984). Practical cone-beam algorithm. *J. Opt. Soc. Am. A-optics Image Sci. Vis.* 1, 612–619. doi:10.1364/josaa.1.000612

Feng, L. (2020). *Identification of traditional Chinese medicines*. Beijing: China Press of Traditional Chinese Medicine.

Feng, S., Jiang, Y., Wang, S., Jiang, M., Chen, Z., Ying, Q., et al. (2015). Molecular identification of dendrobium species (orchidaceae) based on the DNA barcode Its2 region and its application for phylogenetic study. *Int. J. Mol. Sci.* 16 (9), 21975–21988. Epub 20150911. doi:10.3390/ijms160921975

Feng, T., Ge, Y., Xie, Y., Xie, W., Liu, C., Li, L., et al. (2021). Detection of collagen by multi-wavelength photoacoustic analysis as a biomarker for bone health assessment. *Photoacoustics* 24, 100296. Epub 20210826. doi:10.1016/j.pacs.2021.100296

Flouris, K., Jimenez-Del-Toro, O., Aberle, C., Bach, M., Schaer, R., Obmann, M. M., et al. (2022). Assessing radiomics feature stability with simulated ct acquisitions. *Sci. Rep.* 12 (1), 4732. Epub 20220318. doi:10.1038/s41598-022-08301-1

Hussain, Z., Gimenez, F., Yi, D., and Rubin, D. (2017). Differential data augmentation techniques for medical imaging classification tasks. *AMIA Annu. Symp. Proc.* 2017, 979–984. Epub 20180416.

Ma, S., Li, J., Guo, Y., Huang, Y., Chi, X., Wei, Y., et al. (2021). Three-dimensional radiographic and histological tracking of rat mandibular defect repair after inferior alveolar nerve axotomy. *Arch. Oral Biol.* 131, 105252. Epub 20210903. doi:10.1016/j.archoralbio.2021.105252

Ma, Y., Bao, Y., Wang, S., Li, T., Chang, X., Yang, G., et al. (2016). Anti-inflammation effects and potential mechanism of saikosaponins by regulating nicotinate and nicotinamide metabolism and arachidonic acid metabolism. *Inflammation* 39 (4), 1453–1461. doi:10.1007/s10753-016-0377-4

Miao, X. S., Cui, Q. Y., Wang, Z. Y., Liu, X. N., Zhao, A. B., Qiao, Y. J., et al. (2017). Advance in quality assessment of Chinese materia medica using microscopic and morphological methods. *Chin. J. Nat. Med.* 15 (9), 653–663. doi:10.1016/s1875-5364(17)30094-8

Micikevicius, P., Narang, S., Alben, J., Diamos, G., Elsen, E., Garcia, D., et al. (2017). *Mixed precision training*. [arXiv:1710.03740 p.]. Available from: https://ui.adsabs.harvard.edu/abs/2017arXiv171003740M (October 01, 2017).

Palenstijn, W. J., Bédorf, J., Sijbers, J., and Batenburg, K. J. (2017). A distributed astra Toolbox. *Adv. Struct. Chem. Imaging* 2 (1), 19. Epub 20161207. doi:10.1186/s40679-016-0032-z

Prell, D., Kyriakou, Y., and Kalender, W. A. (2009). Comparison of ring artifact correction methods for flat-detector ct. *Phys. Med. Biol.* 54 (12), 3881–3895. Epub 20090602. doi:10.1088/0031-9155/54/12/018

Qian, G.-Z. (2012). *Analysis on saikosaponin of sixteen Bupleurum chinense from shanxi*. Natural Product Research and Development 24 (5), 644–647.

Shen, X. J., Zhang, J. Q., An, Y. L., Yang, L., Li, X. L., Hu, Y. S., et al. (2024). Matlab Language assisted data acquisition and processing in liquid chromatography orbitrap mass spectrometry: application to the identification and differentiation of Radix Bupleuri from its adulterants. *J. Chromatogr. A* 1714, 464544. Epub 20231213. doi:10.1016/j.chroma.2023.464544

Starosolski, Z., Villamizar, C. A., Rendon, D., Paldino, M. J., Milewicz, D. M., Ghaghada, K. B., et al. (2015). Ultra high-resolution *in vivo* computed tomography imaging of mouse cerebrovasculature using a long circulating blood pool contrast agent. *Sci. Rep.* 5, 10178. Epub 20150518. doi:10.1038/srep10178

Su, Y., and Xiao, L. T. (2020). 3d visualization and volume-based quantification of rice chalkiness *in vivo* by using high resolution micro-ct. *Rice (N Y)* 13 (1), 69. Epub 20200916. doi:10.1186/s12284-020-00429-w

van Raamsdonk, L. W. D., Prins, T. W., Meijer, N., Scholtens, I. M. J., Bremer, M., and de Jong, J. (2019). Bridging legal requirements and analytical methods: a review of monitoring opportunities of animal proteins in feed. *Food Addit. Contam. Part A Chem. Anal. Control Expo. Risk Assess.* 36 (1), 46–73. Epub 20190104. doi:10.1080/19440049.2018.1543956

Wong, H. M., Yeung, K. W., Lam, K. O., Tam, V., Chu, P. K., Luk, K. D., et al. (2010). A biodegradable polymer-based coating to control the performance of magnesium alloy orthopaedic implants. *Biomaterials* 31 (8), 2084–2096. Epub 20091229. doi:10.1016/j.biomaterials.2009.11.111

Xie, R., Zhu, Y., Zhang, H., Zhang, P., and Han, L. (2021). Effects and mechanism of pyrolysis temperature on physicochemical properties of corn stalk pellet biochar based on combined characterization approach of microcomputed tomography and chemical analysis. *Bioresour. Technol.* 329, 124907. Epub 20210226. doi:10.1016/j.biortech.2021.124907

Xie, S., Girshick, R., Dollár, P., Tu, Z., and He, K. (2016). *Aggregated residual transformations for deep neural networks*. [arXiv:1611.05431 p.]. Available from: https://ui.adsabs.harvard.edu/abs/2016arXiv161105431X (November 01, 2016).

Yang, F., Dong, X., Yin, X., Wang, W., You, L., and Ni, J. (2017). Radix Bupleuri: a review of traditional uses, botany, phytochemistry, Pharmacology, and toxicology. *Biomed. Res. Int.* 2017, 7597596. Epub 20170516. doi:10.1155/2017/7597596

Yen, M. H., Lin, C. C., Chuang, C. H., and Liu, S. Y. (1991). Evaluation of root quality of Bupleurum species by tlc scanner and the liver protective effects of "Xiao-Chai-Hu-Tang" prepared using three different Bupleurum species. *J. Ethnopharmacol.* 34 (2-3), 155–165. doi:10.1016/0378-8741(91)90033-a

Zhang, Y., Ma, L., Wang, J., Wang, X., Guo, X., and Du, J. (2020). Phenotyping analysis of maize stem using micro-computed tomography at the elongation and tasseling stages. *Plant Methods* 16, 2. Epub 20200104. doi:10.1186/s13007-019-0549-y

frontiers | Frontiers in Pharmacology

TYPE Clinical Trial
PUBLISHED 25 June 2024
DOI 10.3389/fphar.2024.1351871

Check for updates

OPEN ACCESS

EDITED BY
Jian-Bo Yang,
National Institutes for Food and Drug Control, China

REVIEWED BY
Ran Wen,
Hebei Medical University, China
Li Jiang,
Jiangxi University of Traditional Chinese Medicine, China

*CORRESPONDENCE
Rui Li,
crystal005@163.com
Zhao-Yun Zhu,
zzy1370@163.com
Rui Gao,
xyyygr@126.com

†These authors have contributed equally to this work

RECEIVED 07 December 2023
ACCEPTED 05 June 2024
PUBLISHED 25 June 2024

CITATION
Cao W-Y, Liu J-Y, Sun M, Wang J-K, Lu F, Yang Q-N, Zhang W-T, Zi M-J, Zhang B-E, Liu H-B, Wang S-G, Wu Y, Wu R-Z, Wu W-D, Li R, Zhu Z-Y and Gao R (2024), Pharmacokinetics, safety, and efficacy of Fuqi Guben Gao in the treatment of kidney-yang deficiency syndrome: a randomized, double-blind phase I trial.
Front. Pharmacol. 15:1351871.
doi: 10.3389/fphar.2024.1351871

COPYRIGHT
© 2024 Cao, Liu, Sun, Wang, Lu, Yang, Zhang, Zi, Zhang, Liu, Wang, Wu, Wu, Wu, Li, Zhu and Gao. This is an open-access article distributed under the terms of the Creative Commons Attribution License (CC BY). The use, distribution or reproduction in other forums is permitted, provided the original author(s) and the copyright owner(s) are credited and that the original publication in this journal is cited, in accordance with accepted academic practice. No use, distribution or reproduction is permitted which does not comply with these terms.

Pharmacokinetics, safety, and efficacy of Fuqi Guben Gao in the treatment of kidney-yang deficiency syndrome: a randomized, double-blind phase I trial

Wei-Yi Cao[1,2†], Jun-Yu Liu[3,4†], Min Sun[3,4†], Jing-Kun Wang[3,4], Fang Lu[1,2], Qiao-Ning Yang[1,2], Wan-Tong Zhang[1,2], Ming-Jie Zi[1,2], Bai-E Zhang[3,4], Hong-Bin Liu[3,4], Shu-Ge Wang[1,2], Yi Wu[1,2], Rong-Zu Wu[5], Wen-Di Wu[5], Rui Li[1,2*], Zhao-Yun Zhu[3,4*] and Rui Gao[1,2*]

[1]Institute of Clinical Pharmacology of Xiyuan Hospital, National Clinical Research Center for Chinese Medicine Cardiology, China Academy of Chinese Medical Sciences, Beijing, China, [2]NMPA Key Laboratory for Clinical Research and Evaluation of Traditional Chinese Medicine, National Clinical Research Center for Chinese Medicine Cardiology, Beijing, China, [3]Yunnan Province Company Key Laboratory for TCM and Ethnic Drug of New Drug Creation, Yunnan Institute of Materia Medica, Kunming, Yunnan, China, [4]Yunnan Baiyao Group Co., Ltd., Kunming, Yunnan, China, [5]Kunming Municipal Hospital of Traditional Chinese Medicine, Kunming, Yunnan, China

Introduction: Fuqi Guben Gao (FQGBG) is a botanical drug formulation composed of FuZi (FZ; *Aconitum carmichaelii* Debeaux [Ranunculaceae; Aconiti radix cocta]), Wolfberry (*Lycium barbarum* L. [Solanaceae; Lycii fructus]), and Cinnamon (*Neolitsea cassia* (L.) Kosterm. [Lauraceae; Cinnamomi cortex]). It has been used to clinically treat nocturia caused by kidney-yang deficiency syndrome (KYDS) for over 30 years and warms kidney yang. However, the pharmacological mechanism and the safety of FQGBG in humans require further exploration and evaluation.

Methods: We investigated the efficacy of FQGBG in reducing urination and improving immune organ damage in two kinds of KYDS model rats (hydrocortisone-induced model and natural aging model), and evaluated the safety of different oral FQGBG doses through pharmacokinetic (PK) parameters, metabonomics, and occurrence of adverse reactions in healthy Chinese participants in a randomized, double-blind, placebo-controlled, single ascending dose clinical trial. Forty-two participants were allocated to six cohorts with FQGBG doses of 12.5, 25, 50, 75, 100, and 125 g. The PKs of FQGBG in plasma were determined using a fully validated LC-MS/MS method.

Results: FQGBG significantly and rapidly improved the symptoms of increased urination in both two KYDS model rats and significantly resisted the adrenal atrophy in hydrocortisone-induced KYDS model rats. No apparent increase in adverse events was observed with dose escalation. Major adverse drug reactions included toothache, thirst, heat sensation, gum pain, diarrhea, abdominal distension, T-wave changes, and elevated creatinine levels. The PK results showed a higher exposure level of benzoylhypaconine (BHA) than

benzoylmesaconine (BMA) and a shorter half-life of BMA than BHA. Toxic diester alkaloids, aconitine, mesaconitine, and hypaconitine were below the lower quantitative limit. Drug-induced metabolite markers primarily included lysophosphatidylcholines, fatty acids, phenylalanine, and arginine metabolites; no safety-related metabolite changes were observed.

Conclusion: Under the investigated dosing regimen, FQGBG was safe. The efficacy mechanism of FQGBG in treating nocturia caused by KYDS may be related to the improvement of the hypothalamus-pituitary-adrenal axis function and increased energy metabolism.

Clinical Trial Registration: https://www.chictr.org.cn/showproj.html?proj=26934, identifier ChiCTR1800015840.

KEYWORDS

Fuqi Guben Gao, pharmacokinetics, metabonomics, efficacy, kidney-yang deficiency syndrome

1 Introduction

Nocturia, frequent night-time urination, affects up to 60% of people over 65, increasing risks of falls, fractures, depression, and death (Bliwise et al., 2019; Lombardo et al., 2020). Aging and diseases, such as changes in the central nervous system and reduced renal function, are primary causes (Wolff et al., 2021). Traditional Chinese Medicine (TCM) attributes nocturia to kidney-yang deficiency (KYDS), where the kidney, responsible for storing the essence of yin and yang, fails to control water. Warming kidney yang is a common TCM treatment for this condition (Lu et al., 2009; Xu et al., 2019). Fuqi Guben Gao (FQGBG), a botanical drug formulation to treat nocturia caused by KYDS, is derived from the clinical experience in Yunnan Province, China. It is composed of FuZi (FZ; *Aconitum carmichaelii* Debeaux [Ranunculaceae; Aconiti radix cocta]), Wolfberry (*Lycium barbarum* L. [Solanaceae; Lycii fructus]), and Cinnamon (*Neolitsea cassia* (L.) Kosterm. [Lauraceae; Cinnamomi cortex]). In 2013, Kunming Hospital of TCM conducted a randomized double-blind clinical study to evaluate the efficacy and safety of FQGBG in 72 patients with KYDS. The results showed that the effective rate in the treatment group was 95% (Sun et al., 2017). The FZ-Cinnamon pair is commonly used in the clinical treatment of KYDS and has been reported to improve the adrenal cortex function and physical fitness of hydrocortisone-induced KYDS in mice (Qian, 2019). Preclinical pharmacological study results indicated that FQGBG substantially improved polyuria in four kinds of KYDS rat models, including the excessive fatigue, adenine-induced, hydrocortisone-induced, and natural aging types. In addition, the effect observed was faster than positive controls (Gui-fu-di-huang-wan and You-gui-wan). Moreover, FQGBG can significantly counteract hydrocortisone-induced adrenal atrophy in rats with KYDS, increase their adrenocorticotropic hormone response, and significantly prolong the ice-water swimming time of mice with KYDS. Based on the above findings, FQGBG was developed by the Yunnan Institute of Materia Medica and Yunnan Baiyao Group Co., Ltd., and has been approved for clinical trials by the National Medical Products Administration (NMPA, No. 2016L10230) as an investigational agent in Chinese medicine.

The main active metabolites of FZ include three highly toxic diester–diterpene alkaloids: aconitine (AC), mesaconitine (MA), and hypaconitine (HA). According to a previous report, the narrow therapeutic window of AC limits the clinical application of AC-containing botanical drugs; overdosing on AC always induces ventricular tachyarrhythmia and heart arrest. However, emerging evidence shows that low doses of AC or its metabolites could generate cardioprotective effects and are necessary to the clinical efficacy of aconites (Zhou et al., 2021). Thus, owing to this toxicity, FZ must be adequately processed by hydrolyzing AC, MA, and HA into less toxic monoester-diterpene alkaloids, benzoylaconine (BAC), benzoylmesaconine (BMA), and BHA (Singhuber et al., 2009), and its drug safety must be closely monitored. The structural formula of BAC, BMA, BHA, AC, MA, and HA is shown in Figure 1.

Pharmacokinetic (PK) studies help explain and predict various events related to drug efficacy and toxicity. Thus, it is valuable to determine PK parameters in evaluating the rationality and safety of clinical prescriptions (Yan et al., 2018). Metabonomics is a high-throughput detection method for endogenous small molecules and provides information on the entire organism's functional integrity over time following exposure to a perturbation (Lu et al., 2011). It is widely used in mining pathological, pharmacological, and drug safety biomarkers and in establishing disease diagnosis models. Until now, the potential toxic mechanism of Aconitum alkaloids has been studied through metabonomics (Ji et al., 2023).

In this study, we investigated the efficacy of FQGBG in improving the symptoms of kidney-yang deficiency in two types of KYDS model rats, and evaluated the safety of different oral doses of FQGBG through PK parameters, metabonomics and occurrence of adverse reactions in healthy Chinese participants. This study attempts to implement an evaluation model that combines drug exposure, endogenous metabolites, and clinical manifestations, and will provide evidence for the mechanism of exploration of the safety and efficacy of FQGBG in humans.

2 Methods

2.1 Materials

FQGBG comprises FuZi (FZ *Aconitum carmichaelii* Debeaux [Ranunculaceae; Aconiti radix cocta]), Wolfberry (*Lycium barbarum*

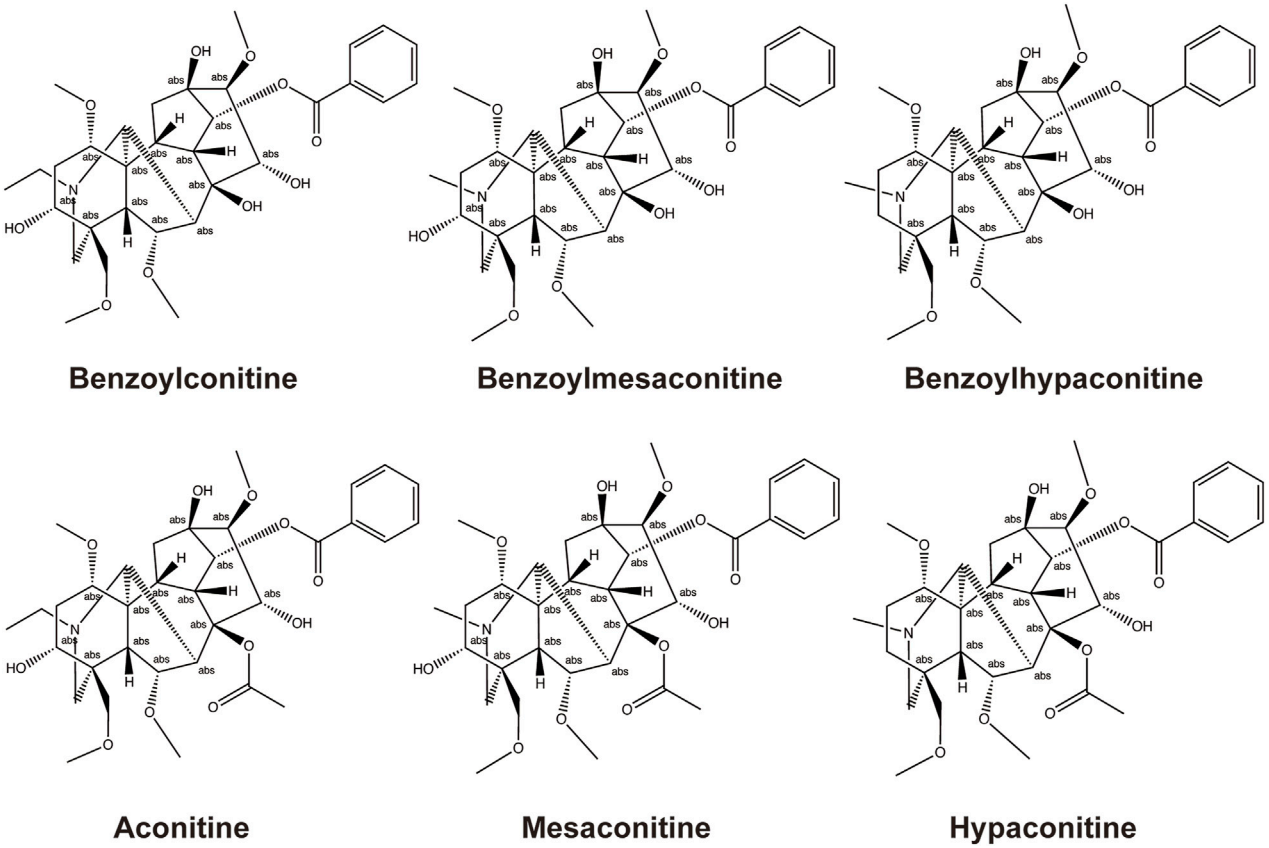


FIGURE 1
Chemical structural formulas of the major diterpene alkaloids in FQGBG.

L. [Solanaceae; Lycii fructus]), and Cinnamon (*Neolitsea cassia* (L.) Kosterm. [Lauraceae; Cinnamomi cortex]). The plants' names were verified at http://mpns.kew.org/mpns-portal/. All pharmaceutical raw materials were processed and quality tested according to the Pharmacopoeia of China (2015). The processing method for FZ involves taking the daughter roots of the Ranunculaceae family plant *Aconitum carmichaelii* Debeaux, immersing them in a bile salts aqueous solution for several days, and then boiling them with the soaking solution until they are thoroughly penetrated. They are then removed, rinsed with water, and longitudinally sliced into pieces about 0.5 cm thick. The slices are further soaked and rinsed with water, and then a coloring liquid is applied to dye the slices a deep tea color. After being dyed, they are steamed until an oily surface and luster appear, and finally, they are dried and sun-dried. Quality control tests for FZ include appearance, thin-layer chromatography (TLC) identification, moisture content, total diester diterpenoid alkaloids, and total monoester diterpenoid alkaloids. The processing method for Wolfberry entails harvesting the red fruit of *Lycium barbarum* L. during the summer and autumn seasons, followed by hot air drying. The fruit is left to air until the skin wrinkles, after which it is sun-dried. Quality control for Wolfberry includes assessment of shape, TLC identification, moisture, total ash content, heavy metals, extractables, polysaccharides of Lycium barbarum, and betaine content. Cinnamon is processed by peeling the bark of *Neolitsea cassia* (L.) Kosterm. in the autumn and allowing it to air dry. Quality control tests for Cinnamon include appearance, TLC identification, moisture content, total ash content, volatile oil, and cinnamaldehyde content. Upon verification, the raw materials FZ (lot 20130731, YP2421601), Wolfberry (lots P20171152, P20190404), and Cinnamon (lots 171,001, Y180301) all met the quality standards of the Pharmacopoeia of China (2015).

The preparation method for FQGBG is as follows: FZ were decocted twice with water, first under a pressure of 0.10 MPa for 2 h and then at atmospheric pressure for 1 h. The filtrates from both decoctions were combined and concentrated to a relative density of 1.1 at 60°C for use. Separately, Cinnamon were ground and subjected to steam distillation for 4 h. The distilled Cinnamon oil was then complexed with β-cyclodextrin at 40°C for 2 h and set aside. The leftover Cinnamon residue and Wolfberry were extracted with hot water at 85°C twice, each for 1 h. This extract was also concentrated to a relative density of 1.1 at 60°C for later use. To finalize the formulation, the two concentrated extracts were blended with honey, potassium sorbate, and span-80. The relative density was adjusted to between 1.3 and 1.4 at 25°C to yield the final product.

FQGBG (25 g per bottle, lot number: ZAA1801/ZEA 1901S) and placebo (25 g per bottle, lot number: ZAB1801/ZEB 1901S) were provided by the Yunnan Institute of Materia Medica and Yunnan Baiyao Group Co., Ltd. (Kunming, Yunnan, China), with an expiration period of 18 months. The content of monoester alkaloids (BMA, BHA, and BAC) in the two batches of FQGBG was 241 μg/g (ZAA1801) and 116 μg/g (ZEA1901S), respectively. The HA, MA, and AC concentration of both batches were lower than the lower limit of

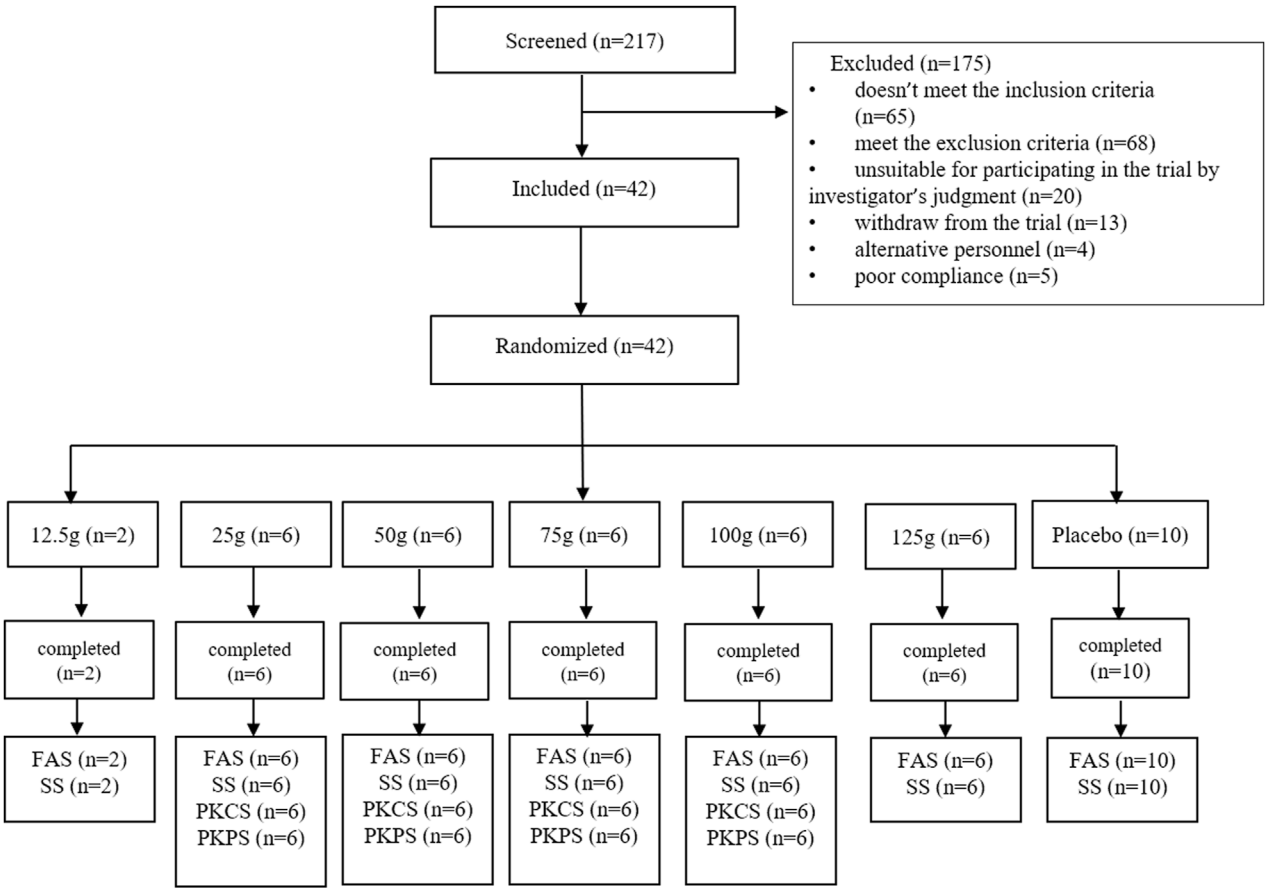


FIGURE 2
Study flowchart.

quantitation. The two drug batches met the draft quality standards. The quality control methods for FQGBG are provided in Supplementary Material S1, which includes three types of identification fingerprinting (TLC, HPLC-UV, and UPLC-QTOF-MS), as well as methods for quantification of six aconitine alkaloids (AC, MA, HA, BAC, BMA, and BHA). Three monoester alkaloids (BAC, BMA, and BHA) are used as efficacy markers. These quality control methods comply with the requirements of the Pharmacopoeia of China (2015).

Gui-fu-di-huang-wan (360 pills per bottle, lot number: 12031565) and You-gui-wan (10 pills per box, lot number: 2013110) were purchased from Beijing Tongren Tang Science and Technology Development Co., Ltd. (Beijing, China). AC (lot 20180316, purity 98.01%) was provided by Yunnan Institute of Materia Medica. MA (lot 110799–201608, purity 98.5%), HA (lot 110789–201609, purity 99.2%), BAC (lot 111794–201705, purity 99.1%), BMA (lot 111795–201604, purity 94.0%), and BHA (lot 111796–201705, purity 98.6%) were purchased from the National Institute for Food and Drug Control (Biomedicine Industry Base, Daxing District, Beijing, China). Norverapamil hydrochloride (lot 1331-063A1, purity 99.1%, internal standard, IS) was purchased from TLC Pharmaceutical Standards (Newmarket, Ontario, Canada). Blank plasma (Bioreclamation IVT, Westbury, NY, United States) was used to prepare the standard curve and quality control samples.

2.2 Study approval

The study protocol was approved by the Human Research Ethics Committees of Xiyuan Hospital, China Academy of Chinese Medical Sciences (2018XL003), and the Chinese Clinical Trial Registry (A phase I clinical trial of Fuqi Gubengao, ChiCTR1800015840, registered 24 April 2018, https://www.chictr.org.cn/showprojEN.html?proj=26934). The clinical study was conducted at Xiyuan Hospital, and all clinical procedures were performed in compliance with the International Conference on Harmonization - Good Clinical Practice and the Declaration of Helsinki.

2.3 Participants

Forty-two healthy Chinese volunteers aged between 18 and 50 years with body mass indices (BMI) between 19.0 and 25.0 kg/m^2 and normal physical examinations, imagological electrocardiogram examinations, and clinical laboratory tests were enrolled in the trial. The exclusion criteria are provided in Supplementary Material S1. All participants provided written informed consent before the start of the study.

2.4 Study design

This phase I, randomized, double-blind, placebo-controlled, single ascending dose clinical trial involved six cohorts with oral doses of 12.5 g (±1 g), 25 g (±1.5 g), 50 g (±2.5 g), 75 g (±3 g), 100 g (±4.5 g), and 125 g (±7 g) FQGBG. As shown in Figure 2, the participants (n = 42) were allocated to the cohorts (eight participants per group, including six with FQGBG and two with placebo, at a 3:1 ratio), except for the first cohort (only two participants were treated with FQGBG). Participants were administered FQGBG or placebo at the respective dose levels with 240 mL water under fasting conditions (overnight fasting for ≥12 h). The procedures of administration were: 10 mL of water was poured into the FQGBG bottle, shook, and blended. The mixture was then poured into a paper cup, after which the above operation was repeated twice. The remaining water was poured into the paper cup and stirred evenly, and the fluid was swallowed at one time.

2.5 Plasma sample collection and preparation

Sampling for PKs was designed based on PK results in our previous study and collected at different time points before and after the administration of FQGBG: at 0, 5, 10, 20, 30, 45 min, 1, 2, 4, 8, 12, 24, 48, 72, 96, and 120 h in four dose groups (25, 50, 75, and 100 g). The preliminary study results indicated that the blood concentration of the three monoester-type alkaloids was reduced to 1/10th of the maximum concentration (C_{max}) at 60–120 h; thus, 120 h after dosing was chosen as the last PK sampling time point. For the metabonomics analysis, blood samples were collected before and after 30 min and 24 h, and urine specimens were collected before and after 24 and 48 h to compare the differences in endogenous metabolites. Blood and urine samples were centrifuged at 1,500 ×g for 10 min at 4°C and the supernatant of the urine was added to preservatives. All sample supernatants were collected and stored at −80°C. Plasma (100 μL) samples spiked with 20 μL of IS were mixed evenly on a shaker. Then, 500 μL ACN containing 0.1% formic acid was added to the sample. Protein precipitation was performed by vortexing the mixture for 10 min and then centrifuging at 4,000 rpm for 10 min at 4°C. Supernatant (150 μL) was added to an equal volume of water containing 0.1% formic acid. The mixture was analyzed using a UPLC-MS/MS method.

2.6 LC-MS/MS conditions

A UPLC system (Waters, Milford, MA, United States) coupled with an MS/MS system (Triple Quad™ 6500, Sciex, Framingham, MA, United States) was applied for the determination of AC, MA, HA, BAC, BMA, and BHA. The data were collected and processed using Analyst software (version 1.6.3, Sciex, Framingham, MA, United States) and Watson LIMS (version 7.4.2 and 7.6SP1). Chromatographic separation was achieved using a Phenomenex Luna Omega Polar C18 column (2.1 × 50 mm, 1.6 μm) at 60°C. The mobile phase comprised water containing 5 mM ammonium acetate and 5% ACN (solvent A) and ACN containing 0.1% formic acid (solvent B). The gradient elution program for AC, MA, and HA was 0–2 min, 68%–50% A; 2–2.2 min, 50%–5% A; 2.2–2.4 min, 5% A; 2.4–2.41 min, 5%–68% A; 2.41–2.5 min, 68% A. The gradient elution program for BAC, BMA, and BHA was 0–2 min, 80%–60% A; 2–2.2 min, 60%–10% A; 2.2–2.4 min, 10% A; 2.4–2.41 min, 10%–80% A; 2.41–2.5 min, 80% A. The flow rate was 0.6 mL/min, and the injection volume was 10 μL.

The mass spectrometer was operated in the positive ion electrospray ionization mode. The analytes were detected using the multiple-reaction monitoring (MRM) mode with m/z transitions at 646.2→586.1 for AC, 632.2→572.1 for MA, 616.2→338.0 for HA, 604.2→554.2 for BA, 590.2→540.2 for BMA, 574.2→542.2 for BHA, and 441.3→165.1 for the IS. The optimized instrumental conditions were gas source temperature, 550°C; ion spray voltage, 5,500 V; entrance potential, 10 V; curtain gas, 40 psi; gas 1, 55 psi; and gas 2, 55 psi.

2.7 Methodological evaluation

The selectivity, calibration standard curve, matrix effect, extraction recovery, precision, accuracy, and stability of the developed method was validated according to the USA Food and Drug Administration (FDA) bio-analytical method validation guidance (U.S. Food and Drug Administration, 2018) (Supplementary Material S1). The calibration standard curves for AC, MA, HA, and BMA ranged from 0.05 to 50 ng/mL, for BAC from 0.1 to 100 ng/mL, and for BHA from 0.01 to 10 ng/mL. The UPLC-MS/MS method for AC, MA, HA, BAC, BMA, and BHA in human plasma produced the required biological quantitative standards. Therefore, this method could be used for the analysis of clinical samples.

2.8 Pharmacokinetic analysis

PK parameters, including the C_{max}, area under the curve (AUC) from administration (t = 0 h) to the last measured concentration (t = 120 h) ($AUC_{0\text{-}t}$), total AUC from administration to infinity ($AUC_{0\text{-}\infty}$), time to reach C_{max} (T_{max}), half-life ($T_{1/2z}$), apparent volume of distribution adjusted for bioavailability (V_z/F), drug clearance (CL_z), mean residence time (MRT) from administration (t = 0 h) to the last measured concentration ($MRT_{0\text{-}t}$), and total MRT from administration to infinity ($MRT_{0\text{-}\infty}$) were calculated by non-compartmental methods using the WinNonlin software (version 8.1, Pharsight Corporation, Mountain View, CA, United States) with the blood concentration data of different participants at different time points.

2.9 Metabonomics analysis

The endogenous metabolites in the plasma and urine samples were analyzed using UPLC coupled with quadrupole time-of-flight mass spectrometry operating in MS^E mode (UPLC-QTOF-MS^E). The sample pretreatment and analysis methods are detailed in Supplementary Material S1. The MassLynx™ 4.1 workstation was used for data acquisition and processing. Progenesis QI (Nonlinear

Dynamics, Newcastle, United Kingdom) was used to select and align the peaks from the metabonomics raw data file. EZinfo 3.0 software (U-Metrics, Version 3.0.3.0; Waters Corporation, Wilmslow, United Kingdom) was used for principal component analysis (PCA), partial least squares-discriminant analysis (PLS-DA), and orthogonal partial least squares-discriminant analysis (OPLS-DA). The variable importance in the projection (VIP) and a Student's t-test was used to screen for significantly changed metabolites before and after administration. Potential biomarkers were identified by comparing the tandem mass spectrometry (MS/MS) fragments with the human metabolome public database (HMDB) (http://www.hmdb.ca/) or the Mass bank database (https://massbank.us/). Metabolite pathway enrichment analysis was obtained using MetaboAnalyst 5.0 (https://www.metaboanalyst.ca/).

2.10 Safety evaluation

Echocardiography, B-mode ultrasound, chest radiography, breath alcohol tests, and infection screening were performed during the screening period. Routine clinical laboratory tests (blood biochemistry, routine blood, routine urine, and routine stool), blood coagulation tests, and testing for microalbuminuria, cystatin C, urine N-acetyl-β-D-glucosaminidase (NAG), troponin T, and N-terminal pro-brain natriuretic peptide (NT-pro-BNP) were performed at baseline and 24, 72, and 120 h after dosing. A 24 h Holter electrocardiogram (ECG) was performed on day 1. ECG and vital signs (blood pressure, pulse, respiratory rate, and body temperature) were recorded at baseline and each day after dosing. Urine and blood pregnancy tests in women of childbearing age were performed at baseline and on the day of completion.

2.11 Adverse events (AEs)

All adverse medical events after dosing, including abnormal laboratory test results, symptoms and diseases, abnormalities, and their clinical significance and relevance to the investigational product, were recorded and evaluated by investigators. Because of the known toxicity of *Aconitum carmichaelii* Debeaux, symptoms of cardiotoxicity, neurotoxicity, and gastrointestinal symptoms were closely monitored.

2.12 Animals

All Sprague–Dawley rats (weighing 190 ± 20 g) were purchased from Guangdong Province Medical Experimental Animal Center (Guangdong, China, license number: SCXK (Yue) 2008-0002). All rats were housed at the Animal Experiment Center of the Yunnan Institute of Materia Medica with free access to food and drinking water (room temperature 20°C–26°C, relative humidity 40%–70%, and 12 h of light/darkness). All animal protocols were approved by the Yunnan Institute of Materia Medica Ethics Committee in conformity to the guidelines for the Care and Use of Laboratory Animals by the National Institutes of Health (Approval No. 2014-08).

2.13 Grouping and modeling of animals

Hydrocortisone-induced KYDS model: After 5 days of acclimatization feeding, 72 male rats were randomly divided into the control group (CON), model group (MOD), Gui-fu-di-huang-wan group (GF, 4.5 g/kg), You-gui-wan group (YG, 4.8 g/kg), low-dose FQGBG group (FQGB-L, 1.29 g/kg), and high-dose FQGBG group (FQGB-H, 2.57 g/kg), with 12 rats in each group. The control group was gavaged with physiological saline, the model group was gavaged with hydrocortisone, and the treatment groups were gavaged with hydrocortisone in the morning and therapeutic drugs in the afternoon, all once daily. The modeling and drug administration were performed simultaneously for 30 consecutive days. The rat model was considered established by observing the appearance of kidney-yang deficiency symptoms in model rats, such as cold fear, huddling, hunchback, mental fatigue, emaciation, etc.

Natural aging KYDS model: 75 male rats were randomly divided into the model group (MOD), GF group (4.5 g/kg), YG group (4.8 g/kg), FQGB-L group (1.29 g/kg), and FQGB-H group (2.57 g/kg) after being raised to 18 months old, with 15 rats in each group. The control group was gavaged with physiological saline, whereas the other groups were gavaged with therapeutic drugs, all once daily for three consecutive months.

2.14 Urine volume

To investigate the effects of hydrocortisone-induced KYDS rats on urine output, rats were placed in metabolic cages for 8 h with free access to water and food at weeks 1, 2, 3, and 4 after the establishment of the model and drug administration. Average urine output was compared with the model group and statistically analyzed. For the natural aging KYDS rats, urine samples were collected for 8 h at weeks 3, 6, 8, 10, and 12 after drug administration. The average urine output was compared with the control group and was statistically analyzed.

2.15 Immune organ index

Following administration on day 30, the hydrocortisone-induced KYDS rats in each group were anesthetized by intraperitoneal injection of 3.5% hydrated chloral hydrate (10 mL/kg). The abdominal cavity was opened, and the adrenals, thymus, and spleen were removed. The immune organs are wiped clean with absorbent paper to remove surface blood and then weighed after removing the surrounding connective tissue. The index of the immune organs is calculated as the ratio of the weight of the immune organ to the weight of the experimental animal.

2.16 Statistical analysis

A descriptive analysis method was adopted to elucidate the demographic characteristics and safety indicators as number, mean, standard deviation, maximum, minimum, and median of each group. The PK parameters were expressed as the mean and standard deviation (SD). GraphPad Prism v.9.1 (GraphPad Software, Inc., San Diego, CA, United States) was used for

TABLE 1 Effects of FQGBG on urine output in hydrocortisone-induced KYDS rats.

Group	Urine volume in 8 h (mL)			
	Week 1	Week 2	Week 3	Week 4
CON	5.2 ± 1.9	4.4 ± 1.4	2.3 ± 2.2	7.8 ± 4.8
MOD	8.4 ± 4.2▼	7.8 ± 4.1▼	8.9 ± 3.7▼	10.2 ± 3.4
GF	6.5 ± 4.3	3.5 ± 2.6**	2.2 ± 2.4**	7.4 ± 2.8*
YG	7.7 ± 3.0	3.6 ± 2.3**	4.2 ± 2.3**	6.6 ± 3.1*
FQGB-H	5.8 ± 2.1*	4.9 ± 3.2*	4.6 ± 4.1**	6.6 ± 3.0*
FQGB-L	4.9 ± 3.1*	4.5 ± 2.5*	4.2 ± 3.2**	7.0 ± 2.6*

Values were presented as mean ± SD (n = 12).
▼ As compared with the control group (CON); ▼$p < 0.05$; ▼▼$p < 0.01$.
* As compared with KYDS, group (MOD); *$p < 0.05$; ** $p < 0.01$.

TABLE 2 Effects of FQGBG on urine output in natural aging KYDS rats.

Group	Urine volume in 8 h (mL)				
	week 3	week 6	week 8	week 10	week 12
MOD	6.0 ± 2.1	3.9 ± 3.6	6.4 ± 2.1	6.0 ± 2.1	3.6 ± 1.7
GF	7.0 ± 3.2	2.3 ± 1.7	4.9 ± 2.6	3.3 ± 2.0**	2.1 ± 1.4*
YG	7.3 ± 3.8	3.1 ± 2.0	5.9 ± 3.4	3.7 ± 2.0**	2.0 ± 1.6*
FQGB-H	4.3 ± 1.9*	2.6 ± 2.2	2.3 ± 1.7**	2.9 ± 1.3**	2.1 ± 1.3*
FQGB-L	8.4 ± 3.9	3.8 ± 4.0	6.3 ± 3.7	4.6 ± 1.7*	2.2 ± 2.0

Values were presented as mean ± SD (n = 15).
*As compared with KYDS, group (MOD); *$p < 0.05$; **$p < 0.01$.

statistical analyses and plotting. Statistical significance was set at $p < 0.05$.

3 Results

3.1 Urine volume observation

As shown in Table 1, compared with the control group, urine output in the hydrocortisone-induced KYDS model group increased at weeks 1 (8.4 ± 4.2 mL/8 h), 2 (7.8 ± 4.1 mL/8 h), and 3 (8.9 ± 3.7 mL/8 h), with significant differences. Urine output at week 4 (10.2 ± 3.4 mL/8 h) also increased, but without a significant difference. The GF and YG groups served as positive control drugs. The GF and YG group inhibited the increase in urine output of the model rats at weeks 2 (GF: 3.5 ± 2.6 mL/8 h, YG: 3.6 ± 2.3 mL/8 h), 3 (GF: 2.2 ± 2.4 mL/8 h, YG: 4.2 ± 2.3 mL/8 h), and 4 (GF: 7.4 ± 2.8 mL/8 h, YG: 6.6 ± 3.1 mL/8 h), with significant differences compared to the model group. The FQGB-L and FQGB-H groups significantly inhibited the increased urine output of the model rats from week 1 to week 4. In the first observation week, the urine output of the FQGB-L group (4.9 ± 3.1 mL/8 h) and the FQGB-H group (5.8 ± 2.1 mL/8 h) was lower than the positive control group (GF: 6.5 ± 4.3 mL/8 h, YG: 7.7 ± 3.0 mL/8 h), indicating that FQGBG acts more rapidly.

For the KYDS natural aging model rats (Table 2), the positive drugs GF and YG showed a reduction in rat urine production at weeks 10 and 12, with significant differences compared to the model group. The FQGB-L group significantly inhibited rat urine production at week 10 (4.6 ± 1.7 mL/8 h), and the FQGB-H group significantly inhibited rat urine production at weeks 3 (4.3 ± 1.9 mL/8 h), 8 (2.3 ± 1.7 mL/8 h), 10 (2.9 ± 1.3 mL/8 h), and 12 (2.1 ± 1.3 mL/8 h). This indicates that the high-dose FQGBG group has a faster onset of action than the positive control group.

3.2 Change of immune organ index

As shown in Table 3, compared with the control group, the adrenal gland (0.088 ± 0.014 mg/g), the thymus (0.78 ± 0.14 mg/g), and the spleen (1.32 ± 0.15 mg/g) showed significant atrophy in hydrocortisone-induced KYDS rats. GF, YG, and FQGBG all had antagonistic effects on adrenal atrophy, but only the FQGB-H group (0.100 ± 0.010 mg/g) showed statistically significant efficacy. GF, YG, and FQGB-H mildly antagonized hydrocortisone-induced thymus atrophy, but there were no significant differences. YG and FQGBG also mildly antagonized hydrocortisone-induced splenic atrophy, but there were no significant differences.

3.3 Pharmacokinetics results

Among all participants, 32 healthy Chinese volunteers in the 25, 50, 75, and 100 g groups were included in the PK study. The mean plasma concentration vs. time profiles of BMA and BHA are shown in Figure 3, and the corresponding major PK parameters are shown in Table 4. The plasma concentrations of AC, MA, HA, and BAC were all below the lower limit of quantification (LLOQ) (50 pg/mL for AC, MA, and HA; 100 pg/mL for BAC). The C_{max} of BMA (C_{max}: 138.57–409.00 pg/mL) was higher than BHA (C_{max}: 84.37–245.67 pg/mL), whereas the $AUC_{0\text{-}t}$ of BMA ($AUC_{0\text{-}t}$: 625.02–4283.40 h × pg/mL) was lower than BHA ($AUC_{0\text{-}t}$: 3471.15–7627.07 h × pg/mL). The results indicate that the overall exposure level of BHA was higher than BMA. The $AUC_{0\text{-}t}$ values of the 50 and 75 g groups of BMA and BHA were similar, suggesting that a saturable absorption was reached after the 50 g treatment. The $AUC_{0\text{-}t}$ values of the 100 g group decreased slightly, reflecting the differences in the drug batches. The T_{max} of BMA (T_{max}: 0.88–1.38 h) was faster than BHA (T_{max}: 0.76–6.38 h), whereas the half-life of BMA ($T_{1/2}$: 14.24–64.03 h) was shorter than BHA ($T_{1/2}$: 43.59–86.27 h). The power function model was used to analyze the associations between PK parameters and the dose in BMA and BHA (Supplementary Figures S2–S4; Supplementary Table S2). The results showed that BMA had linear PK characteristics in the dose range of 25–100 g, and the exposure increase ratio of BHA from 25 to 100 g was lower than the dose increase ratio.

3.4 Metabonomics results

PCA and PLS-Da maps were used to determine whether the administration group was well discriminated from the placebo group. As shown in Figures 4A, B and Supplementary Figure S3, the plasma (24 h post-administration) and urine (48 h post-administration)

TABLE 3 Effects of FQGBG on the immune organ index in hydrocortisone-induced KYDS rats.

Group	Adrenals (mg/g)	Thymus (mg/g)	Spleen (mg/g)
CON	0.132 ± 0.014	1.60 ± 0.32	1.82 ± 0.14
MOD	0.088 ± 0.014▼▼	0.78 ± 0.14▼▼	1.32 ± 0.15▼▼
GF	0.098 ± 0.013	0.90 ± 0.28	1.27 ± 0.18
YG	0.094 ± 0.010	0.83 ± 0.20	1.43 ± 0.43
FQGB-H	0.100 ± 0.010*	0.80 ± 0.24	1.37 ± 0.19
FQGB-L	0.103 ± 0.018	0.69 ± 0.18	1.48 ± 0.18

Values were presented as mean ± SD (n = 12).
▼ As compared with the control group (CON); ▼ $p < 0.05$; ▼▼ $p < 0.01$.
* As compared with KYDS, group (MOD); *$p < 0.05$; **$p < 0.01$.

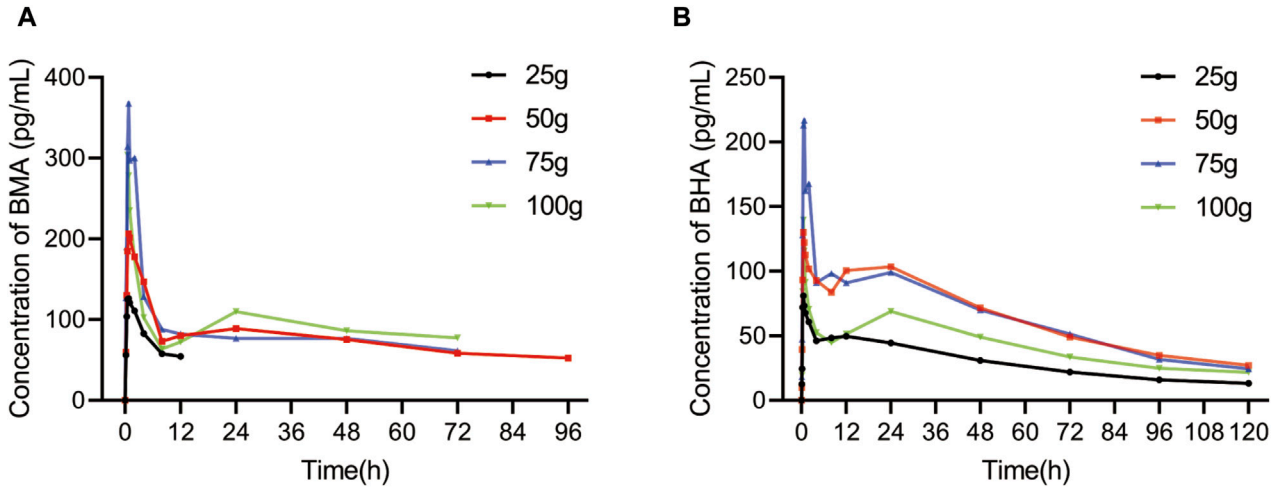


FIGURE 3
Average blood drug concentration-time of BMA **(A)** and BHA **(B)**.

results in each dose group could not be separated from the placebo group; nevertheless, they were well-differentiated among the dose groups. This may be related to the small effect of a single administration on metabolome changes. To search for differential metabolites, metabolites with a VIP ≥1 and $p < 0.05$ were screened by OPLS-DA. FQGBG treatment of 25, 50, 75 and 100 g produced 19, 10, 10 and 6 biomarkers, respectively (Table 5). Among these, the common biomarkers in the different dosage groups were LPC18:0, LPC16:0, L-phenylalanine, palmitic acid, and stearic acid in the plasma sample and 4-acetamidobutanoic acid in the urine sample. The heat map displayed the regulation of biomarkers in the plasma and urine before and after administration (Figure 4C). Upregulated biomarkers in plasma were mainly free fatty acids and LPCs, with metabolic pathway enrichment in mitochondrial β-oxidation of long-chain saturated fatty acids (Figure 4D). Among them, LPC18:0, LPC16:0, palmitic acid, and stearic acid were significantly upregulated in multiple treatment groups (Figure 4E). Downregulated metabolites included L-carnitine, with pathway enrichment mainly focused on fatty acid oxidation-related pathways. This indicated that the changes in plasma metabolites were mainly associated with fatty acid metabolism, mitochondrial β-oxidation, and energy metabolism. In addition, phenylalanine was significantly downregulated in plasma (Figure 4E), suggesting that FQGBG may lead to phenylalanine consumption. In urine, the secondary metabolite of arginine, 4-acetamidobutyric acid, was upregulated after administration (Figure 4E). Furthermore, in the 25 g dose group, ornithine, citrulline, proline, and 4-hydroxyproline were all increased, indicating that the metabolism pathways of arginine and proline may be influenced by FQGBG. Pathway enrichment analysis revealed that biomarkers in urine were mainly associated with tryptophan, purine, arginine, and proline metabolisms, and the urea cycle. In the high-dose group, these biomarkers showed more significant changes (Supplementary Figure S6), suggesting that these metabolites may contribute to understanding the safety and pharmacological effects of FQGBG. All biomarkers were identified by comparison with secondary spectrograms in the HMDB and Massbank databases (Supplementary Figure S7), with two or more characteristic fragment ions as the basis for identification and validation.

3.5 Demographics and safety

Overall, 217 participants were screened, 175 were excluded, and 42 were included. Two participants were assigned to the 12.5 g group, and 30 participants were randomly assigned to the 25, 50, 75, 100, and

TABLE 4 Major PK parameters of BMA and BHA at doses of 25–100 g (Mean ± SD).

Analyte	Parameter	Group of doses			
		25 g	50 g	75 g	100 g
BMA	C_{max} (pg/mL)	138.57 ± 39.25	216.67 ± 75.26	409.00 ± 268.30	321.33 ± 208.62
	AUC_{0-t} (h×pg/mL)	625.02 ± 395.36	4,102.95 ± 3,026.13	4,283.40 ± 2,200.76	2,710.99 ± 2,723.85
	$AUC_{0-\infty}$ (h×pg/mL)	1,963.07 ± 739.08	7,813.99 ± 5,017.74	10,119.87 ± 4,345.04	6,101.52 ± 6,360.16
	T_{max} (h)	1.13 ± 0.70	1.00 ± 0.52	1.38 ± 0.68	0.88 ± 0.56
	$T_{1/2z}$ (h)	14.24 ± 10.26	44.85 ± 36.03	64.03 ± 28.05	32.28 ± 39.99
	V_z/F ($\times10^8$ L)	2.40 ± 0.93	3.76 ± 1.15	6.84 ± 1.81	5.82 ± 3.74
	CL_z/F ($\times10^7$ L/h)	1.35 ± 0.40	1.04 ± 0.95	0.89 ± 0.51	5.27 ± 4.74
	MRT_{0-t} (h)	3.19 ± 1.40	19.33 ± 13.15	17.42 ± 10.58	12.09 ± 13.23
	$MRT_{0-\infty}$ (h)	20.19 ± 14.26	63.93 ± 49.32	87.39 ± 42.24	47.33 ± 56.07
BHA	C_{max} (pg/mL)	84.37 ± 25.69	149.33 ± 49.52	245.67 ± 167.69	148.03 ± 91.16
	AUC_{0-t} (h×pg/mL)	3,471.15 ± 467.60	7,634.24 ± 3,263.18	7,627.07 ± 2,604.34	4,831.67 ± 2,780.52
	$AUC_{0-\infty}$ (h×pg/mL)	5,150.81 ± 1,682.08	9,744.52 ± 4,764.55	9,151.92 ± 3,109.76	6,136.92 ± 3,431.34
	T_{max} (h)	0.76 ± 0.62	6.38 ± 9.77	4.96 ± 9.35	4.46 ± 9.57
	$T_{1/2z}$ (h)	86.27 ± 79.27	49.67 ± 10.28	43.59 ± 4.75	47.72 ± 12.18
	V_z/F ($\times10^8$ L)	5.27 ± 2.50	4.04 ± 1.24	5.59 ± 2.03	13.36 ± 4.55
	CL_z/F ($\times10^7$ L/h)	0.51 ± 0.12	0.60 ± 0.27	0.88 ± 0.28	2.04 ± 0.89
	MRT_{0-t} (h)	43.10 ± 4.89	43.45 ± 6.32	42.81 ± 4.53	41.74 ± 10.29
	$MRT_{0-\infty}$ (h)	114.50 ± 89.49	73.01 ± 16.45	66.29 ± 5.34	71.01 ± 20.86

125 g groups, respectively (Figure 2). Ten participants were assigned to the placebo group. All participants completed the trial and were included in the full analysis set (FAS) and safety analysis set (SS). In addition, 32 participants in the 25, 50, 75, and 100 g groups, who also participated in the PK study, were included in the pharmacokinetics concentration set (PKCS) and pharmacokinetics parameter set (PKPS) analyses. The detailed demographic information and AEs are listed in Tables 6, 7 and Supplementary Table S1. The safety analysis of treatment-emergent adverse events (TEAEs) by system shows varying incidence rates across different dose groups and the placebo. The most common TEAEs included gastrointestinal disorders, with rates of 50% in the 12.5 g group, 33.3% in the 125 g group, and 20% in the placebo group. Investigations of abnormal laboratory results were also notable, especially elevated NAG enzyme levels (33.3%) and positive urine protein (33.3%) in the 75 g group. Cardiac disorders, particularly ventricular extrasystoles, were observed in the 12.5 g (50%) and 25 g (16.7%) groups. General disorders such as heat sensation were frequent in the 125 g group (66.7%). However, the overall incidence of TEAEs and adverse drug reactions (ADRs) were 56.3% in the treatment groups compared to 50% in the placebo group, with no statistical difference observed between the two groups.

4 Discussion

FQGBG contains diterpenoid alkaloids, including diester, monoester, and lipid alkaloids that are both active and toxic. The diester alkaloids have the highest toxicity, and the literature indicates that cardiotoxicity and neurotoxicity are the major toxic reactions of diester diterpenoid alkaloids in *Aconitum carmichaelii* Debeaux (Yang et al., 2018). The AE related to cardiac damage was ventricular premature beat in the 12.5 and 25 g groups. Considering that ventricular premature beats existed at baseline, and there was no remarkable increase in the frequency of ventricular premature beats after dosing or an increased occurrence frequency with dose escalation, the conclusion that the ventricular premature beat was caused by the medication could not be drawn. Other AEs mainly manifested as abnormal laboratory results, but the severity was mild, and AEs had an optimistic prognosis. Elevated NAG enzyme levels and positive urine protein in the 75 g group suggest a possible link to FQGBG's diterpenoid alkaloids, which can be nephrotoxic. These findings may indicate renal stress or damage, particularly at higher doses. In the practical application of TCM, the clinical timing of using "toxic" herbal pieces is particularly crucial. Although the toxic plant metabolites present a risk of harming the body, they can yield significant therapeutic effects when used appropriately. Therefore, the potential renal damage caused by FQGBG might be due to individual intolerance when the drug is applied to healthy subjects, emphasizing the need for careful monitoring and appropriate clinical use. Other AEs mainly manifested as abnormal laboratory results, but the severity was mild, and AEs had an optimistic prognosis. Some AEs may be related to changes in the diet and lifestyle during hospitalization; therefore, whether these AEs were caused by FQGBG, or other

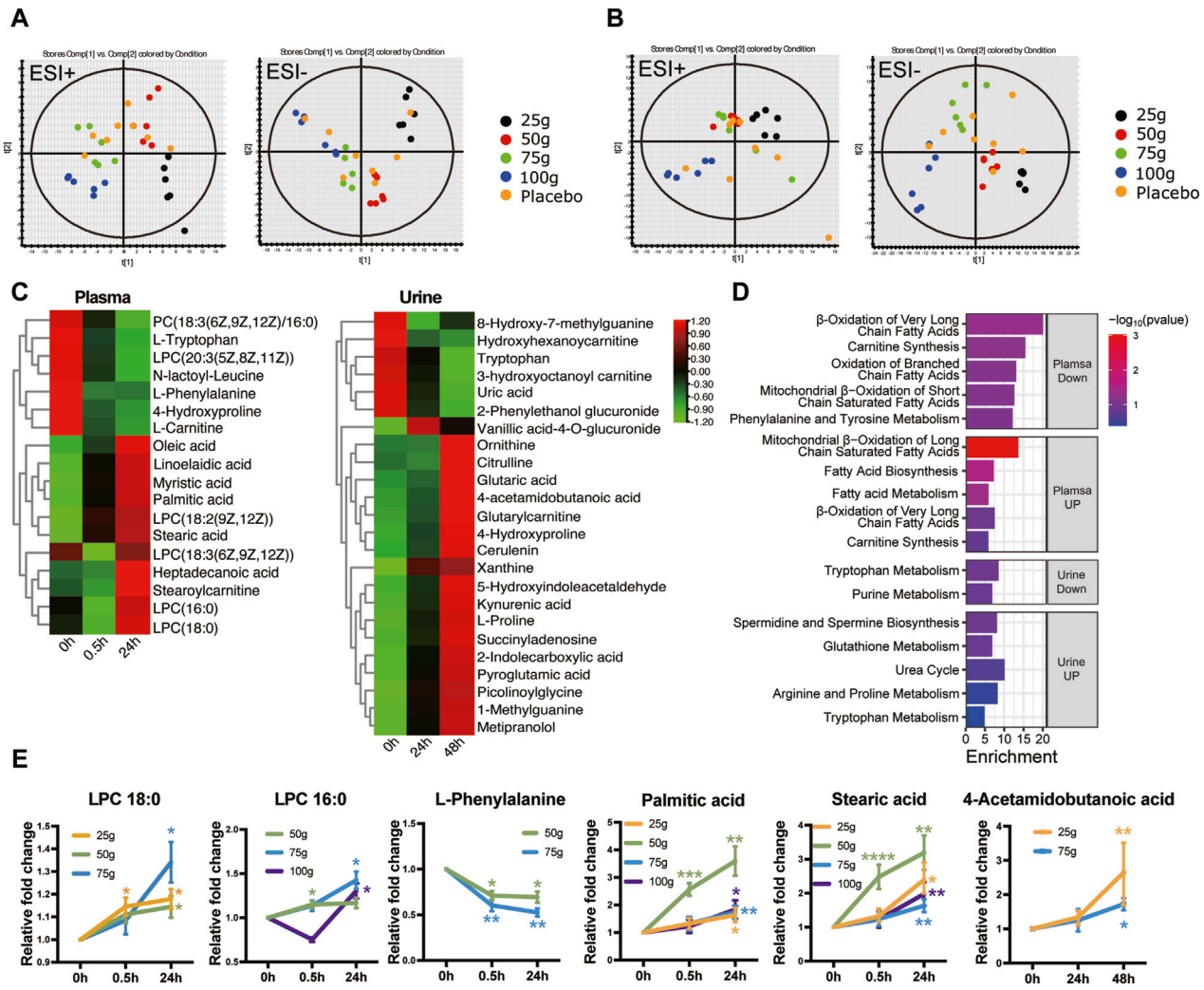


FIGURE 4
Metabonomic characteristics induced by the different dosages of FQGBG. **(A)** PLS-DA scoring plot of plasma collected 24 h after treatment in positive and negative ion modes. (ESI + scores: R2Y = 0.366, Q2 = 0.223; ESI- scores: R2Y = 0.341, Q2 = 0.130). **(B)** PLS-DA scoring plot of urine collected 48 h after treatment in both positive and negative ion modes (ESI + scores: R2Y = 0.655, Q2 = 0.093; ESI- scores: R2Y = 0.720, = 0.232). **(C)** Heat maps illustrate the time-dependent changes of abundance levels of metabolites. **(D)** Metabolite pathway enrichment analysis of upregulated and downregulated biomarkers in plasma and urine, respectively. **(E)** Commonly changed metabolites induced by the different dosages of FQGBG at different time points. *$p < 0.05$, **$p < 0.01$, ***$p < 0.001$.

reasons, is uncertain and further research is needed. FQGBG warms and invigorates the kidney yang; therefore, the primary AEs, including thirst, heat sensation, gum pain, aphtha, feverish palms, insomnia, diarrhea, and abdominal distension, were likely due to the injured body fluid by excessively tonifying the yang and deficient fire flare-ups.

Aconitine alkaloids are the main toxic metabolites and active metabolites of FZ, which have good anti-inflammatory, analgesic, and cardiotonic effects and are widely used in the treatment of various diseases. Among them, a series of diterpenoid alkaloids such as AC, MA, and HA have strong neurotoxic and cardiotoxic effects. In the extraction and preparation process, prolonging high-temperature decoction time can promote the degradation of diester alkaloids into monoester alkaloids, reducing the toxicity and improving the efficacy of the drug (Zhang et al., 2016). When patients experience toxic reactions induced by FZ, the blood concentrations of AC, MA, and HA can reach 0.031, 0.086, and 0.125 ng/mL (Zhang et al., 2019), respectively, which are 0.6, 1.72, and 2.5 times the LLOQ of AC, MA, and HA obtained in this study, whereas the blood concentrations of the three diester alkaloids in this study were all lower than the LLOQ. Furthermore, the blood concentration of the monoester alkaloid, BMA, in FZ poisoning patients, reached 4.665 ng/mL, which is 11.4 times the C_{max} of BMA in this study. The above evidence demonstrates the safety of FQGBG at the studied doses.

The PK behavior of monoester alkaloids of FZ exhibits differences. In this study, the blood concentration of BAC was lower than the LLOQ, which may be related to its fast absorption (T_{max}: 0.31 ± 0.17 h) and low bioavailability (Zhang et al., 2016). BMA is the most abundant monoester alkaloid in FZ, with analgesic and anti-inflammatory effects, and is a potential drug to treat inflammation-related diseases (Zhou et al., 2022). The PK results indicated that BMA is eliminated slowly and that the T1/2z of BMA

TABLE 5 Altered metabolite levels after FQGBG treatment.

Group (g)	No.	m/z	Error (ppm)	Ion	Retention time (min)	Identify	Molecular formula	Sample	*p*-value	Trend
25	1	428.3698	−9.66	ESI+	10.17	Stearoylcarnitine	$C_{25}H_{49}NO_4$	Plasma	0.0004	↑
	2	524.3633	−8.51	ESI+	10.96	LPC (18:0)	$C_{26}H_{54}NO_7P$	Plasma	0.0464	↑
	3	518.3160	−7.42	ESI+	8.86	LPC (18:3 (6Z,9Z,12Z))	$C_{26}H_{48}NO_7P$	Plasma	0.0328	↑
	4	546.3476	−8.19	ESI+	9.85	LPC (20:3 (5Z,8Z,11Z))	$C_{28}H_{52}NO_7P$	Plasma	0.0042	↓
	5	281.2488	0.10	ESI-	10.12	Oleic acid	$C_{18}H_{34}O_2$	Plasma	0.0212	↑
	6	283.2647	0.78	ESI-	10.96	Stearic acid	$C_{18}H_{36}O_2$	Plasma	0.0221	↑
	7	255.2327	−1.98	ESI-	9.81	Palmitic acid	$C_{16}H_{32}O_2$	Plasma	0.0456	↑
	8	144.0658	−7.58	ESI-	3.00	4-Acetamidobutanoic acid	$C_{16}H_{32}O_2$	Urine	0.0020	↑
	9	133.0976	5.85	ESI+	1.02	Ornithine	$C_5H_{12}N_2O_2$	Urine	0.0051	↑
	10	116.0709	4.83	ESI+	1.01	L-Proline	$C_5H_9NO_2$	Urine	0.0068	↑
	11	203.0819	−4.90	ESI-	4.49	Tryptophan	$C_{11}H_{12}N_2O_2$	Urine	0.0075	↓
	12	169.0359	3.32	ESI+	1.47	Uric acid	$C_5H_4N_4O_3$	Urine	0.0108	↓
	13	166.0728	4.83	ESI+	3.44	1-Methylguanine	$C_6H_7N_5O$	Urine	0.0153	↑
	14	384.1156	2.32	ESI+	3.93	Succinyladenosine	$C_{14}H_{17}N_5O_8$	Urine	0.0169	↑
	15	176.0713	5.66	ESI+	6.28	5-Hydroxyindoleacetaldehyde	$C_{10}H_9NO_2$	Urine	0.0229	↑
	16	162.0555	4.75	ESI+	4.79	2-Indolecarboxylic acid	$C_9H_7NO_2$	Urine	0.0254	↑
	17	188.0344	−6.35	ESI-	4.78	Kynurenic acid	$C_{10}H_7NO_3$	Urine	0.0305	↑
	18	131.0344	−6.82	ESI-	3.77	Glutaric acid	$C_5H_8O_4$	Urine	0.0311	↑
	19	132.0659	5.43	ESI+	1.18	4-Hydroxyproline	$C_5H_9NO_3$	Urine	0.0415	↑
50	1	524.3633	−8.51	ESI+	10.96	LPC (18:0)	$C_{26}H_{54}NO_7P$	Plasma	0.0231	↑
	2	166.0862	1.44	ESI+	2.51	L-Phenylalanine	$C_9H_{11}NO_2$	Plasma	0.0441	↓
	3	496.3357	−7.59	ESI+	9.78	LPC (16:0)	$C_{24}H_{50}NO_7P$	Plasma	0.0228	↑
	4	269.2492	0.98	ESI-	10.38	Heptadecanoic acid	$C_{17}H_{34}O_2$	Plasma	0.0112	↑
	5	283.2647	0.78	ESI-	10.96	Stearic acid	$C_{18}H_{36}O_2$	Plasma	0.0045	↑
	6	227.2009	−4.26	ESI-	8.70	Myristic acid	$C_{14}H_{28}O_2$	Plasma	0.0221	↑
	7	279.2325	−2.54	ESI-	9.42	Linoelaidic acid	$C_{18}H_{32}O_2$	Plasma	0.0074	↑
	8	255.2327	−1.98	ESI-	9.81	Palmitic acid	$C_{16}H_{32}O_2$	Plasma	0.0077	↑
	9	182.0678	4.73	ESI+	3.18	8-Hydroxy-7-methylguanine	$C_6H_7N_5O_2$	Urine	0.0334	↓
	10	304.2125	2.92	ESI+	6.60	3-Hydroxyoctanoyl carnitine	$C_{15}H_{29}NO_5$	Urine	0.0460	↓
75	1	132.0661	5.43	ESI+	0.86	4-Hydroxyproline	$C_5H_9NO_3$	Plasma	0.0068	↓
	2	524.3633	−8.51	ESI+	10.96	LPC (18:0)	$C_{26}H_{54}NO_7P$	Plasma	0.0272	↑
	3	756.5519	−2.11	ESI+	12.45	PC (18:3 (6Z,9Z,12Z)/16:0)	$C_{42}H_{78}NO_8P$	Plasma	0.0218	↓
	4	166.0862	1.44	ESI+	2.51	L-Phenylalanine	$C_9H_{11}NO_2$	Plasma	0.0028	↓
	5	205.0978	5.08	ESI+	3.20	L-Tryptophan	$C_{11}H_{12}N_2O_2$	Plasma	0.0063	↓
	6	496.3357	−7.59	ESI+	9.78	LPC (16:0)	$C_{24}H_{50}NO_7P$	Plasma	0.0321	↑
	7	283.2647	0.78	ESI-	10.96	Stearic acid	$C_{18}H_{36}O_2$	Plasma	0.0065	↑

(Continued on following page)

TABLE 5 (*Continued*) Altered metabolite levels after FQGBG treatment.

Group (g)	No.	m/z	Error (ppm)	Ion	Retention time (min)	Identify	Molecular formula	Sample	*p*-value	Trend
	8	255.2327	−1.98	ESI-	9.81	Palmitic acid	$C_{16}H_{32}O_2$	Plasma	0.0069	↑
	9	151.0256	−5.26	ESI-	2.04	Xanthine	$C_5H_4N_4O_2$	Urine	0.0033	↑
	10	144.0658	−7.58	ESI-	3.00	4-Acetamidobutanoic acid	$C_6H_{11}NO_3$	Urine	0.0294	↑
100	1	520.3328	−9.00	ESI+	9.42	LPC (18:2 (9Z,12Z))	$C_{26}H_{50}NO_7P$	Plasma	0.0011	↑
	2	496.3357	−7.59	ESI+	9.78	LPC (16:0)	$C_{24}H_{50}NO_7P$	Plasma	0.0429	↑
	3	283.2647	0.78	ESI-	10.96	Stearic acid	$C_{18}H_{36}O_2$	Plasma	0.0096	↑
	4	255.2327	−1.98	ESI-	9.81	Palmitic acid	$C_{16}H_{32}O_2$	Plasma	0.0212	↑
	5	224.1288	4.70	ESI+	9.02	Cerulenin	$C_{12}H_{17}NO_3$	Urine	0.0289	↑
	6	130.0505	6.97	ESI+	7.26	Pyroglutamic acid	$C_5H_7NO_3$	Urine	0.0086	↑

TABLE 6 Demographics of participants.

	12.5 g	25 g	50 g	75 g	100 g	125 g	Placebo
N	2	6	6	6	6	6	10
Age (years, mean ± SD)	43.5 ± 2.12	36.0 ± 3.69	27.7 ± 1.75	28.0 ± 3.74	30.8 ± 3.13	28.2 ± 2.64	31.6 ± 3.53
Male (*n*, %)	1 (50.0)	3 (50.0)	3 (50.0)	3 (50.0)	3 (50.0)	3 (50.0)	5 (50.0)
Female (*n*, %)	1 (50.0)	3 (50.0)	3 (50.0)	3 (50.0)	3 (50.0)	3 (50.0)	5 (50.0)
Height (cm, mean ± SD)	159.00 ± 1.84	163.73 ± 10.2	168.82 ± 4.66	163.13 ± 7.15	167.25 ± 9.08	163.57 ± 8.92	161.21 ± 8.49
Weight (kg, mean ± SD)	56.750 ± 7.92	62.500 ± 9.81	63.550 ± 9.43	56.450 ± 7.39	62.058 ± 8.04	58.925 ± 7.18	57.705 ± 5.78
BMI (kg/m^2, mean ± SD)	22.45 ± 2.62	23.20 ± 1.61	22.20 ± 2.35	21.13 ± 1.23	22.13 ± 1.81	22.03 ± 2.33	22.20 ± 1.43

N and % represent the number and percentage of subjects; BMI, body mass index; SD, standard deviation.

TABLE 7 Occurrence rate of AEs.

	12.5 g	25 g	50 g	75 g	100 g	125 g	Total	Placebo
N	2	6	6	6	6	6	32	10
TEAE *n* (%)	1 (50.0)	2 (33.3)	2 (33.3)	5 (83.3)	3 (50.0)	5 (83.3)	18 (56.3)	5 (50.0)
ADR *n* (%)	1 (50.0)	2 (33.3)	2 (33.3)	5 (83.3)	3 (50.0)	5 (83.3)	18 (56.3)	5 (50.0)
SAE *n* (%)	0 (0)	0 (0)	0 (0)	0 (0)	0 (0)	0 (0)	0 (0)	0 (0)
SADR *n* (%)	0 (0)	0 (0)	0 (0)	0 (0)	0 (0)	0 (0)	0 (0)	0 (0)

TEAE, treatment-emergent adverse event; ADR, adverse drug reaction; SAE, serious adverse event; SADR, serious adverse drug reaction; Relationships to FQGBG that refer to confirm, probability, and suspicion are defined as ADR.

in the 25–75 g dosage group showed a certain dose dependence (Liu et al., 2014). This suggests that the metabolic enzymes or transporters responsible for BMA's clearance could become saturated at higher doses. This saturation may be related to the influence of other metabolites in FQGBG on the activity of the BMA-metabolizing enzyme CYP3A4 (Dai et al., 2014). Furthermore, Vz/F of BMA gradually increased in the 25–75 g groups, suggesting that higher doses increased the distribution of BMA in the peripheral compartment, which may be related to the increase in $T_{1/2}$.

In contrast, this situation was not observed for BHA, indicating that BHA's metabolic pathways do not experience the same level of saturation within the studied dosage range. Additionally, significant interindividual variability was observed in the PK parameters of BMA and BHA in healthy participants. Our analysis revealed that the CV for most PK parameters of both BMA and BHA exceeded 30%. It is might partly be attributed to the relatively small sample size in our study. A larger sample size would provide a more robust dataset, potentially allowing for a more accurate assessment of the variability and its clinical implications. This study found that the

C_{max}, AUC_{0-t}, and $AUC_{0-\infty}$ of BMA and BHA in the 100 g group were lower than those in the 75 g group. One possible reason for this was that the monoester alkaloid content in the new batch (116 μg/g) was lower than that in the previous batch (241 μg/g) during the clinical trial.

Metabonomics was used to observe the changes in endogenous metabolites in healthy participants after drug administration to evaluate the safety of drugs in humans and explore potential therapeutic targets of drugs. AC is the main plant metabolites in FQGBG, and owing to its known toxicity, it was the focus of the drug safety analysis in this study. Phenylalanine is converted mainly into tyrosine by phenylalanine hydroxylase in the liver; therefore, when MA causes liver damage, this physiological transformation is blocked, resulting in elevated phenylalanine levels (Chen et al., 2022). The upregulation of phenylalanine and tyrosine levels was also associated with inflammation in chronic heart failure, suggesting that phenylalanine can also be an indicator of cardiac function (Cheng et al., 2021). However, our study found that the phenylalanine level was significantly reduced in the 50 and 75 g treatment groups, which may characterize the safety of FQGBG in healthy individuals. AC poisoning also upregulates various amino and fatty acids (Zhang et al., 2019). The abnormal peroxidation of polyunsaturated fatty acids such as arachidonic acid and its metabolites can damage the myocardial mitochondria, leading to cardiac arrhythmia (Cai et al., 2013). However, similar results were not obtained in this study. Therefore, combined with clinical AE observations, metabonomics results can supplement the elucidation of the good safety and tolerability of FQGBG.

The pathogenesis of KYDS involves mainly dysfunction of the hypothalamic-pituitary-target gland axis (adrenal, thyroid, and gonad) marked by cold limbs, polyuria, and slow responses (Chen et al., 2019). Pharmacological results demonstrate that FQGBG can alleviate increased urination in rats with two models of KYDS models (hydrocortisone-induced model and natural aging model) and its efficacy is faster compared to other commonly used TCMs (Gui-fu-di-huang-wan, You-gui-wan) to treat KYDS. In addition, it effectively counteracts hydrocortisone-induced adrenal atrophy in KYDS rat models by hydrocortisone, which suggest that FQGBG primarily exerts its therapeutic effects by counteracting the adrenal dysfunction caused by KYDS, repairing the function of the hypothalamus-pituitary-adrenal axis, and this may be related to the restoration of adrenal responsiveness to pituitary hormones, promoting the release of cortisol and aldosterone, which regulate the water and sodium balance in the kidney. In contrast, altered metabolites in urine, including acetylamino butyric acid, ornithine, guanidinoacetic acid, proline, and 4-hydroxyproline, are all associated with the arginine metabolism pathway. Arginine can regulate the release of adrenocortical hormones and cortisol in patients with diabetes insipidus (Bologna et al., 2020), which may be related to the improvement of polyuria symptoms by FQGBG in KYDS.

Observation of experimental animals, both the FQGBG and the positive drug group improved the symptoms of cold fear, huddling, hunchback, and mental fatigue. This indicates that FQGBG and the positive drug have a certain alleviating effect on the symptoms of decreased energy metabolism and insufficient heat production caused by KYDS. FZ and Cinnamon in FQGBG are TCM that generate heat in the interior body and eliminates cold. Alkaloids in FZ, including fuziline, neoline, and BMA, are identified as β-adrenergic receptor (β-AR) agonists, for regulating the thermogenic function and regulate glucose and lipid metabolism by activating the β3-AR receptor of adipocytes (Gao et al., 2023). Cinnamaldehyde, the main metabolite of Cinnamon, activated PKA signaling, increased thermogenic gene expression levels, and induced phosphorylation of hormone-sensitive lipase (HSL) and Perilipin 1 in primary murine primary adipocytes (Jiang et al., 2017). Therefore, in this study, elevated levels of palmitic acid and stearic acid, which are the main substrates for lipid breakdown and beta-oxidation, may be associated with enhanced lipid breakdown and enhanced energy metabolism induced by FQGBG. Furthermore, upregulation of palmitic acids and stearic acid may also be associated with increased secretory phospholipase (sPLA) activity and degradation of glycerophospholipids. sPLA has been reported to increase the expression of mitochondrial uncoupling markers such as UCP1 and PPAR in brown and white adipocytes of mice (25, 26), thus enhancing mitochondrial oxidation and thermogenesis. sPLA regulates lipolysis in adipocytes by enhancing HSL activity through the ERK signaling pathway (Zhi et al., 2015).

5 Conclusion

The PK and safety of single-dose oral administration of FQGBG were investigated for the first time for healthy Chinese volunteers. The results indicated that the half-lives of FZ monoester alkaloids were prolonged, and there were significant individual differences. Therefore, further evaluation of drug accumulation is needed in PK studies involving continuous administration. Under the experimental dosing regimen, FQGBG was safe in healthy subjects. The pharmacodynamics and metabonomics results suggest that FQGBG exerts its efficacy by improving the function of the hypothalamus-pituitary-adrenal axis, effectively treating the increased urination caused by KYDS, and alleviating the symptoms of cold fear in KYDS rats through enhancing energy metabolism.

Data availability statement

The original contributions presented in the study are included in the article/Supplementary Material, further inquiries can be directed to the corresponding authors.

Ethics statement

The studies involving humans were approved by the Human Research Ethics Committees of Xiyuan Hospital, China Academy of Chinese Medical Sciences. The studies were conducted in accordance with the local legislation and institutional requirements. The participants provided their written informed consent to participate in this study. The animal study was approved by Ethics Committee, Yunnan Institute of Materia Medica. The study was conducted in accordance with the local legislation and institutional requirements. Written informed

consent was obtained from the individual(s) for the publication of any potentially identifiable images or data included in this article.

Author contributions

W-YC: Formal Analysis, Software, Writing–original draft. J-YL: Data curation, Writing–original draft. MS: Conceptualization, Methodology, Writing–original draft. J-KW: Conceptualization, Methodology, Writing–original draft. FL: Supervision, Writing–review and editing. Q-NY: Supervision, Writing–review and editing. W-TZ: Investigation, Writing–review and editing. M-JZ: Investigation, Writing–review and editing. B-EZ: Visualization, Writing–original draft. H-BL: Conceptualization, Methodology, Writing–original draft. S-GW: Visualization, Writing–review and editing. YW: Visualization, Writing–original draft. R-ZW: Software, Validation, Writing–original draft. W-DW: Software, Validation, Writing–review and editing. RL: Writing–review and editing. Z-YZ: Writing–review and editing. RG: Writing–review and editing.

Funding

The author(s) declare that financial support was received for the research, authorship, and/or publication of this article. The work was supported by the Science and Technology Innovation Project, China Academy of Chinese Medical Sciences (CI2021A04703), Fundamental Research Funds for the Central Public Welfare Research Institutes, China Academy of Chinese Medical Sciences (ZZ15-YQ-019), Science and Technology Talent and Platform plan of Yunnan Province (202205AD160044), and Science and Technology Planning Project of Yunnan Province (2014DC036).

Acknowledgments

We thank all the volunteers who participated in the clinical trial, the operation team of Xiyuan Hospital for conducting this trial, and the drug development and production team of Yunnan Institute of Materia Medica and Yunnan Baiyao. We thank the China Academy of Chinese Medical Sciences and Yunnan Province of the People's Republic of China for funding support.

Conflict of interest

Authors J-YL, MS, J-KW, B-EZ, H-BL, Z-YZ were employed by Yunnan Baiyao Group Co., Ltd.

The remaining authors declare that the research was conducted in the absence of any commercial or financial relationships that could be construed as a potential conflict of interest.

Publisher's note

All claims expressed in this article are solely those of the authors and do not necessarily represent those of their affiliated organizations, or those of the publisher, the editors and the reviewers. Any product that may be evaluated in this article, or claim that may be made by its manufacturer, is not guaranteed or endorsed by the publisher.

Supplementary material

The Supplementary Material for this article can be found online at: https://www.frontiersin.org/articles/10.3389/fphar.2024.1351871/full#supplementary-material

References

Bliwise, D. L., Howard, L. E., Moreira, D. M., Andriole, G. L., Hopp, M. L., and Freedland, S. J. (2019). Nocturia and associated mortality: observational data from the REDUCE trial. *Prostate Cancer Prostatic Dis.* 22, 77–83. doi:10.1038/s41391-018-0090-5

Bologna, K., Cesana-Nigro, N., Refardt, J., Imber, C., Vogt, D. R., Christ-Crain, M., et al. (2020). Effect of arginine on the hypothalamic–pituitary–adrenal Axis in individuals with and without vasopressin deficiency. *J. Clin. Endocrinol. Metabolism* 105, dgaa157–e2336. doi:10.1210/clinem/dgaa157

Cai, Y., Gao, Y., Tan, G., Wu, S., Dong, X., Lou, Z., et al. (2013). Myocardial lipidomics profiling delineate the toxicity of traditional Chinese medicine Aconiti Lateralis radix praeparata. *J. Ethnopharmacol.* 147, 349–356. doi:10.1016/j.jep.2013.03.017

Chen, Q., Zhang, K., Jiao, M., Jiao, J., Chen, D., Yin, Y., et al. (2022). Study on the mechanism of mesaconitine-induced hepatotoxicity in rats based on metabonomics and toxicology network. *Toxins* 14, 486. doi:10.3390/toxins14070486

Chen, R., Wang, J., Zhan, R., Zhang, L., and Wang, X. (2019). Fecal metabonomics combined with 16S rRNA gene sequencing to analyze the changes of gut microbiota in rats with kidney-yang deficiency syndrome and the intervention effect of You-gui pill. *J. Ethnopharmacol.* 244, 112139. doi:10.1016/j.jep.2019.112139

Cheng, C.-W., Liu, M.-H., Tang, H.-Y., Cheng, M.-L., and Wang, C.-H. (2021). Factors associated with elevated plasma phenylalanine in patients with heart failure. *Amino Acids* 53, 149–157. doi:10.1007/s00726-020-02933-1

Dai, P.-M., Wang, Y., Ye, L., Zeng, S., Zheng, Z.-J., Li, Q., et al. (2014). Pharmacokinetic comparisons of benzoylmesaconine in rats using ultra-performance liquid chromatography-tandem mass spectrometry after administration of pure benzoylmesaconine and wutou decoction. *Molecules* 19, 16757–16769. doi:10.3390/molecules191016757

Gao, H., Li, Z., Cheng, C., Cui, J., Peng, J., Wang, X., et al. (2023). Fuziline ameliorates glucose and lipid metabolism by activating beta adrenergic receptors to stimulate thermogenesis. *IJMS* 24, 8362. doi:10.3390/ijms24098362

Ji, X., Yang, M., Shen, G., Or, K. H., Yim, W. S., and Zuo, Z. (2023). Safety evaluations of the processed lateral root of Aconitum carmichaelii Debx. And its hepatotoxicity mechanisms in rats. *J. Ethnopharmacol.* 301, 115801. doi:10.1016/j.jep.2022.115801

Jiang, J., Emont, M. P., Jun, H., Qiao, X., Liao, J., Kim, D., et al. (2017). Cinnamaldehyde induces fat cell-autonomous thermogenesis and metabolic reprogramming. *Metabolism* 77, 58–64. doi:10.1016/j.metabol.2017.08.006

Liu, X., Li, H., Song, X., Qin, K., Guo, H., Wu, L., et al. (2014). Comparative pharmacokinetics studies of benzoylhypaconine, benzoylmesaconine, benzoylaconine and hypaconitine in rats by LC-MS method after administration of Radix Aconiti Lateralis Praeparata extract and Dahuang Fuzi Decoction. *Biomed. Chromatogr.* 28, 966–973. doi:10.1002/bmc.3102

Lombardo, R., Tubaro, A., and Burkhard, F. (2020). Nocturia: the complex role of the heart, kidneys, and bladder. *Eur. Urol. Focus* 6, 534–536. doi:10.1016/j.euf.2019.07.007

Lu, C.-C., Jan, Y.-M., Li, T.-C., and Hsieh, C.-L. (2009). Electroacupuncture induces differential effects between yin and yang: a study using cutaneous blood flow and temperature recordings of the hand's dorsum and palm. *Am. J. Chin. Med.* 37, 639–645. doi:10.1142/S0192415X09007120

Lu, X., Xiong, Z., Li, J., Zheng, S., Huo, T., and Li, F. (2011). Metabonomic study on 'Kidney-Yang Deficiency syndrome' and intervention effects of Rhizoma Drynariae extracts in rats using ultra performance liquid chromatography coupled with mass spectrometry. *Talanta* 83, 700–708. doi:10.1016/j.talanta.2010.09.026

Qian, H.-L. (2019). Effects of different Chinese meteria medica pair on regulation of adrenal function in mice with hydrocortisone-induced syndrome. *Chin. Traditional Herb. Drugs*, 2383–2389.

Singhuber, J., Zhu, M., Prinz, S., and Kopp, B. (2009). Aconitum in Traditional Chinese Medicine—a valuable drug or an unpredictable risk? *J. Ethnopharmacol.* 126, 18–30. doi:10.1016/j.jep.2009.07.031

Sun, M., Lin, J., Li, D., Jiang, L., Wu, W., Wang, J., et al. (2017). Clinical trial on 72 patients of kidney-yang deficiency treated with Fuqi Guben Gao. *J. Yunnan Coll. Traditional Chin. Med.* 40, 47–49. doi:10.19288/j.cnki.issn.1000-2723.2017.03.011

U.S. Food and Drug Administration (2018). Bioanalytical method validation guidance for industry. Available at: https://www.fda.gov/regulatory-information/search-fda-guidance-documents/bioanalytical-method-validation-guidance-industry.

Wolff, D. T., Adler, K. A., Weinstein, C. S., and Weiss, J. P. (2021). Managing nocturia in frail older adults. *Drugs Aging* 38, 95–109. doi:10.1007/s40266-020-00815-5

Xu, Y.-X., Luo, H.-S., Sun, D., Wang, R., and Cai, J. (2019). Acupuncture in the treatment of chronic fatigue syndrome based on "interaction of brain and kidney" in TCM: a randomized controlled trial. *Zhongguo Zhen Jiu* 39, 123–127. doi:10.13703/j.0255-2930.2019.02.003

Yan, R., Yang, Y., and Chen, Y. (2018). Pharmacokinetics of Chinese medicines: strategies and perspectives. *Chin. Med.* 13, 24. doi:10.1186/s13020-018-0183-z

Yang, M., Ji, X., and Zuo, Z. (2018). Relationships between the toxicities of radix aconiti lateralis preparata (fuzi) and the toxicokinetics of its main diester-diterpenoid alkaloids. *Toxins* 10, 391. doi:10.3390/toxins10100391

Zhang, H., Sun, S., Zhang, W., Xie, X., Zhu, Z., Chai, Y., et al. (2016). Biological activities and pharmacokinetics of aconitine, benzoylaconine, and aconine after oral administration in rats. *Drug Test. Analysis* 8, 839–846. doi:10.1002/dta.1858

Zhang, Y., Bian, X., Yang, J., Wu, H., Wu, J.-L., and Li, N. (2019). Metabolomics of clinical poisoning by Aconitum alkaloids using derivatization LC-MS. *Front. Pharmacol.* 10, 275. doi:10.3389/fphar.2019.00275

Zhi, H., Qu, L., Wu, F., Chen, L., and Tao, J. (2015). Group IIE secretory phospholipase A_2 regulates lipolysis in adipocytes. *Obesity* 23, 760–768. doi:10.1002/oby.21015

Zhou, C., Gao, J., Qu, H., Xu, L., Zhang, B., Guo, Q., et al. (2022). Anti-inflammatory mechanism of action of benzoylmesaconine in lipopolysaccharide-stimulated RAW264.7 cells. *Evidence-Based Complementary Altern. Med.* 2022, 7008907–7008912. doi:10.1155/2022/7008907

Zhou, W., Liu, H., Qiu, L., Yue, L., Zhang, G., Deng, H., et al. (2021). Cardiac efficacy and toxicity of aconitine: a new frontier for the ancient poison. *Med. Res. Rev.* 41, 1798–1811. doi:10.1002/med.21777

frontiers | Frontiers in Pharmacology

TYPE Original Research
PUBLISHED 22 August 2024
DOI 10.3389/fphar.2024.1386604

Check for updates

OPEN ACCESS

EDITED BY
Jian-bo Yang,
National Institutes for Food and Drug Control, China

REVIEWED BY
Ahmed A. Elmarakby,
Augusta University, United States
Jiuyao Zhou,
Guangzhou University of Chinese Medicine, China
Guoliang Xiong,
Shenzhen Traditional Chinese Medicine Hospital, China

*CORRESPONDENCE
Xiaoli Nie,
nxl117@163.com
Hua Miao,
hmiao77@163.com
Ying-Yong Zhao,
zhaoyybr@163.com

RECEIVED 15 February 2024
ACCEPTED 12 August 2024
PUBLISHED 22 August 2024

CITATION
Li X-J, Wang Y-N, Wang W-F, Nie X, Miao H and Zhao Y-Y (2024) Barleriside A, an aryl hydrocarbon receptor antagonist, ameliorates podocyte injury through inhibiting oxidative stress and inflammation.
Front. Pharmacol. 15:1386604.
doi: 10.3389/fphar.2024.1386604

COPYRIGHT
© 2024 Li, Wang, Wang, Nie, Miao and Zhao. This is an open-access article distributed under the terms of the Creative Commons Attribution License (CC BY). The use, distribution or reproduction in other forums is permitted, provided the original author(s) and the copyright owner(s) are credited and that the original publication in this journal is cited, in accordance with accepted academic practice. No use, distribution or reproduction is permitted which does not comply with these terms.

Barleriside A, an aryl hydrocarbon receptor antagonist, ameliorates podocyte injury through inhibiting oxidative stress and inflammation

Xiao-Jun Li[1,2], Yan-Ni Wang[1], Wen-Feng Wang[3], Xiaoli Nie[2]*, Hua Miao[1]* and Ying-Yong Zhao[1]*

[1]School of Pharmacy, Zhejiang Chinese Medical University, Hangzhou, Zhejiang, China, [2]Department of Nephrology, Integrated Hospital of Traditional Chinese Medicine, Southern Medical University, Guangzhou, Guangdong, China, [3]School of Pharmacy, Heilongjiang University of Chinese Medicine, Harbin, Heilongjiang, China

Introduction: Increasing evidence shows that hyperactive aryl hydrocarbon receptor (AHR) signalling is involved in renal disease. However, no currently available intervention strategy is effective in halting disease progression by targeting the AHR signalling. Our previous study showed that barleriside A (BSA), a major component of *Plantaginis semen*, exhibits renoprotective effects.

Methods: In this study, we determined the effects of BSA on AHR expression in 5/6 nephrectomized (NX) rats. We further determined the effect of BSA on AHR, nuclear factor kappa B (NF-κB), and the nuclear factor erythroid 2-related factor 2 (Nrf2) signalling cascade in zymosan-activated serum (ZAS)-stimulated MPC5 cells.

Results: BSA treatment improved renal function and inhibited intrarenal nuclear AHR protein expression in NX-treated rats. BSA mitigated podocyte lesions and suppressed AHR mRNA and protein expression in ZAS-stimulated MPC5 cells. BSA inhibited inflammation by improving the NF-κB and Nrf2 pathways in ZAS-stimulated MPC5 cells. However, BSA did not markedly upregulate the expression of podocyte-specific proteins in the ZAS-mediated MPC5 cells treated with CH223191 or AHR siRNA compared to untreated ZAS-induced MPC5 cells. Similarly, the inhibitory effects of BSA on nuclear NF-κB p65, Nrf2, and AHR, as well as cytoplasmic cyclooxygenase-2, heme oxygenase-1, and AHR, were partially abolished in ZAS-induced MPC5 cells treated with CH223191 or AHRsiRNA compared with untreated ZAS-induced MPC5 cells. These results indicated that BSA attenuated the inflammatory response, partly by inhibiting AHR signalling.

Discussion: Both pharmacological and siNRA findings suggested that BSA mitigated podocyte lesions by improving the NF-κB and Nrf2 pathways via inhibiting AHR signalling. Therefore, BSA is a high-affinity AHR antagonist that abolishes oxidative stress and inflammation.

KEYWORDS

aryl hydrocarbon receptor, oxidative stress and inflammation, nuclear factor kappa B, Nrf2, chronic kidney disease, podocyte injury, *Plantaginis semen*, barleriside A

1 Introduction

Aryl hydrocarbon receptor (AHR) is a cytoplasmic ligand-mediated transcription factor (Cao et al., 2022; Ouyang et al., 2020). The biological functions of AHR include immune regulation, cell cycle regulation, mucosal barrier function, and organogenesis, which are associated with ligand-mediated receptor activation (da Silva et al., 2022; Ouyang et al., 2020; Wu et al., 2022). AHR can transcribe various drug-metabolizing enzymes including *cytochrome P450 family 1 subfamily A member 1* (*CYP1A1*), *cytochrome P450 family 1 subfamily A member 2* (*CYP1A2*), and *cytochrome P450 family 1 subfamily B member 1* (*CYP1B1*) (Miao et al., 2020). High-affinity AHR ligands have been identified as xenobiotics, such as 2,3,7,8-tetrachlorodibenzo-p-dioxin (Cao et al., 2022). Previous study has suggested that hyperactive AHR signal was implicated in patients with podocyte damage-associated renal disease such as immunoglobulin A nephropathy (IgAN), diabetic kidney disease (DKD) and idiopathic membranous nephropathy (IMN) (Miao et al., 2020). Our previous study showed increased intrarenal AHR mRNA and protein expression in patients with chronic kidney disease (CKD) (Miao et al., 2022). However, no currently available therapy is effective for halting disease progression. Therefore, identification of novel AHR ligands plays a critical role in targeting this enigmatic receptor for the treatment of various diseases.

Mounting evidence suggests that traditional Chinese medicines (TCM) are a key source of new drugs and are used for treatment of various diseases (Newman and Cragg, 2020; Hou et al., 2022; Li, et al., 2022a; Marena et al., 2022; Zhao et al., 2022a; Kong et al., 2023). Natural compounds form TCM were widely used for improving renal function and treating renal injury (Ren et al., 2021; Hu et al., 2022; Zhou et al., 2022; Shao et al., 2023; Sun et al., 2023). Substantial achievements have shown a myriad of natural compounds that can directly modulate AHR signalling (Goya-Jorge et al., 2021). Our previous studies have demonstrated that a number of flavonoids, such as barleriside A (BSA), rhoifolin, 5,7,3′,4′,5′-pentahydroxy flavanone and 5,6,7,8,3′,4′-hexamethoxyflavone, and lignans, including matairesinol and erythro-guaiacylglycerol-β-ferulic acid ether as AHR antagonists, attenuate renal fibrosis by suppressing AHR signalling (Miao et al., 2020; Cao et al., 2022; Miao et al., 2022). In addition, astragaloside IV attenuates renal damage and AHR signalling in mice (Mo et al., 2023). *In vitro* experiments have shown that astragaloside IV suppresses inflammation and AHR signalling in indoxyl sulfate-treated HK-2 cells (Mo et al., 2023). Moreover, a previous study showed that lycopene mitigated Di (2-ethylhexyl) phthalate-induced renal cell injury by suppressing AHR signal (Li et al., 2021). Collectively, naturally derived compounds, such as AHR inhibitors, attenuated renal fibrosis.

Numerous studies have reported that inflammation plays a central role in CKD (Singh et al., 2022; Wang et al., 2023b; Yuan et al., 2022). *Cyclooxygenase-2* (*COX-2*) is produced by transcription factors including AHR and nuclear factor kappa B (NF-ĸB) p65. Several studies have shown that AHR interacts with NF-ĸB in CKD (Addi et al., 2019; Brito et al., 2019; Curran and Kopp, 2022). Our recent study showed that inhibitor of kappa B (IĸB)/NF-ĸB pathway was a downstream target of AHR signal in IMN (Wang et al., 2023b). However, there are no agents that inhibit NF-ĸB pathway by targeting AHR signalling. *Plantaginis semen* is widely used as a diuretic to improve renal function and treat renal diseases in patients (Wen et al., 2023a). Our previous study showed that BSA, a major component of *P. semen*, exhibits renoprotective effects (Miao et al., 2020). In this study, we first determined the effect of BSA on AHR signals in 5/6 nephrectomized (NX) rats. We further revealed that BSA, an AHR antagonist, ameliorated podocyte injury through IĸB/NF-ĸB and kelch-like ECH-associated protein 1 (Keap1)/nuclear factor erythroid 2-related factor 2 (Nrf2) signalling cascade in zymosan activation serum (ZAS)-stimulated MPC5 cells. Our study will uncover that BSA ameliorate podocyte damage-associated renal disease by improving IĸB/NF-ĸB and Keap1/Nrf2 pathways via suppressing hyperactive AHR expression.

2 Materials and methods

2.1 Chemicals, antibodies and reagents

Zymosan A was purchased from Sigma–Aldrich (St. Louis, MO, USA). Primary antibodies, Healthy human and Western quick horseradish peroxidase chemiluminescent substrate were presented in the previous publications (Wang et al., 2023).

2.2 NX-induced CKD rats treated by BSA

Male Sprague Dawley rats were purchased from the Animal Center of the Xi'an Jiaotong University (Xi'an, Shaanxi, China). NX rats were reproduced as described in the previous publication (Miao et al., 2020). Rats were divided into three groups: Sham, NX and NX + BSA (n = 8/group). BSA was administered at 10 mg/kg/day by gastric irrigation for 4 weeks from ninth to 12th week. Urine was collected for 24 h after 12 weeks. All rats were euthanized after anesthetization with 10% urethane. Serum and kidney tissue samples were also collected. The animal care and experiments are approved by Ethics Committee for Animal Experiments of University (No. 20200713-06).

2.3 ZAS preparation and cell treatment

Mouse podocyte cell culture was performed as described in the previous publication (Wang et al., 2023a). C5b-9 was prepared as described in our previous study (Wang et al., 2023a). MPC5 cells were stimulated with 10% ZAS for 24 h in the absence or presence of BSA (20 μM) and CH223191 (10 μM). The treated cells were collected.

2.4 Serum and urine biochemical analysis

Creatinine and urea levels in serum were measured using a Beckman AU680 automatic analyzer. Proteinuria was measured using a Roche Cobas C501 Chemistry Analyzer.

2.5 Quantitative real-time polymerase chain reaction (RT-PCR)

Extracted total RNA, quantitative RT-PCR and specific primers were shown in the previous publications (Miao et al., 2020; Cao et al., 2022; Miao et al., 2022).

2.6 Immunohistochemistry

Kidneys were incubated overnight at 4°C with an anti-AHR primary antibody, and then incubated with a secondary antibody. Analysis was carried out using a light microscope.

2.7 Immunofluorescence

MPC5 cells were incubated with antibodies against podocin, AHR, NF-κB p65, COX-2, Nrf2, and haem oxygenase-1 (HO-1). Details of the immunofluorescence methods are presented in the previous publication (Wang et al., 2023).

2.8 Western blot analysis

Western blot analysis was performed in the previous publication (Cao et al., 2022). The expression levels were normalized to those of α-tubulin and histone H3. The relative levels were quantified using the ImageJ software.

2.9 Statistical analysis

The experimental results are presented as the mean ± standard error of mean. The statistical significance was analyzed using one-way ANOVA using the GraphPad Prism software. The values for $P < 0.05$ were considered statistically significant.

3 Results

3.1 BSA improved kidney function and suppressed nuclei AHR expression in NX-induced CKD rats

Compared to Sham rats, NX rats presented a markedly increase in the serum levels of creatinine and urea, as well as proteinuria levels, while BSA treatment markedly reduced levels of three renal function markers in NX-induced CKD rats (Figure 1A), indicating that BSA improved renal function in NX-induced CKD rats.

Compared to Sham rats, NX rats presented a significant reduction in intrarenal cytoplasmic AHR protein expression in NX-induced CKD rats, which was accompanied by a significant increase in intrarenal nuclei AHR protein expression in NX-induced CKD rats (Figures 1B, C). BSA treatment markedly preserved cytoplasmic AHR protein expression and markedly reduced nuclear AHR protein expression in renal tissues of NX-induced CKD rats (Figures 1B, C). This result was further verified using immunohistochemical analysis (Figure 1D). These data suggest that activating AHR signalling in CKD and AHR may be an effective therapeutic target. BSA is a novel aryl hydrocarbon receptor antagonist.

To elucidate the renoprotective mechanism of BSA, we first determined its effect on ZAS-stimulated MPC5 cells. BSA could markedly inhibit the downregulation of the protein expression of podocin and nephrin in ZAS-treated MPC5 cells in a concentration-dependent manner (10–40 μM) within 24 h (Figures 1E, F). The concentrations of 20 and 40 μM BSA had a stronger effect on the upregulated podocin and nephrin protein expressions than did 10 μM BSA (Figures 1E, F). But, the effect at 20 μM was similar to that observed at 40 μM. Therefore, 20 μM was used for this experiment. Immunofluorescence staining further verified that BSA treatment preserved podocin expression in the ZAS-stimulated MPC5 cells (Figure 1G).

3.2 BSA inhibited AHR signalling in the ZAS-stimulated MPC5 cells

Compared to ZAS-stimulated MPC5 cells, BSA treatment markedly inhibited the mRNA expression of *AHR* and its four target genes, such as *CYP1A1*, *CYP1A2*, *CYP1B1* and *COX-2* in ZAS-induced MPC5 cells (Figure 2A), which was accompanied by reduced AHR nuclear translocation (Figure 2B), which was in line with the protein expression of increasing cytoplasmic AHR and decreasing nuclear AHR (Figures 2C, D). Luciferase assay uncovered that BSA treatment markedly inhibited AHR-driven reporter activity in ZAS-stimulated MPC5 cells (Figure 2E). These data indicate that BSA inhibits activating AHR signalling in ZAS-stimulated MPC5 cells.

3.3 BSA inhibited hyperactive IκB/NF-κB pathway in the ZAS-stimulated MPC5 cells

Compared to ZAS-stimulated MPC5 cells, BSA treatment markedly reduced nuclear p65 expression in ZAS-stimulated MPC5 cells (Figures 3A–C). This is acspanied by markedly inhibiting protein expressions of p-IκBα and p65 downstream target gene products such as COX-2, inducible nitric oxide synthase (iNOS), monocyte chemotactic protein-1 (MCP-1), 12-lipoxygenase (12-LOX), $p67^{phox}$ and $p67^{phox}$ in the ZAS-stimulated MPC5 cells (Figures 3B, C), which were consistent with markedly inhibiting cytoplasm COX-2 protein expression in the ZAS-stimulated MPC5 cells (Figure 3D). Therefore, these data suggest that BSA inhibits the hyperactive IκB/NF-κB pathway in ZAS-stimulated MPC5 cells.

3.4 BSA improved impaired Keap1/Nrf2 pathway in the ZAS-stimulated MPC5 cells

Compared to untreated ZAS-stimulated MPC5 cells, treatment with BSA markedly increased nuclear Nrf2 expression in ZAS-stimulated MPC5 cells (Figures 4A–C). This is also accompanied by markedly reduced protein expression of Keap1 and increased Nrf2 target gene products, such as HO-1, catalase, glutamate-cysteine ligase catalytic subunit (GCLC), glutamate-cysteine ligase modifier subunit (GCLM), manganese superoxide dismutase

10.3389/fphar.2024.1386604

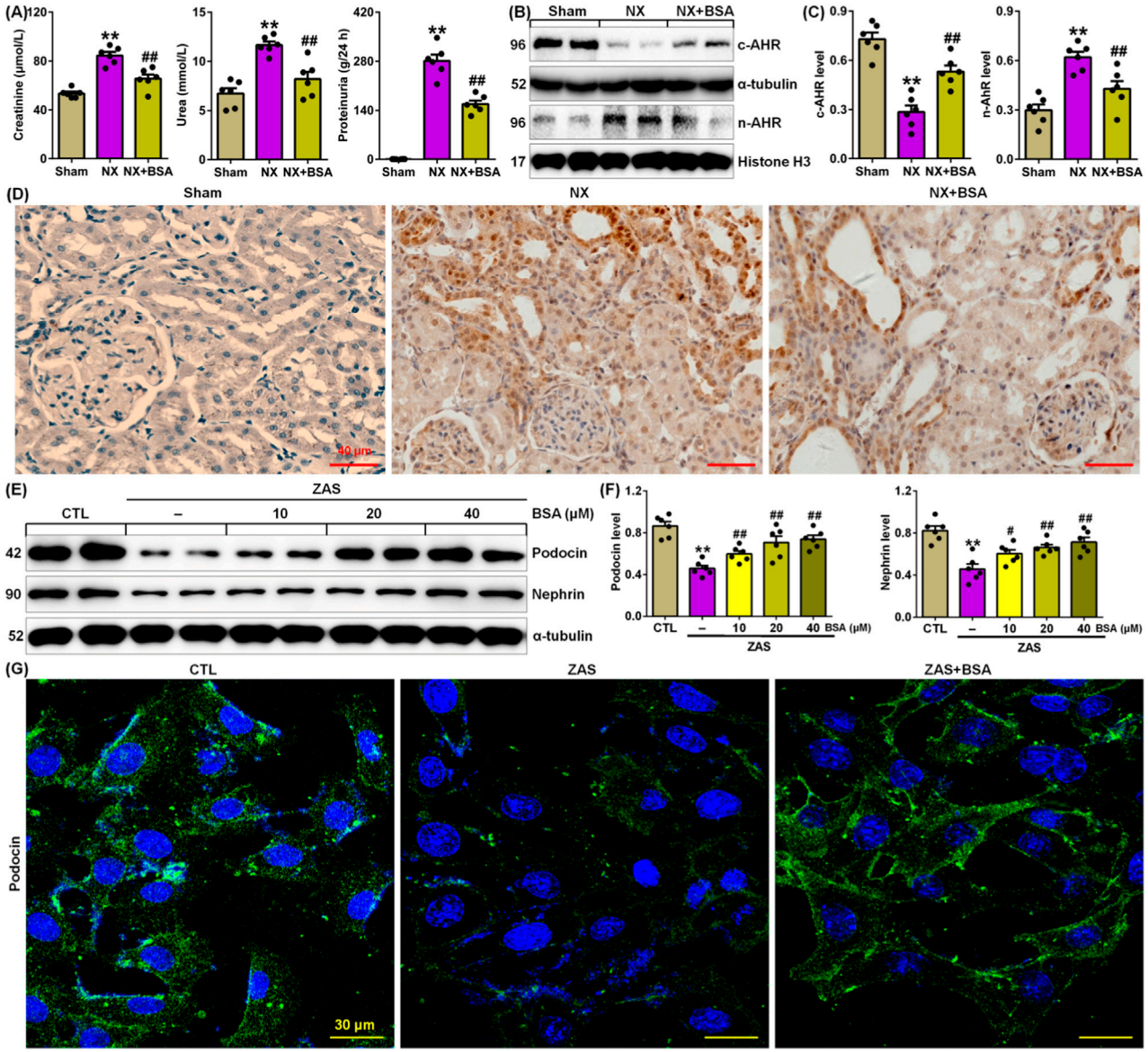


FIGURE 1
BSA inhibits AHR expression in the NX-induced rats. **(A)** Serum levels of creatinine and urea and proteinuria in the control and NX-induced rats with or without BSA. **(B)** Cytoplasm and nuclei AHR protein expression in the renal tissues of control and NX-induced rats with or without BSA. **(C)** Protein levels of cytoplasm and nuclei AHR in the renal tissues of control and NX-induced rats with or without BSA. **(D)** Immunohistochemical analysis with intrarenal anti-AHR antibody in the control and NX-induced rats with or without BSA. **(E)** Protein expression levels of podocin and nephrin in the ZAS-induced MPC5 cells treated with the different concentrations of BSA. **(F)** Quantitative analysis of protein expression of podocin and nephrin in ZAS-induced MPC5 cells treated with the different concentrations of BSA. **(G)** Immunofluorescent analysis with anti-podocin antibody in the control and ZAS-stimulated MPC5 cells with or without BSA. $^{*}P < 0.05$, $^{**}P < 0.01$ compared with sham or CTL; $^{\#}P < 0.05$, $^{\#\#}P < 0.01$ compared with NX or ZAS-stimulated MPC5 cells.

(MnSOD), and nicotinamide adenine dinucleotide phosphate quinone dehydrogenase 1 (NQO-1), in ZAS-stimulated MPC5 cells treated with BSA compared to untreated ZAS-stimulated MPC5 cells (Figures 4B, C). In addition, BSA treatment markedly increased cytoplasmic HO-1 protein expression in ZAS-stimulated MPC5 cells (Figure 4D). These results suggest that BSA improves the impaired Keap1/Nrf2 pathway in ZAS-induced MPC5 cells. Collectively, these results indicate that BSA improves the activating IκB/NF-κB and impaired Keap1/Nrf2 pathway in MPC5 cells.

3.5 BSA ameliorated podocyte injury by improving IκB/NF-κB and Keap1/Nrf2 pathways via AHR signal

We determine whether BSA mitigates MPC5 cell damage by improving IκB/NF-κB and Keap1/Nrf2 pathways via suppressing AHR signalling. BSA treatment downregulated the expression of podocyte-specific proteins in ZAS-mediated MPC5 cells (Figures 5A, B). However, BSA did not significantly upregulate podocyte protein expression in ZAS-induced MPC5 cells treated with

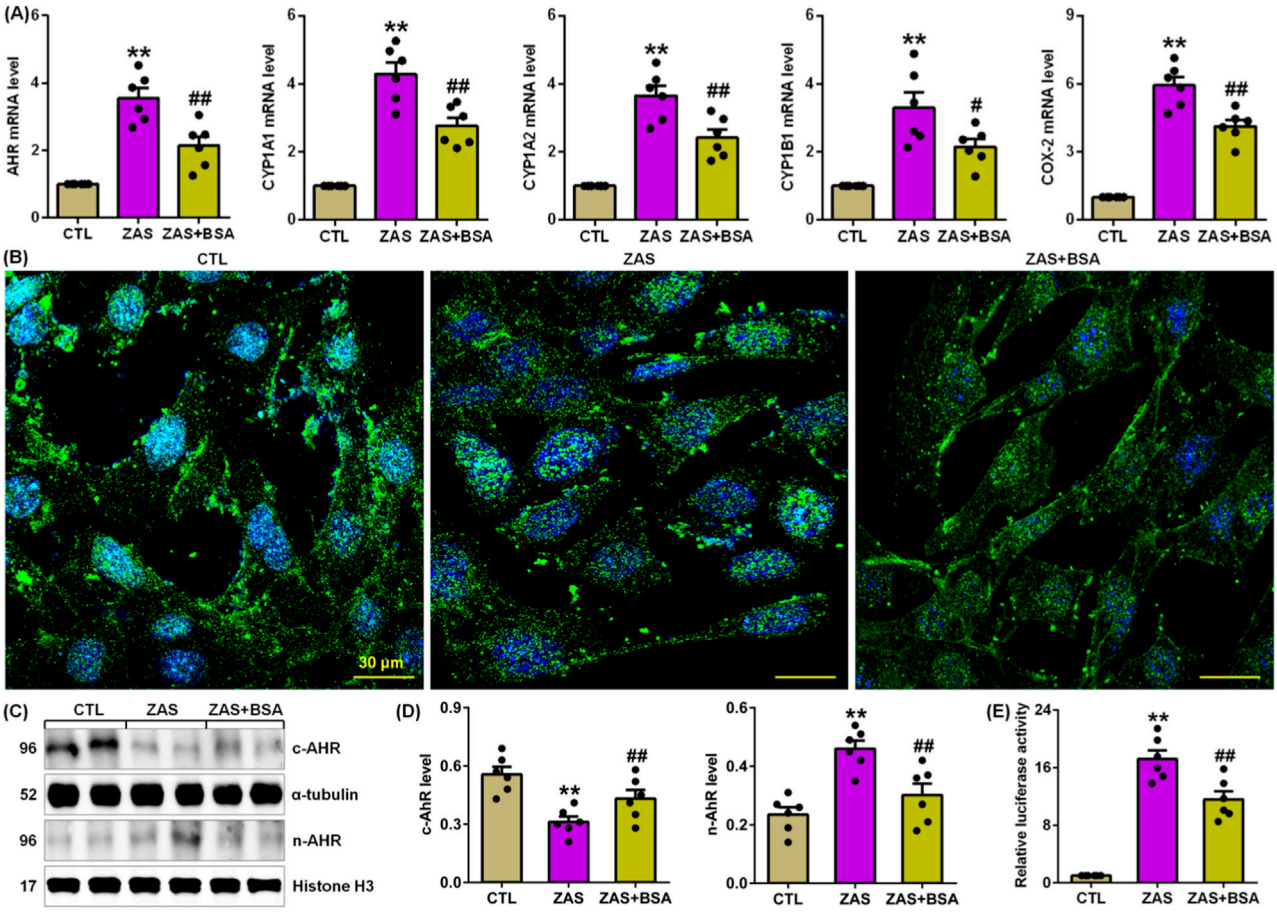


FIGURE 2
BSA inhibits AHR signalling in the ZAS-stimulated MPC5 cells. **(A)** The mRNA levels of *AHR* and its target genes, including *CYP1A1*, *CYP1A2*, *CYP1B1* and *COX-2* in the control and ZAS-stimulated MPC5 cells with or without BSA. **(B)** Immunofluorescent analysis with anti-AHR antibody in the control and ZAS-stimulated MPC5 cells with or without BSA. **(C)** Cytoplasm and nuclei AHR protein expression in the control and ZAS-stimulated MPC5 cells with or without BSA. **(D)** Protein levels of cytoplasm and nuclei AHR in the control and CBSA-induced MN rats with or without MSG. **(E)** Luciferase assay of AHR activation in the control and ZAS-stimulated MPC5 cells with or without BSA. $^{*}P < 0.05$, $^{**}P < 0.01$ compared with CTL; $^{\#}P < 0.05$, $^{\#\#}P < 0.01$ compared with ZAS-stimulated MPC5 cells.

CH223191 compared with only ZAS-mediated MPC5 cells (Figures 5A, B). Similarly, the inhibitory effect of BSA on nuclear NF-κB p65 and Nrf2 as well as cytoplasmic COX-2, MCP-1, HO-1 and catalase was partially abolished in ZAS-mediated MPC5 cells treated with CH223191 compared with only ZAS-induced MPC5 cells (Figures 5C, D). The results were also demonstrated in the ZAS-induced AHR siRNA-transfected MPC5 cells treated with BSA (Figures 6A, D). These results indicate that BSA attenuates inflammatory response via inhibiting AHR signalling. Totally, both pharmacological and siRNA results demonstrate that BSA attenuates podocyte lesion by modulating IκB/NF-κB and Keap1/Nrf2 pathways via suppressing AHR signalling.

4 Discussion

Increasing publications have suggested that TCM improved various diseases by regulating AHR signalling (Wen et al., 2023b; Ying et al., 2024; Zhang et al., 2023; Wang et al., 2024). Accumulated evidence has showed increasing serum AHR activity in CKD patients (Dou et al., 2018; Kim et al., 2013; Kim et al., 2020). Dou et al. demonstrated that CKD patients with stages 3–5 showed strong serum AHR-activating potential and upregulated mRNA levels of *CYP1A1* and *AHR repressor* in whole blood compared to serum from healthy controls (Dou et al., 2018). Kim et al. demonstrated that serum AHR transactivation activity was higher in DKD patients with microalbuminuria and macroalbuminuria than in those with normoalbuminuria (Kim et al. (2013), indicating that high serum AHR transactivation is a high risk factor for DKD. The same research group further demonstrated that serum AHR transactivation activity was increased in non-dialysis CKD patients compared to patients on dialysis, whereas its activity was increased in patients undergoing hemodialysis compared to undergoing peritoneal dialysis (Kim et al., 2020). Hemodialysis treatment could decrease AHR transactivation activity in patients with hemodialysis dialysis (Kim et al., 2020). Some studies have shown hyperactive AHR signalling in renal tissues of CKD patients and animal models (Miao et al., 2020; Miao et al., 2022; Cao et al., 2022; Miao et al., 2024). First, our previous study demonstrated

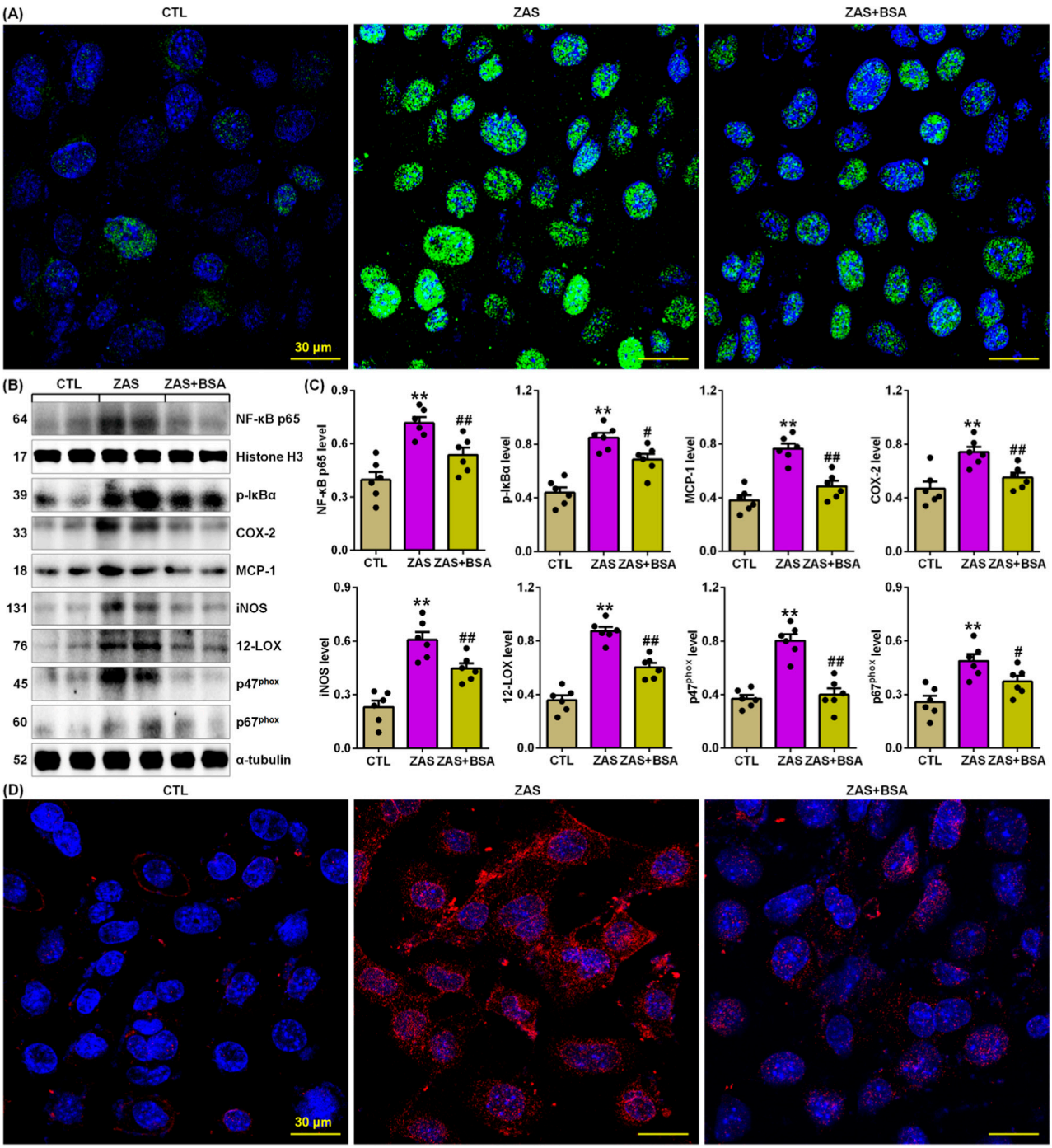


FIGURE 3
BSA inhibits activation of IκB/NF-κB pathway in the ZAS-stimulated MPC5 cells. **(A)** Immunofluorescence analysis with anti-p65 antibody in the control and ZAS-stimulated MPC5 cells with or without BSA. **(B)** Protein expression of p-IκBα and nuclei p65 and its downstream gene products including COX-2, MCP-1, iNOS, 12-LOX, $p47^{phox}$ and $p67^{phox}$ in the control and ZAS-stimulated MPC5 cells with or without BSA. **(C)** Protein levels of p-IκBα, NF-κB p65, COX-2, MCP-1, iNOS, 12-LOX, $p47^{phox}$ and $p67^{phox}$ in the control and ZAS-stimulated MPC5 cells with or without BSA. **(D)** Immunofluorescence analysis with and COX-2 antibody in the control and ZAS-stimulated MPC5 cells with or without BSA. $^{*}P < 0.05$, $^{**}P < 0.01$ compared with CTL; $^{\#}P < 0.05$, $^{\#\#}P < 0.01$ compared with ZAS-stimulated MPC5 cells.

increased intrarenal mRNA expression of *AHR* and its genes, such as *CYP1A1*, *CYP1A2* and *CYP1B1* in CKD patients at five stages, accompanied by elevating AHR nuclear translocation (Miao et al., 2022). Second, our previous study revealed elevated intrarenal AHR nuclear translocation in patients with DKD, IgAN and IMN (Miao et al., 2020). Our latest study further showed increased intrarenal mRNA expression of *AHR* and its genes, including *CYP1A1*, *CYP1A2* and *CYP1B1* in patients with IMN, accompanied by elevated AHR nuclear translocation (Miao et al., 2024; Wang et al., 2023). Similar findings were also

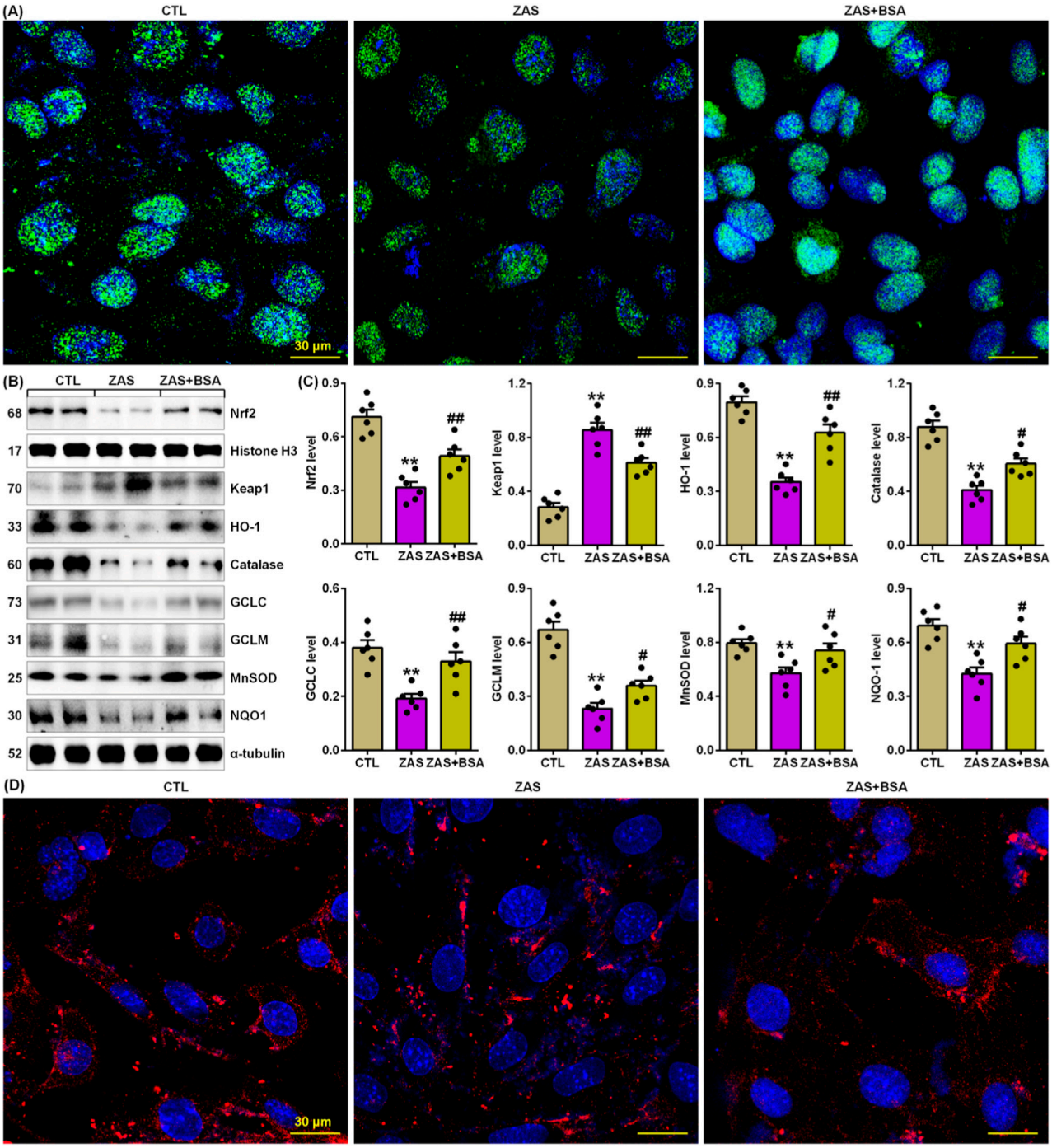


FIGURE 4
BSA improves impairment of Keap1/Nrf2 pathway in the ZAS-stimulated MPC5 cells. **(A)** Immunofluorescence analysis with anti-Nrf2 antibody in the control and ZAS-stimulated MPC5 cells with or without BSA. **(B)** Protein expression of Nrf2, Keap1, HO-1, catalase, GCLC, GCLM, MnSOD and NQO-1 in the control and ZAS-stimulated MPC5 cells with or without BSA. **(C)** Protein levels of Nrf2, Keap1, HO-1, catalase, GCLC, GCLM, MnSOD and NQO-1 in the control and ZAS-stimulated MPC5 cells with or without BSA. **(D)** Immunofluorescence analysis with anti-HO-1 antibody in the control and ZAS-stimulated MPC5 cells with or without BSA. $^{*}P < 0.05$, $^{**}P < 0.01$ compared with CTL; $^{\#}P < 0.05$, $^{\#\#}P < 0.01$ compared with ZAS-stimulated MPC5 cells.

demonstrated in several rat or mice models treated with NX, adenine, unilateral ureteral obstruction and cationic bovine serum albumin (CBSA) (Miao et al., 2020; Cao et al., 2022; Miao et al., 2022). These data show that AHR signalling is activated in various pathological types of CKD. Therefore, AHR is a promising therapeutic target for improving renal function in CKD patients.

Natural products have been demonstrated to be effective therapies for intervention in glomerular-related diseases including glomerulonephritis (Wang et al., 2021; Zhao et al., 2022b; Qin et al., 2023), DKD (Huang et al., 2022; Li et al., 2022b; Liu et al., 2022b; Pei et al., 2022) and IMN (Miao et al., 2024; Wang et al., 2023). In this study, we identified BSA as an AHR

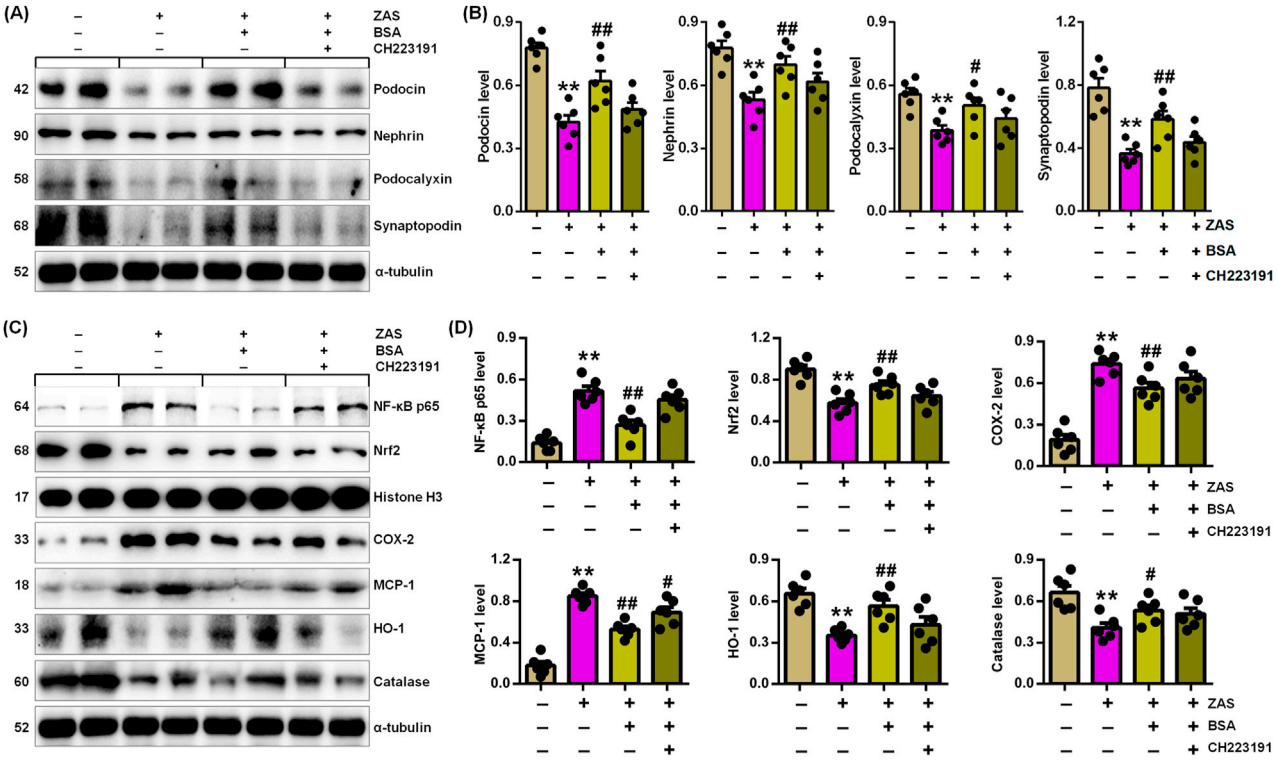


FIGURE 5
BSA inhibits podocyte injury through improving IκB/NF-κB and Keap1/Nrf2 pathways via AHR signalling in the ZAS-induced MPC5 cells with BSA and/or CH223191. **(A)** Podocyte-specific protein expression in the ZAS-induced MPC5 cells with BSA and/or CH223191. **(B)** Podocyte-specific protein levels in the ZAS-induced MPC5 cells with BSA and/or CH223191. **(C)** Protein expression of NF-κB p65, Nrf2, COX-2, MCP-1, HO-1 and catalase in the ZAS-induced MPC5 cells with BSA and/or CH223191. **(D)** Protein levels of NF-κB p65, Nrf2, COX-2, MCP-1, HO-1 and catalase in the ZAS-induced MPC5 cells with BSA and/or CH223191. $^{*}P < 0.05$, $^{**}P < 0.01$ compared with CTL; $^{\#}P < 0.05$, $^{\#\#}P < 0.01$ compared with ZAS-stimulated MPC5 cells.

antagonist and it could ameliorate podocyte lesion through improving IκB/NF-κB and Keap1/Nrf2 pathways (Figure 7). BSA inhibited the mRNA expression of *AHR*, *CYP1A1*, *CYP1A2*, *CYP1B1* and *COX-2* in ZAS-stimulated MPC5 cells, which was accompanied by inhibiting nuclear translocation of AHR. Accumulating evidence suggests that many natural product-derived components can directly regulate AHR signalling. Previous studies have shown that AHR ligands from vegetable extracts mediate *CYP1A1* activity (Zhao et al., 2019). Cruciferous family members, including broccoli, cauliflower, white cabbage, and Brussels sprouts, contain rich sources of AHR ligands, such as indole-3-carbinol and indole-3-acetonitrile (Zhao et al., 2019). Polyphenols are common components of the plant kingdom. Polyphenols are divided into five categories according to their chemical structures: phenolic acids, flavonoids, lignans, tannins and stilbenes. Extensive studies have demonstrated that phenolic acids and flavonoids are the most affluent polyphenolic components in diet and can be classified into flavanols, flavonols, flavones, flavanones, isoflavones, anthocyanins and proanthocyanidins (Zhao et al., 2019).

Recent studies suggested that TCM including Bupi Yishen formula, Dahuang Fuzi decoction and Jian-Pi-Yi-Shen formula attenuated CKD by inhibiting AHR signalling (Mo et al., 2021; Gu et al., 2022; Liu et al., 2022a). Our previous publications have demonstrated that some compounds such as matairesinol, rhoifolin, 5,6,7,8,3′,4′-hexamethoxyflavone, 5,7,3′,4′,5′-pentahydroxy flavanone and erythro-guaiacylglycerol-β-ferulic acid ether attenuated renal fibrosis by suppressing AHR signalling (Miao et al., 2020; Cao et al., 2022; Miao et al., 2022). BSA is a flavonoid glycoside. Previous studies suggested that BSA could decrease the activities of superoxide scavenging and xanthine oxidase, as well as inhibit the protein expression of extracellular matrix proteins, including collagen I, α-smooth muscle actin, and fibronectin in NRK-52E cells mediated by 1-aminopyrene (Karim et al., 2009; Miao et al., 2020). Our previous study showed that BSA inhibited mRNA expression of *AHR*, *CYP1A1*, *CYP1A2* and *CYP1B1* in renal tissues of NX-induced rats and NRK-52E cells mediated by 1-aminopyrene, which was accompanied by the protein expression of upregulated cytoplasmic AHR and downregulated nuclear AHR (Miao et al., 2020). Molecular ligand docking analysis revealed that BSA could bind to the active AHR site and exhibited a strong interaction with AHR. Collectively, the current study and other studies suggest that BSA is an effective AHR antagonist and suppresses AHR expression using *in vivo* and *in vitro* experiments (Figure 7).

Mechanistically, this study further illuminated that treatment with BSA mitigated podocyte lesion by suppressing hyperactive IκB/NF-κB pathway and enhancing impaired Keap1/Nrf2 pathway via

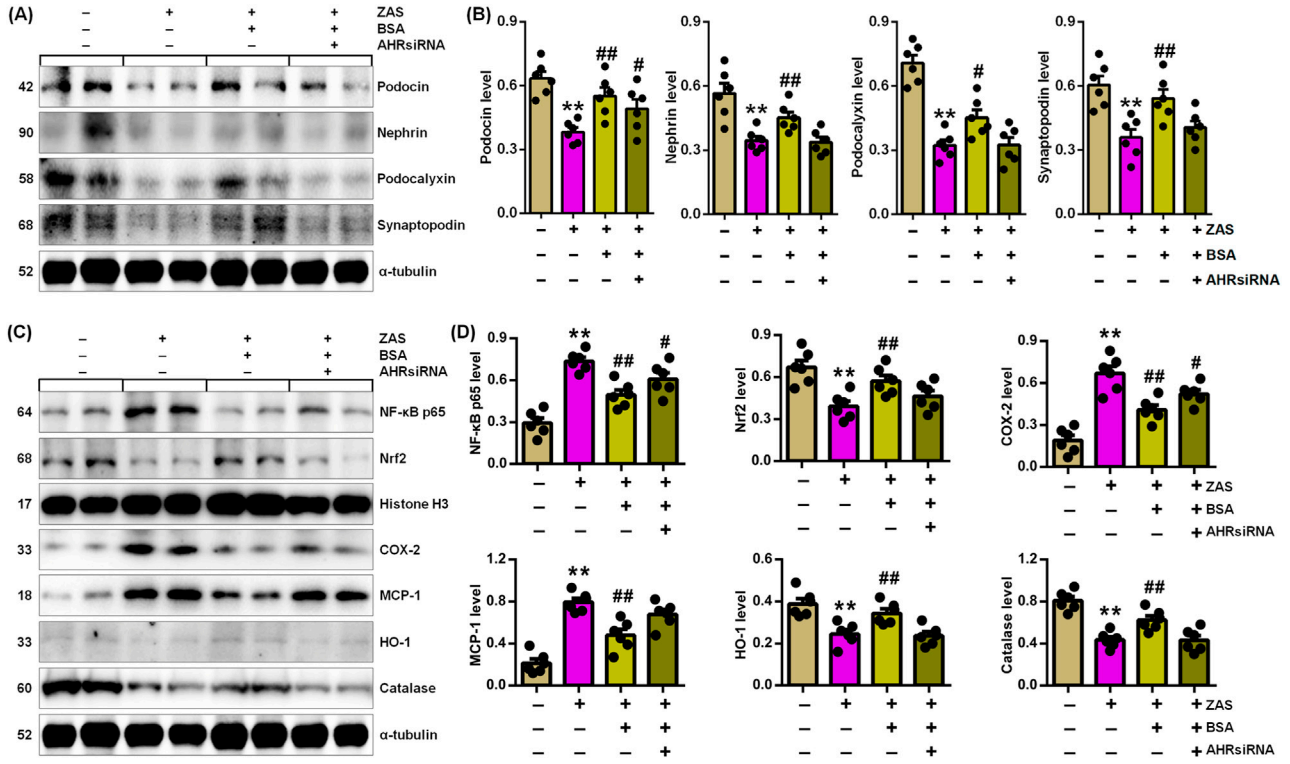


FIGURE 6
BSA inhibits podocyte injury through improving IκB/NF-κB and Keap1/Nrf2 pathways via AHR signalling in the ZAS-induced AHRsiRNA-transfected MPC5 cells treated with BSA. **(A)** Podocyte-specific protein expression in the ZAS-induced AHRsiRNA-transfected MPC5 cells treated with BSA. **(B)** Podocyte-specific protein levels in the ZAS-induced AHRsiRNA-transfected MPC5 cells treated with BSA. **(C)** Protein expression of NF-κB p65, Nrf2, COX-2, MCP-1, HO-1 and catalase in the ZAS-induced AHRsiRNA-transfected MPC5 cells treated with BSA. **(D)** Protein levels of NF-κB p65, Nrf2, COX-2, MCP-1, HO-1 and catalase in the ZAS-induced AHRsiRNA-transfected MPC5 cells treated with BSA. $^{*}P < 0.05$, $^{**}P < 0.01$ compared with CTL; $^{\#}P < 0.05$, $^{\#\#}P < 0.01$ compared with ZAS-stimulated MPC5 cells.

inhibiting AHR signalling in the ZAS-stimulated MPC5 cells (Figure 7). Both oxidative stress and inflammation change expression of a number of genes, including *NF-κB* and *Nrf2*. Our latest study showed that the NF-κB signalling was a downstream target of AHR pathway in IMN (Wang et al., 2023). Several studies have demonstrated that AHR interacts with NF-κB in CKD (Addi et al., 2019; Brito et al., 2019; Curran and Kopp, 2022). Brito et al. reported that increasing AHR protein levels were positively associated with increasing NF-κB protein levels in hemodialysis and non-dialysis-dependent patients (Brito et al., 2019). Our latest study showed increased protein expression of nuclear AHR and cytoplasmic COX-2 in the renal tissues of IMN patients (Wang et al., 2023). In addition, increased protein expression of nuclear AHR and cytoplasmic COX-2 was observed in renal tissues of rats treated with CBSA and ZAS-mediated MPC5 cells (Ma et al., 2023; Wang et al., 2023). Treatment with Moshen granules inhibited their expression in the renal tissues of rats treated with CBSA (Ma et al., 2023). Addi et al. demonstrated that an AHR ligand indole-3 acetic acid mediated activating tissue factor via AHR/NF-κB pathway (Addi et al., 2019). This research group further revealed that COX-2 levels were markedly suppressed in indole-3 acetic acid-induced umbilical vein endothelial cells treated with BAY 11-7082 and CH223191 (Dou et al., 2015). In addition, Lee et al. reported that ochratoxin A-treated HK-2 cells showed increased mRNA expression of *AHR* and its target genes, such as *CYP1A1* and *CYP1A2* representing phase I enzymes, as well as upregulated mRNA expression of phase II enzymes, such as *GCLC*, *NQO1* and *HO-1* by the activation of Nrf2 translocation (Lee et al., 2018). However, AHR deficiency ameliorates oxidative stress-induced macrophage infiltration, activating mesangial cell and kidney fibrosis in DKD mice (Lee et al., 2016).

Accumulated evidence has reported that renoprotective effect of natural products were associated with suppressing AHR, IκB/NF-κB and Keap1/Nrf2 pathways. Dhulkifle et al. reported that treatment with 6-formylindolo(3,2-b)carbazole improved septic acute kidney injury and inflammation by increasing intrarenal mRNA expression of *H O -1* and *NQO1* via *AHR* and *Nrf2* (Dhulkifle et al., 2023). Recent publication showed that Dahuang Fuzi decoction blunted CKD by suppressing AHR/NF-κB pathway (Gu et al., 2022). Moreover, Zhao et al. showed that the beneficial effect of Tangshen formula for NF-κB p-p65 expression was related to AHR inhibition in renal tissues of DKD rats (Zhao et al., 2020). Our earlier publication showed that poricoic acids abolished AHR, IκB/NF-κB and Keap1/Nrf2 pathways in mice with renal fibrosis (Wang et al., 2020). Collectively, this study demonstrated that BSA dampened podocyte lesion partly by modulating IκB/NF-κB and Keap1/Nrf2 pathways via attenuating AHR signalling.

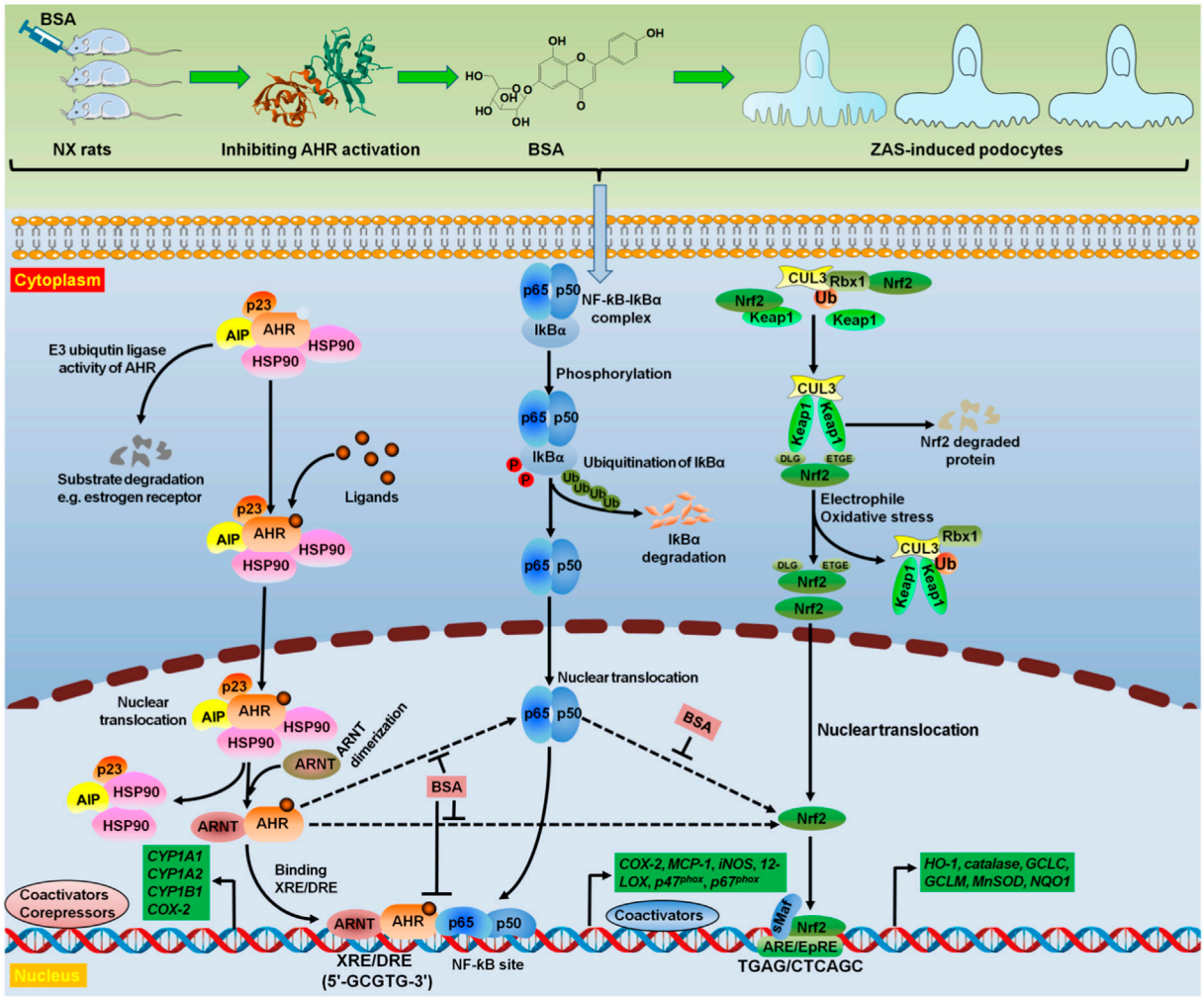


FIGURE 7
BSA as a novel AHR antagonist targeted oxidative stress and inflammation. Treatment with BSA suppressed intrarenal AHR expression at both mRNA and protein levels in NX rats. Hyperactive AHR and IκB/NF-κB pathways and impaired Keap1/Nrf2 pathway were demonstrated in the ZAS-stimulated MPC5 cells. However, treatment with BSA could suppress hyperactive AHR and IκB/NF-κB pathways and enhance impaired Keap1/Nrf2 pathway in the ZAS-stimulated MPC5 cells. Mechanistically, both pharmacological and genetic methods suggested that BSA ameliorated podocyte injury by improving IκB/NF-κB and Keap1/Nrf2 pathways via AHR signalling. Therefore, BSA suppressed intrarenal AHR expression at both mRNA and protein levels by using *in vivo* and *in vitro* experiments. BSA was demonstrated to be as a high-affinity AHR antagonist that abolished oxidative stress and inflammation. AIP, AHR interacting protein; ARE, antioxidant response element; ARE/EpRE antioxidant/electrophile response element; ARNT, aryl hydrocarbon receptor nuclear translocator; CUL3, Cullin3; HSP90, heat shock protein 90; Rbx1, ring-Box 1; sMaf, small musculoaponeurotic fibrosarcoma; Ub, ubiquitin.

5 Conclusion

In conclusion, this study showed that treatment with BSA suppressed AHR expression at both the mRNA and protein levels in the renal tissues of NX rats and ZAS-stimulated MPC5 cells. We further illuminated that BSA mitigated podocyte lesion by suppressing hyperactive IκB/NF-κB pathway and enhancing hypoactive Keap1/Nrf2 pathway via inhibiting AHR signalling in the ZAS-stimulated MPC5 cells. Mechanistically, both pharmacological and genetic results suggested that BSA ameliorated podocyte damage by modulating IκB/NF-κB and Keap1/Nrf2 pathways via AHR signalling. Therefore, BSA is a high-affinity AHR antagonist that abolishes oxidative stress and inflammation. These findings may provide a leading drug for treating podocyte damage-related renal disease through oxidative stress and inflammation.

Data availability statement

The original contributions presented in the study are included in the article/Supplementary Material, further inquiries can be directed to the corresponding authors.

Ethics statement

The animal study was approved by Zhejiang Chinese Medical University. The study was conducted in accordance with the local

legislation and institutional requirements. No potentially identifiable images or data are presented in this study.

Author contributions

X-JL: Data curation, Investigation, Project administration, Supervision, Writing–review and editing. Y-NW: Investigation, Resources, Software, Supervision, Visualization, Writing–review and editing. W-FW: Data curation, Investigation, Supervision, Validation, Writing–review and editing. XN: Software, Supervision, Writing–review and editing. HM: Conceptualization, Funding acquisition, Project administration, Software, Supervision, Visualization, Writing–review and editing. Y-YZ: Conceptualization, Data curation, Funding acquisition, Methodology, Project administration, Software, Supervision, Validation, Writing–original draft.

Funding

The author(s) declare that financial support was received for the research, authorship, and/or publication of this article. This study was supported by the National Natural Science Foundation of China (Nos 82074002, 82274079, and 82274192), the National Key Research and Development Program of China (No. 2019YFC1709405) and the Shaanxi Key Science and Technology Plan Project (No. 2023-ZDLSF-26).

Conflict of interest

The authors declare that the research was conducted in the absence of any commercial or financial relationships that could be construed as a potential conflict of interest.

The author(s) declared that they were an editorial board member of Frontiers, at the time of submission. This had no impact on the peer review process and the final decision.

Publisher's note

All claims expressed in this article are solely those of the authors and do not necessarily represent those of their affiliated organizations, or those of the publisher, the editors and the reviewers. Any product that may be evaluated in this article, or claim that may be made by its manufacturer, is not guaranteed or endorsed by the publisher.

Supplementary material

The Supplementary Material for this article can be found online at: https://www.frontiersin.org/articles/10.3389/fphar.2024.1386604/full#supplementary-material

References

Addi, T., Poitevin, S., McKay, N., El Mecherfi, K. E., Kheroua, O., Jourde-Chiche, N., et al. (2019). Mechanisms of tissue factor induction by the uremic toxin indole-3 acetic acid through aryl hydrocarbon receptor/nuclear factor-kappa B signaling pathway in human endothelial cells. *Arch. Toxicol.* 93 (1), 121–136. doi:10.1007/s00204-018-2328-3

Brito, J. S., Borges, N. A., Anjos, J. S. D., Nakao, L. S., Stockler-Pinto, M. B., Paiva, B. R., et al. (2019). Aryl hydrocarbon receptor and uremic toxins from the gut microbiota in chronic kidney disease patients: is there a relationship between them? *Biochemistry* 58 (15), 2054–2060. doi:10.1021/acs.biochem.8b01305

Cao, G., Miao, H., Wang, Y. N., Chen, D. Q., Wu, X. Q., Chen, L., et al. (2022). Intrarenal 1-methoxypyrene, an aryl hydrocarbon receptor agonist, mediates progressive tubulointerstitial fibrosis in mice. *Acta Pharmacol. Sin.* 43 (11), 2929–2945. doi:10.1038/s41401-022-00914-6

Curran, C. S., and Kopp, J. B. (2022). Aryl hydrocarbon receptor mechanisms affecting chronic kidney disease. *Front. Pharmacol.* 13, 782199. doi:10.3389/fphar.2022.782199

da Silva, J. F., Bolsoni, J. A., da Costa, R. M., Alves, J. V., Bressan, A. F. M., Silva, L. E. V., et al. (2022). Aryl hydrocarbon receptor (AhR) activation contributes to high-fat diet-induced vascular dysfunction. *Br. J. Pharmacol.* 179 (12), 2938–2952. doi:10.1111/bph.15789

Dhulkifle, H., Sayed, T. S., Abunada, H. H., Abulola, S. M., Alhoshani, A., Korashy, H. M., et al. (2023). 6-Formylindolo(3,2-b)carbazole dampens inflammation and reduces endotoxin-induced kidney injury via Nrf2 activation. *Chem. Res. Toxicol.* 36 (3), 552–560. doi:10.1021/acs.chemrestox.3c00002

Dou, L., Poitevin, S., Sallee, M., Addi, T., Gondouin, B., McKay, N., et al. (2018). Aryl hydrocarbon receptor is activated in patients and mice with chronic kidney disease. *Kidney Int.* 93 (4), 986–999. doi:10.1016/j.kint.2017.11.010

Dou, L., Sallee, M., Cerini, C., Poitevin, S., Gondouin, B., Jourde-Chiche, N., et al. (2015). The cardiovascular effect of the uremic solute indole-3 acetic acid. *J. Am. Soc. Nephrol.* 26 (4), 876–887. doi:10.1681/asn.2013121283

Goya-Jorge, E., Jorge Rodríguez, M. E., Veitía, M. S., and Giner, R. M. (2021). Plant occurring flavonoids as modulators of the aryl hydrocarbon receptor. *Molecules* 26 (8), 2315. doi:10.3390/molecules26082315

Gu, M., Ying, P., Miao, Z., Yu, X., Bao, R., Xiao, J., et al. (2022). Treatment of modified Dahuang Fuzi decoction on cognitive impairment induced by chronic kidney disease through regulating AhR/NF-κB/JNK signal pathway. *Evid. Based Complement. Altern. Med.* 2022, 8489699. doi:10.1155/2022/8489699

Hou, J. J., Zhang, Z. J., Wu, W. Y., He, Q. Q., Zhang, T. Q., Liu, Y. W., et al. (2022). Mass spectrometry imaging: new eyes on natural products for drug research and development. *Acta Pharmacol. Sin.* 43 (12), 3096–3111. doi:10.1038/s41401-022-00990-8

Hu, J., Gu, W., Ma, N., Fan, X., and Ci, X. (2022). Leonurine alleviates ferroptosis in cisplatin-induced acute kidney injury by activating the Nrf2 signalling pathway. *Br. J. Pharmacol.* 179 (15), 3991–4009. doi:10.1111/bph.15834

Huang, D., Shen, P., Wang, C., Gao, J., Ye, C., and Wu, F. (2022). Calycosin plays a protective role in diabetic kidney disease through the regulation of ferroptosis. *Pharm. Biol.* 60 (1), 990–996. doi:10.1080/13880209.2022.2067572

Karim, A., Noor, A. T., Malik, A., Qadir, M. I., and Choudhary, M. I. (2009). Barlerisides A and B, new potent superoxide scavenging phenolic glycosides from Barleria acanthoides. *J. Enzyme Inhib. Med. Chem.* 24 (6), 1332–1335. doi:10.3109/14756360902887046

Kim, J. T., Kim, S. H., Min, H. K., Jeon, S. J., Sung, S. A., Park, W. H., et al. (2020). Effect of dialysis on aryl hydrocarbon receptor transactivating activity in patients with chronic kidney disease. *Yonsei Med. J.* 61 (1), 56–63. doi:10.3349/ymj.2020.61.1.56

Kim, J. T., Kim, S. S., Jun, D. W., Hwang, Y. H., Park, W. H., Pak, Y. K., et al. (2013). Serum arylhydrocarbon receptor transactivating activity is elevated in type 2 diabetic patients with diabetic nephropathy. *J. Diabetes Investig.* 4 (5), 483–491. doi:10.1111/jdi.12081

Kong, Y. D., Qi, Y., Cui, N., Zhang, Z. H., Wei, N., Wang, C. F., et al. (2023). The traditional herb *Polygonum hydropiper* from China: a comprehensive review on phytochemistry, pharmacological activities and applications. *Pharm. Biol.* 61 (1), 799–814. doi:10.1080/13880209.2023.2208639

Lee, H. J., Pyo, M. C., Shin, H. S., Ryu, D., and Lee, K. W. (2018). Renal toxicity through AhR, PXR, and Nrf2 signaling pathway activation of ochratoxin A-induced oxidative stress in kidney cells. *Food Chem. Toxicol.* 122, 59–68. doi:10.1016/j.fct.2018.10.004

Lee, W. J., Liu, S. H., Chiang, C. K., Lin, S. Y., Liang, K. W., Chen, C. H., et al. (2016). Aryl hydrocarbon receptor deficiency attenuates oxidative stress-related mesangial cell activation and macrophage infiltration and extracellular matrix accumulation in diabetic nephropathy. *Antioxid. Redox Signal* 24 (4), 217–231. doi:10.1089/ars.2015.6310

Li, C., Jia, W. W., Yang, J. L., Cheng, C., and Olaleye, O. E. (2022a). Multi-compound and drug-combination pharmacokinetic research on Chinese herbal medicines. *Acta Pharmacol. Sin.* 43 (12), 3080–3095. doi:10.1038/s41401-022-00983-7

Li, J., Zhang, J., Yang, M., Huang, X., Zhang, M., Fang, X., et al. (2022b). Kirenol alleviates diabetic nephropathy via regulating TGF-β/Smads and the NF-κB signal pathway. *Pharm. Biol.* 60 (1), 1690–1700. doi:10.1080/13880209.2022.2112239

Li, M. Z., Zhao, Y., Wang, H. R., Talukder, M., and Li, J. L. (2021). Lycopene preventing DEHP-induced renal cell damage is targeted by aryl hydrocarbon receptor. *J. Agric. Food Chem.* 69 (43), 12853–12861. doi:10.1021/acs.jafc.1c05250

Liu, X., Deng, R., Chen, Y., Huang, S., Lu, J., Zheng, L., et al. (2022a). Jian-Pi-Yi-Shen Formula improves adenine-induced chronic kidney disease via regulating tryptophan metabolism and aryl hydrocarbon receptor signaling. *Front. Pharmacol.* 13, 922707. doi:10.3389/fphar.2022.922707

Liu, X. Q., Jiang, L., Li, Y. Y., Huang, Y. B., Hu, X. R., Zhu, W., et al. (2022b). Wogonin protects glomerular podocytes by targeting Bcl-2-mediated autophagy and apoptosis in diabetic kidney disease. *Acta Pharmacol. Sin.* 43 (1), 96–110. doi:10.1038/s41401-021-00721-5

Ma, S.-X., Li, X.-J., Duan, T.-T., Pei, M., Zou, L., Yu, X.-Y., et al. (2023). Moshen granule ameliorates membranous nephropathy by regulating NF-ƙB/Nrf2 pathways via aryl hydrocarbon receptor signalling. *Heliyon* 9 (9), e20019. doi:10.1016/j.heliyon.2023.e20019

Marena, G. D., Ramos, M., Carvalho, G. C., Junior, J. A. P., Resende, F. A., Corrêa, I., et al. (2022). Natural product-based nanomedicine applied to fungal infection treatment: a review of the last 4 years. *Phytother. Res.* 36 (7), 2710–2745. doi:10.1002/ptr.7460

Miao, H., Cao, G., Wu, X. Q., Chen, Y. Y., Chen, D. Q., Chen, L., et al. (2020). Identification of endogenous 1-aminopyrene as a novel mediator of progressive chronic kidney disease via aryl hydrocarbon receptor activation. *Br. J. Pharmacol.* 177 (15), 3415–3435. doi:10.1111/bph.15062

Miao, H., Wang, Y. N., Yu, X. Y., Zou, L., Guo, Y., Su, W., et al. (2024). Lactobacillus species ameliorate membranous nephropathy through inhibiting the aryl hydrocarbon receptor pathway via tryptophan-produced indole metabolites. *Br. J. Pharmacol.* 181 (1), 162–179. doi:10.1111/bph.16219

Miao, H., Wu, X. Q., Wang, Y. N., Chen, D. Q., Chen, L., Vaziri, N. D., et al. (2022). 1-Hydroxypyrene mediates renal fibrosis through aryl hydrocarbon receptor signalling pathway. *Br. J. Pharmacol.* 179 (1), 103–124. doi:10.1111/bph.15705

Mo, Y., Hu, D., Yu, W., Ji, C., Li, Y., Liu, X., et al. (2023). Astragaloside IV attenuates indoxyl sulfate-induced injury of renal tubular epithelial cells by inhibiting the aryl hydrocarbon receptor pathway. *J. Ethnopharmacol.* 308, 116244. doi:10.1016/j.jep.2023.116244

Mo, Y., Jie, X., Wang, L., Ji, C., Gu, Y., Lu, Z., et al. (2021). Bupi Yishen formula attenuates kidney injury in 5/6 nephrectomized rats via the tryptophan-kynurenic acid-aryl hydrocarbon receptor pathway. *BMC Complement. Med. Ther.* 21 (1), 207. doi:10.1186/s12906-021-03376-1

Newman, D. J., and Cragg, G. M. (2020). Natural products as sources of new drugs over the nearly four decades from 01/1981 to 09/2019. *J. Nat. Prod.* 83 (3), 770–803. doi:10.1021/acs.jnatprod.9b01285

Ouyang, L., Yan, B., Liu, Y., Mao, C., Wang, M., Liu, N., et al. (2020). The deubiquitylase UCHL3 maintains cancer stem-like properties by stabilizing the aryl hydrocarbon receptor. *Signal Transduct. Target Ther.* 5 (1), 78. doi:10.1038/s41392-020-0181-3

Pei, D., Tian, S., Bao, Y., Zhang, J., Xu, D., and Piao, M. (2022). Protective effect of salidroside on streptozotocin-induced diabetic nephropathy by inhibiting oxidative stress and inflammation in rats via the Akt/GSK-3β signalling pathway. *Pharm. Biol.* 60 (1), 1732–1738. doi:10.1080/13880209.2022.2116055

Qin, X., Chen, H., Zhu, X., Xu, X., and Gao, J. (2023). Identification of Rab7 as an autophagy marker: potential therapeutic approaches and the effect of Qi Teng Xiao Zhuo granule in chronic glomerulonephritis. *Pharm. Biol.* 61 (1), 1120–1134. doi:10.1080/13880209.2023.2233998

Ren, Q., Tao, S., Guo, F., Wang, B., Yang, L., Ma, L., et al. (2021). Natural flavonol fisetin attenuated hyperuricemic nephropathy via inhibiting IL-6/JAK2/STAT3 and TGF-β/SMAD3 signaling. *Phytomedicine* 87, 153552. doi:10.1016/j.phymed.2021.153552

Shao, Y. F., Tang, B. B., Ding, Y. H., Fang, C. Y., Hong, L., Shao, C. X., et al. (2023). Kaempferide ameliorates cisplatin-induced nephrotoxicity via inhibiting oxidative stress and inducing autophagy. *Acta Pharmacol. Sin.* 44 (7), 1442–1454. doi:10.1038/s41401-023-01051-4

Singh, B., Kumar, A., Singh, H., Kaur, S., Arora, S., and Singh, B. (2022). Protective effect of vanillic acid against diabetes and diabetic nephropathy by attenuating oxidative stress and upregulation of NF-κB, TNF-α and COX-2 proteins in rats. *Phytother. Res.* 36 (3), 1338–1352. doi:10.1002/ptr.7392

Sun, M. Y., Ye, H. J., Zheng, C., Jin, Z. J., Yuan, Y., and Weng, H. B. (2023). Astragalin ameliorates renal injury in diabetic mice by modulating mitochondrial quality control via AMPK-dependent PGC1α pathway. *Acta Pharmacol. Sin.* 44 (8), 1676–1686. doi:10.1038/s41401-023-01064-z

Wang, M., Hu, H. H., Chen, Y. Y., Chen, L., Wu, X. Q., and Zhao, Y. Y. (2020). Novel poricoic acids attenuate renal fibrosis through regulating redox signalling and aryl hydrocarbon receptor activation. *Phytomedicine* 79, 153323. doi:10.1016/j.phymed.2020.153323

Wang, X., Xie, X., Li, Y., Xie, X., Huang, S., Pan, S., et al. (2024). Quercetin ameliorates ulcerative colitis by activating aryl hydrocarbon receptor to improve intestinal barrier integrity. *Phytother. Res.* 38 (1), 253–264. doi:10.1002/ptr.8027

Wang, Y. N., Miao, H., Hua, M. R., Yang, J. Z., Pei, M., Yu, H. X., et al. (2023a). Moshen granule ameliorates membranous nephropathy by blocking intrarenal renin-angiotensin system signalling via the Wnt1/β-catenin pathway. *Phytomedicine* 114, 154763. doi:10.1016/j.phymed.2023.154763

Wang, Y. N., Miao, H., Yu, X. Y., Guo, Y., Su, W., Liu, F., et al. (2023b). Oxidative stress and inflammation are mediated via aryl hydrocarbon receptor signalling in idiopathic membranous nephropathy. *Free Radic. Biol. Med.* 207, 89–106. doi:10.1016/j.freeradbiomed.2023.07.014

Wang, Y. W., Zeng, Q., and Yu, R. H. (2021). Treatment of membranoproliferative glomerulonephritis with traditional Chinese medicine and rituximab: a case report. 8, 3.doi:10.4103/imna.imna_10_21Integr Med Nephrol Androl. 8 3

Wen, S. Y., Wei, B. Y., Ma, J. Q., Wang, L., and Chen, Y. Y. (2023a). Phytochemicals, biological activities, molecular mechanisms, and future prospects of *Plantago asiatica* L. *J. Agric. Food Chem.* 71 (1), 143–173. doi:10.1021/acs.jafc.2c07735

Wen, Y., Zhan, Y., Tang, S., Liu, F., Wu, R., Kong, P., et al. (2023b). Zhizhu decoction alleviates slow transit constipation by regulating aryl hydrocarbon receptor through gut microbiota. *Pharm. Biol.* 61 (1), 111–124. doi:10.1080/13880209.2022.2157020

Wu, S. M., Tsai, J. J., Pan, H. C., Arbiser, J. L., Elia, L., and Sheu, M. L. (2022). Aggravation of pulmonary fibrosis after knocking down the aryl hydrocarbon receptor in the insulin-like growth factor 1 receptor pathway. *Br. J. Pharmacol.* 179 (13), 3430–3451. doi:10.1111/bph.15806

Ying, Y., Song, L. Y., Pang, W. L., Zhang, S. Q., Yu, J. Z., Liang, P. T., et al. (2024). Astragalus polysaccharide protects experimental colitis through an aryl hydrocarbon receptor-dependent autophagy mechanism. *Br. J. Pharmacol.* 181 (5), 681–697. doi:10.1111/bph.16229

Yuan, Q., Tang, B., and Zhang, C. (2022). Signaling pathways of chronic kidney diseases, implications for therapeutics. *Signal Transduct. Target Ther.* 7 (1), 182. doi:10.1038/s41392-022-01036-5

Zhang, C., Fan, S., Zhao, J. Q., Jiang, Y., Sun, J. X., and Li, H. J. (2023). Transcriptomics and metabolomics reveal the role of CYP1A2 in psoralen/isopsoralen-induced metabolic activation and hepatotoxicity. *Phytother. Res.* 37 (1), 163–180. doi:10.1002/ptr.7604

Zhao, H., Chen, L., Yang, T., Feng, Y. L., Vaziri, N. D., Liu, B. L., et al. (2019). Aryl hydrocarbon receptor activation mediates kidney disease and renal cell carcinoma. *J. Transl. Med.* 17 (1), 302. doi:10.1186/s12967-019-2054-5

Zhao, T., Zhang, H., Yin, X., Zhao, H., Ma, L., Yan, M., et al. (2020). Tangshen formula modulates gut microbiota and reduces gut-derived toxins in diabetic nephropathy rats. *Biomed. Pharmacother.* 129, 110325. doi:10.1016/j.biopha.2020.110325

Zhao, Y., Deng, S., Bai, Y., Guo, J., Kai, G., Huang, X., et al. (2022a). Promising natural products against SARS-CoV-2: structure, function, and clinical trials. *Phytother. Res.* 36 (10), 3833–3858. doi:10.1002/ptr.7580

Zhao, Y. L., Zhang, X. H., Guo, F., Wei, Y., Shang, J. H., and Luo, X. D. (2022b). Yi Shen An, a Chinese traditional prescription, ameliorates membranous glomerulonephritis induced by cationic bovine serum albumin in rats. *Pharm. Biol.* 60 (1), 163–174. doi:10.1080/13880209.2021.2021947

Zhou, W., Chen, M. M., Liu, H. L., Si, Z. L., Wu, W. H., Jiang, H., et al. (2022). Dihydroartemisinin suppresses renal fibrosis in mice by inhibiting DNA-methyltransferase 1 and increasing Klotho. *Acta Pharmacol. Sin.* 43 (10), 2609–2623. doi:10.1038/s41401-022-00898-3

frontiers | Frontiers in Pharmacology

TYPE Original Research
PUBLISHED 24 September 2024
DOI 10.3389/fphar.2024.1463864

Check for updates

OPEN ACCESS

EDITED BY
Wei Cai,
Hunan University of Medicine, China

REVIEWED BY
Cynthia G. Suarez,
Finzelberg GmbH & Co., KG, Germany
Laiba Arshad,
Forman Christian College, Pakistan

*CORRESPONDENCE
Bingyue Yang,
bingyyang@126.com

RECEIVED 12 July 2024
ACCEPTED 05 September 2024
PUBLISHED 24 September 2024

CITATION
Zhou K, Peng L, Jing Y, Luo Y, Yan Y, Zhang G, Guo Q and Yang B (2024) Comparison of the difference in the anti-inflammatory activity of two different color types of Farfarae Flos based on *in vitro*, *in vivo* experiments and untargeted metabolomics.
Front. Pharmacol. 15:1463864.
doi: 10.3389/fphar.2024.1463864

COPYRIGHT
© 2024 Zhou, Peng, Jing, Luo, Yan, Zhang, Guo and Yang. This is an open-access article distributed under the terms of the Creative Commons Attribution License (CC BY). The use, distribution or reproduction in other forums is permitted, provided the original author(s) and the copyright owner(s) are credited and that the original publication in this journal is cited, in accordance with accepted academic practice. No use, distribution or reproduction is permitted which does not comply with these terms.

Comparison of the difference in the anti-inflammatory activity of two different color types of Farfarae Flos based on *in vitro*, *in vivo* experiments and untargeted metabolomics

Kexin Zhou[1,2], Liang Peng[1,2], Yiyao Jing[1,2], Yao Luo[1,2], Yonggang Yan[1,2], Gang Zhang[1,2], Qi Guo[1,2] and Bingyue Yang[1,2]*

[1]Shaanxi Qinling Application Development and Engineering Center of Chinese Herbal Medicine, College of Pharmacy, Shaanxi University of Chinese Medicine, Xi'an, China, [2]Key Laboratory for Research of "Qin Medicine" of Shaanxi Administration of Traditional Chinese Medicine, Xi'an, China

Introduction: Due to its remarkable anti-inflammatory pharmacological activity, Farfarae Flos has gained extensive usage in the treatment of various inflammatory diseases such as bronchitis, pneumonia, prostatitis and colitis. And Farfarae Flos come in two color types depending on the color of the flowers: yellowish-white (YW), and purplish-red (PR). However, the difference in anti-inflammatory activity and metabolic profiles between the two flower colors remains unexplored.

Methods: This study aims to explore the difference in the anti-inflammatory potential between YW and PR variants of Farfarae Flos and unravel the mechanisms responsible for the observed differences in anti-inflammatory activity through an integrated approach encompassing untargeted metabolomics and *in vivo*/*vitro* experimental studies. Initially, we verified the contrasting effects of YW and PR on the inhibition of the inflammatory factors interleukin-6 (IL-6) and nitric oxide (NO) by utilizing an *in vitro* RAW 264.7 cell inflammation model. Subsequently, a comprehensive evaluation of the systemic inhibitory capacity of YW and PR on IL-6, Interleukin-10 (IL-10), and tumor necrosis factor-α (TNF-α) was conducted using a validated whole-body mouse model, followed by the analysis of inflammatory factors and histological examination of collected serum, liver, and spleen after 7 days. Furthermore, non-targeted metabolomics profiling was employed to analyze the metabolite profiles of Farfarae Flos with different colors, and quantitative analysis was conducted to identify differential metabolites between YW and PR. The correlation between the anti-inflammatory activities of differentially accumulated metabolites (DAMs) and Farfarae Flos was investigated, resulting in the identification of 48 compounds exhibiting significant anti-inflammatory activity. Additionally, KEGG pathway enrichment analysis was performed to elucidate the underlying mechanisms.

Results: Our findings demonstrate that both YW and PR possess anti-inflammatory abilities, with PR exhibiting significantly superior efficacy. The integration of *in vivo*/*vitro* experiments and non-targeted metabolomics confirmed the exceptional anti-inflammatory potential of PR and solidified its classification as the "purplish-red better" of Farfarae Flos.

Discussion: This study provides valuable insights into the breeding and medical transformation of Farfarae Flos varieties, along with a scientific basis for the establishment of quality standards and the development of new drugs utilizing Farfarae Flos.

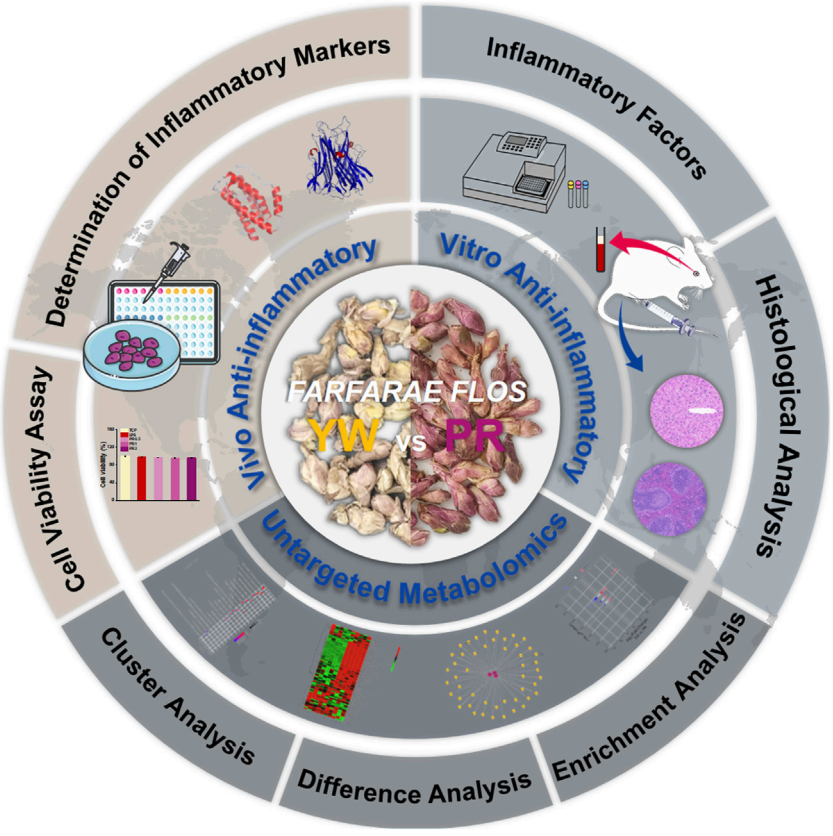
KEYWORDS

Farfarae Flos, anti-inflammatory, non-targeted metabolomics, interleukin-6 (IL-6) inhibition, nitric oxide (NO) inhibition

1 Introduction

Inflammation, a fundamental pathological process triggered by internal or external stimuli, is categorized into acute and chronic inflammation (Kany et al., 2019). Acute inflammation, usually resolves spontaneously, while chronic inflammation is characterized by excessive production of inflammatory factors such as nitric oxide (NO), tumor necrosis factor-α (TNF-α), and interleukin-6 (IL-6) (Kapellos et al., 2019; Tanaka et al., 2020). Inflammatory responses are closely associated with various diseases, including cardiovascular, metabolic diseases, neurodegenerative disorders, and other inflammatory conditions such as chronic gastritis, rheumatoid arthritis, inflammatory bowel disease, and cancer (Pan et al., 2021; Sugimoto et al., 2019). Although a moderate inflammatory response is beneficial for the body's defense against harmful stimuli, excessive or prolonged inflammation can lead to numerous detrimental effects, including fever, redness, tumors, pain and loss of function. In fact, in clinical settings, widely employed anti-inflammatory medications like aspirin and ibuprofen are frequently linked to side effects and allergic responses (Bellón, 2019; Braun et al., 2020; Moore et al., 2019).

In contrast to Western medicines, the use of herbal medicine is steeped in ancient history, with its origins tracing back over millennia (Nunes et al., 2020; Shin et al., 2020). Today, natural and herbal substances continue to receive increasing attention due to their low side effects and cost-effectiveness (Yimer et al., 2019). In recent years, the anti-inflammatory effects of herbal medicine have been extensively studied. Numerous *in vivo*/*vitro* studies have demonstrated that herbal medicine exerts its anti-inflammatory effects by impeding key transcription factors, mitigating the activity of pro-inflammatory cytokines and chemokines, reducing intercellular adhesion molecule expression, and inhibiting the action of pro-inflammatory mediators (Li et al., 2020; Tasneem et al., 2019; Xin et al., 2019).



GRAPHICAL ABSTRACT

Tussilago farfara L., the only plant in the genus *Tussilago* L. in the family Asteraceae, is widely distributed across Asia, Europe and North Africa. The flower buds of *T. farfara* L. commonly known as Farfarae Flos, have long been used in traditional medicine to moisten the lungs, alleviate coughs, reduce phlegm, and lower airway inflammation (Xuan et al., 2020). Moreover, Farfarae Flos exhibits notable anti-inflammatory, anti-allergic, and anti-platelet aggregation properties (Liu et al., 2020). In China, the Farfarae Flos has been used in the form of dried flower buds from ancient times to the present day, and it is used in Chinese medicine as one of the essential medicines for relieving coughs and phlegm and asthma (Jang et al., 2019). In some European countries, indigenous people also use Farfarae Flos to treat coughs and colds. Nevertheless, they are more likely to use the leaves of the herb for the treatment of diseases of the gastrointestinal tract, wounds, burns, urinary and inflammatory damage in the eyes (Kalle et al., 2022). In recent years, Farfarae Flos and related compound preparations have displayed significant therapeutic effects on a wide range of inflammatory conditions, making it a critical species in the development of anti-inflammatory drugs. Numerous studies have identified various compounds in Farfarae Flos, including flavonoids, sterols, phenolic acids, alkaloids, polysaccharides, volatile oils, sesquiterpenoids, triterpenoids, and other bioactive components. The anti-inflammatory effects of key active monomeric components such as sesquiterpenoids (e.g., Tussilagone), flavonoids (e.g., kaempferol), sterols (e.g., ergosterol and β-sitosterol), and organic acids (e.g., chlorogenic acid, isochlorogenic acid, and caffeic acid) have been clinically validated (Chen et al., 2021; Ferrer et al., 2018; Jin et al., 2020; Song et al., 2019; Yang et al., 2020) (Figure 1).

It is well known that Farfarae Flos is dominated by two different colors, purplish-red (PR) and yellowish-white (YW), and the difference between the two colors is obvious and can be easily judged by visual performance. The difference in color often corresponds to variations in pharmacological activity (Zou et al., 2021). Traditionally, the criterion of "purplish-red better" has been employed to evaluate the quality of Farfarae Flos. However, precise studies explaining the regularity behind the superior anti-inflammatory activity of PR compared to YW are lacking. Hence, it is crucial to compare the anti-inflammatory activity between these two colors and conduct an in-depth investigation into the main components and material basis underlying the difference in their anti-inflammatory activity.

In this study, the difference in anti-inflammatory effects between YW and PR through *in vitro* experiments was initially determined. Furthermore, the anti-inflammatory effects of YW and PR were evaluated using a mouse systemic inflammation model, accompanied by histological analysis. Additionally, non-targeted metabolomics analysis was performed to assess the natural differences in metabolite types between YW and PR, and to investigate the reasons for the difference. The presence of differentially accumulated metabolites (DAMs) of YW and PR were annotated into the KEGG pathway, revealing that phenylpropanoid, flavonoid and flavonol, and sesquiterpene metabolism pathways were strongly associated with the anti-inflammatory activity of Farfarae Flos. Moreover, the correlation between anti-inflammatory activities and highly differentially accumulated metabolites (DAMs) of YW and PR was examined. A total of 48 compounds, including flavonoids, sesquiterpenes, sterols, and other compound types, exhibited high correlations with anti-inflammatory activities. These results underscore the correlation between the build up of secondary metabolites and the varying degrees of anti-inflammatory efficacy observed between YW and PR. In conclusion, this study provides comprehensive insights into the patterns and mechanisms underlying the contrasting anti-inflammatory effects of different colors of Farfarae Flos, offering valuable guidance for selecting Farfarae Flos varieties and facilitating its clinical application.

2 Experimental

2.1 Preparation of Farfarae Flos

Farfarae Flos was purchased from Shaanxi Best Enterprise Group. The herb material was identified by Prof. Hu Benxiang. The voucher specimens of Farfarae Flos were preserved in the herbarium of Shaanxi University of Chinese Medicine. All samples were divided into two groups, yellow-white (YW) (Figure 2A) and purplish-red (PR) (Figure 2B), using the color card as a control. Both groups were dried, crushed, and sieved through 40 mesh (pore size 0.425 mm), placed in paper bags and stored in a desiccator at room temperature.

2.2 Chemical solvents

All chemical solvents information can be found in Supplementary Material.

2.3 Preparation of extracts

Took 80 g of each kind of powder from purplish-red and yellowish-white Farfarae Flos, extracted with 85% ethanol for 1 h and filtered while hot, the residue was rinsed three times, concentrated under reduced pressure at 56°C to obtain the extracts of different groups. The extracts were dissolved in distilled water at established concentrations and were recorded as PR for the purplish-red flowers and YW for the yellowish-white flowers.

2.4 Biocompatibility test of YW and PR

Biocompatibility of YW and PR was evaluated by RAW 264.7 cells (Johnson et al., 1983). The cell viabilities of YW and PR were evaluated by alamarBlue® assay. First, RAW 264.7 cells underwent standard thawing procedures and were grown in a humidified incubator containing 5% CO_2 at 37°C for 24 h. The cells were passaged, and after the cells grown to 80% of their maximum density, RAW 264.7 cells were seeded in a 96-well plate at a density of 10,000 cells/well. After being cultured for 24 h, complete mediums containing YW and PR at different concentrations and colors were introduced into the wells. The details of the cytocompatibility evaluation were obtained in the Supplementary Material.

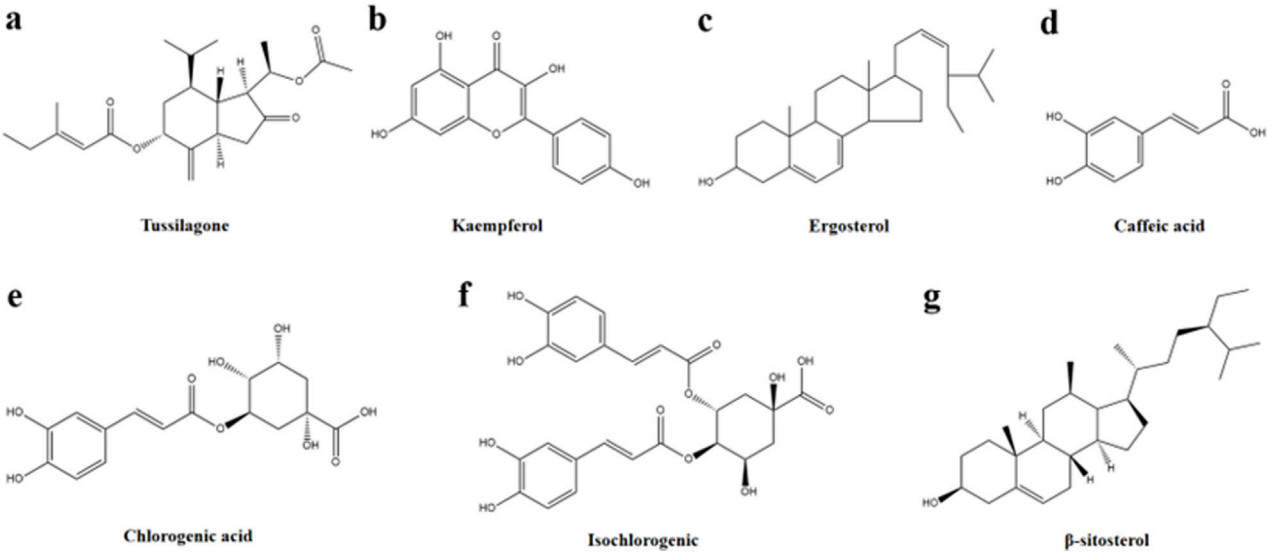


FIGURE 1
Chemical structures of compounds **(A–G)**.

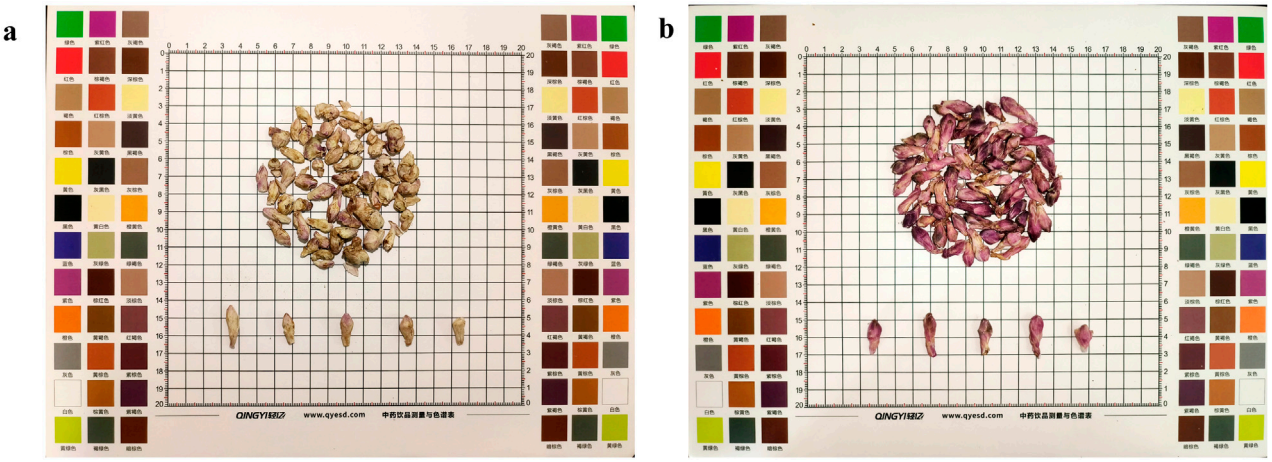


FIGURE 2
(A) A sample of dried YW of Farfarae Flos buds; **(B)** A sample of dried PR of Farfarae Flos buds.

2.5 Animal research

All animals (Kunming mice; 20 ± 2 g; half male and female) were domesticated in the animal laboratory for 7 days before the start of the animal tests. All animal experiments were conducted by the "Regulations on the Administration of Experimental Animals," the Chinese Animal Experiment Guidelines, and internationally accepted ethical principles for the use and care of experimental animals. The animal experiments involved in this study have been approved by the ethics committee (approval number: SUCMDL20220725001).

2.6 NO production assay

RAW 264.7 cells were seeded into 96-well plates at a density of 10,000 cells per well and incubated for 24 h. Subsequently, complete mediums containing YW and PR were introduced into the wells. After being co-incubated for another 24 h, cell suspensions were centrifuged and the cell culture supernatant was obtained. The NO content in the cell culture supernatant was determined by a commercial nitric oxide (NO) content assay. All operations strictly follow the manufacturer's instructions. Optical density (OD) readings of the samples were taken at 530 nm using a microplate reader to determine the NO levels in the supernatant.

2.7 ELISA test

ELISA kits were utilized to quantify the secretion levels of NO, TNF-α, IL-10, and IL-6 in RAW 264.7 cells induced by LPS. Initially, RAW 264.7 cells were plated at a seeding in 96-well plates and allowed to adhere for 12 h. Following attachment, the cells were treated with LPS at a concentration of 1 μg/mL and incubated together for 24 h. After incubation, the cell suspension was harvested and subjected to centrifugation at 1,200 rpm to separate the cell culture supernatant. The concentrations of NO, TNF-α, IL-10, and IL-6 in the supernatant were then determined according to the protocols provided with the ELISA kits. The assay was designed to permit up to 10 replicate measurements for each sample.

2.8 Anti-inflammatory test

After 7 days of adaptation, 90 KM mice were randomly assigned into 9 different groups (n = 10) randomly, including the TCP (tissue culture plate, means this group does not undergo any treatment) group (H_2O), LPS group (H_2O), positive group (Diclofenac Sodium 20 mg/kg), HYW group (High-dose group of YW), MYW group (Middle-dose group of YW), LYW group (Low-dose group of YW), HPR group (High-dose group of PR), MPR group (Middle-dose group of PR) and LPR group (Low-dose group of PR). The dosage of the above experimental groups: high-dose group (5 g/kg), medium-dose group (2.5 g/kg), low-dose group (1.25 g/kg), and all the dosages administered were equivalent to the crude drug. The dose was administered daily at 9:00 a.m. for 7 days. 2 h after the last dose, LPS (5 mg/kg) was injected intraperitoneally into the LPS and dosing groups, and 200 μL of PBS was injected into the TCP (without treatment) group. 2 h later, all mice were anesthetized, blood was taken from the eyes, and the serum was collected after immediate centrifugation. After the blood sampling was completed, the liver and spleen were quickly removed and preserved in a 4% paraformaldehyde solution.

2.9 Histological analysis

Histological analysis was performed by H&E staining. The livers and spleens of the mice were cleaned with saline, preserved in 4% paraformaldehyde, embedded in paraffin, and then sectioned. These sections were subsequently stained using Hematoxylin and Eosin (H&E) and observed and photographed using a microscope.

2.10 Metabolite extraction and UPLC-MS/MS analysis for the untargeted metabolomic analysis

Five samples of about 1 g each were taken from each of the two groups of Farfarae Flos, labeled yellowish-white 1–5 for the YW and purplish-red group 1–5 for the PR, wrapped in tin foil and stored in liquid nitrogen for quick-freezing until use. Take the appropriate amount of samples (50 mg) in a 2 mL EP tube, according to the sample processing method of metabolomics, the 5 groups of samples of YW and PR were further processed, and the detailed processing information, metabolic sample preparation and UPLC MS/MS chromatographic data can be found in the Supplementary Material.

2.11 Bioinformatic analysis of the untargeted metabolomic dataset

The bioinformatic examination of the untargeted metabolomic dataset was conducted using the XCMS and ProteoWizard software suites, alongside the CAMERA and metaX toolboxes, all these tools were implemented by using R software (see Supplementary Material for further details). The annotation of metabolites was facilitated through the use of the online KEGG and HMDB databases. In addition, an in-house library of metabolite fragment profiles was used to validate metabolite identification.

3 Results

3.1 Biocompatibility of YW and PR

Good cytocompatibility is the premise for YW and PR to achieve the medicinal effect. In this study, the biocompatibility of YW and PR was assessed by evaluating the cell viability of RAW 264.7 cells after treatment with these extracts *in vitro*. After 24 h of treatment with complete mediums containing YW and PR, the cell viability of all groups exceeded 90% (Figures 3A–D), indicating that the cell viability was not significantly inhibited by YW and PR treatment. Although the cell viability slightly decreased with increasing concentrations of YW and PR, there were no significant differences compared to the TCP group. Notably, the cell viability of RAW 264.7 cells remained above 90% even at an extract concentration of 2 mg/mL. Additionally, to exclude the impact of lipopolysaccharide (LPS)-induced polarization of RAW 264.7 cells, the cell viability of LPS-treated cells was tested after 24 h. Similarly, the reduction in cell viability after LPS treatment was negligible. Moreover, the cell viability after treatment with YW, PR, and LPS was comparable to that of the TCP group. In conclusion, YW and PR demonstrated favorable cytocompatibility.

3.2 Anti-inflammatory activity of YW and PR

As a cytokine mediating inflammatory immune response, IL-6 plays a critical role in the body's anti-infection immune response. To further confirm the inhibitory effect of Farfarae Flos extracts on inflammation, we evaluated the intracellular IL-6 levels of YW and PR after LPS treatment. IL-6 levels were significantly increased in RAW 264.7 cells after LPS treatment. As shown in Figures 4A–C, both YW and PR significantly reduced intracellular IL-6 levels compared to the LPS-treated group ($p < 0.0001$). The high-dose (2 mg/mL) groups of YW and PR exhibited significantly lower IL-6 levels compared to the medium-dose (1 mg/mL) group and low-dose (0.5 mg/mL) groups of YW and PR, indicating a dose-dependent increase in the anti-inflammatory capacity of both YW and PR. With the increase of the administered concentration, the IL-6 content in the cells showed a negative increase and the cellular inflammatory response was diminished.

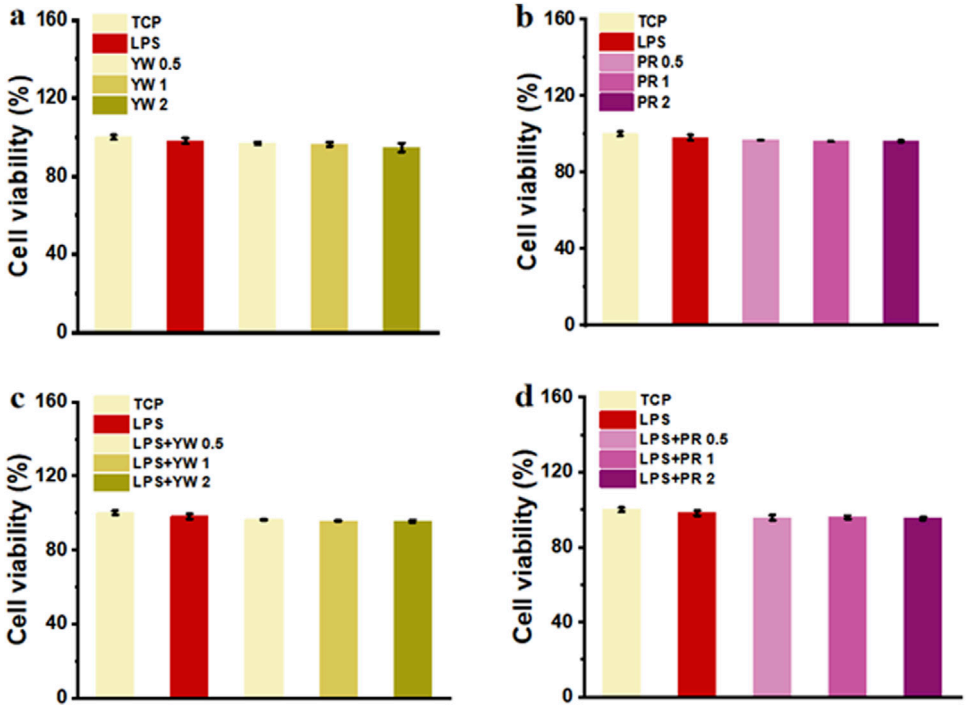


FIGURE 3
(A) Cell viability of YW from various groups; **(B)** Cell viability of PR from various groups; **(C)** Cell viability of YW with LPS treatment from various groups; **(D)** Cell viability of PR with LPS treatment from various groups.

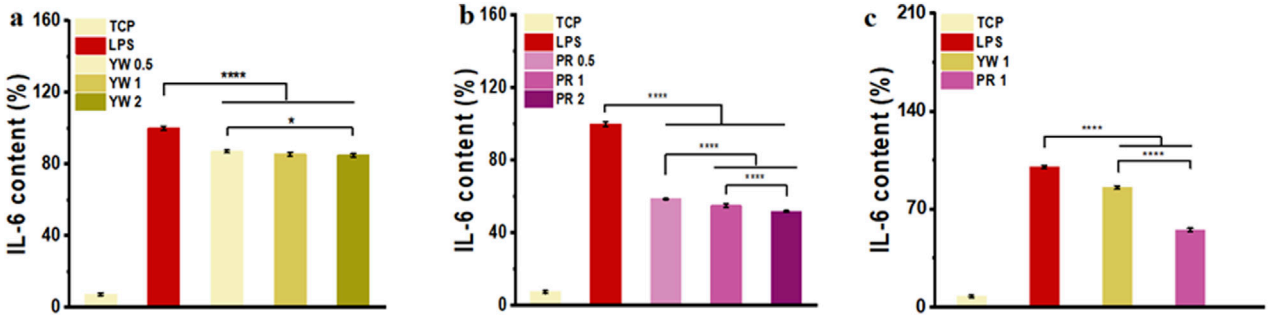


FIGURE 4
IL-6 content in the supernatant of RAW 264.7 cells treated with YW **(A)**, PR **(B)** at 0.5 mg/mL, 1 mg/mL and 2 mg/mL, IL-6 content in the supernatant of RAW 264.7 cells treated with YW and PR **(C)** at 1 mg/mL. (*$p < 0.05$, **$p < 0.01$, ***$p < 0.001$, ****$p < 0.0001$).

Most importantly, at the same concentration of YW, PR demonstrated a significantly greater reduction in IL-6 levels, highlighting its superior anti-inflammatory activity compared to YW ($p < 0.0001$).

Nitric oxide (NO) serves as a signaling molecule with inflammatory properties, regulating various physiological activities. In this study, the ability of YW and PR to scavenge NO was evaluated to verify their anti-inflammatory effects. As illustrated in Figures 5A–C, the LPS-treated group significantly induced NO production in RAW 264.7 cells compared to the TCP group. Compared to the LPS-treated group, both YW and PR were able to reduce the NO concentration significantly ($p < 0.0001$). At concentrations of 0.5 mg/mL, 1 mg/mL, and 2 mg/mL, YW reduced the NO concentration to 9.2 μmol/L, 9.1 μmol/L, and 7.1 μmol/L, respectively, which were significantly lower than the NO concentration in the LPS-treated group (16.8 μmol/L) (Figure 5A). PR also exhibited a dose-dependent increase in the inhibitory effect on NO concentration, with the high-dose group of PR reducing NO concentration to 4.18 μmol/L (Figure 5B), which was not statistically different comparable the TCP group (4.03 μmol/L). Furthermore, a significant difference was observed between YW and PR at high, medium, and low doses ($p < 0.05$). Additionally, when comparing the intracellular NO scavenging abilities of YW and PR at a concentration of 1 mg/mL, PR exhibited significantly stronger

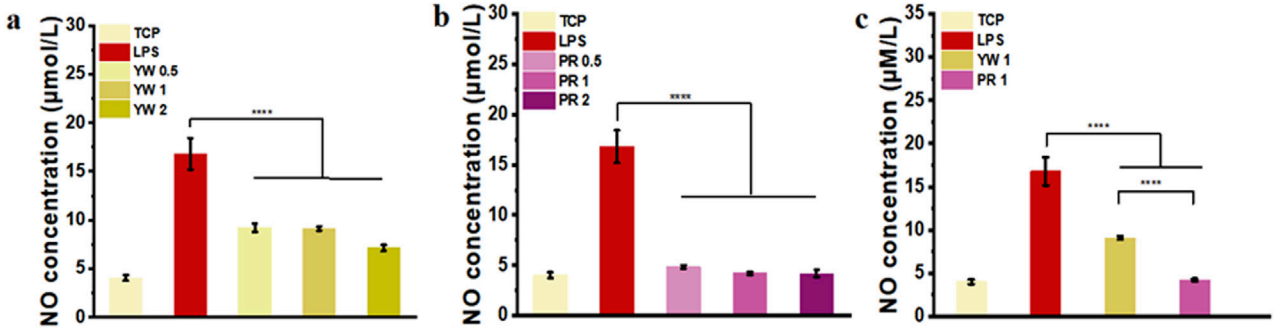


FIGURE 5
NO content in the supernatant of RAW 264.7 cells treated with **(A)** YW and **(B)** PR at concentrations of 0.5 mg/mL, 1 mg/mL and 2 mg/mL, respectively; **(C)** NO concentration in the supernatant of RAW 264.7 cells treated with YW and PR at concentrations of 1 mg/mL. (****$p < 0.0001$).

NO scavenging ability than YW ($p < 0.0001$, Figure 5C). These results confirm that PR had the best NO scavenging capacity, and it is worth mentioning that the reduced NO levels after administration via the high-dose group of PR could even reach the NO levels of the TCP group. Obviously, both YW and PR demonstrated desirable inhibitory effects on inflammation, with PR exhibiting superior anti-inflammatory activity compared to YW.

3.3 Therapeutic effects of the YW and PR on the model of systemic inflammation

Lipopolysaccharide (LPS) is a major component of bacterial outer membranes that causes inflammatory responses in disease and low doses of LPS in mice can induce systemic inflammation. After LPS treatment, the pro-inflammatory cytokines in the mice will increase in a short time. Therefore, to investigate the anti-inflammatory potential of Farfarae Flos, LPS was used to induce systemic acute inflammation in mice. Serum samples from different treatment groups were collected to measure the release of inflammatory cytokines IL-6, TNF-α, and IL-10, serving as indicators of the anti-inflammatory activity of YW and PR. We compared the inhibition of inflammatory factors in LPS-treated mice by YW and PR using mice administered without drugs as the TCP group, mice administered with LPS only as the control group and mice administered with Diclofenac Sodium Sustained Release Tablets as the positive group, as shown in Figures 6A–C. Quantitative data show that in comparison to the LPS control group, Administration of YW and PR at all tested doses suppressed the secretion of the pro-inflammatory cytokines IL-6 and TNF-α in mice. Likewise, all doses of YW and PR promoted the release of the anti-inflammatory cytokine IL-10. Notably, the release of IL-6, IL-10 and TNF-α in PR significantly differed from that in the TCP, control, positive and YW groups ($p < 0.0001$). In comparison to the control, positive control and high-dose group of YW, PR reduced the release of pro-inflammatory cytokine IL-6 by 46.29%, 20.33%, and 31.9%, respectively. The release of pro-inflammatory cytokine TNF-α decreased by 36.58%, 7.64%, and 22.16% correspondingly. Additionally, the expression of the anti-inflammatory factor IL-10 increased by 29.63%, 5.3%, and 14.86%. Consistent with the results in Section 3.2, the ability of YW and PR to regulate inflammatory factors in mouse serum improved with increasing doses. Moreover, PR demonstrated a superior anti-inflammatory effect on LPS-induced systemic inflammation in mice compared to YW, with the high-dose group of PR even outperforming the positive group. These results align with the findings of previous *in vitro* experiments. Hence, PR exhibits notable anti-inflammatory activity and holds significant therapeutic and clinical application potential. Further investigation is necessary at the molecular level to elucidate any differences in the anti-inflammatory activity between YW and PR and the underlying mechanisms.

3.4 Histological analysis

Histological sections of normal liver tissues showed normal lobular structure with central veins and radial hepatic cords accompanied by intact hepatocytes with a homogeneous distribution of cytoplasm. The control group showed marked morphological changes and fibrosis, as indicated by disruption of the histological structure, fibrous extension, formation of large fibrous septa, pseudobulbar separation and fibrous accumulation. Additionally, substantial hepatocyte degeneration, necrosis, hepatic sinusoidal dilatation, inflammatory cell infiltration, and cytoplasmic vacuole formation were observed. Treatment with YW and PR resulted in noticeable improvements in liver structure, as evidenced by reduced hepatic injury, inhibited hepatocyte degeneration and necrosis, and significant restoration of liver structure and function (Figure 7). Importantly, PR exhibited better protection against liver and spleen injury compared to YW.

3.5 Difference in metabolic components between YW and PR analyzed by UPLC-MS/MS

Our findings revealed that both YW and PR exhibited anti-inflammatory effects. However, PR demonstrated significantly superior activity compared to YW. Notably, the high-dose group of PR displayed the highest level of anti-inflammatory activity. Despite these results, the underlying mechanism responsible for

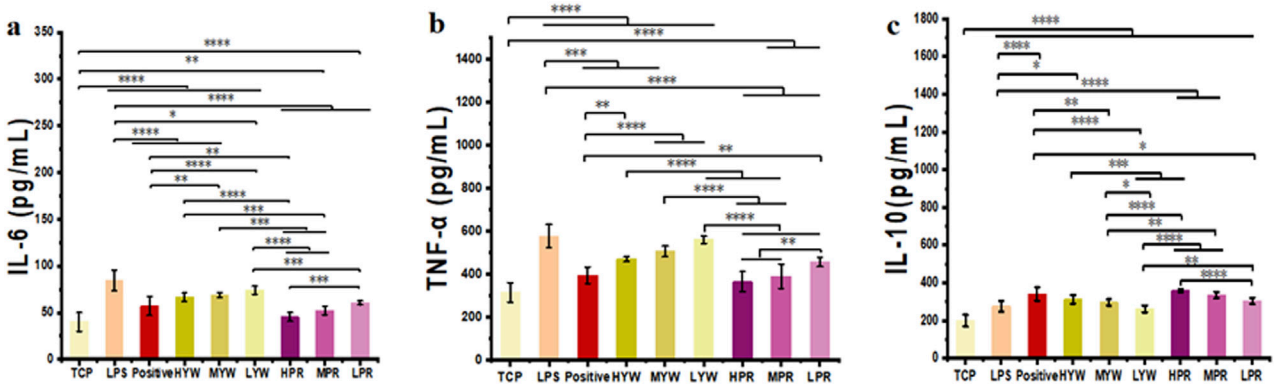


FIGURE 6
Content of **(A)** IL-6, **(B)** TNF-α and **(C)** IL-10 in mouse serum of TCP, control group, positive group and YW and PR (n = 10). (*$p < 0.05$, **$p < 0.01$, ***$p < 0.001$, ****$p < 0.0001$).

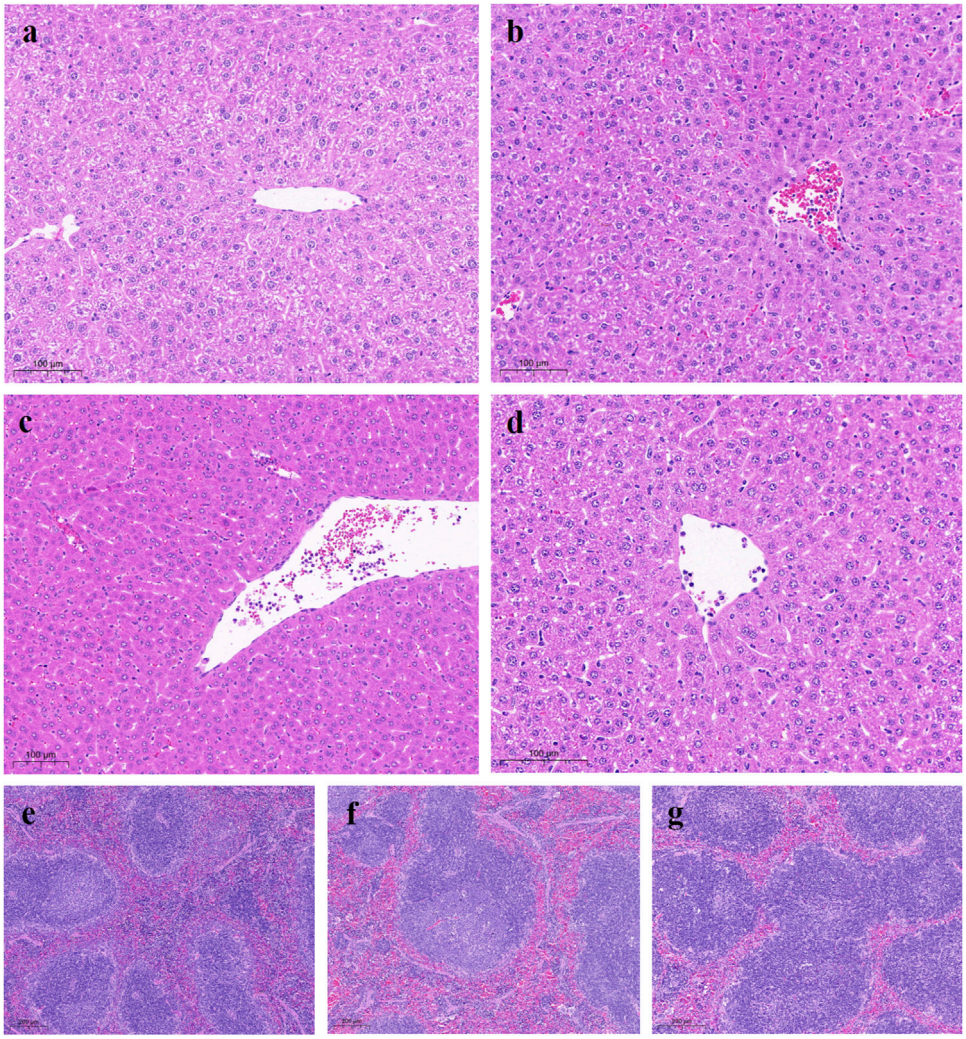


FIGURE 7
Representative microscopic images of H&E stained liver sections from all study groups. **(A)** Liver TCP group: liver showing normal tissue of hepatocytes and hepatic lobules; **(B)** Control group: mice liver with hepatocytes, most of which had cytoplasmic vacuoles; **(C)** High-dose group of YW: gradual recovery of hepatocytes; **(D)** High-dose group of PR: hepatic lobule structure was clearly restored; **(E)** Spleen TCP group; **(F)** Spleen positive group; **(G)** High-dose group of PR.

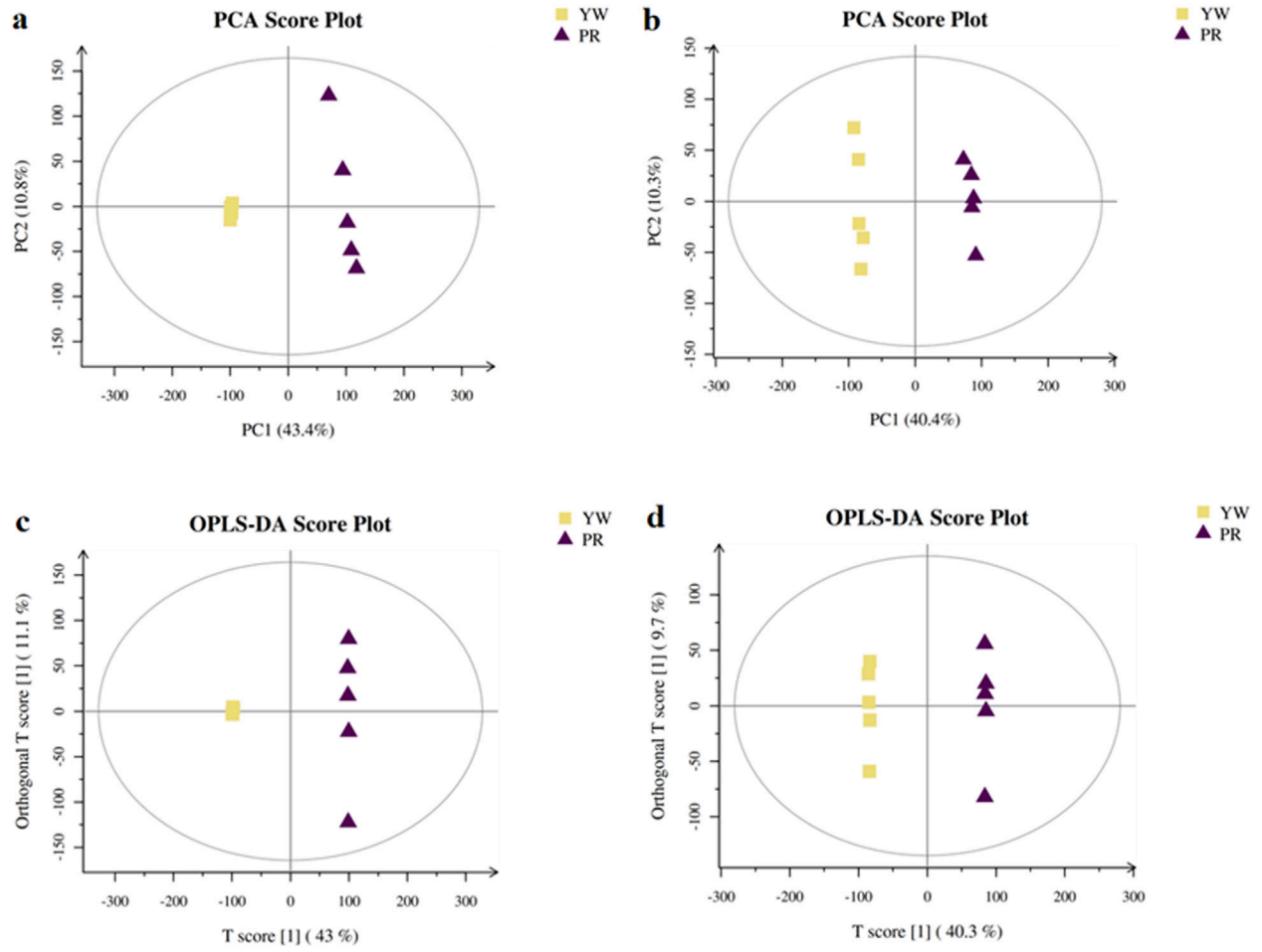


FIGURE 8
PCA scores plot of YW and PR in positive ion **(A)** and negative ion **(B)**; The OPLS-DA score plots in the positive ion mode **(C)** and negative ion mode **(D)**.

the difference in activity between YW and PR remains elusive. To gain further insight into the anti-inflammatory activity of Farfarae Flos at the molecular level, we employed an untargeted metabolomics approach to analyze the metabolite profiles of YW and PR.

3.5.1 Principal component analysis (PCA)

In this study, we investigated the metabolic differences between YW and PR using UPLC-MS/MS analysis. First, we performed unsupervised pattern recognition principal component analysis (PCA) to compare the overall distribution trends of secondary metabolites and assess whether there were any differences between YW and PR. As depicted in Figures 8A, B, the PCA 2D plots clearly showed two distinct clusters corresponding to YW and PR based on their spectral features. PR mainly clustered along the positive axis of PC1, while YW predominantly clustered along the negative axis of PC1. The coefficient of variation (CV) values were below 30%, indicating good reproducibility. In both positive and negative ion modes, PC1 and PC2 accounted for a significant amount of the variation, demonstrating that YW and PR could be easily differentiated. There was no overlap between the YW and PR clusters, suggesting substantial differences in metabolite profiles between the two groups. Thus, the PCA analysis confirmed a significant distinction in the metabolites of YW and PR.

3.5.2 Orthogonal partial least squares discriminant analysis (OPLS-DA)

To delve deeper into the metabolic distinctions between YW and PR, we used OPLS-DA as our analytical method. High predictability (Q^2) is a key parameter representing the predictive ability of the model, when $Q^2 > 0.9$ and the goodness of fit is strong, the OPLS-DA analytical model as well as the VIP values (Variable Importance Projections) generated by the model are stable, reliable and valid. As shown in Figures 8C, D, the Q^2 value of 0.957 indicated a clear separation between YW and PR metabolites, confirming a distinct trend of separation in their metabolite profiles.

3.6 Screening of differential metabolites, functional annotation, and enrichment analysis between the groups

Next, we conducted differential metabolite screening, functional annotation, and enrichment analysis to identify the most

10.3389/fphar.2024.1463864

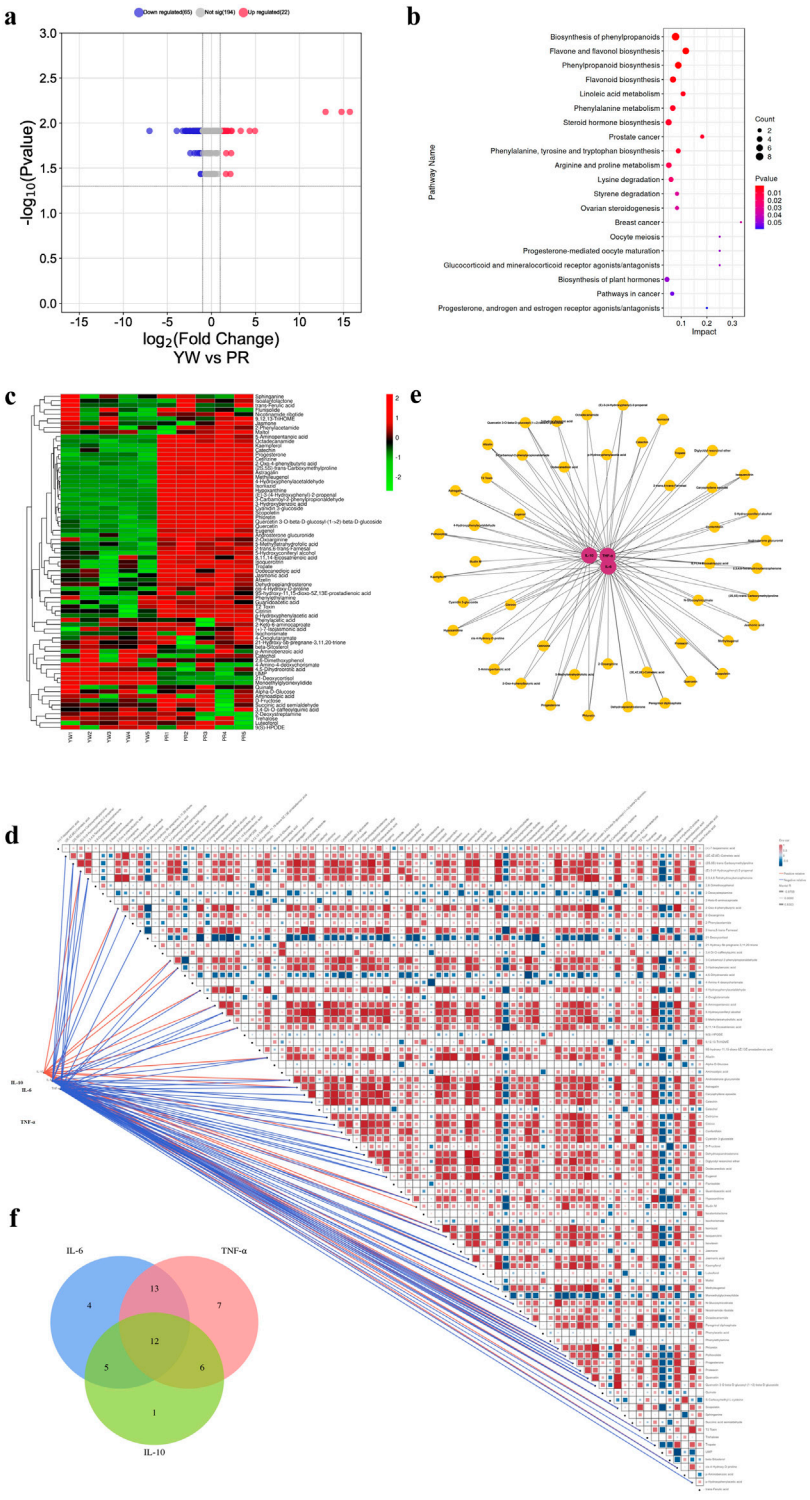


FIGURE 9
(A) Volcano plot of differential metabolites between YW and PR. Blue indicates downregulation, red indicates upregulation; **(B)** Pathway map of the top 20 KEGG metabolites annotated by DAMs; **(C)** Clustering heatmap of 87 DAMS. Green indicates downregulation, red indicates upregulation; **(D)** Correlation network diagram of 87 DAMs with three inflammatory factors (IL-6, TNF-α, IL-10); **(E)** Network map between metabolites and anti-inflammatory capacity. Red circles indicate different inflammatory factors, yellow circles indicate different metabolites, and the line connecting two circles indicates correlation ($r \geq 0.7$, $p < 0.028$); **(F)** Correlation of metabolites with three inflammatory factors in the Venn plot.

representative differential metabolites between YW and PR. Using UPLC-MS/MS qualitative and quantitative analysis, we identified 281 differential metabolites in YW and PR (VIP values ≥1, Fold change ≥2, $p \leq 0.05$). Compared with PR, the 87 DAMs in the samples of YW changed significantly. The volcano plot provided an overview of the distribution of differentially expressed metabolites, showcasing upregulated metabolites highlighted in red and downregulated metabolites depicted in blue, which can also serve as the functional analysis of metabolic pathways. As shown in Figure 9A, among the differential metabolites, 22 metabolites upregulated and 65 metabolites downregulated. These changed metabolites included flavonoids, alkaloids, phenolic acids, nucleotides, and their derivatives.

To gain insight into the biological functions associated with these differential metabolites, we performed KEGG metabolic pathway enrichment analysis using Metabo Analyst 5.0. The top 20 metabolic pathways enriched are represented as enrichment bubble plots as shown in Figure 9B.

3.7 Correlation analysis of the secondary metabolites in Farfarae Flos and their anti-inflammatory activity

Furthermore, we examined the correlation between the 87 DAMs and the anti-inflammatory activities (IL-6, TNF-α, and IL-10) to gain further insight into the anti-inflammatory components present in Farfarae Flos by using Spearman correlation coefficients. The clustering heatmap (Figure 9C) and correlation network diagram (Figure 9D) depicted the relationships between the 87 differential metabolites and the three inflammatory factors (IL-6, TNF-α, and IL-10). We identified 48 metabolites that were significantly correlated with anti-inflammatory activities ($|r| \geq 0.7$, $p < 0.028$), covering various compound types such as alkaloids, flavonoids, sterols, sesquiterpenes, coumarins, and others (Figure 9E). Analysis using Spearman correlation indicated that there was a positive correlation between 24 distinct metabolites and the anti-inflammatory cytokine IL-10. Conversely, 47 distinct metabolites showed a negative correlation with the pro-inflammatory cytokines IL-6 and TNF-α. Additionally, 12 differential metabolites showed correlations with all three inflammatory factors (Figure 9F). Table 1 provides the names and classifications of these 12 metabolites, including six flavonoids and flavonols, one coumarin, one sterol, one sesquiterpene, and three other compounds. Among them, Quercetin exhibited the highest correlation coefficient with IL-6 ($|r| = 0.977$), N-Glucosylnicotinate showed the highest correlation coefficient with TNF-α ($|r| = 0.966$), and the flavonoids Quercetin 3-O-beta-D-glucosyl-(1->2)-beta-D-glucoside, Afzelin, and Isoquercitrin displayed the highest correlation coefficients with IL-10 ($r = 0.830$). Based on the correlation analysis and multiple factors, we speculate that the differential content of these compounds may contribute to the observed differences in the anti-inflammatory capacity and pharmacological effects between YW and PR. In addition to flavonoids, alkaloids, and sesquiterpenes, coumarins (e.g., Scopoletin) and sterols (e.g., Progesterone) may also play significant roles as anti-inflammatory substances in Farfarae Flos.

4 Discussion

In recent years, the identification and quality control of medicinal flowers have remained crucial in botanical medicine research (Hadizadeh et al., 2022; Jeyaraj et al., 2022). Farfarae Flos has emerged as a valuable resource for anti-inflammatory drug development due to its rich content of various anti-inflammatory active ingredients such as flavonoids, sesquiterpenoids, and sterols (Yang et al., 2022). However, there is still a need for further exploration of its anti-inflammatory potential. The lack of uniform evaluation criteria for medication selection in clinics and limited understanding of the differences in anti-inflammatory activity between the two most common colors, yellowish-white (YW) and purplish-red (PR), necessitate further investigation. Although previous studies have explored that Farfarae Flos exerts anti-inflammatory effects through the regulation of Nrf2, NF-κB, and NLRP3 inflammasome (Aralbaeva et al., 2017; Kim et al., 2006; Xu et al., 2022), the underlying mechanisms contributing to the differential anti-inflammatory activity of different colors based on secondary metabolomics remain unexplored. Hence, to standardize the clinical use of Farfarae Flos and ensure efficacy and safety, there is an urgent need to investigate the variation in anti-inflammatory activity between YW and PR and understand the potential underlying mechanisms from the perspective of secondary metabolite accumulation.

In this study, we established a cellular inflammation model by inducing RAW 264.7 macrophages with lipopolysaccharide (LPS). The results demonstrated that both YW and PR effectively inhibit the release of inflammatory factors IL-6 and NO, and indicating initial differences in anti-inflammatory effects between the two variants. Furthermore, in an experimental model of systemic inflammation in mice, we observed that both YW and PR suppressed the release of pro-inflammatory cytokines IL-6 and TNF-α while promoting the release of the anti-inflammatory factor IL-10 in the serum of mice. Histological analysis confirmed that both YW and PR ameliorated liver and spleen damage induced by systemic inflammation. Notably, all of these results proved that PR consistently exhibited superior anti-inflammatory effects compared to YW, but the mechanisms underlying these differences in activity have not been found.

The metabolomics approach provided a valuable opportunity for a comprehensive investigation into the metabolic variations exhibited by Farfarae Flos collected at different stages, raw and processed Farfarae Flos (Cao et al., 2021; Li et al., 2018; Li et al., 2017). Therefore, we employed an untargeted metabolomic approach to analyze the metabolite profiles of YW and PR, aiming to further elucidate the anti-inflammatory activities of Farfarae Flos at the molecular level. The PCA and OPLS-DA results showed a large population difference and high separation between YW and PR, which further verified that there were significant anti-inflammatory activity differences between YW and PR in terms of characterization. Meanwhile, we also screened all the differential metabolites in YW and PR and found 281 differential metabolites. Screening these metabolites with VIP values ≥1, Fold change ≥2, $p \leq 0.05$, 22 metabolites displayed elevated levels in YW compared to PR, while 65 metabolites

TABLE 1 12 DAMs were screened out that are closely related to inflammatory factors.

Number	Compounds	Classifications
1	Quercetin 3-O-beta-D-glucosyl-(1->2)-beta-D-glucoside	Flavonoids and Flavonols
2	Phloretin	
3	Kaempferol	
4	Isoquercitrin	
5	Astragalin	
6	Afzelin	
7	Scopoletin	Coumarins
8	Progesterone	Sterols
9	Polhovolide	Sesquiterpenes
10	Hypoxanthine	Others
11	(E)-3-(4-Hydroxyphenyl)-2-propenal	
12	Androsterone glucuronide	

exhibited decreased levels. KEGG pathway analysis of these 87 differentially accumulated metabolites revealed enrichment in phenylpropanoid, flavonoid, flavonol, and sesquiterpene biosynthesis pathways. In our study, we identified that the biosynthesis of phenylpropanoids, flavonoids and flavonols, and sesquiterpenes represented key metabolic pathways contributing to the variation in metabolites observed between PR and YW. Among these, the phenylpropanoid biosynthesis pathway was found to be particularly significant (Zhang et al., 2021), This pathway encompasses the production of a variety of compounds, including lignans, phenylpropanoids, flavonoids, coumarins, and other substances, and it serves as a source of precursors for many of the plant's secondary metabolites. The phenylpropanoid pathway not only plays a pivotal role in plant growth and reproduction but also is involved in the plant's defense mechanisms against both biotic and abiotic environmental stresses (Lavhale et al., 2018). Moreover, they contribute to plant reproduction by the accumulation of flavonol and anthocyanin pigments in floral parts (Rahim et al., 2023). Significance analysis of KEGG allowed the identification of the main biological functions of the different metabolites. This information provides a foundation for further biological studies on Farfarae Flos. The results of conjoint analysis with anti-inflammatory activity showed that 48 DAMs out of 87 DAMs were significantly correlated with the anti-inflammatory activity of Farfarae Flos, as evidenced by the inhibition of pro-inflammatory cytokines IL-6 and TNF-α and promotion of anti-inflammatory cytokine IL-10. It is worth mentioning that our study unveiled the potential anti-inflammatory activity of coumarins (e.g., Scopoletin) and sterols (e.g., Progesterone) in addition to the established role of flavonoids, alkaloids, and sesquiterpenes in Farfarae Flos.

Our study highlights the excellent qualities of PR, particularly its superior anti-inflammatory activity. Experimental evidence has consistently demonstrated higher content of indicator components and greater anti-inflammatory activity in PR compared to YW, and explores the underlying mechanisms contributing to the important quality characteristic 'purplish-red better' of Farfarae Flos. Our experimental results will guide the subsequent clinical use of Farfarae Flos, for instance, in the treatment of inflammation, PR should be considered the primary choice. We speculate that the synergistic accumulation of key active ingredients and the regulation of effective secondary metabolites during bud development may be the main reasons for the quality of Farfarae Flos. While this study focused on exploring the difference in anti-inflammatory activity between YW and PR through a combination of *in vivo*/*vitro* experiments and non-targeted metabolomics, and confirmed that these differences may be related to the accumulation of secondary metabolites in YW and PR, but failed to provide explanations for the reasons for the difference in anti-inflammatory activity in terms of signaling pathways and other underlying molecular mechanisms. These potential mechanisms will be clarified in our next study.

5 Conclusion

Our study compared the difference in anti-inflammatory activity and accumulation of secondary metabolites between two distinct colors of Farfarae Flos using a comprehensive approach that incorporated *in vivo*/*in vitro* experiments alongside metabolomics analysis. It was confirmed that both YW and PR could inhibit the release of NO, IL-6, and TNF-α, while enhancing the expression of IL-10. Furthermore, they exhibited the capacity to mitigate inflammation-induced liver and spleen cell damage, thereby exerting significant anti-inflammatory properties. Notably, PR exhibited superior anti-inflammatory activity compared to YW. These differences in anti-inflammatory activity were closely associated with the accumulation of plant secondary metabolites. Our findings may provide the experimental basis for the clinical application of Farfarae Flos, and have promising implications for the selection of varieties and quality evaluation of Farfarae Flos.

Data availability statement

The raw data supporting the conclusion of this article will be made available by the authors, without undue reservation.

Ethics statement

The animal study was approved by the Shaanxi University of Chinese Medicine. The study was conducted in accordance with the local legislation and institutional requirements.

Author contributions

KZ: Data curation, Formal Analysis, Methodology, Project administration, Writing–original draft. LP: Formal Analysis, Methodology, Writing–original draft. YJ: Formal Analysis, Writing–review and editing. YL: Formal Analysis, Writing–review and editing. YY: Formal Analysis, Validation, Writing–review and editing. GZ: Formal Analysis, Validation, Writing–review and editing. QG: Supervision, Writing–review and editing. BY: Conceptualization, Data curation, Funding acquisition, Methodology, Writing–review and editing.

Funding

The author(s) declare financial support was received for the research, authorship, and/or publication of this article. This research was financially supported by (1) The National Natural Science Foundation of China (Grant No. 82204578). (2) General Project of Natural Science of Shaanxi Provincial Department of Science and Technology (2021JQ-733). (3) Shaanxi University of Traditional Chinese Medicine (2020 GP06). (4) Subject Innovation Team of Quality Control and Resources Development of "Qin drug" of Shaanxi University of Chinese Medicine (2019-QN01).

Conflict of interest

The authors declare that the research was conducted in the absence of any commercial or financial relationships that could be construed as a potential conflict of interest.

Publisher's note

All claims expressed in this article are solely those of the authors and do not necessarily represent those of their affiliated organizations, or those of the publisher, the editors and the reviewers. Any product that may be evaluated in this article, or claim that may be made by its manufacturer, is not guaranteed or endorsed by the publisher.

Supplementary material

The Supplementary Material for this article can be found online at: https://www.frontiersin.org/articles/10.3389/fphar.2024.1463864/full#supplementary-material

References

Aralbaeva, A. N., Mamataeva, A. T., Zhaparkulova, N. I., Utegalieva, R. S., Khanin, M., Danilenko, M., et al. (2017). A composition of medicinal plants with an enhanced ability to suppress microsomal lipid peroxidation and a protective activity against carbon tetrachloride-induced hepatotoxicity. *Biomed. Pharmacother.* 96, 1283–1291. doi:10.1016/j.biopha.2017.11.085

Bellón, T. (2019). Mechanisms of severe cutaneous adverse reactions: recent advances. *Drug Saf.* 42 (8), 973–992. doi:10.1007/s40264-019-00825-2

Braun, J., Baraliakos, X., and Westhoff, T. (2020). Nonsteroidal anti-inflammatory drugs and cardiovascular risk–a matter of indication. *Semin. Arthritis Rheum.* 50, 285–288. doi:10.1016/j.semarthrit.2019.07.012

Cao, J., Lu, Z., Qin, X., and Li, Z. (2021). Chemical comparison of the raw and processed Farfarae Flos by liquid chromatography-mass spectrometry based metabolomic approach. *J. Mass Spectrom.* 56 (2), e4697. doi:10.1002/jms.4697

Chen, S., Dong, L., Quan, H., Zhou, X., Ma, J., Xia, W., et al. (2021). A review of the ethnobotanical value, phytochemistry, pharmacology, toxicity and quality control of Tussilago farfara L.(coltsfoot). *J. Ethnopharmacol.* 267, 113478. doi:10.1016/j.jep.2020.113478

Ferrer, D. B., Venskutonis, P. R., Talou, T., Zebib, B., Ferrer, J. M. B., and Merah, O. (2018). Identification and *in vitro* activity of bioactive compounds extracted from Tussilago farfara (L.) plant grown in Lithuania and France. *Free Radicals Antioxid.* 8 (1), 40–47. doi:10.5530/fra.2018.1.7

Hadizadeh, H., Samiei, L., and Shakeri, A. (2022). Chrysanthemum, an ornamental genus with considerable medicinal value: a comprehensive review. *S. Afr. J. Bot.* 144, 23–43. doi:10.1016/j.sajb.2021.09.007

Jang, H., Ko, H., Song, K., and Kim, Y. S. (2019). A sesquiterpenoid from Farfarae Flos induces apoptosis of MDA-MB-231 human breast cancer cells through inhibition of JAK–STAT3 signaling. *Biomolecules* 9 (7), 278. doi:10.3390/biom9070278

Jeyaraj, E. J., Lim, Y. Y., and Choo, W. S. (2022). Antioxidant, cytotoxic, and antibacterial activities of Clitoria ternatea flower extracts and anthocyanin-rich fraction. *Sci. Rep.* 12 (1), 14890. doi:10.1038/s41598-022-19146-z

Jin, C., Ye, K., Luan, H., Liu, L., Zhang, R., Yang, S., et al. (2020). Tussilagone inhibits allergic responses in OVA-induced allergic rhinitis Guinea pigs and IgE-stimulated RBL-2H3 cells. *Fitoterapia* 144, 104496. doi:10.1016/j.fitote.2020.104496

Johnson, H., Northup, S., Seagraves, P., Garvin, P., and Wallin, R. (1983). Biocompatibility test procedures for materials evaluation *in vitro*. I. Comparative test system sensitivity. *J. Biomed. Mater. Res.* 17 (4), 571–586. doi:10.1002/jbm.820170403

Kalle, R., Pieroni, A., Svanberg, I., and Sõukand, R. (2022). Early citizen science action in ethnobotany: the case of the folk medicine collection of Dr. Mihkel Ostrov in the territory of present-day Estonia, 1891–1893. *Plants* 11 (3), 274. doi:10.3390/plants11030274

Kany, S., Vollrath, J. T., and Relja, B. (2019). Cytokines in inflammatory disease. *Int. J. Mol. Sci.* 20 (23), 6008. doi:10.3390/ijms20236008

Kapellos, T. S., Bonaguro, L., Gemünd, I., Reusch, N., Saglam, A., Hinkley, E. R., et al. (2019). Human monocyte subsets and phenotypes in major chronic inflammatory diseases. *Front. Immunol.* 10, 2035. doi:10.3389/fimmu.2019.02035

Kim, M.-R., Lee, J. Y., Lee, H.-H., Aryal, D. K., Kim, Y. G., Kim, S. K., et al. (2006). Antioxidative effects of quercetin-glycosides isolated from the flower buds of Tussilago farfara L. *Food Chem. Toxicol.* 44 (8), 1299–1307. doi:10.1016/j.fct.2006.02.007

Lavhale, S. G., Kalunke, R. M., and Giri, A. P. (2018). Structural, functional and evolutionary diversity of 4-coumarate-CoA ligase in plants. *Planta* 248, 1063–1078. doi:10.1007/s00425-018-2965-z

Li, J., Zhang, Z.-Z., Lei, Z.-H., Qin, X.-M., and Li, Z.-Y. (2018). NMR based metabolomic comparison of the antitussive and expectorant effect of Farfarae Flos collected at different stages. *J. Pharm. Biomed. Anal.* 150, 377–385. doi:10.1016/j.jpba.2017.12.028

Li, S., Liu, X., Chen, X., and Bi, L. (2020). Research progress on anti-inflammatory effects and mechanisms of alkaloids from Chinese medical herbs. *J. Evidence-Based Complement. Altern. Med.* 2020, 1303524. doi:10.1155/2020/1303524

Li, Z., Li, J., Zhang, Z., Mi, X., Du, G., and Qin, X. (2017). NMR-based metabolomic analyses for the componential differences and the corresponding metabolic responses of three batches of Farfarae Flos. *Chemom. Intell. Lab. Syst.* 165, 1–10. doi:10.1016/j.chemolab.2017.03.010

Liu, C., Wu, H., Wang, L., Luo, H., Lu, Y., Zhang, Q., et al. (2020). Farfarae Flos: a review of botany, traditional uses, phytochemistry, pharmacology, and toxicology. *J. Ethnopharmacol.* 260, 113038. doi:10.1016/j.jep.2020.113038

Moore, N., Duong, M., Gulmez, S. E., Blin, P., and Droz, C. (2019). Pharmacoepidemiology of non-steroidal anti-inflammatory drugs. *Therapies* 74 (2), 271–277. doi:10.1016/j.therap.2018.11.002

Nunes, C. d.R., Barreto Arantes, M., Menezes de Faria Pereira, S., Leandro da Cruz, L., de Souza Passos, M., Pereira de Moraes, L., et al. (2020). Plants as sources of anti-inflammatory agents. *Molecules* 25 (16), 3726. doi:10.3390/molecules25163726

Pan, L., Xie, W., Fu, X., Lu, W., Jin, H., Lai, J., et al. (2021). Inflammation and sarcopenia: a focus on circulating inflammatory cytokines. *Exp. Gerontol.* 154, 111544. doi:10.1016/j.exger.2021.111544

Rahim, M. A., Zhang, X., and Busatto, N. (2023). Editorial: phenylpropanoid biosynthesis in plants. *Front. Plant Sci.* 14, 1230664. doi:10.3389/fpls.2023.1230664

Shin, S. A., Joo, B. J., Lee, J. S., Ryu, G., Han, M., Kim, W. Y., et al. (2020). Phytochemicals as anti-inflammatory agents in animal models of prevalent inflammatory diseases. *Molecules* 25 (24), 5932. doi:10.3390/molecules25245932

Song, K., Ha, I. J., and Kim, Y. S. (2019). A strategy for identification and structural characterization of oplopane-and bisabolane-type sesquiterpenoids from Tussilago farfara L. by multiple scan modes of mass spectrometry. *J. Chromatogr. A* 1602, 188–198. doi:10.1016/j.chroma.2019.05.012

Sugimoto, M. A., Vago, J. P., Perretti, M., and Teixeira, M. M. (2019). Mediators of the resolution of the inflammatory response. *Trends Immunol.* 40 (3), 212–227. doi:10.1016/j.it.2019.01.007

Tanaka, M., Toldi, J., and Vécsei, L. (2020). Exploring the etiological links behind neurodegenerative diseases: inflammatory cytokines and bioactive kynurenines. *Int. J. Mol. Sci.* 21 (7), 2431. doi:10.3390/ijms21072431

Tasneem, S., Liu, B., Li, B., Choudhary, M. I., and Wang, W. (2019). Molecular pharmacology of inflammation: medicinal plants as anti-inflammatory agents. *Pharmacol. Res.* 139, 126–140. doi:10.1016/j.phrs.2018.11.001

Xin, Q., Yuan, R., Shi, W., Zhu, Z., Wang, Y., and Cong, W. (2019). A review for the anti-inflammatory effects of paeoniflorin in inflammatory disorders. *Life Sci.* 237, 116925. doi:10.1016/j.lfs.2019.116925

Xu, L.-T., Wang, T., Fang, K.-L., Zhao, Y., Wang, X.-N., Ren, D.-M., et al. (2022). The ethanol extract of flower buds of Tussilago farfara L. attenuates cigarette smoke-induced lung inflammation through regulating NLRP3 inflammasome, Nrf2, and NF-κB. *J. Ethnopharmacol.* 283, 114694. doi:10.1016/j.jep.2021.114694

Xuan, X., Sun, Z., Yu, C., Chen, J., Chen, M., Wang, Q., et al. (2020). Network pharmacology-based study of the protective mechanism of conciliatory anti-allergic decoction on asthma. *Allergol. Immunopathol.* 48 (5), 441–449. doi:10.1016/j.aller.2019.12.011

Yang, L., Jiang, H., Wang, S., Hou, A., Man, W., Zhang, J., et al. (2020). Discovering the major antitussive, expectorant, and anti-inflammatory bioactive constituents in Tussilago farfara L. based on the spectrum–effect relationship combined with chemometrics. *Molecules* 25 (3), 620. doi:10.3390/molecules25030620

Yang, L., Yu, S., Qin, X., and Li, Z. (2022). Analysis of inter-individual variability of antitussive effect of Farfarae Flos and its fecal metabolites based on gut microbiota. *J. Pharm. Biomed. Anal.* 217, 114836. doi:10.1016/j.jpba.2022.114836

Yimer, E. M., Tuem, K. B., Karim, A., Ur-Rehman, N., and Anwar, F. (2019). Nigella sativa L.(black cumin): a promising natural remedy for wide range of illnesses. *J. Evidence-Based Complement. Altern. Med.* 2019, 1528635. doi:10.1155/2019/1528635

Zhang, S., Li, C., Gu, W., Qiu, R., Chao, J., Pei, L., et al. (2021). Metabolomics analysis of dandelions from different geographical regions in China. *Phytochem. Anal.* 32 (6), 899–906. doi:10.1002/pca.3033

Zou, Q., Wang, T., Guo, Q., Yang, F., Chen, J., and Zhang, W. (2021). Combined metabolomic and transcriptomic analysis reveals redirection of the phenylpropanoid metabolic flux in different colored medicinal Chrysanthemum morifolium. *Ind. Crops Prod.* 164, 113343. doi:10.1016/j.indcrop.2021.113343

frontiers | Frontiers in Pharmacology

TYPE Review
PUBLISHED 15 November 2024
DOI 10.3389/fphar.2024.1479963

Check for updates

OPEN ACCESS

EDITED BY
Zhichao Xu,
Northeast Forestry University, China

REVIEWED BY
Le-Le Zhang,
Chengdu University, China
Zhi Chai,
Shanxi University of Chinese medicine, China

*CORRESPONDENCE
Liangjun Guan,
guanlj3@163.com
Shunli Xiao,
xiaosl3@163.com

RECEIVED 13 August 2024
ACCEPTED 31 October 2024
PUBLISHED 15 November 2024

CITATION
Shu L, Li K, Yang S, Hu M, Ming X, Yan B, Guan L and Xiao S (2024) A review on ethnobotany, phytochemistry, and pharmacology of the genus *Duhaldea* DC.
Front. Pharmacol. 15:1479963.
doi: 10.3389/fphar.2024.1479963

COPYRIGHT
© 2024 Shu, Li, Yang, Hu, Ming, Yan, Guan and Xiao. This is an open-access article distributed under the terms of the Creative Commons Attribution License (CC BY). The use, distribution or reproduction in other forums is permitted, provided the original author(s) and the copyright owner(s) are credited and that the original publication in this journal is cited, in accordance with accepted academic practice. No use, distribution or reproduction is permitted which does not comply with these terms.

A review on ethnobotany, phytochemistry, and pharmacology of the genus *Duhaldea* DC

Liangyin Shu[1,2], Kailin Li[1,2], Suyu Yang[3], Mengdie Hu[1], Xinrong Ming[1], Bingyuan Yan[2], Liangjun Guan[1]* and Shunli Xiao[1]*

[1]School of Pharmaceutical Sciences, Hunan University of Medicine, Huaihua, China, [2]School of Pharmacy, Shandong Second Medical University, Weifang, China, [3]School of Pharmacy, Baotou Medicai College, Baotou, China

The botanical drugs of genus *Duhaldea* DC. have been traditionally utilized in folk medicine for the treatment of a wide array of illnesses, encompassing fractures, bone wounds, carbuncles and poisoning, bronchitis, bruises, giddy with hypertension of qi, and lung deficiency cough. The genus *Duhaldea* DC. comprises 15 species widespread in Central, East, and Southeast Asia and 7 species (2 endemic) in China. The review aims to provide a systematic overview of ethnopharmacology, phytochemistry, and pharmacology of *Duhaldea* DC. and to explore the future therapeutic potential and scientific potential of this genus. The data were systematically collected from books and scientific databases such as PubMed, Web of Science, Google Scholar, CNKI, and doctoral and master's theses. To date, a total of 352 metabolites have been isolated from this genus, and terpenoids, flavonoids, phenylpropanoids, and inositol angelates are the primary contributors to the pharmacological activities of *Duhaldea* DC. The crude extracts and isolated phytochemical metabolites from this genus have been shown to exhibit various pharmacological activities, including anti-inflammatory, antimicrobial, anti-osteoporotic, anticancer, and antioxidant activities. Despite notable advancements in our understanding of the chemical constituents and pharmacological properties of *Duhaldea* DC., it is absolutely crucial to conduct additional research into the pharmacology and toxicology of these species to definitively ascertain their safety, efficacy, and quality.

KEYWORDS

***Duhaldea* DC., ethnobotany, pharmacology, phytochemistry, traditional uses**

1 Introduction

Previously, plants of the genus *Duhaldea DC.* were considered to belong to the genus *Inula* L. (Cheng et al., 2014a; Li, 2017). However, in the last decade or so, plant taxonomists have concluded that these plants should become a separate genus under the family Asteraceae, and the scientific name of the genus has been revised to *Duhaldea* DC (Wu and Peter, 2011). *Duhaldea* DC consists of 15 species, mainly shrubs or perennial botanical drugs. The genus is widely distributed in Asia, with seven species in China, of which two are endemic (Wu and Peter, 2011). The stem is erect. The leaves are alternate and densely hairy. The capitulum is often solitary or found in dense terminal corymbs. It has multiple total bracts, with white edge

TABLE 1 Summary of the ethnobotanical uses of the genus *Duhaldea* DC (species name, plant part, country, uses, mode of administration, and associated references).

Species	Plant part used	Uses	References
D. wissmannian	Root	Infantile malnutritional stagnation	*Synopsis of Chinese Ethnic Medicine* (in Chinese)
D. nervosa	Root or whole	Treatment of rheumatic diseases such as rheumatic ostealgia, beriberi edema, and rheumatic arthritis Treatment of digestive system diseases such as dyspepsodynia, cacochylia, dyspepsia abdominal distension, chronic gastritis, and esophagus cancer Treating fractures and bone wounds Treatment of other diseases such as cold, sputum cough, ardent fever, pain in waist and lower extremities, neuralgia, and mammitis	Long (2004), *Dian Nan Ben Cao* (in Chinese), *Yunnan Selected Chinese Materia Medica* (in Chinese), *Yunnan Simao Selected Chinese Materia Medica* (in Chinese), *Synopsis of Chinese Ethnic Medicine* (in Chinese), and *Compendium of Chinese Traditional Medicine Resources* (in Chinese)
D. cappa	Leaf, root, or whole plant	Treatment of a variety of painful diseases such as rheumatic pain in waist and lower extremities, rheumatic ostealgia, toothache, dyspepsodynia, rheumatic arthralgia, and nervous headache Treatment of multiple inflammatory conditions such as kidney inflammation edema, infantile pneumonia, gastritis, vesical catarrh, amygdalitis, bronchitis, gingivitis, mammitis, and hepatitis Treatment of parasitic infectious diseases such as bilharziasis, malaria, and acariasis Treatment of other diseases injuries from falls, fractures, contusions and strains, hemorrhage, cold cough, ardent fever, itchy skin, infantile fever, neuroticism, sore and furuncle, puerperal cold, irregular menses, tuberculosis, snakebite, diarrhea, postpartum cold, and hemorrhoids	*Yunnan Selected Chinese Materia Medica* (in Chinese), *Yunnan Simao Selected Chinese Materia Medica* (in Chinese), *Chinese Ethnic Materia Medica Monographs* (in Chinese), *Synopsis of Chinese Ethnic Medicine* (in Chinese), and *Compendium of Chinese Traditional Medicine Resources*
D. pterocaula	Root	Treatment of ulcerative carbuncle pyogenic infections, tracheitis, injuries from falls, fractures, contusions and strains, deficiency of vital energy, dizziness, cough due to lung deficiency, dysentery, tinnitus, insomnia, fluster, splenic organ swelling, anemofrigid cold, dizziness, cold, and tuberculosis of bones and joints	Chunli et al. (2021), *Compendium of Chinese Traditional Medicine Resources* (in Chinese), and *Synopsis of Chinese Ethnic Medicine* (in Chinese)
D. eupatorioides	Root	Treatment of malnutritional stagnation	*Synopsis of Chinese Ethnic Medicine* (in Chinese)

flowers. The disk florets are bisexual, either yellow or whitish. The achenes are ellipsoid and hairy, with an epidermis featuring elongated crystals (Ding and Jin, 2017).

Species in the genus *Duhaldea* DC. are traditionally used for the treatment of stomachache, relieving rheumatism, fractures, bone wounds, asthma, headache, rheumatism, peptic ulcers, loose motions, indigestion, bronchitis, angeitides, vasculitis, and dizziness (Long, 2004; Yan et al., 2011; Jyoti et al., 2017; Huang et al., 2021a). *Duhaldea* DC. species are rich in sesquiterpene lactones, sesquiterpenes, phenylpropanoids, inositol derivatives, triterpenes, and flavonoids, which authenticate their medicinal importance (Baruah et al., 1982; Yan et al., 2010; Cheng et al., 2014b; Wu et al., 2015; Zheng et al., 2015). Anti-inflammatory, piscicidal, anti-osteoporotic, and anticancer activities exhibited by various extracts and metabolites isolated from the genus *Duhaldea* DC. showed its pharmacological importance (Yoshida et al., 1995; Xie et al., 2007; Wang et al., 2013; Tai et al., 2014). *D. nervosa* and *D. cappa* are the most popular, widely utilized, and highly investigated species in the genus despite the relatively low number of other species within the genus, which are more or less underexplored. This species is an important medicinal species extensively used in Asian countries to treat stomachache and rheumatism (Yan et al., 2011).

This review aims to establish a relationship between traditional uses and scientific studies by critically assessing the available literature on ethnopharmacology, phytochemistry, and pharmacology, possible mechanisms of action, and toxicology of the plant species from the genus *Duhaldea* DC. Furthermore, this review also highlights the various research gaps for the better exploitation of this genus and provides a baseline for future research studies. Related scientific literature studies up to March 2024 were collected from the following databases: PubMed, Elsevier, Web of Science, Springer, ScienceDirect, Wiley, ACS, CNKI, and doctoral and master's theses. The search terms included "Duhaldea," "rubricaulis," "wissmanniana," "lachnocephala," "forrestii," "nervosa," "cappa," "pterocaula," "eupatorioides," "cuspidata," "griffithii," "latifolia," "revoluta," "simonsii," "xiaoheiyao," "caoweiling," and "baimianfeng." The collected data from different sources were comprehensively summarized for botany, ethnopharmacology, phytochemistry, pharmacology, and toxicology of the genus *Duhaldea* DC. ChemDraw 20.0 was used to extract the chemical metabolites. The PubChem database (https://pubchem.ncbi.nlm.nih.gov) was used to confirm the chemical classifications and structures, and iPlant (https://www.iplant.cn/) was used to verify the names of the plants.

2 Traditional uses and ethnopharmacology

Botanical drugs have been used to treat an array of conditions by humans since ancient days (Schulz et al., 2001). *Duhaldea* DC species are widely distributed in Asia. The botanical drug uses of the genus *Duhaldea* DC are summarized in Table 1.

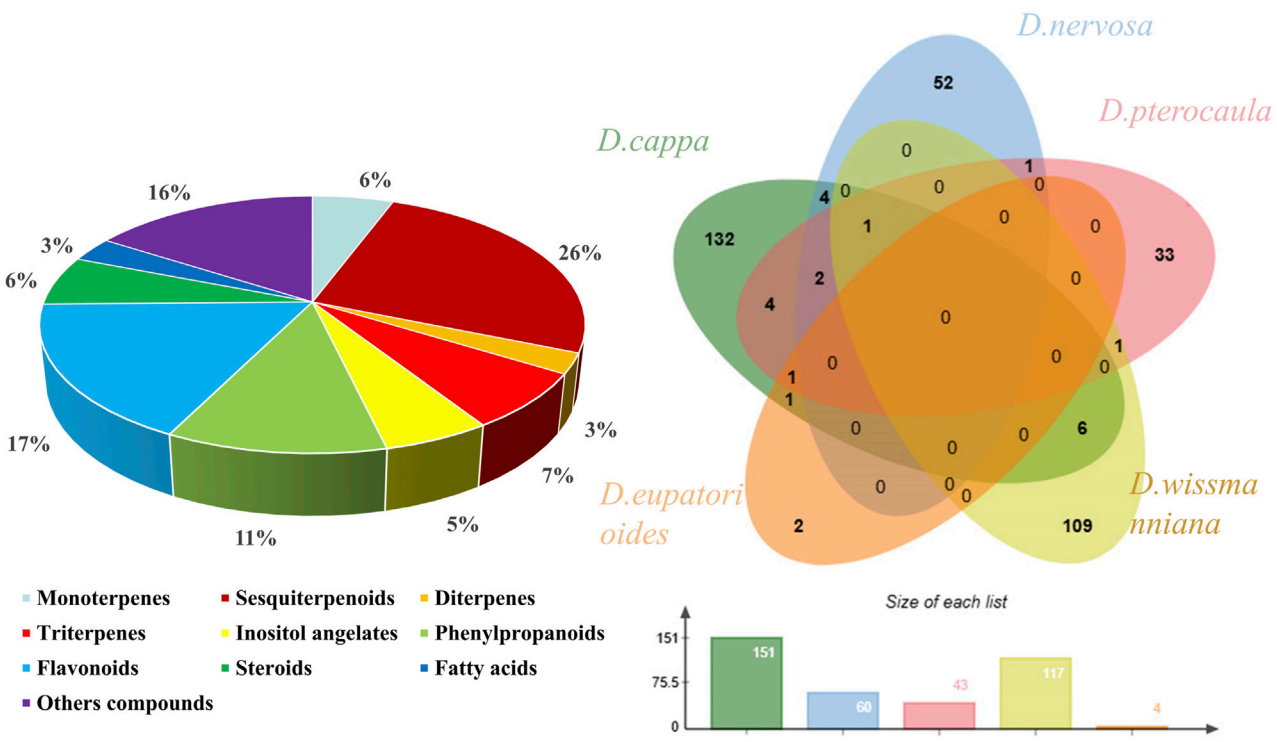


FIGURE 1
Chemical classes and proportions of phytochemical metabolites isolated and characterized from the genus *Duhaldea* DC.

3 Phytochemistry

3.1 Preliminary phytochemical screening

Early phytochemical studies of *Duhaldea* DC. were conducted in the 1990s and revealed the presence of saponins in the sesquiterpenoids of this species (Baruah et al., 1980; Goswami et al., 1984). Large sesquiterpenoids were also recently identified in the alcohol extract of *D. wissmanniana* (Cheng et al., 2013; Cheng et al., 2014b). Other studies in subsequent years have led to the isolation and identification of phenylpropanoids, flavonoids, inositol angelates, phenolic metabolites, phenolic, monoterpenes, diterpenes, and triterpenes from acetone, chloroform, methanol, and ethanol extracts of *D. cappa* (Wang et al., 2012; Zhou, 2017). Moreover, a study on the chemical metabolites of the root of *D. cappa* resulted in the extraction and characterization of a mixture of five ceramide metabolites from this species (Guo et al., 2007). In the past few decades, liquid chromatography–mass spectrometry (LC-MS), especially ultra-high-performance liquid chromatography–high-resolution mass spectrometry (UHPLC-HRMS), has become the most powerful and reliable analytical instrument in the detection and characterization of metabolites from traditional Chinese medicine, drug, or biological samples (Wei et al., 2020). UHPLC-HRMS is an advanced form of an analytical technique used to separate and identify the complex mixture of metabolites found in botanical drugs. It is important to make generalization about the fragmentation pathways of reference metabolites using the HRMS technique to speculate the identity of potential metabolites in genus *Duhaldea* DC. (Ma et al., 2022). In the study of the chemical composition of the whole botanical drug and inflorescence of *D. nervosa*, UHPLC-Q-Exactive Orbitrap mass spectrometer and UHPLC-QTOF-MS/MS were used, and 149 chlorogenic acid derivatives and 34 metabolites were finally identified, respectively (Wei et al., 2020; Wei et al., 2022). UHPLC-Q-Exactive Orbitrap mass spectrometer and UHPLC-QTOF-MS/MS were used in the study of the chemical composition of *D. cappa*, and 68 chlorogenic acid derivatives and 12 metabolites were finally identified, respectively (Peng et al., 2017; Peng et al., 2021).

3.2 Chemical composition

Detailed phytochemical studies on *Duhaldea* DC. have revealed in an array of secondary metabolites. Many researchers, especially in the past 40 years, have discovered new metabolite structures from *Duhaldea* DC. To date, a total of 393 chemical metabolites have been reported from *Duhaldea* DC. species, including sesquiterpenoids, monoterpenes, diterpene, triterpenes, inositol angelates, phenylpropanoids, flavonoids, phenolic metabolites, and ceramide metabolites (Figure 1). The detailed information on these metabolites is summarized in Supplementary Table S1.

3.2.1 Monoterpenes

Monoterpenes belong to a large and diverse group of naturally occurring metabolites. The basic structure of monoterpenes, or monoterpenoids, consists of two linked isoprene units. They might be cyclized and oxidized in a variety of ways. Due to their

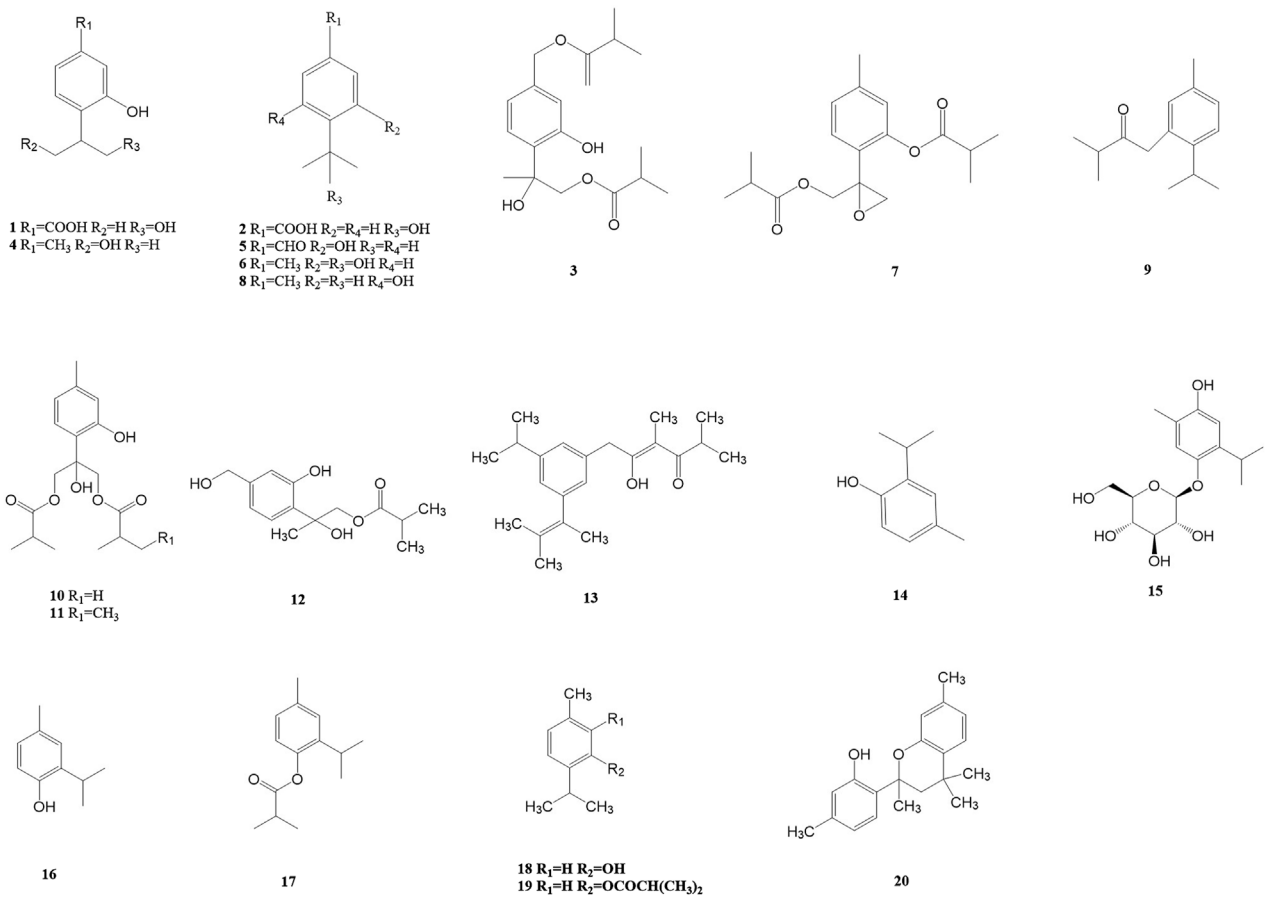


FIGURE 2
Structures of monoterpenes (metabolites 1–20).

low molecular weight, many of them exist in the form of essential oils. Many monoterpenes and their derivatives have anti-inflammatory, antimicrobial, anticonvulsant, analgesic, antiviral, anticancer, antituberculosis, and antioxidant biological activities (Zielińska Błajet and Feder Kubis, 2020). A total of 20 monoterpenes (1–20) have been reported from the genus *Duhaldea* DC., and Figure 2 shows their chemical structures.

3.2.2 Sesquiterpenoids

In the study of chemotaxonomy based on secondary metabolites from the Asteraceae family, sesquiterpene lactones, which are used as taxonomic markers, are a more studied class of secondary metabolites. More than 4,000 sesquiterpene lactones with around 30 different skeletons have been reported from several tribes of Asteraceae (Wu et al., 2006). A total of 90 sesquiterpenoids (21–110) have been reported from the genus *Duhaldea* DC., and Figure 3 shows their chemical structures.

3.2.3 Diterpenes

Diterpenes are the product of the mevalonic acid biosynthesis pathway. Some diterpenes have antiviral activity, such as kirkinine, *Excoecaria* toxin (anti-HIV), jiadifenoic acids JP (anti-Coxsackie virus), briaexcavatolide U, briaexcavatin L (anti-HCMV), genkwanin P, laurifolioside A (anti-HBV), linearol, isosidol (anti-HPIV-2), and debromoaplysiatoxin (anti-CHIKV) (Wardana et al., 2021). A total of nine diterpenes (111–119) have been reported from the genus *Duhaldea* DC., and their chemical structures are shown in Figure 4.

3.2.4 Triterpenes

Triterpenoids are a class of terpenoids with a basic skeleton of 30 carbon atoms consisting of six isoprene units, which exist in the plant body in free form or in the form of glycosides or esters combined with sugars, and have a wide range of biochemical activities, such as anti-inflammatory and antitumorigenic activities (Gill et al., 2016; Miranda et al., 2022). At the same time, triterpenes play a vital role in the formation of structures in plant membranes, which stabilize the phospholipid bilayers in the cell membranes (Liby et al., 2007). A total of 25 triterpenoids (120–144) have been reported from the genus *Duhaldea* DC., and their chemical structures are shown in Figure 5.

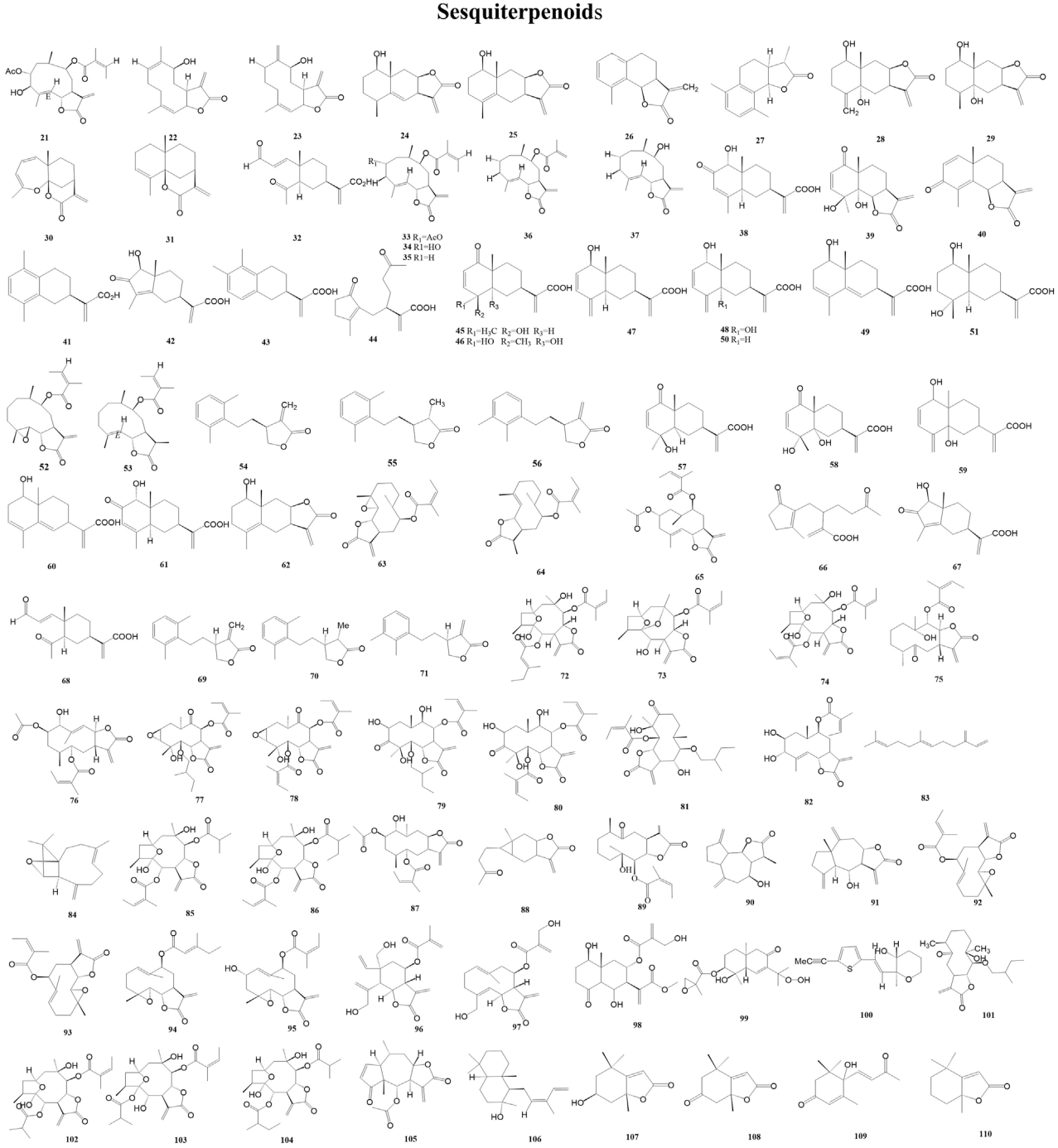


FIGURE 3
Structures of sesquiterpenoids (metabolites 21–110).

3.2.5 Inositol angelates

Inositol, also known as cyclohexane hexanol, is widely distributed in animals and plants and is a growth factor for animals and microorganisms. It was first isolated from the heart muscle and liver. Muscle inositol is an essential nutrient source for birds and mammals, and a deficiency of muscle inositol can, for example, cause symptoms such as hair loss in mice and periocular abnormalities in rats. Furthermore, inositol deficiency may be involved in the pathogenesis of diseases, such as metabolic syndrome, spina bifida (a neural tube defect), polycystic ovary syndrome, and diabetes (Marine and Christophe, 2013; Kiani et al., 2021; Dorina et al., 2023). A total of 19 inositol angelates (145–163) have been reported from the genus *Duhaldea* DC., and their chemical structures are shown in Figure 6.

3.2.6 Phenylpropanoids

Phenylpropanoids form a class of metabolites with a core structure consisting of a phenyl group attached to a three-carbon

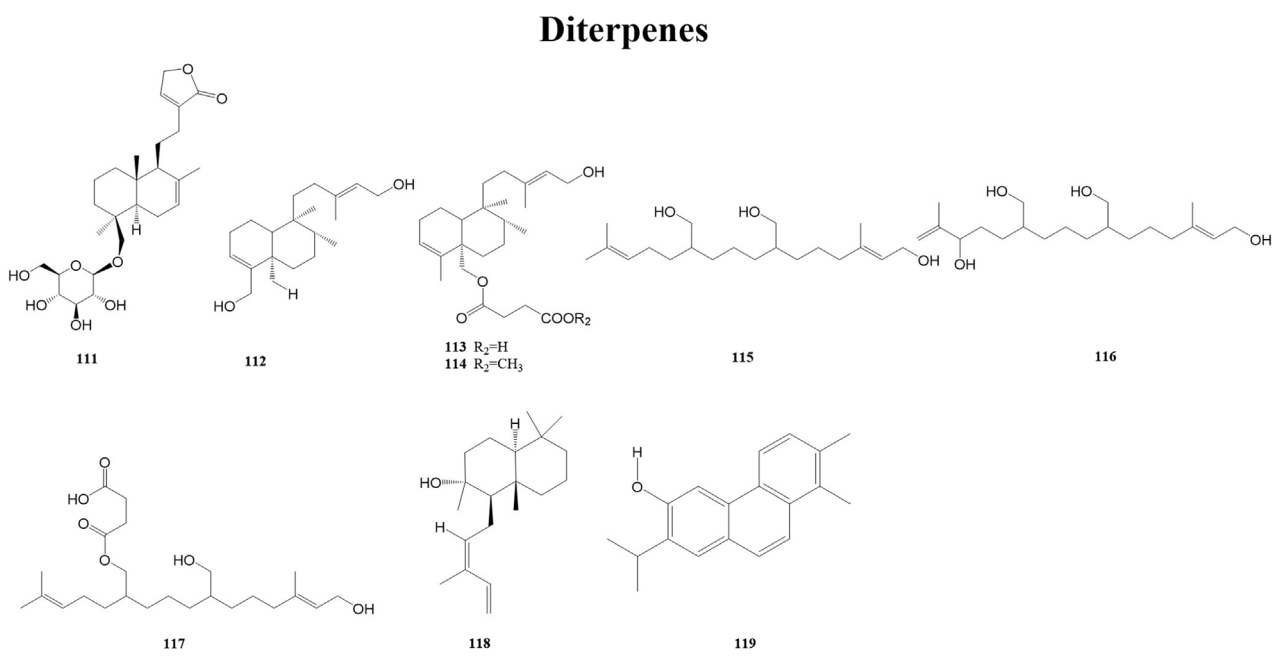


FIGURE 4
Structures of diterpenes (metabolites 111–119).

chain. This C6–C3 carbon skeleton is usually obtained from the enzymatic deamination of the aromatic amino acid phenylalanine. Phenylpropanoids, owing to their antimicrobial and antioxidant activities, are applied in pharmaceutical products as a preservative. Currently, in many countries, phenylpropanoid derivatives have been approved as food additives and active metabolites in skincare products (Neelam et al., 2020). A total of 39 phenylpropanoids (164–202) have been reported from the genus *Duhaldea* DC., and their chemical structures are shown in Figure 7.

3.2.7 Flavonoids

Flavonoids are a group of polyphenolic metabolites produced in plants as secondary metabolites. Flavonoids are a class of yellow pigments derived from 2-phenylchromanone as the mother nucleus, including the isomers of flavonoids and their hydrogenation and reduction products, i.e., a series of metabolites with C6-C3-C6 as the basic carbon framework. Flavonoids are widely found in fruits, vegetables, and other food crops. They have favorable biochemical effects on multiple diseases (e.g., cardiovascular disease and atherosclerosis), as well as other bioactivities (e.g., anti-inflammatory, antiviral, and antioxidant activities) (Serafini et al., 2010; Fardoun et al., 2020; Badshah et al., 2021; Shen et al., 2022). A total of 61 flavonoids (203–263) have been reported from the genus *Duhaldea* DC., and their chemical structures are shown in Figure 8.

3.2.8 Steroids

Steroid is a general term for a large group of cyclopentane-thickened fully hydrogenated phenanthrene derivatives that are widely distributed in living organisms. Steroids are widely known for their potent anti-inflammatory and immune-modulating activities (Neilsen et al., 2014). A total of 22 steroids (264–285) have been isolated from the genus *Duhaldea* DC., and their chemical structures are shown in Figure 9.

3.2.9 Fatty acids

Fatty acids are carboxylic acids with a typical RCOOH structure, containing a methyl end, a hydrocarbon chain (R), and a carboxylic terminus. Fatty acids have both a systematic and a common name (e.g., octadecanoic and stearic). Fatty acids play multiple roles in humans and other organisms. At the same time, fatty acids are a substantial part of lipids, one of the three major metabolites of biological matter (along with proteins and carbohydrates) (Tvrzicka et al., 2011). A total of 11 fatty acids (286–296) have been reported from the genus *Duhaldea* DC., and their chemical structures are shown in Figure 10.

3.2.10 Other metabolites

In addition to the above metabolites, *Duhaldea* DC. also contains phenolic acids, chlorogenic acid, organic acids, and polyols. These metabolites are categorized as other because they rarely exert similar pharmacological effects as a class of metabolites or they occur less frequently in the genus. For example, Wang et al. isolated and purified a novel water-soluble polysaccharide (DNP-1) from the root of *D. nervosa* via column chromatography (Wang et al., 2023). This is the only isolation of polysaccharides that we have found in our research searches of this genus. A total of 56 other metabolites (297–352) have been reported from the genus *Duhaldea* DC., and their chemical structures are shown in Figure 11.

10.3389/fphar.2024.1479963

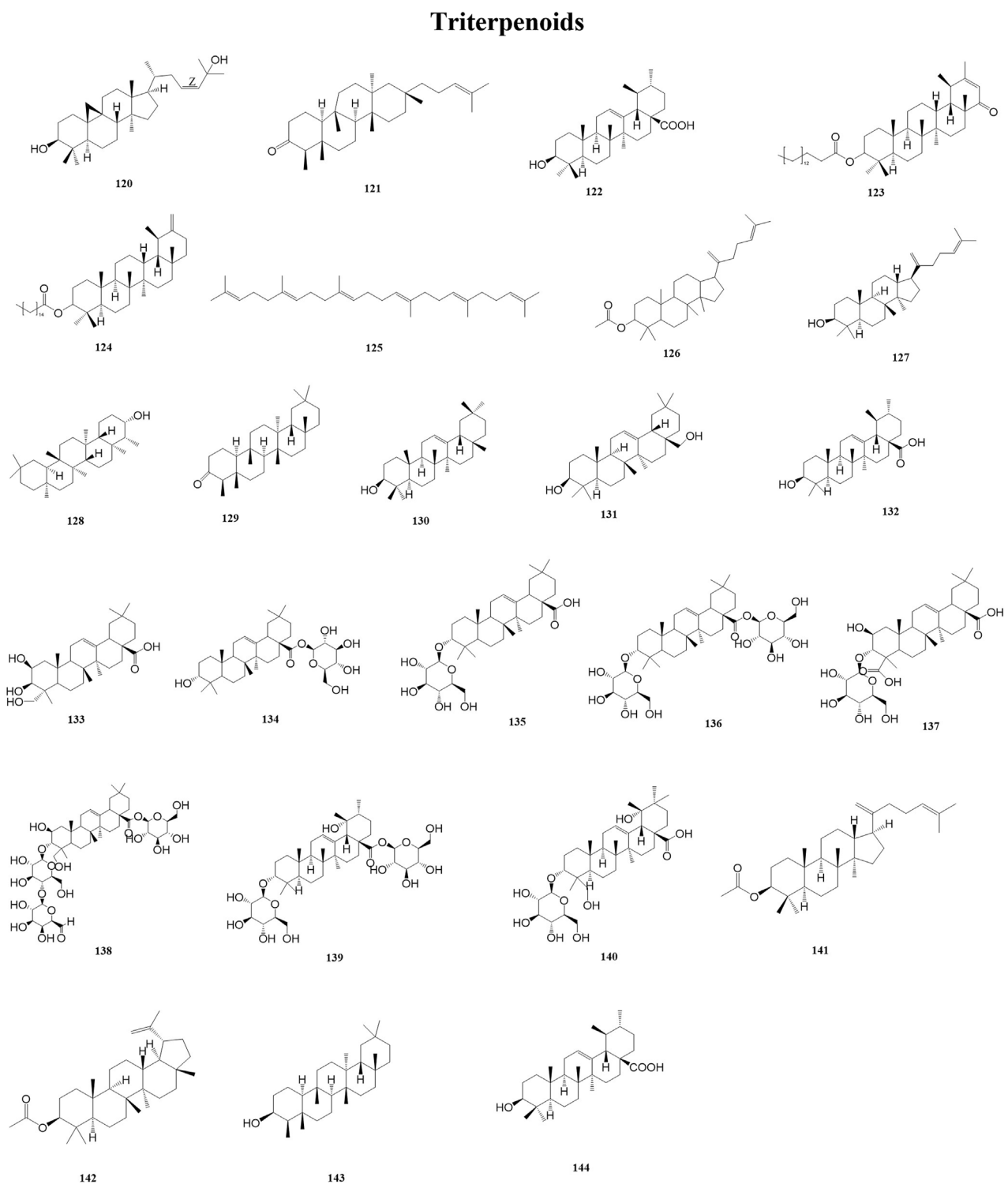


FIGURE 5
Structures of triterpenes (metabolites 120–124).

4 Pharmacology

Present-day research and the study of historical texts have shown that whole plants or their respective plant parts have been used to treat or alleviate different illnesses. Currently, botanical drugs are also used in the conventional system of medicine, where plants and associated phytochemicals are being actively explored for their direct use as pharmaceutical agents. At the same time, it can be noted that the plant is used as a medicine and food, is usually

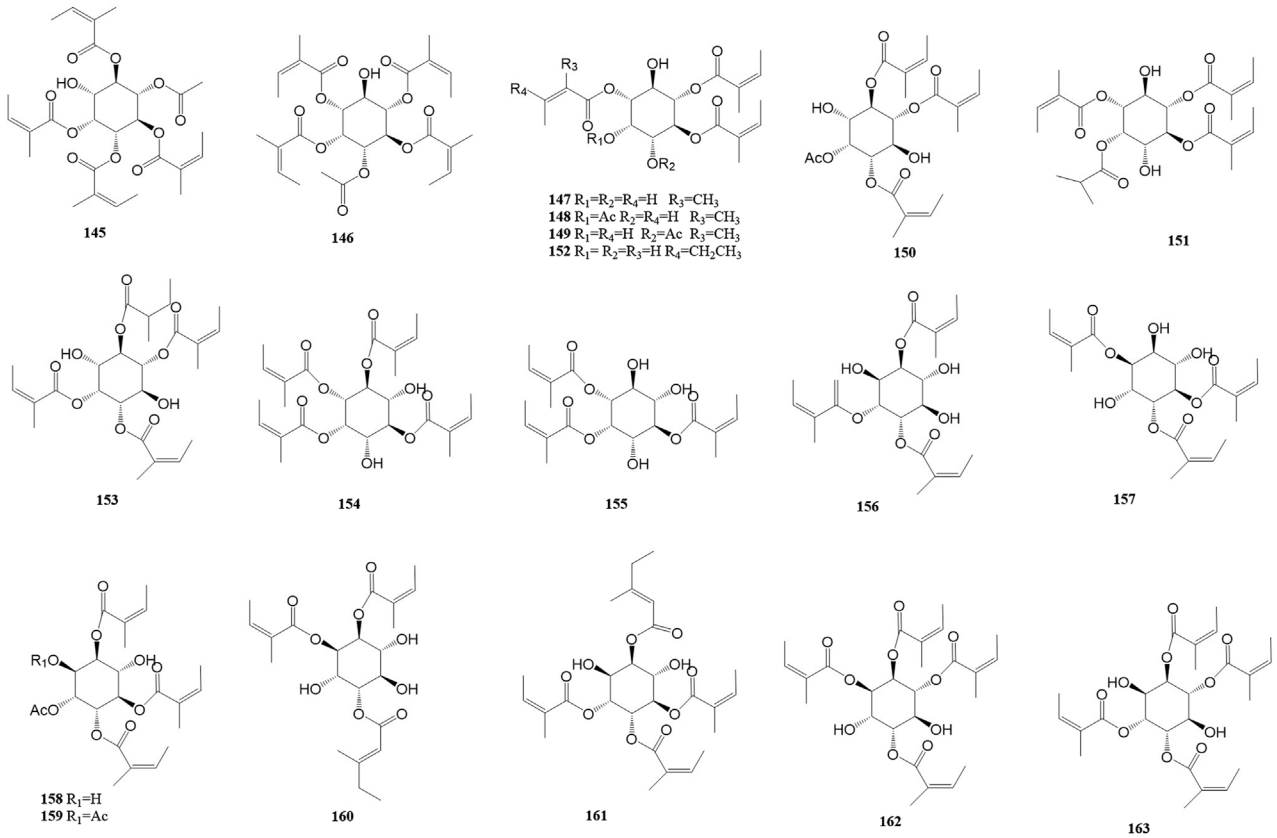


FIGURE 6
Structures of inositol angelates (metabolites 145–163).

used as a spice and seasoning in food, and also prevents and controls some diseases in people.

The genus *Duhaldea* DC. has long been used therapeutically in different countries in Asia due to its wide range of biological and pharmacological activities. The broad-spectrum ethnomedicinal uses of the different species of *Duhaldea* DC. have led to the initiation of several pharmacological investigations, such as anti-inflammatory, antioxidant, antitumor, and antibacterial activities. A brief summary of these pharmacological effects is given in Figure 12. An overview of the modern pharmacological studies on these species is detailed in the following sections.

4.1 Anti-inflammatory activity

Inflammation is a defensive response of the body to stimulation, manifested by redness, swelling, heat, pain, and dysfunction. In immune cells, macrophages are the main cell type involved in the inflammatory process. RAW 264.7 macrophages are a good model for screening anti-inflammatory drugs. The modern pharmacology of *Duhaldea* DC has proven to have significant anti-inflammatory effects, and its main material basis of anti-inflammation is sesquiterpenoids. A total of 21 eudesmane and germacrane derivatives were isolated from *D. wissmannian*. These isolates exhibited significant inhibitory effects on lipopolysaccharide (LPS)-induced nitric oxide (NO) production in RAW 264.7 macrophages (20, 5, 0.5, and 0.1 μM), with aminoguanidine as a positive control (Cheng et al., 2013; Cheng et al., 2014b). Wang et al. screened a total of 35 monomers isolated from *D. wissmannian*, including sesquiterpenoids, monoterpenes, and flavonoid lignans, for their inhibitory effects on NO metabolism in LPS-induced RAW 264.7 macrophages. Four concentration gradients of 50, 10, 2, and 0.4 μM were used to determine the metabolic inhibition rate and cytotoxicity of each monomer metabolite on NO, and 1β-hydroxy-alantolactone and inulicin were used as a positive control. The results showed that the sesquiterpenoids containing α-methylene-γ-lactone fragments exhibited strong NO metabolism inhibition, and some flavonoid lignans and myo-inositol derivatives also showed some anti-inflammatory activities (Wang, 2013). The *D. wissmannian* eudesmane-derivatized sesquiterpene, Chengwissmanolide A (IC_{50} = 0.38 μM), showed stronger or similar NO inhibitory activity to the positive drug aminoguanidine (0.20 or 0.37 μM) (Cheng, 2012). Four new sesquiterpenes, pterocaullins A–D (1–4), along with 10 known metabolites isolated from the whole plants of *D. pterocaula*, were tested for their inhibitory effects against LPS-induced NO production in RAW 264.7 macrophages using parthenolide (10 μM) as a positive control. Pterocaullin B exhibited promising anti-inflammatory activity, with an IC_{50} value of 7.03 μM (Zhu et al., 2019).

10.3389/fphar.2024.1479963

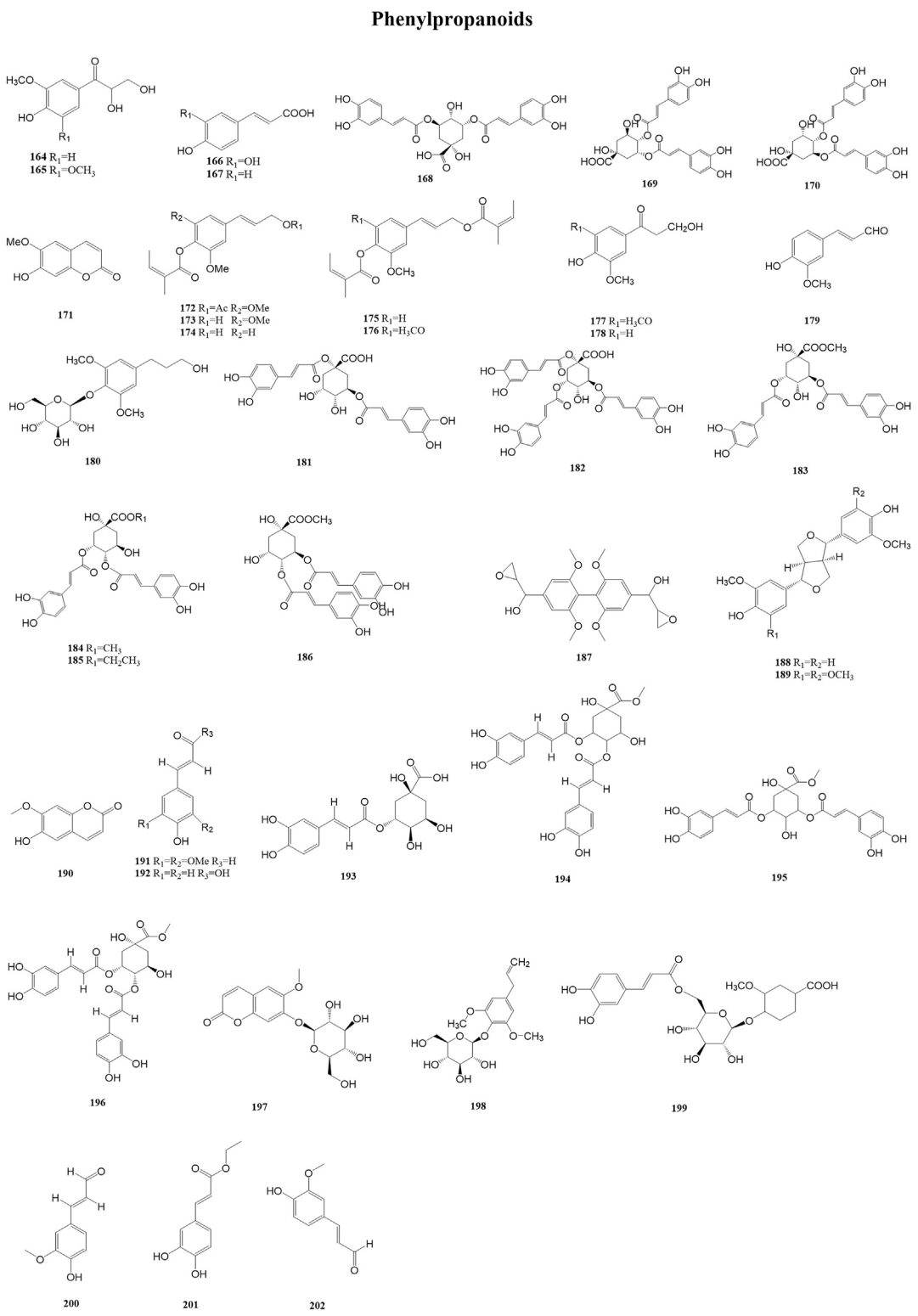


FIGURE 7
Structures of phenylpropanoids (metabolites 164–202).

Other types of metabolites in the genus also have good anti-inflammatory activity. A new polysaccharide, DNP-1, was isolated from *D. nervosa* and inhibited the concentrations of NO, TNF-α, MCP-1, IL-2, and IL-6 pro-inflammatory factors in LPS-induced RAW 264.7 cells at concentrations of 50, 100, and 150 μg/mL (Wang et al., 2023). Wang et al. isolated 17 metabolites from *D. wissmannian,* and the anti-inflammatory activity of RAW 264.7 macrophages against LPS-induced NO production was also



FIGURE 8
Structures of flavonoids (metabolites 203–263).

evaluated. Metabolites 3-acetate-1,2,4,5-tetrakis(2-methyl-2-butenoate) inositol, 2,3-dehydrosilychristin, hydnocarpin, 8-hydroxy-7,9-di-isobutyryloxythymol, and 7-hydroxy-8,9-bis(isobutyryloxy)thymol showed moderate activities, with IC_{50} values of 13.3, 19.6, 23.3, 10.8, and 10.1 μM, respectively. On the other hand, 4-acetate-1,2,3,5-tetrakis (2-methyl-2-butenoate) inositol, 23-*o*-acetylsilychristin A, isohydnocarpin, silybin B, and isosilybin A exhibited weak activities, with IC_{50} values of 32.6, 36.7, 48.2, 50.5, and 50.5 μM, respectively (Wang et al., 2013).

The metabolite (4R,5R,6S,7S,9S,10R)-9-angeloyloxy-4,5-epoxygermacra-11 (13)-en-12,6-olide, isolated from *D. wissmannian*, demonstrated potent inhibition of NO with an IC_{50} value of 1.04 ± 0.07 μM. Aminoguanidine served as the positive control and exhibited its inhibition with an IC_{50} value of 0.79 ± 0.05 μM (Cheng et al., 2014b). Maoxiucaioside A obtained from *D. nervosa*. has a significant inhibitory effect on the release of TNF-α, IL-6, and IL-1β, with IC_{50} values of 17.90 ± 2.29 μM, 19.45 ± 2.16 μM, and 18.54 ± 1.30 μM, respectively, slightly lower than those of dexamethasone (Li et al., 2023). The metabolites derived from *D. nervosa,* i.e., nervolan A, nervolan B, nervolan C, coniferyl diangelate, and sinapyl diangelate, were evaluated for their inhibitory effects on LPS-induced NO production in RAW 264.7 cells. The results demonstrated that these metabolites exhibited mild inhibitory activities against NO production, with IC_{50} values of 33.31, 15.43, 21.32, 16.19, and 33.56 μM, respectively (Yan et al., 2010). The five known analogs, isolated from *D. cappa*, exhibited anti-inflammatory activities against the production of NO in RAW 264.7 cells stimulated by LPS. Their IC_{50} values ranged from 7 to 23 μM, with celecoxib (IC_{50} 1.6 μM) serving as the positive control (Wu et al., 2015).

The *D. cappa* methanolic extract (75 and 150 mg/kg) showed reduction in the rat paw edema, significant inhibition of the cotton pellet-induced granulomas in rats, and potential immunomodulatory activity in all the assays performed (Jyoti

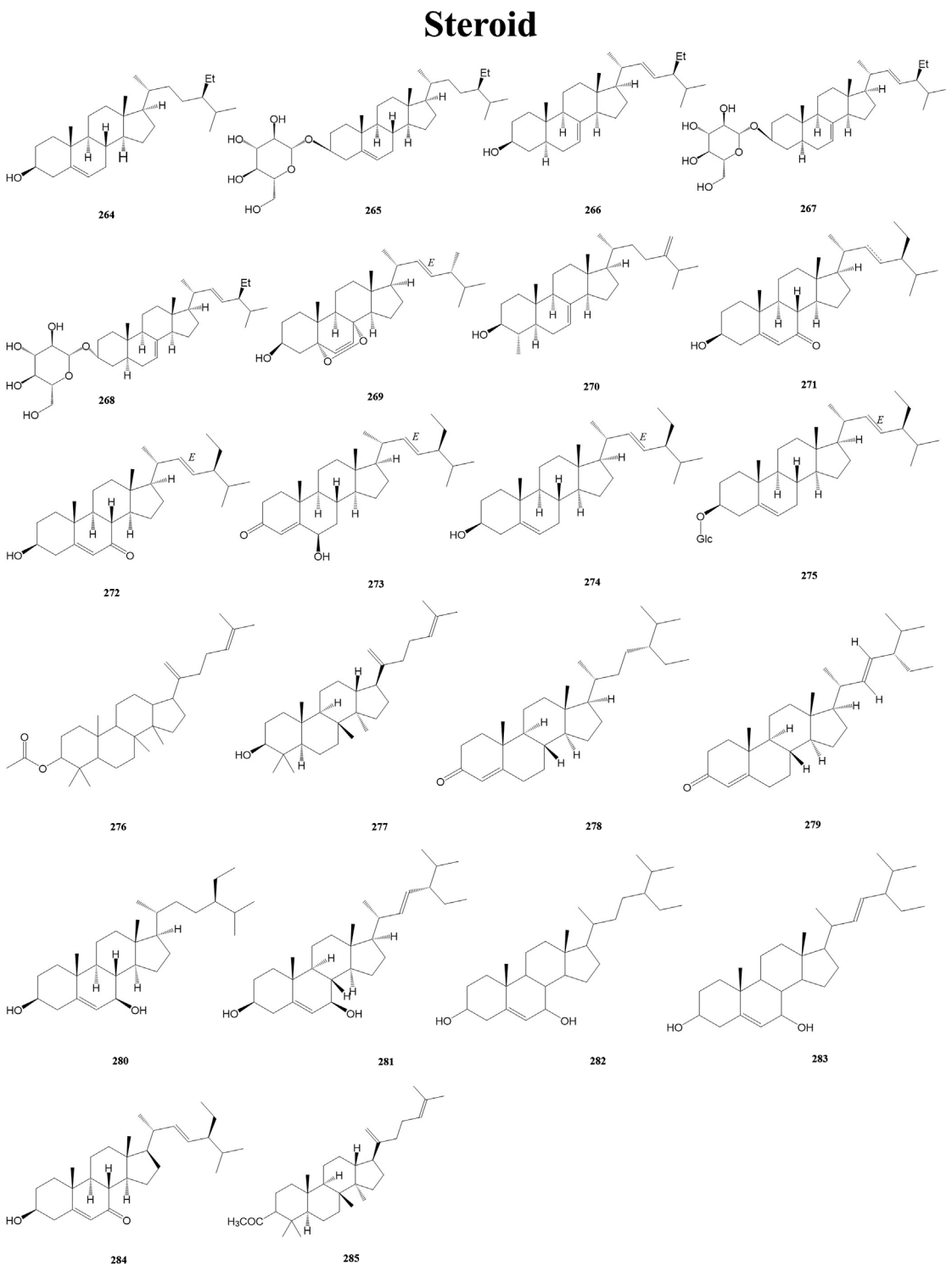


FIGURE 9
Structures of steroids (metabolites 264–285).

et al., 2017). The *D. cappa* root ethanol extract (5 g/kg) significantly inhibited xylene-induced ear swelling and acetic acid-induced capillary permeability in mice and has certain anti-inflammatory effects (Mo et al., 2012), and 60% ethanol fraction of *D. cappa* is the main anti-inflammatory constituent (Gong et al., 2018; Wang et al., 2018). The *D. cappa* aqueous extract (24 g/kg) also improved the inflammatory response of severe pneumonia rats, which may be related to the inhibition of the TLR2/MyD88/NF-κB signaling pathway (Aizaizi et al., 2018). The *D. cappa* aqueous extract (24 g/kg) can improve inflammation of severe pneumonia induced by *Klebsiella pneumoniae* by blocking p38 MAPK and NF-κBp65 signaling pathways (Li, 2017).

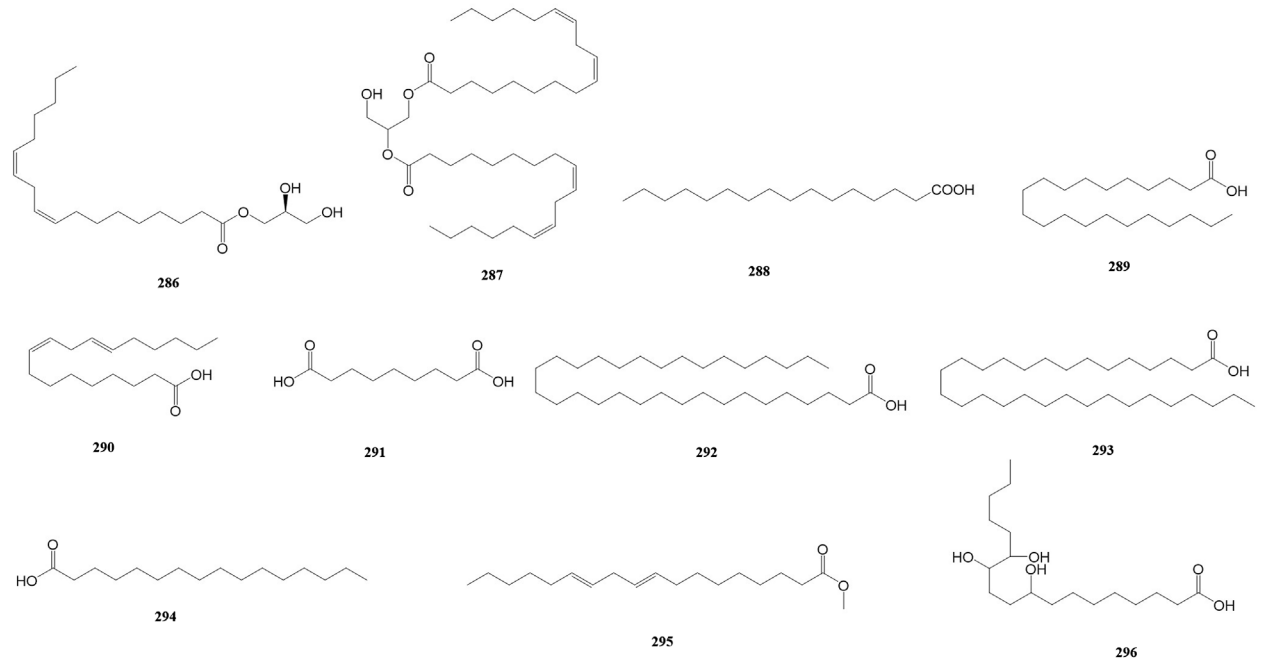


FIGURE 10
Structures of fatty acids (metabolites 286–296).

4.2 Antitumor activity

Tumors are formed by the proliferation of local tissue cells under the action of various tumorigenic factors. According to the cell characteristics of tumors and the degree of harm to the body, tumors are divided into benign tumors and malignant tumors. Cancer, a malignant tumor, has become the second leading fatal disease after cardiovascular and cerebrovascular diseases and seriously threatens human health and life. Modern pharmacological studies have shown that *Duhaldea* DC. has certain anticancer effects, and its main anticancer substance is sesquiterpenoids. Cheng et al. evaluated all 21 isolates; these isolates showed no significant toxicity in RAW 264.7 macrophages at concentrations up to 20 μM. Metabolites (5*R*,7*R*,10*S*)-4,5-epoxy-4,5-secoeudesma-1,3-dien-12,5-olide, 3-oxoeudesma-1,4,11 (13)-trien-12,6β-olide, haageanolide, and 11,13-dehydroisohyposantonin had strong inhibitory effects on NO, with IC_{50} values of 0.68, 0.68, 0.97, and 0.65 μM, respectively. Moreover, the cytotoxicity assay in four human tumor cell lines suggested that new metabolites (5*R*,7*R*,10*S*)-4,5-epoxy-4,5-secoeudesma-1,3-dien-12,5-olide, (2*R*,4*E*,6*R*,7*S*,9*S*,10*R*)-2-acetoxy-9-angeloyloxygermacra-4,11(13)-dien-12,6-olide, 4E-9β-angeloyloxy-2α-hydroxy-7α,10αH-germacra-4,11(13)-dien-12,6α-olide (4*E*,6*R*,7*S*,9*S*,10*R*)-9-angeloyloxygermacra-4,11 (13)-dien-12,6-olide, 4*E*-9β-methacryloxy-7α,10αH-germacra-4,11 (13)-dien-12,6α-olide, 4*E*-9β-hydroxy-7α,10αH-germacra-4,11 (13)-dien-12,6α-olide, and 3-oxoeudesma-1,4,11 (13)-trien-12,6β-olide showed strong toxicity against HepG2, PC-3, and MGC-803 cells (Cheng et al., 2013). Five germacrane-type sesquiterpene lactones (ineupatolide D, ineupatolide E, dvaricin B, nepalolide C, and inculacappolide) were isolated from *D. cappa* showed moderate inhibitory effects on A431, A549, BGC-823, HL-60, HT-29, and MCF-7 cancer cell lines with IC_{50} values ranging from 2.1 to 36.3 μM, and doxorubicin was used as the positive control (Wu et al., 2017). The cytotoxicity assay showed that inulacappolide has anti-proliferative effects against human cervical cancer (HeLa), human leukemia (K562), and human nasopharyngeal carcinoma (KB) cell lines, with IC_{50} values of 1.2 mM, 3.8 mM, and 5.3 μM, respectively (Xie et al., 2007). The sesquiterpene metabolite ineupatorolide B, isolated from *D. cappa*, exhibited potent growth-inhibitory activity against HeLa cells, whereas its activity against MM1-CB melanoma cells was weaker. The mechanism by which ineupatorolide B exerts its growth-inhibitory effects may involve the activation of PKCα, leading to an enhancement of the retrotranscriptional activation capacity of NFAT (Mei et al., 2015).

As a medicinal plant, this genus not only serves as a flavorful seasoning but also inhibits the production of carcinogens in food. Cheng et al. discovered that the electrophilic metabolites act as creatinine inhibitors to reduce the generation of heterocyclic aromatic amines. Their research reveals that the rhizome of *D. nervosa*, when used as a spice, can inhibit the production of carcinogens in food (Cheng et al., 2023). *D. nervosa* shows greater potential as a functional food for cancer prevention and anticancer effects. Under the condition of simulated gastric fluid *in vitro*, the stem and leaf extracts of *D. nervosa* can effectively remove nitrite and block the production of nitrosamines (Yuan et al., 2021).

4.3 Antioxidant activity

An increasing body of research indicates that antioxidants play a crucial role in mitigating the effects of aging as free radicals and oxidants contribute to cellular and tissue degradation, impair metabolic functions,

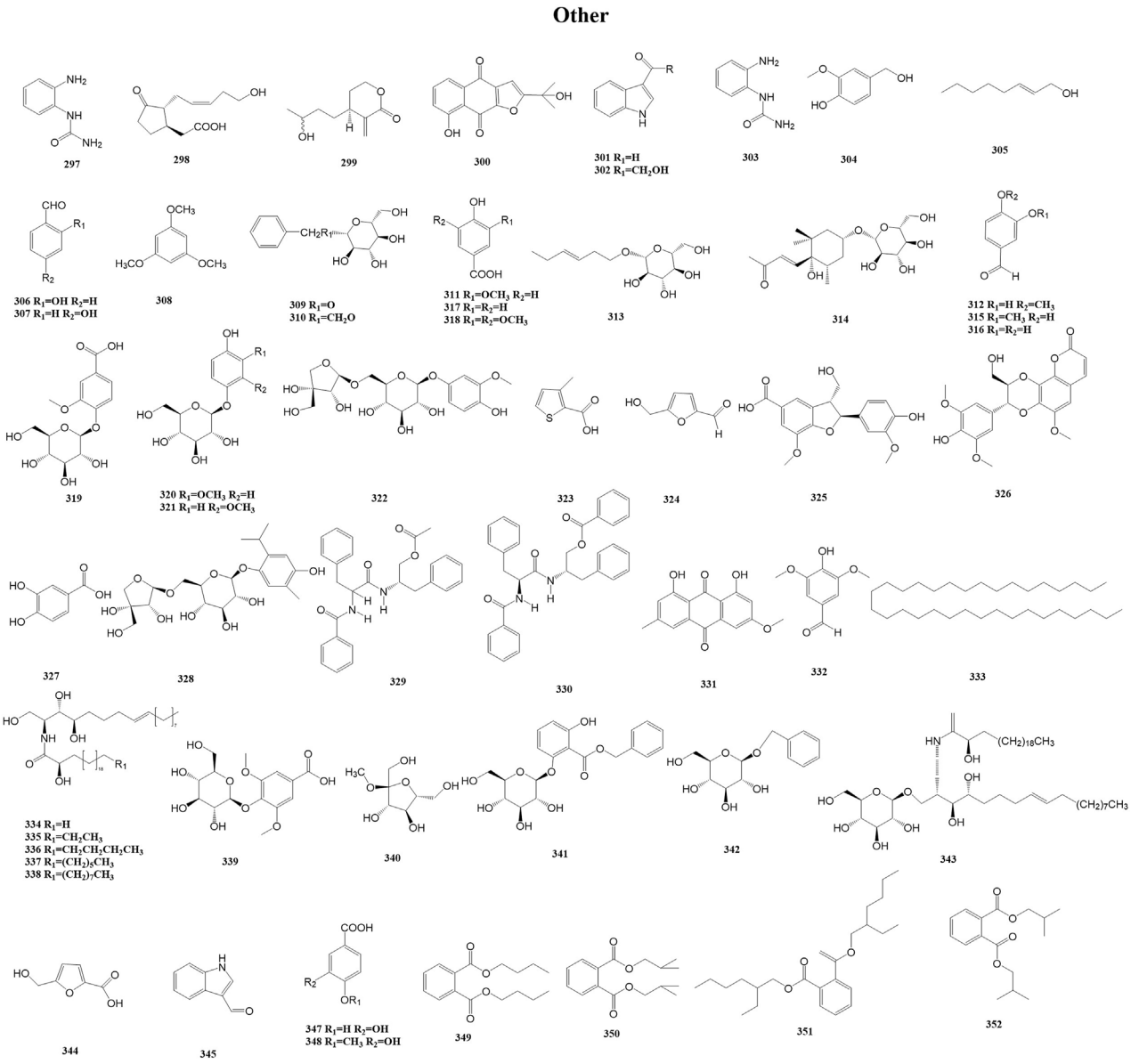


FIGURE 11
Structures of other metabolites (metabolites 297–352).

and are associated with various health issues. Cheng et al. compared the chemical space and antioxidant activities of ethanol extracts from different parts of *D. nervosa*. Findings support the traditional use of its roots and indicate thymol di-isobutyrate as a major functional factor. The results showed that significant correlations and extracts upregulated the mRNA expression of antioxidant response actors in H_2O_2-challenged HepG2 cells, hence also cueing the potential antioxidant activity of other parts (Cheng et al., 2020). He et al. compared the antioxidant effects of ultrasonic alcoholic extracts from different parts of the plant through *in vivo* and *ex vivo* experiments. *In vitro*, the extract amount was positively correlated with the clearing effect of free radicals at certain drug concentrations, with VC as the positive drug. *In vivo*, control and aging model groups had different treatments, while the experimental group had low, medium, and high (300, 600, and 1,200 μg g^{-1}·d^{-1})-dose intragastric administrations. The results showed good free radical scavenging and antioxidant capacity, with the underground part having a significantly higher antioxidant effect than the aboveground part (He et al., 2016). Yang et al. investigated the antioxidant activity of polysaccharides from aboveground and below-ground parts of *D. nervosa* and total flavonoid of *D. nervosa* and found that the reducing ability of polysaccharide and flavonoid, the inhibiting ability of superoxide anion free radical, and the scavenging ability of the DPPH radical were greater than that of para-rutin at high concentration, and the antioxidant ability was higher than that of rutin with the increase in concentration. They show a high scavenging rate of hydroxyl radicals (Tao et al., 2015; Tao et al., 2016). Kalola et al. used the DPPH radical scavenging assay, superoxide radical scavenging assay, measurement of reducing power, and measurement of the effect on lipid peroxidation in rat liver homogenates, and butylated hydroxytoluene, gallic acid, and ascorbic acid were used as the positive control. The results showed that the *D. cappa* methanolic extract and the

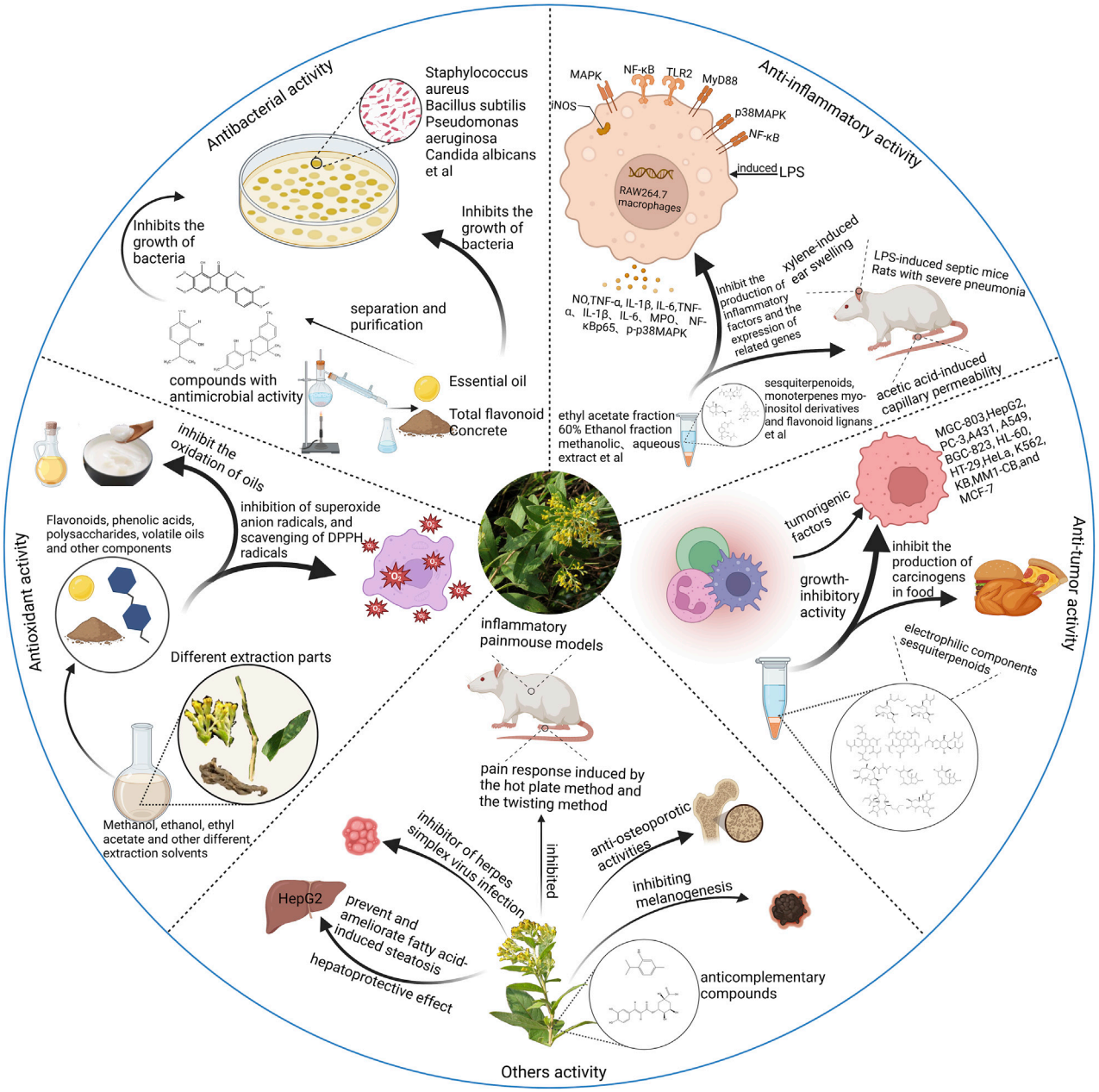


FIGURE 12
Brief description of the various pharmacological actions of the genus *Duhaldea* DC.

ethyl acetate-soluble fraction exhibited higher antioxidant activity (Kalola and Shah, 2006). The volatile oil (310–520 mg/L) of *D. cappa* has some scavenging ability for both hydroxyl radicals (positive control: mannitol and thiourea) and superoxide anion radicals (positive control: VC), but the scavenging activity of hydroxyl radicals is stronger (Liu et al., 2009a). *D. nervosa* extracts (0.05 g/g) can also effectively inhibit the oxidation of oils (Liu et al., 2011).

4.4 Antibacterial activity

Antimicrobial activity is an important indicator for screening natural metabolites for their potential to become antibiotics. Ethanol extracts (10 μg/mL) and petroleum ether extracts (10 μg/mL) of *D. nervosa* significantly inhibited *Staphylococcus aureus* and *Bacillus subtilis* (Liu et al., 2011). The essential oil derived from *D. cappa* comprises approximately 50% sesquiterpene hydrocarbons. Streptomycin (30 μg/disk) and erythromycin (15 μg/disk) were used as positive controls, while hexane was taken as a negative control, and at the concentration of 1,000 μL/mL, it has a significant inhibitory effect on *Enterococcus faecalis*, *Klebsiella pneumoniae*, *Xanthomonas viripennis*, and *B. subtilis* (Priydarshi et al., 2016). The antimicrobial activity of the flavonoid extracts from *D. cappa* was studied against nine microorganisms. The results showed that the minimal inhibitory concentration (MIC) of the *D. cappa* flavonoids to *Sarcina lutea* was the best with a ratio of 0.0039 g/mL; the MIC of *E. faecalis*, *B. subtilis*,

and *S. aureus* was 0.1250 g/mL; the MIC of *Escherichia coli*, *Salmonella typhimurium*, and *Salmonella* paratyphi A was 0.5000 g/mL but no obvious inhibitory effect on *Proteus vulgaris* and *Candida albicans* (Liu W. et al., 2010). Liu et al. showed that the MIC values of roots, stems, and leaves against *S. aureus* were 15.63, 62.5, and 62.5 mg/mL, respectively, while the MIC values of roots, stems, and leaves against *Pseudomonas aeruginosa* were 15.63, 31.25, and 62.5 mg/mL, respectively (Liu et al., 2009b). The antimicrobial effects of different extracts from different parts of *D. cappa* on different bacteria were compared, among which the glacial acetic acid extract had the best antimicrobial effect, the root and leaf extracts had better antimicrobial effects than the stem extract, and the extracts had better inhibitory effects on Gram-positive than Gram-negative bacteria (Liu S. et al., 2010). The growth of 15 plant pathogenic fungi and 4 bacteria could be inhibited by 100 mg/mL of thymol isolated from *D. cappa* (Xie et al., 2012). By comparing the various extraction and separation fractions of the ethanol extract of *D. cappa*, the chloroform:acetone 10:0 fraction of the ethyl acetate extract exhibited the most significant antibacterial activity at a concentration of 2.0 mg/mL, followed by the ethyl acetate extract and the chloroform:acetone 9:1 fraction (Li et al., 2020).

4.5 Others' activity

The electrophilic metabolites (0.5, 2.0, and 8.0 μg/mL) of *D. nervosa* attenuated hepatic steatosis in FFA-treated HepG2 cells. Studies suggest that it improved hepatic lipid metabolism disorder, Krebs cycle activity, oxidative phosphorylation, and the cellular and mitochondrial redox status. Additionally, 10-isobutyryloxy-8,9-epoxythymol isobutyrate activates the Nrf2-ARE signaling pathway by upregulating Nrf2 expression and promoting Nrf2 nuclear translocation (Cheng et al., 2022). Dong et al. found that the ethyl acetate fraction of *D. nervosa* (0.5–2.0 μg/mL) effectively reduced hepatic lipid accumulation and ROS production, lowered TG and TC levels, and enhanced antioxidant enzyme activity. The depletion of electrophilic components reduced its efficacy and regulatory effects on lipid metabolism and redox-related gene expression (Dong et al., 2020).

The ethyl acetate fraction of *D. pterocaula* (40 mg/kg, 100 μL) demonstrated potent analgesic effects in inflammatory pain mouse models and caused no anti-nociceptive tolerance (Huang et al., 2021b). The alcoholic extract of the *D. cappa* root (5 g/kg) significantly inhibited the pain response induced by the hot plate method and the twisting method in mice and had some analgesic effects (Mo et al., 2012). Kiran et al. and Yupei et al. developed a hepatotoxicity model through the intraperitoneal injection of carbon tetrachloride suspended in sterile oil or D-GalN. Silymarin at a dosage of 100 mg/kg and bifendate at 0.2 g/kg were identified as positive control drugs. The dosages for the water extract of *D. cappa* were administered at 9.8 g/kg, 19.5 g/kg, and 39.0 g/kg and 200 mg/kg and 400 mg/kg, and the effects on hepatotoxicity were assessed after a 10-day treatment period. The aqueous extract of *D. cappa* chrysanthemum showed a hepatoprotective effect against carbon CCl4 and D-GalN-induced hepatotoxicity in rats (Kiran et al., 2017; He et al., 2019). Yang et al. screened a PXR-HepG2 cell model with high expression of the pregnane X receptor. A negative control group (DMSO group, 0.1%), a drug treatment group (25, 50, and 100 mg/L), and a positive control group were treated with the pregnane X receptor agonist rifampicin (10 μmol/L) for 24, 48, and 72 h, respectively. Yang et al. showed that *D. cappa* can affect the expression of P450 enzymes in primary rat hepatocytes and HepG2 cells with high expression of the pregnane X receptor (Chang et al., 2020).

The methanol and dichloromethane extracts of *D. cappa* are potent inhibitors of herpes simplex virus infection *in vitro*. The *D. cappa* methanol extract exhibited significantly higher anti-herpes simplex virus (HSV) activity than the *D. cappa* dichloromethane extract as it inhibited more than 50% of the virus. The 50% effective doses of the *D. cappa* methanol extract against HSV-1 and HSV-2 were determined to be 720.1 ± 32.7 μg/mL and 529.2 ± 5.2 μg/mL, respectively (Nikomtat et al., 2011). The 12 isolated triterpenoids were screened for their anti-osteoporotic activities, and the metabolites oleanoic acid 3-O-(β-D-glucopyranosyl)-28-O-β-D-glucopyranosyl ester and 2β-hydroxyolean-3-O-(β-D-glucopyranosyloxy)-12-en-23, 28-dioic acid showed good anti-osteoporotic activities with IC_{50} values of 86.3 and 51.6 μg/mL, respectively, and their inhibitory effects were slightly lower than those of the positive control, teriparatide (45.6 μg/mL) (Tai et al., 2014). Fujita et al. studied the mechanism of action of 5–15 μM inulavosin isolated from *D. nervosa* (Compositae) in inhibiting melanogenesis, reducing the melanin content without affecting the enzymatic activities or the transcription of tyrosinase or Tyrp1 in B16 melanoma cells (Hideaki et al., 2009). Wen et al. evaluated the anti-complementary effects of blossoms of *D. nervosa* extracts based on the classical pathway. Their results showed that chlorogenic acid, 3,5-dicaffeoylquinic acid, 1,5-dicaffeoylquinic acid, and thymol were the major anti-complementary metabolites in the blossoms of *D. nervosa* (Wen et al., 2019).

5 Conclusion and future perspectives

The genus *Duhaldea* DC. has been used in traditional medicine to treat fractures, bone wounds, carbuncle and poison, bronchitis, bruises, giddy with hypertension of qi, and lung deficiency cough. Five species of the genus *Duhaldea* DC. have been reported to have various applications in traditional systems of medicine in several Asian countries. However, ethnobotanical data are sometimes hard to find, and it is difficult to access sources. Therefore, although the authors have made great efforts to cover the available literature as rigorously as possible, there may be possibilities that some publications, reports, or books on traditional medicinal uses of the genus *Duhaldea* DC. escaped our exploration. Available data indicate that over 352 metabolites have been identified from this genus, including terpenoids, flavonoids, phenylpropanoids, inositol angelates, chalcones, phenolics, and ceramide metabolites. The genus *Duhaldea* DC. is associated with various pharmacological activities, including anti-inflammatory, antimicrobial, anti-osteoporotic, anticancer, and antioxidant activities. Despite the fruitful phytochemical and pharmacological studies on genus *Duhaldea* DC., there are still several key issues to be resolved regarding the need for further development of genus *Duhaldea* DC.

At present, the genus *Duhaldea* DC. comprises 15 species widespread in Central, East, and Southeast Asia. However, only three (*D. wissmannian*, *D. nervosa*, and *D. cappa*) of the plants in the genus have been more extensively studied. In the future, more attention needs to be paid to underexplored plants in the study of this genus; these underexplored plant species could be promising candidates for further research.

Regrettably, aside from the systematic characterization and separation of plant metabolites conducted by Wang and Cheng

et al. on *D. wissmannian* (Cheng, 2012; Wang, 2013), most other phytochemical investigations related to this species remain relatively fragmented. Phytochemistry seeks to identify valuable new plant metabolites. There exist considerable gaps in the study of the chemistry within this genus, making the systematic characterization and separation of its metabolites an urgent priority. Simultaneously, plant metabolites encompass not only various small-molecule metabolites but also macromolecular metabolites such as polysaccharides and peptides, which exhibit remarkable pharmacological activities. However, it is disheartening to note that among the extensive studies conducted on this genus, only Wang et al. realized this aspect (Wang et al., 2023).

Although advancements have been achieved in understanding the chemical and pharmacological characteristics of the genus *Duhaldea* DC., several concerns remain. Notably, the majority of pharmacological investigations on plant metabolites have been conducted exclusively *in vitro*, leading to a low confidence level regarding the validity of such simplistic *in vitro* studies demonstrating activity. Likewise, certain pharmacological assessments of extracts from this genus have only confirmed their efficacy *in vitro*. The current study mainly focused on the pharmacological activity profile of the extracts and isolated metabolites of the genus *Duhaldea* DC, while the mechanism of action was less studied, and targets and channels of action of the active metabolites corresponding to diseases were not scientifically elucidated. Modern scholars can consider using network pharmacology, data mining, and virtual screening to predict the targets, receptors, and pathways of their chemical metabolites related to pharmacological activities. At the same time, the molecular mechanisms and relationships between the active metabolites of the genus and the potential pharmacological activities are validated through high-quality and well-designed *in vivo* and *in vitro* and clinical studies.

In terms of pharmacological effects, most of them have focused on the anti-inflammatory, antitumor, antioxidant, and other effects, but at present, there are few modern pharmacological studies of the traditional effects of FI in the treatment of diseases. These ignore the modern pharmacological interpretation of traditional applications. In the future, pharmacologic studies of the genus *Duhaldea* DC can focus on indications in its traditional applications and should also provide a modern pharmacological explanation for the traditional application of the genus *Duhaldea* DC. At the same time, it should be noted that the plants of the genus *Duhaldea* DC are used as both medicine and food, and the pharmacological effects of the application in food and the effect on the inhibition of some disease-causing factors in food, as well as the prevention and control of some diseases.

Finally, *Duhaldea* DC species possess various biological activities, which can be applied to clinical medicine with further research. In addition, with the advancements observed recently in analytical techniques and quality control methods, among which the improvement and update in chromatography techniques and molecular identification methods, it is inevitable that new quality markers and quality control measures may be adopted for the better quality assessment of traditional botanical drug medicine in the future.

Plants of the genus *Duhaldea* DC as traditional plant medicines have made outstanding contributions in treating diseases and maintaining physical health. In this study, the ethnopharmacology, phytochemistry, and pharmacological effects of the genus *Duhaldea* DC were systematically elaborated to obtain a comprehensive understanding of the genus *Duhaldea* DC and reveal the shortcomings of the current research studies. In response to these shortcomings, this study provides guidance for future research on the genus *Duhaldea* DC, providing an effective scientific basis for expanding the pharmacological effect of *Duhaldea* DC, explaining the traditional application of *Duhaldea* DC, developing new drugs rationally, ensuring drug safety, controlling drug quality, and adapting *Duhaldea* DC to clinical application.

Author contributions

LS: conceptualization, data curation, formal analysis, investigation, methodology, resources, software, validation, and writing–original draft. KL: conceptualization, visualization, and writing–original draft. SY: formal analysis, investigation, and writing–original draft. MH: investigation, resources, and writing–original draft. XM: conceptualization, software, and writing–original draft. BY: software and writing–original draft. LG: data curation, project administration, and writing–review and editing. SX: data curation, funding acquisition, project administration, supervision, and writing–review and editing.

Funding

The author(s) declare that financial support was received for the research, authorship, and/or publication of this article. This study was supported by the Science and Technology Innovation Program of Hunan Province (No. 2022RC1228).

Conflict of interest

The authors declare that the research was conducted in the absence of any commercial or financial relationships that could be construed as a potential conflict of interest.

Publisher's note

All claims expressed in this article are solely those of the authors and do not necessarily represent those of their affiliated organizations, or those of the publisher, the editors, and the reviewers. Any product that may be evaluated in this article, or claim that may be made by its manufacturer, is not guaranteed or endorsed by the publisher.

Supplementary material

The Supplementary Material for this article can be found online at: https://www.frontiersin.org/articles/10.3389/fphar.2024.1479963/full#supplementary-material

References

Aizaizi, A., Zhu, W. C., and Patihan, K. (2018). Effect and mechanism of aqueous Inula Cappa aqueous extract on serum inflammatory factors in rats with severe pneumonia. *J. Clin. Exp. Med.* 17 (16), 1708–1711. doi:10.3969/j.issn.1671-4695.2018.16.008

Badshah, S. L., Faisal, S., Muhammad, A., Poulson, B. G., Emwas, A. H., and Jaremko, M. (2021). Antiviral activities of flavonoids. *Biomed. Pharmacother.* 140, 111596. doi:10.1016/j.biopha.2021.111596

Baruah, R. N., Sharma, R. P., Baruah, J. N., Mondeshka, D., Hertz, W., and Watanabe, K. (1982). Ineupatoriol, a thiophene analogue of ichthyothereol, from Inula eupatorioides. *Phytochemistry* 21 (3), 665–667. doi:10.1016/0031-9422(82)83161-0

Baruah, R. N., Sharma, R. P., Thyagarajan, G., Herz, W., Govindan, S. V., and Blount, J. F. (1980). Unusual germacranolides from Inula eupatorioides. *J. Org. Chem.* 45 (24), 4838–4843. doi:10.1021/jo01312a007

Chang, Y., Fei, S., Junqi, H., Yonglin, W., Yongjun, L., Yanyu, L., et al. (2020). Effect of active constituents from inula cappa on the protein expression of CYP3A4 in HepG2 cells with high PXR expression. *Guizhou Yike Daxue Xuebao* 45 (10), 1137–1142. doi:10.19367/j.cnki.2096-8388.2020.10.004

Cheng, X. (2012). *Studies on bioactive secondary metabolites from four plants of inula genus*. Doctor: Shanghai Jiao Tong University.

Cheng, X., Ma, J., Amadou, I., Zhao, W., Chen, Y., Zhang, C., et al. (2023). Electrophilic components from Xiaoheiyao (rhizomes of Inula nervosa Wall.) alleviate the production of heterocyclic aromatic amines via creatinine inhibition. *Food Chem.* 404, 134561. doi:10.1016/j.foodchem.2022.134561

Cheng, X., Shao, W., Zhang, S., Wang, G., Shan, L., Shen, Y., et al. (2014a). Winolides A–C, bioactive sesquiterpene lactones with unusual 5, 6-secoeudesmane frameworks from Inula wissmanniana. *RSC Adv.* 4 (64), 33815–33818. doi:10.1039/c4ra05131a

Cheng, X., Shoude, Z., Chunhui, W., Jie, R., Jiangjiang, Q., Xue, T., et al. (2013). Bioactive eudesmane and germacrane derivatives from Inula wissmanniana Hand.-Mazz. *Phytochemistry* 96, 214–222. doi:10.1016/j.phytochem.2013.10.006

Cheng, X., Tu, P., Dong, W., Yu, B., Xia, S., Muskat, M. N., et al. (2022). Electrophilic thymol isobutyrate from Inula nervosa Wall.(Xiaoheiyao) ameliorates steatosis in HepG2 cells via Nrf2 activation. *J. Funct. Foods* 88, 104895. doi:10.1016/j.jff.2021.104895

Cheng, X., Wang, C., Wei, P., Zhang, X., Zeng, Q., Yan, S., et al. (2014b). New sesquiterpenic acids from Inula wissmanniana. *Fitoterapia* 95, 139–146. doi:10.1016/j.fitote.2014.03.013

Cheng, X., Zhao, W., Dong, W., and Le, G. (2020). Chemical space charting of different parts of inula nervosa wall.: upregulation of expression of Nrf2 and correlated antioxidants enzymes. *Molecules* 25 (20), 4789. doi:10.3390/molecules25204789

Chunli, H., Lehao, w., Yang, Y., Huizi, J., and Yan, Z. (2021). The anti-inflammatory activity and mechanisms of Inula pterocaula extract in LPS-induced inflammatory responses in RAW 264.7 macrophages. *Dalian Gongye Daxue Xuebao* 40 (04), 253–259. doi:10.19670/j.cnki.dlgydxxb.2021.0404

Ding, B., and Jin, C. (2017). *Flora of wenzhou*. China Forestry Publishing House.

Dong, W., Yuge, J., Shufang, X., Congcong, C., Wei, Z., and Xiang-rong, C. (2020). Study on intervention effects of electrophilic components from Xiaoheiyao against free fatty acid-induced steatosis in HepG2 cells. *Packag. Food Mach.* 36 (3), 24–33. doi:10.13652/j.issn.1003-5788.2020.03.005

Dorina, G., E, J. A., Szilárd, V., Alex, V., Zoltán, S., Julia, S., et al. (2023). Inositol is an effective and safe treatment in polycystic ovary syndrome: a systematic review and meta-analysis of randomized controlled trials. *Reprod. Biol. Endocrin* 21 (1), 10. doi:10.1186/s12958-023-01055-z

Fardoun, M. M., Maaliki, D., Halabi, N., Iratni, R., Bitto, A., Baydoun, E., et al. (2020). Flavonoids in adipose tissue inflammation and atherosclerosis: one arrow, two targets. *Clin. Sci.* 134 (12), 1403–1432. doi:10.1042/CS20200356

Gill, B. S., Kumar, S., and Navgeet, M. (2016). Triterpenes in cancer: significance and their influence. *Mol. Biol. Rep.* 43, 881–896. doi:10.1007/s11033-016-4032-9

Gong, Z., Li, M., Xiong, D., Wu, L., Liu, T., Lan, Y., et al. (2018). Evaluation of anti-inflammatory activity of inula cappa extract based on inflammation model *in vitro* and *in vivo*. *Nat. Prod. Res.* 29 (12), 2050. doi:10.16333/j.1001-6880.2017.12.009

Goswami, A. C., Baruah, R. N., Sharma, R. P., Baruah, J. N., Kulanthaivel, P., and Herz, W. (1984). Germacranolides from inula cappa. *Phytochemistry* 23 (2), 367–372. doi:10.1016/S0031-9422(00)80334-9

Guo, Q., Yang, J., and Liu, J. (2007). Studies on the chemical constituents from Inula cappa (II). *J. Chin. Med. Mat.* 30 (1), 35–37. doi:10.13863/j.issn1001-4454.2007.01.015

He, A., She, C., Zeng, J., and Peng, S. (2016). Comparison study on *in vitro* and *in vivo* antioxidant activities of Inula nervosa Wall. extracts from different parts. *Chin. Pharmacol. Bull.*, 79–83. doi:10.3969/j.issn.1001-1978.2016.01.017

He, Y., Wu, Q., Huang, L., Su, Y., Yao, X., Wu, D., et al. (2019). Protective effect of InuIa cappa (buch.-ham) DC. Water extract on CCl4 and D-GalN induced acute liver injury in mice. *Sci. Technol. Eng.* 19 (23), 42–46. doi:10.3969/j.issn.1671-1815.2019.23.007

Hideaki, F., Tomonori, M., Takayuki, K., Sadaki, Y., Akitsugu, Y., Masaru, H., et al. (2009). Inulavosin, a melanogenesis inhibitor, leads to mistargeting of tyrosinase to lysosomes and accelerates its degradation. *J. Invest. Dermatol* 129 (6), 1489–1499. doi:10.1038/jid.2008.376

Huang, C., Changsheng, D., Yanan, Z., Yang, Y., Huizi, J., and Yan, Z. (2021a). Duhaldea pterocaula (franch.) anderb. Attenuates nociception and inflammation via GABAA receptors. *Front. Pharmacol.* 12, 753128. doi:10.3389/fphar.2021.753128

Huang, C., Dong, C., Zhu, Y., Yu, Y., Jin, H., and Zhang, Y. (2021b). Duhaldea pterocaula (franch.) anderb. Attenuates nociception and inflammation via GABAA receptors. *Front. Pharmacol.* 12, 753128. doi:10.3389/fphar.2021.753128

Jyoti, K., Rahul, S., Arti, P., K, L. S., and B, S. M. (2017). Anti-inflammatory and immunomodulatory activities of Inula cappa roots (Compositae). *J. Complement. Integr. Med.* 14 (3), 20160083. doi:10.1515/jcim-2016-0083

Kalola, J., and Shah, M. (2006). Actividad de barrido de los radicales libres de Inula cappa. *Ars Pharm.* 47 (4), 385–401. doi:10.30827/ars

Kiani, A., Paolacci, S., Calogero, A., Cannarella, R., Di Renzo, G., Gerli, S., et al. (2021). From Myo-inositol to D-chiro-inositol molecular pathways. *Eur. Rev. Med. Pharm.* 25 (5), 2390–2402. doi:10.26355/eurrev_202103_25279

Kiran, K. A., Kumar, S., and Sharma, P. K. (2017). Hepatoprotective activity of Inula cappa DC. Aqueous extract against carbon tetrachloride induced hepatotoxicity in Wistar rats. *Int. Res. J. Pharm.* 8, 14–19. doi:10.7897/2230-8407.08013

Li, F. (2017). Anti-inflammatory effect of inula cappa aqueous extract on Klebsiella pneumoniae-induced severe pneumonia in rats. *World Chin. Med.* 12 (10), 2438–2442. doi:10.3969/j.issn.1673-7202.2017.10.041

Li, W., Yang, Y., Wu, J., Jiang, S., Yang, Y., Guo, T., et al. (2023). A new labdane diterpenoid glycoside and other constituents from Inula nervosa (Asteraceae) and their chemotaxonomic importance. *Biochem. Syst. Ecol.* 109, 104662. doi:10.1016/j.bse.2023.104662

Li, Y., Li, T., Chen, Z., Wang, R., Li, B., Dong, F., et al. (2020). Study on antibacterial activity of extracts from roots of inula cappa. *Chin. Arch. Tradit. Chin. Med.* 38 (01), 24–27. doi:10.13193/j.issn.1673-7717.2020.01.006

Liby, K. T., Yore, M. M., and Sporn, M. B. (2007). Triterpenoids and rexinoids as multifunctional agents for the prevention and treatment of cancer. *Nat. Rev. Cancer* 7 (5), 357–369. doi:10.1038/nrc2129

Liu, P., Yang, G., Tian, X., Zhang, Y., Li, F., and Wang, F. (2011). Antioxidating effects of Inula nervosa Wall. ex DC. on the edible oils and its antimicrobial activity. *Sci. Technol. Food Ind.* 32 (10), 187–189. doi:10.13386/j.issn1002-0306.2011.10.026

Liu, S., Chen, J. J., Li, J., Chen, F., and Deng, L. (2010). Antmi icrobial effects of inula cappa O rganic SolventExtrac ts. *Liaoning J. Tradit. Chin. Med.* 37 (03), 398–400. doi:10.13192/j.ljtcm.2010.03.19.liushg.087

Liu, S., Hu, X., Liu, X., and Deng, L. (2009a). Chemical campositin of the essental oil fram inula cappa and their effects on free radicals scavenging. *J. Anhui Agric. Univ.* 37 (26), 12536–12537+12666. doi:10.13989/j.cnki.0517-6611.2009.26.148

Liu, S., Li, J., Chen, F., Liu, X., and Deng, L. (2009b). Studies on the antinicrobial activities of aqueous fram inula cappa DC *in vitro*. *Lishizhen Med. Mat. Med. Res.* 20 (12), 3072–3074. doi:10.3969/j.issn.1008-0805.2009.12-3072-02

Liu, W., Ge, T., Liu, S., and Liu, X. (2010). Extraction of flavonoids from inula cappa and its antibacterial activity. *Hubei. Agric. Sci.* 49 (02), 426–429. doi:10.14088/j.cnki.issn0439-8114.2010.02.072

Long, S. (2004). Clinical experience of "maoshoucai" for treating traumatic injury. *JMPCM* 12, 231–232.

Ma, J., Li, K., Shi, S., Li, J., Tang, S., and Liu, L. (2022). The application of UHPLC-HRMS for quality control of traditional Chinese medicine. *Front. Pharmacol.* 13, 922488. doi:10.3389/fphar.2022.922488

Marine, L. C., and Christophe, O. S. (2013). Potential role and therapeutic interests of myo-inositol in metabolic diseases. *Biochimie* 95 (10), 1811–1827. doi:10.1016/j.biochi.2013.05.011

Mei, D., Takaki, H., Bin, C., Qingwen, S., Siming, W., Kazuko, K., et al. (2015). Protein kinase Cα-mediated cytotoxic activity of ineupatorolide B from Inula cappa DC. in HeLa cells. *Int. J. Oncol.* 47 (5), 1839–1844. doi:10.3892/ijo.2015.3172

Miranda, R. d.S., de Jesus, B. d.S. M., da Silva Luiz, S. R., Viana, C. B., Adao Malafaia, C. R., Figueiredo, F. d.S., et al. (2022). Antiinflammatory activity of natural triterpenes—an overview from 2006 to 2021. *Phytother. Res.* 36 (4), 1459–1506. doi:10.1002/ptr.7359

Mo, J., Xu, M., Yang, D., and Huang, Z. (2012). Experimental study on anti-inflammatory and analgesic effects of ethanol extracts of Dong-medicine Inula cappa. *Chin. J. Exp. Tradit. Med. Form.* 18, 258–260. doi:10.13422/j.cnki.syfjx.2012.21.021

Neelam, E., Khatkar, A., and Sharma, K. K. (2020). Phenylpropanoids and its derivatives: biological activities and its role in food, pharmaceutical and cosmetic industries. *Crit. Rev. Food Sci. Nutr.* 60 (16), 2655–2675. doi:10.1080/10408398.2019.1653822

Neilsen, E., William, K., and David, A. (2014). Steroids: pharmacology, complications, and practice delivery issues. *Ochsner J.* 14 (2), 203–207.

Nikomtat, J., Meepowpan, P., and Tragoolpua, Y. (2011). Inhibition of Inula cappa (Ham. ex D. Don) DC. extracts on herpes simplex virus infection *in vitro*. *Afr. J. Microbiol.* 5 (24), 4049–4058. doi:10.5897/AJMR10.387

Peng, G., Xiong, D., Li, M., Wu, L., Chen, T., Li, Y., et al. (2017). Analysis of chemical constituents of effective components of Inula cappa. *J. Anhui. Agri. Sci.* 45 (29), 131–133. doi:10.13989/j.cnki.0517-6611.2017.29.041

Peng, J., Xie, J., Shi, S., Luo, L., Li, K., Xiong, P., et al. (2021). Diagnostic fragment-ion-based for rapid identification of chlorogenic acids derivatives in Inula cappa Using UHPLC-Q-Exactive orbitrap mass spectrometry. *J. Anal. Methods Chem.* 2021, 6393246. doi:10.1155/2021/6393246

Priydarshi, R., Melkani, A. B., Mohan, L., and Pant, C. C. (2016). Terpenoid composition and antibacterial activity of the essential oil from Inula cappa (Buch-Ham. ex. D. Don) DC. *J. Essent.* 28 (2), 172–176. doi:10.1080/10412905.2015.1090935

Schulz, V., Hänsel, R., and Tyler, V. E. (2001). *Rational phytotherapy: a physician's guide to herbal medicine*. Psychology Press, 1–39.

Serafini, M., Peluso, I., and Raguzzini, A. (2010). Flavonoids as anti-inflammatory agents. *Proc. Nutr. Soc.* 69 (3), 273–278. doi:10.1017/S002966511000162X

Shen, N., Wang, T., Gan, Q., Liu, S., Wang, L., and Jin, B. (2022). Plant flavonoids: classification, distribution, biosynthesis, and antioxidant activity. *Food Chem.* 383, 132531. doi:10.1016/j.foodchem.2022.132531

Tai, Z., Chen, C., Qin, B., Cai, L., and Xu, Y. (2014). Studies on triterpenoid saponins from inula pterocaula. *J. Kunming Univ. Sci. Technol. Nat. Sci.* 39 (05), 70–75. doi:10.3969/j.issn.1007-855x.2014.05.014

Tao, Y., Lei, H., Guoqiang, F., Peipei, S., and Pinhua, L. (2015). Antioxidant activity of total flavonoids from sanicula astrantiifolia wolff. *Mod. Agric. Sci. Technol.* (17), 311–313+316. doi:10.3969/j.issn.1007-5739.2015.17-0311-03

Tao, Y., Tingting, L., Fen, Y., Fang, W., and Pinhua, L. (2016). Polysaccharides contents and antioxidant activity of Sanicula astrantiifolia Wolff. *Sci. Technol. Cereal. Oil. Food* 24 (03), 55–58. doi:10.16210/j.cnki.1007-7561.2016.03.012

Tvrzicka, E., Kremmyda, L.-S., Stankova, B., and Zak, A. (2011). Fatty acids as biocompounds: their role in human metabolism, health and disease-a review. part 1: classification, dietary sources and biological functions. *Biomed. Pap. Med. Fac. Palacky. Univ. Olomouc* 155 (2), 117–130. doi:10.5507/bp.2011.038

Wang, A., Li, M., Sun, J., Xiong, F., Chen, T. T., Wu, L., et al. (2018). Study on the antibacterial and anti-inflammatory activities of extracts from inula cappa (DC.). *Shizhen Guo Yi Guo Yao* 29 (07), 1580–1584. doi:10.3969/j.issn.1008-0805.2018.07.014

Wang, C., Zhang, X., Wei, P., Cheng, X., Ren, J., Yan, S., et al. (2013). Chemical constituents from Inula wissmanniana and their anti-inflammatory activities. *Arch. Pharmacal Res.* 36, 1516–1524. doi:10.1007/s12272-013-0143-1

Wang, C. H. (2013). *Studies on the constituents from inula wissmanniana and quallty control of inula cappa. master*. Shanghai Jiao Tong University.

Wang, F., Li, X., Sun, Q., Yao, S., Ke, C., Tang, C., et al. (2012). Sesquiterpene lactones from Inula cappa. *Phytochem. Lett.* 5 (3), 639–642. doi:10.1016/j.phytol.2012.06.012

Wang, Z., Ma, X., Shi, S., He, S., Li, J., Wilson, G., et al. (2023). Structural characterization and anti-inflammatory activity of a novel polysaccharide from Duhaldea nervosa. *Polymers* 15 (9), 2081. doi:10.3390/polym15092081

Wardana, A. P., Aminah, N. S., Rosyda, M., Abdjan, M. I., Kristanti, A. N., Tun, K. N. W., et al. (2021). Potential of diterpene compounds as antivirals, a review. *Heliyon* 7 (8), e07777. doi:10.1016/j.heliyon.2021.e07777

Wei, C., Kailin, L., Pei, X., Kaiyan, G., Lian, Z., Jianbo, Y., et al. (2020). A systematic strategy for rapid identification of chlorogenic acids derivatives in Duhaldea nervosa using UHPLC-Q-Exactive Orbitrap mass spectrometry. *Arab. J. Chem.* 13 (2), 3751–3761. doi:10.1016/j.arabjc.2020.01.007

Wei, L., Zhiqi, W., Dong, W., Yulin, H., Mengchu, L., Jianping, G., et al. (2022). Analysis of chemical constituents and study on anti-complement activity in the inflorescences of inula nervosa. *Chin. Tradit. Pat. Med.* 44 (07), 2401–2405. doi:10.3969/j.issn.1001-1528.2022.07.061

Wen, Z., Huang, W., Long, W., Gong, J., and Wu, D. (2019). *In vitro* anticomplementary activity and quality evaluation of dried blossoms of Inula nervosa Wall. from different geographical origins. *Biomed. Chromatogr.* 33 (12), e4682. doi:10.1002/bmc.4682

Wu, J., Tang, C., Cai, Y., Ke, C., Lin, L., Yao, S., et al. (2017). Cytotoxic germacrane-type sesquiterpene lactones from the whole plant of Inula cappa. *Chin. Chem. Lett.* 28 (5), 927–930. doi:10.1016/j.cclet.2016.11.011

Wu, J., Tang, C., Yao, S., Zhang, L., Ke, C., Feng, L., et al. (2015). Anti-inflammatory inositol derivatives from the whole plant of Inula cappa. *J. Nat. Prod.* 78 (10), 2332–2338. doi:10.1021/acs.jnatprod.5b00135

Wu, Q., Shi, Y., and Jia, Z. (2006). Eudesmane sesquiterpenoids from the Asteraceae family. *Nat. Prod. Rep.* 23 (5), 699–734. doi:10.1039/B606168K

Wu, Z., and Peter, R. (2011). *Flora of China*. Beijing: Science Press.

Xie, H., Chen, H., Cao, B., Zhang, H., and Zou, Z. (2007). Cytotoxic germacranolide sesquiterpene from Inula cappa. *Chem. Pharm. Bull.* 55 (8), 1258–1260. doi:10.1248/cpb.55.1258

Xie, H., Wang, J., Chen, Z., Yuan, G., Li, Q., and Qin, L. (2012). Antimicrobial compound isolated from inula cappa and its inhibitory characteristics. *Nat. Prod. Res. Dev.* 24 (11), 1534–1537. doi:10.16333/j.1001-6880.2012.11.021

Yan, L., Cheng, X., Zeng, Q., Qin, J., Zhang, W., and Jin, H. (2011). Phytane and neoclerodane diterpenes from the aerial parts of Inula nervosa Wall. *Biochem. Syst. Ecol.* 39 (4-6), 700–703. doi:10.1016/j.bse.2011.06.001

Yan, L., Huang, Y., Fu, J., Qin, J., Zeng, Q., Zhu, Y., et al. (2010). Three new phenylpropanoids from inula nervosa wall. *Helv. Chim. Acta* 93 (7), 1418–1421. doi:10.1002/hlca.200900432

Yoshida, T., Mori, K., and Guangxin, H. (1995). Inulavosin, a new thymol dimer with piscicidal activity from Inula nervosa. *Heterocycles* 9 (41), 1923–1926. doi:10.1002/CHIN.199552231

Yuan, Z., Hongyan, Z., Ling, X., and Mengli, L. (2021). Scavenging and disconnecting effects on nitrosation reaction by extracts of stem and leaf of inula nervosa wall. *Southwest China J. Agric. Sci.* 34 (10), 2145–2150. doi:10.16213/j.cnki.scjas.2021.10.012

Zheng, L., Hao, X., Yuan, C., Huang, L., Zhang, J., Dong, F., et al. (2015). Study on chemical constituents of Inula cappa. *China J. Chin. Mater Med.* 40 (4), 672–678. doi:10.4268/cjcmm20150419

Zhou, W. (2017). Chemical constituents of Inula cappa. *J. Chin. Pharm. Sci.*, 25–30. doi:10.11669/cpj.2017.01.005

Zhu, S., Chunli, H., Yongzhen, X., Yangguo, X., Guojing, W., Weidong, Z., et al. (2019). Pterocaullins A– D, four sesquiterpene lactones from Inula pterocaula. *Phytochem. Lett.* 33, 70–76. doi:10.1016/j.phytol.2019.07.010

Zielińska Błajet, M., and Feder Kubis, J. (2020). Monoterpenes and their derivatives—recent development in biological and medical applications. *Int. J. Mol. Sci.* 21 (19), 7078. doi:10.3390/ijms21197078

frontiers | Frontiers in Pharmacology

TYPE Original Research
PUBLISHED 28 January 2025
DOI 10.3389/fphar.2025.1538837

Check for updates

OPEN ACCESS

EDITED BY
Zhichao Xu,
Northeast Forestry University, China

REVIEWED BY
Shijun Xu,
Chengdu University of Traditional Chinese Medicine, China
Ling Tang,
Southern Medical University, China
Jidong Fang,
The Pennsylvania State University, United States

*CORRESPONDENCE
Lili Huang,
huanglili@hljucm.edu.cn

RECEIVED 03 December 2024
ACCEPTED 09 January 2025
PUBLISHED 28 January 2025

CITATION
Wu J, Sun H, Zhao Y, Lian L, Bian H, Guo Y, Li D and Huang L (2025) The spectrum-efficacy correlation of Kai-Xin-San for cognition of $A\beta_{42}$ transgenic *Drosophila* and verification of its active ingredients.
Front. Pharmacol. 16:1538837.
doi: 10.3389/fphar.2025.1538837

COPYRIGHT
© 2025 Wu, Sun, Zhao, Lian, Bian, Guo, Li and Huang. This is an open-access article distributed under the terms of the Creative Commons Attribution License (CC BY). The use, distribution or reproduction in other forums is permitted, provided the original author(s) and the copyright owner(s) are credited and that the original publication in this journal is cited, in accordance with accepted academic practice. No use, distribution or reproduction is permitted which does not comply with these terms.

The spectrum-efficacy correlation of Kai-Xin-San for cognition of $A\beta_{42}$ transgenic *Drosophila* and verification of its active ingredients

Jinfu Wu[1], Hang Sun[1], Yiyang Zhao[1], Lian Lian[1], Hongsheng Bian[1], Yong Guo[2], Dan Li[2] and Lili Huang[1]*

[1]College of Pharmacy, Heilongjiang University of Chinese Medicine, Harbin, China, [2]Shineway Pharmaceutical Group Co., Ltd., Shijiazhuang, China

Introduction: This study aims to establish the fingerprint spectra of Kai-Xin-San (KXS) and investigate its spectrum-effect relationship in treating Alzheimer's disease (AD).

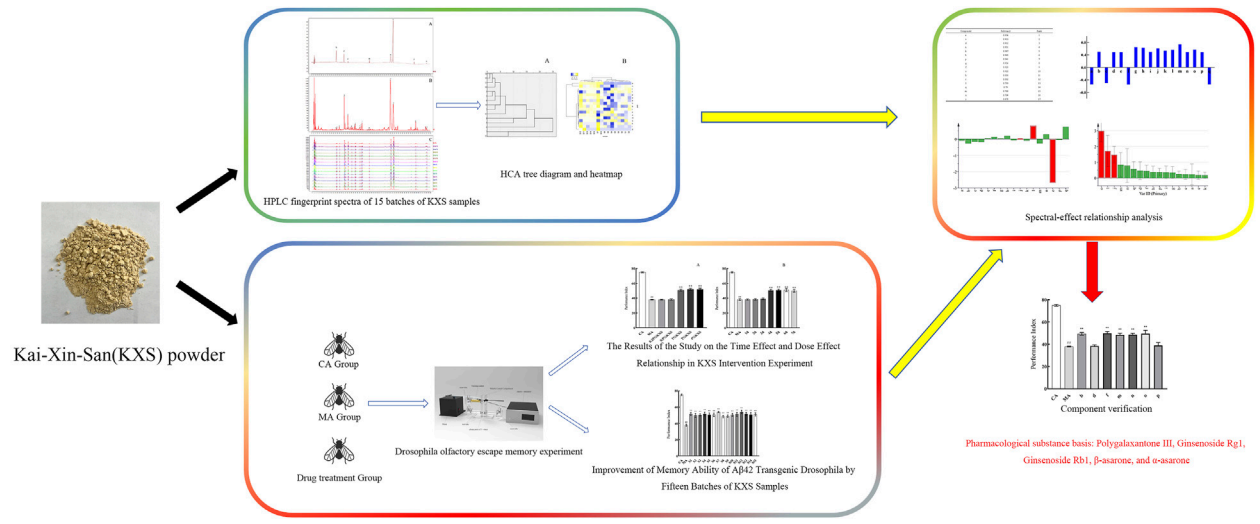
Methods: Initially, the fingerprints of 15 batches of KXS were established and analyzed using HPLC, with the method's precision, stability, and repeatability thoroughly evaluated. Subsequently, the effects of the 15 batches of KXS were assessed in an olfactory escape memory experiment, utilizing $A\beta_{42}$ transgenic *drosophila* as a model. Finally, the spectrum-effect relationship between the KXS fingerprint and memory improvement was analyzed, with the active ingredients subjected to validation testing.

Results: The results identified seventeen common peaks in the fingerprint, and eight active components were determined: polygalaxanthone III, 3-6-disinapoylsucrose, ginsenoside Rg1, ginsenoside Rb1, β-asarone, α-asarone, dehydrotumulosic acid, and dehydropachymic acid. Treatment with KXS (1%, for 4 days) significantly enhanced the performance index of $A\beta_{42}$ flies in the olfactory experiment. Both spectrum-effect analysis and validation tests indicated that polygalaxanthone III, ginsenoside Rg1, ginsenoside Rb1, β-asarone, and α-asarone were positively correlated with the performance index and improved the performance index in the olfactory experiment. The HPLC fingerprint method for KXS demonstrated excellent precision, accuracy, and reproducibility, making it suitable for quality evaluation and control of KXS. Polygalaxanthone III, ginsenoside Rg1, ginsenoside Rb1, β-asarone, and α-asarone are identified as potential active ingredients of KXS for anti-AD effects.

Discussion: These findings provide an experimental basis for developing new drugs based on KXS and its active ingredient combinations.

KEYWORDS

Kai-Xin-San, spectrum-efficacy relationship, Alzheimer's disease, pharmacodynamic material basis, HPLC, Aβ42 transgenic *Drosophila*



GRAPHICAL ABSTRACT

1 Introduction

Alzheimer's disease (AD), a degenerative disorder of the central nervous system, is characterized by its insidious onset and age-related progression (Liu et al., 2024b). Clinically, the hallmark features of AD include memory decline and cognitive impairment (Huang et al., 2024). The incidence of AD increases significantly with age; among individuals over 65 years old, the incidence ranges from 4% to 7%, while for those over 85, it rises dramatically by 20%–30% (Lopez-Lee et al., 2024). According to the International Alzheimer's Association, globally, a new case of AD is diagnosed every 3 s, underscoring its status as a major public health concern with severe implications for human wellbeing (Liu et al., 2024a). This highlights the urgent need to develop effective treatments for AD.

The pathological mechanisms underlying AD are highly complex, and its precise etiology remains unclear. Aβ and tau proteins are pivotal in the disease's pathogenesis. Additionally, chronic inflammation, mitochondrial dysfunction, oxidative stress-induced neuronal damage or apoptosis, and other factors contribute significantly to the development of AD (Bero et al., 2011; Li et al., 2011; Ma et al., 2011; Dong et al., 2022; Kim et al., 2024). Current therapeutic drugs show limited efficacy, often targeting only one or a few elements of the disease's pathological processes, such as reducing amyloid-protein deposition (Tabor and Holtzman, 2023) or inhibiting neuronal apoptosis (Xu et al., 2021). However, these treatments do not effectively halt disease progression. Moreover, medications like acetylcholinesterase inhibitors (e.g., donepezil) and NMDA receptor antagonists (e.g., memantine) can cause side effects, including nausea, vomiting, and cardiac arrhythmia (Buck et al., 2024; Egunlusi and Joubert, 2024).

Drosophila melanogaster is widely utilized as a genetic model organism due to its short life cycle, rapid reproduction, and well-mapped genome. Numerous AD models have been established by expressing AD-related proteins in the brains of flies. $A\beta_{42}$ transgenic *drosophila*, which expresses the human $A\beta_{42}$ protein in its brain, exhibits reduced learning and memory capabilities, a shortened lifespan, and degenerative changes in brain regions (Iijima-Ando and Iijima, 2010). This model serves as a powerful tool for studying $A\beta_{42}$ and evaluating potential anti-AD drugs.

Traditional Chinese medicine (TCM) achieves therapeutic effects through multi-target and multi-perspective interventions, enabling comprehensive regulation and modulation of complex disease mechanisms. Compared to chemical drugs, TCM generally exhibits better tolerance and lower toxicity, offering significant therapeutic advantages in treating complex chronic diseases like AD (Ding et al., 2022). Kai-Xin-San (KXS), originally recorded in Bei Ji Qian Jin Yao Fang by Sun Simiao during the Tang Dynasty, is primarily used for treating mental restlessness, amnesia, insomnia, and severe palpitations (Yan et al., 2024). Modern pharmacological studies have demonstrated that KXS possesses anti-AD (Xu et al., 2023), antidepressant (Wang Y. T. et al., 2024), anti-inflammatory (Bai et al., 2022), and sleep-disorder-improving properties. Its anti-AD effects are achieved through various mechanisms, such as reducing amyloid-β (Aβ) protein deposition (Wang H. et al., 2024), upregulating protein kinase B phosphorylation levels (Jiao et al., 2022), improving mitochondrial dysfunction (Wang et al., 2023), and exerting neuroprotective effects (Zhang et al., 2023). The four herbal ingredients in KXS have also been studied for their anti-dementia properties. Research indicates that the primary active components with anti-AD effects include saponins in ginseng and polygala, oligosaccharide esters in polygala, phenylpropanoid compounds such as asarone in acorus gramineus, and triterpenic acids in poria (Park et al., 2019; Meng et al., 2021; Yuan et al., 2021; Zeng et al., 2021; Xu et al., 2023). However, the chemical complexity of KXS and the variability in medicinal efficacy due to factors such as origin, storage, and harvest season present challenges for quality consistency and reproducibility.

Evaluating the quality of TCM requires comprehensive, macroscopic, and non-linear analytical approaches. The HPLC fingerprint spectrum, as a quality control method, meets this

requirement effectively (Xu et al., 2022). However, HPLC fingerprint does not directly associate these components with therapeutic efficacy. Establishing a spectrum-effect relationship to connect fingerprint profiles with drug efficacy is essential for elucidating the pharmacodynamic material basis of TCM and developing effective quality control methods. This approach integrates chemical composition, pharmacological action, and disease relevance (Xu et al., 2022).

In this study, the HPLC technique was utilized to develop a fingerprint profile for KXS. Using an $A\beta_{42}$ transgenic *drosophila* model and memory performance as indicators, the spectrum-effect relationship was analyzed through grey relational analysis, bivariate correlation analysis, and partial least-squares regression. This analysis clarified the pharmacodynamic material basis of KXS, established quality standards, and ensured consistency in quality and therapeutic efficacy. Furthermore, these findings provide a solid foundation for the development of new drugs and the optimization of preparation techniques.

2 Materials and methods

2.1 Composition, source, and preparation of KXS sample solution

KXS is composed of ginseng, polygala, poria and acorus gramineus, with a proportion of 1:1:2:1, according to the Notice by the National Administration of Traditional Chinese Medicine of China.

Ginseng is the dried root and rhizome of *Panax ginseng* C. A. Mey. of the Araliaceae family. Polygala is the dried root of *Polygala tenuifolia* Willd. of the Polygalaceae family. Poria is the dried sclerotium of *Poria cocos* (Schw.) Wolf, a fungus of the Polyporaceae family. Acorus is the dried rhizome of *Acorus tatarinowii* Schott of the Araceae family. The above-mentioned medicinal materials were all provided by Shineway Pharmaceutical Group Co., Ltd., with a total of 15 batches (S1-S15).

Accurately weigh 1 g of KXS, add 5 mL of 95% methanol, and record the weight. Heat the mixture under reflux for 30 min, then allow it to cool. Re-weigh the solution and adjust to the original weight using 95% methanol. Mix thoroughly, filter, and collect the filtrate for use.

2.2 Preparation of chemicals and reference solutions

Polygalaxanthone III (DST230425-089), 3-6-disinapoylsucrose (DST210510-022), ginsenoside Rg1 (DSTDR000902), ginsenoside Rb1 (DSTDR000603), β-asarone (DSTDA001901), α-asarone (DST201025-044), dehydrotumulosic acid (DSTDQ010202), dehydropachymic acid (DSTDQ010101) were purchased from Dest Biotechnology Co., Ltd. (Sichuan, China). Acetonitrile (20240701, TEDIA) and methanol (20240628, TEDIA) were obtained from DiMa Technology Co., Ltd. (Beijing, China).

Dissolve an appropriate amount of the relevant components in 95% methanol to prepare the test solution. The concentrations of polygalaxanthone III, 3-6-disinapoylsucrose, ginsenoside Rg1, ginsenoside Rb1, β-asarone, α-asarone, dehydrotumulosic acid and dehydropachymic acid are 0.74 mg. mL^{-1}, 0.76 mg. mL^{-1}, 0.59 mg. mL^{-1}, 0.35 mg. mL^{-1}, 0.85 mg. mL^{-1}, 1.42 mg. mL^{-1}, 0.61 mg. mL^{-1} and 0.58 mg. mL^{-1}, respectively.

2.3 *Drosophila* strains, sources, and rearing conditions

Wild type W^{1118}, Elav-Gal4, and UAS-$A\beta_{42}$ *drosophila* were all provided by the Core Facility of *Drosophila* Resource and Technology, CEMCS, CAS.

Main groups: I Control group with the same genetic background (CA): Select male *drosophila* from the first generation of Elav-Gal4 virgin *drosophila* and W^{1118} male *drosophila* hybrid offspring. II $A\beta_{42}$ group (MA): Red-eyed straight-winged males were selected from the progeny generation of Elav-Gal4 virgin *drosophila* and UAS-$A\beta_{42}$ male *drosophila* (Elav/Y; UAS-Aβ/+, $A\beta_{42}$ *drosophila*) (Tue et al., 2020).

Standard *drosophila* Medium: The flies culture medium consists of cornmeal, soybean flour, sucrose, maltose, agar, yeast, and water. Specifically, it contains 6.7 g of cornmeal, 0.8 g of soybean flour, 4.0 g of sucrose, 4.2 g of maltose, 1.0 g of agar, 2.5 g of yeast, and 100 mL of water. Besides, sodium benzoate, with a dosage of 0.1 g, is selected as the preservative. The flies were maintained at a temperature of 25°C, with 60% humidity, under a 12-h light and 12-h dark cycle. The medium was refreshed every 3–4 days for passaged flies.

KXS-Containing Medium: Following the method for preparing Chinese medicine-containing medium described in previous research (Zhang et al., 2016), the KXS-containing medium was prepared with concentrations ranging from 0.25% to 4%. Before each administration, the *drosophila* were fasted for 3 h.

2.4 Analysis conditions of HPLC

The HPLC chromatographic analysis was performed using a Waters e2695 HPLC-DAD system (Waters, United States) equipped with a Waters Symmetry C_{18} chromatographic column (4.6 × 250 mm, 5 μm) (Waters, United States). For gradient elution, the mobile phases consisted of acetonitrile solution (organic phase C) and 0.2% phosphoric acid aqueous solution (organic phase D), with a flow rate of 1 mL min^{-1}. The temperature of the chromatographic column was maintained at 30°C. The injection volume was set to 20 μL, and the chromatograms were detected at a wavelength of 203 nm. The gradient elution program was as follows: 0–2 min, 10–12%C; 2–10 min, 12–14%C; 10–14 min, 14–15%C; 14–21 min, 15–16%C; 21–23 min, 16–18%C; 23–33 min, 18–26%C; 33–48 min, 26–30%C; 48–58 min, 30–35%C; 58–68 min, 35–37%C; 68–78 min, 37%C; 78–93 min, 37–50%C; 93–103 min, 50–74%C; 103–115 min, 74–82%C; 115–120 min, 82–10%C.

2.5 HPLC method validation

The KXS sample test solution (S1) was prepared following the procedure described in Section 2.1. Six consecutive injections were performed under the conditions outlined in Section 2.4 to assess the

precision of the instrument. The S1 test solution was injected at intervals of 0, 2, 4, 8, 12, and 24 h to evaluate sample stability. Additionally, six separate test solutions of S1 samples were prepared and injected to assess sample reproducibility.

2.6 Chromatographic peak identification

The reference solution, prepared as described in Section 2.2, was analyzed using the chromatographic system. The retention time of the reference peak was recorded, and the retention times of the reference components in the sample solution were determined by comparison with the recorded reference peak retention times.

2.7 Fingerprint similarity analysis

Fifteen batches of KXS samples were analyzed using the standardized HPLC method. The resulting chromatographic data were exported in CDF format and processed using the Similarity Evaluation System for Chromatographic Fingerprints of Traditional Chinese Medicines (version 2012).

2.8 Hierarchical cluster analysis

Systematic cluster analysis was performed using SPSS statistical software (IBM, United States). The between-groups linkage method was employed to analyze the chromatographic peak area data from the fingerprint spectra of 15 batches of KXS. The similarity between samples was measured using the Euclidean distance.

2.9 Behavioral experiments

2.9.1 *Drosophila* olfactory escape memory experiment

The experimental apparatus was provided by SANS Biotechnology Co., Ltd. (Supplementary Figure S1). The experiments were conducted in an environment maintained at a constant temperature of 25°C and humidity of 60%, under dark infrared conditions.

The olfactory escape memory experiment consisted of two phases: the training phase and the testing phase (Yu et al., 2024). In the training phase, a four-step process was followed. First, 100 flies were placed into the training tubes to adapt for at least 90 s. Second, the flies were exposed to CS + gas (4-methylcyclohexanol, MCH, Sigma, 104191) and synchronously subjected to 1.5-s pulses of 60 V electric shocks delivered every 3.5 s for a total of 12 pulses. Third, fresh air was introduced for 45 s to clear any residual CS + gas. Finally, the flies were exposed to CS- gas (3-octanol, OCT, Sigma, 218405) for 1 min without electric shocks. After the training phase, the testing phase was conducted immediately to examine the flies' instantaneous memory. Flies that had undergone the training phase were moved to the choice point of the T-maze, which contained two arms exposed to CS + gas and CS- gas, respectively. The flies were allowed to choose between the two arms based on olfactory cues within 2 min. Afterward, the flies were anesthetized with CO_2, and the numbers of flies in the CS + gas and CS- gas arms were recorded.

The performance index (PI) was used to evaluate the memory performance of flies. The calculation formula is as follows:

$$PI = [Number(CS-) - Number(CS+)] \div [Number(CS-) + Number(CS+)] \times 100$$

The average value of PI was calculated from the PI of fourteen batches flies in olfactory escape memory experiment (n = 14).

2.9.2 Investigation of time-effect and dose-effect relationships in KXS intervention experiments

Using the experimental method described in "2.9.1," an investigation was conducted to determine the effective dosage concentration and administration duration of KXS. Specifically, five concentrations of KXS—0.25%, 0.5%, 1%, 2%, and 4%—were examined. Administration at these concentrations was carried out for 4 days. Additionally, the study explored the effects of different durations of continuous dosing (1 day, 2 days, 3 days, 4 days, and 5 days) at a fixed concentration of 1% KXS.

2.9.3 Improvement effect of different batches of KXS samples on memory ability

The $A\beta_{42}$ transgenic *drosophila* were divided into fifteen groups, and each group received drugs from a specific batch. Following the experimental method outlined in "2.9.1," the number of *drosophila* in the respective gas environments was recorded for each group, and the PI for memory was calculated.

2.10 Spectrum-effect relationship analysis

The spectrum-effect relationship, which refers to the connection between the peak areas of the common peaks in KXS and its effect on enhancing cognitive ability, was established using grey relational analysis, bivariate correlation analysis, and partial least squares regression analysis.

2.11 Statistical analysis

Data are presented as mean ± SD. SPSS was used for statistical analysis, and GraphPad (United States) was employed for graphing. One-way ANOVA was conducted for data analysis. Statistical significance was indicated by $P < 0.05$.

3 Results

3.1 HPLC method validation

Using the α-asarone peak (peak 0) as the reference, the relative standard deviation (RSD) for precision ranged from 0% to 0.6%, for reproducibility from 0.1% to 0.5%, and for stability from 0% to 1.3%. The results showed that the RSD of the relative peak area of each chromatographic peak in the fingerprint chromatogram was less than 2%. The HPLC method demonstrated excellent accuracy, and

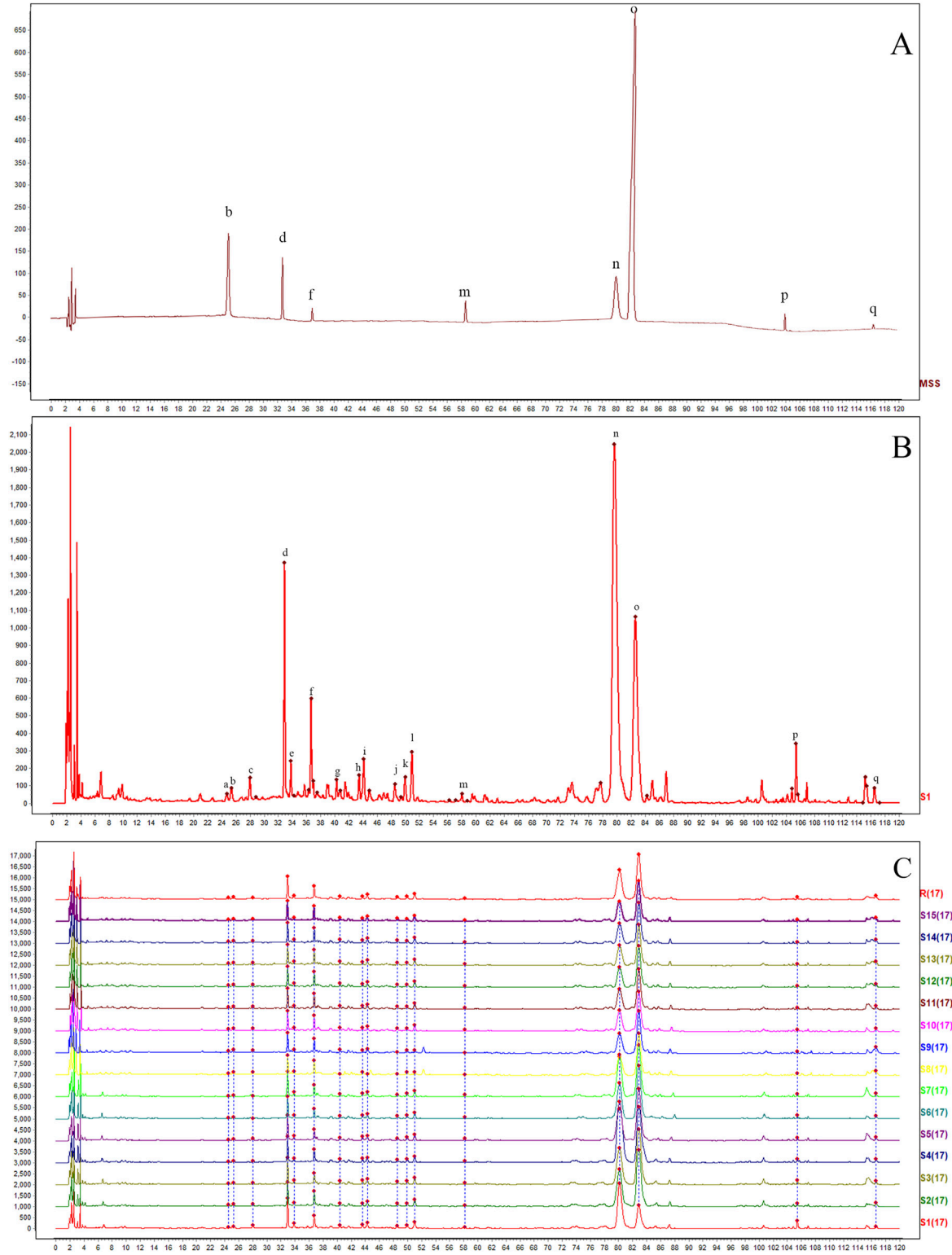


FIGURE 1
HPLC fingerprints of 15 batches of Kai-Xin-San **(A)** Mixed reference substance solution, **(B)** KXS sample and **(C)** 15 batches of KXS. b: polygalaxanthone III; d: 3-6-disinapoylsucrose; f: ginsenoside Rg1; m: ginsenoside Rb1; n: β-asarone; o: α-asarone; p: dehydrotumulosic acid; q: dehydropachymic acid.

TABLE 1 The relative peak areas of 17 common peaks in HPLC fingerprints of Kai-Xin-San.

Sample	a	b	c	d	e	f	g	h	i	j	k	l	m	n	o	p	q
S1	0.01	0.03	0.02	0.17	0.02	0.09	0.02	0.03	0.05	0.03	0.04	0.07	0.01	0.63	1.00	0.03	0.05
S2	0.02	0.03	0.02	0.17	0.02	0.09	0.02	0.03	0.05	0.02	0.04	0.07	0.01	0.62	1.00	0.03	0.05
S3	0.01	0.03	0.02	0.17	0.02	0.09	0.02	0.03	0.05	0.04	0.04	0.07	0.01	0.63	1.00	0.03	0.04
S4	0.01	0.03	0.02	0.17	0.02	0.09	0.02	0.03	0.04	0.04	0.04	0.07	0.02	0.62	1.00	0.02	0.05
S5	0.01	0.03	0.02	0.17	0.02	0.09	0.02	0.03	0.05	0.03	0.04	0.06	0.02	0.63	1.00	0.03	0.04
S6	0.01	0.03	0.02	0.17	0.02	0.09	0.02	0.03	0.05	0.03	0.04	0.06	0.02	0.63	1.00	0.03	0.03
S7	0.01	0.03	0.01	0.16	0.02	0.08	0.02	0.03	0.04	0.03	0.04	0.06	0.02	0.58	1.00	0.03	0.03
S8	0.02	0.03	0.02	0.17	0.02	0.09	0.02	0.02	0.05	0.01	0.04	0.03	0.00	0.63	1.00	0.03	0.04
S9	0.02	0.03	0.02	0.17	0.02	0.09	0.02	0.03	0.05	0.01	0.04	0.03	0.01	0.63	1.00	0.03	0.04
S10	0.02	0.03	0.01	0.15	0.02	0.08	0.02	0.03	0.04	0.03	0.04	0.06	0.01	0.56	1.00	0.02	0.03
S11	0.02	0.03	0.01	0.17	0.02	0.08	0.02	0.03	0.04	0.03	0.04	0.06	0.01	0.58	1.00	0.03	0.04
S12	0.02	0.03	0.01	0.16	0.02	0.08	0.02	0.03	0.04	0.03	0.04	0.06	0.01	0.59	1.00	0.03	0.03
S13	0.01	0.03	0.02	0.16	0.02	0.08	0.02	0.03	0.04	0.03	0.04	0.06	0.01	0.59	1.00	0.03	0.04
S14	0.02	0.03	0.02	0.16	0.02	0.08	0.02	0.03	0.04	0.03	0.04	0.06	0.01	0.59	1.00	0.03	0.04
S15	0.02	0.03	0.02	0.16	0.02	0.08	0.02	0.03	0.04	0.03	0.04	0.06	0.01	0.59	1.00	0.03	0.04
RSD (%)	22.42	3.60	9.03	3.95	4.21	5.91	4.37	7.01	3.73	32.02	4.20	19.96	30.91	4.12	0.00	2.86	15.44

Note: The o-peak is regarded as the characteristic peak.

TABLE 2 The relative retention times of 17 common peaks in HPLC fingerprints of Kai-Xin-San.

Sample	a	b	c	d	e	f	g	h	i	j	k	l	m	n	o	p	q
S1	0.29	0.30	0.35	0.41	0.42	0.46	0.50	0.54	0.55	0.60	0.62	0.64	0.72	1.03	1.00	1.32	1.46
S2	0.29	0.30	0.35	0.41	0.42	0.45	0.50	0.54	0.55	0.60	0.63	0.63	0.72	1.03	1.00	1.31	1.45
S3	0.30	0.30	0.35	0.41	0.41	0.45	0.50	0.54	0.55	0.60	0.63	0.63	0.72	1.03	1.00	1.32	1.45
S4	0.29	0.29	0.34	0.40	0.42	0.45	0.50	0.54	0.54	0.60	0.61	0.63	0.72	1.03	1.00	1.31	1.44
S5	0.30	0.31	0.35	0.41	0.41	0.46	0.50	0.54	0.55	0.60	0.62	0.62	0.72	1.03	1.00	1.32	1.46
S6	0.29	0.30	0.35	0.41	0.42	0.45	0.50	0.54	0.55	0.60	0.62	0.63	0.72	1.03	1.00	1.31	1.45
S7	0.29	0.30	0.35	0.41	0.42	0.46	0.50	0.54	0.55	0.61	0.62	0.64	0.73	1.04	1.00	1.33	1.46
S8	0.29	0.30	0.35	0.41	0.42	0.46	0.51	0.55	0.55	0.61	0.63	0.64	0.73	1.03	1.00	1.33	1.47
S9	0.29	0.30	0.35	0.41	0.42	0.46	0.50	0.54	0.55	0.61	0.63	0.64	0.73	1.04	1.00	1.33	1.47
S10	0.29	0.30	0.35	0.41	0.42	0.46	0.51	0.55	0.55	0.61	0.62	0.64	0.73	1.04	1.00	1.33	1.47
S11	0.29	0.30	0.34	0.41	0.42	0.46	0.50	0.54	0.55	0.61	0.62	0.64	0.73	1.03	1.00	1.32	1.46
S12	0.29	0.30	0.35	0.41	0.42	0.46	0.50	0.54	0.55	0.61	0.63	0.64	0.73	1.04	1.00	1.33	1.47
S13	0.29	0.30	0.35	0.41	0.42	0.46	0.50	0.54	0.55	0.61	0.62	0.64	0.73	1.05	1.00	1.33	1.46
S14	0.29	0.30	0.35	0.41	0.42	0.46	0.50	0.54	0.55	0.61	0.62	0.64	0.73	1.04	1.00	1.32	1.46
S15	0.29	0.30	0.34	0.41	0.42	0.46	0.50	0.54	0.55	0.60	0.62	0.63	0.73	1.05	1.00	1.32	1.46
RSD (%)	0.80	1.10	0.30	0.40	0.80	0.50	0.60	0.60	0.50	0.50	0.80	0.70	0.70	0.70	0.00	0.50	0.60

Note: The o-peak is regarded as the characteristic peak.

TABLE 3 The non-common peak area ratio of HPLC fingerprint of 15 batches of Kai-Xin-San.

Sample	Rate (%)	Sample	Rate (%)	Sample	Rate (%)
S1	4.40	S6	6.77	S11	5.55
S2	6.97	S7	8.33	S12	5.56
S3	5.34	S8	8.40	S13	5.75
S4	6.05	S9	8.58	S14	6.12
S5	7.44	S10	8.77	S15	6.64

TABLE 4 The similarity of HPLC fingerprint of 15 batches of Kai-Xin-San.

Sample	Similarities	Sample	Similarities	Sample	Similarities
S1	0.887	S6	0.998	S11	0.991
S2	0.999	S7	0.999	S12	0.991
S3	0.999	S8	0.997	S13	0.991
S4	0.98	S9	0.994	S14	0.991
S5	1	S10	0.989	S15	0.992

the KXS sample solution remained stable for up to 24 h. These findings confirm that the developed HPLC fingerprint method has superior reproducibility.

3.2 Establishment of fingerprint spectra for fifteen batches of KXS

As illustrated in Figure 1, chromatograms were obtained for the mixed reference solution (Figure 1A), the KXS test samples (Figure 1B), and each batch of KXS (Figure 1C) under the specified chromatographic conditions. By comparing the ultraviolet spectra and the retention times of the reference substance peaks, 17 common peaks were identified within the 0–120 min range. Eight components were identified: polygalaxanthone III (b), 3-6-disinapoylsucrose (d), ginsenoside Rg1 (f), ginsenoside Rb1 (m), β-asarone (n), α-asarone (o), dehydrotumulosic acid (p), and dehydropachymic acid (q). Peak o, with the largest area in the fingerprint spectrum, was designated as the characteristic peak following chromatographic system analysis. The relative peak areas of each common peak are listed in Table 1, relative retention times in Table 2, and the proportion of non-common peak areas in Table 3. Variations in the RSD of relative peak areas reflect differences in the compound content among batches.

3.3 Fingerprint similarity analysis

To assess sample similarity, a comparative analysis was performed between the fingerprint chromatograms of the 15 KXS batches and a reference chromatogram. The similarity range for the batches compared to the reference fingerprint was between 0.887 and 1, as detailed in Table 4. Most samples exhibited high similarity, with values close to or exceeding 0.99. For example, batches S2, S3, S6, and S7 showed similarities above 0.99, while S5 reached 1, indicating consistent chemical composition and relative content among these batches. This suggests stable quality and a well-controlled production process. However, batch S1, with a similarity of 0.887, displayed relatively lower similarity. This may point to minor differences in raw materials, processing, or storage, causing slight variations in chemical components. Despite this, the similarity remained high overall, indicating that the deviations were within an acceptable range.

3.4 Hierarchical clustering analysis (HCA)

The study employed the HCA function in SPSS statistical software (IBM, USA) and used the inter-group linkage method to analyze the fingerprints of 15 batches of KXS. HCA was applied to assess the correlation of the KXS HPLC fingerprints, and testing was performed using Heatmapper (http://www.heatmapper.ca/) (Xu et al., 2022). The HCA dendrogram (Figure 2A) and heatmap (Figure 2B) were generated. Each color unit in the heatmap corresponds to a matrix representing a numerical value. As seen in Figure 2, four clusters were identified. S1, S2, S3, S5, S6, S10, S11, S13, S14, and S15 form one group; S9 and S8 form another group; S4 forms a separate group; and S12 and S7 form a final group. The HCA results indicate that the different batches of KXS samples share similar fingerprints, but the peak areas of the chemical components differ, suggesting variations in the content of the chemical components. HCA can effectively differentiate samples at the chemical level.

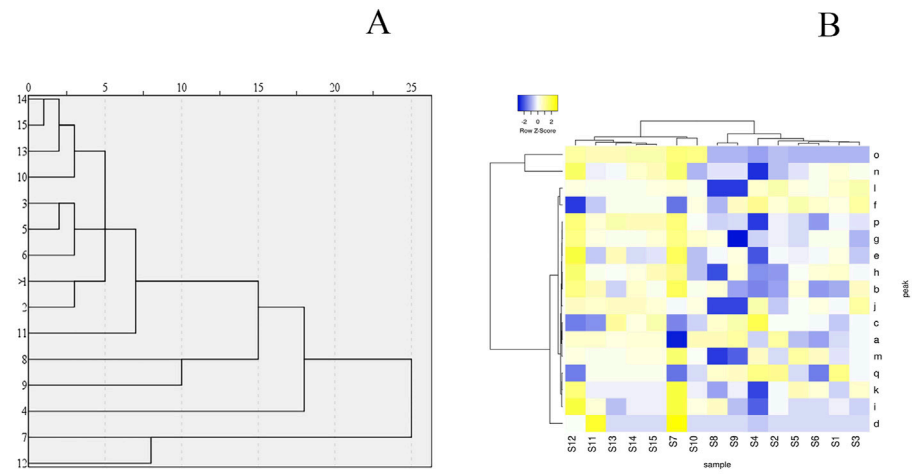


FIGURE 2
The hierarchical clustering analysis for common peak areas in Kai-Xin-San HPLC fingerprint **(A)** Dendrogram and **(B)** heat map.

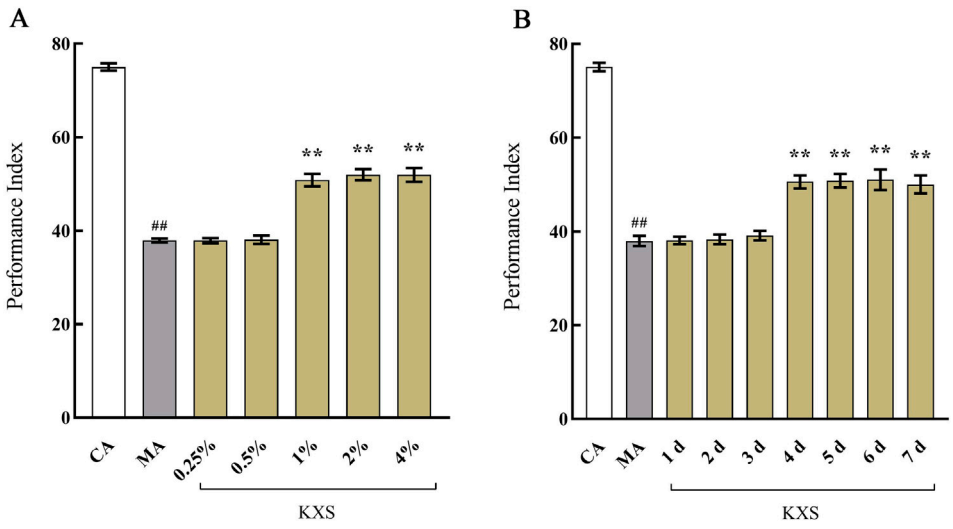


FIGURE 3
The effects of Kai-Xin-San on the performance index of I of $A\beta_{42}$ transgenic *drosophila* **(A)** Different concentration and **(B)** different duration. CA: Control group with the same genetic background. MA: $A\beta_{42}$ transgenic group. n = 14 per group. Data are presented as Mean ± SD. Compared with the CA, $^{\#\#}P < 0.01$; compared with the MA, $^{**}P < 0.01$.

3.5 Results of the study on the time effect and dose effect relationship in KXS intervention experiment

The experiments demonstrated that, except for the 0.25% and 0.5% KXS groups, which were ineffective, all other concentrations of KXS significantly enhanced the PI of $A\beta_{42}$ transgenic *drosophila* (Figure 3A). Similarly, except for the groups treated for 1, 2, and 3 days, all other treatment duration groups also showed improvements in PI (Figure 3B). Based on these results, the optimal administration concentration was determined to be 1% KXS, with a treatment duration of 4 days.

3.6 Improvement of memory ability in $A\beta_{42}$ transgenic *Drosophila* by fifteen batches of KXS samples

As shown in Figure 4, the 15 batches of KXS samples all demonstrated an enhancement effect on cognitive impairment in $A\beta_{42}$ transgenic *drosophila*. However, there were variations among the different samples in the extent of cognitive improvement. This discrepancy may be attributed to the differences in the chemical composition of the samples. Therefore, the spectrum-effect relationship was further investigated.

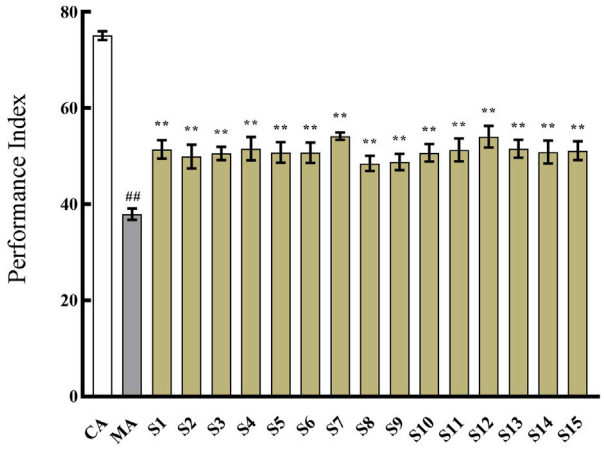


FIGURE 4
The effect of 15 batches of Kai-Xin-San on the performance index of $A\beta_{42}$ transgenic *drosophila*. CA: Control group with the same genetic background. MA: $A\beta_{42}$ transgenic group. S1~S15: Kai-Xin-San samples S1~S15. n = 14 per group. Data are presented as Mean ± SD. Compared with the CA, $^{\#\#}P < 0.01$; compared with the MA, $^{**}P < 0.01$.

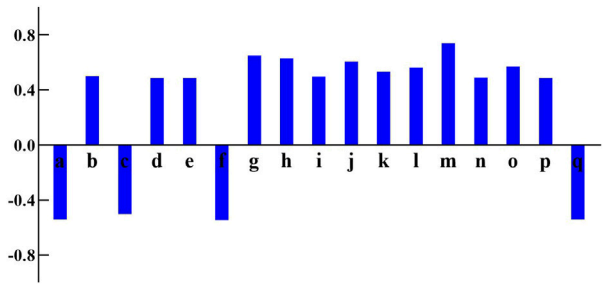


FIGURE 5
The correlation coefficients between peaks area and performance index of 17 common peaks in Kai-Xin-San HPLC fingerprints.

3.7 Spectral effect relationship analysis

3.7.1 Grey relational analysis (GRA)

GRA is a multifactorial statistical technique used to determine the strength of the association between each chemical constituent and drug efficacy. The correlation coefficient ranges from 0 to 1, with higher values indicating a stronger correlation with the improvement of cognitive impairment. A higher correlation coefficient suggests a stronger connection between the constituent and the drug efficacy, making it more likely to be a significant active substance. The chemical constituents with a correlation coefficient exceeding 0.8 are e (0.954), i (0.953), d (0.952), n (0.951), k (0.947), b (0.945), p (0.941), g (0.936), f (0.928), o (0.922), h (0.886), and c (0.862). These results suggest that these constituents may be potential active substances for the treatment of AD.

3.7.2 Bivariate correlation analysis (BCA)

The purpose of BCA is to examine the linear association between two variables. The pearson correlation coefficient is used to measure the degree of correlation between elements and drug efficacy. The higher the absolute value of this coefficient, the stronger the correlation. The data used is both reliable and representative. In this study, the BCA tool in SPSS statistical software (IBM, United States) was utilized to evaluate the correlation between the chromatographic peak area values and the PI. As shown in Figure 5, the components m, g, h, j, l, o, b, i, n, k, d, e, and p show a positive correlation with the cognitive improvement effect and may be potential active components for the treatment of AD.

3.7.3 Partial least - Squares regression (PLSR)

In order to investigate the comprehensive influence of peak areas on the PI of flies, PLSR analysis was conducted using software SIMCA-14.1 (Sartorius Stedim, Sweden). As shown in Figures 6A, B, in this model, when R^2 and Q^2 are both greater than 0.5, it indicates that the model not only fits the data well but also has a certain degree of accuracy in predicting new data, demonstrating good generalization ability. Thus, the model is considered to have a favorable fit. Using a VIP value greater than 1 as the criterion for screening potential active components, when the VIP value exceeds 1, the chemical component contributes significantly to the model. Additionally, 200 permutation tests were conducted. The intersection point of the Q^2 regression line and the y-axis is located on the negative semi-axis, indicating that the model is not over-fitted and that the model validation result is valid (see Figure 6C). The results show that the VIP values of o, l, and j are all greater than 1, suggesting that these three components are related to the improvement of cognitive impairment. Therefore, these components may be potential active ingredients of KXS in the treatment of AD.

3.8 Component verification

Based on the results of the above spectrum-effect relationship analysis, b, c, d, e, f, g, h, i, j, k, l, m, n, o, and p may be potential active ingredients of KXS. Among these, seven identified ingredients were selected for subsequent verification to further analyze the impact of a single ingredient on the PI of $A\beta_{42}$ transgenic *drosophila*. As described in Figure 7, the PI values of the 15 batches of KXS increased by an average of 35% compared to the MA. However, the PI of polygalaxanthone III, ginsenoside Rg1, ginsenoside Rb1, β-asarone, and α-asarone increased by 30.26%, 31.60%, 27.36%, 28.55%, and 30.74%, respectively. Compared to KXS, the PI growth rate of these active ingredients decreased to varying degrees.

4 Discussion

In our study, the HPLC fingerprint of KXS was successfully established, demonstrating good separation and repeatability. Eight chemical components were identified, which were derived from the four Chinese medicinal herbs constituting KXS. Polygalaxanthone III, ginsenoside Rg1, ginsenoside Rb1, β-asarone, and α-asarone may be the potential active ingredients of KXS in the treatment of AD.

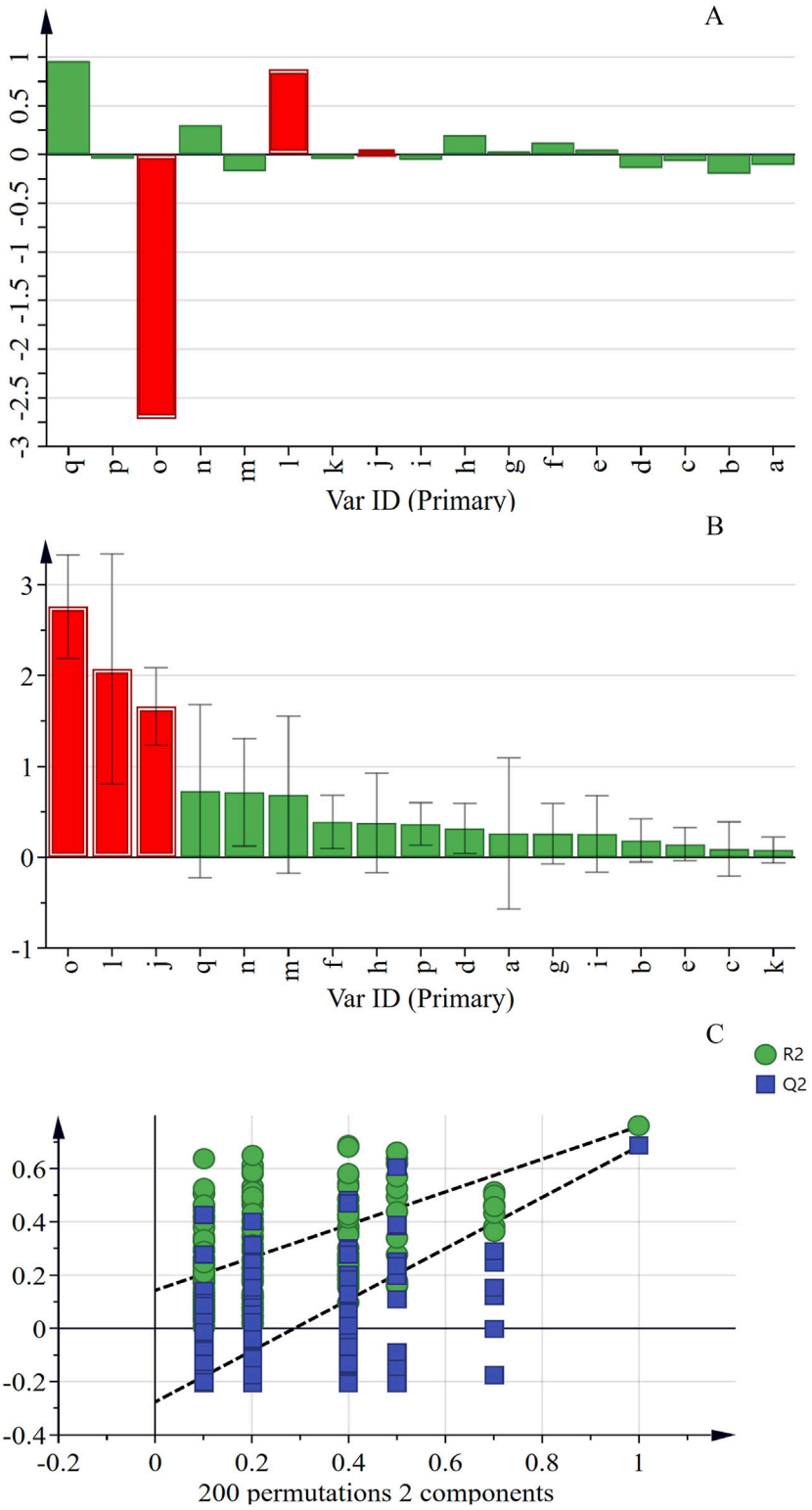


FIGURE 6
The PLSR analysis between peaks area and performance index of 17 common peaks in Kai-Xin-San HPLC fingerprints **(A)** Coefficients, **(B)** VIP **(C)** PLSR model.

These results can serve as a foundation for controlling the quality standards of KXS on one hand and provide an experimental basis for the development of new drugs combining KXS and its active ingredients on the other hand.

Due to the complex composition of traditional Chinese medicine, the presence of more common peaks in its fingerprint spectra allows for more comprehensive quality control. Previous studies (Lv et al., 2016; Lin et al., 2021; Yin et al., 2021; Yang et al., 2022; Shan et al., 2023)

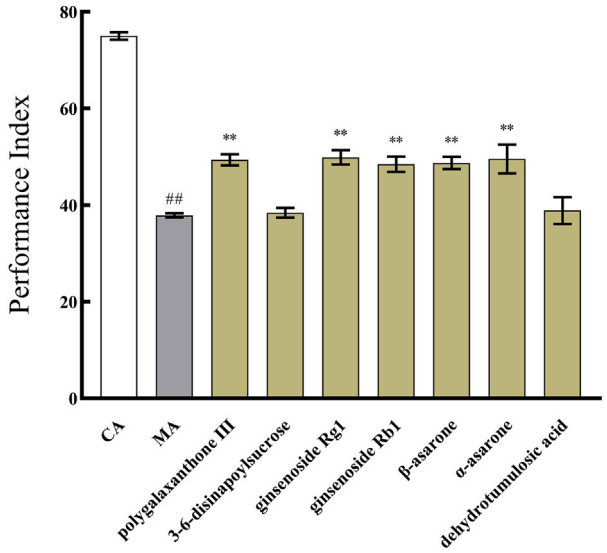


FIGURE 7
The effect of identified seven components of Kai-Xin-San on the performance index of $A\beta_{42}$ transgenic *drosophila*. CA: Control group with the same genetic background. MA: $A\beta_{42}$ transgenic group. n = 14 per group. Data are presented as Mean ± SD. Compared with the CA, $^{\#\#}P < 0.01$; compared with the MA, $^{**}P < 0.01$.

established the fingerprint spectra of KXS, but the number of common peaks and the identification of components were relatively limited, failing to comprehensively reflect the characteristics of its chemical components. In contrast, the fingerprint spectra established in our study identified seventeen common peaks and eight components, effectively controlling the internal quality of KXS in a more comprehensive and systematic manner. Furthermore, the eight identified components all originated from the four Chinese medicinal herbs constituting KXS. Unlike previous studies, the active ingredients identified did not include those from ginseng (Lv et al., 2016) or poria cocos (Shan et al., 2023). As previously reported (Lv et al., 2016; Yang et al., 2022; Shan et al., 2023; Shang et al., 2024), our findings further confirm that the growth environment of the medicinal materials used in KXS influences its quality.

The $A\beta_{42}$ transgenic *drosophila* model has been widely utilized for screening potential drugs for the treatment of AD (Iijima et al., 2004). Our study found that KXS exhibited a dose-dependent anti-AD effect in $A\beta_{42}$ transgenic *drosophila*. Unlike traditional preparation methods, where KXS is typically extracted using water and methanol in pharmacodynamic studies (Shan et al., 2023; Su et al., 2023; Shang et al., 2024; Yan et al., 2024), in our study, KXS powder was dissolved directly into the *drosophila* culture medium. This approach ensured consistency with the classical preparation method, allowing us to explore the efficacy of KXS in a genetically manipulable and short-life-cycle model.

The spectrum-effect relationship provides an effective strategy for identifying active substances in Chinese medicine formulas. The spectrum-effect relationship analysis of KXS demonstrated that seven identified components were associated with the anti-$A\beta_{42}$ effect. Further component-verification experiments revealed that polygalaxanthone III, ginsenoside Rg1, ginsenoside Rb1, β-asarone, and α-asarone improved the memory abilities of $A\beta_{42}$ transgenic *drosophila*. Previous studies have shown that polygalaxanthone III (Park et al., 2019; Deng et al., 2020; Du et al., 2022; Xie et al., 2023), β-asarone (Meng et al., 2021; Balakrishnan et al., 2022), α-asarone (Zeng et al., 2021; Venkatesan, 2022), ginsenoside Rg1 (Sun et al., 2022; Wang et al., 2023; Deng et al., 2024), and ginsenoside Rb1 (Yang et al., 2020; Changhong et al., 2021; Yuan et al., 2021; Shalaby et al., 2023) all exhibited anti-AD pharmacological activities. Despite previous studies suggesting that 3-6-disinapoylsucrose exhibited anti-AD effects (Yuan et al., 2021), our study failed to demonstrate such effects. This discrepancy may be attributed to variations in the animal model used, the drug preparation method, and the administered dosage.

Nevertheless, this study has certain limitations. Under the current experimental paradigm, it is challenging to precisely determine whether KXS and its components affect the encoding stage of learning, the formation or maintenance stage of short-term memory, or both. Therefore, it may be necessary to conduct more paradigm in olfactory escape memory experiment to study the effect of KXS on improving cognition. Although the *drosophila* model has advantages in studying certain basic neurobiological processes, it has limitations in exploring long-term memory and differentiating between various memory systems. To more comprehensively evaluate the impact of KXS and its components on long-term memory, future research could employ rodent models for multi-stage and multi-type memory tests.

5 Conclusion

This study successfully established the KXS fingerprint method, which demonstrated precision, stability, and reproducibility. At the same time, the study also identified the key active ingredients of KXS that play an anti-AD role: polygalaxanthone III, ginsenoside Rg1, ginsenoside Rb1, β-asarone, and α-asarone. As a classic prescription in traditional Chinese medicine, KXS holds significant research potential, provided that quality is comprehensively monitored and effectively controlled. On the one hand, based on the pathological mechanism of AD, it is recommended to conduct further research into the anti-AD mechanism of KXS to provide a theoretical basis for its clinical application. On the other hand, the active ingredients of KXS can be combined to develop new drugs for the treatment of AD.

Data availability statement

The raw data supporting the conclusions of this article will be made available by the authors, without undue reservation.

Ethics statement

The manuscript presents research on animals that do not require ethical approval for their study.

Author contributions

JW: Data curation, Formal Analysis, Writing–original draft. HS: Data curation, Formal Analysis, Writing–original draft. YZ: Formal

Analysis, Investigation, Writing–original draft. LL: Formal Analysis, Investigation, Writing–original draft. HB: Investigation, Methodology, Writing–original draft. YG: Formal Analysis, Investigation, Writing–original draft. DL: Investigation, Methodology, Writing–original draft. LH: Writing–review and editing.

Funding

The author(s) declare that financial support was received for the research, authorship, and/or publication of this article. This research was funded by the Natural Science Foundation of Heilongjiang Province of China (No. LH 2022H086), Heilongjiang Provincial Undergraduate Institutions for Excellent Young Teachers Basic Research Program (YQJH2023152), Heilongjiang Province Touyan Team, Key Laboratory of the Ministry of Education—North Medicine Fundamental and Applied Research Open Fund, the Scientific Research Fund of Heilongjiang University of Chinese Medicine, and the Doctoral Innovation Fund of Heilongjiang University of Chinese Medicine (2015bs08).

Acknowledgments

The authors wholeheartedly thank the various funds and co-authors for their invaluable help and support in this study. Their munificent financial support and contributions have been essential in propelling the research forward, and we deeply appreciate their efforts.

Conflict of interest

Authors YG and DL were employed by Shineway Pharmaceutical Group Co., Ltd.

The remaining authors declare that the research was conducted in the absence of any commercial or financial relationships that could be construed as a potential conflict of interest.

Generative AI statement

The authors declare that no Generative AI was used in the creation of this manuscript.

Publisher's note

All claims expressed in this article are solely those of the authors and do not necessarily represent those of their affiliated organizations, or those of the publisher, the editors and the reviewers. Any product that may be evaluated in this article, or claim that may be made by its manufacturer, is not guaranteed or endorsed by the publisher.

Supplementary material

The Supplementary Material for this article can be found online at: https://www.frontiersin.org/articles/10.3389/fphar.2025.1538837/full#supplementary-material

References

Bai, G., Jing, S., Cao, H., Qiao, Y., Chen, G., Duan, L., et al. (2022). Kai-Xin-San protects depression mice against CORT-induced neuronal injury by inhibiting microglia activation and oxidative stress. *Evid. Based Complement. Altern. Med.* 2022, 5845800. doi:10.1155/2022/5845800

Balakrishnan, R., Cho, D. Y., Kim, I. S., Seol, S. H., and Choi, D. K. (2022). Molecular mechanisms and therapeutic potential of α- and β-asarone in the treatment of neurological disorders. *Antioxidants (Basel)* 11 (2), 281. doi:10.3390/antiox11020281

Bero, A. W., Yan, P., Roh, J. H., Cirrito, J. R., Stewart, F. R., Raichle, M. E., et al. (2011). Neuronal activity regulates the regional vulnerability to amyloid-β deposition. *Nat. Neurosci.* 14 (6), 750–756. doi:10.1038/nn.2801

Buck, A., Rezaei, K., Quazi, A., Goldmeier, G., Silverglate, B., and Grossberg, G. T. (2024). The donepezil transdermal system for the treatment of patients with mild, moderate, or severe Alzheimer's disease: a critical review. *Expert Rev. Neurother.* 24 (6), 607–614. doi:10.1080/14737175.2024.2355981

Changhong, K., Peng, Y., Yuan, Z., and Cai, J. (2021). Ginsenoside Rb1 protected PC12 cells from $A\beta_{25-35}$-induced cytotoxicity via PPARγ activation and cholesterol reduction. *Eur. J. Pharmacol.* 893, 173835. doi:10.1016/j.ejphar.2020.173835

Deng, X., Qiu, Z., Chen, X., Liu, J., Wang, X., Li, J., et al. (2024). Exploring the potential mechanism of ginsenoside Rg1 to regulate ferroptosis in Alzheimer's disease based on network pharmacology. *Eur. J. Pharmacol.* 979, 176859. doi:10.1016/j.ejphar.2024.176859

Deng, X., Zhao, S., Liu, X., Han, L., Wang, R., Hao, H., et al. (2020). Polygala tenuifolia: a source for anti-Alzheimer's disease drugs. *Pharm. Biol.* 58 (1), 410–416. doi:10.1080/13880209.2020.1758732

Ding, M. R., Qu, Y. J., Hu, B., and An, H. M. (2022). Signal pathways in the treatment of Alzheimer's disease with traditional Chinese medicine. *Biomed. Pharmacother.* 152, 113208. doi:10.1016/j.biopha.2022.113208

Dong, Y., Yu, H., Li, X., Bian, K., Zheng, Y., Dai, M., et al. (2022). Hyperphosphorylated tau mediates neuronal death by inducing necroptosis and inflammation in Alzheimer's disease. *J. Neuroinflammation* 19 (1), 205. doi:10.1186/s12974-022-02567-y

Du, L. J., Zhang, X. N., Li, S. S., Sun, Y. F., Jin, H. Z., Yan, S. K., et al. (2022). Network pharmacological investigation into the mechanism of Kaixinsan powder for the treatment of depression. *Metab. Brain Dis.* 37 (8), 2903–2914. doi:10.1007/s11011-022-01067-5

Egunlusi, A. O., and Joubert, J. (2024). NMDA receptor antagonists: emerging insights into molecular mechanisms and clinical applications in neurological disorders. *Pharm. (Basel)* 17 (5), 639. doi:10.3390/ph17050639

Huang, Y. Y., Gan, Y. H., Yang, L., Cheng, W., and Yu, J. T. (2024). Depression in Alzheimer's disease: epidemiology, mechanisms, and treatment. *Biol. Psychiatry* 95 (11), 992–1005. doi:10.1016/j.biopsych.2023.10.008

Iijima, K., Liu, H. P., Chiang, A. S., Hearn, S. A., Konsolaki, M., and Zhong, Y. (2004). Dissecting the pathological effects of human Abeta40 and Abeta42 in Drosophila: a potential model for Alzheimer's disease. *Proc. Natl. Acad. Sci. U. S. A.* 101 (17), 6623–6628. doi:10.1073/pnas.0400895101

Iijima-Ando, K., and Iijima, K. (2010). Transgenic Drosophila models of Alzheimer's disease and tauopathies. *Brain Struct. Funct.* 214 (2-3), 245–262. doi:10.1007/s00429-009-0234-4

Jiao, Y. N., Zhang, J. S., Qiao, W. J., Tian, S. Y., Wang, Y. B., Wang, C. Y., et al. (2022). Kai-Xin-San inhibits tau pathology and neuronal apoptosis in aged SAMP8 mice. *Mol. Neurobiol.* 59 (5), 3294–3309. doi:10.1007/s12035-021-02626-0

Kim, S., Chun, H., Kim, Y., Kim, Y., Park, U., Chu, J., et al. (2024). Astrocytic autophagy plasticity modulates Aβ clearance and cognitive function in Alzheimer's disease. *Mol. Neurodegener.* 19 (1), 55. doi:10.1186/s13024-024-00740-w

Li, S., Jin, M., Koeglsperger, T., Shepardson, N. E., Shankar, G. M., and Selkoe, D. J. (2011). Soluble Aβ oligomers inhibit long-term potentiation through a mechanism involving excessive activation of extrasynaptic NR2B-containing NMDA receptors. *J. Neurosci.* 31 (18), 6627–6638. doi:10.1523/JNEUROSCI.0203-11.2011

Lin, R., Yin, J., Wu, M., Ding, H., Han, L., Yang, W., et al. (2021). Global identification and determination of the major constituents in Kai-Xin-San by ultra-performance liquid chromatography-quadrupole-Orbitrap mass spectrometry and gas chromatography-mass spectrometry. *J. Pharm. Biomed. Anal.* 206, 114385. doi:10.1016/j.jpba.2021.114385

Liu, Y., Tan, Y., Zhang, Z., Yi, M., Zhu, L., and Peng, W. (2024a). The interaction between ageing and Alzheimer's disease: insights from the hallmarks of ageing. *Transl. Neurodegener.* 13 (1), 7. doi:10.1186/s40035-024-00397-x

Liu, Y., Xiao, X., Yang, Y., Yao, R., Yang, Q., Zhu, Y., et al. (2024b). The risk of Alzheimer's disease and cognitive impairment characteristics in eight mental disorders: a UK Biobank observational study and Mendelian randomization analysis. *Alzheimers Dement.* 20 (7), 4841–4853. doi:10.1002/alz.14049

Lopez-Lee, C., Torres, E. R. S., Carling, G., and Gan, L. (2024). Mechanisms of sex differences in Alzheimer's disease. *Neuron* 112 (8), 1208–1221. doi:10.1016/j.neuron.2024.01.024

Lv, C., He, B., Sui, Z., Li, Q., and Bi, K. (2016). Identification and determination of the major constituents in Kai-Xin-San by UPLC-Q/TOF MS and UFLC-MS/MS method. *J. Mass Spectrom.* 51 (7), 479–490. doi:10.1002/jms.3773

Ma, T., Hoeffer, C. A., Wong, H., Massaad, C. A., Zhou, P., Iadecola, C., et al. (2011). Amyloid β-induced impairments in hippocampal synaptic plasticity are rescued by decreasing mitochondrial superoxide. *J. Neurosci.* 31 (15), 5589–5595. doi:10.1523/JNEUROSCI.6566-10.2011

Meng, M., Zhang, L., Ai, D., Wu, H., and Peng, W. (2021). β-Asarone ameliorates β-amyloid-induced neurotoxicity in PC12 cells by activating P13K/Akt/Nrf2 signaling pathway. *Front. Pharmacol.* 12, 659955. doi:10.3389/fphar.2021.659955

Park, H., Kang, S., Nam, E., Suh, Y. H., and Chang, K. A. (2019). The protective effects of PSM-04 against beta amyloid-induced neurotoxicity in primary cortical neurons and an animal model of Alzheimer's disease. *Front. Pharmacol.* 10, 2. doi:10.3389/fphar.2019.00002

Shalaby, A. M., Alnasser, S. M., Ahmed Khairy, D., Alabiad, M. A., Alorini, M., Jaber, F. A., et al. (2023). The neuroprotective effect of ginsenoside Rb1 on the cerebral cortex changes induced by aluminium chloride in a mouse model of Alzheimer's disease: a histological, immunohistochemical, and biochemical study. *J. Chem. Neuroanat.* 129, 102248. doi:10.1016/j.jchemneu.2023.102248

Shan, X., Yang, X., Li, D., Zhou, L., Qin, S., Li, J., et al. (2023). Research on the quality markers of antioxidant activity of Kai-Xin-San based on the spectrum-effect relationship. *Front. Pharmacol.* 14, 1270836. doi:10.3389/fphar.2023.1270836

Shang, B., Jia, S., Zhang, T., Gao, F., Lu, M., Chen, K., et al. (2024). Study on the chemical constituents and mechanism of Kai-Xin-San based on UPLC-Q-Exactive MS and network pharmacology. *J. Ethnopharmacol.* 322, 117652. doi:10.1016/j.jep.2023.117652

Su, S., Chen, G., Gao, M., Zhong, G., Zhang, Z., Wei, D., et al. (2023). Kai-Xin-San protects against mitochondrial dysfunction in Alzheimer's disease through SIRT3/NLRP3 pathway. *Chin. Med.* 18 (1), 26. doi:10.1186/s13020-023-00722-y

Sun, Y., Yang, Y., Liu, S., Yang, S., Chen, C., Lin, M., et al. (2022). New therapeutic approaches to and mechanisms of ginsenoside Rg1 against neurological diseases. *Cells* 11 (16), 2529. doi:10.3390/cells11162529

Tabor, G. T., and Holtzman, D. M. (2023). Current status of amyloid-targeting immunotherapies for Alzheimer's disease. *Sci. Transl. Med.* 15 (721), eadk9993. doi:10.1126/scitranslmed.adk9993

Tue, N. T., Dat, T. Q., Ly, L. L., Anh, V. D., and Yoshida, H. (2020). Insights from *Drosophila melanogaster* model of Alzheimer's disease. *Front. Biosci. (Landmark Ed)* 25 (1), 134–146. doi:10.2741/4798

Venkatesan, K. (2022). Anti-amnesic and anti-cholinesterase activities of α-asarone against scopolamine-induced memory impairments in rats. *Eur. Rev. Med. Pharmacol. Sci.* 26 (17), 6344–6350. doi:10.26355/eurrev_202209_29660

Wang, H., Zhou, L., Zheng, Q., Song, Y., Huang, W., Yang, L., et al. (2024a). Kai-Xin-San improves cognitive impairment in D-gal and $A\beta_{25-35}$ induced ad rats by regulating gut microbiota and reducing neuronal damage. *J. Ethnopharmacol.* 329, 118161. doi:10.1016/j.jep.2024.118161

Wang, N., Yang, J., Chen, R., Liu, Y., Liu, S., Pan, Y., et al. (2023). Ginsenoside Rg1 ameliorates Alzheimer's disease pathology via restoring mitophagy. *J. Ginseng Res.* 47 (3), 448–457. doi:10.1016/j.jgr.2022.12.001

Wang, Y. T., Wang, X. L., Lei, L., Guo, Z. Y., Hu, D., Wang, Z. Z., et al. (2024b). Efficacy of Chinese herbal formula Kai-Xin-San on rodent models of depression: a systematic review and meta-analysis. *J. Ethnopharmacol.* 321, 117492. doi:10.1016/j.jep.2023.117492

Xie, Y., Yang, Y., Yuan, X., Liu, Y., and He, X. (2023). Herb pair of Polygala tenuifolia Willd and Acorus tatarinowii Schott decoction attenuates seizures and alleviates anxiety in mice: evidence for modulating inflammation, alleviating oxidative stress and mediating GABA pathway. *Pak J. Pharm. Sci.* 36 (2), 565–577. doi:10.36721/PJPS.2323.36.2.REG.565-577.1

Xu, C., Wu, J., Wu, Y., Ren, Z., Yao, Y., Chen, G., et al. (2021). TNF-α-dependent neuronal necroptosis regulated in Alzheimer's disease by coordination of RIPK1-p62 complex with autophagic UVRAG. *Theranostics* 11 (19), 9452–9469. doi:10.7150/thno.62376

Xu, N., Li, M., Wang, P., Wang, S., and Shi, H. (2022). Spectrum-effect relationship between antioxidant and anti-inflammatory effects of Banxia Baizhu Tianma decoction: an identification method of active substances with Endothelial cell protective effect. *Front. Pharmacol.* 13, 823341. doi:10.3389/fphar.2022.823341

Xu, Y. M., Lu, F. M., Xu, H. C., Zhang, J., Hei, S. Y., Qiu, Y. H., et al. (2023). Kai-Xin-San improves cognitive impairment via Wnt/β-Catenin and IRE1/XBP1s signalings in APP/PS1 mice. *Rejuvenation Res.* 26 (3), 105–115. doi:10.1089/rej.2022.0063

Yan, C., Yang, S., Shao, S., Zu, R., Lu, H., Chen, Y., et al. (2024). Exploring the anti-ferroptosis mechanism of Kai-Xin-San against Alzheimer's disease through integrating network pharmacology, bioinformatics, and experimental validation strategy *in vivo* and *in vitro*. *J. Ethnopharmacol.* 326, 117915. doi:10.1016/j.jep.2024.117915

Yang, L., Liang, J., Zheng, Q., Zhou, L., Xiong, Y., Wang, H., et al. (2022). A comparative study of serum pharmacochemistry of Kai-Xin-San in normal and AD rats using UPLC-LTQ-Orbitrap-MS. *Pharm. (Basel)* 16 (1), 30. doi:10.3390/ph16010030

Yang, R., Jiang, X., He, X., Liang, D., Sun, S., and Zhou, G. (2020). Ginsenoside Rb1 improves cognitive impairment induced by insulin resistance through Cdk5/p35-NMDAR-IDE pathway. *Biomed. Res. Int.* 2020, 3905719. doi:10.1155/2020/3905719

Yin, J., Lin, R., Wu, M., Ding, H., Han, L., Yang, W., et al. (2021). Strategy for the multi-component characterization and quality evaluation of volatile organic components in Kaixin San by correlating the analysis by headspace gas chromatography/ion mobility spectrometry and headspace gas chromatography/mass spectrometry. *Rapid Commun. Mass Spectrom.* 35 (21), e9174. doi:10.1002/rcm.9174

Yu, H., Liu, D., Zhang, Y., Tang, R., Fan, X., Mao, S., et al. (2024). Tissue-specific O-GlcNAcylation profiling identifies substrates in translational machinery in Drosophila mushroom body contributing to olfactory learning. *Elife* 13, e91269. doi:10.7554/eLife.91269

Yuan, J., Wang, H., Wang, Y., Wang, Z., Huo, Q., Dai, X., et al. (2021). Rapid identification of 3,6'-Disinapoyl sucrose metabolites in Alzheimer's disease model mice using UHPLC-orbitrap mass spectrometry. *Molecules* 27 (1), 114. doi:10.3390/molecules27010114

Zeng, L., Zhang, D., Liu, Q., Zhang, J., Mu, K., Gao, X., et al. (2021). Alpha-asarone improves cognitive function of APP/PS1 mice and reducing $A\beta_{42,}$ P-tau and neuroinflammation, and promoting neuron survival in the Hippocampus. *Neuroscience* 458, 141–152. doi:10.1016/j.neuroscience.2020.12.026

Zhang, X., Sun, Y., Yu, Q., Zeng, W., Zhang, Y., Zeng, M., et al. (2023). Jia-Wei-Kai-Xin-San treatment alleviated mild cognitive impairment through anti-inflammatory and antiapoptotic mechanisms in SAMP8 mice. *Mediat. Inflamm.* 2023, 7807302. doi:10.1155/2023/7807302

Zhang, Z. Q., Degejin, D., Geng, D., Zhang, Q., Tian, Y., Xi, Y., et al. (2016). Pharmacodynamic study on insomnia-curing effects of Shuangxia Decoction in *Drosophila melanogaster*. *Chin. J. Nat. Med.* 14 (9), 653–660. doi:10.1016/S1875-5364(16)30077-2

frontiers | Frontiers in Pharmacology

TYPE Systematic Review
PUBLISHED 17 April 2025
DOI 10.3389/fphar.2025.1508015

Check for updates

OPEN ACCESS

EDITED BY
Wing Lam,
Yale University, United States

REVIEWED BY
Bhuchitra Singh,
Johns Hopkins University, United States
Cui Bomiao,
Sichuan University, China

*CORRESPONDENCE
Lirong Ren,
2554750789@qq.com
Yuan Yuan,
mdd30530@163.com
Yini Zhu,
yzhu15@seu.edu.cn

†These authors have contributed equally to this work

RECEIVED 08 October 2024
ACCEPTED 31 March 2025
PUBLISHED 17 April 2025

CITATION
Zhang Y, Wei J, Gao C, Feng S, Wang H, Chai J, Zhu Y, Yuan Y and Ren L (2025) The efficacy and safety of Chinese herbal medicine Shugan Sanjie decoction in the treatment of uterine fibroids: a systematic review and meta-analysis. *Front. Pharmacol.* 16:1508015. doi: 10.3389/fphar.2025.1508015

COPYRIGHT
© 2025 Zhang, Wei, Gao, Feng, Wang, Chai, Zhu, Yuan and Ren. This is an open-access article distributed under the terms of the Creative Commons Attribution License (CC BY). The use, distribution or reproduction in other forums is permitted, provided the original author(s) and the copyright owner(s) are credited and that the original publication in this journal is cited, in accordance with accepted academic practice. No use, distribution or reproduction is permitted which does not comply with these terms.

The efficacy and safety of Chinese herbal medicine Shugan Sanjie decoction in the treatment of uterine fibroids: a systematic review and meta-analysis

Yang Zhang[1†], Junfan Wei[1†], Chanchan Gao[2†], Shenyang Feng[1], Haiying Wang[1], Junjie Chai[1], Yini Zhu[3]*, Yuan Yuan[1]* and Lirong Ren[1]*

[1]The Seventh Clinical Medical College of Guangzhou University of Chinese Medicine, Shenzhen, China, [2]Department of Oncology, Zhongda Hospital Affiliated to Southeast University, Nanjing, China, [3]Department of Microbiology and Immunology, Medical School of Southeast University, Nanjing, China

Background: Shugan Sanjie Decoction (SGSJ) is a commonly used Chinese medicine prescription for the treatment of uterine fibroids (UFs). However, there is still a lack of evidence for its effects and safety. To systematically assess the efficacy and safety of SGSJ in conjunction with Mifepristone [MFP] or Leuprolide acetate [LA] for the treatment of UFs, thereby providing a reference for clinical medication.

Objective: To systematically assess the efficacy and safety of SGSJ in combination with MFP or LA for the treatment of UFs, thereby providing a basis for clinical medication decisions.

Methods: Eight digital medical databases were systematically searched to identify randomized controlled trials (RCTs) evaluating the use of SGSJ combined with MFP or LA for the treatment of UFs. The search spanned from the inception of each database to July 2024. Risk of Bias (ROB) 2.0 and RevMan 5.3 software were utilized for systematic review and meta-analysis. Eligible studies comprised RCTs comparing SGSJ plus MFP or LA with MFP or LA alone. The primary outcome was the Clinical Effective Rate (CER). Secondary outcomes included (1) Uterine Fibroid Volume (UFV) (2), Uterine Volume (UV) (3), Serum Sex Hormone Levels [Follicle-Stimulating Hormone (FSH), Luteinizing Hormone (LH), Estradiol (E2), Progesterone (P)], and (4) Traditional Chinese Medicine Syndrome Scores (TSS).

Results: The meta-analysis comprised 12 RCTs with 952 participants. The results of meta-analysis showed that the total effective rate of SGSJ or combined with MFP or LA in the treatment of UFs [RR = 1.26, 95% CI (1.19, 1.34), $P < 0.00001$], which was statistically significant compared with the MFP or LA group and superior to the MFP or LA group ($P < 0.05$).

Conclusion: At present, there are evidence shows that SGSJ combined with MFP or LA improves CER, reduces UFV, and modulates sex hormone levels. However, due to the poor methodological quality and high heterogeneity of the included trials, our conclusions should be interpreted with caution. Future studies should prioritize rigorous RCTs with standardized treatment protocols, extended follow-up, and comprehensive safety assessments to identify SGSJ as a reliable treatment option for UFs.

Systematic Review registration: https://www.crd.york.ac.uk/PROSPERO/view/CRD42024506017

KEYWORDS

Chinese herbal medicine, shugan sanjie decoction, uterine fibroids, systematic review, meta-analysis

1 Introduction

Uterine fibroids (UFs), also known as uterine leiomyoma, are common benign monoclonal tumor affecting women of childbearing age (Stewart et al., 2017; De La Cruz and Buchanan, 2017; Ning et al., 2020), with risk factors including age, family history, hypertension (Mitro et al., 2024), obesity, diet, vaginal microbiota changes, environment, and so on (5–7). Patients with UFs always present different symptoms depending on the location and volume of the UFs. The closer the UFs are to the endometrium, the more severe the symptoms they cause, including excessive menstrual flow, prolonged menstrual periods, and in severe cases, may lead to a women being chronically anemic (Laughlin-Tommaso and Stewart, 2018; Lee and Stewart, 2023; Syed, 2022). In addition, UFs can lead to pelvic pain, frequent urination, urinary urgency, abdominal distension, abdominal pain and infertility in female patients (Lee and Stewart, 2023; Donnez and Dolmans, 2016).

The prevalence of UFs has been studied to be as high as 80%, but the actual prevalence may be higher considering the undiagnosed presence of asymptomatic patients (Laughlin-Tommaso and Stewart, 2018; Vannuccini et al., 2024). Current treatments for UFs are categorized as non-surgical and surgical (Marsh et al., 2024), with hysterectomy remaining the primary surgical treatment method, accounting for 75% of cases (Stewart et al., 2016). However, hysterectomies result in the loss of fertility in women of childbearing age and put women at increased risk for cardiovascular disease, cognitive impairment in later life, mental health and other diseases (Manyonda et al., 2020). And the high cost of surgery causes family economic burden and affects family harmony (Stewart et al., 2021; Walker and Stewart, 2005; Tulandi, 2007). Therefore, pharmacologic therapy among nonsurgical treatments has become the primary choice of many patients and physicians. Current pharmacologic measures include progesterone receptor modulators (PRMs), tranexamic acid, gonadotropin-releasing hormone (GnRH) agonists, and other symptom-relieving medications (mainly oral contraceptives, levonorgestrel, and intrauterine devices). Hormone therapy is usually the treatment of choice for most women, and studies have shown it to be effective in reducing UFs size and relieving clinical symptoms (Ali et al., 2023). There are certain adverse effects of drug therapy. For example, a large number of patients still suffer from adverse effects such as regeneration of UFs and endometrial hyperplasia, and patients need to increase drug dose due to long-term drug resistance (Fu et al., 2020; Stewart and Nowak, 2022). Therefore, researchers have sought safer alternative medications for the treatment of UFs. Conventional Western medical treatments have issues such as surgical risks and drug side effects, making Traditional Chinese Medicine (TCM), with its characteristics of multiple targets and low toxicity, a research hotspot (Zhang et al., 2010).

Shugan Sanjie Decoction (SGSJ) has the effect of soothing liver and clearing collaterals. Recently, the research on SGSJ for the treatment of UFs is increasing (Zhai, 2017). However, none of the articles have comprehensively evaluated the efficacy and safety of SGSJ for the treatment of UFs, which has resulted in limited evidence supporting SGSJ as an effective treatment option for UFs. Therefore, this study conducted a meta-analysis of randomized controlled trials (RCTs) of SGSJ for the treatment of UFs with the aim of systematically evaluating the efficacy and safety of SGSJ for the treatment of UFs, and providing a basis for the clinical treatment of UFs.

2 Materials and methods

The present study adhered to the Preferred Reporting Items for Systematic Reviews and Meta-Analyses (PRISMA) guidelines (Page et al., 2021) (Figure 1).

2.1 Protocol registration

The present study followed the protocol registered in the International Prospective Register of Systematic Reviews (PROSPERO) (https://www.crd.york.ac.uk/prospero/), registration number: CRD42024506017. No personal data were collected for this study and ethical approval was not required.

2.2 Search strategy

We searched RCTs in the following eight databases from January 2024 to July 2024, including PubMed, Web of Science, Embase, Chinese Scientifc Journals Database (VIP), China National Knowledge Infrastructure (CNKI), Cochrane Library, ScienceDirect, Allied and Complementary MedicineDatabase (AMED), Wanfang, and Chinese Biological Medical Database (CBM). The following search terms were used in combination (Leiomyoma OR Fibroid Tumor OR Fibromyoma OR Fibroid OR Fibroid Uterus OR Fibroma, Uterine OR Fibroids, Uterine OR Leiomyoma, Uterine) AND (shugansanjie tang OR shugansanjie decoction) AND (Randomized Controlled Trials as Topic OR Clinical Trials, randomized OR Trials, Randomized Clinical OR Controlled Clinical Trials, Randomized).

2.3 Inclusion and exclusion criteria

2.3.1 Types of studies

We included RCTs that have been published in both Chinese and English to evaluate the efficacy and safety of SGSJ in the treatment of UFs.

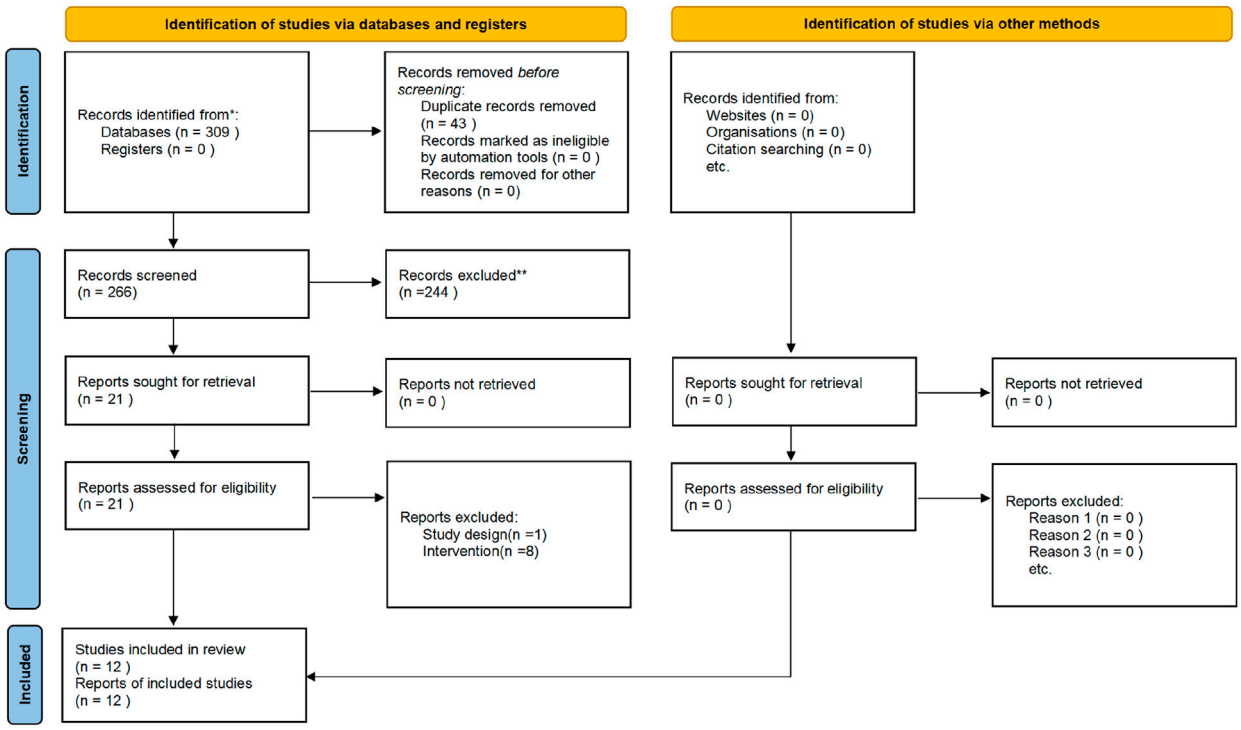


FIGURE 1
PRISMA flow chart of the selection process.

2.3.2 Types of participants

Patients diagnosed with UFs, aged ≥18 years old.

2.3.3 Types of interventions and comparators

This systematic review included studies on SGSJ and combination therapy (SGSJ and Mifepristone [MFP] or Leuprolide acetate [LA]). To ensure the reproducibility of the results, all herbal ingredients of SGSJ were described in accordance with the ConPhyMP (Consensus for Pharmacological Intervention of Medicinal Plants) guidelines. Botanical authentication, including species names, family, and identification methods, was documented where available. The following medication groups were compared in this study: a) the SGSJ and modified SGSJ groups with MFP or LA; b) the SGSJ group with placebo (same taste, shape, color, and odor as SGSJ) group; and c) combination therapy (SGSJ plus Western medicine) group with MFP or LA. In addition, SGSJ is composed of Bupleurum falcatum L [Apiaceae; Bupleuri radix], Cyperus rotundus L [Cyperaceae; Cyperi rhizoma], Salvia miltiorrhiza Bunge [Lamiaceae; Salviae miltiorrhizae radix et rhizoma], Paeonia lactiflora Pall [Paeoniaceae; Paeoniae radix rubra], Prunus persica (L.) [Rosaceae; Persicae semen], Corydalis yanhusuo [Papaveraceae; Corydalis rhizoma], Glycyrrhiza glabra L [Fabaceae; Glycyrrhizae radix et rhizoma], Commiphora myrrha (T.Nees) Engl [Burseraceae; Myrrha], Boswellia sacra Flück [Burseraceae; Olibanum], Conioselinum anthriscoides 'Chuanxiong' [Apiaceae; Chuanxiong rhizoma], Typha angustifolia L [Typhaceae; Typhae pollen], and Panax notoginseng (Burkill) F.H.Chen [Araliaceae; Notoginseng radix et rhizoma].

2.3.4 Types of outcome measures

Clinical effective rate (CER) was the primary outcome. CER: The sum of the percentages of women with UFs that achieved cured, observably effective and effective. Cured: Clinical symptoms and signs disappeared completely, and B-ultrasound showed that UFs disappeared completely; Observably effective: The clinical symptoms improved significantly or basically disappeared, and the volume of myoma was reduced by ≥ 50%; Effective: Conscious symptoms improved, B-ultrasound showed myoma volume reduced by 25%–50%; Ineffective: Symptoms and signs did not improve, and B-ultrasound showed no reduction of fibroid volume or <25%. Secondary outcome measures (Stewart et al., 2017): Uterine fibroid volume (UFV) (De La Cruz and Buchanan, 2017). Uterine volume (UV) (Ning et al., 2020). Serum sex hormone levels [follicle-stimulating hormone (FSH), luteinizing hormone (LH), estradiol (E_2), progesterone (P)] (Mitro et al., 2024). TCM syndrome scores (TSS).

2.3.5 Exclusion criteria

The exclusion criteria for this study were as follows (Stewart et al., 2017): outcome indicators cannot be obtained (De La Cruz and Buchanan, 2017); repeated publications (Ning et al., 2020); incomplete data (Mitro et al., 2024); therapeutic measures combinated with other kinds of complementary and alternative treatments, such as acupuncture and moxibustion.

TABLE 1 Summary characteristics of the included studies.

First author (year) [ref.]	Study design	Sample (T/C)	Age (T/C, years)	Interventions		Treatment duration	Outcomes	Funding
				Treatment	Comparator			
Haiyan Wu, 2021 (34)	RCT	30/30	47.61 ± 1.45/ 47.12 ± 2.72	SGSJ + MFP (10 mg/d, qd)	MFP (10 mg/d, qd)	12 weeks	CER	NR
Yanxia Chen, 2020 (35)	RCT	48/48	37.96 ± 4.63/ 38.47 ± 5.12	SGSJ + MFP(10 mg/d, qd)	MFP (10 mg/d, qd)	12 weeks	CER, UFV, UV, TSS	NR
Yanan Liu, 2020 (33)	RCT	41/40	36.32 ± 2.15/ 36.25 ± 2.06	SGSJ + MFP(10 mg/d, qd)	MFP (10 mg/d, qd)	2 weeks	CER, UFV	NR
Baozhen Wang, 2021 (41)	RCT	43/42	36.25 ± 2.06/ 41.56 ± 3.38	SGSJ + MFP(10 mg/d, qd)	MFP (10 mg/d, qd)	3 months	TSS, P	NR
Wei Ma, 2023 (36)	RCT	44/44	32.01 ± 5.42/ 31.85 ± 5.39	SGSJ + LA (3.75 mg/m, qw)	LA (3.75 mg/ m, qw)	3 months	CER, UFV, UV, E_2, LH, FSH	NR
Wenting Chen, 2022 (37)	RCT	37/37	43.99 ± 11.34/45.10± 15.34	SGSJ + MFP(10 mg/d, qd)	MFP (10 mg/d, qd)	3 months	CER, UFV, P	NR
Mingyuan Xu, 2022 (38)	RCT	16/16	33.27 ± 0.16/ 33.28 ± 0.31	SGSJ + MFP(10 mg/d, qd)	MFP (10 mg/d, qd)	3 months	CER, E_2, LH, FSH, P	NR
Junyan Fan, 2021 (42)	RCT	60/60	40.62 ± 2.51/ 40.38 ± 2.64	SGSJ + MFP(10 mg/d, qd)	MFP (10 mg/d, qd)	12 weeks	CER, UFV, TSS	NR
Fumei Zhang, 2023 (39)	RCT	31/31	42.35 ± 3.52/ 42.32 ± 3.42	SGSJ + MFP(10 mg/d, qd)	MFP (10 mg/d, qd)	3 months	CER, UFV, P	NR
You Zhai, 2017 (25)	RCT	51/51	41.95 ± 6.02/ 42.58 ± 5.82	SGSJ + MFP(10 mg/d, qd)	MFP (10 mg/d, qd)	12 weeks	CER, UFV, P	NR
Bo Zhang, 2020 (43)	RCT	26/26	33 ± 0.8	SGSJ + MFP(10 mg/d, qd)	MFP (10 mg/d, qd)	12 weeks	UFV, TSS, P	NR
Li Zhou, 2019 (40)	RCT	50/50	41 ± 2.7/ 40 ± 2.5	SGSJ + MFP(10 mg/d, qd)	MFP (10 mg/d, qd)	8 weeks	CER, UFV, UV, E_2, LH, FSH, TSS	NR

Note. Ref., reference; T, treatment grouping; C, comparator grouping; NR, not recorded.

2.4 Study selection and data extraction

In this study, two independent evaluators, YZ and JW, searched the studies according to the search strategy and created a new database using the EndNote software to manage the studies. The title, keywords, abstract and the full text of the literature were screened by YZ and CG and the reasons for exclusion were recorded for further review. If two evaluators could not reach a consensus, the third evaluator (YZ or LR) would arbitrate. Data were collected by two reviewers (HW and JC), including the first author, publication date, number of included studies, sample size of trial group, treatment protocol details of trial group, treatment protocol of control group, follow-up time, post-treatment examination results, and adverse events were extracted. The extracted information was filled into the form we designed in advance, and the extracted data was cross-checked by two other reviewers (SF and YY) to ensure the accuracy of the data. If the information in the included article is unclear, it will be confirmed by the reviewer (LR) after inquiring by email.

2.5 Reporting quality assessment

To ensure the reproducibility and accurate interpretation of studies involving medicinal plant extracts, we employed the ConPhyMP (Heinrich and Jalil, 2023; Heinrich et al., 2022) checklist as a tool for assessing the quality of the 12 articles included in this study. Two researchers, SF and JC, independently extracted information from two checklists while being unaware of each other's evaluations. A score of "1" or "0" was assigned based on whether the RCTs reported the relevant section/topic. A score of "0" indicated that the corresponding section/topic was not mentioned, whereas a score of "1" indicated that it was described by the author in their study (Heinrich and Jalil, 2023; Heinrich et al., 2022). Table 2, Table 3 presents both the number and percentage of ConPhyMP checklist items reported in these included studies.

2.6 Risk of bias assessment

YZ and JW evaluated the quality of the included RCTs literature using the Cochrane risk bias assessment tool ROB 2.0 (Sterne et al., 2019), which included five types of bias involving randomization bias, bias from established interventions, bias from missing outcome data, bias from outcome measurements, and bias from selectively reported outcomes. Any disagreements are agreed upon after discussion with the other two reseachers (YZ and LR).

TABLE 2 ConPhyMP checklist of information for reporting plant material and its initial processing.

Section/Topic	Item no.	Checklist item	n	ConPhyMP% (n/12)
Title and abstract	1	A clear and concise title including an informative abstract and balanced summary	11	91.7
Description of the botanical drug and taxonomic authentication	2	Botanical or morphological authentication of the plant material (desirable is a combination with DNA barcoding, e.g., PCR, RFLP, genome sequencing) and the information must be included in a separate section of Material and Methods, if applicable, combined with the information required under item 3	0	0
Description of the extract and extraction process	3	A separate section in Material and Methods, covers the relevant information on the material investigated, including the full species name(s), authorites and family; e.g., Salvia miltorrhiza Bunge [Lamiaceae; Salviae miltorrhizae radix et rhizoma], and on the processing and extraction of the crude drug including the traditional processing of the material used medicinally (fumigation, steaming, roasting, cooking, frying, *etc.*).	0	0
Documentation of the legal basis for collection and processing	4	Full compliance with the Nagoya protocol, CITES, and all associated treaties including phytosanitary regulations	12	100
Description of product characteristics, in case of a finished (commercial) product	5	Information on the characteristics of the commercial products including batch number and date of production/best by information and regulatory status.	0	0

2.7 Data synthesis

Statistical analysis was carried out by RevMan 5.3 software (Wu et al., 2018), and the measurement indicators of the effects of the count data usually included Relative Risk (RR) and Odds Ratio (OR). Standardized Mean Difference (MD) and standardized Mean Difference (SMD) were used to describe effect sizes. In this study, RR or SMD were used. Both with 95% Confidence Interval (CI) to complete the analysis. The statistical heterogeneity among all studies was evaluated by X^2 and I^2 test with $\alpha = 0.05$. When $P > 0.1$ and $I^2 \leq 50\%$ of all studies, the included studies were considered to have no heterogeneity, and the Fixed effect model was adopted for analysis. When $P \leq 0.1$ and $I^2 > 50\%$, the included studies were considered heterogeneous, and random effect model was adopted for analysis (Huedo-Medina et al., 2006). If there is a large heterogeneity in the study, the source is initially explored through subgroup analysis, or further explored through sensitivity analysis. Sensitivity analysis was performed by sequentially removing each included study to assess the robustness of the meta-analysis results. Subgroup analyses were conducted based on disease duration (>12 months vs <12 months), treatment duration (>8 weeks vs. ≤8 weeks), medication combinations (SGSJ + MFP vs. SGSJ + LA) and doses of combined MFP (MFP≥20 mg/d vs. MFP <20 mg/d).

2.8 Quality assessment of the evidence

According to the outcome indicators, the quality of evidence in the included RCTS was evaluated using GRADE (Guyatt et al., 2008) (Grading of Recommendations, Assessment, Development and Evaluations) pro 3.6 software, which was divided into four levels: high, medium, low and very low, and the level of evidence was strictly evaluated.

3 Results

A total of 309 articles were searched in this study. Using literature management software, 43 duplicate articles were eliminated. By screening the titles, keywords, and abstracts, 244 articles with different study types, including animal experiments, experience, reviews, and research reviews, were eliminated. By screening the full text, 9 studies with inconsistent intervention types, study participants, study comparators and study outcome measures were deleted. A total of 12 articles were included in the final meta-analysis (Figure 1).

3.1 Study characteristics

12 RCTs involving 952 participants were included (Figure 1). All studies were conducted in China and published between 2017 and 2023. Among the included studies, one compared combination of SGSJ and LA with LA alone, while eleven compared combination of SGSJ and MFP with MFP alone. Regarding the dosage form and route of administration for SGSJ, all 12 studies utilized oral decoctions. For MFP and LA, eleven studies investigated oral tablets, and one study examined subcutaneous administration of LA. In a single study, the sample size ranged from 16 to 60 patients, and the treatment duration varied from 2 weeks to 3 months. Concerning the diagnostic criteria for UFs, four studies did not specify the basis, three adopted the 2017 Chinese Expert Consensus on the Diagnosis and Treatment of UFs, two referred to obstetrics and gynecology textbooks, one followed NCCN-2018 guidelines, and two used the 1994 Chinese Clinical Diagnosis and Treatment Criteria for UFs. Regarding the syndrome types of UFs, all 12 studies identified qi stagnation and blood stasis syndrome. See Table 1 for details.

TABLE 3 ConPhyMP checklist of items for conducting and reporting analytical methods relevant for extract type A.

Section/Topic	Item no.	Checklist item	n	ConPhyMP% (n/12)
Type of extract	1	A – Confirm that the species or botanical drug under investigation is covered in a monograph in one of the national or regional pharmacopoeias	12	100
Preferred/main methods for extract characterisation/ chemical analysis	2a*	The description of the active ingredients in the botanical drug (if known) or analytical marker compounds as defined	12	100
	2b*	An analysis as defined in the monograph is needed if the extract has not been supplied with a certificate	0	0
	2c*	If the preparation was purchased, the manufacturer and certificate of analysis need to be included	0	0
	2a#	Triple chemical fingerprinting methods, each with one or more detection parameters	0	0
	2b#	Quantification of at least two marker compounds (unless this is not feasible, evidence needs to be provided), and justification of the choice of markers (if applicable)	0	0
Alternative methods for extract characterisation/chemical analysis	3a	Single chemical fingerprinting method with at least three different detection parameters (i.e., altered detection parameters, like TLC/HPTLC with different staining reagents and/or UV excitation wavelengths, HPLC-DAD/ LCDAD with different wavelengths). The same applies to coupling MS or NMR to chromatographic techniques	0	0
	3b	Quantification of at least two marker compounds (unless this is not feasible, evidence needs to be provided), and justification of the choice of markers (if applicable)	0	0
Use of reference standards	4	(a) Direct overlay of the chromatogram of the sample with that of an officially specified reference standard (if applicable) (b) Chromatographic fingerprinting: Direct overlay of the chromatogram of the sample with that of official reference standards of the powdered plant material or the dry extract from the plant material	0	0
Comparison of different extracts/samples of the same plants	5	(a) Direct comparison of the chromatographic/ spectroscopic system and/or scoring system for "similarity" to be followed	0	0

*Compliance with pharmacopoeial standards to be followed.
#Including either the preferred or alternative approaches for characterisation.

3.2 Reporting quality

Table 2 provides an overview of the plant materials and their initial information checklist treatment of the included studies reveals, indicating that 38.3% of the items were reported. Upon reviewing the titles, it was found that only one study (Liu, 2020) lacked a clear and concise title (item 1). Additionally, none of the studies reported botanical or morphological identification of plant materials (item 2), relevant information on survey materials (including complete species name, authority, and family) (item 3), or information on the characteristics of commercial products (including batch number, production date, and regulatory status) (item 5). However, twelve studies were fully compliant with the Nagoya Protocol, CITES, and all relevant treaties, including the Plant Health Regulations (item 5).

Table 3 summarizes the analytical methods related to Class A extracts. In all the included studies, botanical drugs were documented in regional monographs or national pharmacopoeias (item 1). The active constituents of all the botanical drugs were identified (item 2a*). However, eight ConPhyMP items were not addressed in any of the literature (0%): the extract lacked a certificate (item 2b*), the manufacturer and assay certificate were not provided (Item 2c*), the use of triple fingerprinting was not mentioned (item 2a#), the quantification of at least two labeled compounds was not reported (item 2b#), single chemical fingerprinting with varying detection parameters was not described (Item 3a), the quantification of at least two labeled compounds was not specified (item 3b), reference standards were not utilized (item 4), and comparisons between different extracts or samples of the same substance were not conducted (item 5).

3.3 Risk of bias assessment

The risk of bias is illustrated in Figures 2, 3.

3.3.1 Random sequence generation

Among the included studies, eight studies (Zhai, 2017; Wu, 2021; Chen, 2020; Ma, 2023; Chen, 2022; Xu, 2022; Zhang, 2023; Zhou, 2019) utilized the random number table method, two studies

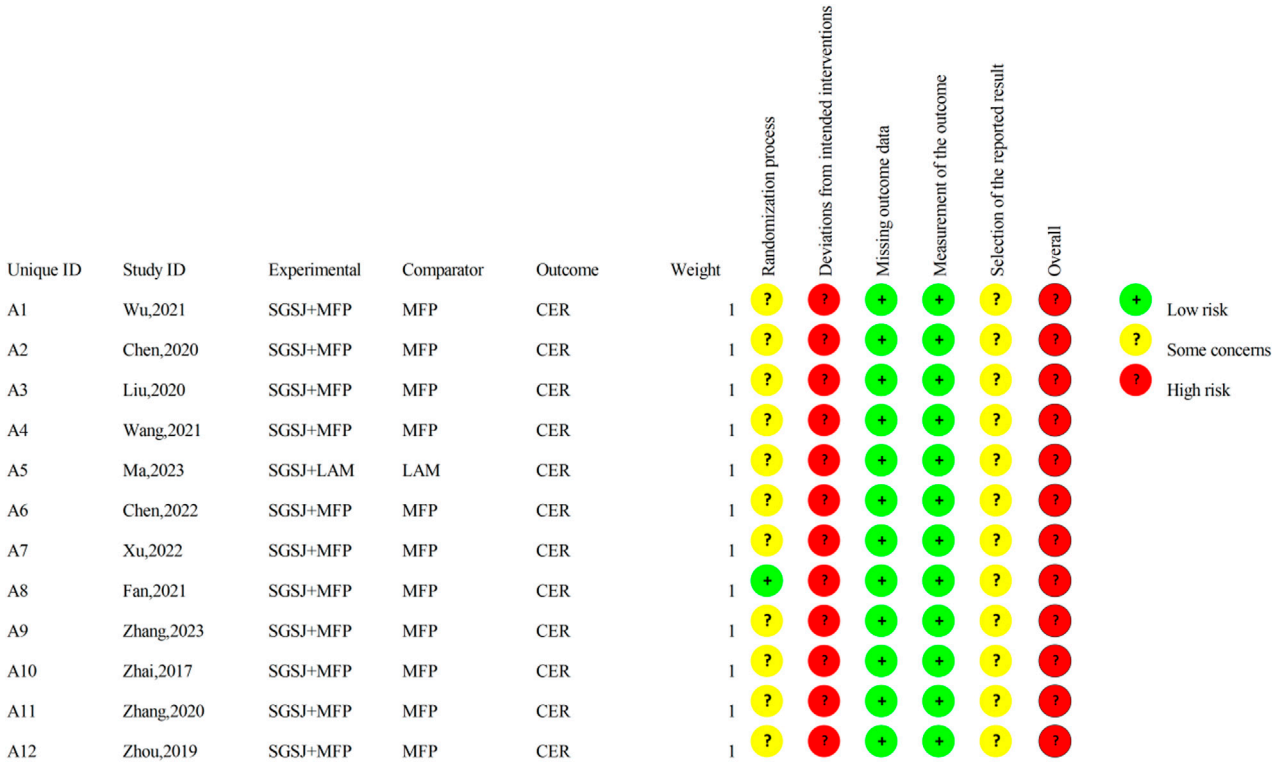


FIGURE 2
Risk-of-bias graph.

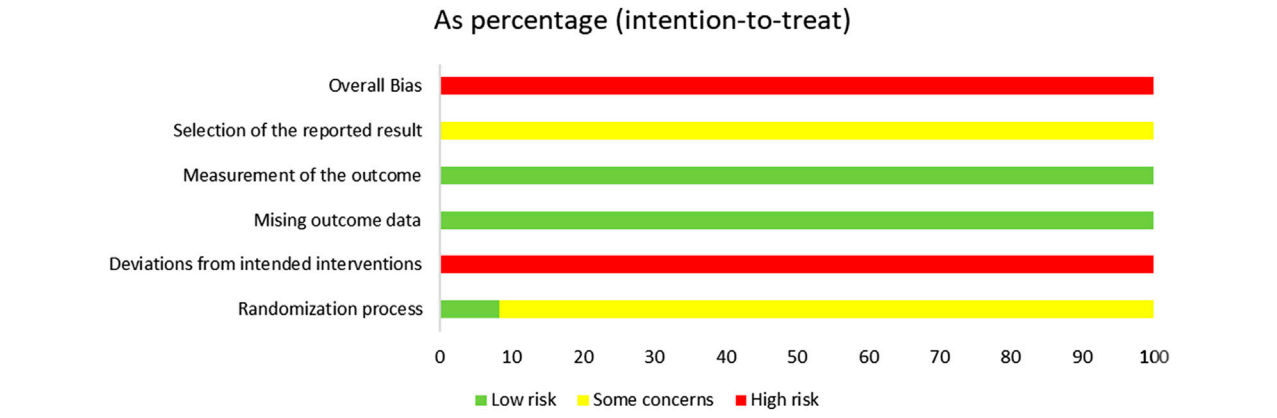


FIGURE 3
Risk-of-bias summary.

(Liu, 2020; Wang, 2021) employed the lottery randomization method, which were evaluated as having a low risk of bias. The remaining two studies (Fan, 2021; Zhang, 2020) did not specify the exact randomization method and were therefore assessed as having an unclear risk of bias.

3.3.2 Allocation concealment

Among the 12 studies, only one study explicitly reported the concealment of allocation in the experiment, while the remaining 11 studies failed to provide such information. Consequently, one study (Fan, 2021) was rated as having a low risk of bias, whereas the risk of bias in the remaining 11 studies remained unclear.

3.3.3 Blinding of participants and personnel

Of the 12 studies, only one (Fan, 2021) reported the implementation of double-blinding, however, it failed to provide a detailed description of the blinding method. Given that SGSJ was significantly different in appearance from MFP and LA, blinding participants and personnel to group allocation was not feasible. Consequently, all studies were evaluated as having a high risk of bias.

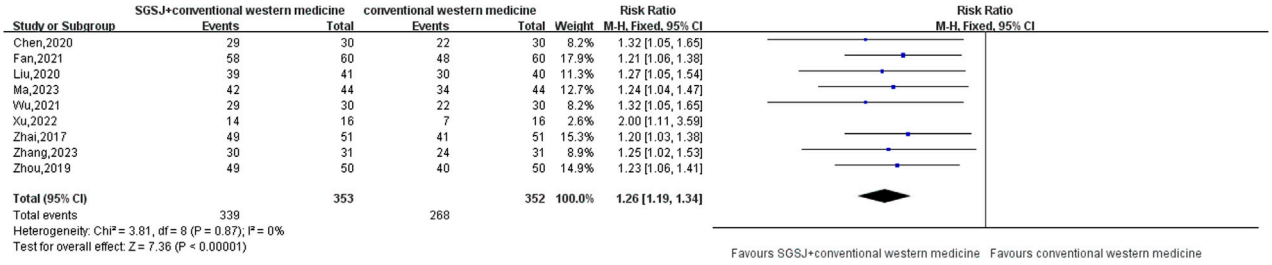


FIGURE 4
Forest plot of the clinical efficiency rate.

3.3.4 Blinding of outcome assessment

Twelve studies failed to provide detailed descriptions regarding the blinding of outcome assessors; consequently, all twelve studies were rated as having an unclear risk of bias.

3.3.5 Incomplete outcome data

All 12 studies reported complete outcome data and were evaluated as having a low risk of bias.

3.3.6 Selective reporting

Due to the absence of explicit blinding, it was not feasible to ascertain whether the researchers had selectively reported the intervention after becoming aware of it. Consequently, all 12 studies were deemed to be at a high risk of bias.

3.3.7 Overall bias

There was one instance of high risk of bias, two instances with unclear risks of bias, and two instances classified as low risks that were also cost-effective. Consequently, the overall assessment indicated a high risk of bias.

3.5 Meta-analysis results

3.5.1 CER

10 studies (Zhai, 2017; Liu, 2020; Wu, 2021; Chen, 2020; Ma, 2023; Chen, 2022; Xu, 2022; Zhang, 2023; Zhou, 2019; Fan, 2021) compared the total response rate of the test group and the control group, involving a total of 815 patients, most of which classified their CER as effective (effective, observably effective, cured) and ineffective. This data type is a binary variable, and RR combined effect size is selected. Heterogeneity test $P = 0.87$, $I^2 = 0\%$, the conclusion is that there is no significant heterogeneity among the studies, so the fixed-effect model is selected for combined analysis. As shown in Figure 4, there was a statistically significant difference in the total effective rate between the SGSJ combined with MFP or LA group and the MFP or LA group [RR = 1.26, 95% CI (1.19, 1.34), $P < 0.00001$], which indicated that the SGSJ combined with MFP or LA group had a higher overall clinical effectiveness rate than the MFP or LA group in treating UFs. The results of sensitivity analysis by one-by-one elimination method showed no significant change, indicating that the study results were relatively stable.

3.5.2 UFV

Nine studies (Zhai, 2017; Liu, 2020; Chen, 2020; Ma, 2023; Chen, 2022; Zhang, 2023; Zhou, 2019; Fan, 2021; Zhang, 2020) reported changes in the volume of UFs before and after the treatment of SGSJ combined with MFP including 388 cases in the SGSJ combined with MFP group and 387 cases in the MFP group. Heterogeneity test $P < 0.00001$, $I^2 = 97\%$, so the random effects model was adopted. As shown in Figure 5, there was a statistically significant difference in the volume of UFs between the SGSJ combined with MFP group and the SGSJ combined with MFP group [MD = −18.23, 95% CI (−22.50, −13.97), $P < 0.00001$], indicating that combined treatment could reduce the volume of UFs in patients more effectively. Sensitivity analysis was performed on these 9 literature, and no literature interfered with the results of this meta-analysis, indicating that this study has good stability. Subgroup analysis was conducted according to the duration of disease, the duration of disease was >12 months in 4 studies and <12 months in 3 studies. ① > 12 months: UFV in the SGSJ combined with MFP group was lower than that in the MFP group, the difference was statistically significant [MD = -13.10.95% CI (−13.91, −12.28), $P < 0.00001$]. ② < 12 months: UFV in the SGSJ combined with MFP group was lower than that in the MFP group, and the difference was statistically significant [MD = -20.27.95% CI (−21.89, −18.65), $P < 0.00001$], as shown in Figure 6. However, the pooled analysis showed significant statistical heterogeneity (chi-square = 205.29, degrees of freedom = 6; $I^2 = 97\%$). Subgroup analysis was conducted according to the duration of treatment. ① > 8 weeks: UFV in SGSJ combined with MFP group was lower than that in MFP group, the difference was statistically significant [MD = -17.89.95% CI (−23.40, −12.37), $P < 0.00001$]; ②≤8 weeks: UFV in the SGSJ combined with MFP group was lower than that in the MFP group, and the difference was statistically significant [MD = −19.41.95% CI (−30.16, −8.66), $P < 0.00001$], as shown in Figure 7. However, the pooled analysis showed significant statistical heterogeneity (chi-square = 263.43, degrees of freedom = 8; $I^2 = 97\%$). Significant heterogeneity ($I^2 = 97\%$) persisted despite subgroup analyses based on disease duration and treatment duration, suggesting that other unconsidered factors (e.g., patient demographics, treatment adherence) may influence UFV outcomes.

3.5.3 UV

Three studies (Chen, 2020; Ma, 2023; Zhou, 2019), with 284 participants, reported the effect of SGSJ in combination with MFP or LA compared with MFP or LA alone. Heterogeneity test $P = 0.45$, $I^2 = 0\%$, fixed effect model was used for meta-analysis. The

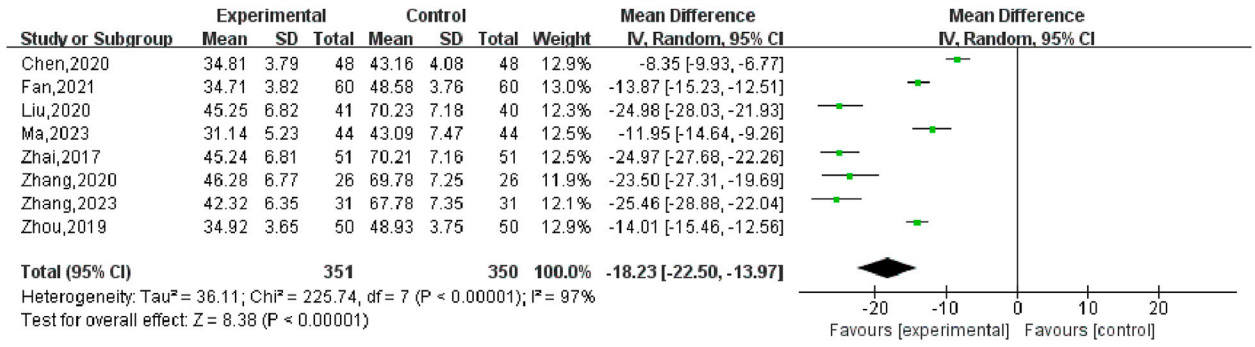


FIGURE 5
Forest plot of the UFs volume.

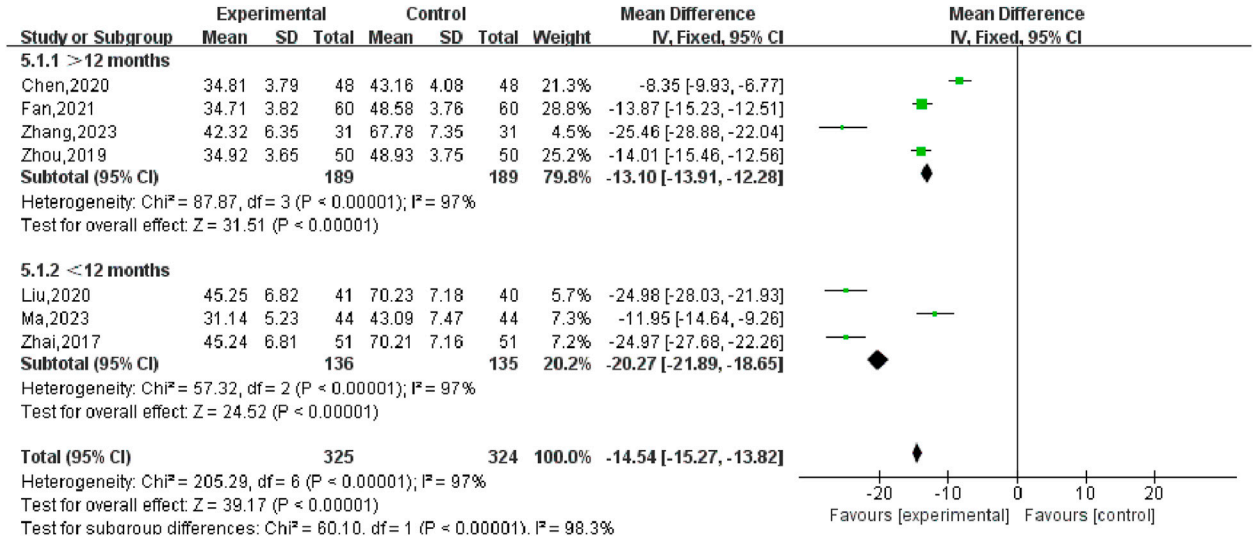


FIGURE 6
Forest plot of UFs volume disease course subgroup analysis.

results showed that there was a statistically significant difference in UV between the SGSJ combined with MFP or LA group and the MFP or LA group [MD = −18.52, 95% CI (−19.99, −17.06), P < 0.00001] (Figure 8). The results of sensitivity analysis showed no significant change, indicating that the research results were relatively stable.

3.5.4 TSS

Four studies (Chen, 2020; Wang, 2021; Fan, 2021; Zhang, 2020) reported the changes of Qi-stagnation and blood-stasis syndrome scores before and after treatment, including 177 cases in the SGSJ combined with MFP group and 176 cases in the MFP group. Heterogeneity test P = 0.09, I^2 = 59%, so the random effects model was used for meta-analysis. As shown in Figure 9, there was a significant statistically difference in symptom scores between the SGSJ combined with MFP group and the MFP group [MD = −5.43, 95% CI (−6.27, −4.60), P < 0.00001], which suggested that the SGSJ combined MFP group had a greater change in qi stagnation and blood stasis scores than the MFP group. Sensitivity analysis showed that when excluded (Fan, 2021), heterogeneity was reduced to 0%, but this did not overturn our conclusions, and the results were relatively stable.

3.5.5 Follicle-stimulating hormone (FSH)

Three studies (Ma, 2023; Xu, 2022; Zhou, 2019) reported changes in FSH values in patients before and after treatment, including 220 participants. Heterogeneity test P < 0.00001, I^2 = 98%, so the random effects model was used for meta-analysis, as shown in Figure 10, there was a statistically significant difference in symptom scores between the SGSJ combined with MFP or LA group and the MFP or LA group [MD = −3.89, 95% CI (−5.96, −1.81), P < 0.00001], which suggested that the SGSJ combined with MFP or LA group showed a greater change in FSH values than the MFP or LA group. Due to the large heterogeneity in the studies, we performed subgroup analysis based on the types of western medicines combined by SGSJ, with 1 study combining LA and 2 studies combining MFP. ① Combined with LA: the FSH of observation group was lower than that of control group, and the difference was

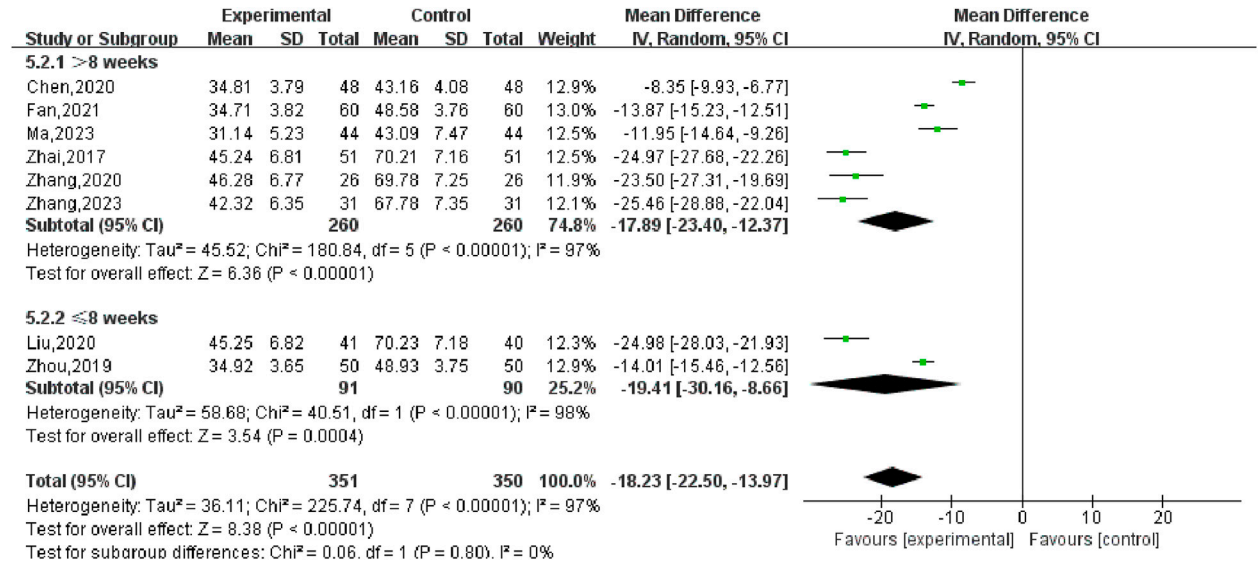


FIGURE 7
Forest plot of UFs volume treatment subgroup analysis.

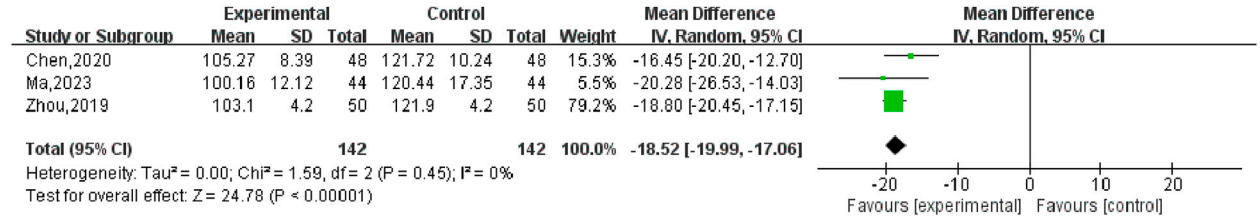


FIGURE 8
Forest plot of uterine volume.

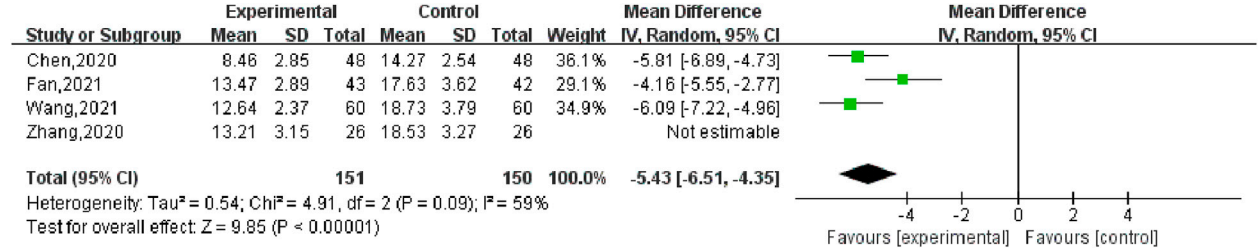


FIGURE 9
Forest plot of TCM syndrome scores.

statistically significant [MD = −2.07.95% CI (−2.06, −1.54), P < 0.00001]; ② Combined with MFP: the FSH in the observation group was lower than that in the control group, and the difference was statistically significant [MD = −3.89.95% CI (−5.96, −1.81), P < 0.00001], as shown in Figure 11. However, the pooled analysis showed significant statistical heterogeneity (chi-square = 109.49, degrees of freedom = 2; I^2 = 98%). FSH was more significantly reduced in the combined with MFP group compared to the combined with LA group, suggesting a possible drug-dependent interaction.

3.5.6 Luteinizing hormone (LH)

Three (Ma, 2023; Xu, 2022; Zhou, 2019) studies compared post-treatment LH levels in experimental and control groups, involving a total of 220 patients. Heterogeneity test P < 0.00001, I^2 = 100%, so the random effects model was used for meta-analysis, as shown in

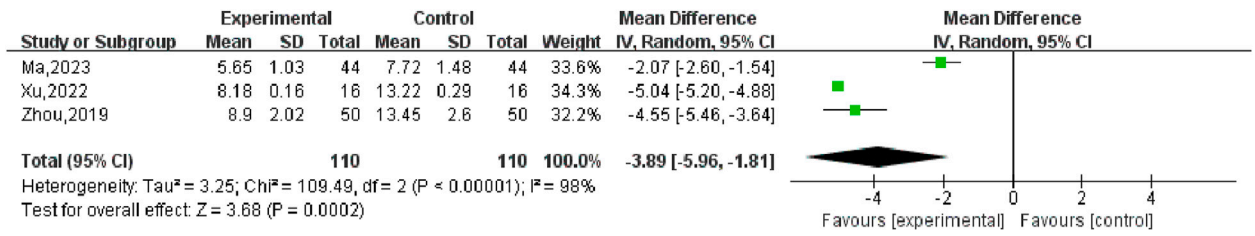


FIGURE 10
Forest plot of follicle-stimulating hormone.

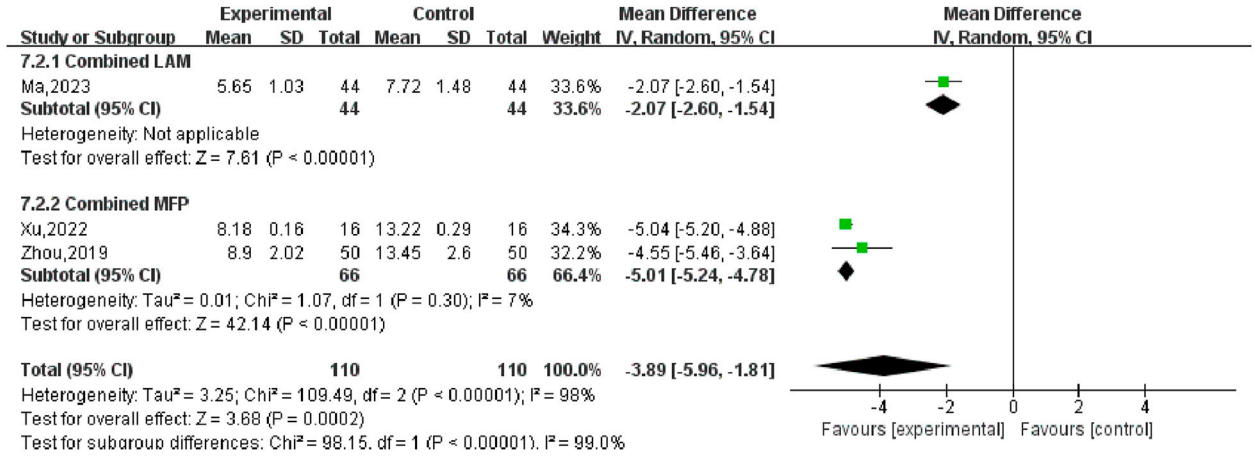


FIGURE 11
Forest plot of follicle-stimulating hormone combined drug use subgroup analysis.

Figure 12, there was a statistically significant difference in symptom scores between the SGSJ combined with MFP or LA group and the MFP or LA group [MD = −3.57, 95% CI (−6.70, −0.44), $P < 0.00001$], which indicated that SGSJ combined with MFP or LA can significantly reduce the LH levels of patients. After sensitivity analysis, literature was removed one by one, and the final combined effect size did not change in direction, and the random effect model was used to merge. We performed a subgroup analysis based on based on the types of western medicines combined by SGSJ, with 1 study combining LA and 2 studies combining MFP. ① Combined with LA: LH in the observation group was lower than that in the control group, and the difference was statistically significant [MD = −1.12, 95% CI (−1.49, −0.75), $P < 0.00001$]; ② Combined with MFP: LH in the observation group was lower than that in the control group, and the difference was statistically significant [MD = −4.91.95% CI (−5.86, −3.97), $P < 0.00001$]. The results showed that TH was more significantly reduced in the combined with MFP group compared to the combined with LA group, suggesting a possible drug-dependent interaction (Figure 13).

3.5.7 Progesterone (P)

Six studies (Wang, 2021), including 407 participants, reported the effect of combination therapy *versus* MFP alone in treating P. The heterogeneity of the pooled analysis was high ($P < 0.00001$, $I^2 = 98\%$), so the random effects model was used in the meta-analysis. Comprehensive results show that the combined treatment can decrease the P [MD = 4.46, 95% CI (4.61, 4.32), $P < 0.00001$], (Figure 14). When Wang (2021) was excluded, the heterogeneity was reduced to 0%, but this did not overturn our conclusions, and the findings were relatively stable. We performed subgroup analyses based on different doses of combined MFP, with 2 studies having oral MFP≥20 mg/d and 4 studies having oral MFP <20 mg/d ① ≥20 mg/d: diamond shape across the inefficacy line, indicating that the difference between the experimental group and the control group was not statistically significant, that is, SGSJ combined with MFP or LA was no more effective in reducing P than the control group [MD = −0.42, 95% CI (−1.27, 0.43), $P < 0.00,001$]; ② < 20 mg/d: P in the observation group was lower than that in the control group, and the difference was statistically significant (MD = −4.59.95% CI (−4.73, −4.44), $P < 0.00,001$), as shown in Figure 15. Subgroup analysis showed that SGSJ combined with lower MFP doses (<20 mg/d) significantly reduced P levels, whereas no significant reduction was observed with higher MFP doses (≥20 mg/d).

3.5.8 Estradiol (E_2)

Three studies, including 220 participants, reported the effects of combination therapy *versus* conventional western drug therapy alone on E_2. The heterogeneity of the pooled analysis was high ($P < 0.0001$, $I^2 = 96\%$), so the random effects model was used in the

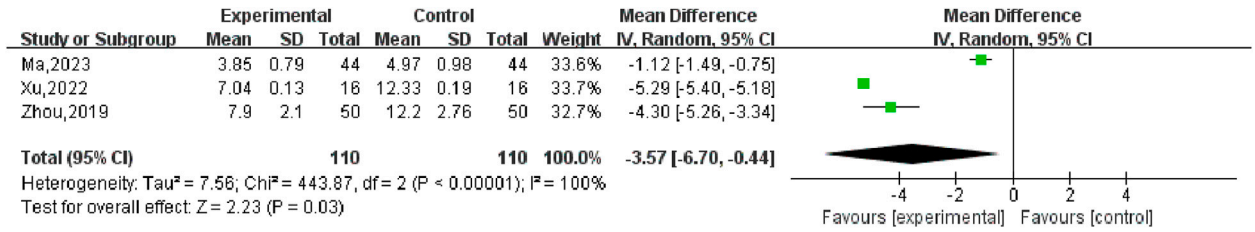


FIGURE 12
Forest plot of luteinizing hormone.

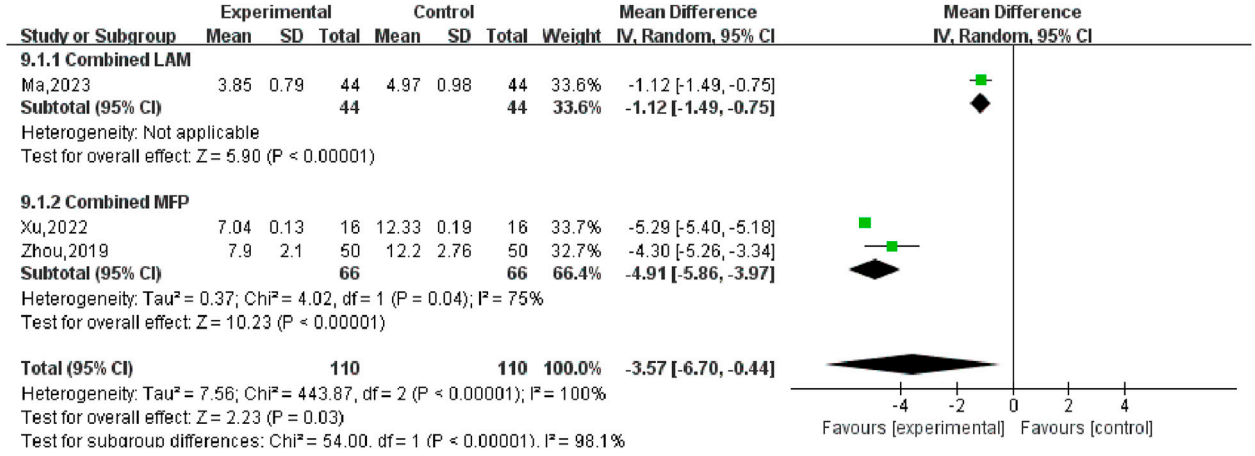


FIGURE 13
Forest plot of luteinizing hormone combined drug use subgroup analysis.

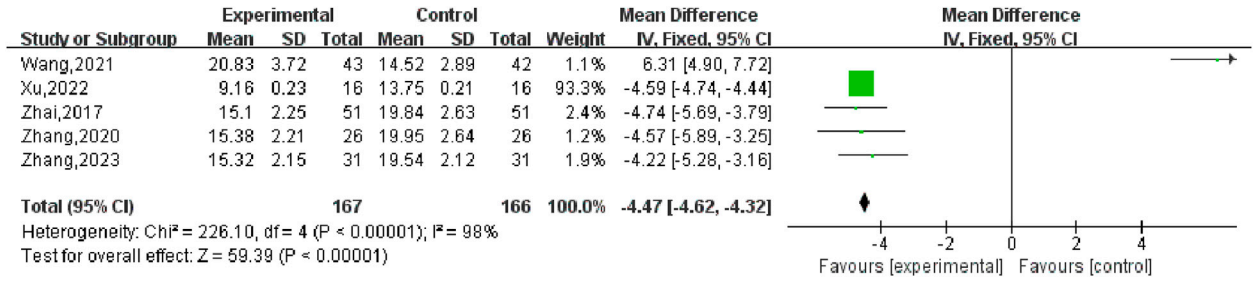


FIGURE 14
Forest plot of progesterone.

meta-analysis. The comprehensive results showed that the difference between combined treatment and MFP or LA alone was not statistically significant E_2 [Smd = −1.72.95% CI (−4.12, −0.68), $P < 0.00001$] (Figure 16). Sensitivity analysis showed that after removing [Xu, 2022] (Xu, 2022), the heterogeneity was reduced to 0%, which overruled our conclusion, indicating that the stability of the results of E_2 meta-analysis was poor.

3.5.9 Publication bias

In this meta-analysis, we tested publication bias by drawing funnel plots of eight outcome indicators, including total CER, UFV change, UV change, E_2, P, LH and FSH levels, and TSS. In the funnel plots drawn by total clinical response rate, scatter points were more symmetrical, and there is little possibility of publication bias. The funnel plot of the other 7 outcome indicators showed asymmetric discrete distribution with publication bias.

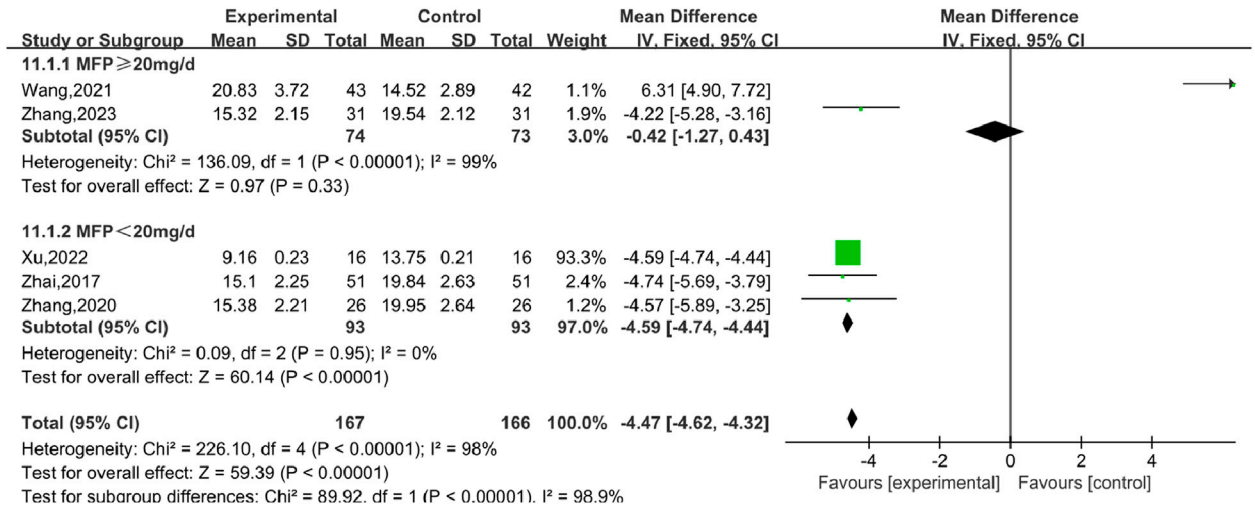


FIGURE 15
Forest plot of progesterone MFP dosage subgroup analysis.

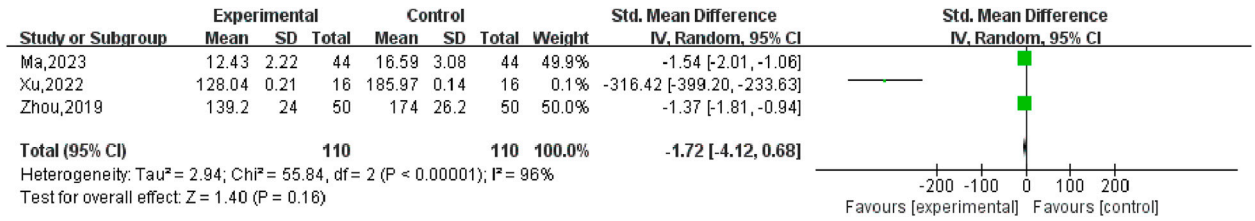


FIGURE 16
Forest plot of estradiol.

3.6 GRADE assessment

All studies included in this study were meta-analyzed and GRADE evidence assessment was evaluated. Problems of bias risk, limitation and inconsistency were found in the evaluation, due to the risk of bias in aspects such as low quality and accuracy of the literature, so that all the research studies were not eligible for GRADE upgrade and at least one was eligible for downgrade. Therefore, in the end, the highest GRADE evidence evaluation included in this study was only three of medium quality, and there were a lot of low-quality, very low-quality evidence. The quality of the evidence was reduced due to the risk of bias, inconsistency and imprecision. High heterogeneity between studies and unclear randomization methods resulted in low GRADE scores. It has long been a phenomenon that the quality evaluation of Chinese medicine research studies on methodology is generally not high. Due to the low quality of the studies, the trust of clinicians in research has decreased, which is one of the limitations of this study.

4 Discussion

UFs are common benign gynecologic tumors in women of fertility age (Donnez et al., 2012). Surgery and endocrine therapy may cause severe physical and psychological trauma, including impaired physiological function and body image problems (Dolmans and Donnez, 2024). Due to the untolerable side effects of conventional treatments, TCM has become a research hotspot for its multi-targeting and low-toxicity properties. However, differences in treatment methods and outcome assessment have limited the dissemination of existing TCM studies (Shi et al., 2023). In this study, evidence-based medicine and meta-analysis were used to evaluate the efficacy and safety of SGSJ for UF. However, the findings should be interpreted with caution due to methodological limitations and significant heterogeneity of the included studies.

The sensitivity analysis revealed that specific studies (e.g., Wang, 2021) had a disproportionate impact on heterogeneity. This may be due to differences in patient populations, intervention protocols, or outcome assessment methods.

4.1 Summary of evidence

To the best of our knowledge, this study represents the pioneering systematic review and meta-analysis evaluating the efficacy and safety of SGSJ combined with MFP or LA in the treatment of UFs in China. A total of 12 randomized controlled

trials, encompassing 952 patients, were included in this analysis. The findings suggest that SGSJ in combination with MFP or LA significantly increases the CER and reduces the UFV compared with MFP or LA alone, demonstrating superior therapeutic efficacy. However, these findings should be interpreted with caution due to significant heterogeneity between studies and methodological quality limitations.

The results of meta-analysis showed that the overall CER of SGSJ combined with MFP or LA was higher than that of the control group. In addition, secondary outcome indicators, including UFV, UV, sex hormone levels (FSH, LH, P), and TSS, were significantly improved in the treatment group compared with the control group. However, there was no significant change in E_2 levels.

Subgroup analyses showed that longer treatment duration (>8 weeks) resulted in greater UFV reduction and higher CER, as well as a significant reduction in heterogeneity, suggesting that sustained intervention may improve therapeutic efficacy. In addition, patients with UFs ≤12 months showed greater improvement than those with UFs ≤12 months, suggesting that SGSJ may exert a better therapeutic effect in early intervention. Subgroup analyses based on different drug combinations showed that SGSJ + MFP had more pronounced benefits in reducing UFV and modulating sex hormone levels compared with SGSJ + LA, and less heterogeneity was observed in the SGSJ + MFP subgroup, suggesting that the combination may be more consistently effective. In addition, MFP dose played a role in modulating the therapeutic effect, as high doses (≥20 mg/d) were associated with better regulation of P levels but also increased heterogeneity, whereas low doses (<20 mg/d) showed moderate efficacy with fewer reported adverse events, highlighting the need to optimize dosing strategies.

In addition, the high degree of heterogeneity observed in UFV (I^2 = 97%) and hormone-related outcomes (FSH, LH, P levels, I^2 > 90%) suggests that there is a great deal of variation between studies. Subgroup analyses based on treatment duration, disease duration, and drug combinations (SGSJ + MFP vs. SGSJ + LA) helped to minimize heterogeneity to some extent, but did not fully resolve it. This suggests that other factors, such as individual patient response variability and adherence differences, may influence the results. Future studies should standardize the dose and duration of treatment for MFP to minimize variability.

With regard to safety, limited adverse event data were available, with only one study reporting mild side effects such as rash and mild vaginal bleeding. In addition, the combination of SGSJ and MFP was associated with fewer adverse events than MFP alone, suggesting a potential protective effect of SGSJ against MFP-related side effects. However, the long-term safety of SGSJ remains uncertain due to limited reports of adverse reactions and lack of long-term follow-up data.

4.2 Reporting quality

Compliance with the ConPhyMP tool was suboptimal in RCTs of SGSJ combination therapy for UFs. The average proportion of ConPhyMP tool usage across all included studies was only 38.3% and 20%, respectively. Specific issues identified include (Stewart et al., 2017): inadequate descriptions of plant materials, lacking botanical or morphological identification, which hinders readers' understanding of the morphological structure and functional relationships of botanical drugs (De La Cruz and Buchanan, 2017); omission of full species names, authorities, and family information, which impairs patients' ability to accurately identify botanical drugs (Ning et al., 2020); lack of detailed information about commercial products, reducing transparency and affecting readers' assessment of safety. Regarding the ConPhyMP for extract type A, the following deficiencies were noted (Stewart et al., 2017): absence of a certificate for the extract (De La Cruz and Buchanan, 2017); lack of manufacturer and analytical certificates (Ning et al., 2020); failure to perform triple chemical fingerprinting of botanical drugs (Mitro et al., 2024); quantification of at least two labeled compounds was not conducted (Yang et al., 2022); none of the reports utilized a single chemical fingerprinting method (Silberzweig et al., 2016); labeled compounds were not quantified, and no justification was provided for these omissions. The inconsistent reporting of SGSJ components across studies weakens the reliability of results. Future research should adhere to international standards (e.g., ConPhyMP) to provide consistent botanical authentication, extraction details, and quality control measures.

4.3 The impact of bias risk on outcomes

4.3.1 Selection bias and performance bias

Only one study (Fan, 2021) reported the implementation of blinding procedures. The remaining studies did not provide detailed protocols regarding blinding, concealment of the randomization process, or sample size calculations. Non-transparent randomization methods and inadequate concealment of group assignments may have resulted in imbalanced baseline characteristics between groups. What's more, the persistence of high heterogeneity in UFV outcomes, even after subgroup analysis, suggests potential confounding factors such as individual patient response variability and differing intervention adherence. Further research is needed to investigate additional factors that may influence treatment response, such as baseline fibroid characteristics, hormonal status, and genetic variations. Additionally, the absence of blinding for participants and research personnel could have led to differential intensities of adjunctive therapy or care provided to the intervention and control groups. For instance, patients in the placebo group might have exhibited reduced adherence due to awareness of their group allocation. Consequently, the combined effect size may be either overestimated or underestimated. In unblinded studies, the treatment effect in the intervention group may be exaggerated by a placebo effect or observer expectations. Future studies should ensure strict blinding of participants and assessors to minimize performance and detection bias. In addition, appropriate allocation concealment methods (e.g., sealed opaque envelopes or centralized randomization) should be used to improve methodological quality.

4.3.2 Reporting bias and measurement bias

The efficacy evaluation indicators in all studies were insufficiently comprehensive, with critical outcomes such as menstrual volume, long-term efficacy, and recurrence rate

remaining underreported. Standardized tools for assessing menstrual volume were not utilized. Consequently, the impact of the interventions on long-term outcomes remains unclear. Incomplete information for clinical decision-making: The absence of key outcomes may mislead clinical practice and decision-making.

4.3.3 Follow-up bias and time effect bias

None of the studies provided long-term follow-up data exceeding 6 months. The high rate of loss to follow-up, coupled with the lack of intention-to-treat analyses, may have led to an underestimation of adverse events or recurrence rates. Short-term treatment effects might not accurately represent sustained efficacy or delayed side effects of the intervention. Consequently, this could result in an overestimation of short-term benefits (e.g., an intervention that is initially effective but subsequently fails) and inadequate safety assessments for identifying long-term adverse effects.

4.4 Implications for research

In view of the risk of bias mentioned, we proposes several recommendations for future research. Firstly, future RCTs should provide detailed descriptions of their randomization methods, encompassing simple, block, stratified, and cluster randomization techniques. Secondly, it is advised that experimental studies on botanical drugs adhere strictly to the ConPhyMP checklist in both design and reporting. Additionally, rigorous blinding procedures must be implemented to ensure blinding of participants, researchers, and observers. However, the preparation and evaluation of TCM placebos present greater challenges compared to chemical drugs due to the unique taste and diverse odors of TCM formulations. Consequently, future research should explore the development of safe and comparable TCM placebos. Furthermore, all adverse events in each study group should be meticulously documented in accordance with the CONSORT 2010 Statement (48), and the duration of clinical trials should be extended to assess the long-term safety of SGSJ in treating UFs. In addition, future studies should systematically evaluate the dose-response relationship between MFP and SGSJ to refine the optimal treatment protocols.

4.5 Strengths and limitations

Our study possesses several notable strengths. Firstly, despite the increasing number of clinical studies investigating the treatment of UFs, there has been no systematic review or meta-analysis focusing on the combination of SGSJ and MFP or LA for UFs. This study represents the first comprehensive evaluation of SGSJ, thereby addressing a significant gap in the evidence base for its use in treating UFs. Secondly, our interpretation of the results is conducted with a high degree of caution. We conducted subgroup analyses to identify sources of heterogeneity and performed sensitivity analyses and publication bias tests. Additionally, we incorporated both subjective (CER, TSS) and objective (UFV, UV, LH, FSH, E_2, P, and adverse effects) outcome measures.

Although best efforts have been made to refine the methodology of this study, inevitably there are still several limitations of our study. First, Adverse drug effects are inadequately recorded, only one study (Ma, 2023) reported adverse effects, and none included monitoring of liver and kidney function, hormone levels, or long-term complications such as cancer risk. This significantly limits the reliability of any safety conclusions drawn. Second, the follow-up duration was insufficient: all studies had a follow-up period of less than 6 months, precluding an accurate assessment of both the persistence of efficacy and potential long-term toxicity. In addition, the study populations were highly homogeneous: all studies were conducted in China, which may restrict the generalizability of the findings to other ethnic groups or healthcare systems.

Finally, the most significant limitation of this study is the lack of efficacy in assessing drug safety. This is mainly attributed to the following reasons: firstly, only one study (Ma, 2023) reported adverse effects, while the remaining studies provided no data on adverse events. This absence of information may stem from selective reporting bias or inadequate monitoring protocols. Secondly, none of the studies included long-term follow-up periods exceeding 6 months. What's more, the reporting of Chinese medicine components is inconsistent (such as lack of botanical identification and standardized extract information), affecting the credibility of the results. Consequently, several critical safety questions remain unaddressed (Stewart et al., 2017): Long-term organ toxicity: it remains unclear whether cumulative damage to liver and kidney function exists with SGSJ (De La Cruz and Buchanan, 2017). Effects on hormone homeostasis: it still unclear whether long-term use leads to abnormal fluctuations in FSH or LH levels (Ning et al., 2020). Reproductive and pregnancy risks: Insufficient data on exposure during pregnancy to assess potential effects on fetal development.

5 Conclusion

At present, there are evidence shows that SGSJ combined with MFP or LA improves CER, reduces UFV, and modulates sex hormone levels. However, due to the poor methodological quality and high heterogeneity of the included trials, our conclusions should be interpreted with caution. Future studies should prioritize rigorous RCTs with standardized treatment protocols, extended follow-up, and comprehensive safety assessments to identify SGSJ as a reliable treatment option for UFs.

Data availability statement

The original contributions presented in the study are included in the article/supplementary material, further inquiries can be directed to the corresponding authors.

Author contributions

YaZ: Data curation, Writing – original draft, Writing – review and editing, Conceptualization, Formal Analysis, Methodology, Visualization. JW: Data curation, Writing – original draft,

Writing – review and editing, Conceptualization, Validation. CG: Data curation, Methodology, Supervision, Conceptualization, Formal analysis, Writing–review and editing. SF: Writing – review and editing, Data curation, Methodology. HW: Data curation, Writing – review and editing, Visualization. JC: Writing – review and editing, Data curation, Visualization. YiZ: Data curation, Methodology, Supervision, Conceptualization, Formal analysis, Validation, Writing–review and editing. YY: Writing – review and editing, Conceptualization, Project administration, Supervision, Validation, Writing – original draft. LR: Supervision, Writing – original draft, Writing – review and editing, Conceptualization, Formal Analysis, Methodology, Resources.

Funding

The author(s) declare that no financial support was received for the research and/or publication of this article.

Conflict of interest

The authors declare that the research was conducted in the absence of any commercial or financial relationships that could be construed as a potential conflict of interest.

Generative AI statement

The author(s) declare that no Gen AI was used in the creation of this manuscript.

Publisher's note

All claims expressed in this article are solely those of the authors and do not necessarily represent those of their affiliated organizations, or those of the publisher, the editors and the reviewers. Any product that may be evaluated in this article, or claim that may be made by its manufacturer, is not guaranteed or endorsed by the publisher.

References

Ali, M., Ciebiera, M., Wlodarczyk, M., Alkhrait, S., Maajid, E., Yang, Q., et al. (2023). Current and emerging treatment options for uterine fibroids. *Drugs* 83 (18), 1649–1675. doi:10.1007/s40265-023-01958-6

Chen, L., Chen, H., Yang, Q., Jiang, Y., Liu, L., Yu, H., et al. (2022). Guizhi Fuling Capsule inhibits uterine fibroids growth by modulating Med12-mediated Wnt/β-Catenin signaling pathway. *J. Ethnopharmacol.* 290:115115. doi:10.1016/j.jep.2022.115115

Chen, W. (2022). Clinical effect of Shugan Sanjie Decoction on the syndrome of qi stagnation and blood stasis in uterine fibroids. *Inn. Mong. J. Traditional Chin. Med.* 41 (03), 24–25. doi:10.16040/j.cnki.cn15-1101.2022.03.030

Chen, Y. (2020). Effect of Shugan Sanjie Decoction on uterine volume and menstrual volume in patients with uterine fibroid syndrome of Qi stagnation and blood stasis. *Chin. J. Ethnomedicine Ethnopharmacy* 29 (20), 117–119.

De La Cruz, M. S., and Buchanan, E. M. (2017). Uterine fibroids: Diagnosis and treatment. *Am. Fam. Physician* 95 (2), 100–107. Cited in: Pubmed; PMID 28084714.

Dolmans, M. M., and Donnez, J. (2024). Solving the mysteries surrounding uterine fibroids: are we almost there? *Fertil. Steril.* 122(1):4–5. Declaration of Interests M.M.D. has nothing to disclose. J.D. has nothing to disclose. Epub 20240511. doi:10.1016/j.fertnstert.2024.05.144

Donnez, J., and Dolmans, M. M. (2016). Uterine fibroid management: from the present to the future. *Hum. Reprod. Update*. 22(6):665–686. Epub 20160727. doi:10.1093/humupd/dmw023

Donnez, J., Tomaszewski, J., Vázquez, F., Bouchard, P., Lemieszczuk, B., Baró, F., et al. (2012). Ulipristal acetate versus leuprolide acetate for uterine fibroids. *N. Engl. J. Med.* 366(5):421–432. doi:10.1056/NEJMoa1103180

Fan, J. (2021). Clinical study of Shugan Sanjie Decoction treating syndrome of Qi-stagnation and blood-stasis in uterine fibroids. *Shenzhen J. Integr. Traditional Chin. West. Med.* 31 (12), 74–76. doi:10.16458/j.cnki.1007-0893.2021.12.031

Fu, Y., Fan, Y., Fan, W., Lv, Y., Ai, S., and Yu, C. (2020). Efficacy and safety of traditional Chinese herbal formula combined with western medicine for uterine fibroid: a protocol for systematic review and meta-analysis. *Med. Baltim.* 99, e22039(36). doi:10.1097/md.0000000000022039

Guyatt, G. H., Oxman, A. D., Vist, G. E., Kunz, R., Falck-Ytter, Y., Alonso-Coello, P., et al. (2008). GRADE: an emerging consensus on rating quality of evidence and strength of recommendations. *Bmj.* 336, 1170–1173. 924-6. doi:10.1136/bmj.39504.506319.80

Harris, H. R., Petrick, J. L., and Rosenberg, L. (2022). The epidemiology of uterine fibroids: where do we go from here? *Fertil. Steril.* 117(4):841–842. Epub 20220309. doi:10.1016/j.fertnstert.2022.01.037

Heinrich, M., and Jalil, B. (2023). From the CONSORT to the ConPhyMP statement and beyond-how to ascertain best practice. *Front. Pharmacol.* 14:1338710. doi:10.3389/fphar.2023.1338710

Heinrich, M., Jalil, B., Abdel-Tawab, M., Echeverria, J., Kulić, Ž., McGaw, L. J., et al. (2022). Best Practice in the chemical characterisation of extracts used in pharmacological and toxicological research-The ConPhyMP-Guidelines. *Front. Pharmacol.* 13:953205. doi:10.3389/fphar.2022.953205

Huedo-Medina, T. B., Sánchez-Meca, J., Marín-Martínez, F., and Botella, J. (2006). Assessing heterogeneity in meta-analysis: Q statistic or I2 index? *Psychol. Methods*. 11(2):193–206. doi:10.1037/1082-989x.11.2.193

Langton, C. R., Harmon, Q. E., and Baird, D. D. (2024). Family history and uterine fibroid development in black and african American women. *JAMA Netw. Open*. 7(4):e244185. Conflict of Interest Disclosures: None reported. Epub 20240401. doi:10.1001/jamanetworkopen.2024.4185

Laughlin-Tommaso, S. K., and Stewart, E. A. (2018). Moving toward individualized medicine for uterine leiomyomas. *Obstet. Gynecol.* 132(4):961–971. doi:10.1097/aog.0000000000002785

Lee, S., and Stewart, E. A. (2023). New treatment options for nonsurgical management of uterine fibroids. *Curr. Opin. Obstet. Gynecol.* 35(4):288–293. doi:10.1097/gco.0000000000000880

Liu, Y. (2020). Effect of Shugan Sanjie Decoction on lesion volume and hemodynamics in patients with uterine fibroids. *Pract. Clin. J. Integr. Traditional Chin. West. Med.* 20 (13), 75–76. doi:10.13638/j.issn.1671-4040.2020.13.037

Ma, W. (2023). Clinical effect of Shugan Sanjie Decoction combined with leuprelin on patients with uterine fibroids of Qi stagnation and blood stasis. *Shenzhen J. Integr. Traditional Chin. West. Med.* 33 (9), 42–45. doi:10.16458/j.cnki.1007-0893.2023.09.012

Manyonda, I., Belli, A. M., Lumsden, M. A., Moss, J., McKinnon, W., Middleton, L. J., et al. (2020). Uterine-artery embolization or myomectomy for uterine fibroids. *N. Engl. J. Med.* 383(5):440–451. doi:10.1056/NEJMoa1914735

Marsh, E. E., Wegienka, G., and Williams, D. R. (2024). Uterine fibroids. *Jama*. 331(17):1492–1493. doi:10.1001/jama.2024.0447

Meng, W., Lin, W. L., Yeung, W. F., Zhang, Y., Ng, E. H. Y., Lee, Y. P. E., et al. (2022). Randomized double-blind trial comparing low dose and conventional dose of a modified traditional herbal formula Guizhi Fuling Wan in women with symptomatic uterine fibroids. *J. Ethnopharmacol.* 283:114676. Epub 20210922. doi:10.1016/j.jep.2021.114676

Mitro, S. D., Wise, L. A., Waetjen, L. E., Lee, C., Zaritsky, E., Harlow, S. D., et al. (2024). Hypertension, cardiovascular risk factors, and uterine fibroid Diagnosis in midlife. *JAMA Netw. Open*. 7(4):e246832. doi:10.1001/jamanetworkopen.2024.6832

Ning, G., Zhang, X., Zhang, Q., Wang, Z., and Liao, H. (2020). Real-time and multimodality image-guided intelligent HIFU therapy for uterine fibroid. *Theranostics*. 10(10):4676–4693. Competing Interests: The authors have declared that no competing interest exists. Epub 20200326. doi:10.7150/thno.42830

Page, M. J., McKenzie, J. E., Bossuyt, P. M., Boutron, I., Hoffmann, T. C., Mulrow, C. D., et al. (2021). The PRISMA 2020 statement: an updated guideline for reporting systematic reviews. *Bmj.* 372:n71. Epub 2021/03/31. doi:10.1136/bmj.n71

Shi, S., Luo, L., Peng, F., and Yu, C. (2023). Potential mechanism of Taohong Siwu Decoction in uterine fibroid treatment based on integrated strategy of network pharmacology and experimental verification. *Chin. Med.* 18(1):95. The authors declare that they no competing interests. Epub 20230802. doi:10.1186/s13020-023-00809-6

Silberzweig, J. E., Powell, D. K., Matsumoto, A. H., and Spies, J. B. (2016). Management of uterine fibroids: a focus on uterine-sparing interventional techniques. *Radiology*. 280(3):675–692. doi:10.1148/radiol.2016141693

Sterne, J. A. C., Savović, J., Page, M. J., Elbers, R. G., Blencowe, N. S., Boutron, I., et al. (2019). RoB 2: a revised tool for assessing risk of bias in randomised trials. 366:l4898, Available online at: www.icmje.org/coi_disclosure.pdfanddeclare. doi:10.1136/bmj.l4898

Stewart, E. A., Cookson, C. L., Gandolfo, R. A., and Schulze-Rath, R. (2017). Epidemiology of uterine fibroids: a systematic review. *Bjog*. 124(10):1501–1512. Epub 20170513. doi:10.1111/1471-0528.14640

Stewart, E. A., Laughlin-Tommaso, S. K., Catherino, W. H., Lalitkumar, S., Gupta, D., and Vollenhoven, B. (2016). Uterine fibroids. *Nat. Rev. Dis. Prim.* 2:16043. Epub 20160623. doi:10.1038/nrdp.2016.43

Stewart, E. A., Missmer, S. A., and Rocca, W. A. (2021). Moving beyond reflexive and prophylactic gynecologic surgery. *Mayo Clin. Proc.* 96(2):291–294. doi:10.1016/j.mayocp.2020.05.012

Stewart, E. A., and Nowak, R. A. (2022). Uterine fibroids: hiding in plain sight, 37, 16, 27. doi:10.1152/physiol.00013.2021

Syed, Y. Y. (2022). Relugolix/estradiol/norethisterone (norethindrone) acetate: a review in symptomatic uterine fibroids. *Drugs*. 82(15):1549–1556. doi:10.1007/s40265-022-01790-4

Tulandi, T. (2007). Treatment of uterine fibroids--is surgery obsolete? *N. Engl. J. Med.* 356(4):411–413. doi:10.1056/NEJMe068281

Vannuccini, S., Petraglia, F., Carmona, F., Calaf, J., and Chapron, C. (2024). The modern management of uterine fibroids-related abnormal uterine bleeding. *Fertil. Steril.* 122(1):20–30. doi:10.1016/j.fertnstert.2024.04.041

Walker, C. L., and Stewart, E. A. (2005). Uterine fibroids: the elephant in the room. *Science*. 308(5728):1589–1592. doi:10.1126/science.1112063

Wang, B. (2021). Effect of Shugan Sanjie decoction on TCM syndrome score and P level in patients with hysteromyoma Qi stagnation and blood-stagnation syndrome. *Contemp. Med.* 27 (11), 79–81.

Wu, H. (2021). Therapeutic effect of Shugan Sanjie Decoction on the syndrome of uterine fibroid qi stagnation and blood stasis. *Women's Health* (30).

Wu, Y., Zhang, C., Chen, Y., and Luo, Y. J. (2018). Association between acute mountain sickness (AMS) and age: a meta-analysis. *Mil. Med. Res.* 5(1):14. Ethics approval and consent to participate: not applicable. competing interests: The authors declare that they have no competing interests. Epub 20180511. doi:10.1186/s40779-018-0161-x

Xu, M. (2022). Clinical effect analysis of Shugan Sanjie Decoction in the treatment of uterine fibroids with Qi stagnation and blood stasis syndrome. *Electron. J. Pract. Gynecol. Endocrinol.* 9 (11), 72–74.

Yang, Q., Ciebiera, M., Bariani, M. V., Ali, M., Elkafas, H., Boyer, T. G., et al. (2022). Comprehensive review of uterine fibroids: developmental origin, pathogenesis, and treatment. *Endocr. Rev.* 43(4):678–719. doi:10.1210/endrev/bnab039

Zhai, Y. (2017). Clinical study on the treatment of hysteromyoma with qi stagnation and blood stasis syndrome by shugan Sanjie tang. *ACTA Chin. Med.* 32(12):2516–2518. doi:10.16368/j.issn.1674-8999.2017.12.653

Zhang, B. (2020). Clinical study on shugan Sanjie decoction in treating hysteromyoma with qi zhi xue yu zheng. *Clin. study Shugan Sanjie Decoction Treat. hysteromyoma Qi Zhi Xue Yu Zheng* 36 (23), 105–106.

Zhang, F. (2023). Clinical observation of Shugan Sanjie Decoction treating syndrome of qi stagnation and blood stasis in uterine fibroids. *Clin. observation Shugan Sanjie Decoction Treat. syndrome qi stagnation blood stasis uterine fibroids* 39 (10), 1940–1941.

Zhang, Y., Peng, W., Clarke, J., and Zhishun, L. (2010). Acupuncture for uterine fibroids. *Cochrane Database Syst. Rev.* 2010. doi:10.1002/14651858.CD007221.pub2

Zhou, L. (2019). Clinical observation on 50 cases of uterine fibroid qi stagnation and blood stasis syndrome treated by integrated traditional Chinese and Western medicine. *Chin. J. Ethnomedicine Ethnopharmacy* 28 (5), 86–88.

Frontiers in Pharmacology

Explores the interactions between chemicals and living beings

The most cited journal in its field, which advances access to pharmacological discoveries to prevent and treat human disease.

Discover the latest Research Topics

See more →



Frontiers

Avenue du Tribunal-Fédéral 34
1005 Lausanne, Switzerland
frontiersin.org

Contact us

+41 (0)21 510 17 00
frontiersin.org/about/contact